MTR-TYPE NUCLEAR REACTOR SAFETY ANALYSIS

(this page is intentionally left blank)

THE USE OF EXPERIMENTAL DATA IN AN MTR-TYPE NUCLEAR REACTOR SAFETY ANALYSIS

By

SIMON E. DAY, B.SC., M.ENG.

A Thesis

Submitted to the School of Graduate Studies

in Partial Fulfilment of the Requirements

for the Degree

Doctor of Philosophy

McMaster University

DOCTOR OF PHILOSOPHY (2006) McMaster University

(Engineering Physics) Hamilton, Ontario

TITLE: The Use of Experimental Data in an MTR-Type Nuclear Reactor Safety Analysis

AUTHOR: Simon E. Day, B.Sc. (Saint Mary's University), M.Eng. (McMaster Univesity)

SUPERVISOR: Professor William J. Garland

NUMBER OF PAGES: 698

ABSTRACT

Reactivity initiated accidents (RIAs) are a category of events required for research reactor safety analysis. A subset of this is unprotected RIAs in which mechanical systems or human intervention are not credited in the response of the system. Light-water cooled and moderated MTR-type (*i.e.*, aluminum-clad uranium plate fuel) reactors are self-limiting up to some reactivity insertion limit beyond which fuel damage occurs. This characteristic was studied in the Borax and Spert reactor tests of the 1950s and 1960s in the USA.

This thesis considers the use of this experimental data in generic MTR-type reactor safety analysis. The approach presented herein is based on fundamental phenomenological understanding and uses correlations in the reactor test data with suitable account taken for differences in important system parameters.

Specifically, a semi-empirical approach is used to quantify the relationship between the power, energy and temperature rise response of the system as well as parametric dependencies on void coefficient and the degree of subcooling. Secondary effects including the dependence on coolant flow are also examined. A rigorous curve fitting approach and error assessment is used to quantify the trends in the experimental data.

In addition to the initial power burst stage of an unprotected transient, the longer term stability of the system is considered with a stylized treatment of characteristic power/temperature oscillations (chugging). A bridge from the HEU-based experimental data to the LEU fuel cycle is assessed and outlined based on existing simulation results presented in the literature. A cell-model based parametric study is included.

The results are used to construct a practical safety analysis methodology for determining reactivity insertion safety limits for a light-water moderated and cooled MTR-type core.

(this page is intentionally left blank)

SUMMARY

Reactivity initiated accidents (RIAs) are a category of events required for research reactor safety analysis. A subset of this is unprotected RIAs in which mechanical systems or human intervention are not credited in the response of the system. Light-water cooled and moderated MTR-type (*i.e.*, aluminum-clad uranium plate fuel) reactors are self-limiting up to some reactivity insertion limit beyond which fuel damage occurs. This characteristic was studied in the Borax and Spert reactor tests of the 1950s and 1960s in the USA.

The wealth of data from these reactor tests show that the self-limiting response of such a reactor is highly predictable and is consistent for a wide range of system parameters such as plate spacing, fuel loading, and core size. This is illustrated in the correlated data plots of maximum power (P_{max}), energy generated to the time of maximum power (E_{tm}), and the maximum fuel plate surface temperature rise (ΔT_{max}) for the different test cores as functions of the transient reciprocal period (α_o). The reciprocal period is a convenient index for a transient, related to the size of the initiating reactivity insertion. The three parameters P_{max}, E_{tm}, and ΔT_{max} are all indicators of the proximity and approach to the onset of fuel damage.

For an HEU MTR-type core the self-limiting response in the short period range is governed primarily by coolant voiding producing negative reactivity feedback. In this sense the self-limiting response is dependent on the voiding characteristics of the core which in turn are dependent upon the nuclear characteristics (*e.g.*, void coefficient), the heat transfer characteristics (*e.g.*, thermal resistance and heat transport) of the fuel and coolant, and the initial conditions of the system (*e.g.*, initial temperature). For LEU fuel the self-limiting behaviour is further strengthened by negative fuel temperature feedback.

Various degrees of fuel damage have been observed in the range of periods less than 10 msec ($\alpha_o > 100\ sec^{-1}$). These various types and degrees of fuel damage are directly tied to maximum fuel plate temperatures and progress in severity with shortening reactor period and increasing maximum temperature. Onset of fuel damage is considered a safety limit since breaching of the fuel plate cladding represents a compromise of a level of containment for radiation release to the environment.

Safety analysis is interested in predicting the maximum reactivity insertion which does not result in meeting or exceeding this temperature safety limit. The approach presented herein uses correlations in the reactor test data with suitable account taken for differences in important system parameters.

Specifically, a semi-empirical approach is used to quantify the parametric dependencies on void coefficient and the degree of subcooling. Secondary effects including the dependence on coolant flow are also examined.

The analysis is based primarily on the HEU step insertion test data. Further analysis, extending the results to ramp-style insertion events and the LEU fuel cycle are included, as is consideration of post insertion stability of the core.

The identification and quantification of trends and dependencies in the data confirm the generic applicability of the reactor test results to MTR-type cores for safety analysis purposes.

The results are used to construct a practical safety analysis methodology for determining reactivity insertion safety limits for a light-water moderated and cooled MTR-type core. This methodology is applicable to any such system and represents an alternative or complimentary approach to PSA analysis. Fuel damage information has been collected and used to construct a framework for deriving safety limits for reactivity insertion events.

This work also represents an extensive summary and assessment of the full scale reactor tests carried out in Borax I and the Spert Project. Details of the test cores are included as is the summary test data and a history of the projects.

ACKNOWLEDGEMENTS

No man is an island. I have many people I would like to acknowledge.

On the academic side I would like to thank my committee members, not only for valuable discussion and support but also for showing remarkable endurance. Jim Donnelly was one of the professionals who taught me my first reactor physics, in particular associated with computer simulation. His experience and advice with respect to the PARET simulations and LEU fuel analysis is greatly appreciated. Dave Jenkins ("I don't believe we've met") and Dave Jackson showed patience and enthusiasm for the project which was very important. Although not officially part of my supervisory committee I would also like to thank Fred Hoppe for his guidance and the many interesting conversations over in Hamilton Hall which revolved around applied statistics and the refined and sophisticated aspects of chalk. Thanks Fred! You are all good guys.

This project grew from a seed planted during work on the McMaster Nuclear Reactor Safety Analysis Report update in 2000-2002. I owe special thanks to Charles Blahnik who I consider my mentor. I enjoyed all of our chalk board discussions. Without Charles I may never have started down this path.

The reactor physics community is thinly spread over great distances. Special thanks to the guys down at Argonne National Laboratory; in particular Nelson Hanan for locating the old PARET benchmark input files, Jim Snelgrove for information on fuel damage and material properties, and Bill Woodruff who was always on hand, when not cross-country skiing, to field questions regarding his simulation work on the Spert data. Also thanks to Ron Ellis from down at Oak Ridge, and Tom Newton at MIT who were always available for reactor physics and related discussions. A global society of reactor physicists!

I would also like to acknowledge the tremendous work performed by the scientists and engineers of the Borax and Spert Projects: "If I have seen further [than certain other men] it is by standing upon the shoulders of giants," (Sir Isaac Newton). It truly was a pleasure and an inspiration to read through the old reports.

A special thanks must also be extended to the Thode Library staff, in particular Shawn Leslie, Brigitte Maier, and Helen Creedon (from Interlibrary Loans at Mills Library) who were always very accommodating, whether it was letting me into the catacombs of Thode Library in search of old journals or hunting, ordering, or copying technical reports from INEL. Thank you!

I would also like to thank Elvira Evangelista formerly of the Engineering Physics office who always took good care of me on the administrative side and always provided a smile and encouragement. Also thanks to Fran Allen and more recently Marylin Marlow. Thank you to Mike Butler and Chris Heysel from MNR who were very understanding about flexibility in my work schedule and for a crucial period of work relief to really crack the project open.

Finally, I would like to thank my supervisor, Bill Garland. I remember a senior student once saying that Bill let you go on a long lease that was firmly attached at both ends. I think that is a good description. Thanks Bill for sticking by me and always backing me up. Thanks for being my supervisor. I enjoyed the project and the years that went by and particularly enjoyed our chats in your office which quite often were about much more than nuclear reactor safety analysis. I consider you my friend as well as my supervisor.

Also on the personal side of things, I would like to thank Rob Leger from my research group for many enjoyable lunches, Marcelo Pomerantz for encouragement and keeping me up to date on Futbol Argentino (Boca!), and Dr. Gail Frost who always dropped a line to make sure I kept beavering away at things and didn't miss the latest scores from England. Thanks also to the rest of my friends for their support, encouragement, or simply for timely distraction throughout the course of this project. Even if you didn't really understand what I was doing (or why) you didn't let long stretches of silence get in the way!

Thanks to my family: the first Dr. Day (my Dad) who encouraged the higher education route; the second Dr. Day (my brother Graeme) who was an excellent study partner on family Christmas holidays and a fellow doctoral candidate during some of the run in (I can sure look up to my little brother who really has it going); my sister Tara and my Mum who always provided understanding and gentle voices and the occasional pep-talk when I needed them the most; the Mercuri clan who have opened their homes and hearts to me; and finally, Sandy and Mackenzie who have made our home a sanctuary and bring great joy and love to my life. Yes, "the book" is done. I love you all.

Simon

FOREWORD

So much energy from a tiny little piece of matter! Harnessing the power of the atom for peaceful uses, as the world proposed after World War II, was and remains a great feat of engineering.

With the promise of energy generation without the production of greenhouse gases or particulate pollution, nuclear power is set to help solve or alleviate two of the largest problems tied to the conventional fossil fuel industry and facing the world today. The issues related to mining and mankind's greed for resources still exist but the nuclear industry at least may help manage air and ocean pollution while a proper solution is identified. Nuclear power should certainly be considered as a component of a sustainable, or at least less self-consuming civilization. Imagine not having to live through countless "smog days" each summer or having to hear about natural gas explosions or environmentally disastrous oil spills. That is not all as in addition to the energy applications nuclear facilities produce medical radioisotopes and provide a plethora of academic and industrial research opportunities.

With this tremendous power comes just as imposing responsibilities. The nuclear fuel cycle is not closed so it is not a completely clean energy source. The debate of what to do with, or more specifically, how to take care of the radioactive inventory of spent nuclear fuel is an ever present issue. While acknowledging the issues associated with spent nuclear fuel management, this should not detract from the possible benefits associated with containing fuel waste in solid form compared to spreading it thinly (or even not so thinly as evident from looking at the horizon on summer days in Southern Ontario) throughout the atmosphere, such as in the case of fossil fuel power plants.

However, the most notorious and most recognized negative image of the nuclear industry is not the fuel cycle but rather the consequences of a severe nuclear accident. There have been several nuclear accidents as the industry grew at an extraordinary rate from chalkboards in the 1940s to power producing test reactors in the late 1960s to full operational commercial power plants in the 1970s. The most infamous of these, and the one with the largest environmental impact was the April 1986 accident at one of the four Chernobyl power units. A combination of poor design, poor construction, mis-operation, and a conflict between political and scientific interests resulted in a large fraction of the radioactive inventory contaminating the surrounding area.

Responsibility extends from the designers, the construction crews, the operators, and the teachers through all those associated with a nuclear facility. There will always

be a risk of an accident happening. However, it is possible that through careful and conscientious design and operation, a respect for the science and pride in doing a good job, this risk can be made very small. One aspect of minimizing this risk is the acquisition and assimilation of knowledge about a nuclear facility. The better your understanding of your facility the greater your ability to operate and use it in a safe and responsible manner.

Although basic nuclear science research now reaches into dozens of disciplines, the pioneering work of the nuclear industry should not be confined to the archives as it still represents the fundamental building blocks for present day research and development. With this idea at the forefront the full-scale reactor experiments of the 1950s and 1960s are revisited with an eye to application of their results to present day safety analysis for plate-fuelled water-moderated research reactors.

This thesis is presented as a small contribution to the knowledge base for the nuclear industry. In a way it is specific to a certain reactor type but the presented methodology may be applied to different systems. This project represents an extension and hopefully an improvement in the area of safety analysis.

NOMENCLATURE

AECL	Atomic Energy of Canada Limited
ANL	Argonne National Laboratory
APPR	Army Package Power Reactor (*aka*, P-Core)
Borax	Boiling Water Reactor Experiments
BSR	Bulk Shielding Reactor
CABRI	Swimming Pool Reactor Test Facility in Cadarache, France
CANDU	Canada Deuterium Uranium, power reactor design
CDC	Capsule Driver Core
DBA	Design Basis Accident
HEU	High Enrichment Uranium
IAEA	International Atomic Energy Agency
LEU	Low Enrichment Uranium
LWR	Light Water Reactor
MNR	McMaster Nuclear Reactor
MTR	Materials Testing Reactor
MTR-type	rectangular plate-fuel
NRTS	National Reactor Testing Station, Idaho, USA
ORNL	Oak Ridge National Laboratory
PPF	Power Peaking Factor
PSA	Probabilistic Safety Assessment
PWR	Pressurized Water Reactor
RERTR	Reduced Enrichment for Research and Test Reactors
RIA	reactivity initiated accident
SAR	safety analysis report
SCRAM	fast trip mechanical emergency shutdown system (safety control rod axe man)
SEU	Slightly Enriched Uranium
SL-1	Stationary Low Power Reactor 1 (*aka*., Argonne Low Power Reactor, ALPR)
Spert	Special Power Excursion Reactor Tests
SOE	Safe Operating Envelope
TREAT	Transient Reactor Test Facility
US AEC	United States Atomic Energy Commission
Chugging	oscillatory power and temperature operation
D-test	destructive test
msec	milli-second, *i.e.*, 10^{-3} seconds
mk	milli-k, unit of reactivity, 1 mk = 0.001 in terms of multiplication factor

MW	mega-watt, *i.e.*, 10^6 watts
$	dollar, unit of reactivity, \$1 / β . 7 mk
τ	reactor period, *i.e.*, power *e*-folding time
τ_o	asymptotic reactor period
α	reciprocal reactor period, *i.e.*, $1/\tau$
α_o	asymptotic reciprocal reactor period, *i.e.*, $1/\tau_o$
β	delayed neutron fraction
Λ	neutron generation time
ℓ	prompt neutron lifetime
λ	neutron precursor decay constant
ρ	reactivity
ρ_{in}	reactivity insertion
E_{tm}	energy generation to the time of maximum power
E_{tot}	total energy generation
ED	energy density
k	multiplication factor
P_{max}	maximum power
PD	power density
pr_{max}	maximum pressure
T_{max}	maximum temperature
ΔT_{max}	maximum temperature rise
T_{sub}	degree of subcooling
T_{tm}	temperature at the time of maximum power
V_f	fuel meat volume

TABLE OF CONTENTS

(this page is intentionally left blank)

CHAPTER 1 - INTRODUCTION

TABLE OF CONTENTS

LIST OF FIGURES

1 INTRODUCTION

Given the dynamics and potential consequences of a nuclear reactor accident, safety analysis is a required and necessary aspect of the design and operation of such a facility.

Part of the approach of safety analysis of a nuclear reactor involves the identification of event sequences, tied to operation and design, which can lead to accident situations. The quality of such an approach depends upon the thoroughness of the analysis in covering all possible scenarios. In conjunction with this event-sequence development is the identification of engineering limits inherent to the nuclear reactor. One type of limit is associated with runaway reactivity-initiated accidents which, although considered rare or "incredible" in most cases, are treated in safety analyses in an effort to evaluate the maximum hazards to the reactor and the general public. This limit involves the maximum reactivity perturbations (size and speed) which the system can survive, both with and without credit to shutdown safety systems. In the latter case, the inherent properties of the reactor determine the course of the accident.

The work herein is based on revisiting the experimental data set derived from the full-scale reactor transient test projects conducted in the USA during the 1950s and 1960s. The data set is extensive and contains not only information on general behaviour of reactor cores under runaway transient conditions but also information on the dependence of this behaviour on variation of certain system parameters.

1.1 Outline of the Thesis

1.1.1 Objective

The objective of this thesis is to develop a methodology for deriving reactivity limits for unprotected accident situations for a plate-fuelled water-moderated research reactor. The relevance of this work is to (a) provide more information about a certain type of nuclear reactor which can lead to better safety culture *via* procedures, operations, and general knowledge, (b) to put rare accident events into the perspective of reactivity thresholds and serious consequences, and (c) to provide an alternative or supplemental method to conventionally used simulation and probability-based analysis techniques.

1.1.2 Hypothesis

The hypothesis of this work is two-fold. Firstly, it is hypothesized that the existing experimental data set, can be interpolated and extrapolated using physical judgement of the self-limiting characteristics of plate-fuel water-moderated reactor systems, to derive reactivity limits precluding the onset of fuel damage in an unprotected accident situation.

Secondly, it is also hypothesized that current kinetic simulation codes, previously benchmarked against experimental transient data for these types of reactors, but admittedly lacking in fundamental thermal and hydraulic capabilities, can be used to provide a bridge in the experimental data between different uranium-enrichment fuel cycles, thus making the derived reactivity limits applicable to fuel-cycle converted or converting facilities.

1.1.3 Document Summary

The composition of the rest of the document is as follows:

The remainder of this chapter is broken into two sections. The first provides some background to plate-fuelled water-moderated research reactors with special attention given to the full-scale reactor tests of the 1950s and 1960s. This helps put the reactor test data used in this study into the context of modern nuclear facilities. The rest of Chapter 1 briefly reviews the different approaches to, or aspects of, safety analysis as they pertain to this project.

In Chapter 2 the physical mechanisms associated with the self-limiting behaviour of certain research reactor systems are discussed. The self-limiting system response to a reactivity perturbation is then described.

In Chapter 3 the experimental data set and the experimental details of the reactor tests are examined. This includes various considerations in using the experimental results.

Chapter 4 contains analysis investigating parametric dependencies found in the test data. Specifically, the analysis accounts for variation in core size, power distribution, and voiding, subcooling, and coolant flow characteristics.

In Chapter 5 the additional aspect of stability with respect to accident situations is considered. This is related to additional limits and is incorporated into the overall

methodology.

Chapter 6 extents the analysis of Chapter 4 to include fuel cycles of reduced uranium enrichment.

Chapter 7 presents a full methodology for determining reactivity limits for generic plate-fuelled water-moderated reactors and includes an example walkthrough of the methodology using the McMaster Nuclear Reactor (MNR).

Finally, Chapter 8 summarizes the conclusions of this work.

1.2 Background

This section provides some history and background to plate-fuelled water-moderated reactors. Included is a chronology of the full-scale reactor experiments.

1.2.1 MTR-Type Reactors

Research and Test Reactors were developed as an aid to the power reactor industry in the post Second World War era of Atoms for Peace. One of the first North American facilities was the Materials Testing Reactor (MTR) built in the early 1950s at the National Reactor Testing Station (NRTS) in Idaho, USA (Fig. 1-1 , Ref. 1-1). The MTR first went critical in 1952 and was operated until 1970. The primary design purpose of the MTR was to test materials and nuclear industry components in high-intensity radiation. It was a light-water-cooled and -moderated facility using UAl plate-type fuel. The term “MTR-type facility” is now used in a generic sense to describe any plate-fuelled light-water reactor system. The term refers to the type of core of the nuclear reactor, (*i.e.*, fuel, coolant, moderator) and is applied to both pool-type and tank-type systems.

MTR-type fuel consists of a uranium metal, often with a dispersing agent, in the form of a thin sheet (referred to as the fuel “meat”), clad on both sides, most commonly with aluminum. These fuel plates are on the order of one to two millimetres thick. A group of plates are held together by metal side-plates, with space for coolant flow between adjacent plates, constituting a rectangular fuel assembly. A schematic of an MTR-type plate fuel assembly is shown in Figure 1-2. The outer dimensions are usually close to 8 cm by 8 cm horizontally with a 60 cm fuelled vertical height. The exact thickness of the fuel meat, clad and coolant channels can vary between specific

fuel designs. For example, fuel has been used with as little as 10 plates per assembly and as many as 24 plates per assembly. The current MNR fuel design has 18 plates, the inner 16 of which contain fuel.

An MTR-type core contains these rectangular fuel assemblies in a grid pattern (Fig. 1-3). Depending upon the loading, enrichment, exact design of the fuel, reflector properties, and operational requirements, an MTR-type core typically contains anywhere from 20 to 70 fuel assemblies. Presently MNR operates with about 30 standard-fuel assemblies and six partial control-fuel assemblies.

MTR-type reactors are characterized by self-limiting properties. Under an increase in temperature these systems will tend to reduce power which subsequently reduces temperature, stabilizing the system. This self-limiting feature is strongest upon production of steam within the fuel assemblies *via* boiling when the coolant reaches saturation temperature. These "negative feedback" characteristics are an inherent safety feature of such designs and are what were investigated in the full-scale reactor experiments.

1.2.2 Self-Limiting Characteristics of Water Moderated Reactors

The full-scale reactor experiments conducted as part of the Borax (Boiling Water Reactor Experiments) and Spert (Special Power Excursion Reactor Tests) projects identified the strong self-limiting characteristics inherent in MTR-type reactor systems. (Note: despite Borax and Spert being acronyms, the convention of only capitalizing the first letter, as done in the original technical reports, is adopted herein.)

This reactor design relies on a set of basic phenomena to mitigate reactivity insertions:

- fuel plate expansion which forces water out of the coolant channels and increases the metal to water ratio of the system,
- water moderator expansion (leading to a density reduction), similarly increasing the metal to water ratio in the system,
- once the fuel plate temperature becomes high enough, water moderator boiling which provides a large negative void feedback effect, and
- fuel temperature increase providing negative Doppler reactivity feedback effect.

The speed of the power excursion dictates the relative timing and importance of these self-limiting phenomena as the fuel temperature increase is a prompt effect while the moderator expansion and voiding phenomena rely on heat transfer from the fuel material to the water. For fast power excursions the time associated with this heat transfer plays a crucial role in the response of the system. In the case of short period transients the moderator boiling and fuel temperature effects are most important, and are therefore the main focus of this thesis.

Although the inherent safety of such systems is remarkably strong, limits to the ability of an MTR-type core to self-limit a fast power excursion do exist and have been observed in both test and accident situations. Thus, the understanding of these limits and the ability to apply this knowledge to specific reactors is a useful and important exercise.

1.2.3 The Full-Scale Reactor Experiments

With the booming nuclear industry of the time (early 1950s) and the flexibility of operation and application of MTR-type facilities, many such reactors were built both for industrial and academic purposes. Several of these were built at university institutions including NC State (1953), Penn State (1955), University of Michigan (1956) and McMaster University (1959). Some of these facilities are still in operation today.

With the push on to develop power reactors the industry was growing by leaps and bounds, jumping well ahead on the learning curve of basic nuclear reactor theory. As part of the effort to keep pace, a major experimental program was put in place by the US Atomic Energy Commission (AEC) to investigate the safety characteristics of reactors (Ref. 1-2). One of the starting points of this program was with MTR-type cores. The majority of reactor test data comes from the Borax and Spert projects which operated between 1953 and 1970 at which point the main focus of the nuclear industry shifted from research reactors to power reactors, fast reactors, and fusion technology.

The data set collected during the Borax and Spert Projects represents a wealth of knowledge regarding the self-limiting characteristics of MTR-type systems under a variety of conditions. The results are well documented and publicly available. From the results of the Borax and Spert experiments an understanding of the safety characteristics of heterogeneous light water reactors has been and can be further

developed.

The following sections briefly describe the Borax and Spert projects. Detailed descriptions of the Borax I and Spert reactors are found in Appendix A. The associated data from the reactor tests are summarized in Appendix B.

1.2.3.1 The Borax Experiments

The first reactor test project, Borax, was operated by Argonne National Laboratory (ANL) and was located at the NRTS, Idaho, USA (Fig. 1-4, Ref. 1-3).

A series of reactors were built on the Borax site, the first of which, Borax I, was an MTR-type system. A photo and a schematic of the Borax I facility are shown in Figures 1-5 and 1-6. The objective of the Borax I experiments was to investigate the transient and steady-state boiling characteristics of light-water cooled and moderated reactors.

Transient tests were initiated by rapidly adding extra "reactivity" into the core by ejecting an absorber rod. The power was then allowed to increase on an exponential period (*i.e.*, the time it takes for the reactor power to increase by a factor of e . 2.72) related to the size of the initial reactivity insertion. The reactor would eventually produce enough negative reactivity feedback to halt the power excursion and reduce the power to a relatively low level. The majority of the negative reactivity feedback was produced by boiling the water between the fuel plates. The transients were allowed to evolve for up to about 20 seconds before being manually shutdown by insertion of the control rods. The general transient test sequence, common to both the Borax and Spert tests, is shown in Figure 1-7 (Ref. 1-4).

During the summer and fall of 1953, over 70 tests of a "run away" nature were conducted. Most of these tests were initiated with the coolant temperature at saturation but two test series were performed with the initial coolant temperature below the boiling point (this difference in temperature with respect to the saturation temperature of the light water is referred to as subcooling). Gradual increases in the magnitude of the inserted reactivity were made based on extrapolation of preceding test results.

Despite the highest peak power being in the range of 2600 mega-watts (MW) for all experiments conducted during 1953, the maximum fuel plate temperature remained below the damage threshold, *i.e.*, the melting point of the aluminum cladding

material (. 600EC). (Note: typical MTR-type reactor operating power is on the order of a few MW.)

During the short period transients the steam production often resulted in violent ejection of water from the core and even the reactor vessel itself. The associated pressures were enough to mechanically deform some of the fuel plates. These plates could be bent back into shape but continued testing on the weakened plates resulted in deformation even under milder pressure conditions. As a result the transient testing in 1953 was discontinued in favour of the investigation of the characteristics of operation under steady-state boiling conditions. An oscillatory behavior related to the fraction of voids in the core was noted during these tests which would later be investigated further in the Spert experiments. The steady-state boiling tests were continued in 1954 in a replacement reactor (Borax II), more suited to these operating conditions. The 1953 Borax I tests are described in detail in Reference 1-5.

In the spring of 1954, the subcooled transient experiments in Borax I were continued and it was decided to investigate the possibility of a threshold of self-shutdown ability and the possibility of fuel damage in the temperature range of the melting point of the fuel cladding material. On July 22, 1954, the Borax I reactor was destroyed by a pressure pulse following a transient with a 2.6 msec period. This test was originally intended only to melt a small fraction (about 4%) of the fuel plates (Fig. 1-8, Ref. 1-6). Fuel plate fragments were scattered over an area of 200 to 300 feet from the reactor (there was no containment building). The 1954 Borax I tests are described in detail in Reference 1-7.

The Borax I experiments demonstrated that "voiding is a most effective, reliable, and rapid power-limiting process, capable of protecting properly designed reactors against reactivity excursions which produce reactor periods shorter than 5 ms." (Ref. 1-5) Just as importantly, it was found that the results of a reactivity insertion are predictable from milder tests and the existence of a reactivity threshold for the ability to self-limit a reactivity insertion was identified. In addition, the phenomenon of "chugging", *i.e.*, coupled voiding/power oscillations, related to the stability of boiling operation was first observed.

The Borax project was continued with the construction of the Borax II facility, built in late 1954 to replace the first reactor. Borax II used the same control trailer and many of the same parts, salvaged from Borax I. The core was about twice the size of the Borax I core. This reactor included flow and pressurization systems and operated at 300 psi pressure. Transient testing was continued in Borax II but not to

the extent as in Borax I (Ref. 1-8).

In March of 1955, the second reactor, Borax II, was modified with the addition of a steam turbine-generator to become Borax III. On July 17, 1955 electricity from Borax III was first used to power the town of Arco, Idaho (population 1200) for the first time. This was the first time a city had been powered entirely by nuclear power. Borax III was operated until mid-1956. The first three Borax cores used highly enriched uranium (HEU) aluminum alloy fuel, clad in aluminum.

On December 3, 1956, Borax IV achieved first criticality. It was operated until June 1958. Borax IV was also a pressurized facility, operating at 300 psi and was used primarily to test high thermal capacity fuel materials (ceramics). It used the same plant and components as Borax III. The last Borax reactor, Borax-V, was used as an electrical power experiment and operated between February 1962 and August 1964. The Borax reactors and their programs are described briefly on the ANL-West website (Ref. 1-9).

1.2.3.2 The Spert Experiments

The Spert Project, also located at the NRTS (Fig. 1-4) and sponsored by the US AEC, was run by the nuclear division of the Phillips Petroleum Company. It was initiated in 1954 and continued through 1970. In total four Spert reactors were built and multiple cores were tested between these, at times concurrently operating, facilities.

The first phase of the Spert Project focussed on exploratory studies of the transient behaviour of light-water reactors under atmospheric and ambient conditions. The test procedure and the measured parameters were similar to those associated with the Borax experiments (see Fig. 1-7). General tests with both step and ramp insertions and varying reactor conditions were performed as were more specific tests designed to study specific shut-down mechanisms. In addition, upon discovery of large self-induced oscillations, similar to those reported from the Borax I tests, the Spert Project was broadened to include stability testing.

By 1960, a large amount of data had been collected from the exploratory phase of the program concerned mainly with typical research reactor operating conditions. Emphasis shifted first to studying the effects of elevated temperature, pressures and forced flow, more typical of power reactor systems and then to the study of low enrichment uranium (LEU) oxide rod-type cores. In addition, a destructive test program was designed and initiated first with HEU plate-fuel and then with LEU rod-

fuel. Finally, by the mid-1960s, the emphasis of the project shifted for a final time. The integral core experiments were discontinued in favour of the subassembly testing program where fuel samples could be studied under severe conditions without damage to the rest of the core, which was used as a driver. These driver cores were used in the Spert reactors while a separate facility was readied to take over the subassembly test program. The Spert Project is outlined in References 1-10, 1-11, and 1-12 and many associated quarterly technical reports. A brief summary of the experimental program for each Spert reactor follows.

Spert I first went critical on July 11, 1955. Similar to the Borax I facility, it was light water cooled and moderated, and operated under atmospheric pressure conditions. Testing began with the objective of repeating and extending the exploratory transient tests started in Borax I. Studies of the variation of the void coefficient were included as were stability tests.

The first core in Spert I, designated the "A-core" was composed of highly-enriched aluminum-clad MTR-type plate-fuel assemblies. Testing on the A-core continued until May 24, 1957, and included 606 transient tests, most of which were initiated by step insertions of reactivity at ambient temperatures. In addition some ramp reactivity insertions tests, stability tests, and tests investigating the effects of the size of the hydrostatic head, characteristics of the moderator, initial power level, and other miscellaneous factors were performed.

The A-core was replaced with the "B-core" series in July 1957. The Type-B fuel assemblies were created with removable plates so that the number of fuel plates per assembly and the spacing between them could be varied. The objective of the B-core series of tests was to investigate the effect of changes in the void coefficient on the transient behaviour. Three different B-cores were studied, the B-24/32, B-16/40 and B-12/64 configurations. Following the B-cores, other plate-fuel cores were tested in Spert I including the stainless-steel clad Army Package Power Reactor (APPR) core, also designated the P-18/19 core, and the stainless-steel clad Bulk Shielding Reactor II (BSR-II) core borrowed from the Oak Ridge National Laboratory (ORNL).

In February 1961, the first LEU core was loaded into a Spert reactor. The original plans had called for testing of a low-enrichment plate-type core, similar to that used in Borax IV (Ref. 1-12) but these were altered to use a rod-type uranium-oxide fuel typical of that used in power reactors. The core was designated the SA-592 core in Spert I. The objectives of the LEU oxide testing program were to investigate the additional effects of reduced conductivity of the fuel material and the increased

prompt negative reactivity feedback due to the Doppler effect.

Following the testing of the LEU SA-592 core in Spert I, the D-12/25 (HEU, UAl plate-type) core was installed. An integral (*i.e.*, involving the entire core as opposed to a subassembly test where the core is only used as a driver) destructive test was carried out on November 5, 1962 (Fig. 1-9). Following this test, the Spert I facility was repaired and reused in further LEU rod-type core tests. Two potentially destructive tests were carried out with the Spert I OC-core (very similar to the SA-592 core). The first was conducted on November 10, 1963 and the second on April 14, 1964. Finally, the Capsule Driver Core (CDC) was installed in Spert I for preliminary testing before it was moved to Spert IV. Spert I was deactivated in September of 1964.

Spert II was designed to be able to house cores cooled and moderated by different materials, namely light and heavy water. Provisions were made to accommodate higher temperatures and pressures and both upward and downward coolant flow. Construction of Spert II was started in August 1957 and after numerous delays given a lower priority compared to the Spert I and Spert III facilities, it was completed on February 1, 1960. It first went critical with a light-water moderated core in March 1960 and with a heavy-water moderated core in August 1960. Initial testing was with the B-12/64 core moderated and cooled with light water. This was the same core design as used in Spert I. Upon completion of this test series the light water was replaced by heavy water. Two heavy-water moderated core configurations were studied, one close-packed, similar to those used in Spert I and Spert III, and the second expanded. Tests continued until the end of 1964.

Because of the rapidly expanding US power program, precedence during construction was given to Spert III ahead of Spert II. The Spert III construction was completed ahead of the Spert II construction and operation was handed over to Phillips Petroleum Company on October 23, 1958. First criticality was achieved on December 19, 1958. Provisions for high temperature, high pressure, forced coolant flow and heat removal were included in the facility. Spert III was designed primarily to investigate transient behaviour under conditions more typical of power reactors systems, *i.e.*, high temperature, pressure and forced coolant flow. A test series was conducted on the stainless-steel clad C-19/52 HEU plate-fuel core, which was completed by the end of 1964. Spert III endured a long shutdown from October 26, 1961 until January 1964 due to the failure of the pressure vessel. In January, 1965, the C-19/52 core was replaced with the E-core with which testing on LEU oxide rod-type fuel was continued.

The Spert IV facility was designed to continue the stability testing program started in Spert I. Spert IV was built as a pool-type reactor rather than a tank-type reactor and included provisions for forced flow and heat removal. It first went critical on July 24, 1962 with the aluminum-clad D-12/25 plate fuel core, similar to that used in Spert I. The stability program was continued until the spring of 1964 at which point the facility was used for mock-up experiments for the Power Burst Facility (PBF) and later for the subassembly testing program using the Capsule Driver Core (CDC) in the interim while the graphite-moderated and pulse-operated Transient Reactor Test (TREAT) Facility was being readied.

1.2.3.3 Other Experiments

The Borax and Spert experiments represent the majority of full-scale reactor experiments of this type. In addition to these projects the January 3, 1961 accident at the Army-operated SL-1 (Stationary Low Power Reactor 1), also located at the NRTS, has relevance to the self-limiting behaviour of MTR-type cores. This accident resulted from mishandling of the central control rod and led to a large fast reactivity insertion. The SL-1 core was destroyed and the power excursion, recorded on the reactor instrumentation and calculated from data acquired in the recovery process, shared many similar characteristics to the Borax and Spert destructive tests. Information on the SL-1 system and accident is included in Appendices A and B.

Other experimental programs relevant to MTR-type reactor safety have been performed. Tests similar to the Spert HEU plate-fuel transient experiments were carried out at the CABRI swimming-pool reactor facility in Cadarache, France (Refs. 1-13, 1-14). Also of relevance are: (i) the subassembly testing program carried out in the latter stages of the Spert Project and continued in the Transient Reactor Test Facility (TREAT) which investigated fuel sample behaviour under severe power excursion conditions, and (ii) transient heat transfer experiments which were conducted in Grenoble, France, the United States and the United Kingdom (Refs. 1-13, 1-14, 1-15). The results of these tests may compliment the Borax and Spert data but are not included in this work.

1.2.4 Non-Proliferation and the RERTR Program

Although research and test reactors represent an established technology, the topic of safety analysis is currently an active research area.

In 1978 a non-proliferation (safeguards against the spread of bomb-grade nuclear

material, *i.e.*, HEU fuel) initiative was started at ANL by the US Department of Energy (DOE) to convert the existing light-water and other research reactors from the use of HEU to LEU fuel. This program is called the Reduced Enrichment for Research and Test Reactors (RERTR). Annual meetings are held to report progress on conversion projects and to discuss the latest reduced enrichment technology. The present mandate is to convert all US and Russian supplied research reactors from HEU to LEU fuel cycles within ten years as of 2002. This involves safety evaluations needed to implement the conversions (Ref. 1-16).

To this point a considerable amount of work has been conducted with respect to safety analysis concerns related to such a fuel conversion. The International Atomic Energy Agency (IAEA) has funded projects which have produced two guidebooks on this topic (Refs. 1-17, 1-18).

The current research and test reactor community may still be dominated by, but is not limited to, 30 to 50 year old facilities. Prompted by the lucrative and growing field of medical isotope production, construction of new small reactors is underway, including two of the Canadian MAPLE design and one traditional MTR-type reactor in Sydney, Australia. Other research reactors have either recently been built or are planned in Germany (FRM-II), Russia (PIK) and France (at Cadarache).

Although not explicitly a goal of the RERTR program, a benefit of the fuel cycle conversion from HEU to LEU is the improved inherent safety which is associated with a significant Doppler feedback contribution. This self-limiting characteristic of LEU light-water systems is prompt in nature and along with the strong void feedback of these systems is a primary self-limiting mechanism.

1.3 Aspects of Safety Analysis

This section outlines the concept of safety in relation to an operating facility and reviews different aspects and approaches to safety analysis.

The bottom line for operation of a nuclear facility is to avoid exposure of workers and the general public to radiation. This may result from operational hazards, such as working in high radiation fields from equipment or handling materials, or more dramatically from accidental radiation releases.

The largest radioactive inventory in a nuclear reactor is contained in the fuel of the

operating core. Uranium is fissioned, producing not only energy but also a distribution of radioactive nuclei called fission products. These are the fragments of the fissioned uranium (or other actinide) nuclei. These fission products have a wide range of radioactive half-lives, ranging from very short-lived species (micro-seconds to minutes), through those with half-lives on the order of hours and days, to those which have half-lives of many years.

The fission product inventory is kept contained by the physical characteristics of the fuel, which is typically sheathed by a cladding material. This cladding is designed to maintain its integrity through the exposure life and as a result represents the first stage of containment of the fission products. Events which lead to fuel cladding failure such as cracking, melting or other ruptures will lead to fission product release. The limiting accident, in terms of the maximum hazard, is complete disassembly of the reactor core which results in the release of the entire fission product inventory.

Safe operation of a nuclear facility is ensured by careful and experienced design, operation, maintenance and regulation. Additionally, a long chain of independent failures are required to place a nuclear reactor in an unsafe state. In this sense it is very unlikely that an accident of any notable consequence will occur in a properly constructed and operated nuclear reactor. In addition to attention to proper normal operation, regulations on the nuclear industry require facilities to provide a safety analysis report (SAR). This work often includes the identification and analysis of the worst case "credible" accident scenario. This is commonly referred to as the "design basis accident" (DBA) for a new facility or a "design assessment accident" for an existing facility.

One class of accident scenarios is reactivity initiated accidents (RIAs) which are events in which a reactivity insertion places the reactor in a super-critical state and the power increases. If left unchecked this situation has the potential to ultimately result in fuel damage and radiation release to the environment. The worst case scenario is core disassembly. This was in fact the DBA for the Spert reactor hazard summary reports (*e.g.*, Ref. 1-19).

Typically, instead of considering core disassembly or even fuel damage as the DBA, event sequences (in the form of "event trees") are developed which identify the most likely, most serious scenarios.

1.3.1 The Safety Analysis Concept

Operations of a nuclear reactor from the standpoint of safety is illustrated in the concept diagram of Figure 1-10. For normal operations, the reactor conditions are kept within a safe operating envelope (SOE), shown as the inner circle in Figure 1-10.

The SOE represents a conservative limit on power, flow rates, temperatures and reactivities and is enforced *via* administrative controls. Physically, such limits can be associated with the onset of boiling or maximum fuel or coolant temperatures.

Beyond the SOE is a second limit associated with the onset of fuel damage. This is shown as the middle circle on Figure 1-10. This boundary, unlike the SOE, is directly associated with a physical damage threshold. The exact definition of the onset of fuel damage may vary slightly depending on the type of system and the regulatory limits on such a system. For example, fuel centerline melting, fuel clad blistering, and fuel clad melting, are all examples of putting this limit into practice. They may occur under different physical conditions but all represent the same concept which is the release of radioactivity from the nuclear fuel. In this sense, the SOE can be thought of as starting at the onset of fuel damage limits but then adding significant conservative margins. The onset of fuel damage limits are defined by the system behaviour under accident conditions such as flow blockage, reactivity-initiated power excursions and loss of coolant scenarios.

Beyond the onset of fuel damage limit is another limit, representing the acceptable dose to the facility staff and the general public. This is shown as the outer circle on Figure 1-10. This is the bottom line and represents the maximum hazards of such a facility. It is defined by the containment characteristics of the facility, the exclusion zone (if any) and the dispersion behaviour of any releases.

During a safety analysis of a nuclear reactor, various accident events are considered. Each event is associated with a certain set of conditions which place it somewhere on the phase space defining the SOE, the onset of fuel damage and the acceptable dose limits. The placement of each event with respect to these limits, shown as an "x" on Figure 1-10, determines its severity. The design and operation of nuclear facilities are such that events which fall further out from the middle of the concept diagram (Figure 1-10), *i.e.*, further from normal operating conditions, are associated with significantly smaller probabilities of occurrence.

The nuclear industry is tightly regulated. Although the chances of a severe accident are extremely low, regulations require the nuclear industry to consider rare events. The rationale being that the associated consequences are important enough to warrant treatment of such scenarios in safety-analysis work. This is somewhat inconsistent with respect to other industries such as air transportation, natural gas and oil supply and transportation, and mining for which catastrophic accidents have occurred on a much higher frequency, often with debatably more severe consequences.

This thesis is concerned with the second of the three boundaries shown in Figure 1-10, the onset of fuel damage. More specifically, the derivation of reactivity limits associated with this boundary.

1.3.2 The PSA-Cutoff

The concept of risk is an integral part of the modern day nuclear industry. The analytical approach to this concept is referred to as probabilistic safety assessment (PSA) and involves combining the consequence of an event (*e.g.*, the radioactive exposure of the general public) with the probability of said event occurring over a given time frame. Through the use of sequences and reliability data, fault trees and event trees are constructed which lead to the assignment of probabilities for certain chains of events. In this way the "risk" associated with a nuclear facility is quantified. It is customary to consider events with frequencies of occurrence of less than one in one million per year (*i.e.*, $< 10^{-6}$ events per year) as rare events. The usual methodology of a safety analysis is to explicitly analyse any event with a frequency of greater than 10^{-6} events per year but to only identify events with frequencies less than 10^{-6} events per year. This is called the PSA-cutoff, and answers the question of "what if" with "chances are it won't happen."

To reduce the risk of accidents, the nuclear industry practices the philosophy of defence in depth by equipping a nuclear reactor with multiple, independent safety shutdown systems and multiple, independent barriers to radioactive release. The engineered safety shutdown systems are built to be able to mitigate accident conditions in a fast and reliable manner. The reliability of such systems results in the probability of a severe accident, in which the shutdown systems fail to deal with the problem, being extremely low, well beyond 10^{-6} events per year. As a result, anticipated transients without shutdown intervention by the engineered safety systems are often dealt with to the extent of proclaiming them rare events from a PSA point of view.

An interesting characteristic is evident when comparing power and research (and test) reactors. Research reactor systems, by design, tend to be more simple than power reactors and are not operated under such extreme conditions of temperature or pressure. As a result, it is common that a research reactor relies on a single emergency shutdown system while power reactors are typically required to have more than one fast-acting emergency shutdown system. This is the case in MNR, where the only safety-shutdown system is the addition of absorber (SCRAM) rods. It should be noted that there are multiple, diverse signalling systems to actuate these shutdown rods. From a PSA standpoint, what is lacking in redundancy in research reactor shutdown systems is made up for by the robustness and reliability of such systems. In the case of many research reactor designs, inherent safety characteristics may be thought of as an additional safety shutdown system.

PSA analysis therefore presents part of the picture. This approach is often thought of as inadequate from the general public's point of view and is an inherent and ongoing problem of public perception of the nuclear industry. Even from a scientific point of view the PSA-cutoff is not particularly satisfying.

1.3.3 Accident Analysis

The other main part of safety analysis is event or accident analysis, which explicitly analyses the initiating events and considers them in relation to limits of the system and the resulting consequences. One class of event is a reactivity initiated accident (RIA) which can be further classified as either "protected" or "unprotected". The former credits the actions of mechanical safety systems (*e.g.*, SCRAM rod insertion) while the latter relies completely on inherent characteristics of the core.

This type of analysis puts the "limiting" initiating events into context with the inherent limits of the system, *i.e.*, to compare input reactivity limits defined by operations and procedures with the physical limits related to the onset of fuel damage. In terms of RIAs these physical limits are the reactivity thresholds for the onset of fuel damage. Typically, limiting step (instantaneous) and ramp (gradual) additions of reactivity are considered.

Accident analysis therefore extends the PSA approach by answering the "what if" question.

1.3.4 Simulation of Power Excursions

One of the objectives of the Spert Project was to develop analytical tools to simulate power excursions in research and power reactors. Most of the early work was with the "shutdown model", based on the Fuchs' model, in which the major assumption is that the shutdown effect is proportional to the energy release of a transient (see for example, Ref. 1-20). This approach lumps the affects of the various feedback mechanisms into one "shutdown coefficient" and while generating some useful empirical correlations does not independentlylend itself to much of a physical understanding of the self-limiting characteristics of the MTR-type systems in question. (Note: the Shutdown Model is used in conjunction with the experimental data in Chapter 4.)

Post Spert, development of analytical methods continued based on more mechanistic methods, with attempts to simulate the Spert transients being met with somewhat limited and varying success (Refs. 1-21, 1-22, 1- 23). This eventually led to the creation of codes such as PARET which has been further developed at ANL and represents the state of the art in coupled physics and thermal-hydraulics kinetic analysis for research reactors (Refs. 1-24, 1-25). PARET models have been compared to selected transients from Spert I, Spert II, and Spert IV including the Spert I D-core destructive tests and has also been used in calculations for the IAEA 10 MW benchmark core for generic transient analysis core conversion studies (Refs. 1-26, 1-27, 1-28). Other groups have also modelled Spert experiments, including Atomic Energy of Canada Ltd. (AECL) using the code TANK (Ref. 1-29). The objective of modelling the Spert experiments is to validate the desired code systems for application to other research reactor systems.

The accuracy of simulation of severe unprotected transients rests in the ability to model transient heat transfer associated with complex hydrodynamic states within the core. The associated governing equations for transient heat transfer contain heat transfer coefficients which are dependent upon the local conditions of the media. The validity of a solution is reliant upon knowledge of these coefficients. There is a lack of a fundamental understanding of the transient heat transfer process and as a result these parameters are only known in empirical form. The existing empirical correlations are often based on steady-state data or on transient experiments in which the conditions are quite different from those existing in an MTR-type reactor core.

Similarly, the mechanism of transient void formation and the associated hydrodynamics are also modelled in an empirical manner which is a notable

simplification of complex processes. Transient heat transfer experiments and simulation approaches for MTR-type reactors are summarized in References 1-14, 1-15 and 1-24. The lack of reliable transient thermal-hydraulic data and theory are recognized limitations for simulation tools (Ref. 1-26).

Given the issues, simulation models are commonly adjusted to fit to experimental data. However, the use of heat transfer correlations and other fitting parameters does not lend itself to an understanding of underlying physical processes and development of a generic quantitative theory or to quantitative application of the results to other systems. Benchmarking success has also been limited to accident response only up to the time of peak power and the onset of significant coolant boiling. In any event attempts to identify reactivity limits with respect to fuel damage have been made in terms of simulation of unprotected RIAs (Refs. 1-30, 1-31). Most of the weight of modern-day safety analysis is placed on this sort of simulation.

Comparisons of the Borax I and Spert I A data show that although the qualitative behaviour is the same, marked differences in quantitative response between similar MTR-type systems exist (Ref. 1-32). Therefore, in the absence of additional experimental data, simulation models and results from a benchmarked problem should only be applied to other systems at best in a relative sense and failing that in a qualitative manner.

However, even with all of the recognized complexities and limitations associated with the modelling of transients, simulation still represents a powerful analysis tool. Although absolute results may be hard to justify, relative changes and parametric studies can provide important trend analysis to be used in conjunction with the existing theory and the experimental data set.

With this in mind the reactor experiments provide data which has captured the link between local and core distributed characteristics and integral core behaviour. This is the beauty of the experimental results and the key to unlocking the information will also open the door to improvements in simulation methods.

1.3.5 Previous Uses of the Reactor Test Data

In addition to providing data for code benchmarking, the experimental results have been used previously in the context of MTR-type reactor safety analysis. These instances are outlined below.

The Ford Nuclear Reactor (FNR) quotes a total step insertion limit of 0.18 %k/k (18 mk) from an initial temperature of 21EC in their hazards evaluation for their 1957 and 1984 SARs (Refs. 1-33, 1-34). This is based on published work by Luckow and Widdoes (Ref. 1-35) which develops a subcooling relation from the Borax I data. Sensitivity to other parameters is treated qualitatively.

MIT used correlations based on some of the test data to arrive at a similar maximum reactivity insertion limit in their 1970 and recent SAR updates (Refs. 1-36, 1-37). This analysis takes into account variations in the void coefficient of reactivity but treats other parametric variations in a conservative but qualitative manner.

A reactivity limit was also quoted in the MNR 1970 SAR (Ref. 1-38) but no parametric analysis was included with the limiting value simply taken directly from the Borax I destructive test. This represents a misuse of the test data as the Borax limit is not necessarily conservative with respect to MNR. In 2002 the MNR SAR was updated (Ref. 1-39) and the maximum reactivity limit analysis was extended to include a subcooling adjustment similar to that used by FNR as well as a parametric adjustment with respect to power distribution. Other differences were treated in conservative or qualitative manners.

These examples represent partial use, and in one case misuse, of the reactor test data. The work herein represents a more complete parametric study and develops a more complete SAR methodology based on deriving reactivity limits from the test data. This area of research has been identified as missing from or under-developed in current safety analysis approaches for research and test reactors (Ref. 1-40). MTR-type reactors still operate around the world, in North American, South America, Europe and Asia with new facilities a possibility. Thus, the relevance of this work to the nuclear industry is underlined.

1.4 References

1-1. "Experimental Power and Test Reactors", US AEC Technical Report TID-4562, November 1956.

1-2. R. H. Graham, D. G. Boyer, "AEC Steps Up Reactor Safety Experiments", Nucleonics, v. 14, n. 3, pp. 45-47, March 1956.

1-3. SL-1 Report Task Force, "IDO Report on the Nuclear Incident at SL-1 Reactor, January 3, 1961 at the National Reactor Testing Station", US AEC Technical Report IDO-19302, January 1962.

1-4. W. E. Nyer, S. G. Forbes, F. L. Bentzen, G. O. Bright, F. Schroeder, T. R. Wilson, "Experimental Investigations of Reactor Transients", US AEC Technical Report IDO-16285, Phillips Petroleum Co., April 20, 1956.

1-5. J. R. Dietrich, D. C. Layman, "Transient and Steady State Characteristics of a Boiling Reactor. The Borax Experiments, 1953", ANL-5211 (also listed as AECD-3840), Argonne National Laboratory, USA, February 1954.

1-6. T. P. McLaughlin, S. P. Monahan, N. L. Pruvost, V. V. Frolov, B. G. Ryazanov, V. I. Sviridov, "A Review of Criticality Accidents, 2000 Revision", LANL Technical Report LA-13638, Los Alamos National Laboratory, Los Alamos, New Mexico, U.S.A., May 2000.

1-7. J. R. Dietrich, "Experimental Investigation of the Self-Limitation of Power During Reactivity Transients in a Subcooled, Water-Moderated Reactor. Borax I Experiments, 1954", ANL-5323, (also listed as AECD-3668), Argonne National Laboratory, USA, 1954

1-8. J. R. Dietrich, "Experimental Determinations of the Self-Regulation and Safety of Operating Water-Moderated Reactors", in the Proceedings from the First International Conference on the Peaceful Uses of Atomic Energy, Geneva, 1955, Argonne National Laboratory, v. 13, pp. 88-101.

1-9. "Reactor Homepage" website, Argonne National Laboratory, http://www.anlw.anl.gov/anlw_history/reactors/.

1-10. W. E. Nyer, S. G. Forbes, "Spert Program Review", US AEC Technical Report IDO-16415, Phillips Petroleum Co., September 27, 1957.

1-11. J. C. Haire, Jr., "A Summary Description of the SPERT Experimental Program", Nuclear Safety, v. 2, n. 3, March 1961, pp. 15-23.

1-12. W. E. Nyer, S. G. Forbes, "Spert Program Review", US AEC Technical Report IDO-16634, Phillips Petroleum Co., October 19, 1960.

1-13. H. B. Smets, "Reactor Safety Research - Water Reactor Behavior During Rapid Power Variations Subject of International Meeting", Nuclear News, v. 9, n. 7, pp. 32-33, 1966.

1-14. M. Nyer, "Study of Thermal and Hydraulic Phenomena Accompanying a Rapid Power Excursion on a Heating Channel", PhD dissertation from Grenoble University, France, 1967, published as Oak Ridge National Laboratory Technical Report ORNL/TR-89/34.

1-15. R. P. Morgan, "A Review and Discussion of Literature Concerning Transient Heat Transfer and Steam Formation", US AEC Technical Report IDO-17226, Phillips Petroleum Co., March 1967.

1-16. A. Travelli, "Status and Progress of the RERTR Program in the Year 2002", in the Proceedings from the 2002 International Meeting on Reduced Enrichment for Research and Test Reactors, November 3-8, 2002, Bariloche, Argentina.

1-17. "Research Reactor Core Conversion from the use of Highly Enriched Uranium to the use of Low Enriched Uranium Fuels Guidebook", International Atomic Energy Agency Technical Document IAEA-TECDOC-233, Vienna, Austria, 1980.

1-18. "Research Reactor Core Conversion Guidebook", International Atomic Energy Agency Technical Document IAEA-TECDOC-643, Vienna, Austria, April 1992.

1-19. G. O. Bright, J. E. Grund,"Hazards Summary Report for Spert II", US AEC Technical Report IDO-16491, Phillips Petroleum Co., February 17, 1959.

1-20. S. G. Forbes, F. L. Bentzen, P. French, J. E. Grund, J. C. Haire, W. E. Nyer, and R. F. Walker, "Analysis of Self-Shutdown Behavior in the Spert I Reactor", US AEC Technical Report IDO-16528, Phillips Petroleum Co., July 23, 1959.

1-21. W. J. Turner, "Calculation of 'Spert' Transients", Journal of Nuclear Energy, v. 22, 1968, pp. 397-409.

1-22. B. E. Clancy, J. W. Connolly, B. V. Harrington, "An Analysis of Power Transients Observed in SPERT I Reactors. Part I: Transients in Aluminum Plate-Type Reactors Initiated at Ambient Temperature", AAEC/E345, Australian Atomic Energy Commission, 1975.

1-23. B. E. Clancy, J. W. Connolly, B. V. Harrington, "An Analysis of Power Transients Observed in SPERT I Reactors. Part II: Dependence of Burst Parameters on Initial Temperature and Core Moderation", AAEC/E383, Australian Atomic Energy Commission, 1976.

1-24. C. F. Obenchain, "PARET - A Program for the Analysis of Reactor Transients", US AEC Technical Report IDO-17282, Phillips Petroleum Co., January 1969.

1-25. R. S. Smith, "PARET Code Revisions", ANL Intra-Laboratory Memo to A. Travelli, Argonne National Laboratory, December 7, 1987.

1-26. W. L. Woodruff, "A Kinetics and Thermal-Hydraulics Capability for the Analysis of Research Reactors", Nuclear Technology, v.64, February 1984, pp. 196-206.

1-27. W. L. Woodruff, "The PARET Code and the Analysis of the SPERT I Transients", ANL/RERTR/TM-4, Proceedings of the International Meeting on Research and Test Reactor Core Conversions from HEU to LEU Fuels, 1982.

1-28. W. L. Woodruff, N. A. Hanan, J. E. Matos, "A Comparison of the RELAP5/MOD3 and PARET/ANL Codes with the Experimental Transient Data from the Spert IV D-12/25 Series", from the Proceedings of the 1997 International Meeting on Reduced Enrichment for Research and Test Reactors, Jackson, Wyoming, USA, October 5-10, 1997.

1-29. R. J. Ellis, "The Reactor Kinetics Code TANK: A Validation against selected SPERT 1B Experiments", IAEA SM-310/103, in Proceedings of the IAEA International Symposium on Research Reactor Safety, Operations, & Modifications (held at Chalk River Laboratories, October 23-27, 1989), Atomic Energy of Canada Limited report, AECL-9926, Vol. 2, pp. 395-409,

March 1990.

1-30. A. M. Mirza, S. Khanam, N. M. Mirza, "Simulation of Reactivity Transients in Current MTRs", Annals of Nuclear Energy, v. 25, n. 18, pp. 1465-1484, 1998.

1-31. J. E. Matos, K. E. Freese, "Safety Analyses for HEU and LEU Equilibrium Cores and HEU-LEU Transition Core for the IAEA Generic 10 MW Reactor", IAEA-TECDOC-643, Vol. 2: Analysis, App. A-F, Vienna, Austria, April 1992.

1-32. W. E. Nyer, S. G. Forbes, F. L. Bentzen, G. O. Bright, F. Schroeder, T. R. Wilson, "Transient Experiments with the Spert I Reactor", Nucleonics, v. 14, n. 6, pp. 44-49, June 1956.

1-33. Ford Nuclear Reactor - Description and Operation, Michigan Memorial Phoenix Project, University of Michigan, June 1957.

1-34. Safety Analysis, Ford Nuclear Reactor, Michigan Memorial Project, University of Michigan, Docket 50-2, License R-28, 1984.

1-35. W. K. Luckow, L. C. Widdoes, "Predicting Reactor Temperature Excursions by Extrapolating Borax Data", Nucleonics, v. 14, n. 1, pp. 23-25, January 1956.

1-36. Safety Analysis Report for the MIT Research Reactor (MITR-II), MITNE-115, October 1970.

1-37. Safety Analysis Report for the MIT Research Reactor, draft version of Chapter 13, *circa* November 2002.

1-38. McMaster Nuclear Reactor, Safety Analysis Report, Hamilton, Ontario, Canada, 1972.

1-39. McMaster Nuclear Reactor Safety Analysis Report, McMaster University, Hamilton, Ontario, Canada, February 2002.

1-40. Wm. J. Garland, C. Heysel, "McMaster Nuclear Reactor Safety Analysis Methodology Overview", presented at the IAEA Technical Meeting on Safety Analysis for Research Reactors, Vienna, Austria, June 3-7, 2002.

1.5 Figures

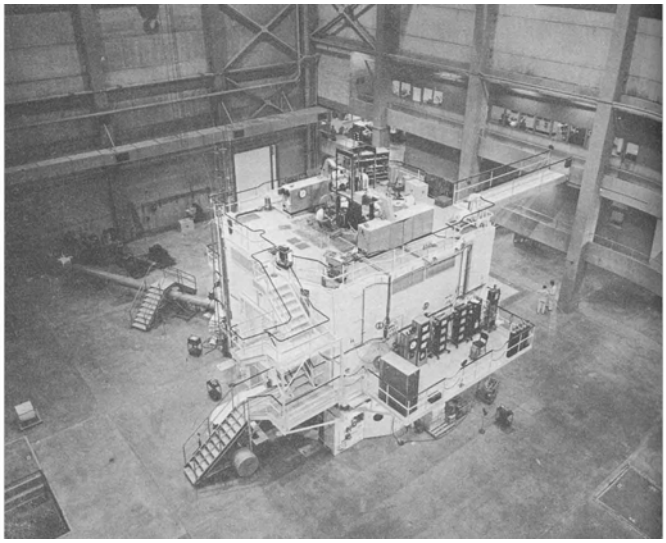

Figure 1-1: View of the MTR from the crane operator's cab (Ref. 1-1).

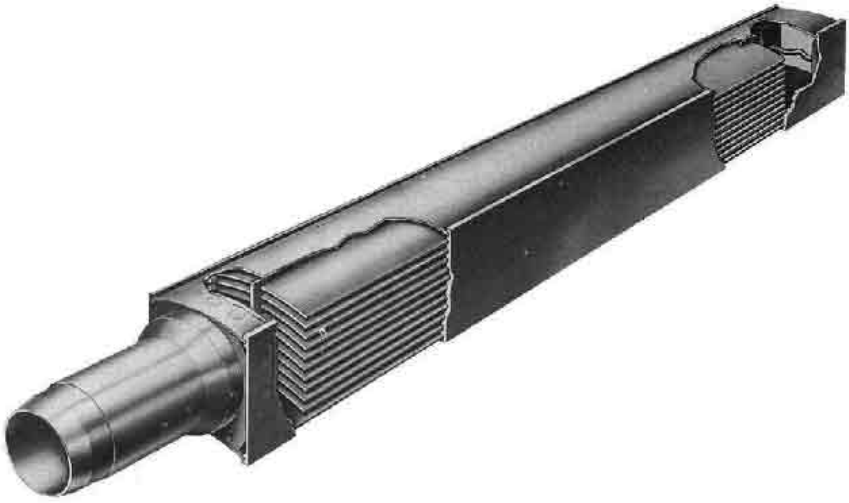

Figure 1-2: Schematic of an MTR-type Plate Fuel Assembly. Cutaway Sections show Fuel Plates.

Figure 1-3: Overhead Photograph of the MNR Core. The man on the left is holding a fuel assembly (Photo courtesy of Tom Boschler).

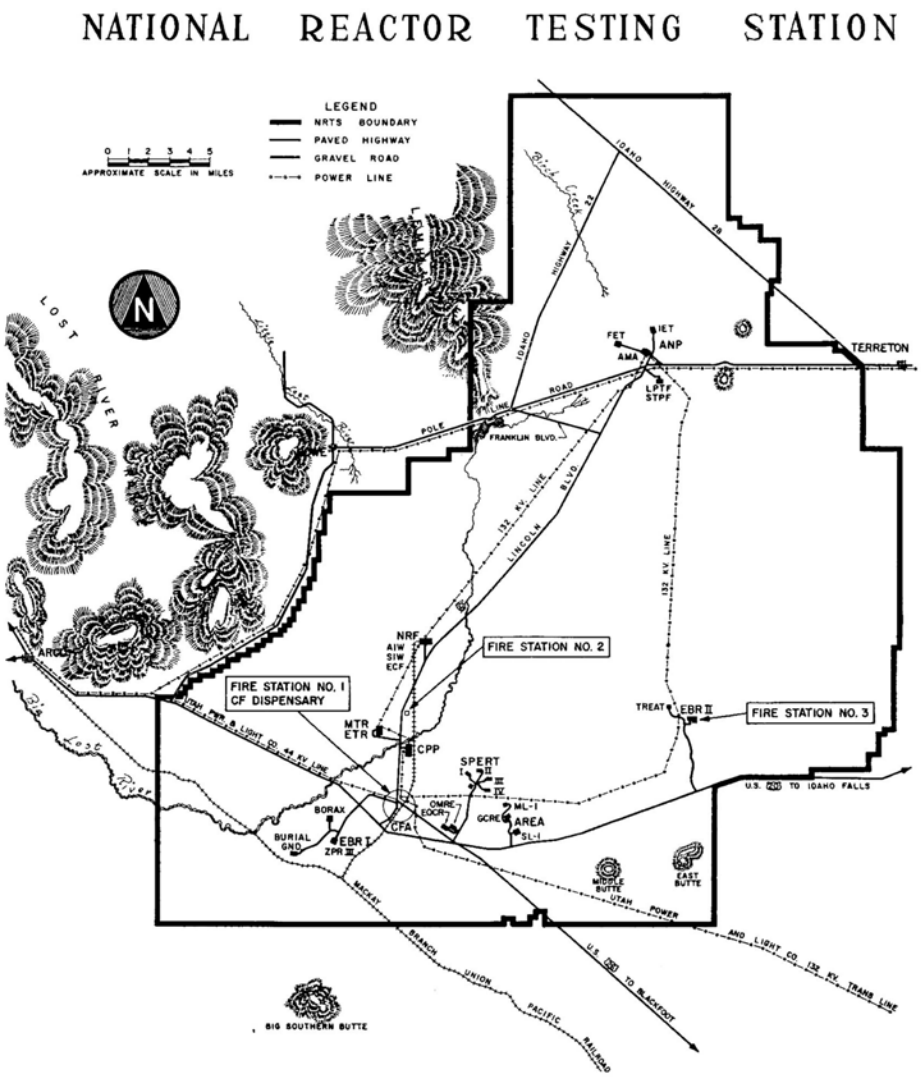

Figure 1-4: Site Plan of the National Reactor Testing Station (NRTS) in Idaho, USA, *circa* 1962 (modified from Ref. 1-3).

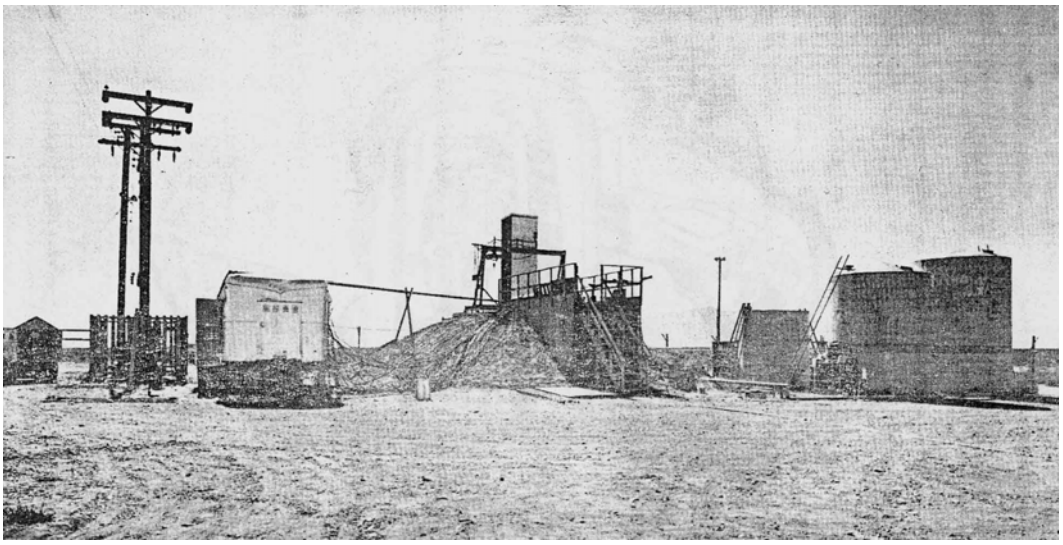

Figure 1-5: Borax I Site at the National Reactor Testing Station, Idaho, USA, *circa* 1954. The view is toward the reactor through the pump pit. The trailer on the left contains the recording instruments. Tanks on the right hold a supply of shield water and deionized reactor water. (Ref. 1-7)

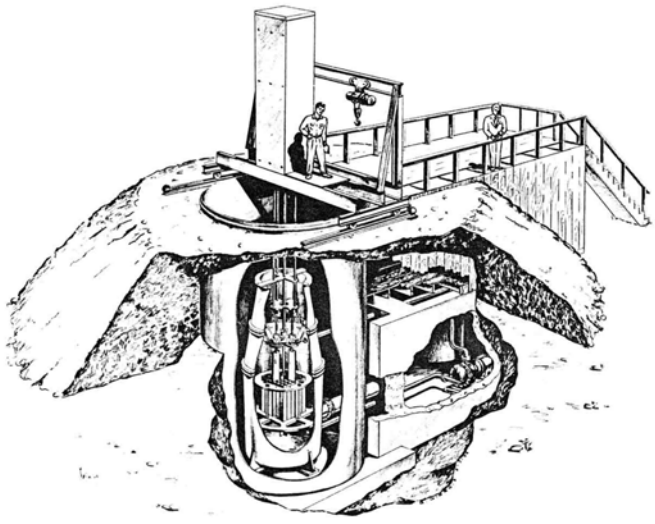

Figure 1-6: Cutaway Drawing of the Borax I Reactor Showing Partial Underground Location. (Ref. 1-7)

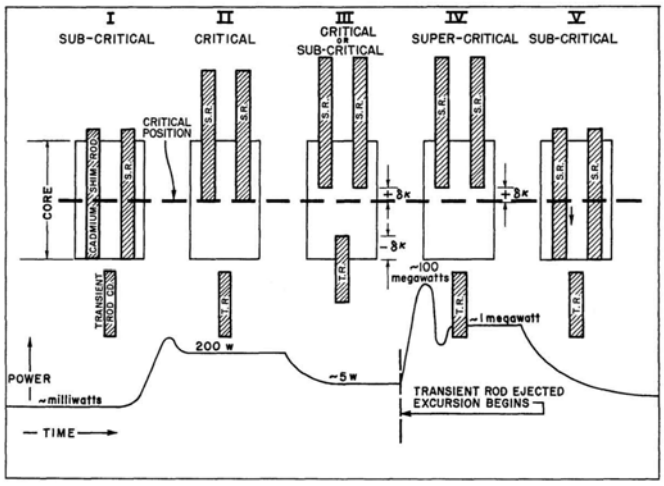

TRANSIENT TEST SEQUENCE

Figure 1-7: Schematic Drawing of the Transient Test Sequence used in the Borax and Spert Experiments (Ref. 1-4)

Figure 1-8: Steam and Water Expulsion from Borax I during the July 22, 1954 Destructive Test (Ref. 1-6)

Figure 1-9: Steam and Water Expulsion from the Spert I Destructive Test on November 5, 1962 (Ref. 1-4)

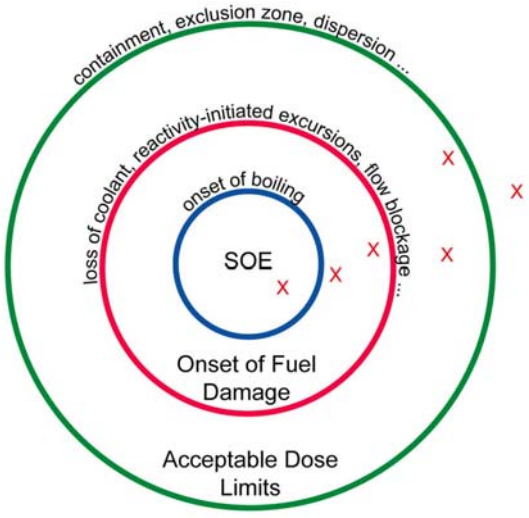

Figure 1-10: Safety Concept Diagram

(this page is intentionally left blank)

CHAPTER 2 - SELF-LIMITING CHARACTERISTIC OF WATER-MODERATED REACTORS

TABLE OF CONTENTS

LIST OF TABLES

LIST OF FIGURES

2 SELF-LIMITING CHARACTERISTICS OF WATER-MODERATED REACTORS

2.1 Dynamics of a Nuclear Reactor

2.1.1 The Nuclear Energy Cycle

In a nuclear fission reactor, energy is produced in and around the reactor core from the fissioning (splitting) of heavy nuclei. This energy appears as kinetic energy of the fission reaction products which, *via* the slowing down collisions of these particles with the media, manifests itself as heat. On the order of 85% (Ref. 2-1) of the fission energy is deposited in the fuel material with the remainder deposited in the surrounding materials.

A typical research reactor may operate at a power of several megawatts (MW) with a core slightly smaller than a cubic metre. To maintain safe temperatures while operating at power, cooling must be provided to carry the heat produced away from the core. This is commonly done with a liquid coolant such as light water. Natural convection may be adequate to cool a relatively low power facility while forced (*e.g.*, pumped) coolant flow is needed to maintain low temperatures for higher power level systems.

A schematic of a typical MTR-type swimming-pool reactor heat transport system is shown in Figure 2-1. The reactor cooling systems usually comprise both a "primary" and a "secondary" side. The primary system circulates coolant through the core and carries the heat away to be transferred to the secondary system *via* a heat exchanger. The use of two coolant loops provides a containment barrier to the environment for trace radioactivity in the primary water. A power reactor system will use the energy contained in the coolant system to produce power by turning a turbine with steam, however, a typical research reactor will simply dump the produced energy to the atmosphere *via* a cooling tower type system. Flow rates associated with various power levels are adopted to keep the fuel and core structure at safe temperatures during operation.

Many accident situations revolve around scenarios in which the core materials increase in temperature. This may be due to the power increasing or to a loss of cooling capacity. As materials increase in temperature their properties change. Some of these changes compromise the containment of the radioactive byproducts of the fission process. In this sense for safety reasons it is crucial to maintain a cool reactor

core.

2.1.2 Neutron Multiplication

The concepts of neutron multiplication, generation time, reactivity and period are explained in most introductory texts on nuclear reactor analysis (*e.g.*, Refs. 2-2, 2-3, 2-4, 2-5). A brief outline follows.

The nuclear fission chain reaction is driven and sustained by neutrons. A neutron fissions a heavy element nucleus (*e.g.*, uranium) producing energy and more neutrons. As such, the power level of a reactor core is proportional to the neutron population. A stable neutron population is associated with a stable power. If the neutron population is allowed to die away the power likewise decreases and the reactor shuts down. Conversely, if the neutron population increases the power level proportionally increases.

A reactor core in which the neutron population, or power, is stable at a certain level is referred to as "critical". One that cannot sustain a chain reaction is referred to as "subcritical" and one in which the chain reaction is increasing in magnitude is called "supercritical". A critical state represents a normal mode of operation. From a safety standpoint an unchecked supercritical situation is to be avoided and a subcritical mode is required as a safe shutdown state.

The propagation of the neutron population of a reactor core can be described as neutron "multiplication". A "multiplication factor", given the notation k, can be defined as the ratio of successive neutron generations, *i.e.*,

$$multiplication\ factor, k \equiv \frac{neutron\ generation\big|_{i+1}}{neutron\ generation\big|_{i}}$$

or the ratio of the neutron production rate to neutron loss rate at a given instant in time, *i.e.*,

$$multiplication\ factor, k \equiv \left.\frac{neutron\ production\ rate}{neutron\ loss\ rate}\right|_{i}$$

where i is an index for neutron generations. Regardless of which definition is

preferred, a multiplication factor of unity is associated with a stable critical system, less than unity represents a subcritical system, and greater than unity represents a supercritical system.

Therefore, it is the neutron production and loss rates (*e.g.*, fission, absorption, leakage) which determine the stability or instability of a fission chain reaction. Changes in the reactor core configuration, material composition, and temperature all affect these neutron production and loss rates. These changes may occur as a result of manual mechanical intervention (*e.g.*, movement of control rods) or inherent changes in state properties (*e.g.*, heating up of the system with increasing power).

Using the definition of the multiplication factor, it is evident that the change in the neutron population for one generation is given by,

$$\Delta N = kN - N$$

where N is the neutron population for a given generation and kN is the resulting population for the subsequent generation for a system under conditions leading to a multiplication factor of k. Therefore, the change in neutron population per time associated with one generation is,

$$\frac{\Delta N}{\Delta t} = \frac{(k-1)N}{\Lambda}$$

where Λ is the neutron generation time, *i.e.*, the time from fission for the average neutron to either leak from or be absorbed by the system. By considering this as a differential equation (*i.e.*, changing the Δ's to differentials), it is clear that the time behaviour of the neutron population is governed by an exponential relation to time and has the solution,

$$N(t) = N_0 e^{\frac{\delta k}{\Lambda} t}$$

where the excess multiplication factor, *i.e.*, (k-1), has been written as δk. This indicates that in the case of a supercritical system, *i.e.*, $k > 1$, the neutron population will increase by a factor of e . 2.72 every $\Lambda/\delta k$ seconds. This time is referred to as the "reactor period" or simply the "period". Note, that for a decrease in multiplication factor, *i.e.*, $k < 1$, the period is negative which means that the exponent

of the exponential is negative and physically that the neutron population and power will decrease with time.

2.1.3 Neutron Generation Time

Physically, the generation time can be thought of as comprising the time for: (a) the fission process, (b) the slowing down or thermalization time of the neutrons which are "born" at high energies, and (c) the diffusion time of the thermalized neutrons until they are absorbed or escape from the system.

Most of the neutrons from fission, *i.e.*, on the order of 99.25%, appear practically instantaneously after the fission event and are referred to as "prompt" neutrons. The thermalization and diffusion time therefore are the major contributors to the "lifetime" of these neutrons. Typical prompt neutron lifetimes in thermal U-235-based light water reactors are on the order of 10^{-4} or 10^{-5} seconds. The prompt neutron lifetime is determined by the core design and primarily depends on the material used for the moderator and reflector.

Importantly for reactor control, a fraction of the fission neutrons, *i.e.*, on the order of 0.75%, appear significantly after the fission event from the decay of fission products, called precursors. These neutrons are referred to as "delayed". The fraction of delayed neutrons is designated β and is an intrinsic property of the fissile material. In terms of the multiplication factor for a critical system β . 0.007. Although the fraction of delayed neutrons is small, the significant delay times, from fractions of a second up to many tens of seconds, is enough to increase the average neutron lifetime to the order of 0.1 seconds, *i.e.*, a factor of 10^3 or 10^4, making reactor control possible.

2.1.4 Reactivity

A change in neutron multiplication is referred to as a change in "reactivity". A change in the system properties which increases the multiplication is said to be a source of "positive reactivity" while a change which reduces the neutron multiplication of the system is said to be a source of "negative reactivity". An "addition" of positive or negative reactivity into a critical system will place the system into a supercritical or subcritical state, respectively. Examples of such situations include the movement of control absorber rods, fuel assemblies or samples in or around the core. Positive or negative reactivity can be thought of as analogous to pressing your foot down or taking it off the accelerator peddle of a car.

More formally, reactivity is a commonly used parameter in neutron kinetic analysis and is defined as:

$$\rho \equiv \frac{k-1}{k} = \frac{\delta k}{k}$$

This is simply a convenient way of expressing the excess multiplication from the governing neutron kinetic equations. The differences between ρ and δk should be kept in mind when comparing measurements and calculations, especially when k is significantly different than unity.

Various units are assigned to measure reactivity, including $\%\Delta k/k$, milli-k (mk), pcm and dollars ($). The equivalent $\Delta k/k$ for each of these units are shown below:

$$\begin{aligned} 1\,\%\,\Delta k/k &= 0.01 \\ 1\,mk &= 0.001 \\ 1\,pcm &= 0.00001 \\ 1\,\$ &= \beta \approx 0.007 \end{aligned}$$

Herein, we will adopt the units of milli-k for reactivity.

2.1.5 Reactor Period

The exponential characteristic governing the neutron dynamics depends on the excess multiplication (reactivity), the neutron generation time, and the relationship between the two.

For small positive changes in reactivity, *i.e.*, $\rho << \beta$, the influence of the delayed neutrons is what dominates the dynamic response of the nuclear reactor system. For example, an increase in reactivity of 2 mk in a system with a neutron generation time of 0.1 seconds will produce a reactor period, τ, of,

$$\begin{aligned} &for\ \rho = 0.002 \\ &\tau = \frac{\Lambda}{\delta k} = \frac{\Lambda}{\rho k} = \frac{0.1\,\text{sec}}{(0.002)(1.002)} \approx 50\,\text{sec} \end{aligned}$$

This is a relatively slow time frame during which automatic control systems and manual operations can easily be performed.

For severe accident situations the change in reactivity may be considerably larger. As the size of the reactivity addition approaches β the influence of the delayed neutrons is greatly reduced. When $\rho \$ \beta$ the reactor can maintain the chain reaction on prompt neutrons alone. This situation is referred to as "prompt critical" or "prompt supercritical". In this case the generation time reduces to the prompt neutron lifetime. As a comparative example to the case above, the period resulting from a reactivity addition in excess of β by 2 mk in a system with a prompt neutron lifetime of 50 μsec is,

$$\rho - \beta = 0.002$$

$$\tau \approx \frac{\ell}{\rho - \beta} = \frac{5 \times 10^{-5} \text{ sec}}{0.002} = 25 \text{ msec}$$

This is obviously too fast a dynamic for manual intervention so reactor safety must rely on early detection and fast acting shutdown systems as well as design and procedures to avoid such situations. The size of the delayed neutron fraction determines the relationship between a reactivity insertion and prompt criticality. The delayed neutron fraction is a property of the fissile material, *i.e.*, fissioning isotope, and as a result may vary slightly with core burnup distribution.

A rigorous relation between the prompt neutron lifetime, the delayed neutron characteristics, the reactivity, and the resulting reactor period can be derived from the governing time dependent neutron equations. By assuming separability of the spatial and temporal components of the solution, this relation is described by the Inhour Equation (Ref. 2-4),

$$\rho_{in} = \frac{\omega\ell}{1+\omega\ell} + \frac{1}{1+\omega\ell}\sum_i \frac{\omega\beta_i}{\omega+\lambda_i}, \quad \textit{where the largest } \omega = \frac{1}{\tau_0}$$

where λ_i and β_i are the average decay constant and delayed neutron fraction associated with the delayed neutron precursor group "i". It is conventional to treat the delayed neutron fraction as a series of groups representative of decay times over the range of about 0.1 seconds to about 80 seconds. Each group leads to transient components in

the dynamic response of the system, which die out fairly quickly thus establishing the fundamental mode of the solution. The fundamental mode is associated with the "stable" or "asymptotic" reactor period.

From the above discussion the important point is that small reactivity perturbations to a critical system lead to power transients with periods on the order of many seconds. Comparatively, larger reactivity additions, near and above β, lead to much faster transients, with periods in the range of msec. The full-scale reactor experiments investigated power excursions with periods in this shorter range, down to a few msec. This range is associated with the limits of effectiveness of the inherent safety characteristics of MTR-type systems. This is included in the calculations in Chapter 7.

With respect to analysis of the results from the full-scale reactor experiments, the data are documented in terms of the reactor period of each transient. Therefore, the reactor period is used as the characteristic parameter in the analysis herein. With knowledge of the system dependent prompt neutron lifetime and the delayed neutron data, all of which can be measured and calculated, the reactivity limit associated with a specific period limit for a specific system can be determined from fundamental relations as shown above.

2.2 Negative Feedback

Light-water-moderated uranium-fuelled reactors are characterized by inherent sources of negative reactivity, *i.e.*, as the temperature of these systems increases changes in the state of the system produce negative reactivity. Thus, in the case of increasing power, the temperature of the system tends to increase which adds negative reactivity which in turn reduces the power. This negative feedback is an inherently safe system property. The concept of reactivity feedback is shown schematically in Figure 2-2 (Ref. 2-4).

The speed at which negative reactivity can be produced and the magnitude of such negative reactivity defines the effectiveness of such self-limiting behaviour.

These feedback mechanisms are all grounded in basic nuclear reaction properties and should be thought of in terms of the production and loss of neutrons. Such a phenomenological approach allows for a deeper physical understanding of the situation.

2.2.1 Fuel Temperature Feedback

Increases in fuel temperature changes the multiplication of the system *via*: (i) fuel plate expansion and subsequent displacement of water moderator, (ii) changes in the neutron spectrum with the thermal temperature of the system, and (iii) increased neutron reaction rates as a result of Doppler broadening of energy dependent reaction probabilities. The first factor has a similar effect to that due to moderator density changes. The second factor is a result of the thermal neutron spectrum being in equilibrium with the system. This changes with the system temperature, causing changes in the average nuclear reaction probabilities and possibly even in chemistry, both of which affect the reaction rates of the neutrons with the various materials in and around the reactor core.

With regards to Doppler broadening, the fuel material temperature affects the reaction properties of the neutron and heavy nucleus (*e.g.*, uranium). Reaction probabilities are referred to as "cross sections" from an analogy of a neutron hitting (or missing) a target "area". Cross sections for many heavy isotopes, including common fuel materials such as uranium and plutonium, are characterized by sharp increases in value over very small energy ranges. These spikes in the reaction probability with respect to energy are called resonances as they are determined by the constructive "resonant" overlapping of the nuclei and neutron quantum wave properties. Resonances are typical in the epithermal range of energies above an electron volt (eV - an electron volt is a unit of energy equal to the change in energy of an electron in passing through a potential difference of 1 volt. 1 eV = 1.60219 $\times 10^{-19}$ Joules). Examples of cross sections as functions of energy (of the neutrons) are shown in Figure 2-3 For U-235, the main fissioning isotope in a typical reactor, and Figure 2-4 For U-238, the most naturally abundant uranium isotope. The main component up to about 1 MeV of the U-238 total cross section is parasitic absorption, *i.e.*, that which does not produce a fission reaction.

As the fuel temperature increases, the heavy nuclei vibrations in the solid structure increase. This alters the relative motion between the incident neutrons and the target nuclei producing a wider distribution with respect to energy. As a result, resonance peaks in the cross section energy spectra become broader over energy and the resulting overall reaction rate increases. Changes in reaction rates lead to changes in the reactivity of the system. These reactivity changes due to resonance broadening of the fuel cross sections are referred to as Doppler reactivity feedback.

For light water moderated reactors with LEU fuel these first two factors are relatively

minor in comparison to that associated with the third factor, Doppler broadening. As it turns out, the increase in the U-238 parasitic absorption rate, *i.e.*, that which does not produce fission, dominates under increased temperatures. As a result the neutron balance swings towards more "losses" relative to "production" and the result is an increased source of negative reactivity. Since the most dominant isotope in this respect is U-238 this feedback mechanism is negligible for highly enriched uranium (HEU) fuel cycles, *i.e.*, U-235 content increased to greater than 90% with the balance being mostly U-238, but becomes dominant for low enrichment uranium (LEU) systems, *i.e.*, those in which the U-235 content is less than 20% and therefore there is significantly more U-238.

It should be noted that for reactors based on different moderators (*e.g.*, D_2O or graphite) and natural enrichment fuel, the U-238 Doppler effect may be small compared to other factors. This is the case in CANDU power reactors where neutron thermalization takes place mainly away from the fuel. In this case the net fuel temperature feedback is actually positive due to the contribution of spectrum hardening and the Pu-239 isotope resonance near the upper part of the thermal range.

As a large portion of the fission energy, *i.e.*, ~ 85%, is deposited directly in the fuel, a fuel temperature increase is associated with a prompt reactivity feedback effect during a power excursion.

So, in summary:

- the majority of the energy produced from fission is deposited promptly in the fuel material,
- an increase in fission rate results in an increase in fuel temperature,
- the increase in fuel temperature increases various neutron-nucleus reaction rates *via* Doppler broadening of cross section resonances, and
- in MTR-type systems which contain significant amounts of U-238 this results in a negative source of reactivity.

2.2.2 Moderator Temperature & Void Feedback

The other mentioned feedback effects are related to the "moderation" and leakage of the neutrons in and from the light water system. Light water plays multiple roles in the MTR-type core. It provides:

- the main heat removal medium; as energy from fission is transferred to the water coolant which subsequently flows, either by natural circulation or forced means, out of the core,
- a radiological shield; a foot of light water attenuates about 90% of thermal neutrons,
- a reflector; by scattering neutrons which are exiting the system back into the core, and
- a moderator for the neutron population.

Fission neutrons, *i.e.*, those produced by the fission process, are created with relatively high energies, on the order of 2-3 MeV. However, the neutron/uranium fission process proceeds most efficiently, *i.e.*, the fission cross sections are much larger, at lower neutron energies, *i.e.*, typically in the range of a few eV or less. Materials of low atomic number, such as hydrogen, carbon or oxygen preferentially interact with neutrons in scattering reactions in which the neutron loses energy to the nucleus. The lighter the nucleus the larger the average energy transfer per collision event. In this way, a scattering material "moderates" the neutron energy from high (2-3 MeV) to low (a few eV or less), thus facilitating the fission reaction process. Without the light water in an MTR-type core the fission chain reaction doesn't "go". On the other hand, without the light water inventory the main heat sink is also missing which is fine only if the reactor is "off" and already "cool".

The negative feedback from reduced coolant/moderator density is due to both increased leakage and loss of moderation. A decrease in water density in the core leads to an increase in leakage of neutrons from the core as there is less scattering material to contain the neutron population. This leads to a further reduction in neutron multiplication *via* increased losses, thus negative reactivity. The decrease in density also reduces the amount of moderating material in the core. In a thermal system such as a typical U-235 fuelled research reactor, this leads to a reduction in neutron production and therefore negative reactivity.

Increases in system temperature therefore increase the leakage and decrease the moderation by removing light water *via*: (i) a decrease in the light water density, and (ii) when things get hot enough, steam production. Experiments have confirmed that moderator expulsion *via* steam formation is the dominant feedback mechanism in HEU MTR-type systems (Ref. 2-6).

To some extent the moderator temperature feedback mechanism is a prompt effect in that on the order of 15% of the fission energy is deposited in the coolant/moderator

and structural material *via* neutrons, gamma and beta particles. However, the majority of the moderator temperature and void feedback are delayed mechanisms during a power excursion as both rely on heat transfer from the fuel to the coolant/moderator material. Voiding is a fast acting feedback mechanism once saturation temperatures are reached as a result of the change in density between the liquid and vapour phases of light water and steam, and can be treated as a threshold effect.

So, in summary:

- as the temperature of the light water coolant increases the density decreases, *i.e.*, there are less atoms of light water per unit volume,
- with less atoms of light water per unit volume the scattering reactions with the neutrons decreases,
- as a result of the reduction in scattering events, the neutrons, on average, are not moderated to as low an energy, *i.e.*, the average energy of the neutrons remains higher,
- the higher energy neutron population and less scattering collisions results in more leakage from the core, reducing the multiplication factor of the core, thus producing a negative reactivity effect,
- the higher energy neutrons fission less with the fuel material, further reducing the multiplication factor of the core, thus producing more negative reactivity, and
- if the coolant reaches boiling (saturation) temperature these effects are greatly magnified as the steam volume replaces the liquid coolant.

2.2.3 Fuel Relocation

Fuel relocation represents the ultimate negative reactivity feedback mechanism. A critical configuration is achieved by bringing together a sufficient mass of fissile material in balance with structural, cooling, reflecting, and moderating materials. This is what is achieved when fuel assemblies are loaded into a core grid and control rods are subsequently partially withdrawn to produce a multiplication factor of unity, *i.e.*, $k = 1.000$. Typically, spreading out a critical configuration will produce negative reactivity.

In a severe accident scenario, the removal of fissile material from the system will terminate the fission chain reaction and therefore the power excursion. Possible mechanisms include the melting of fuel plates which subsequently "drop out" of the bottom of the core, or in a more extreme situation, blowing apart of the core as a result of internal pressure production. The result is a subcritical configuration.

2.2.4 Other Minor Contributions & Discounted Mechanisms

Other factors such as radiolytic gas production (Ref. 2-7) and the hypothesis of the production of highly-absorbing poison isotopes (Ref. 2-8) during the power pulse have been discounted as major feedback mechanisms by specific studies in the full-scale reactor experiments. No other hypothesized feedback mechanisms have been shown to be part of the self-limiting behaviour of MTR-type systems.

2.3 General Characteristics of an Unprotected Power Excursion

A feature of MTR-type systems in general, including MNR, is that the design results in negative temperature and coolant void coefficients of reactivity (see Section 2.2). For HEU fuel, the Doppler feedback with increasing temperature is practically negligible but this effect is substantial in LEU fuel with the significant U-238 content. Increasing temperature also reduces the coolant/moderator density *via* fuel plate expansion, heating of the single phase coolant/moderator, and once boiling commences, steam production, *i.e.*, voiding of the coolant/moderator.

Two questions relevant to rapid and large positive reactivity insertions are:

- Is the amount of negative reactivity produced large enough to compensate for the initial insertion of positive reactivity, and
- Is there enough time before the fuel reaches a damage threshold for the feedback mechanisms to limit the excursion?

Simulation and measurements of local void coefficients indicate that the available compensating reactivity is substantial. While the full scale reactor tests demonstrate that for HEU MTR-type systems coolant voiding reactivity feedback is delivered rapidly and is effective in self-limiting reactivity-driven transients up to a certain limit on reactivity. For LEU fuel, the self-limiting characteristics of the system are enhanced by a significant prompt negative fuel temperature feedback mechanism.

The reactor experiments also show that fuel damage and even core disassembly can result, given a large enough and fast enough reactivity insertion. Therefore, the answers to the above two questions are: yes, below certain reactivity limits.

In addition to the rate and magnitude of the initial reactivity insertion, the timing and magnitude of the various feedback effects will determine the system behaviour. Given that most of the energy produced by fission is contained within the fuel and effectively is deposited instantaneously, the change in temperature of the fuel meat is therefore a "prompt" effect. Conversely, the heat transfer from the fuel meat to the coolant depends upon the thermal conductivity of the fuel and cladding and the heat transfer coefficient at the cladding/coolant interface. Even for thin MTR-type fuel plates with high thermal conductivity, the temperature change of the coolant following a power excursion is considered a "delayed" effect relative to the temperature change in the fuel meat. The timing and magnitude of the feedback effects for an MTR-type system are summarized in Table 2-1.

The following sections describe the power, temperature and hydraulic response associated with the self-limitation of reactivity insertion accidents.

2.3.1 Power Behaviour

An idealized power response to a step-reactivity insertion in an HEU MTR-type system is shown in Figure 2-5.

The phenomena behind the different regions of the power trace are explained in Reference 2-9 and are based not only on the results from the Borax experiments but also on the continuation of that work in the Spert I experiments. For now the prompt Doppler feedback is put to the side as the experimental data set from the full-scale reactor tests on MTR-type plate fuel did not include this parameter. Adjustments due to Doppler feedback in LEU fuel will be considered later in this section.

For very rapid positive reactivity insertions, the resulting power initially increases exponentially on a certain period (see region (1) in Figure 2-5). Period refers to the asymptotic reactor period which is the rate of exponential power increase following the reactivity insertion before feedback mechanisms come into effect. This period is a function of the inserted reactivity and is dependent on both the prompt and delayed neutron characteristics of the specific reactor (Fig. 2-6) which in turn are dependent on the design and the fuel cycle of the reactor. Roughly speaking, transients can be referred to as fast, intermediate and slow depending on the period,

τ, *i.e.*,

- 300 msec # τ (slow)
- 35 msec # τ # 300 msec (intermediate or "transition")
- τ # 35 msec (fast)

These ranges reflect different modes of self-limiting behaviour of the test cores which is reflected in the experimental data. Behaviour with respect to range of period is discussed in more detail in Chapter 3. The fast range is associated with shutdown *via* boiling for transients from ambient initial temperature.

Following the establishment of the initial period, the power continues to rise almost exponentially until the inherent feedback mechanisms of the system can provide enough negative reactivity to compensate for the excess positive reactivity (see region (2) of Figure 2-5). The power rise continues and slows slightly from the initial exponential as materials start to increase in temperature but before voiding of the coolant begins (see region (3) of Figure 2-5). This stage is more noticeable in slower transients. The breakaway from exponential rise usually occurs about a decade below peak power (Ref. 2-10). Heat transfer is mainly by conduction and large thermal gradients (upwards of 100's of degrees centigrade for very short period transients) exist across the fuel plate and into the boundary layer of the coolant.

For large positive reactivity insertions, *i.e.*, short periods, the fuel plate temperatures exceed the coolant saturation temperature and steam voids are produced in the coolant channels. The extent to which the fuel plate surface temperature exceeds the saturation temperature of the coolant, *i.e.*, the degree of superheat, depends on the period of the transient. The shorter the period the more the superheat.

In transients which are severe enough to induce voiding, the power reaches a peak value as the coolant begins to void (see region (4) of Figure 2-5). Significant boiling at this point produces enough negative reactivity to limit the excursion. This void feedback is the dominant negative feedback mechanism for extreme power excursions in HEU systems. Power then decreases even more quickly than the initial power rise (*i.e.*, exponential on the asymptotic reactor period) as there is large voiding in the core (see region (5) of Figure 2-5), and hence a negative reactivity that is larger in absolute value than the initial positive insertion.

In general, the peak power, total energy, and fuel plate temperatures associated with the initial power pulse increase with increasing rate and magnitude of the initial

reactivity insertion.

Following the initial positive reactivity insertion, the reactor core then seeks a new equilibrium power level at which the negative feedback derived from fuel temperature increase, thermal moderator expansion, and void content compensate the initial reactivity insertion. Due to the time lag in the thermal process of void formation, energy is often built up beyond that needed to produce enough void to compensate for the initial reactivity insertion. Thus excess voiding is created in the core and the power trace initially undershoots this eventual equilibrium level (see region (6) of Figure 2-5). The power remains at this low level while the core is voided, determined mainly by the decay of the precursors (Ref. 2-9). This undershoot in power increases as the period of the transient decreases. For slow and intermediate transients the power may not undershoot the new equilibrium level at all, certainly not if voiding is not involved in the self-limiting process.

At this stage of the transient the delayed neutron source from the delayed precursors formed in the initial power peak continues to build up and to contribute more to the power level. Also, the core refills to a certain extent as the power and fuel plate surface temperatures have decreased due to the massive voiding of the core. As a result the power increases towards the new equilibrium value associated with steady-state boiling at which the feedback mechanisms just compensate for the initial reactivity insertion (see region (7) of Figure 2-5).

Depending upon the hydraulics of the system, the power may then settle into a stable yet noisy equilibrium level on the order of a fraction of a MW to several MW (see region (8) of Figure 2-5). The exact power level will depend upon the initial reactivity insertion as this determines the amount of compensating reactivity which must be held in voids in the system. The noise in the power response associated with this stage of the transient is due to boiling in the coolant channels. A steady boiling mode of operation may continue for a timescale on the order of seconds to minutes before developing into larger magnitude oscillations, or indefinitely for less severe transients, depending on the void fraction in the core required for reactivity compensation. Typically power oscillations in the steady-state boiling mode are less than a few percent of the mean power. For larger duration situations, on the order of minutes, the equilibrium power has time to adjust to lower values due to increasing temperature of the system and increased fission product poisoning (Ref. 2-11).

The amount of void in the system will be determined by how much initial positive reactivity must be compensated. For void contents above a certain percentage, the

steady-state boiling will develop into larger oscillations about the equilibrium power level (see region (9) of Figure 2-5). These oscillations in the power are driven by periodic voiding and refilling of the coolant channels, first creating negative reactivity and then as the core refills, a positive reactivity insertion (see region (10) of Figure 2-5).

Although, in some cases, these power oscillations can be small in amplitude, *e.g.*, < ± 50% about a mean power level, they can in more severe circumstances reach magnitudes on the order of the initial power pulse in a short period step reactivity insertion transient. For the purposes of this report, power oscillations are defined, based on their magnitudes as follows:

- "small" if they are < ± 50% of the mean power value, and
- "large" if they are > ± 50% of the mean power value.

The fully developed large amplitude oscillatory power behaviour, contained in the latter category above, is referred to as "chugging" (Ref. 2-1). Often a system will pass through a transition region of small oscillations between steady boiling and large amplitude chugging. In the case of chugging these power peaks are qualitatively similar to the initial power pulse associated with a step reactivity insertion transient.

The "envelope of oscillations" can be quite irregular about the equilibrium power level and the magnitudes of the power peaks of the oscillations can be as great as the initial power peak due to a step reactivity insertion (Refs. 2-9, 2-12). As the coolant refills the core, positive reactivity is re-introduced to the system causing the oscillation power peaks. Therefore, the refilling is effectively a positive reactivity insertion. The magnitude and the rate of rise of these oscillation power peaks are therefore dependent on the amount of voiding/refilling and the refilling time of the coolant.

The stylized transient response shown in Figure 2-5 is typical of a step, or instantaneous, insertion of positive reactivity into an HEU system. Step reactivity insertions are associated with scenarios such as the ejection or rapid removal of an absorber rod, or the fast insertion of a fuel assembly or experimental sample into the reactor core.

Ramp reactivity insertions by their nature introduce the initial positive reactivity more slowly to the system. Typical ramp rates of insertion are related to the speed of absorber rod motor withdrawal, the gradual filling of a voided region *via* leakage,

or of the controlled addition or removal of fuel assemblies or experimental samples. For a ramp insertion, increases in temperature and the associated feedback effects are notable during the time of the reactivity insertion. As a result, the timing and size of the initial power burst is dependent on the reactivity insertion rate and the initial power (Refs. 2-13, 2-14). A lower initial power level will delay the timing of and increase the rise rate (smaller minimum period) and magnitude of the initial power burst.

For relatively fast ramp reactivity insertion rates the power behaviour is similar to that for a step reactivity insertion to the extent that an initial power pulse occurs with a maximum power greater than the post-pulse equilibrium power level. A comparison of power and period (actually reciprocal period) for step and ramp insertions is shown in Figure 2-7 (Ref. 2-15). For slower transients, however, the initial power pulse is small, if present at all, and does not necessarily represent a maximum power value compared to the post-pulse equilibrium power level. In this sense, for a ramp reactivity insertion, the post-initial-power-pulse behaviour can be associated with the limiting power and temperatures of the transient. A stylized comparison of step, fast ramp and slow ramp initial power behaviour is shown in Figure 2-8.

The post-initial-power-pulse behaviour, *i.e.*, steady state boiling and possible chugging characteristics of the ramp and step insertion transients are similar and are not affected by the ramp rate and initial power.

With respect to safety analysis, chugging must be considered for both the long term behaviour of a system following a step reactivity insertion (Figure 2-5) and also as the long term behaviour of a system following a ramp or other gradual reactivity insertion. In fact, chugging may represent the limiting characteristic of a ramp or other gradual insertion scenarios from the standpoint of maximum power and limiting fuel temperature.

Up until this point, the discussion has been directly applicable to HEU MTR-type systems. The self-limiting behaviour of such systems is significantly altered when the fuel material is switched to LEU. In an LEU system, the power rise associated with a step reactivity insertion will begin to deviate from an exponential almost immediately as the Doppler feedback effect, resulting from the high U-238 content of this fuel, is prompt in nature.

For the same initial reactivity insertion the initial power pulse will be smaller in

magnitude for an LEU system compared to an HEU system due to the additional negative reactivity feedback from the Doppler mechanism. Also, for power pulses of the same amplitude those associated with the LEU system would be expected to be broader due to the more continuous feedback mechanism compared to the voiding response which is a threshold effect. These effects are shown schematically in Figure 2-9.

With respect to the post power peak response of the system there is no reason to believe that an LEU system will not behave in a similar manner as an HEU system. Therefore, the steady state boiling and chugging modes previously described should be typical of an LEU system. The transition between steady boiling and oscillatory behaviour is a function of the reactivity held in voids and therefore will occur at comparatively larger initial reactivity insertions for the LEU system since a larger fraction of the reactivity is compensated by the Doppler feedback. It is also reasonable to believe that the power peaks associated with chugging in an LEU system will be qualitatively similar to the initial power pulse for an LEU system.

The characteristics of the power response of a reactivity insertion also depends upon various system parameters such as initial temperature, pressure, and coolant circulation mode. The sensitivity of the system response to these parameters amongst others is encapsulated in the experimental data set.

The associated temperature response of the system and a more developed discussion of the hydraulics associated with the different regions of the transient response are contained in the following sections.

2.3.2 Temperature Behaviour

It may be helpful when constructing a picture of the temperature response during a fast power excursion to consider the steady state boiling heat transfer curve (Fig. 2-10). Although experiments have shown considerable difference between steady state and transient heat transfer rates (Ref. 2-16), this figure illustrates the trends in heat transfer for the different stages or extents of boiling.

The important ideas to take from the steady state boiling heat transfer curve are the following:

- Heat transfer increases markedly once boiling starts (compare regions (I) and (II) of Figure 2-10). This is due to the mixing

of the coolant caused by the process of steam formation. Experiment has shown that heat transfer during boiling is insensitive to the flow velocity of the coolant (Ref. 2-17).

- Heat Transfer decreases significantly as the system moves from nucleate boiling to film boiling (region (III) of Figure 2-10). This is due to the heated surface becoming covered by steam rather than liquid for which there is a much lower conductivity.
- As the surface temperature is increased in the film boiling region (see region (IV) of Figure 2-10) heat transfer increases as driven by both conduction through the steam layer and radiative processes.
- The maximum heat flux achievable in the nucleate boiling region (see region (II) of Figure 2-10) is also associated with a point in the film boiling region (see region (IV) of Figure 2-10). This indicates that small changes in heat flux can result in large changes in temperature. The jump from the nucleate to film boiling regions is referred to as "critical heat flux" (CHF) or "dryout" and can result in sudden increases in temperature up to temperatures near the melting point of the solid material.

An idealized fuel plate surface temperature response to a step-reactivity insertion in an HEU MTR-type system is shown in Figure 2-11. This is the temperature response associated with a power history such as that shown in Figure 2-5 during and following the initial power pulse. The fuel plate temperature can be thought of as an integral of the power of the excursion, modified by a time dependent heat loss to the reactor coolant/moderator and structure.

Initially, the temperature increase is approximately adiabatic as little or no energy has time to be transferred to the coolant (see region (1) of Figure 2-11). Given the power and energy deposition with respect to time and the approximately constant specific heat of the fuel, the surface temperature of the fuel plate increases exponentially with time of the transient (Ref. 2-1).

For a severe enough transient, *i.e.*, for a large enough reactivity insertion resulting in a short enough period, the fuel plate temperature will overshoot the saturation temperature of the coolant, *i.e.*, superheat (see region (2) of Figure 2-11). The amount of superheat depends on the speed of the transient compared to the time

constant for heat transfer to the coolant. The superheat may be as much as 150EC prior to noticeable boiling, which is greater than that associated with slow superheat which is typically no greater than ~ 15EC (Ref. 2-9).

The temperature rise continues exponentially until the feedback effects begin to be significant (corresponding to region (3) in Figure 2-5). At the point where the surface temperature of the fuel plate is high enough to produce boiling in the coolant, the rate of temperature rise decreases. This is the result of increased heat transfer from the fuel plate to the coolant *via* nucleate boiling (see region (3) of Figure 2-11).

Often the characteristic surface temperature curve will show a temperature setback after the region characterised by nucleate boiling and just prior to a significant increase in temperature. This setback, (see region (4) of Figure 2-11) is associated with the large heat transfer required to produce a large volume of steam. With the now large volume of steam in the core, most of the plate surface is steam blanketed and subsequently the rate of heat transfer is significantly reduced. During this stage the surface temperature increases rapidly (see region (5) of Figure 2-11) and is analogous to the critical heat flux (CHF) state often used as a safety criterion for power reactor limits. Data and photographic evidence from capsule tests support this description of the heat transfer and boiling processes (Ref. 2-18).

The void reactivity produced from the steam generation arrests the power excursion. With the energy source removed the temperature rise of the fuel plate surface is halted. The temperature remains high and only decreases slowly (see region (6) of Figure 2-11) as the core is still voided and heat transfer from the vapour blanketed fuel plate surface to the coolant is low. This continues until the core begins to refill with water, increasing the heat transfer and reducing the fuel plate surface temperature (see region (7) of Figure 2-11). Enough compensating feedback is retained by the system in the form of elevated temperatures and void content to prevent further power increase.

The fuel plate surface temperature approaches the saturation temperature of the coolant at this point. Further perturbations may be seen as a result of steady state boiling of the coolant water or driven by power oscillations as a result of periodic voiding and refilling of the core in the chugging mode of operation. Plate surface temperature fluctuations during steady state (nucleate) boiling are typically 2EC to 3EC about a mean of slightly above the saturation temperature (Ref. 2-11). For chugging, the temperature will oscillate with the size of the oscillations determined by the amount of reactivity being returned to the system upon refill. The stability of

the temperature during chugging will depend upon the energy balance for this mode of operation.

In many safety analyses the occurrence of CHF or dryout (see Fig. 2-10) is assumed to lead to a temperature jump leading to a temperature to beyond the melting point of the cladding material. This is obviously not necessarily the case in an unprotected reactivity driven power excursion in an MTR-type system as shown from the full scale reactor experiment data. Therefore, for this type of reactor, the use of dryout as a safety limit for severe accidents is overly conservative.

The following general remarks can be made with regards to the period of the power excursion:

- $\tau \$ 50$ msec (slow): the fuel plate surface temperature will have a maximum close to the saturation temperature of the coolant as boiling heat transfer is sufficient to cool the plates *i.e.*, regions (2) to (5) in Figure 2-11 are not significant.
- 10 msec $\# \tau \#$ 50 msec (intermediate): the maximum temperature increases with decreasing period as the film blanketing plays a significant role in the temperature response of the fuel plate, as shown in regions (5) to (7) in Figure 2-11.
- $\tau \#$ 10 msec (fast): the maximum fuel plate surface temperature is mainly limited by the total energy production, *i.e.*, regions (2) to (4) in Figure 2-11 are not significant as boiling heat transfer has little effect on heat removal from the plate.

The preceding discussion has been with respect to the fuel plate surface temperature. Figure 2-12 shows an idealized fuel plate surface and fuel plate centre, *i.e.*, meat, temperature response to a step-reactivity insertion power excursion. The same relationship is shown in Figure 2-13 for a transient performed in the Spert I D-12/25 core during the destructive test series. The plate surface temperature trace in this figure is from a thermocouple reading while the central temperature trace is calculated using the measured plate surface temperatures and the power traces as the boundary conditions and source term respectively (Ref. 2-19).

Similar relationships were found from experimental thermocouple results on bare and insulated sections of the same fuel plate in the Borax I reactor (Ref. 2-20) with the insulated plate data approximating the temperature behaviour of the interior of the

plate.

Under steady state conditions there is only a slight temperature gradient over the thin fuel plates, *e.g.*, on the order of a few degrees depending on the operating conditions. This is a characteristic of the high conductivity material and thin dimension of the plates. However, during a step reactivity insertion where the period of the power is on the order of milliseconds, large thermal gradients, on the order of 100's of degrees Celsius, can be established. This is shown by conductive heat calculations and supported by post-test examination of melted fuel plates, such as from the Borax I destructive test in which some recovered fragments showed fuel plate sections with intact clad from which the molten fuel meat had apparently flowed out.

At the beginning of a reactivity driven power excursion there is little or no thermal gradient across the fuel plate. This is shown in Figure 2-12 with both the surface and centre curves starting from the same point. Both curves initially progress close to the total energy deposition as little heat is being lost from the plates.

As the transient progresses, the two curves begin to diverge, indicating that a temperature gradient is being established across the fuel plate. The magnitude of the thermal gradient will be affected by the speed of the transient (period), the thermal conductivity of the fuel and clad material, the thickness of the clad material, and the coolant conditions (boundary conditions). The explanation of this dynamic distribution is that the energy is deposited directly in the fuel meat in the centre of the plate and despite the high thermal conductivity of both the meat and the cladding material, the time constant associated with the heat transfer is still long compared to the reactor period.

Once boiling begins, the fuel plate surface temperature increases at a lower rate than the fuel plate centre. A large thermal gradient is established which may reach hundreds of degrees. Depending on whether the central temperatures reach the melting point of aluminum and the fuel alloy, the plate centre temperature trace will show small plateau regions due to the melting and subsequent freezing of the material (these are not shown in Figure 2-12).

Once the core is voided, the power excursion is arrested and the energy source is effectively removed. The plate centre temperature begins to decrease around the same time as the plate surface temperature shoots up given that the plate surface is vapour blanketed and the heat transfer to the coolant is markedly decreased. The temperature distribution within the plate then begins to flatten shown by the two

traces converging in Figure 2-12. Upon refilling of the core, the fuel plate surface temperature drops more rapidly. Assuming no further source of positive reactivity, both curves approach the saturation temperature of the coolant and steady state or quasi-steady state conditions with little thermal gradient.

The dynamics of the temperature distribution in the fuel plate are relevant to safety limits and the destructive mechanism in that the tensile strength of the plate is significantly reduced upon heating to temperatures typical of short period power excursions (Ref. 2-19). This is discussed in more detail in Section 2.4.

With respect to the temperature distribution in the coolant, as the fuel plate surface temperature rises, large thermal gradients are established over the boundary layer of the coolant next to the fuel plate. This is a result of the conduction-only heat transfer (Ref. 2-19) and the differences in heat capacity of the plate and the water. The specific heat of the fuel plates is approximately a third of the specific heat of the water (Ref. 2-21). Calculations indicate that the significant temperature rise in the coolant, prior to boiling, is confined to a thin layer close to the fuel plate surface, on the order of tenths of a millimetre which is only 10% of the typical coolant channel thickness (Refs. 2-9, 2-22) (see Figure 2-14). Boiling/voiding producing shutdown reactivity occurs with the bulk temperature of the coolant well below saturation temperature.

2.3.3 Hydraulic Behaviour Including Chugging

The hydraulic behaviour related to the self-limiting response during a reactivity induced power excursion has been noted with regards to the power related feedback (Section 2.3.1) and the temperature related heat transfer (Section 2.3.2). This section focusses on the hydrodynamics associated with the post-initial-power-peak behaviour of the system.

Steady-state boiling is possible in these systems for natural circulation and upward flow operation. This has been demonstrated in the Borax experiments (Ref. 2-1) and the Spert IV Stability test series (Ref. 2-11).

For either of these coolant circulation conditions, the upward buoyancy force on the void generated in the coolant channel acts to accelerate the coolant flow rate, thus providing improved heat removal from the core. The increased heat removal resulting from the buoyancy enhanced flow can therefore limit the degree of boiling and establish an equilibrium condition. This is shown pictorially in Figure 2-15. The

associated power response of the system is rather noisy in nature but variations about the mean power level are typically less than a few percent. An example of a power trace during steady-state boiling is shown in Figure 2-16, taken from the Borax I results and shows the characteristically "bumpy" power trace associated with this mode of operation.

For relatively small reactivity insertions, leading to steam contents in the core below a certain percent volume, the system can continue in this mode of operation indefinitely. The exact power level associated with self-limiting steady-state boiling depends on the fuel assembly geometry and power density characteristics of the core but can be on the order of several megawatts. This is an important point demonstrating that boiling in MTR-type coolant channels does not necessarily lead to complete voiding of the channel.

Above a certain void fraction the system can no longer operate in a steady boiling mode. The voiding becomes large in amplitude filling the entire breadth of the coolant channel. The steam production forces the water from the coolant channel driven by the pressure difference associated with the difference in volume between the liquid and vapour phases (steam occupies approximately 900 times the volume of liquid water at a atmospheric pressure). Once the steam has expanded, forcing the coolant from the channel, the water refills the coolant channel, driven by the buoyancy forces on the void, the hydrostatic water head above the core and any forced circulation. Meanwhile, the power excursion has been arrested by the negative void feedback, thus removing the heat source in the fuel plates. The refilling water then cools the fuel plate but also increases the reactivity of the system. In this way the power excursion and the related hydrodynamic cycle is repeated and an oscillatory mode of operation is established. A pictorial representation of chugging in a fuel plate assembly for natural circulation or upward flow is shown in Figure 2-17.

Unlike the random fluctuations associated with steady boiling, this oscillatory behaviour is characterized by a definite frequency. The associated power oscillations, which are driven by the reactivity decrease (with voiding) and increase (with refilling) also show a definite frequency and amplitude of oscillation.

The amplitude of these power oscillations depends upon the extent of the voiding and refilling of the coolant channels, and the magnitude of the associated reactivity. Large scale voiding and refilling is referred to as "chugging" and can result in power oscillations on the order of magnitude of the initial power pulse of an equivalent step

reactivity insertion of reactivity.

No experimental data are available regarding steady state boiling or chugging in a system with forced downward flow. From basic principles, for forced downward flow the system can only enter into the flow chugging mode of operation due to the opposing directions of the flow and buoyancy forces. For given downward flow conditions, as boiling commences the upward buoyancy force on the void in the coolant channel will effectively slow the flow rate by increasing the flow resistance in the channel. As a result the flow rate decreases. Subsequently, the residence time of the coolant in the channel increases and the extent of boiling increases. Increased void fraction will further decrease the flow rate. This is a self propagating situation leading to large amplitude voiding. This is shown pictorially in Figure 2-18. The rest of the hydrodynamic cycle is similar to that for the case of natural circulation or upward flow chugging but the refill may be preferentially from the top down as aided by the forced flow direction.

2.3.4 The Relationship Between Power, Temperature and Hydraulics

As evident from the descriptions in the preceding sections the power distribution, temperature distribution and hydraulic state of the reactor core prior to and during a power excursion are all coupled. Consideration of one of these aspects necessarily involves the others. For example, the power distribution determines the temperature distribution in the reactor as does the hydraulic properties related to heat transfer. The temperature drives the feedback mechanisms which effect the power distribution and response. The hydraulics are coupled to the power and temperature characteristics *via* the transition from single phase to two-phase (voiding) states and also the voiding dynamics associated with steady-state boiling and chugging drives the power response by determining the reactivity balance of the system.

An example of the relationship between the power and fuel plate temperature is shown in Figure 2-13 for a 9.5 msec period transient in the Spert I D-12/25 core. Of note is that the maximum fuel temperatures occur after the maximum power which is consistent with the delay in the heat transfer from plate to coolant.

In situations in which negative reactivity is held in steam voids in the coolant, MTR-type systems are susceptible to power oscillations. Upon exceeding a certain void fraction in the coolant channels, the channels void a large fraction of the total coolant volume and enter into a voiding/refilling cycle. The power oscillations are driven by the reactivity changes associated with this voiding (negative reactivity insertion) and

refilling (positive reactivity insertion). The fuel plate temperature likewise is driven through oscillations due to the changing rate of fission energy production and heat transfer conditions. An example of the power and temperature oscillations are shown in Figure 2-19. The relation between the power and temperature during the oscillations is similar to a repeating pattern of the initial power pulse for a step insertion

It should also be recognized that fuel plate temperatures are local quantities while power in an integral core property. The exact timing of local temperature behaviour compared to the power behaviour will therefore depend on the relationship between the local perturbations and the integral core response. These relations, and their sensitivity to variation in system parameters, are what are captured in the data from the full scale reactor experiments. Simulation, in place of the experimental results, is understandably a difficult proposition as all three areas must be modelled faithfully in order for any of the three to yield accurate results.

The coupled temperature, hydraulic, and power behaviour characteristic of MTR-type systems, allows for rapid, reliable and effective limiting of the power excursion, without fuel damage for power excursions up to a certain threshold. With respect to this threshold, if enough initiating positive reactivity is inserted fast enough into the system then the resulting period of the power rise will be short enough, or in other words the power rise will be fast enough, so that the temperature of the fuel will reach damage thresholds (*e.g.*, melting temperature) before enough negative reactivity can be produced to arrest the power excursion. In this case, local fuel damage or widespread core damage will result.

2.3.5 Inherent *vs.* Mechanical Shutdown

Although not a primary goal of this thesis, a comparison of protected (*i.e.*, mechanical shutdown system protected) *vs.* unprotected transient response for an MTR-type core is an interesting exercise which helps put the self-limiting characteristics of such systems into a context of safety analysis. Although mechanical-shutdown and inherent-self-limiting properties will differ between systems, the general features of the analysis are applicable to MTR-type systems in general.

In an MTR-type system rapid absorber rod insertion provides shutdown coverage in the event of a power excursion. In these situations the absorber rods are either motor-driven (called a “reverse”) or more quickly dropped (called a “trip” or

"SCRAM") into the core. Relatively low power and power-rate reverse and trip set points, and the fast action of such systems typically mitigate a power transient before the point at which self-limiting mechanisms are noticeable. This is evident in simulation results of both HEU and LEU cores for reasonably large and rapid reactivity insertions (*i.e.*, $1.5/0.5 sec). Examples of this are found in Reference 2-23.

The comparison of inherent and mechanical shutdown was studied as part of the Spert Project with the BSR-II core (Refs. 2-24, 2-25, 2-26, 2-27). These tests involved step insertions of reactivity from low power conditions. The results from the BSR-II tests show that down to short periods the mechanical shutdown system is more effective than inherent shutdown effects, *i.e.*, the mechanical systems mitigate the transient before inherent processes take effect. This is shown in Figure 2-20, where protected tests produce a lower maximum power than the unprotected tests for transients of a given period. Tests with different types of mechanical protection (*i.e.*, rod reversal, different numbers of rod drops on power level and period) are considered. At some point however, for some short period, the effectiveness of the mechanical shutdown system is no greater than the inherent self-limiting mechanisms and beyond this (shorter periods) the inherent characteristics self-limit the transient before the mechanical shutdown system can take effect.

The exact period where the two shutdown "systems" are equally effective depends on the trip point setting, the time delay characteristics of the mechanical shutdown system, and the strength of the inherent shutdown mechanisms. For the BSR-II core, where the shutdown rods were spring-loaded for downward release, this period was found to be approximately 4.5 msec for a high-power level trip set at 100 kW, which is in the region of fuel damage for this specific core. For gravity drop systems the "takeover" of inherent shutdown may be expected at slightly longer periods.

The effectiveness of the mechanical shutdown system was found to be most sensitive to the delay time, assuming a large amount of reactivity being available for shutdown. The mechanical shutdown system delay time is comprised of both electronic and actuation components. The former is the time for the electronic scram signal to trigger the system and the latter is the time for the mechanism to provide enough negative reactivity to stop the power rise, *i.e.*, the time for the rods to be inserted far enough into the core to terminate the power excursion. In the BSR-II system the electronic component of the delay time was made short, on the order of 5 msec, while the actuation time was found to be the major contributor to the delay time, on the order of 25 msec. These delay time components will vary from system to system.

A simple model was developed as part of the analysis to explore this sensitivity to delay time in the action of the mechanical shutdown system.

The model used in the Spert Project analysis is based on a constant delay time assumption, *i.e.*, the delay time is assumed constant with varying period and the negative reactivity is inserted as a step function. The step function assumption approximates the *s*-shape of the rod worth curve. The inherent shutdown mechanisms were not credited in the simple analytical model. With a constant delay time, the power simply behaves as,

$$P_{\max} = P_{trip} e^{\alpha t_d}$$

where P_{max} is the maximum power, P_{trip} is the power at the time of the trip signal, α is the reciprocal period and t_d is the constant delay time. Experimental measurements for mechanical shutdown system protected transient tests agree well with this model. The effect of delay time on the peak power is illustrated in Figure 2-21 which shows the trend in maximum power for systems with delay times varying by two orders of magnitude. The results are shown relative to the associated self-limited case and also to fuel damage thresholds.

2.4 Fuel Damage

The bottom line safety concern in a nuclear reactor accident is radiation exposure to workers and the public resulting from radiation release to the environment. The radiation released in an accident is some fraction of the radioactive inventory built up within the nuclear fuel as produced from the fission process. This inventory is contained within the fuel by the solid nature of, and the cladding on, the fuel material. The cladding boundary represents the first level of containment for a nuclear reactor core. Fuel damage is associated with a breach of this primary level of containment and as a result the onset of fuel damage represents a safety limit.

Despite the strong self-limiting characteristics of water-moderated plate-type cores, fuel damage has been observed to occur in the case of very fast, *i.e.*, very short period, transients. For an unprotected reactivity insertion, fuel damage occurs when the self-limiting characteristics cannot mitigate the transient before material property thresholds have been exceeded.

Various degrees and types of fuel damage were observed and studied during the Borax and Spert reactor tests. The subset of the fuel damage data is summarized in Chapter 3. The severity of the damage ranges from relatively minor mechanical deformations of the fuel plates to extensive fuel plate melting and core disassembly. In addition, irradiation and manufacturing flaws can also lead to fuel plate blistering at temperatures below the melting point of the clad. The degree of damage depends on the speed (*i.e.*, the period) of the transient, determined by the size of the initial reactivity insertion as well as the system parameters affecting the self-limiting ability of the core in question. The onset and degree of fuel damage appears very similar between cores, despite a wide variation in system parameters.

The physics of the fuel damage mechanisms, the types of damage, the core disassembly scenario and mechanism, and pertinent safety limits are described in the following sections. Further information on fuel damage experience and the destructive characteristic of MTR-type cores can be found in References 2-28, and 2-29.

2.4.1 Types and Physics of Fuel Damage

Fuel damage is caused by temperature increases in the fuel plates coupled in some situations by pressure generation within the core.

Under normal operating conditions the heat removal capability in a typical MTR-type reactor is such that peak fuel temperatures remain well below coolant saturation temperature and temperature drops across the fuel plates are only on the order of a few degrees centigrade. However, under accident conditions the heat removal capability can be compromised, either mechanically, *e.g.*, coolant channel blockage, or by the dynamics of the scenario, *e.g.*, in the case of fast power excursions.

During unprotected short period power excursions large amounts of energy are deposited primarily in the fuel meat in very short time intervals raising plate temperatures and establishing temperature gradients up to hundreds of degrees centigrade between the fuel meat centerline and the clad-coolant surface.

These temperature increases cause physical changes in the plate materials, such as a decrease in the tensile strength of the clad material, thermal stresses as a result of differing rates of thermal expansion, and phase changes (*e.g.*, melting). The seriousness and consequences of such changes depend on the magnitude of the temperature rise produced in the plate material during the excursion. Pressure

generation as a result of steam generation within the core, or in a more extreme case, by vaporization of the fuel meat within a fuel plate, in combination with the reduced strength of the fuel plates results in various types and degrees of fuel damage.

The Borax and Spert reactor tests and the few cases of reactor accidents in similar cores provide information on the different types and degrees of damage expected in MTR-type cores. The different types of fuel damage can be classified as:

- fuel plate clad blistering
- mechanical deformation of the fuel plates
- fuel plate clad melting

All three types of damage were experienced during the reactor tests and range in degree from practically inconsequential localized damage to widespread damage throughout the core. These types of damage are progressive in terms of severity and extent with shortening reactor period. Further decrease in the reactor period may in addition lead to core disassembly which represents the most severe damage scenario for an MTR-type core.

The physics behind the different types of damage are discussed in the following sections with reference to the experimental observations.

Understanding of the types of damage, the associated mechanisms, and the conditions leading to the onset of damage allow for the definition of safety limits as part of severe accident analysis methodology. These limits are defined with respect to fuel damage data in Chapter 7.

2.4.1.1 Clad Blistering

Blistering was observed in both the Spert I P-core and the Spert III C-core following short period power excursions. Examples of this damage are shown in Figures 2-22 and 2-23. The blistering was noted near the flux peak regions of the fuel plates but was not found on all plates exceeding a given temperature. The fuel in both of these cores was stainless-steel clad and the blistering in both cases has been attributed to manufacturing defects.

In the case of the Type-P fuel, metallurgical examination revealed that pre-existing faults in the fuel, due to manufacturing errors, resulted in inter-granular corrosion. This corrosion led to cracking under the thermal stresses of the short period

transients, water ingress and finally to blistering during subsequent transient testing. It should be noted that the same fuel did not blister during blister tests in which water was not present.

Similar metallurgical examination of the Type-C fuel did not indicate the same flaw in the fuel but rather suggested that blistering of this fuel may have been caused by a second fabrication factor, fuel meat inhomogenieties (fuel stringers into the clad).

Further details on the P-core and C-core blistering damage can be found in References 2-30, 2-31, 2-32, and 2-33.

No blistering was observed in experiments on the Al-clad plate fuel, suggesting that it was free of these manufacturing flaws. Modern day MTR-type fuel is not expected to suffer from these fabrication flaws given the methods and quality assurance programs in place for fuel manufacturers.

While not closely associated with more severe fuel damage, the rupture of blisters (as experienced with the P-core testing, Ref. 2-33) results in the release of fission product gases. Post irradiation blister testing on MTR-fuel indicates that irradiated plate-fuel is susceptible to clad blistering as a result of fission product accumulation (Refs. 2-34, 2-35, 2-36)

The onset of blistering is associated with a fuel plate clad surface temperature below and up to the melting point of the clad material. Fuel exposure during the reactor tests was insignificant compared to the fuel cycle length of research reactors explaining why blistering was not observed on the Al-clad test fuel.

2.4.1.2 Mechanical Deformation

Fuel damage in terms of mechanical deformation results from a loss of fuel plate elasticity as the plate temperature is raised, coupled with stress and strain induced by non-uniform thermal expansion and external pressure generation from coolant voiding within the core. This type of fuel damage occurs while the fuel plate is still in a solid material state and prior to melting damage discussed in the next section (Section 2.4.1.3). Deformation in the form of fuel plate bowing and rippling was observed in many of the reactor test cores.

This type of damage is typical of short period transients with periods or around 10 msec and shorter. For example, minor plate deformation was found in the Borax fuel

for transients with periods less than 10 msec and severe bowing was noted for a 5 msec transient. The exact period at which deformation damage first occurs will vary with the specific core and is not noted exactly for many of the experimental cases reported in the literature. For the Spert I A core it was observed that:

> "7 msec transients could be performed routinely with only minor mechanical distortions of the core," and "Core damage at 5 msec was limited to modest distortions." (Ref. 2-37)

This sort of period range seems typical and consistent with damage observations in a number of the other test cores. The onset of relatively minor deformation was noted in the Spert I D-core and the Spert IV D-core for transients with periods less than 9 msec (Ref. 2-38) and 10 msec respectively (Ref. 2-39).

The degree of plate deformation is proportional to the speed of the transient, increasing from minor plate bowing (over the length of the plate), to more pronounced and localized bowing and even plate rippling for shorter period transients. An example of a bowed and rippled fuel plate from the Spert III C-19/52 core is shown in Figure 2-24.

Whereas the self-limiting behaviour was found to be closely similar between the Spert Al-clad and the SS-clad plate cores, the SS-clad plate cores were found to be more susceptible to mechanical damage in terms of warping of the fuel plates. The same types and progression of damage were observed in the SS-clad cores but with onsets associated with lower clad temperatures and longer transient periods.

This is attributed to the differences in thermal conductivity between Al and SS. The lower thermal conductivity of the latter leads to larger thermal gradients, more non-uniform expansion, and increased thermal stresses over the fuel plate for a given transient. Calculations for the SS-clad Type-P fuel show that a transient with a period of 5 msec can lead to a gradient on the order of 540EC (1000EF) between the center of the plate and the plate surface which can, in turn, lead in turn to thermal stresses beyond the elastic limit and permanent deformation (Ref. 2-31). This is consistent with the observed fuel damage in the SS-clad test cores.

Warping and rippling of the stainless-steel-clad fuel plates was found to occur as a result of step insertion induced transients resulting in reactor periods shorter than 15 to 20 msec (Ref. 2-33). Severe bowing resulting in almost complete coolant channel blockage has been observed in transients with periods on the order of 5 msec.

In the case of the Borax tests, the mechanical damage was quite dramatic with the normally concave plates being reversed in curvature.

> "After these experiments the core was disassembled, and the bent plates were pounded roughly back into shape, but they were no longer very strong." (Ref. 2-1)

The maximum fuel surface temperatures for these tests did not approach the melting point of the cladding (Ref. 2-21). The minor plate bowing damage found in the Spert I D-core fuel is associated with maximum fuel plate surface temperatures of approximately 400EC (Ref. 2-40). More severe deformation is tied to higher clad surface temperatures. For maximum clad surface temperatures of between 550EC and 650EC the plates develop rippling which becomes "square topped" and causes fracturing of the clad (Ref. 2-40).

In addition to mechanical plate deformation resulting from the initial power burst of a step insertion initiated transient, mechanical damage was also observed in the Spert I A-core as a result of chugging oscillations:

> "The violent nature of these tests is indicated not only by the power behavior and the expulsion of water from the reactor vessel, but also by damage to the fuel assemblies. In several assemblies, fuel plates were actually torn loose from the brazed-on side plates and the assemblies suffered mechanical deformations such that they could no longer be placed in the reactor grid structure." (Ref. 2-41)

Although, in most cases, not of an immediate concern with regards to radiation release these mechanical deformations can lead to reduced coolant flow and the generation of a hot spot on the fuel. This in turn can lead to localized fuel plate melting and is thought to have possibly played a part in localized melting of a single plate in both the Spert I B-12/64 and Spert IV D-12/25 cores. It is also possible that severe plate deformation may play a part in the core destructive mechanism (see Section 2.4.2). Therefore, mechanical plate deformation can be classified as a precursor and possible contributor to more severe fuel plate damage which results in radioactive inventory release.

2.4.1.3 Clad Melting

Fuel plate clad melting represents a breach of the containment offered by the fuel

plate cladding, and, after blistering, is associated with the next stage of significant fission product release. The melting point of aluminum clad is typically on the order of 600EC, varying slightly with the specific alloy. For Al-6061, the standard reactor grade cladding material used in the US, the solidus point is 585EC (Ref. 2-35).

Clad melting can occur in two very different scenarios: (i) locally as a result of coolant flow blockage or fuel fabrication defects while the rest of the core is significantly below the melting point of the clad material, and (ii) independent of flow blockage or defects, during a very fast (short period) transient when the temperature increases of the clad exceeds the melting point before the energy can be transferred to the coolant.

In the first case, clad melting is not necessarily related to a reactivity insertion scenario or any power increase. Of course, a positive power excursion may very well create the required temperatures for melting in a blockage scenario. Clad melting due to flow blockage was experienced in the Engineering Test Reactor (ETR) on December 12, 1961 (Ref. 2-42), while clad melting as a result of fuel fabrication defects was experienced in the Westinghouse Testing Reactor (WTR) on April 3, 1960 (Ref. 2-43). Neither of these two accidents were initiated by a transient power increase.

Localized and isolated fuel plate melting was experienced in both the Spert I B-12/64 core (Ref. 2-44) and the Spert IV D-12/25 core (Ref. 2-39). In both cases, a hole was melted in a single plate of a single fuel assembly during step initiated reactivity insertion tests which were not expected to produce fuel damage (Figs. 2-25, 2-26). Neither of these two instances of plate melting were part of a sequence or progression to more severe or widespread core damage. In fact in both cases, the plate damage went undetected during subsequent transient testing and did not noticeably influence the self-limiting behaviours of the test cores.

In both cases this localized and isolated plate melting may have been due to fabrication flaws or previously existing mechanical damage causing blockage of the adjacent coolant channel. Metallurgical analysis of the B-12/64 plate indicates a non-symmetric temperature distribution over the melted part of the plate pointing to a blockage type situation. Coolant channel blockage may have played a role in both of these cases, although testing with the B-12/64 core did not include periods short enough to expect anything other than minor fuel plate deformation. These incidents illustrate that the occurrence of plate melting is not necessarily self propagating and does not necessarily lead to core disassembly.

In any case, fuel plate melting can indeed occur in the absence of any channel blockage or defects in the fuel plates, and solely as a result of temperature increases during fast transients. This scenario was studied in the "destructive test series" conducted in the Spert I D-12/25. The transient tests in question were performed just prior to the final destructive test in which the core was damaged beyond further testing. This test series included progressively shorter period transients and fuel plate melting was observed for the tests with periods of 5 msec and 4.6 msec.

In the absence of pre-existing channel blockage or fuel defects, clad melting occurs centred around the hot spot of the core, typically the geometric centre of the core near the axial flux peak, when the maximum fuel plate surface temperature exceeds the melting point of the clad material. This is illustrated in the melt patterns of the non-destructive 5-msec and 4.6-msec period transients in the Spert I D-12/25 core (Figs. 2-27, 2-28, 2-29, 2-30).

Typical melting from the Spert I D-12/25 5-msec test is shown in Figures 2-31 and 2-32. The extent of the region of melting becomes progressively larger with shortening periods. While the melted clad may remain on the plate in the area of melting, holes and some fuel relocation can result. Plate fracturing was observed on melted plates in these tests. Additionally, in combination with the mechanical deformation typical of transients in this period range, fusing of adjacent fuel plates may result (Fig. 2-33).

Unlike the local instances of melting in the Spert I B- and Spert IV D-cores discussed above, these melting situations are closely related to more severe and widespread core damage. While not necessarily triggering the core destructive mechanism (core disassembly did not occur for the 5-msec and 4.6-msec tests in which melting was observed), indications are that the margin between onset of clad melting and the threshold for core disassembly is small in terms of transient period. The melt patterns in these cases are closely tied to the plate destruction patterns observed in the core disassembly cases.

The core destructive mechanism and the related fuel damage are discussed in further detail in Section 2.4.2.

2.4.2 Core Disassembly and the Destructive Mechanism

For short enough periods, exceeding those associated with onset of clad blistering, and onset of fuel plate deformation, an MTR-type light water core is susceptible to

violent core disassembly. This accident scenario involves destruction of the core as a result of a large pressure pulse generated by steam formation. The magnitude of the pressure pulse associated with the core disassembly scenario is much larger than those expected during self-limitation of transients *via* steam formation.

Core disassembly occurs when the self-limiting mechanisms can not mitigate the transient before the threshold for the destructive mechanism is exceeded. It is associated with possible damage to the structure of the facility and significant radiological release beyond the containment barrier of the fuel cladding.

Three instances of MTR-type core disassembly provide a database of information. These are the two destructive tests (D-tests) performed on the Borax I and Spert I D-12/25 cores, and the SL-1 reactor accident.

2.4.2.1 Damage Description

The damage associated with the core disassembly includes extensive fuel plate melting and disintegration, ejection of coolant water, relocation of the fuel, and significant damage to the core structure. As a result of the Borax I destructive test a major fraction of the core was melted, the core was completely disassembled, the reactor tank was burst, most of the shield tank contents were ejected, and the one ton (~1000 kg) control drive mechanism was thrown 30 ft into the air. Below are some interesting excerpts regarding the Borax I destructive test:

> "In a very short time after the release of the central control rod a column of what appeared to be dark grey smoke was ejected from the reactor to a height of some 80 feet. The difference in appearance between this material and the silvery-white mixture of steam and water which had been ejected during the slower-period 1953 experiments was striking. Shortly thereafter the sound of a medium sharp detonation reached the control trailer, and a slight tremor of the trailer was felt. In a few seconds the smoke cleared away, and it was apparent that the entire superstructure of the reactor, containing the control rod mechanism, had been carried away." (Ref. 2-20)

> “The explosive force of the excursion broke the reactor tank and completely disassembled the reactor core. Some of the fuel elements and fuel element fragments remained in the shield tank and the pump pit, while others were blown completely out, the smaller fragments

travelling as far as 200 feet." (Ref. 2-20)

> "A second phenomenon shown by the high speed camera is the presence of pieces of material in the ejected debris which seem to be emitting light of sufficient intensity to be plainly visible, even though the excursion was made in bright sunlight. It has been postulated that these may be hot fragments of fuel element which are burning in air." (Ref. 2-20)

> "Although the explosion was spectacular, its effects were comparable to those which could be caused by a moderate amount of chemical explosive." (Ref. 2-21)

Estimates of the equivalent amount of chemical explosive are reported as 6 to 17 lbs of TNT to achieve the same magnitude of damage, and 70 lbs of TNT to achieve the same energy release (Ref. 2-20).

In the Borax I core, only one fuel assembly was left containing most of its fuel plates following the destructive test. The post-destructive-test map of the Spert I D-core is shown in Figure 2-34 and the melt pattern is shown in Figure 2-35. In the SL-1 accident forty-seven percent of the fuel in the central 16 assemblies was destroyed while over the entire core 20% of the fuel was destroyed (Ref. 2-45). A schematic of the destroyed plates in SL-1 is shown in Figure 2-36 and a photo of the post-accident core is shown in Figure 2-37.

Damage to the fuel/core was found to vary with radial location, with relatively less melting on the core periphery compared to the centre of the core. In general, the central portions of the fuel plates were melted and subsequently disintegrated, leaving the tops and bottoms of the plates and the unfueled strips of cladding on each side. There did not appear to be any radial direction bias in the damage distribution.

Examination of the fuel debris suggests that in both the Borax and Spert I D-core destructive tests fuel meat was molten and "flowed" out of the partially intact cladding on the central fuel plates (Fig. 2-38). In some assemblies the fuel plates looked to have melted and been torn away from the side plates while in others the plates appeared to be "neatly stripped" from the side plates (Fig. 2-39). In contrast, in the SL-1 accident, the fuel meat appeared to have "exploded away" from the cladding (Ref. 2-28). This difference in behaviour is discussed below.

Outside of the melted region of the core, mechanical deformation of the assemblies was severe. An example of this is shown in Figure 2-40 from the Spert I D-core recovery (Ref. 2-46). As mentioned previously the damage to the core structure and facility in all three cases was significant.

Similar "spongy type fuel material" was noted in all three cases during the post-excursion examinations of the debris. This was a predominant form of the damaged fuel indicating a relatively fast cooling rate of molten fuel metal in contact with water or water-vapour. This further indicates the rapid termination of all energy generation once the core is disassembled.

The radiological releases associated with these excursions are documented in References 2-20, 2-40, and 2-45. It should be kept in mind that the Borax I and Spert I D-cores were practically "clean", *i.e.*, very little in the way of fission product buildup and none of the three reactor facilities incorporated a containment structure.

2.4.2.2 Destructive Mechanism

As discussed in Section 2.3.5, the self-limiting mechanisms characterising an MTR-type core are separate from the mechanism behind core disassembly. Data from both the Borax I and Spert I D-core destructive tests show that the cores in fact did self-limit the nuclear reaction prior to the core disassembly.

In the case of Borax I, although the destructive pressure pulse was observed prior to the time of maximum power, indications are that the nuclear transient was self-limited prior to core disassembly, apparently by the same self-limiting mechanisms as for non-destructive transients of longer period. This was evidenced by the high-speed motion picture recording of a blue flash being extinguished before ejection of core material from the reactor tank. Data from the Spert I D-core destructive test clearly show that the transient was self-limited before the occurrence of the destructive pressure pulse. The power at the time of the pulse (~15 msec after peak power) had already dropped to approximately five percent of the maximum value (Fig. 2-41). The differences in timing of the pressure pulse relative to the time of peak power are due to the triggering of the destructive mechanism which depends on the local fuel plate temperature distribution. This is discussed in more detail below.

The three excursions are associated with asymptotic reactor periods and reactivity insertions of 2.6 msec/33 mk (Borax I), 3.2 msec/25 mk (Spert I D), and 3.6 msec/24

mk (SL-1). The transient data associated with these three excursions are summarized in Table 2-2. All of the transient data with the exception of pressure generation can be extrapolated from longer period tests. It therefore appears that self-limiting mechanisms are still applicable during destructive excursions and that the violent disassembly of the core arises as a consequence of different conditions in the core and a different mechanism, not found in the longer period tests.

The exact "onset" period and reactivity of the core destructive mechanism was not identified, only that these transients were beyond the core disassembly threshold. For the Borax I core this threshold is somewhere between 14 and 2.6 msec corresponding to an initiating reactivity addition of between 11 mk and 33 mk. For the Spert I D-core this threshold is between 4.6 and 3.2 msec, corresponding to an initiating reactivity addition between 19 mk and 25 mk. Both of these period/reactivity ranges are applicable to initially low power, ambient temperature conditions.

What is also known are the characteristics of the core on previous non-destructive tests (in the case of Borax I and Spert I D) and the damage and state of the core resulting from the destructive excursion. Given the phenomenological understanding of the shutdown mechanisms and the state of the core prior to disassembly, the core disassembly mechanism can be postulated. This is described herein.

Core disassembly is caused by a large pressure pulse produced from what is referred to as a "steam explosion". Analysis of structural damage shows that this pressure pulse originates in the central portion of the core (*i.e.*, the hottest section of the core). The pressure pulse is generated by the very rapid and large scale voiding of the coolant similar to that produced for longer period transients as part of the self-limiting response of the MTR-type core but different in that the magnitude is much larger.

The hypothesis herein is that the sudden and extensive increase in steam formation occurs due to a sudden and extensive increase in heat transfer area between the hot plate material and the coolant. Specifically this is the release of hot fuel meat (molten or vapour) into the coolant, resulting from a breach of the cladding material. The sudden bringing into contact of the hot fuel meat (much hotter than the clad surface) and the coolant discontinuously increases the steam formation compared to longer period self-limitation mechanisms in which the plate integrity is maintained.

Calculations have shown that the tensile strength of the Spert Type-D fuel plates is significantly degraded at the time of the destructive pressure pulse, *i.e.*, essentially

negligible at the core hot spot and only 6% of its initial strength at the core periphery (Ref. 2-19). Given the weakened state of the core due to the elevated fuel plate temperature, this suggests that the generated pressure destroys the integrity of adjacent plates and the mechanism is self propagating. That is, the fragmentation of additional fuel creates more steam and adds to the pressure pulse.

For both the Borax I and Spert I D-core the hypothesis is that this mechanism is triggered by the release of molten fuel from the plates once the clad is breached by melting. This fits with the evidence from the post-accident examination of the damaged and destroyed fuel plates in which the meat had apparently "flowed" from the plates, leaving much of the cladding still intact.

Unlike the Borax I damage evidence, the fuel meat in the SL-1 destructive excursion looked like it had "virtually exploded away from its clad" (Ref. 2-45). This presents evidence as to the internal temperature distribution in the fuel plates at the time of core disassembly and suggests a higher temperature in the SL-1 plates.

Analysis of the three excursions (Ref. 2-28) shows that internal temperatures in the SL-1 fuel plates may have exceeded the vaporization temperature of the fuel meat while the clad surface temperature was only 420EC, below the melting point of the clad. These calculated SL-1 fuel temperatures are consistent with the amount of Al-H_2O reaction product found in the core debris (Ref. 2-28). An applicable temperature distribution is shown schematically in Figure 2-42. In this case the fuel meat centerline temperature exceeds vaporization temperature. The clad surface may or may not have reached the melting point at this time for this suggested triggering mechanism.

This is in contrast to the Borax I and Spert I D cases where the melting point of the cladding surface is reached well before the temperature of the fuel meat reaches vaporization. The internal temperature distribution of the hot fuel plate in these cases is schematically represented in Figure 2-43. In this case the fuel meat centerline is molten when the clad surface temperature exceeds the melting point.

The differences occur due to the differences in plate and clad thickness and thermal conductivities, *i.e.*, the SL-1 meat and clad were both significantly thicker and more highly loaded than the Borax and Spert plates. This suggests that bursting of fuel plates occurred in the SL-1 accident in contrast to the Borax I and Spert I D behaviour.

Discussion of this dependence on clad thickness is given in Reference 2-28 including thermal calculations for an exponential energy deposition. Similar calculations of the transient temperature distributions within the fuel plates and loss of tensile strength calculations given in Reference 2-19.

What initially triggers the plate fragmentation may be the pressure generated from the self-limiting coolant voiding or even the re-wet of the plates during the unstable hydrodynamic state of the core during and following self-limitation of the nuclear transient. This latter possibility fits with evidence from molten metal-water experiments conducted to investigate the Borax and Spert I D-core destructive test mechanism, which show that molten metal is violently disrupted and dispersed by the impact of water (Refs. 2-47, 2-48).

In any event, the destructive mechanism appears consistent within the two destructive tests and the destructive accident in the three different reactors, with the exception of the exact details of release of the fuel meat into the coolant. Fuel plate deformation, while not likely required for a core disassembly reaction to occur, likely can contribute to such an event by creating not only local "initiation sites" for melting but also blocking pressure release avenues *via* the coolant channels and enhancing the damage of adjacent plates and assemblies. It is reasonable to assume that cores with pre-existing plate deformation and weakened plates *via* mechanical deformation may be more susceptible to core disassembly or at least to more extensive damage.

While fuel plate surface melting may not necessarily precede the destructive pressure pulse (dependent on fuel plate geometry and thermal characteristics) it appears to be the case for typical fuel plate thicknesses associated with the test reactor fuel and modern MTR-type fuel, *i.e.*, clad thickness # 0.051 cm and meat thickness # 0.051 cm. Indications are that the margin between fuel clad surface melting and core disassembly is small and, pending further analysis on the role of plate deformation, tensile strength thresholds, and internal plate melting distributions, is presently left as future work.

The destructive mechanism points to maximum temperature limits and a "global" state of the core. Localized damage, including melting and fuel relocation, has been seen to happen in isolated incidents (Spert I B- and Spert IV D-core tests) and does not necessarily lead to further core damage or degradation of the self-limiting ability of the core. The high fuel temperatures associated with core disassembly can only be generated from short period reactivity initiated events. As such, non-RIA events, such as coolant channel blockage are not related to this type of core damage and are

associated with local fuel damage only.

It should be noted that the driving factor is not a metal-water chemical reaction for which the term "steam explosion" is otherwise associated. The topic of metal-water chemical reactions is addressed in Section 2.4.2.3.

More information on the destructive mechanism for MTR-type fuel may be available from testing carried out in the Transient Reactor Test (TREAT) facility in Idaho, and the Nuclear Safety Research Reactor (NSRR) facility in Japan. Both are pulsed systems in which fuel samples can be studied. The pulse width between these two facilities varies with the former characterized by a pulse width between 0.3 and 1 second and the latter by a pulse width between 25 and 100 msec (Ref. 2-49).

2.4.2.3 Metal-Water Reaction

An additional factor worth mentioning is the exothermic Al-H_2O reaction of interest to light-water-cooled and moderated reactor accident analysis, *i.e.*,

$$2\,Al + 3\,H_2O \rightarrow Al_2O_3 + 3\,H_2 + 231\times10^3\ cal/mol\ of\ Al_2O_3\ formed,$$
$$or\ 18\ MW\text{-}sec/kg\ of\ Al\ metal\ reacting$$

This Al-H_2O reaction is discussed in Reference 2-45 in the context of the SL-1 accident and the Borax and Spert I D-core destructive tests.

The experimental and post-accident analysis of the fuel debris provides estimates of the extent of this reaction. These estimates indicate that only a fraction of the total energy generation is from the Al-H_2O chemical reaction, *i.e.*, about 3.5 MW-sec or 10% of the nuclear energy generation in the Spert I D-core destructive test (Ref. 2-50) and approximately 24 ± 10 MW-sec or one fifth of the total nuclear energy generated in the SL-1 accident (Ref. 2-45). Additionally, examination of the fuel debris reveals that the destroyed fuel is primarily in small to medium particle form if not still part of a fuel plate and that cooling of the fuel particles is rapid. Both of these characteristics are not favourable to the Al-H_2O reaction which requires very high temperatures of the molten material and finely particularized material to be self-sustaining.

As a result, it can be concluded that the temperatures and physics are such that the environment created during an MTR-type core disassembly event is not conducive

to a self-propagating Al-H_2O reaction.

Therefore, this reaction is not the cause of the "steam explosion" but rather a by-product of the core disassembly. The energy generated by the Al-H_2O reaction constitutes a fraction of the total energy production (most of which comes from the nuclear reaction) and varies with system specifics related to temperature distributions and magnitudes achieved in the excursion.

It should also be noted that the presence of fuel melting is not enough to initiate the Al-H_2O reaction. For example, no evidence of metal-water reaction was found in the ETR blockage accident analysis (Ref. 2-42).

2.5 References

2-1. J. R. Dietrich, D. C. Layman, "Transient and Steady State Characteristics of a Boiling Reactor. The Borax Experiments, 1953", ANL-5211 (also listed as AECD-3840), Argonne National Laboratory, USA, February 1954.

2-2. J. R. Eaton, Electrons, Neutrons and Protons in Engineering, Pergammon Press Ltd., 1st Edition, 1966.

2-3. S. Glasstone, M. C. Edlund, The Elements of Nuclear Reactor Theory, D. Van Nostrand Company Ltd., 1952.

2-4. J. J. Duderstadt, L. J. Hamilton, Nuclear Reactor Analysis, John Wiley & Sons, 1976.

2-5. S. Glasstone, A. Sesonske, Nuclear Reactor Engineering, 3rd Edition, Krieger Publishing Co., 1981.

2-6. J. C. Haire, Editor, "Quarterly Technical Report - Spert Project - April, May, June, 1959", US AEC Technical Report IDO-16584, Phillips Petroleum Co., April 12, 1960.

2-7. J. A. Norberg, "Quarterly Progress Report - January, February, March, 1959 - Reactor Projects Branch", US AEC Technical Report IDO-16539, Phillips Petroleum Co., November 20, 1959.

2-8. G. O. Bright, Editor, "Quarterly Technical Report - April, May, June, 1958 - Reactor Projects Branch", US AEC Technical Report IDO-16489, Phillips Petroleum Co., January 19, 1959.

2-9. W. A. Horning and H. C. Corben, "Theory of Power Transients in the Spert I Reactor, Final Report", US AEC Technical Report IDO-16446, Ramo-Wooldridge Corp. for the Phillips Petroleum Co., August 20, 1957.

2-10. A. H. Spano, R. W. Miller, "Spert I Destructive Test Program Safety Analysis Report", US AEC Technical Report IDO-16790, Phillips Petroleum Co., June 15, 1962.

2-11. J. G. Crocker, Z. R. Martinson, R. M. Potenza, L. A. Stephan, "Reactor Stability Tests in the Spert IV Facility", US AEC Technical Report IDO-

17088, Phillips Petroleum Co., July 1965.

2-12. F. Schroeder, "Stability Tests with the Spert-I Reactor", US AEC Technical Report IDO-16383, Phillips Petroleum Co., July 1, 1957.

2-13. W. E. Nyer, S. G. Forbes, F. L. Bentzen, G. O. Bright, F. Schroeder, T. R. Wilson, "Experimental Investigations of Reactor Transients", US AEC Technical Report IDO-16285, Phillips Petroleum Co., April 20, 1956.

2-14. S. G. Forbes, F. L. Bentzen, P. French, J. E. Grund, J. C. Haire, W. E. Nyer, R. F. Walker, "Analysis of Self-Shutdown Behaviour in the Spert I Reactor", US AEC Technical Report IDO-16528, July 23, 1959.

2-15. T. J. Thompson, J. G. Beckerly, editors, The Technology of Nuclear Reactor Safety, Vol. 1, "Reactor Physics and Control", Chapter 7, W. E. Nyer, "Mathematical Models of Fast Transients", The MIT Press, 1964.

2-16. R. P. Morgan, "A Review and Discussion of Literature Concerning Transient Heat Transfer and Steam Formation", US AEC Technical Report IDO-17226, Phillips Petroleum Co., March 1967.

2-17. P. A. Lottes, et al., "Boiling Water Reactor Technology. Status of the Art Report. Volume I. Heat Transfer and Hydraulics", US AEC Technical Report ANL-6561, Argonne National Laboratory, February 1962.

2-18. R. W. Miller, "An Experimental Study of Transient Boiling during Spert I Power Excursions", Transactions of the American Nuclear Society, v.4, n.1, June 1961, p.69.

2-19. J. E. Houghtaling, Alain Sola, A. H. Spano, "Transient Temperature Distributions in the Spert I D-12/25 Fuel Plates During Short-Period Power Excursions", US AEC Technical Report IDO-16884, Phillips Petroleum Co., June 1964.

2-20. J. R. Dietrich, "Experimental Investigation of the Self-Limitation of Power During Reactivity Transients in a Subcooled, Water-Moderated Reactor. Borax-I Experiments, 1954", ANL-5323, (also listed as AECD-3668), Argonne National Laboratory, USA, 1954.

2-21. J. R. Dietrich, "Experimental Determinations of the Self-Regulation and Safety of Operating Water-Moderated Reactors", in the Proceedings from the First International Conference on the Peaceful Uses of Atomic Energy, Geneva, 1955, Argonne National Laboratory, v. 13, pp. 88-101.

2-22. H. L. McMurray, A. V. Grimaud, "Temperature Distribution in a Fuel Plate with Exponentially Rising Power. Part II - Results Based on Asymptotic Solutions", US AEC Technical Report IDO-16311, Phillips Petroleum Co., January 5, 1955.

2-23. J. E. Matos, E. M. Pennington, K. E. Freese, W. L. Woodruff, "Safety-Related Benchmark Calculations for MTR-Type Reactors with HEU, MEU and LEU Fuels", ANL, IAEA-TECDOC-643, v.3, Appendix G-1, 1992.

2-24. F. L. Bentzen, "The Merits of Inherent Shutdown Vs Mechanical Shutdown of a Plate-Type Water-Moderated and -Reflected Reactor In a Runaway Condition", Transactions of the American Nuclear Society, v.3, n.2, 1960, pp.429-430.

2-25. F. Schroeder, editor, "Quarterly Technical Report - Spert Project - April, May, June, 1960", US AEC Technical Report IDO-16640, Phillips Petroleum Co., April 7, 1961.

2-26. F. L. Bentzen, "The Merits of Inherent Shutdown Vs Mechanical Shutdown of a Plate-Type Water-Moderated and -Reflected Reactor In a Runaway Condition", US AEC Technical Report IDO-16722, Phillips Petroleum Co., November 3, 1961.

2-27. L. A. Stephan, "Transient Tests of the BSR-II Core in the Spert I Facility", US AEC Technical Report IDO-16768, Phillips Petroleum Co., April 5, 1963.

2-28. Flight Propulsion Laboratory Department, "Additional Analysis of the SL-1 Excursion", US AEC Technical Report IDO-19313, General Electric Company, November 21, 1962.

2-29. T. J. Thompson, J. G. Beckerly, editors, The Technology of Nuclear Reactor Safety, Vol. 1, "Reactor Physics and Control", Chapter 11, T. J. Thompson, "Accidents and Destructive Tests", The MIT Press, 1964.

2-30. F. L. Bentzen, editor, "Quarterly Progress Report - October, November, December, 1958 - Reactor Projects Branch", US AEC Technical Report IDO-16537, Phillips Petroleum Co., September 1, 1959.

2-31. A. H. Spano, editor, "Quarterly Technical Report - Spert Project - July, August, September 1959", US AEC Technical Report IDO-16606, Phillips Petroleum Co., July 11, 1960.

2-32. F. Schroeder, editor, "Quarterly Technical Report - Spert Project - October, November, December, 1960", US AEC Technical Report IDO-16687, Phillips Petroleum Co., June 1, 1961.

2-33. R. E. Heffner, "Damage to Stainless Steel Fuel in Spert Reactors", US AEC Technical Report IDO-16729, Phillips Petroleum Co., November 22, 1961.

2-34. J. M. Beeston, R. R. Hobbins, G. W. Gibson, W. C. Francis, "Development and Irradiation Performance of Uranium Aluminide Fuels in Test Reactors", Nuclear Technology, v.49, June 1980, p.136.

2-35. R. P. Taleyarkhan, "Analysis and Modelling of Fission Product Release from Various Uranium-Aluminum Plate-Type Reactor Fuels", Nuclear Safety, v.33, n.1, pp.6-22, January-March 1992.

2-36. "Safety Evaluation Report related to the Evaluation of Low-Enriched Uranium Silicide-Aluminum Dispersion Fuel for Use in Non-Power Reactors", U.S. Nuclear Regulatory Commission Technical Report NUREG-1313, July 1988.

2-37. W. E. Nyer, S. G. Forbes, "Spert Program Review", US AEC Technical Report IDO-16634, Phillips Petroleum Co., October 19, 1960.

2-38. J. Dugone, D. D. Wieland, "Fuel Plate Experience During the Spert I Destructive Test Series with an Aluminum-Clad, Plate-Type Core", US AEC Technical Report IDO-16885, Phillips Petroleum Co., July 1963.

2-39. J. G. Crocker, L. A. Stephan, "Reactor Power Excursion Tests in the Spert IV Facility", US AEC Technical Report IDO-17000, Phillips Petroleum Co., August 1964.

2-40. R. W. Miller, Alain Sola, R. K. McCardell, "Report of the Spert I Destructive Test Program on an Aluminum, Plate-Type, Water-Moderated Reactor", US AEC Technical Report IDO-16883, Phillips Petroleum Co., June 1964.

2-41. F. Schroeder, "Stability Tests with the Spert-I Reactor", US AEC Technical Report IDO-16383, Phillips Petroleum Co., July 1, 1957.

2-42. F. R. Keller, "Fuel Element Flow Blockage in the Engineering Test Reactor", US AEC Technical Report IDO-16780, Phillips Petroleum Co., May 10, 1962.

2-43. Capt. A. Nelson Tardiff, "Some Aspects of the WTR and SL-1 Accidents", US AEC Technical Report IDO-19308, April 9, 1962.

2-44. G. O. Bright, editor, "Quarterly Progress Report - January, February, March, 1958 - Reactor Projects Branch", US AEC Technical Report IDO-16452, Phillips Petroleum Co., September 10, 1958.

2-45. SL-1 Project, "Final Report of SL-1 Recovery Operation", US AEC Technical Report IDO-19311, General Electric Company, July 27, 1962.

2-46. F. Schroeder, editor, "Quarterly Technical Report - Spert Project - October, November, December, 1962", US AEC Technical Report IDO-16890, Phillips Petroleum Co., May 17, 1963.

2-47. R.W. Wright, G.H. Humberstone, "Dispersal and Pressure Generation by Water Impact upon Molten Aluminum", Transactions of the American Nuclear Society, Vol. 9, 1966, pp 30.5-:306.

2-48. K. Darby, R.C. Pottinger, N.J.M. Rees, R.G. Turner, "The Thermal Interaction between Water and Molten Aluminum under Impact Conditions in a Strong Tube", Engineering of Fast Reactors for Safe and Reliable Operation, Vol. II., Karlsruhe, Oct. 1973.

2-49. V. Georgevich, R. P. Taleyarkhan, S. Navarro-Valenti, S. H. Kim, "Thermally Induced Dispersion Mechanisms for Aluminum-Based Plate-Type Fuels Under Rapid Transient Energy Deposition", ORNL Conference Paper CONF-950828-26, National Heat Transfer Conference, Portland, Oregon, USA, August 1995.

2-50. F. Schroeder, editor, “Quarterly Technical Report - Spert Project - January, February, March, 1963", US AEC Technical Report IDO-16893, Phillips Petroleum Co., May 20, 1963.

2.6 Tables

Table 2-1: Summary of Feedback Characteristics for MTR-type Systems

Mechanism	Sign	Timing	Magnitude	
			HEU	LEU
Doppler	negative	prompt	negligible	large
Void	negative	delayed	large	large
Coolant Temperature	negative	mostly delayed	small	small
Reflector Temperature	positive	long delay	small	small

Table 2-2: Transient Summary Data for the Destructive Power Excursions

Destructive Power Excursions

Core	reactivity (mk)	period (msec)	alpha (sec-1)	Pmax (MW)	Etot (MW-sec)	Tmax Clad (deg C)	Tmax Meat (deg C)
Borax I	32.6	2.6	385	13,000 - 20,000	135	> 690	1093 - 1650
Spert I D-12/25	24.9	3.2	313	2250	30.7	> 615	1360
SL-1	24 +/- 3	3.6 +/- 0.5	278	16,000 - 19,000	133 +/- 10	> 640	945 - 1050

Data is taken from the following technical reports: ANL-5323 (Borax), IDO-16883 (Spert), IDO-19313 (SL-1)
reactivity = estimated inserted reactivity causing the asymptotic or minimum period
Tmax Clad = maximum clad surface temperature
Tmax Meat = maximum (estimated) fuel meat temperature
estimated uncertainty is indicated when reported
The Spert I D-12/25 reactivity insertion is reported as 3.55 $, and converted to mk using 7 mk/$.
SL-1 reactivity and period values are estimated from post-accident analysis of probably rod positions

2.7 Figures

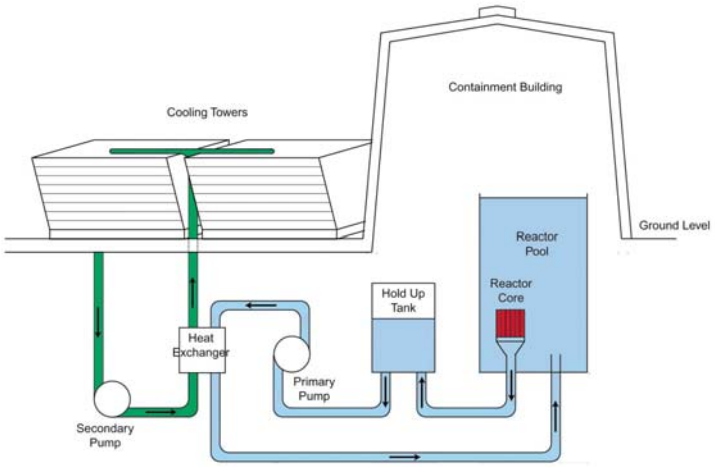

Figure 2-1: McMaster Nuclear Reactor Cooling Systems

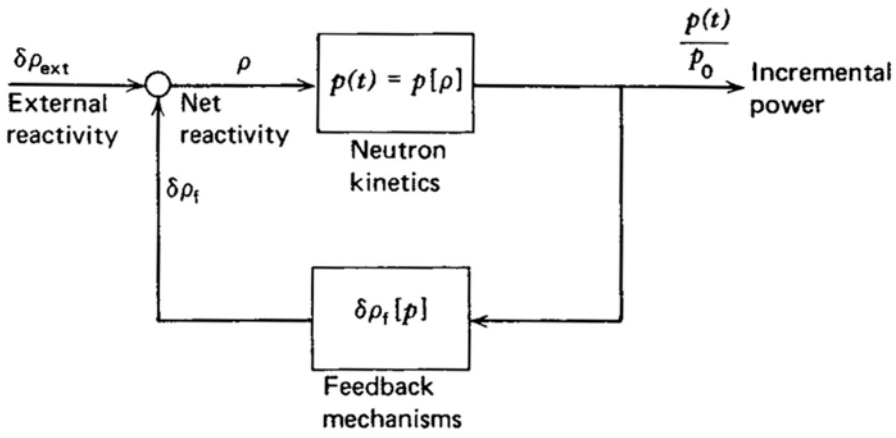

Figure 2-2: Closed-Loop Concept Diagram of Reactivity Feedback (Ref. 2-4)

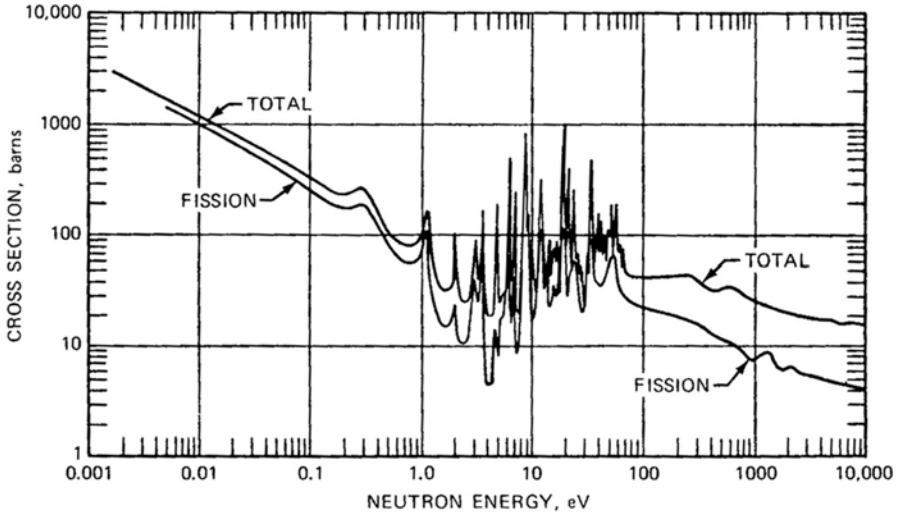

Figure 2-3: Microscopic Total and Fission Cross Sections for U-235 as a Function of Energy (Ref. 2-5)

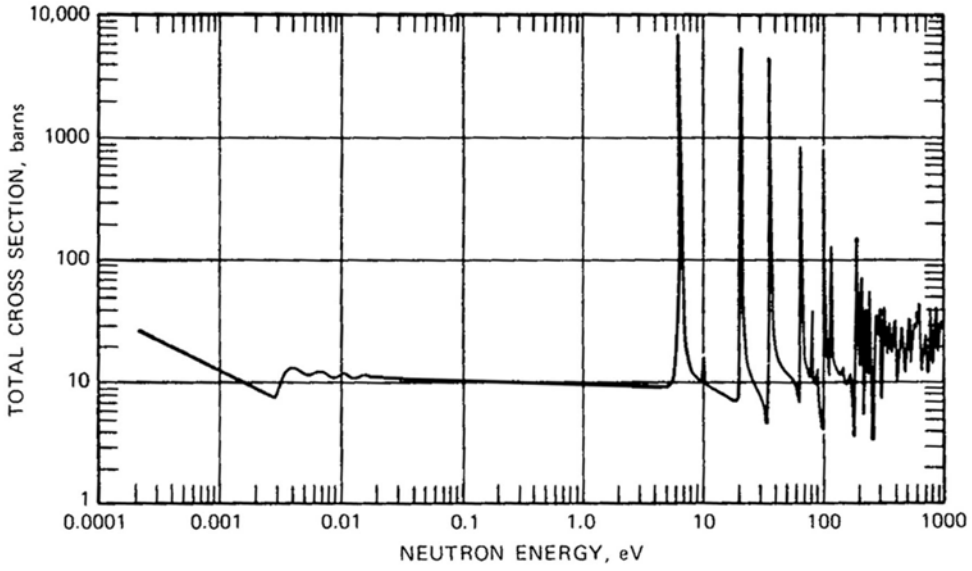

Figure 2-4: Microscopic Total Cross Section for U-238 as a Function of Energy (Ref. 2-5)

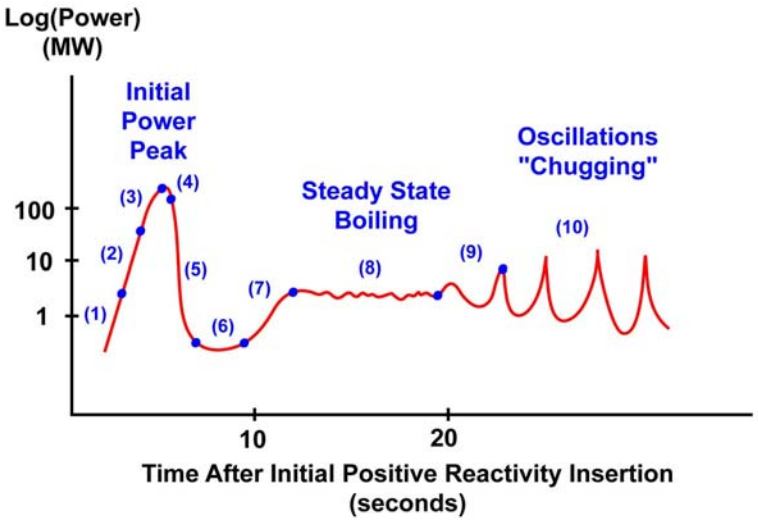

Figure 2-5: Idealized Power against Time for a Step Reactivity Insertion

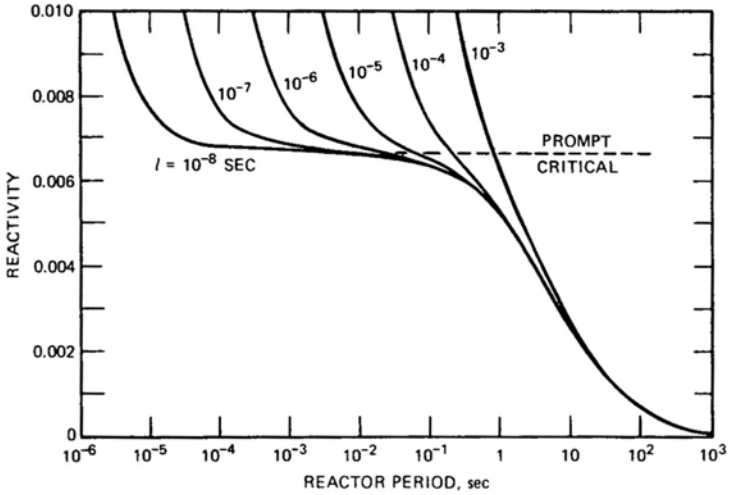

Figure 2-6: Relationship Between Reactor Period and Reactivity for Various Prompt Neutron Lifetimes (Ref. 2-5)

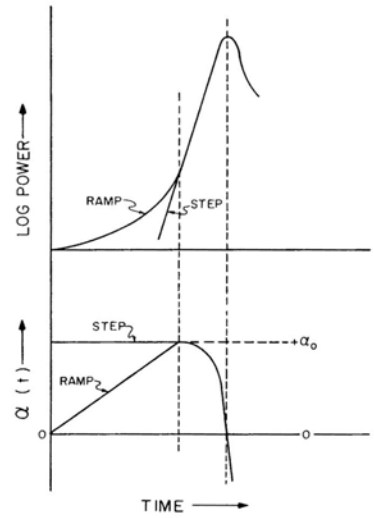

Figure 2-7: Power and Reactivity Behaviour for Step and Ramp Transients (Ref. 2-15)

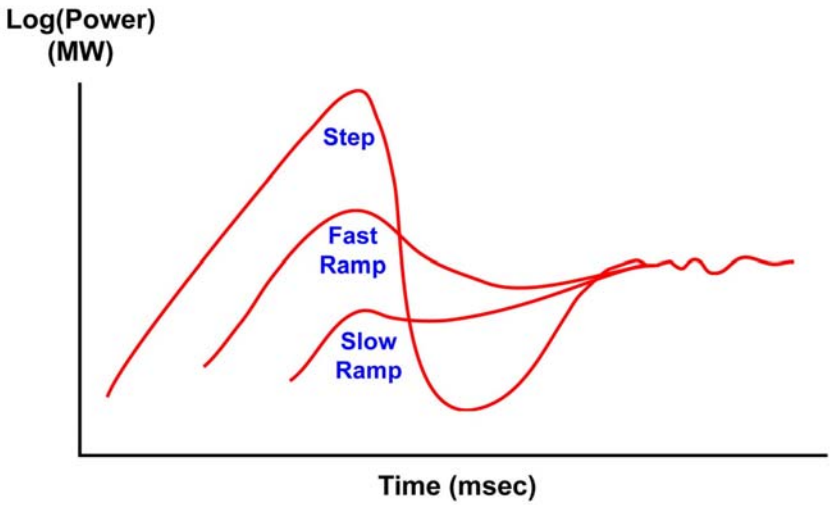

Figure 2-8: Schematic Comparison of Step and Ramp Insertion Initial Power Pulse Behaviour

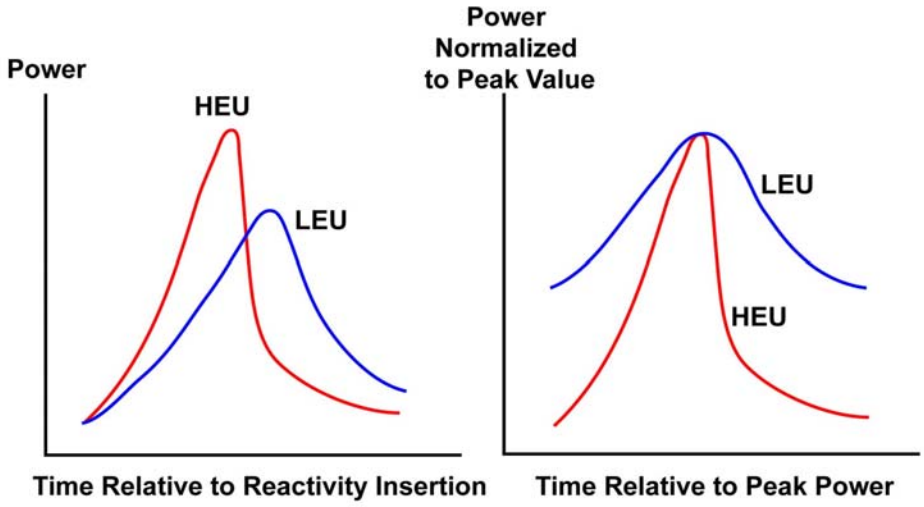

Figure 2-9: Schematic Comparison of HEU and LEU System Initial Power Pulse Behaviour: Magnitude and Timing (left), Pulse Shape (right)

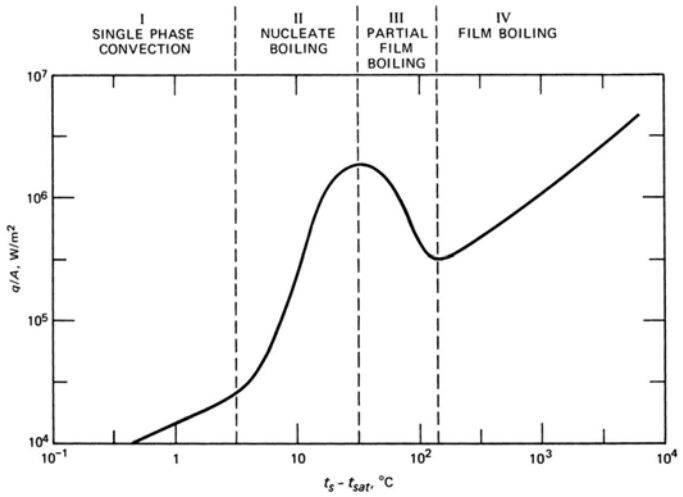

Figure 2-10: Variation of Heat Flux with Surface-Liquid Temperature Difference in Pool Boiling (Ref. 2-5)

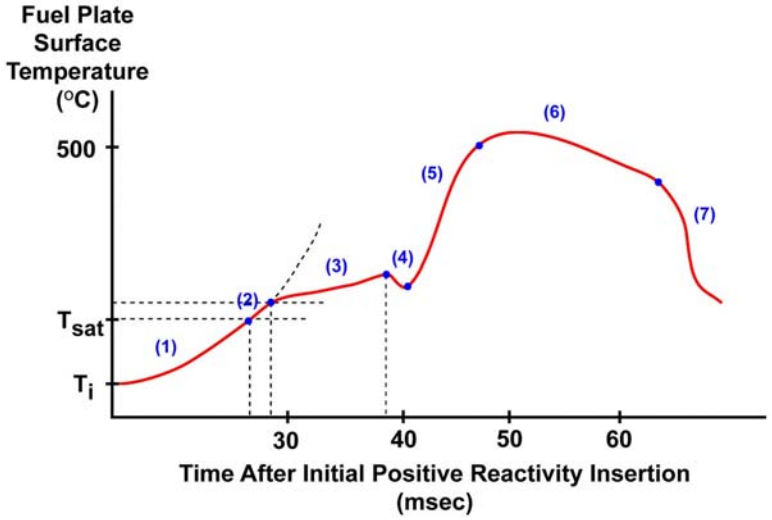

Figure 2-11: Idealized Plate Surface Temperature against Time for a Step Reactivity Insertion

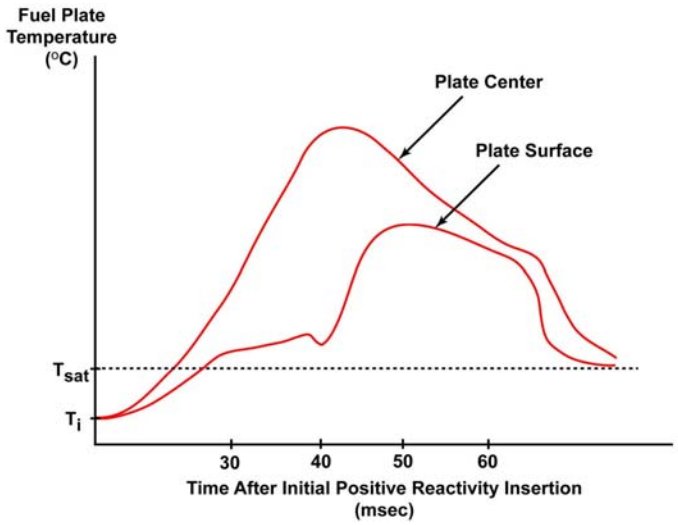

Figure 2-12: Idealized Plate Surface and Centre Temperature against Time for a Step Reactivity Insertion

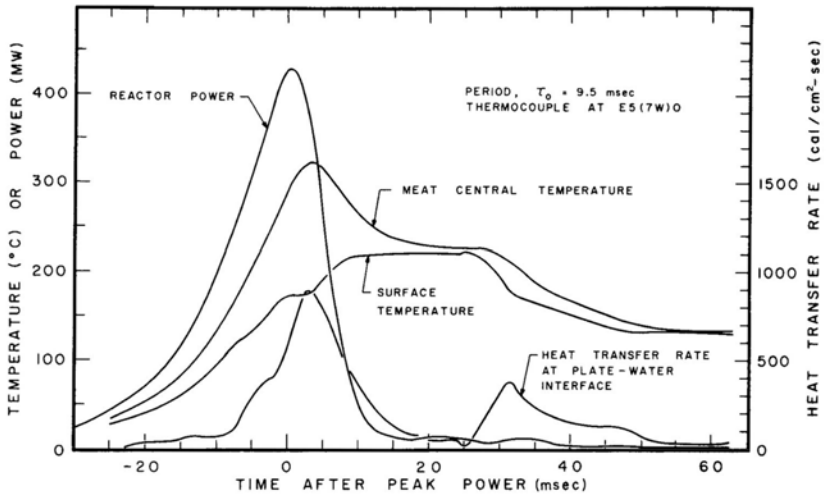

Figure 2-13: Transient Data and Calculated Central Meat Temperature from a 9.5-msec Period Step-Insertion Power Excursion in Spert I D-12/25 (Ref. 2-19)

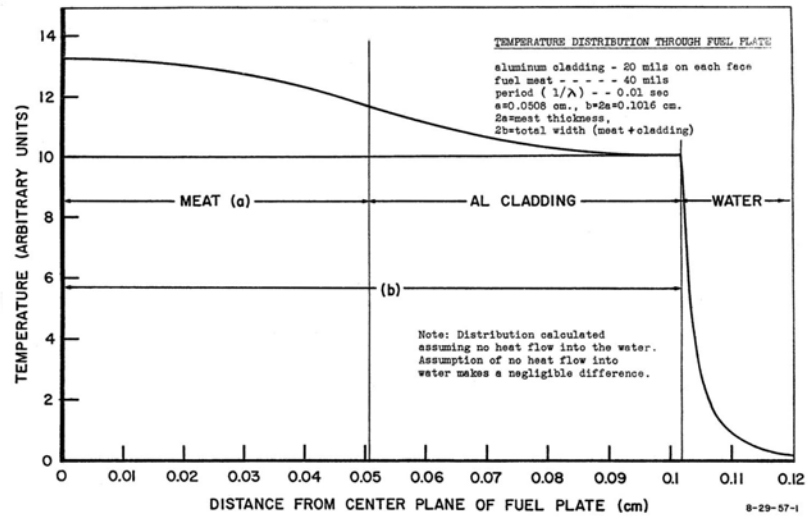

Figure 2-14: Calculated Fuel Plate and Coolant Channel Temperature Distribution During an Exponential Power Rise (Ref. 2-22)

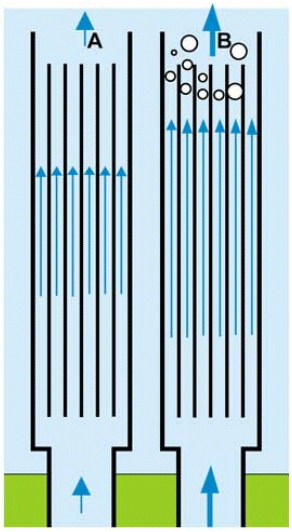

Figure 2-15: Pictorial Representation of Steady Boiling Flow in a Plate Fuel Assembly

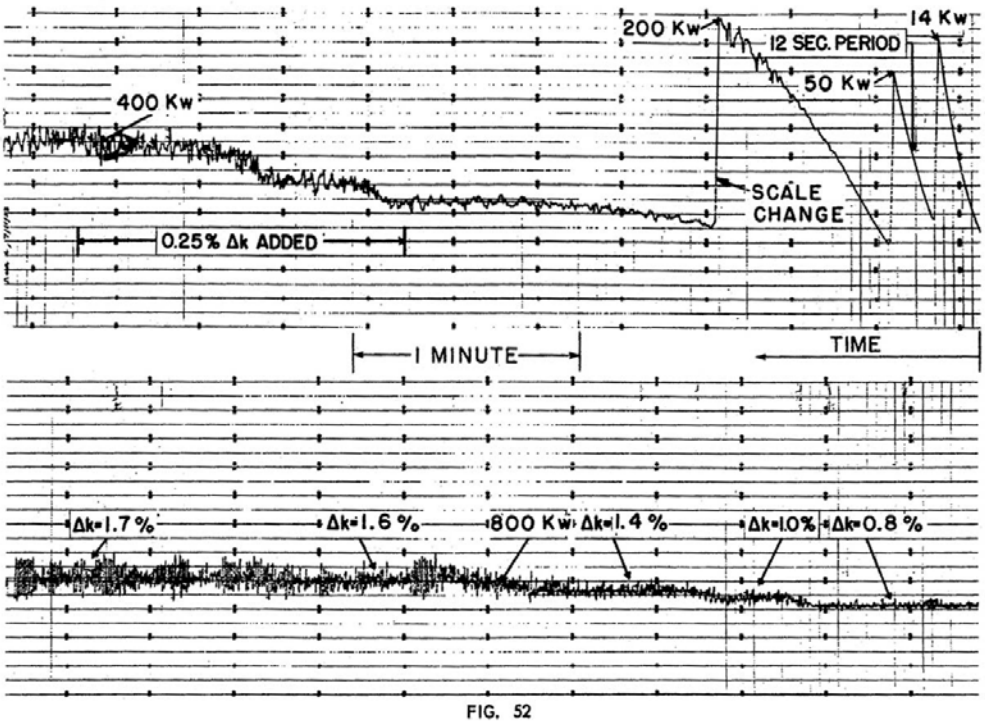

FIG. 52

POWER CHART SHOWING APPROACH TO POWER AND BOILING OPERATION AT ATMOSPHERIC PRESSURE (RUN 2, 9/18/53)

THE REACTOR TEMPERATURE WAS INITIALLY AT SATURATION. THE REACTOR WAS BROUGHT UP TO POWER ON A 12-SECOND PERIOD WHICH LEVELED OFF INTO STEADY OPERATION AS BOILING BEGAN. FURTHER REACTIVITY ADDITIONS WERE MADE TO INCREASE POWER. THE Δk NOTATIONS INDICATE REACTIVITY COMPENSATED BY STEAM.

THE CHARTS ARE FROM A BROWN ELECTRONIK RECORDER SHOWING OUTPUT OF COMPENSATED ION CHAMBER. ZERO IS AT BOTTOM OF CHART. PEN SPEED IS HIGH ENOUGH TO SHOW AMPLITUDE OF VARIATIONS WITH REASONABLE ACCURACY. THERE IS A TIME GAP OF ABOUT A MINUTE BETWEEN UPPER AND LOWER CHARTS, DURING WHICH A SCALE CHANGE WAS MADE.

Figure 2-16: Steady State Boiling Time Trace from the Borax I Tests (Ref. 2-1)

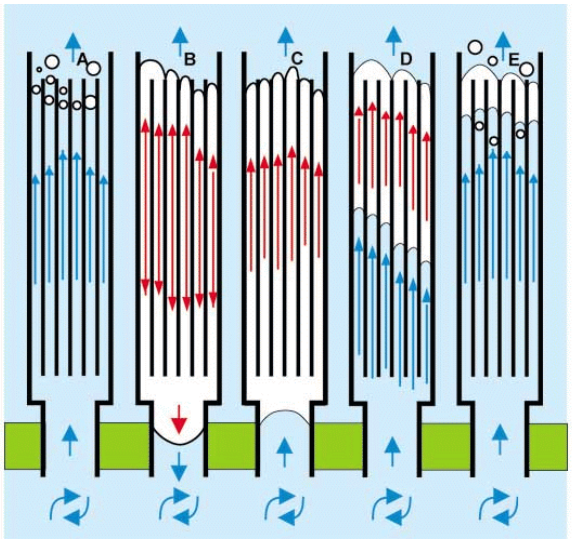

Figure 2-17: Pictorial Representation of Chugging Flow Oscillations in a Plate Fuel Assembly with Upward Coolant Flow

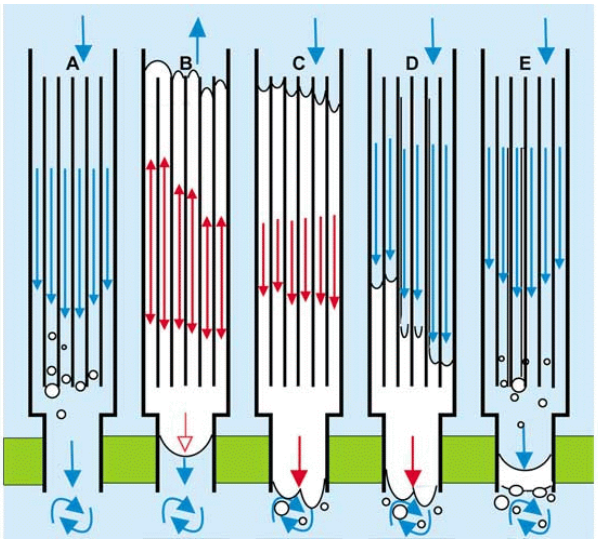

Figure 2-18: Pictorial Representation of Chugging Flow Oscillations in a Plate Fuel Assembly with Downward Coolant Flow

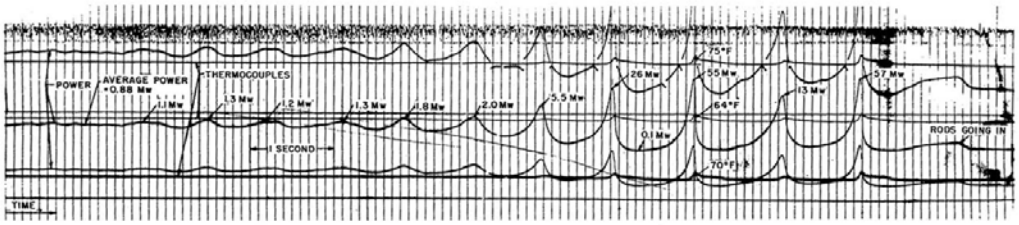

FAST GALVANOMETER RECORDS SHOWING TRANSITION FROM OSCILLATORY BOILING TO "CHUGGING" AT ATMOSPHERIC PRESSURE. 2.6% k_{eff} COMPENSATED BY STEAM (END OF RUN 2, 9/18/53)

THE THREE POWER RECORDS ARE FROM ION CHAMBERS OF DIFFERENT SENSITIVITIES, ON LOGARITHMIC SCALE. THE UPPERMOST TRACE IS UNRELIABLE BECAUSE OF A STICKING GALVANOMETER. THE TOP TEMPERATURE TRACE IS FROM THE CENTER OF FUEL PLATE 4. THE MIDDLE TRACE IS FROM THE CENTER OF PLATE 1, AND THE LOWEST TRACE FROM THE SURFACE OF PLATE 1.

Figure 2-19: Chugging Power and Temperature Trace from the Borax I Tests (Ref. 2-1)

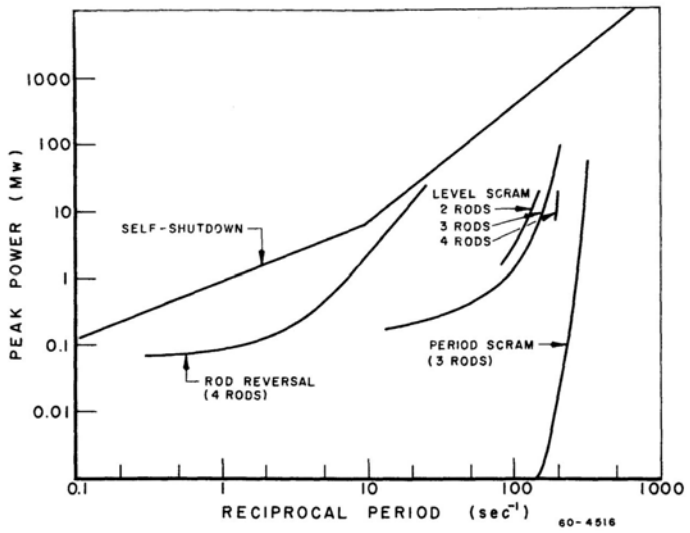

Figure 2-20: Power Data from the Spert I BSR-II Core for Self-Shutdown and Protected Transient Tests (Ref. 2-25)

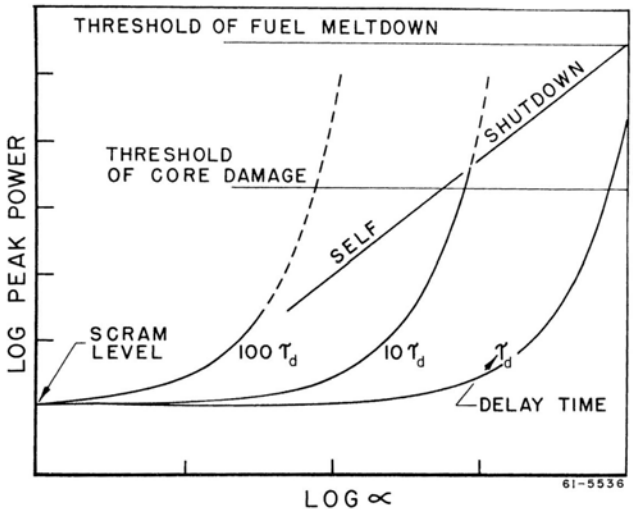

Figure 2-21: Effect of Delay Time on Mechanical Shutdown System Effectiveness (Ref. 2-26)

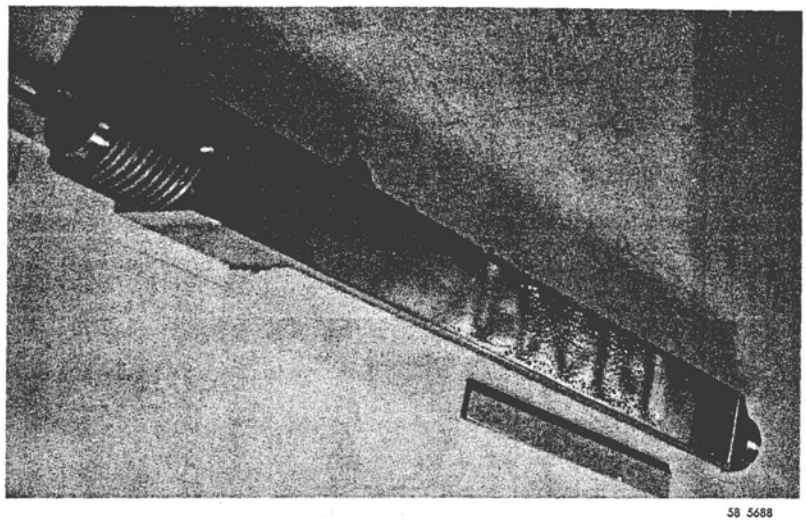

Figure 2-22: Spert I Type-P Blistered and Warped Fuel Assembly (Ref. 2-30)

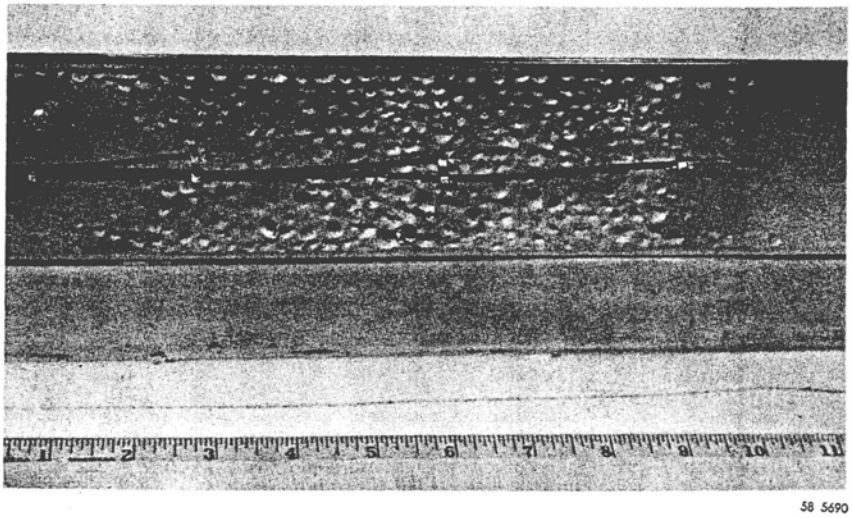

Figure 2-23: Blisters on a Spert I Type-P Fuel Assembly (Ref. 2-30)

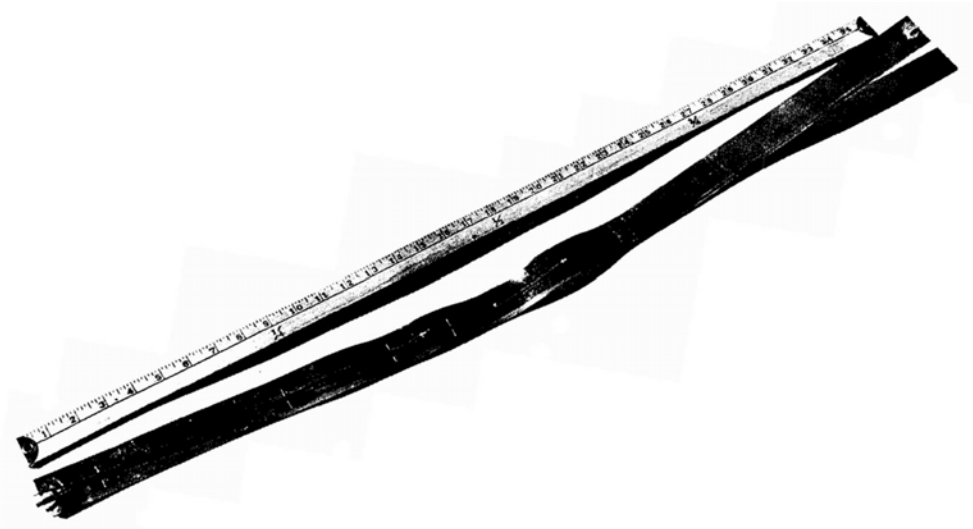

Figure 2-24: Bowed and Rippled Plate from the Spert III C-Core (Ref. 2-33)

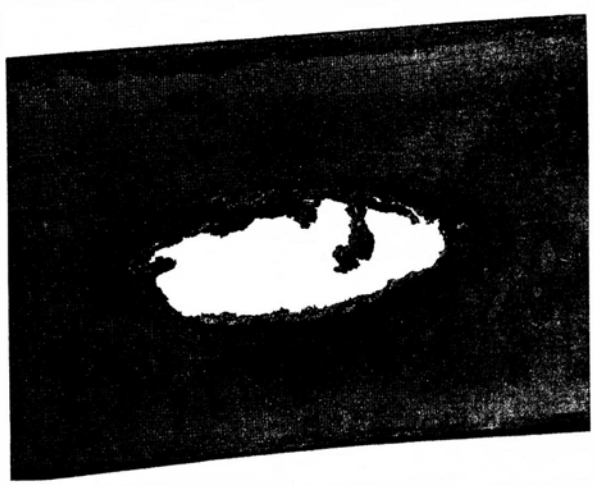

Figure 2-25: Hole Melted in Spert I B-12/64 Fuel Plate (Ref. 2-44)

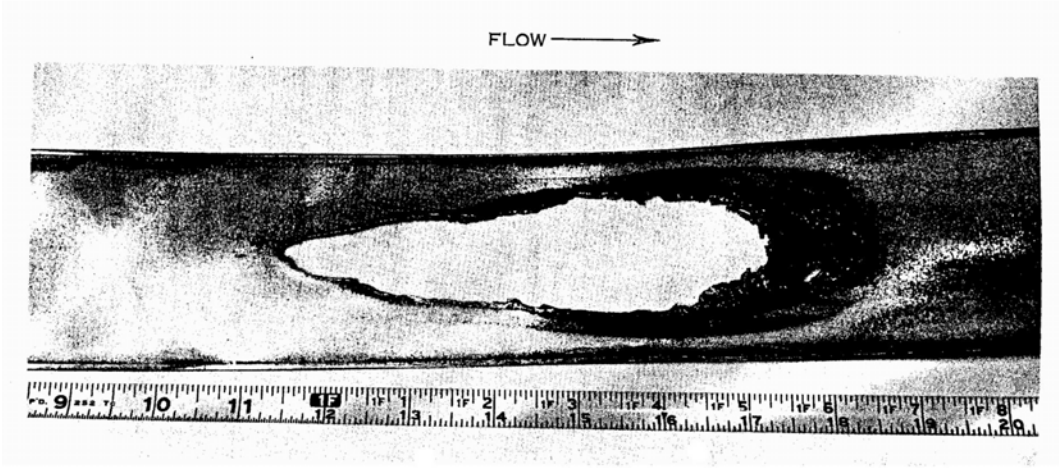

Figure 2-26: Hole Melted in Spert IV D-12/25 Fuel Plate (Ref. 2-39)

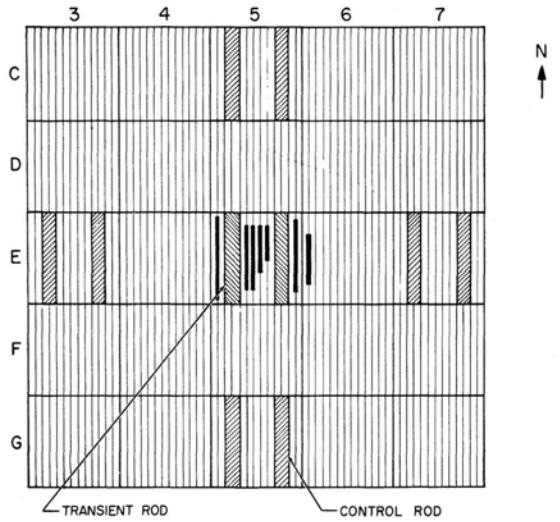

Figure 2-27: Horizontal Melt Pattern from the Spert I D-core 5 msec test (Ref. 2-40)

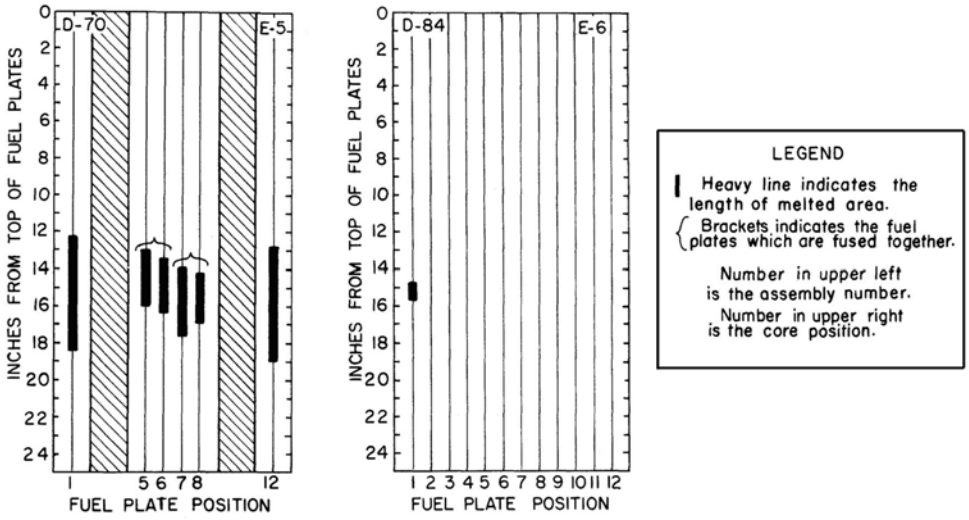

Figure 2-28: Vertical Melt Pattern from the Spert I D-core 5 msec test (Ref. 2-40)

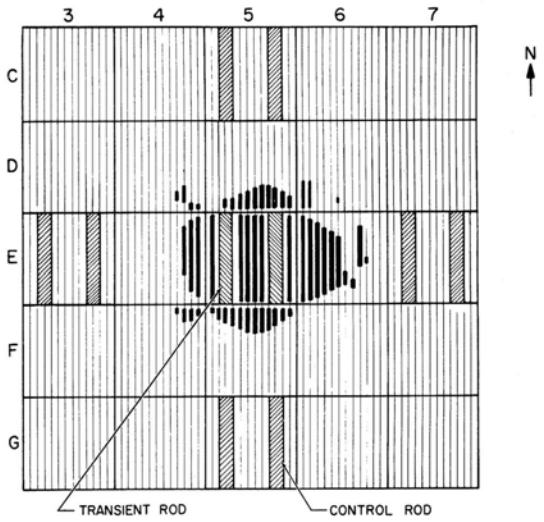

Figure 2-29: Horizontal Melt Pattern from the Spert I D-core 4.6 msec test (Ref. 2-40)

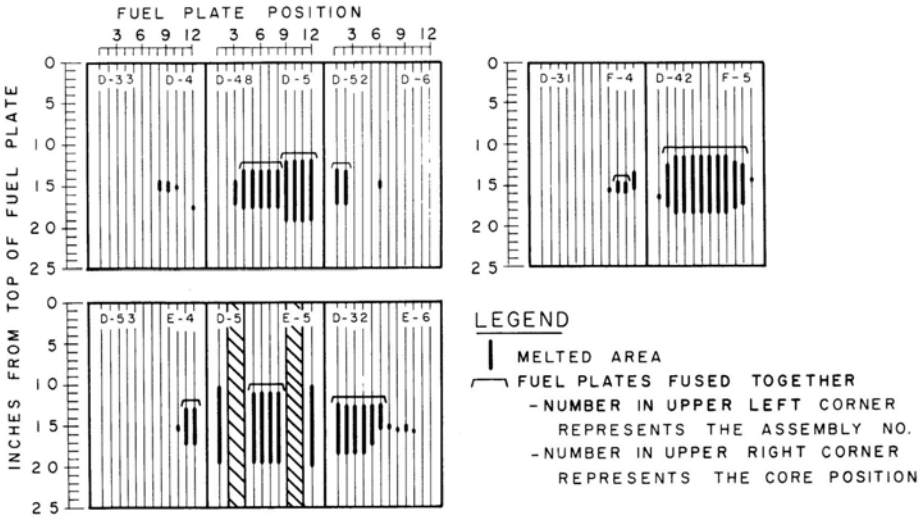

Figure 2-30: Vertical Melt Pattern from the Spert I D-core 4.6 msec test (Ref. 2-40)

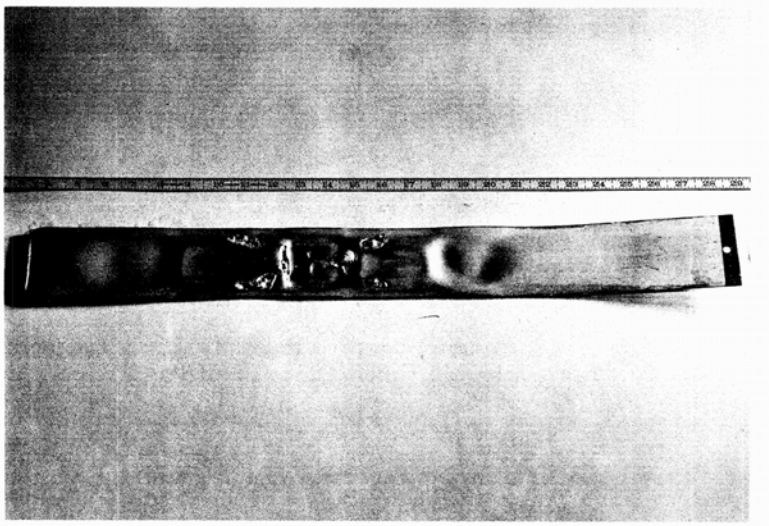

Figure 2-31: Melted Plate from the Spert I D-core 5 msec test (Ref. 2-38)

Figure 2-32: Closeup of Melting from the Spert I D-core 5 msec test (Ref. 2-38)

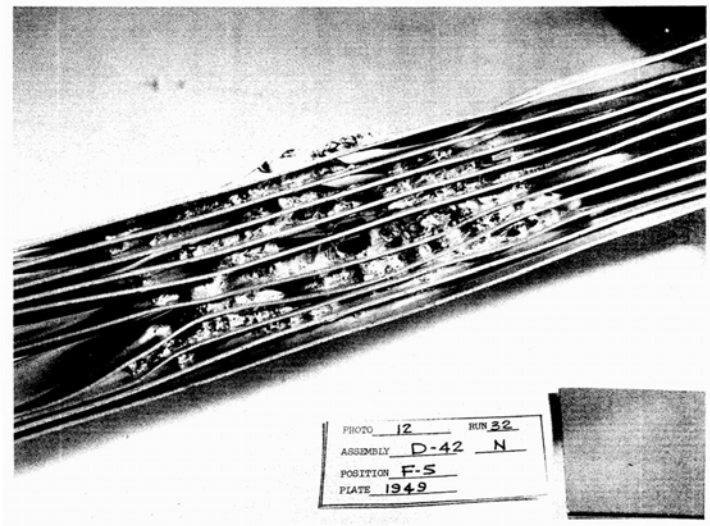

Figure 2-33: Melted and Fused Plates from the Spert I D-core 4.6 msec test (Ref. 2-38)

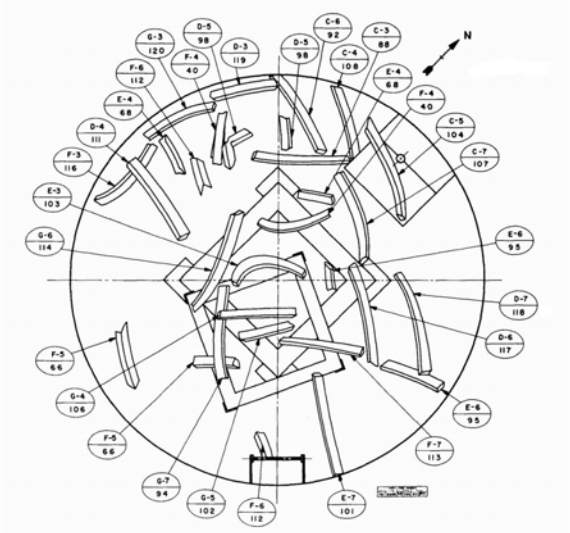

Figure 2-34: Core Displacement Map from the Spert I D-core D-test (Ref. 2-38)

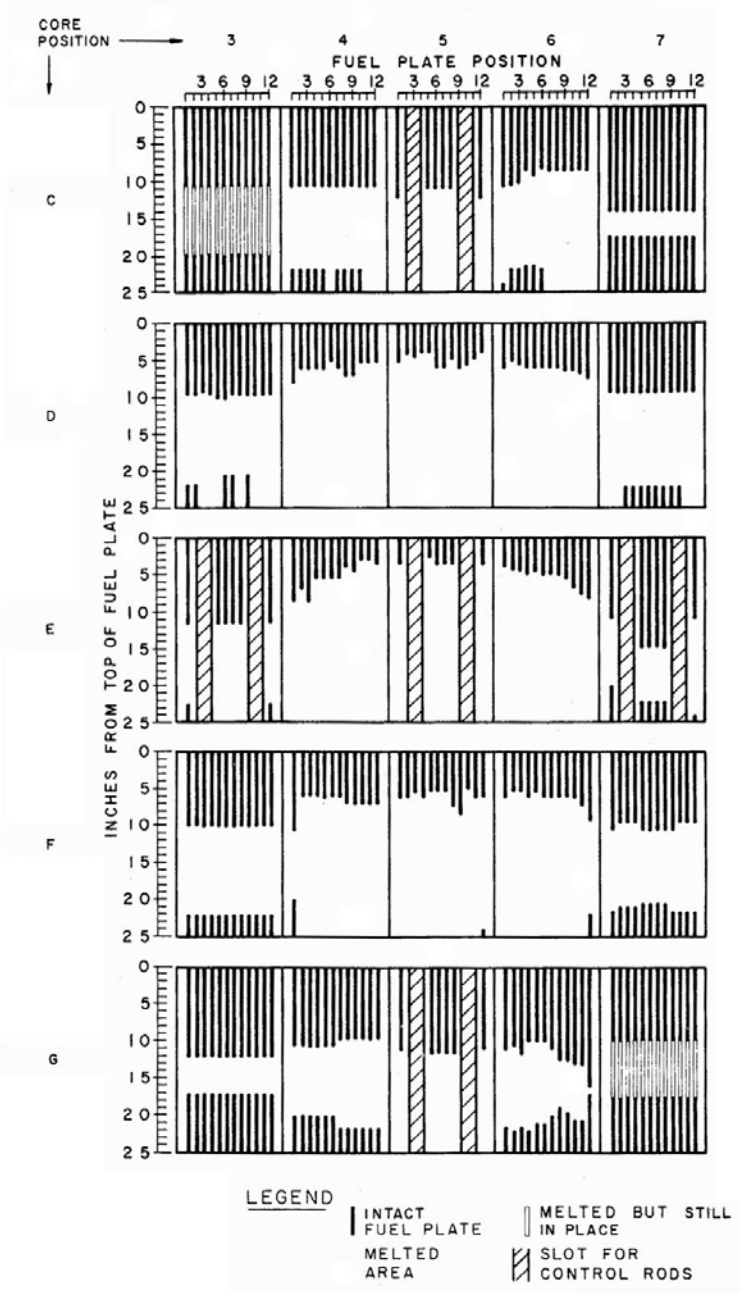

Figure 2-35: Vertical Melt Pattern from the Spert I D-core D-test (Ref. 2-40)

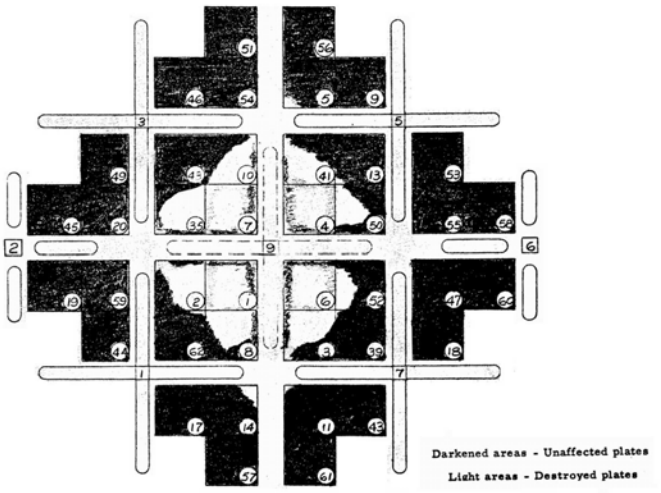

Figure 2-36: Fuel Destruction Map for the SL-1 Accident (Ref. 2-45)

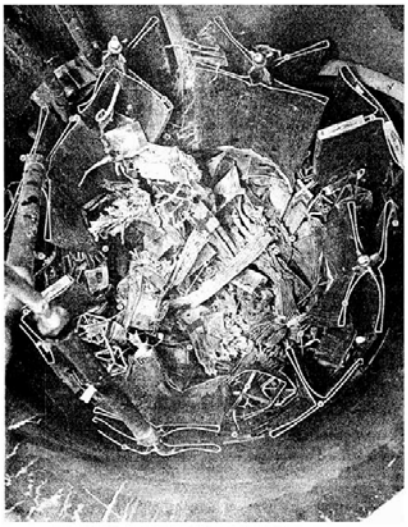

Figure 2-37: Photo of SL-1 Post-Accident Core (Ref. 2-45)

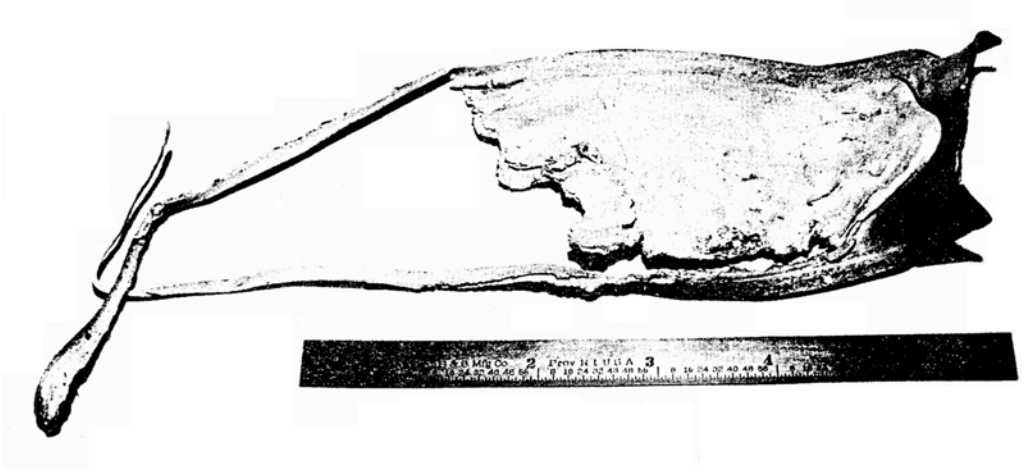

Figure 2-38: Recovered Fuel Plate from the Borax I D-test (Ref. 2-20)

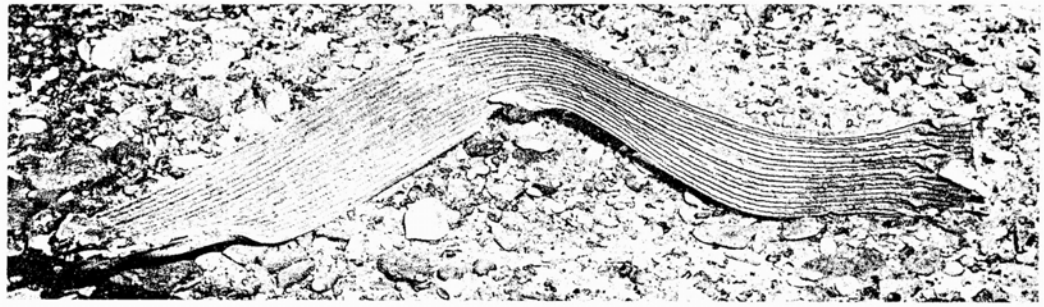

Figure 2-39: Recovered Side Plate from the Borax I D-test (Ref. 2-20)

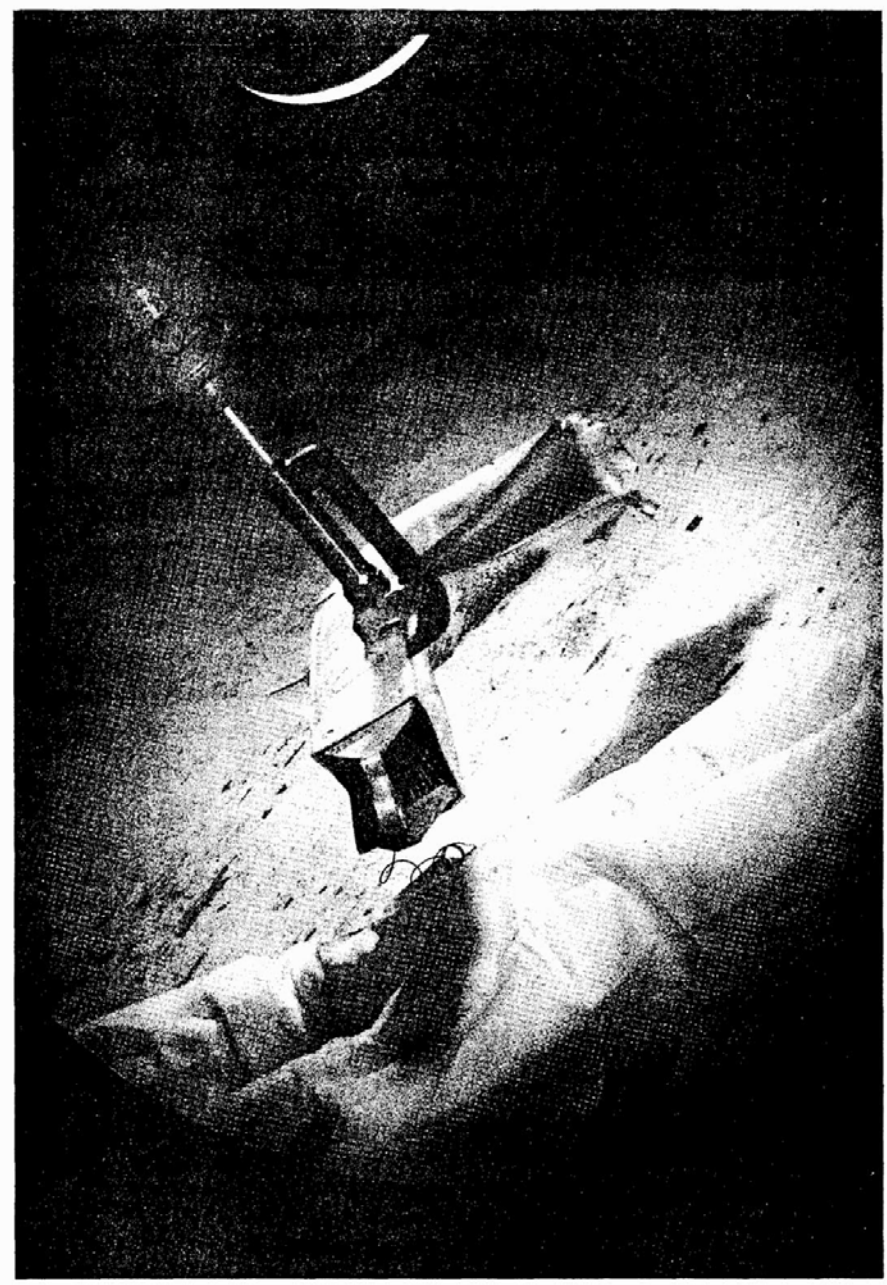

Figure 2-40: Recovered Fuel Assembly from the Spert I D-core D-test (Ref. 2-46)

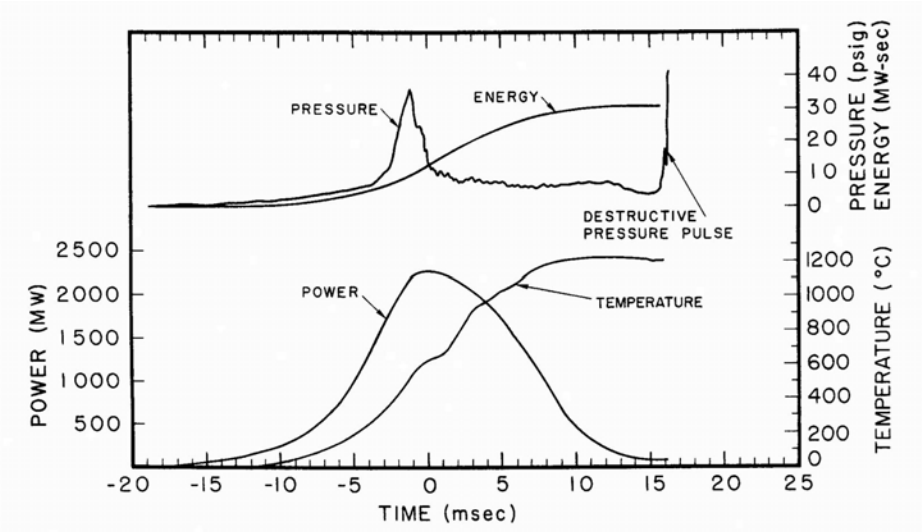

Figure 2-41: Power, Energy, Temperature and Pressure Time Traces from the Spert I D-core D-test (Ref. 2-40)

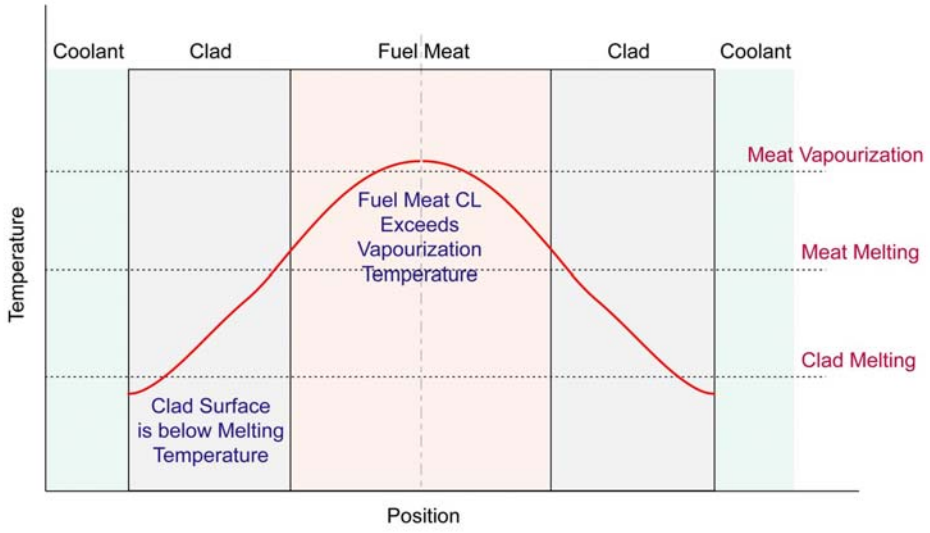

Figure 2-42: Thick Plate Temperature Distribution at Time of Core Disassembly

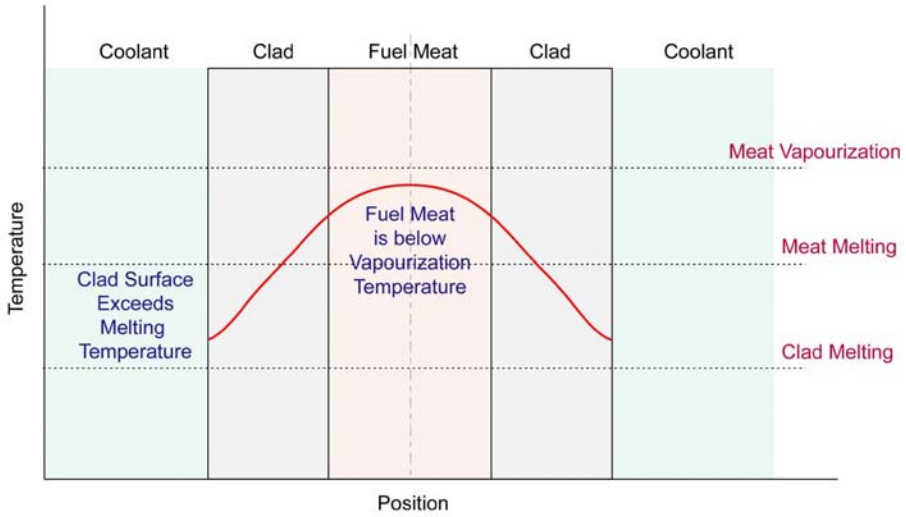

Figure 2-43: Thin Plate Temperature Distribution at Time of Core Disassembly

CHAPTER 3 - THE EXPERIMENTAL DATA SET: ASSESSMENT

TABLE OF CONTENTS

LIST OF TABLES

LIST OF FIGURES

(this page is intentionally left blank)

3 THE EXPERIMENTAL DATA: ASSESSMENT

To properly apply the results of the full scale reactor tests to present day MTR analysis, a familiarity with the experimental technique, the systems, what data are available, and a general understanding of the test results is required. The objective of this chapter is to provide this information and thereby form a foundation for the analysis methodology used and presented in Chapters 4, 5, 6, and 7.

The information contained in this chapter is sufficient to allow for proper assessment of the test data, and to provide enough background so that the analyst can combine results from the various test systems and test series.

Section 3.1 outlines what tests were performed, what was measured and how the data were collected, describes the form of the data, and indicates some general relationships between the measured quantities as well as providing a general assessment of the completeness of the experimental data set. Section 3.2 identifies and assesses the subsets of the test data associated with the primary parametric dependencies. These parametric dependencies are the subject of the analysis of Chapters 4, 5, and 6. Section 3.3 highlights some important points which must be considered when using the data, and discusses uncertainty estimates on the measurements. It also contains some important points on the use of the experimental data.

The information in this chapter is supplemented by Appendix A "Description of the Systems" which presents a brief summary of the technical specifications and nuclear characteristics of each test system, and Appendix B "The Experimental Data: Summary" which provides a description of the various test series and includes the relevant transient summary data in table format.

3.1 General Description of the Data

3.1.1 Test Summary

Data were collected for a wide range of reactivity additions, nuclear parameters, and initial system conditions in several different reactor cores, the majority of which were HEU Al-clad plate-fuel type. In addition HEU stainless-steel-clad plate-type cores were studied as were slightly enriched rod-type oxide cores, the latter representative of power reactor fuel *circa* 1960. In order to combine the results from the various

test series and systems, the reference point of the measurements, the type of measurements, and the reactor system from which the measurements were derived must be considered. Details on the different reactor systems are included in Appendix A.

The test cores can be classified into one of three groups:

- aluminum-clad HEU plate-fuel cores,
- stainless-steel-clad HEU plate-fuel cores, and
- stainless-steel-clad LEU rod-fuel cores.

A listing of the systems, indicating the main objective of the associated testing, is given in Table 3-1.

Only H_2O cooled cores are considered in this thesis. An additional series of H_2O-cooled, aluminum-clad plate-fuel cores were installed in Spert II using the Type-B fuel, however, no kinetic testing was carried out on these cores as they were assembled solely in preparatory work for the Spert II D_2O test program. As a result they are not included in any detail herein. Transient testing on D_2O-cooled and -moderated HEU plate-fuel cores in the Spert II facility are reported in References 3-1, 3-2, 3-3, and 3-4.

Although not part of the experimental program the SL-1 reactor is included in this list as the destructive accident at this facility is relevant to the test results. Similarly, the IAEA 10MW benchmark reactor, which is a simulation problem, is included as the work on this compliments the experimental data set.

The results of the full scale reactor tests have been reported in varying degrees of completeness mostly in technical reports for both the Borax and Spert projects and also to some degree in journal publications. The experimental data, as located, are included in Appendix B, mostly in tabular form.

Three types of tests make up the reactor experiments, these are:

- step reactivity insertion initiated transients
- ramp reactivity insertion initiated transients, and
- stability tests

The self-limiting behaviour observed in all three of these test types is fundamentally

related through an understanding of the self-limiting mechanisms themselves. Therefore, information from one type of test acts to compliment the understanding of the other types of tests. The reactor response to ramp reactivity insertions is found to be comparable to that to step reactivity insertions when considered from a certain perspective, and the stability tests serve to complete the self-limiting behaviour picture for both step and ramp insertion situations.

The step reactivity insertion initiated transients, or "step tests", represent the majority of the experiments conducted both in the Borax I and the Spert facilities and as a result make up most of the data used in this thesis. Tables 3-2, 3-3, and 3-4 summarize the step test series for the aluminum-clad plate-type, stainless-steel plate-type, and oxide rod-type cores, respectively.

Ramp reactivity insertions were conducted in the Spert I A-, B-12/64, and oxide rod-cores as well as the stainless-steel clad Spert III C-core. In addition, a single protected startup transient test was carried out in the Spert I BSR-II core. Ramp reactivity additions were also made in the Borax I and Spert IV D cores as part of stability test series. The ramp insertion test series are summarized in Table 3-5.

Stability tests were conducted in the Borax I, Spert I A-17/28, B-12/64 and the Spert IV D-12/25 cores. A summary of the stability tests is given in Table 3-6.

Significant sensitivity to various system parameters have been identified and the respective data subsets associated with variation of these parameters are treated in more detail in Section 3.2.

3.1.2 Transient Test Measurables

The primary variables measured in the full-scale reactor transient experiments were power, temperature, and pressure. These were recorded as functions of time over the course of each transient.

Measurement of the transient power is important as it is related to the reactivity of the system. Power as a function of time allows for calculation of reactivity as a function of time indicating the size and timing of reactivity feedback effects. Also from the power measurement, the asymptotic reactor period, *i.e.*, the speed of the power excursion, is measured while the time integral of the power provides a measurement of the nuclear energy generation during the transient.

Measurement of the reflector, coolant, and fuel-plate temperatures provides information on the total energy generation, transient temperature distribution and energy partition throughout the core, the transient heat transfer rates, and the nature of the heat transfer, *e.g.*, onset of boiling at a specific point in the core. In addition, the fuel plate temperature measurements provide an indication of the proximity to damage thresholds as well as the location, extent, and severity of expected damage in a given transient.

Pressure, like the temperature measurements, indicates the onset of boiling in the core, relevant to the type and timing of reactivity feedback mechanisms. It is also an indicator of the destructive mechanism of MTR-type cores.

3.1.3 Instrumentation and Measurement

In general the test data were measured in the same manner and using the same technology throughout both the Borax and Spert projects. This is not surprising as the Spert Project was created as a continuation of the Borax I tests at the NRTS. When changes were made from one core to the next, these were generally in terms of refinement rather than principle. The general approach to the instrumentation and measurement is outlined herein.

The logistics of the instrumentation of these tests are impressive. The transients produced power changes from milli-watt to giga-watt range, while surface temperatures of fuel plates increased by hundreds of degrees centigrade; all of this taking place on exponential periods as short as a few milliseconds. The response of the instrumentation is remarkable.

The same general equipment layout was adopted in both the Borax and Spert Projects. Due to the potentially destructive nature of the reactor tests, the test reactors were built in the middle of the Idaho desert. Control, monitoring, and recording of the data from the tests were conducted from remote locations. The conditioning components of the data channel were slightly removed (on the order of a couple of hundred feet) from the reactor, while the control and recording equipment was located in an even more remote control centre (half a mile from the reactors for the Spert Project).

> ***"These (3000-foot) signal cables are lying on the desert and are covered with earth about 1/3 of their total length."*** (From Reference 3-5, discussing troubleshooting of "hum and noise" in the Spert I A

transient systems.)

Each reactor system was outfitted with both operational and transient instrumentation, which were similar but with additional resolution and a higher frequency response for the latter. It is the transient instrumentation associated with the specific measurables that is discussed in the following sections. The Borax I and Spert I transient instrumentation block diagrams are given in Figures 3-1 and 3-2, respectively. The instrumentation of the other Spert reactors was similar to that shown in Figure 3-2 (Ref. 3-6).

Each power, temperature, or in general any transducer instrumentation can be thought of in terms of the idea of a data channel, consisting of a detector and its associated conditioning, transmission and recording equipment. A typical data channel is shown schematically in Figure 3-3. The "detector" in the data channel is the piece of equipment being used to convert the physical phenomenon of interest into an electrical signal, *i.e.*, an ion chamber, a thermocouple, or a pressure gauge. Calibration and testing of the conditioning, transmission and recording equipment was done on a routine basis throughout the test programs by replacing the detector in the data channel with a known current source (Ref. 3-7). The entire data channel has been considered in the uncertainty estimates discussed in Section 3.3.3.

Common to each type of measurement, each signal was recorded in real time as an analog signal on a channel of a recording oscillograph where signals were recorded as time traces on photographic paper (Ref. 3-8). In the later tests data were also recorded on magnetic tape. Two examples of the raw data are shown in Figures 3-4 and 3-5, the first for a typical step transient from subcooled conditions and the second from the destructive test, both conducted in Borax I. After recording, time traces were then interpreted as part of the data reduction.

Details with respect to instrumentation for specific cores are summarized in Table 3-7 and can be used in conjunction with the details of the system descriptions given in Appendix A. The reactor cores are presented in chronological order in Table 3-7 to illustrate the evolution of the instrumentation throughout the tests. The impact of the differences in instrumentation or measurement methodology between test systems on the resulting data must be taken into consideration when assessing the specific data sets. This is discussed in Section 3.3.

Further information on the electronics of the data collection and the calibration and measurement methods are given in References 3-7, 3-9, and 3-10, and the references

listed in Table 3-7.

3.1.3.1 Power, Period, Reactivity and Energy

Power measurements were based on radiation leakage from the core and were made using out-of-core detectors. The most common type of power detector used in the reactor tests was an out-of-core boron-lined ionization chamber. These provided most of the power measurements for the Borax and Spert tests. Later in the Spert tests, specifically by the Spert I D-core test series, miniature boron-lined ion chambers and semi-rad chambers, placed nearer the core, were also used to compliment the standard ion chambers.

Calibration of the ion chambers was typically done calorimetrically by comparing the chamber readings to electrical heater input producing the same system temperature rise at a variety of power levels (Refs. 3-7, 3-9). Sensitivity of chamber readings to void volume in and around the core was found to be small (Refs. 3-7, 3-11). Wire activation and insulated fuel plate temperature measurements (Refs. 3-8, 3-12) were also used in the calibration process. Calibration specifics are discussed further in Section 3.3.1.

Typically, multiple detectors were used simultaneously and independently, each associated with either a linear or logarithmic amplifier. Thus power was measured on both linear and logarithmic scales as a function of time during each excursion test. The power measurement equipment evolved during the reactor tests from using only logarithmic amplification (Borax I) to exclusively linear amplification (by the Spert I P-core tests). The linear-scale power records are more accurate and this is reflected in the uncertainty estimates discussed in Section 3.3.3.

The range for different chambers was set to provide overlapping coverage over the many (typically five or six) decades of expected power range of transients of varying severity. This was achieved by moving the detectors in relation to their distance to the core.

The reactor period was measured from the power time traces. For the tests initiated by step reactivity insertions, the initial asymptotic exponential period was measured. This is the period of the exponential power rise at the beginning of a transient test, after the initial “prompt jump” response, and before the feedback effects become evident prior to the initial power peak.

The steepest slope on the log power trace, spanning a minimum of one decade of change, was determined. In the Borax tests the portion of the power trace considered for the period determination was that from the time of completion of the rod ejection to the beginning of the deviation from the exponential rise. Similarly, in the Spert tests, the portion of the power trace considered for these measurements was from 1% of the maximum deflection of the signal (maximum power) to the peak power.

For ramp tests, which often did not produce an exponential power rise, the minimum period was measured. This was also associated with the initial power pulse, if present. The period was also measured for some of the power oscillations associated with chugging.

The power traces were also used to calculate the reactivity of the system as a function of time during the transient. This was achieved by using the measured power trace as input into point kinetics equations and backing out the reactivity trace. The reactivity of the system, derived from the power history is not to be confused with the initial reactivity insertion. The inserted reactivity was measured from rod worth data and the change in rod positions and is not dependent on the transient power measurements.

The third main quantity determined from the power measurements was energy generation, determined by integration of the power time traces. This was typically checked by comparison with both foil or flux wire activation as well as bulk temperature changes of the system. Differences in the Borax and Spert definitions of energy are discussed in Section 3.3.1.

3.1.3.2 Temperature

Temperature measurements were made using thermocouples placed in various locations throughout the reactor: (i) in the reflector to measure the initial temperature of system and also to provide temperatures for energy balance calculations, (ii) between fuel plates in the coolant channels used primarily in the stability tests in Spert IV, and (iii) attached directly to the fuel plates.

With respect to fuel plate temperature measurement, the thermocouples were attached either to the surface or buried in the interior of the fuel plates. The term “surface” thermocouple should be used loosely as, depending upon the method of attachment, these could actually be buried to a significant depth in the cladding. A 10-mil (0.010"), or smaller, diameter chromel-alumel thermocouple was the most commonly

used as it achieved the desired response time as well as providing adequate robustness. Various methods of attaching the thermocouples were used over the course of the reactor tests as the technology evolved.

The three main ways in which thermocouples were secured to fuel plates for the reactor experiments were *via*: (i) a plug method, (ii) peening, and (iii) spot welding.

Thermocouples attached *via* the "plug" method were truly interior type as in this method of attachment part of the plate is cut away, the thermocouple welded to the fuel meat, and then the cut region refilled by a plug. An example is shown in Figure 3-6. This type of thermocouple was used only in Borax I.

Although thermocouples attached by "peening" were considered "surface" thermocouples in the literature, they are also an interior type. The method of "peening" involves creating parallel scratches in the fuel plate cladding about ½" long and to a depth at least of the thickness of the thermocouple wire and at most the thickness of the cladding. The wire is then inserted into the scratches and is covered with the cladding material (shown in Figure 3-7 and discussed in Reference 3-9).

Thermocouples welded to the outer cladding surface are truly "surface" thermocouples. In this method of attachment the thermocouple leads are simply spot welded to the surface of the fuel plate (Fig. 3-8). The chromel-alumel type of thermocouple was found to be the most reliable. Typically thermocouples were attached to multiple fuel plates and at multiple heights on the same plate (*e.g.*, Fig. 3-9).

The specific thermocouple type and attachment method for each system are noted in Table 3-7 and their impact on the data is discussed in Section 3.3.2.

3.1.3.3 Pressure

At the time of the reactor tests the available pressure instrumentation was too large to fit in the coolant channels so was typically placed around the core, often in the end boxes of the fuel assemblies. This introduced complexities such as averaging over many coolant channel and attenuation of the pressure source. As a result the pressure measurements were of a mainly qualitative nature and are treated as secondary to the power and temperature measurements. Discussion of the pressure measurements from a large portion of the Spert tests is found in Reference 3-13.

3.1.3.4 Additional Instrumentation

Additional instrumentation included radiation area monitors, flow meters, strain and displacement detectors, and photographic equipment. These are noted throughout the referenced technical reports and are summarized in Table 3-7 for each system.

Data from these additional sources have primarily contributed to an understanding of the self-limiting behaviour of the MTR-type systems and although of interest to this subject are not treated to any great extent herein.

3.1.4 Form of the Data

The results of the full-scale reactor tests have been reported in varying degrees of completeness mostly in technical reports for both the Borax and Spert projects and also to some degree in journal publications. The experimental data as reported exists in three main formats:

- time traces,
- tabulations of the summary data, and
- correlated data plots.

The time traces are the most fundamental data records for the tests. These are reported having already been processed from the original oscillograph or magnetic tape records. The time traces show the evolution of the primary quantities (power, temperature and pressure) during the transient as well as in many cases, the calculated energy. In some cases the calculated total reactivity or compensating reactivity of the system is also included. An example of a time trace, taken from the Spert I A step insertion test series is shown in Figure 3-10.

The most easily observable part of the power excursion test is the initial power burst. This is a common feature of step-insertion initiated transients and of relatively fast-ramp-insertion initiated transients. The characteristics of the initial power burst provide a general indication of the behaviour of the system during the power excursion.

The commonly measured quantities, of which many are related to the initial power burst are as follows:

T_i The initial temperature of the reactor system, usually uniform, measured from thermopiles in and about the core, (EC).

τ The asymptotic or minimum reactor period, measured from the power time trace, (msec).

P_{max} The maximum power measured during the test, the peak power of the initial burst of a step or ramp test, or equilibrium or chugging values for ramp and stability tests, (MW).

E_{tm} The generated energy to the time of peak power measured from the power time trace, (MW-sec).

This quantity was not reported for the Borax tests. It is defined in the Spert tests as the energy generated from 1% of the peak power value to the time of maximum power, (Ref. 3-7).

E_{tot} The "total" energy generated during a test measured from the power time trace, (MW-sec).

This quantity is defined slightly differently in the Borax and Spert Projects. In the Borax Project the "total" energy is defined as the energy release up to the time the power reaches its first minimum (Ref. 3-12). If the power did not go through a peak before reaching an equilibrium level or termination of the test then no total energy value was specified. For the Spert Project the "total" energy is defined as the energy release from 1% of the peak power value to 1% of the peak power on the decline of power or at the time of scram, whichever occurred first (Ref. 3-7).

T_{tm} The fuel plate temperature at the time of peak power, measured from fuel plate thermocouples, (EC).

T_{max} The maximum fuel plate temperature recorded during the power excursion, measured by fuel plate thermocouples, (EC).

pr_{max} The maximum pressure recorded during the power excursion, (psi or psig).

These quantities, referred to as "transient summary data quantities", can all be extracted from the time traces of power, temperature and pressure. In most cases this processing has already been done and these results are reported for each test in

tabular form. The transient summary data tables for each test series of the Borax and Spert Projects are included in Appendix B.

The third form in which the test data are reported is as series of correlated data plots, examples of which from the Spert I A-core step test series are shown in Figures 3-11, 3-12, and 3-13. These are plots of the transient summary quantities against reciprocal reactor (asymptotic) period. The reciprocal period, α_o, is commonly used as an index for discussion of the test results as it is a directly observable quantity related to the reactivity insertion (a large value of α_o is associated with a large initial reactivity insertion) and also appears in kinetics theory equations.

For this report the data are taken from the transient summary data tables when available and when not are extracted from the correlated data plots (preferentially) and the individual time traces (as a last resort). Of additional interest are the initial temperature and pressure of the system, the height of the hydrostatic head above the core, and the coolant flow conditions for each test. This information is often described in the technical reports which contain the summary test data.

It should be adopted as good practice and is the author's recommendation to cross-reference the transient summary data, as tabulated, with both the correlated data plots and the individual test time traces. Consideration of the correlated data plots provides an indication of the range and extent of the test series as well as the quality of the data, reflected by the scatter of the data points. Consideration of the individual time traces allows for an assessment of the behaviour of the given test. Any irregular behaviour will be apparent here and the test can be checked for completeness, *e.g.*, if the temperature is still rising at the time of termination of the test then the "maximum" temperature listed for the test does not truly represent the maximum temperature reached during the power excursion.

The "initial burst" data are the most commonly reported results for the reactor experiments as they capture a large part of the behaviour of the system during the transient. The quality of the burst data is also found to be high, resulting from the fact that the conditions surrounding the initial part of the transient were the most controllable. Post burst data are subject to variability both in definition and due to the more complex behaviour of the system during this stage. As a result, the burst data are the most strongly correlated data to the initial asymptotic period (at the beginning of a transient) or equivalently to the reciprocal of the period.

Additional information for ramp-insertion-initiated and stability tests, for which at

least part of the focus is on the post-initial-power-burst behaviour can be found in the text of the technical reports and in the individual test time traces.

3.1.5 Correlations in the Data

Despite the variations in many system parameters and the identified sensitivities to such variations, the overall behaviour of all of the MTR-type cores studied during the reactor tests is remarkably similar.

Certain aspects of the self-limiting behaviour and characteristics of the transient response of MTR-type systems are associated with specific ranges of reactor period. Herein, three ranges of period are considered:

- τ # 35 msec (short), (α_o $29 sec^{-1})
- 35 msec < τ < 300 msec (transition), (29 sec^{-1} > α_o > 3.3 sec^{-1})
- τ $ 300 msec (long), (α_o # 3.3 sec^{-1})

The behaviour of the reactor systems within and between these period ranges is illustrated in plots of maximum power, energy, and maximum fuel temperature against reciprocal reactor period (Figs. 3-11, 3-12, 3-13). The short period range is defined as that for which self-shutdown of HEU cores at ambient conditions is *via* coolant voiding from boiling.

As seen in these figures, the reactor response is highly predictable as it is strongly correlated to α_o. The transition zone is defined as the "break" range between the long and short period ranges and occurs in the region of reactivity insertions on the order of β. These characteristics are common for all of the test cores.

This section briefly explains the obvious correlations in the test data. The important points to take from this discussion are:

- The transient response of an MTR-type system following a reactivity insertion of a given rate and magnitude is highly predictable from the knowledge of the system behaviour following reactivity insertions of other rates and magnitudes.
- The transient response, including the limits on the system (maximum temperatures), is well captured by the power burst summary data.
- The individual measured quantities are related allowing for

consideration of partially reported data sets.

These points have contributed to an understanding of the fundamental physical mechanisms driving the self-limiting ability of MTR-type reactors and allow for the development of an analysis methodology based on the quantitative use, including both interpolation and extrapolation, of the experimental data set.

3.1.5.1 Peak Power

The peak power during a transient and the speed of the power rise (decreasing period and increasing α_o) both increase with increasing size of the initial reactivity insertion. Peak power, P_{max}, is strongly correlated with α_o. In general, three regions of behaviour are associated with three ranges of α_o: (i) small α_o, or long period which is a slower power rise time, (ii) a transition region around the point where the initial reactivity insertion causes the system to go prompt critical ($\rho_{in} = \beta$), and (iii) for large α_o, or short periods. The short period range is of primary interest to this study as it is associated with the onset of fuel damage.

The long and short period ranges are characterized by typical slopes on a $\ln(P_{max})$ *vs.* $\ln(\alpha_o)$ plot which is similar for different systems (roughly unity and two for an HEU MTR-type system for the long and short period ranges respectively). An example of this from the Spert I A step tests is shown in Figure 3-11. The location of the transition between the long and short period ranges on a P_{max} *vs.* α_o plot depends on the relationship between period and reactivity for the given system (*i.e.*, on parameters such as the delayed neutron fraction and the prompt neutron lifetime).

Although the variation of system parameters and initial test conditions affect the magnitude of the power rise following a reactivity insertion (*i.e.*, the position of the P_{max} *vs.* α_o curves) the same general trends are evident for all HEU MTR-type Al-plate cores as illustrated in Figure 3-14. In fact the same trends (*i.e.*, shape of the curves) as seen in the Al-clad cores are evident in the stainless-steel-clad cores and even the LEU rod-type cores.

3.1.5.2 Energy to Time of Peak Power

The energy release to the time of peak power, E_{tm}, is used as a measurement of the energy release in a transient. It is also strongly correlated to the reciprocal reactor period as shown for the Spert I A-core in Figure 3-12 and for all of the HEU Al-clad plate cores in Figure 3-15. The different period ranges of behaviour are also

indicated on this diagram. The transition period range is characterized by a decrease in energy release to time of peak power with shortening period (increasing α_o). This "dip" is typical of all cores studied in the reactor tests and results due to the reduction in conductive heat loss as the transient speed is increased. Eventually radiative heat transfer processes (losses) dominate as the E_{tm} data again increases with increasing α_o. Again, the short period range is of primary interest in this study.

The total energy release is not as strongly correlated to the reactor period (or α_o) as E_{tm} as it depends more on the post-power-peak behaviour of the system which is not as directly related to the initial asymptotic reactor period of the excursion. Also the somewhat arbitrary definition of the total energy allows for different ends points to the measurement which contributes to the scatter in the data (termination point is either the time at which the power reaches 1% of peak power on the decline or the time of SCRAM, a rather arbitrary cutoff, whichever came first).

3.1.5.3 Burst Shape Parameter

The peak power, P_{max}, and the energy released to the time of peak power, E_{tm}, are correlated which can be seen from Figures 3-14 and 3-15 as the system with the highest peak power also has the highest energy release to the time of peak power, *etc*.

There is also an almost linear relationship between energy and the product of power and period (MW-sec) for step initiated transients. As the period gets shorter the power pulse gets higher and narrower. However the shape of the pulse, with time measured in terms of periods, does not change greatly over a wide range of period as shown in Figure 3-16. This figure shows the power bursts against time in terms of period for various Spert I A periods between 2.1 sec and 7 msec, showing the similar shape for periods of less than about 40 msec. The total energy of the initial power pulse is roughly equal to the peak power multiplied by twice the period of the excursion (Ref. 3-8).

The shape of the initial power pulse can also be seen *via* a plot of peak power against energy release to time of peak power or in a plot of E_{tm} *vs.* P_{max}/α_o. The ratio $(E_{tm}\,\alpha_o)/P_{max}$ is called the Burst Shape Parameter (BSP) and is included in the tabulation of the data in Appendix B.

In HEU Al-clad cores the BSP changes noticeably between long and short period ranges as for short period transients coolant voiding is a dominant shutdown mechanism resulting in a faster rate of shutdown, *i.e.*, the power pulse is cut off at a

faster rate. In this sense the BSP lends information about the behaviour of the system. For the short period range this parameter is relatively constant and is similar for all HEU Al-clad cores indicating that the power rise and the shutdown mechanisms which govern the self-shutdown (power decrease) are consistent (Fig. 3-17).

3.1.5.4 Fuel Plate Temperature

The maximum fuel temperature data are used directly in the analysis methodology presented herein. Importantly this quantity, T_{max}, is found to be related to the burst data (P_{max}, E_{tm}, T_{tm}), and is also found to be predictable from and correlated to the reactor period.

Behaviour of the fuel plate temperature with period is shown in Figure 3-18 as a series of time traces. The general trends in the temperature data with period are evident in correlated data plots of T_{tm} and T_{max} *vs.* α_o, but upon first inspection there is considerable scatter in the data points, particularly in the short period range. This is apparently due to a combination of factors including type and exact location of the thermocouples used for the measurements as well as proper consideration of any variability in initial temperature conditions. For further discussion see Section 3.3.2. Consideration of the temperature rise from only equivalent thermocouple locations reduces the scatter in the temperature data and results in a reasonably correlated variable with respect to the asymptotic reactor period. See for example Figures 3-13 and 3-19 for the Spert I A- and D-core tests from low power ambient conditions, respectively.

The temperature rise at the time of peak power is linearly proportional to the maximum temperature rise during the transient for a given type of test (*e.g.*, step, or ramp of set characteristics). This is shown in Figure 3-20 for the Spert I A ambient step tests. This indicates that the maximum temperature rise, neglecting any long term stability effects, is indeed primarily dictated by the initial power pulse during a step initiated power excursion. This is not surprising since the energy release generating the temperature rise is primarily during the initial power peak of a step reactivity insertion initiated transient.

The relationship between T_{max} and E_{tm} is shown in Figure 3-21, particularly in the short period range of transients.

The temperature at the time of peak power, T_{tm}, shows similar correlations as found

for T_{max}. Whereas T_{max} is of primary importance with respect to damage considerations, T_{tm} provides information on the shutdown mechanisms responsible for the self-limiting behaviour, indicating the presence or lack of void-related shutdown from boiling. As can be seen from a plot of T_{tm} *vs.* α_o for the HEU Al-clad cores (Fig. 3-22) the short period range (for α_o $ 15 sec) is related to the maximum fuel plate surface temperature reaching the coolant saturation temperature at the time of peak power, *i.e.*, coolant voiding *via* boiling becoming the primary shutdown mechanism.

For all of the HEU aluminum-clad cores, with widely varying system parameters, the maximum temperature rise results are all within a factor of two for a given period in the short period range (Fig. 3-23). The inter-relations of the T_{max} data for the different cores differ in some cases compared to the associated relations for power and energy release for the same cores due, at least in part, to the differences in parameters related to the size of the shutdown coefficients (*i.e.*, the void coefficient for these HEU cores) of reactivity and power density distribution for the different cores (Ref. 3-14).

Factors accounting for the relation between temperature response in one core compared to that in other cores make up part of the analysis methodology (Chapter 4).

3.1.5.5 HEU Stainless-Steel-Clad and LEU Rod Core Data

The majority of the reactor tests were conducted on HEU aluminum-clad plate fuel cores and are the focus of this thesis. However, useful information can also be extracted from the tests on the HEU stainless-steel-clad plate-fuel and the LEU oxide-rod-fuel cores, both of which showed similar trends in the burst parameters from step insertion transients.

The stainless-steel-clad plate cores showed the same general self-limiting behaviour as the aluminum-clad plate cores. In fact, despite the variation in cladding and other system parameters, the burst parameter data from the stainless-steel-clad plate core tests lie within the extremes of the aluminum-clad plate core data (Figs. 3-24, 3-25, 3-26). It should be noted that the burst data from the Spert I BSR-II core are almost identical to the Spert I P-core results (Ref. 3-15).

The LEU oxide-rod cores shared markedly different self-limiting behaviour compared to the HEU plate cores. The different response being due to the large prompt Doppler feedback contribution of the LEU fuel and also the much smaller

heat transfer of the oxide fuel. Even so, the peak power and generated energy data show similar trends with respect to reactor period as in the HEU plate cores (Figs. 3-3-27, 3-28). The fuel temperature results, however, were significantly different as the surface temperature rise at the time of peak power in the oxide-rod fuel was on the order of only a few degrees, illustrating the self-limiting behaviour being almost entirely due to Doppler feedback. The maximum fuel surface temperatures were also well below those found for the HEU plate fuel at comparable periods.

The specifications and test-series results for the HEU stainless-steel-clad plate and the LEU oxide rod cores are included in Appendices A and B.

3.1.5.6 Ramp Insertions of Reactivity

To this point, step insertions of reactivity have dominated the discussion. A second important scenario is that in which the reactivity addition occurs over a noticeable time period. One example of this is the "startup accident" which is a common safety analysis accident scenario and involves the motor driven withdrawal of the control rod bank from the core. The reactivity addition rate is determined by the worth of the control rods and the withdrawal rate. Transients generated by this type of reactivity addition are classified as ramp reactivity insertion initiated transients or more simply "ramp insertions".

The system response to a ramp insertion has been discussed in Chapter 2. Provided the reactivity addition rate is sufficient it is characterised by a power burst and accompanying temperature rise, similar to that found for a step insertion transient. The longer term stability of the system is independent of the manner in which the reactivity is added.

The investigation of ramp insertion transients in the reactor test program included studying the sensitivity with respect to both reactivity addition rate and initial power. The maximum power of the generated burst was found to increase with increasing reactivity addition rate and decrease with increasing initial power over the range of parameters studied. The behaviour was similar for the HEU Al-plate and stainless-steel-plate as well as the LEU oxide rod cores (Refs. 3-16, 3-17, 3-18, 3-19).

In terms of the initial power burst and associated maximum fuel temperature, step insertion transients are always more severe than ramp insertion transients when considering the same total reactivity insertion, *i.e.*, the faster the reactivity is added the more severe the resulting transient. However, when compared on the basis of an

"effective reactor period" the system responses are found to be roughly equivalent.

This "effective reactor period" is the asymptotic initial period in the case of a step insertion (determined by the magnitude of the inserted reactivity) and the minimum period during a ramp insertion (determined by the reactivity addition rate).

This equivalence, based on equating periods is demonstrated for HEU Al-plate, HEU stainless-steel-plate, and LEU rod-cores in plots of the P_{max} *vs.* α_o (Figs. 3-29, 3-30, 3-31, 3-32). Although of note that the peak power results from the ramp tests are slightly higher than the associated results from the step tests, the data agree within a factor of two with the largest discrepancies in the long period range and a convergence of the ramp and step results as the period is shortened.

This equivalence is also, importantly, applicable to the energy and temperature burst parameters (Refs. 3-18, 3-20). This is expected given the correlations between the burst parameters in the step tests and the fact that the same shutdown mechanisms are involved in both the step and ramp insertion transients. The temperature equivalence is illustrated in a pair of time traces from the Spert III C-core test series for periods of 40 msec and 17 msec (Figs. 3-33, 3-34). The energy and temperature equivalence is also shown in the LEU oxide rod-fuel results in a series of correlated data plots of E_{tm}, T_{tm}, and T_{max} *vs.* α found in Reference 3-18.

Analytical work based on the energy feedback model supports this ramp *vs.* step equivalence (Ref. 3-14). Also the same relative insensitivities with respect to elevated pressure and forced coolant flow rate for short period tests were found for ramp insertions as for step insertions (Refs. 3-18, 3-21)

On this basis, the burst parameters from a ramp insertion transient have been found to be approximately equivalent to those in a step insertion transient. This is an important conclusion as the equivalence simplification allows the same methodology, based on correlating maximum burst parameters to periods and reactivity, to be used on both types of reactivity insertions. In other words, the potentially destructive period, as predicted from step insertion transient data, also applies to the potentially destructive ramp insertion transient on the basis of comparable asymptotic and minimum periods.

In addition to the analysis of the initial power burst, the longer-term stability of the system must be considered. This aspect of the system response to a ramp reactivity insertion is not correlated to the step insertion response in the same manner as the

initial burst parameters and must be considered separately. Previously, only the initial burst has been considered when treating ramp insertion reactivity events.

3.1.6 Completeness of the Data Set

The majority of the tests were step initiated transients. Common to all cores, these were initiated by rapid ejection of the central transient rod. The typical test sequence from the Spert I tests, and applicable to the other test reactors is shown in Figure 3-35. Most of the sensitivity analysis to various system parameters was conducted using step insertion tests.

Two other types of tests were also conducted as part of the experimental programs: (i) ramp initiated transients, initiated by withdrawal of the control rod bank at a fixed rate, and (ii) stability tests which were concerned with the longer term response of the system and were initiated either by step or ramp reactivity insertions.

The variations with a number of system parameters were studied. The specific parameter dependencies investigated included: void reactivity coefficient, plate/channel geometry, hydrostatic head, initial reactor/coolant temperature, system pressure, and system flow conditions. There is a lack of data on variation of initial power levels, especially high initial power level. There are no data on downward flow conditions and LEU plate-type cores were not studied.

Two factors determine the completeness of the experimental data set: (i) the extent of the experimental program, and (ii) the quality of the measurements. A brief assessment summary of data set, in these terms, is presented below:

Parameter	**Extent of Testing**	**Quality of the Results**
T_i = ambient	extensive	good
T_i = saturation	extensive	good
Subcooling	moderate	fair
Initial Power	almost all from low power	-
hydrostatic head	limited	qualitative except from Spert IV D tests

void coefficient	minimal	good, but mostly combined with other effects
coolant flow	limited to upflow, and by D-type fuel design	fair
clad material	Al & SS	good, but mostly combined with other effects
LEU	limited to SEU rod fuel	-
reactivity addition rate	steps and a few ramp rates, supplemented by ANL simulation	good
PWR conditions	tested at high pressures and temperatures with flow	good
Stability	limited	quality fair, limited mainly to power data
Fuel Damage	extensive	good but mostly qualitative

It is possible to form subsets of the step test data to examine specific parameter variation, *e.g.*, subcooling, and void coefficient. Some of these subsets are more complete than others. The subsets with respect to variation in void coefficient, subcooling, fuel damage, LEU enrichment, and stability are discussed in more detail in Section 3.2.

The ramp data are mainly qualitative in nature with the argument based on the ramp and step data equivalence. This has been shown in previously published analysis and is adopted herein with the qualifier that long term stability (*i.e.*, chugging) must be considered (see Chapter 5).

The reactor tests in total provide a large amount of information on the general topic of shutdown mechanisms which can be used to develop a methodology for analysis of self-limiting power excursions. This area of study is relevant to severe accident

analysis which is part of a modern day SAR and such a methodology is developed in Chapter 7 of this thesis. Quantitative relations can also be developed from the experimental data for the variation of certain system parameters in the application to specific MTR systems. In other cases, the quality of the data can only suggest a conservative bounding approach with regards to other system parameters.

Although some parts of the data are not of a high enough quality or abundance to be used in a quantitative manner the underlying understanding of the mechanisms suggests simulation approaches which can be used in the absence of the experimental data, *e.g.*, for extension to LEU plate fuel.

3.2 Subsets of the Data

The self-limiting ability of the MTR-type cores were found to be sensitive to variations in the degree of initial subcooling, the size of the void reactivity feedback which varies with plate spacing and metal-to-water ratio of the core, and the Doppler feedback reactivity of the core which varies with fuel enrichment. The relevant subsets of the experimental data associated with variations in these parameters are outlined in the following sections. In addition, the data subsets with respect to stability/chugging operation, and fuel damage are similarly summarized.

Analysis with respect to these dependencies are reported in Chapter 4.

3.2.1 Subcooling

Subcooling is defined as the difference between saturation temperature and the initial coolant temperature of the system, *i.e.*,

$$T_{Subcooling} \equiv T_{Saturation}^{Coolant} - T_{Initial}^{Coolant}$$

A lower initial coolant temperature, or similarly, a higher coolant saturation temperature (as is the case with higher pressure at the core elevation in a pool reactor), leads to a higher degree of subcooling.

Subcooling was found to be an important parameter in the study of the self-limiting ability of HEU MTR-type systems during the Borax I experiments (Ref. 3-8) and was also investigated in the Spert Project. The applicable test series from both projects

are summarized below.

3.2.1.1 Borax I subcooling series

As part of the Borax I experiments a test series was conducted specifically to investigate the effect of subcooling on the transient response. Two different period transients were studied (22msec and 13msec) at various degrees of subcooling. The degree of subcooling was varied from zero (*i.e.*, the core initially at coolant saturation) to 22EC for the 13 msec transient series and 78EC for the 22 msec transient series. These two degrees of subcooling correspond to initial temperatures of approximately 80EC (13 msec series) and 30EC (22 msec series) depending on the saturation temperature which is not explicitly stated. Both periods are considered in the "short period range" but are in the less severe sub-range and do not result in temperatures approaching the melting temperature of the aluminum cladding. The subcooling test series was conducted as part of the 1953 experiments and is reported in Reference 3-8.

The test results are in terms of total energy produced and maximum fuel plate temperature as functions of subcooling and are summarized in Appendix B. Temperature measurements were recorded from three thermocouples, two centre-plug-type and one surface-welded-type, all located on the axial centerline of two plates in the instrumented assembly located in grid position 21 (the hot position in the core). The associated maximum power results have not been located for these transient tests.

In addition to the specific subcooling tests conducted with the Borax I core, step initiated transients for varying periods were performed from both ambient and saturation coolant conditions. The ambient test series, conducted in 1954 (Ref. 3-12), cover a range of periods from 33 msec to 2.6 msec ($30\ sec^{-1} < \alpha_o < 385\ sec^{-1}$). The saturation test series covers a period of range from 30 msec to 5 msec ($33\ sec^{-1} < \alpha_o < 200\ sec^{-1}$) and are reported in Reference 3-8. Maximum power and maximum temperature are reported for these tests although both are not reported for all of the tests. The transient summary data are summarized in Appendix B.

These two initial temperature conditions represent the upper and lower bounds of subcooling in Borax I and can be used as a further reference for the subcooling test series. The broader range of periods in the ambient and saturation test series demonstrates the subcooling effect at shorter periods, up to the onset of damage period range.

3.2.1.2 Spert I B-Core Test Series

The effect of subcooling was also studied as part of the Spert I B-Core tests. The Spert I B-Core data are in a different form than the Borax I subcooling data in that the degree of subcooling was held constant for transient tests of varying period as opposed to varying the degree of subcooling while holding the transient period constant. The data thus spans a range of periods and lends itself to P_{max}, E_{tm} and ΔT_{max} *vs.* α_o plotting.

Tests were conducted over a wide range of transient periods, extending from the long period range of transients down to the short period range. The shortest periods achieved in these tests are in the 10 to 15 msec range, *i.e.*, longer than periods associated with fuel damage. The data are from Reference 3-22 and are reproduced in Appendix B.

The Spert I B-24/32 core step insertion tests were conducted from initial temperatures of 20EC to 28EC, 40EC, 60EC, 80EC, and 96EC. Those with the B-16/40 core were conducted from initial temperatures of 20EC, 50EC, 80EC, and 95EC, and those with the B-12/64 core tests were conducted from initial temperatures of 20EC, 40EC, 60EC, 80EC, and 95EC. The data subsets for elevated initial temperatures (lower degrees of subcooling) are not as extensive as those for initially ambient temperature (~20EC). When only the short period range is considered this further reduces the amount of data to only a few experimental points. Typically two or three data points are available per initial temperature. Only a single test was conducted at 40EC, 60EC, and 80EC with the B-12/64 core.

The temperature measurements for these tests are all reported as the maximum recorded temperature for each test but are from different thermocouples. It should be noted that the thermocouples used in Spert I B were of the peened variety, making inter-comparison between different thermocouples difficult due to variation in reading.

3.2.1.3 Other Spert Subcooling Data

There are three additional subsets of data with relevance to the effect of subcooling analysis. One is a series of step initiated transients performed with the Spert IV D-12/25 core. These tests were conducted from an initial temperature of approximately 20EC with either a two foot or an 18 foot hydrostatic head (*i.e.*, depth of water above the core). While not designed to investigate the effect of subcooling,

an increase in hydrostatic head increases the coolant saturation temperature, and thus the degree of subcooling, for a given initial temperature.

Increasing the hydrostatic head from two to 18 feet increases the saturation temperature by about 11EC. Most of the Spert IV D-core tests were performed with a hydrostatic head of 18 feet and only three transients in the short period range are reported for a reduced hydrostatic head of two feet. This data subset is included in the Spert IV D-core summary data in Appendix B.

Step tests from both ambient and saturation initial conditions were also performed on the Spert I A-core. This data set was not located until late in this study and is not included in Appendix B or the analysis. These tests are reported in Reference 3-23.

The other supplementary data subset is from the Spert III C-19/52 core tests. This is a stainless steel clad core so application of this data requires accounting for the difference in clad material on the transient response.

The Spert III C-core tests were conducted under atmospheric pressure conditions, with no coolant flow besides natural circulation, from a variety of initial temperatures ranging from 19EC to 34EC and also at 60EC, 82EC, and 90EC. The number of tests were limited at each temperature although in some cases a considerable range of periods were studied. Data are reported from a variety of thermocouple positions further reducing the amount of equivalent temperature data at each degree of subcooling as a function of transient period. The subcooling data subset from the Spert III C-core is included in Appendix B.

3.2.2 Void Reactivity

The step insertion tests on the Spert I B-cores demonstrate the significance of the size of the void coefficient of reactivity on the self-limiting response of the system. The watery B-12/64 core has the smallest uniform void coefficient of reactivity and a small but positive central void coefficient. The B-24/32 core has the largest uniform and central void coefficient. The B-16/40 core which had alternate large and small coolant channels is associated with both uniform and central void coefficients intermediate to those of the other two B-cores

For ambient, low power initial conditions the P_{max}, E_{tm}, and ΔT_{max} results are enveloped by the B-12/64 core (highest values) and the B-24/32 core (lowest values).

Test series under atmospheric pressure, low power, natural coolant circulation conditions were conducted at various initial degrees of subcooling. The ambient temperature tests are comparable to those from the other test cores.

Void coefficient information also exists for the other test cores. As a result the data for tests from equivalent initial conditions can be compared on the basis of void reactivity for all of the test cores.

3.2.3 LEU Fuel

The LEU data subset is limited to rod-type uranium-oxide stainless-steel-clad cores. The results illustrate the effect of Doppler feedback as the primary self-limiting mechanism. However, due to the relative low conductivity of this fuel type compared to aluminum clad dispersion fuel (*e.g.*, U_3Si_2-Al/Al) plate fuel the effect of moderator expulsion *via* boiling is suppressed which will not be the case in the latter fuel type. Therefore, information on the Doppler feedback mechanism may be obtained from the Spert tests but the case of higher conductivity LEU plate fuel is not available. As such LEU plate fuel represents a gap in the experimental data set.

The LEU oxide rod-fuel data subset is summarized in and the data are included in Appendix B. Tests were conducted on three cores:

- Spert I SA-592
- Spert I OC-592
- Spert III E-core

Most of the LEU tests (those from Spert I) were conducted from ambient temperature, atmospheric pressure, low power conditions, with natural circulation coolant flow and under a two-foot hydrostatic head. The Spert III E-core tests extend the test conditions to those more applicable to power reactor operation, *i.e.*, higher temperature and pressure with forced coolant flow. Data reporting is extensive with power, energy, and temperature data available for the various transient periods. The time traces of the Spert I tests are also available in the cited references in Appendix B. Ramp transients were also investigated with the Spert I OC-592 core. These are also included in Appendix B.

The period range of the LEU tests extends that investigated with the HEU plate fuel, in that shorter periods were investigated with the Spert I OC-592 core. Two tests, with periods of 2.2 msec and 1.55 msec were included in this test series. Both

resulted in rod rupture. The 2.2 msec test is predictable from step tests with longer periods as fuel rupture was just post-power-peak. The 1.6 msec period test resulted in rod rupture prior to extrapolated time of peak power so represents a different combination of shutdown mechanisms.

The point of the LEU fuel testing was to investigate the effectiveness of the Doppler shutdown mechanism. The low heat transfer properties of the UO_2 and stainless steel clad as well as the low surface to volume ratio of the rods results in a long thermal time constant (on the order of seconds) for this fuel. This allowed for the isolation of the Doppler effect for short period transients. In the short period region with these cores it was determined that the power bursts were limited, almost entirely, by the Doppler feedback.

This test data subset demonstrates the effectiveness of the Doppler mechanism of feedback. With respect to plate fuel, simulation data are available in the literature to help bridge the gap in the experimental data set. This is discussed in more detail in Chapter 6.

Additionally, the fuel failure characteristics of the rod-type oxide fuel was shown to be primarily rupture which did not result in large scale core damage but was rather limited to local hot fuel-rods. This is different from the higher conductivity plate fuel cores.

3.2.4 Stability

The power and temperature stability was investigated for some of the test cores. Some of the data are from the post initial pulse parts of step test records while others are from specifically designed ramp insertion tests. These tests are summarized and assessed in the following sections.

3.2.4.1 Stability Test Summary

The Borax stability and chugging data set consists of time trace of power and temperature for a few tests at saturation initial temperatures. One of these tests was from initially steady boiling conditions while a series of step tests are reported showing oscillatory behaviour. The magnitudes of the oscillations are small for both the power and temperature. All tests were terminated by rod insertion after less than 10 seconds of operation. It appears that the boiling test was still developing into chugging upon test termination. For subcooled conditions, time traces are reported

for two step tests. The first illustrates small amplitude power oscillations while the second shows a damped secondary power and temperature peak. The time traces for all of these tests are included in Appendix B.

The Spert I A-core tests were by far the most extreme of any of the tests studying chugging, in that the chugging was allowed to develop for large amplitude oscillation envelopes. This test series investigated the sensitivity to the size of the hydrostatic head above the core. For two tests a chugging oscillation envelope was established for about a minute in duration. For a subsequent test the oscillation envelope was not fully established as the test was terminated for fear of exceeding safe limits. Unfortunately the data set is incomplete for these tests in the sense that the accompanying temperature oscillations are not reported. Safety limits were apparently related to the magnitude of the power oscillations. Total reactivity insertion (*via* a ramp), initial power, chugging power and frequency are all indicated for these tests. Tests were performed from both saturation and ambient conditions. It is noted that problems with reproducibility were encountered in this test series and quantitative results represent a sort of average of the 40 odd tests conducted (Ref. 3-24).

Stability information is also available for a testing using the B-12/64 core, specifically a series of three ramp tests from ambient initial temperature and for five step tests from saturation. The ambient test is described in the text of one of the technical reports (Ref. 3-17) and the saturation test time traces are available in a data summary report for general step insertion testing on the B-12/64 core (Ref. 3-22). The ambient test duration was longer than 40 seconds while the saturation test records are the run-outs of step insertion tests and were terminated between 10 and 20 seconds after initiation. The data are included in Appendix B.

The final stability testing was conducted using the Spert IV D-12/25 core. Most of this testing focussed on the onset of chugging with variation in hydrostatic head (2" and 18"), input reactivity, and coolant flow (natural circulation and upward forced flow). All oscillations were small and full chugging was not developed. Both power and fuel plate surface temperature are reported in the form of time traces. Additionally, coolant temperature at a number of axial positions in a channel are recorded in the form of a time trace for one of the tests. Stability testing was terminated due to restrictions in the design of the Type-D fuel assemblies which caused approach to safety limits prior to the onset of large oscillations in power and temperature under forced flow conditions.

A summary of the stability tests which are related to chugging behaviour is given in Table 3-6.

3.2.4.2 Completeness of the Data Set

Overall, the stability subset of the experimental data is sparse. This subset is made up of tests from Borax I, Spert I A-17/28 and B-12/64, and Spert IV D-12/25.

Gaps exist in the data set from lack of testing and failure to report data, while the quality and extent of the data set was hampered by a poor control of some system parameters such as the initial temperature of the system and the hydrostatic head above the core. There is also a lack of data with respect to variations in initiating reactivity so a complete set of maximum power and temperature with respect to reactivity or period is not available. Unfortunately for some of the tests the fuel plate temperature data are omitted and only the power results are reported.

There is also a lack of data available on the specifics of the voiding dynamics, related to the voiding mechanism within a single channel as well as how many coolant channels and assemblies were voiding and refilling during oscillatory behaviour. Axially spaced fuel plate surface and coolant thermocouples provide some data but these data are mainly reported for pre-chugging behaviour in Spert IV D-12/25.

Chugging was only partially investigated under forced upward flow conditions and not at all under forced downward flow conditions.

It should be noted that under large amplitude voiding conditions errors in the ion chamber power measurements may be introduced. However, for maximum power readings, *i.e.*, before large scale voiding on each oscillation, the precision of the ion chamber readings should be comparable to that associated with the step and ramp transient power pulses.

Despite the limited data, the combination of all the stability information from these tests is enough to provide information for developing a picture of the physics behind the chugging phenomenon. This is developed into a methodology for deriving quantitative safety limits in Chapter 5.

3.2.4.3 Sensitivities to System Parameters

Tests were conducted to investigate the effects of varying the height of the

hydrostatic head over the core, the upward coolant flow rate and the inlet water temperature. However, these variables were not properly controlled during the testing so results must be treated mainly as qualitative.

Differences in the amplitude of the power oscillations for tests with different hydrostatic heads was investigated in the Spert I A-core testing. The variability in results may be due to the lack of control of this variable during the tests as water was lost from the system during the large amplitude voiding and the retained water was recognized as "frothy" indicating that the refilling coolant probably contained a significant void fraction. This may have minimized the reactivity insertion and result in smaller oscillation amplitudes as seen in the results for the two-foot hydrostatic head tests.

Dependency on coolant flow is limited to the data from the Spert IV D-core tests, specifically the comparison of two tests, one with natural circulation and one with forced upward flow.

Qualitatively the dependence on bulk temperature can be seen from the Borax I data in that for the same reactivity input the system can show chugging tendencies at saturation conditions while remaining stable at subcooled temperatures. This was also seen in the Spert IV D-core tests when in one test the bulk temperature was allowed to rise from 20EC to 70EC at which point instabilities were observed. This is also evident in the Spert I A-core results.

3.2.4.4 Closing Remarks Regarding the Stability Experimental Data

The following chugging characteristics are noted from the reported data:

- MTR-type reactors are susceptible to chugging behaviour in situations where compensating reactivity is held in coolant voids.
- Oscillations commence once the void content in the coolant channels exceeds a certain threshold value.
- The reactivity changes induced by coolant voiding and refilling drive the power oscillations.
- Refill can be from the top or the bottom of the core depending upon the direction of coolant flow and any obstructions.
- Amplitude of the oscillations increase with amount of excess reactivity inserted into the system.

- The power peaks become narrower with increasing excess reactivity inserted into the system.
- Oscillations can be either of small or large amplitude, the latter is referred to as "chugging".
- For large amplitude oscillations, *i.e.*, chugging, parallel coolant channels void and refill in phase and are coupled to the power oscillations.
- As in the case of the initial power pulse of a step insertion transient, fuel plate temperature oscillations accompany and slightly lag the power oscillations.
- The power and temperature oscillations occur on a definite frequency, on the order of 0.5 to 2.0 cycles per second depending on system parameters.
- Although the magnitude of the power oscillations vary in an irregular manner they show no tendency to be damped or to diverge over the timescale of the testing.
- The power oscillations are qualitatively similar to the initial power pulse generated in a step reactivity insertion transient.
- Chugging is sensitive to variations in bulk reactor temperature, hydrostatic head, and coolant flow distribution.

This information is incorporated in the analysis of Chapter 5.

3.2.5 Fuel Damage

The reactor tests were designed to investigate the self-limiting characteristics of MTR-type cores for a wide range of transient periods up to and including those associated with fuel damage. Given the monetary cost, the radiological consequences and the irreversible nature (in many cases) associated with fuel damage, the fuel damage tests were carefully planned and added as a progression from less severe transients. In some cores the fuel damage range of transients were avoided and in others investigation of this range was kept until the end of a core test program.

Damage ranging from mechanical deformation to extensive fuel plate melting was observed in many of the test cores. The severity and extent becoming progressively larger with decreasing reactor period. In the following sections the damage tests are summarized by core.

3.2.5.1 Borax I

Permanent deformation of fuel plates was noted in the short period testing of the Borax I reactor (Refs. 3-8, 3-25). This was attributed to the steam pressures generated during rapid coolant voiding. The specific transients for which this occurred are not noted in the literature the mechanical damage was noted as from transients with periods in the range of 10 msec to 5 msec. The tests which produced the damage were conducted before the "Subcooling Test Series" during 1953 step initiated transients from saturation coolant temperatures.

The 13 msec period subcooling tests produced a reoccurrence of the mechanical damage and this is the reason why the subcooling test series was not extended to shorter periods. It should be noted that previously tests of period 13 msec did not produce mechanical damage but did in this case due to the weakened state of the plates. The transient tests were discontinued at this point in favour of steady state boiling tests. Reference 3-26 misleadingly reports the onset of damage for the Borax I core as approximately 20 msec without explaining the prior weakening damage tests.

A single destructive test was carried out with the Borax I reactor. This resulted in complete disassembly of the reactor core, extensive melting of the fuel meat and aluminum cladding and widespread mechanical deformation of the assemblies and core structure. The test results are summarized in Appendix B and are described both qualitatively and quantitatively in Reference 3-12. Additional description of the damage observed as a result of the destructive test is given in Reference 3-25.

3.2.5.2 Spert I A-Core

Fuel damage associated with the step initiated Spert I A transients is not reported in any detail. A passing remark in Reference 3-26 indicates the degree and threshold of mechanical damage, presumably in the Spert I A core (only the A- and B-core tests had been conducted at the time of writing of the report) associated with periods of 7 msec and less.

No further details of the damage have been located. The only other mention of fuel damage in the Spert I A-core is associated with stability tests in which mechanical plate damage resulted during chugging oscillations (Ref. 3-24).

There is no mention of plate melting during the stability tests.

3.2.5.3 Spert I B-Cores

The B-core testing was limited to periods of about 10 msec or longer. These are longer periods than those associated with mechanical deformation and more severe damage in the other test cores.

However, one occurrence of fuel damage in the B-12/64 core was reported (Ref. 3-27). During void coefficient tests in which some of the fuel was removed from the core, a 2" by 1" hole was discovered in a single fuel plate. The hole was completely through the fuel plate and had apparently gone unnoticed during transient tests subsequent to the damage based on above normal activity measurements. The cause of the damage was not conclusively determined and did not affect the transient performance of the core.

3.2.5.4 Spert I D-Core

Investigation of fuel damage thresholds and a second destructive test were the prime objectives of the testing on the Spert I D-core. Fuel plate damage was observed for periods on the order of 9 msec and shorter (Ref. 3-28). Around 9 msec the damage was limited to relatively minor mechanical distortion in the form of plate bowing. This progressed to more localized and pronounced bowing, and then to rippling as the periods were subsequently shortened. To investigate the damage range of periods, tests were performed with periods of 6.4, 6.0, 5.0, 4.6, and 3.2 msec, the latter being the destructive test. Severe plate deformation was observed as a result of all of these tests and plate melting was observed in the 5.0, 4.6, and 3.2 msec period tests.

The three tests which resulted in fuel melting (5.0, 4.6, and 3.2 msec periods) are reported in successive quarterly reports from the Spert Project (Refs. 3-11, 3-29, 3-30, 3-31). The information in these quarterly reports is also summarized in Reference 3-32, which also includes additional analysis on the destructive test program in Spert I D. Time traces of the transient tests, fuel melt patterns and analysis and photographs of the fuel damage are all found in this latter reference. Additional information regarding the temperature measurements from these tests and the entire D-core test series is given in Reference 3-33. Further examination of the fuel damage from these tests including metallurgical analysis and qualitative comparison to damage from the Borax I, SL-1, ETR, and WTR reactors is reported in Reference 3-28.

The transient summary data for all of these tests are included in Appendix B.

3.2.5.5 Spert IV D-Core

Although the test program with the Spert IV D-core was not planned to investigate fuel damage ranges, a single occurrence of fuel damage was observed during testing with high coolant flow rates. A hole was melted in one of the outer plates of the central hot assembly of the core. This is reported in two quarterly technical reports (Refs. 3-34, 3-35) as well as in the Spert IV D-core summary report (Ref. 3-36).

This instance of plate damage was isolated and was attributed to plate deformation, restricting one of the narrow coolant channels on the outside of the fuel assembly. The melted plate, as in the case of the B-12/64 core plate melt did not appear to influence the transient behaviour of the core and was in fact not detected during subsequent tests.

Fuel plate deformation, in the form of bowing and rippling, was noted for transients with periods less than 15 msec (Ref. 3-36). Deformations were found to be minor for transients of 10 msec period.

3.2.5.6 SL-1

The SL-1 reactor accident provides additional information regarding fuel damage and core disassembly in MTR-type reactors. An extensive damage assessment and analysis is reported in Reference 3-37 which includes photos of the fuel damage, a plate damage schematic map of the core and metallurgical analysis results. The transient characteristics in terms of peak power, energy generation and temperature rises are included in this report and further discussed in Reference 3-38. The degree of the potential Al/H_2O reaction is also discussed in these two references.

When considering the SL-1 accident information the differences between this system and those of the Borax and Spert cores should be considered. The specifications of the SL-1 core are included in Appendix A.

3.2.5.7 Stainless-Steel-Clad Plate-Cores

Mechanical deformation, similar to that observed with the Al-clad plate cores, was found in the three stainless-steel-clad Spert plate-cores included in the reactor tests.

Fuel plate warping, in the form of bowing and rippling, was observed in each of the Spert I P-18/19, Spert I BSR-II, and Spert III C-19/52 cores for transients with periods in the region of 14 msec. In the P-core a transient of this speed was found to generate clad surface temperatures of 210EC. This rippling/warping onset was used as the limit to the testing of the Spert I BSR-II core which was to be subsequently returned to and used by ORNL. The mechanical damage observed in the stainless-steel-clad Spert cores is summarized and discussed in Reference 3-39, as well as in a series of quarterly reports from the Spert Project (Refs. 3-40, 3-41, 3-42, 3-43).

In addition to fuel plate warping, blistering of the clad surface was noted in both the P-18/19 and C-19/52 cores. In the P-18/19 core this followed testing of a 5 msec transient, generating clad surface temperatures of 300EC in the regions of blistering (which were not the "hot spots" in the core for this test) (Refs. 3-39, 3-40). Similar blistering was observed in the Spert III C-19/52 core (Ref. 3-39) and while not attributed to intergranular corrosion is also attributed to fabrication issues of fuel homogeneity (Refs. 3-39, 3-43).

3.2.5.8 Stainless-Steel-Clad LEU Rod-Fuel Cores

The fuel rod experience from the Spert LEU rod-type test cores is not directly applicable to fuel damage in MTR-type plate-fuel cores. Rod damage ranging from discolouration and bowing to rod bursting was observed during the short period transient testing and the attempted destructive tests.

The behaviour of this type of core is very different from the plate-fuel cores as a result of the very different heat transfer characteristics of the system. The heat transfer time constant for the rod fuel is significantly longer than that for the plate fuel and as a result larger thermal gradients and minimal clad surface temperature rise occurs. Planned destructive tests on the Spert I OC were unsuccessful with fuel damage somewhat locally limited to bursting of a two fuel rods in each of the two shortest period tests (2.2 msec and 1.6 msec periods).

Experience with fuel rod damage is reported in References 3-20, 3-44, and 3-45. Thermal stresses associated with these short period transients are reported in Reference 3-35.

3.2.5.9 Other Reactor Fuel Damage Information

Additional information on fuel damage which has relevance to MTR-type reactors is associated with the fuel melting accident in the Westinghouse Testing Reactor, WTR (Ref. 3-46), the flow blockage accident resulting in fuel melting in the Engineering Test Reactor, ETR (Ref. 3-47), and results of the TREAT Project.

The onset of mechanical fuel damage in the form of bowing of plates, in heavy-water MTR-type cores, was observed to occur for periods five to ten times longer and for reactivity additions approximately twice as large when compared to light-water MTR-type cores (Ref. 3-1). This is the result of differences in prompt neutron lifetime, feedback coefficients, and heat transfer characteristics between the two types of cores.

3.3 Remarks on the Use of the Data

This section contains information relevant to the practical use of the experimental data from the reactor tests. Sections 3.3.1 and 3.3.2 identify differences in the measurement methods of different test series for the power/energy and temperature data, respectively. These factors must be accounted for in order to legitimately compare data from one test series to data from another - the analyst must be aware when comparing “apples to oranges”.

Section 3.3.3 contains information on the uncertainty associated with the experimental data and Sections 3.3.4 and 3.3.5 discuss the transient tests with respect to actual event scenarios and limitations in the data.

Given the nature of safety analysis for severe accident scenarios, a conservative bounding approach is adapted herein when using the data and developing a methodology.

3.3.1 Power/Energy Normalization

Although the power measuring equipment used in the Borax tests was similar to that used in the Spert tests, significant differences in the power calibration of this equipment leads to different definitions of power (and energy).

In the Borax test program, the ion chambers were calibrated against energy

measurements based on fuel plate temperature rise during the transient (first before the appearance of feedback effects and later from insulated plates). These methods are described in both References 3-8 and 3-12. In comparison, the Spert power calibration was based on bulk system temperature measurements, considering the entire reactor as a calorimeter (Refs. 3-7, 3-9).

It is not clear if the Borax power/energy normalisation used for the power excursion tests was also adopted for the steady boiling tests as additional calibration procedures similar to those used in the Spert Project were reported for these tests.

As a result of the differences in calibration, all power (and energy) results reported in References 3-8 and 3-12 represent only the prompt energy deposited as heat in the fuel plates, which is roughly 85% of the total nuclear energy generated (the remainder is approximately 7% deposited elsewhere in the system and 8% from delayed energy generation). The Spert results represent all nuclear energy generated.

In addition the Borax power and energy results, being based on energy density, have been normalized to a 30-standard-assembly core, taking into account the various plate loading and number of assemblies used during the tests (see Appendix A).

Therefore, in order to properly compare Borax I and Spert power and energy measurements the Borax I results should be considered to be from a 30-assembly core and be scaled by a factor of roughly 1/0.85. This is the standard adopted herein. It should be noted that this correction has not been applied for comparisons previously reported in the literature, specifically in the Spert Project technical reports (see for example Figure 3-19 in Reference 3-16).

In addition, when comparing Borax I and Spert total energy values, E_{tot}, the slightly different definitions used for this quantity should be kept in mind (see Section 3.1.4). The individual time traces from the Spert transients in question should be examined to see if the power trace reached a minimum of 1% of the peak power on the decline from the initial pulse. If this point was not reached then the E_{tot} value represents the integral to the termination (*via* SCRAM) of the test and this quantity is not comparable to the associated Borax results.

3.3.2 Thermocouple Specifics

One of the aspects of application of the temperature data from the reactor tests is to gain insight into transient heat transfer as part of the self-limiting shutdown

mechanisms of the reactor. Another aspect is the behaviour of the "hot spot" in the reactor in relation to fuel damage thresholds. Therefore, the usefulness of the temperature data and the ability to compare and combine data from different test series relies on the knowledge of where in the temperature distribution across a fuel plate and throughout the reactor core the measurement is being made.

As noted in Section 3.1.4, a noticeable amount of scatter exists in the fuel plate temperature measurements from the reactor tests, especially for the short period range of transients (see for example Figure 3-13). This scatter can be attributed, at least in part, to the specifics of the thermocouples from which the measurements were made.

There are two main factors to consider when working with the fuel plate temperature measurements from the reactor tests. These are:

- the location of the thermocouple in the core, *i.e.*, which assembly, fuel plate and location on the fuel plate is the thermocouple located, and
- the attachment method of the thermocouple to the fuel plate

Both have been found to vary between cores and within test series, and are related to the position of the thermocouple in relation to the temperature gradient within the fuel and the core. The location and type of the thermocouple is generally noted in the results from the each test.

These two factors are considered separately in the following discussion. The variation in the temperature readings with the variation in these factors allows for uncertainty estimates to be placed on the temperature data and assessment of the temperature data set as a whole.

Other contributions to the scatter of temperature data may have resulted from variations in the initial temperature of the system, resulting in slightly different subcooling.

An example of the potential misuse of temperature data is shown in Figure 3-36 in which the thermocouples of various types (surface and buried) and different locations (different plates in the instrumented assembly) in Borax I are compared with peened thermocouples from Spert I A. As discussed below these measurements are not necessarily comparable.

3.3.2.1 Thermocouple Location

For a typical test series in any given core, temperature measurements from thermocouples at different positions are reported.

The temperature at any given point in the core is determined by both the power density or energy deposition distribution and the heat removal characteristics at the various locations. For MTR-type fuel under natural coolant circulation conditions the heat removal is similar for each plate in the core and therefore the temperature distribution is proportional to the power density distribution, which in turn is roughly proportional to the thermal flux distribution. As the thermal flux distribution (measured for each core using flux wires) varies considerably from one assembly location to another, from one plate to another, and even axially from one position on a plate to another, it is not surprising that the temperature measurements from a thermocouple at position A will be different from a thermocouple at position B for a given power transient. The "hot spot" in the core corresponds to the peak thermal flux position (all else equal).

Therefore, some of the scatter in the temperature results can be eliminated if the variation in thermocouple position is considered. The easiest way to do this is by simply considering measurements from only one thermocouple position, or from equivalent (same thermal flux) positions. For example, the temperature data from the Spert I A test series is shown in Figure 3-13 with the various thermocouple locations indicated. Consideration of only thermocouples at locations 44-012+0, 55+0, and 55-172+0, and removal of points associated with a suspected instrument range setting error (Ref. 3-7), results in much less scatter of the data points.

The consideration of only single or equivalent thermocouple locations reduces the size of the data set considerably in some cases. In order to utilize more of the data, the measurements from different thermocouple locations can theoretically be scaled with the power density (or thermal flux) distribution. In the case of the reactor experiments, the flux distribution was usually measured in the initial static tests for each core and can be found in the references cited in Appendix A. For the above case, unfortunately, no power density distribution is reported for the Spert I A core which is needed to normalize the thermocouple readings. A rough estimate may be made using the Spert I B flux wire results or derived from simulation.

This scaling should be kept in mind in all instances with regards to the maximum temperature achieved in a given test as in some instances the thermocouple positions

were not at or near the hot spot in the core. For example, with respect to the Borax I temperature data, the temperature measurements were made from thermocouples located on the core axial centerline. This location is slightly offset from the axial power peak. Therefore, to consider the maximum fuel plate temperature from these tests, the data should be adjusted.

A second example is also taken from the Borax I tests. For the destructive test, for which the instrumented fuel assembly was moved from the hot core location (grid position 21) to a lower flux location (grid position 26). The change in thermal flux ratio is roughly 1.39 to 1.04 (measured on the static core loading which had two less assemblies). Assuming that temperature rise is proportional to thermal flux, this approximate change in flux ratio can be used here to scale the temperature results, *i.e.*,

$$\Delta T_{21} = \frac{1.39}{1.04} \Delta T_{26}$$

In the above the right hand side is a product of the measured fuel plate temperature rise in the "off-peak" location (*i.e.*, core position 26) and the thermal flux ratio between this position and the hot position (*i.e.*, core position 21). The left hand side therefore represents the maximum fuel plate temperature rise. This adjustment also assumes constant specific heat of the fuel material and proportional heat removal.

Information needed for flux scaling of the temperature measurements can be obtained *via* standard static simulation methods leading to the calculation of power peaking factors (*PPF*s). Factors such as loading pattern, location of flux traps and absorbers, assembly design, and burnup distribution all affect the *PPF*s. In some cases the local, radial, and axial *PPF*s are found to be quite considerable (Ref. 3-48). An example of the variation of the axial *PPF* with changes in control rod bank position in the MNR core is shown in Figure 3-37. A similar distribution is expected with respect to the control rod positions in the fresh-fuel test cores.

In cases with uniform heat removal throughout the core, consideration of the power density (or flux distribution) is sufficient for temperature scaling. However, in the case of nonuniform heat removal this second distribution must also be considered. An example of the importance of this factor is taken from the Spert IV D-core tests, in which the narrow outer coolant channels led to fuel damage (melting) in the outer fuel plate of an assembly during tests with flow. The restricted flow in these narrow channels accentuated the power/cooling mismatch locally while the rest of the core

remained cooled. Similar and even more severe transients with only natural circulation using this same type of fuel did not result in melting in this core location (Refs. 3-34, 3-35).

A related issue worth mentioning is that in a given test series for each test the maximum fuel temperature is reported. In many cases these readings are from various thermocouples locations.

From a neutronic standpoint there is no reason to believe that the hot spot will change from one test to another with the exception of a small shift due to the differing position of the control rod bank - in the case of the Borax and Spert cores, this shift would be upwards axially as the control rod bank is withdrawn to a greater extent to provide larger reactivity insertions, and subsequently shorter period transients, upon ejection of the transient rod.

A variety of possibilities exist to explain the differing thermocouple locations being associated with the hot spot of the same core. These include the failure of a given thermocouple during a test series, or the loss of a particular signal or data record for a given test. Information is not given for the state and extent of the thermocouple set for each test so these assumptions are based on speculation. Local boiling effects are observed to contribute a certain amount of "noise" on the temperature time traces but the large scale behaviour should remain the same for the specific locations in the core (*e.g.*, the "hot spot" in the core should enter the film boiling first for any given transient).

3.3.2.2 Attachment Style

The two most common methods of attachment for thermocouples to the fuel plates are by welding to the outer clad surface and by peening into the interior of the plate (see Section 3.1.3, Instrumentation and Measurement).

During a fast transient, significant thermal gradients are established within the fuel plates, with the majority of the energy deposited in the fuel meat and subsequently conducted to the surface of the cladding. It has been found that just as the position of the thermocouple in relation to the core coordinate system is important, so is the position of the thermocouple in terms of the depth to which it is buried in the cladding (Refs. 3-33, 3-49, 3-50). Temperature data varies between different thermocouples peened to different depths, and more significantly between true surface and buried thermocouples. In this sense, this factor is akin to the

thermocouple position as it relates to a different location in the temperature distribution of the core and can lead to errors in comparative as well as absolute temperature measurements.

As a result, the different methods of thermocouple attachment lead to both uncertainties in absolute and comparative measurements.

The peening depth of typical thermocouples (0.005" diameter wires) used in Spert I A and B was noted to vary up to several thousandths of an inch within the (0.020" thick) cladding, *i.e.*, a significant fraction of the clad thickness from one thermocouple to another (Refs. 3-7, 3-51). The attachment style of the thermocouples for all of the test cores is indicated in Table 3-7.

Discussion of the uncertainties related to the thermocouple attachment style are discussed in detail in Section 3.3.3.

3.3.3 Error Assessment

This section summarizes these uncertainties in the measured and calculated quantities comprising the reactor test data from both the Borax and Spert tests. The literature reporting the reactor test data, which for the most part is comprised of ANL and IDO technical reports, has been assessed to identify the various uncertainties in the test data. The information is in general limited to error estimates on the type of measurement rather than an uncertainty on each data point. When not available for a given data set estimates from similar systems are used. For example, given that the same procedures and instrumentation was used in the Spert I A- and B-cores the uncertainties on the data measured in the B-core are likely identical to those associated with and reported for the data measured in the A-core.

The various sources of error include:

(i) precision of the measuring equipment,
(ii) the method of calibration of the measurements,
(iii) the method of measurement of the data,
(iv) data reduction, and
(v) the physics of the transient conditions themselves.

Standard error propagation techniques are employed in this section to derive overall uncertainties.

It is useful for analysis purposes to separate the overall uncertainty in the test data into random and systematic components. In the same context it is also useful to note the form of the uncertainties on the test data. Absolute uncertainties, for example those associated with a fixed precision on a scale, will be constant over the range of the data, *e.g.*, ± 2EC from the precision to which the temperature recording scale can be read. In comparison, relative uncertainties, *e.g.*, ± 5%, will increase with increasing value of the quantity measured.

These two types and the form of these uncertainties are considered in different aspects of the curve fitting and regression analysis of Chapter 4.

A final note worth mentioning is with regards to comparing data from different test series from different reactor cores. A careful review of the method of measurement and the physics of the situation will indicate the equivalence of the measured quantities. This is particularly relevant to the comparison of power and energy data between the Borax and Spert tests, and is relevant to variation in the systematic errors of the temperature test data.

In the following subsections the primary data measureables are discussed in terms of uncertainty estimates and these are summarized in Table 3-8.

3.3.3.1 General Measurements

In general the response and resolution of the instrumentation used in the Spert Project was reported to be such that a transient with a period down to 1-msec can be followed with "negligible distortion", *i.e.*, within one or two percent (Refs. 3-10, 3-16). This time constant is related to the ion-collection time for the ion chambers (Ref. 3-9) and the response time of the thermocouples. This is a faster period than any of the transient tests produced, including those resulting in fuel damage and core disassembly.

Since the Borax I instrumentation system and procedures were similar to those used in the Spert Project it is not unreasonable to assume roughly the same degree of uncertainty in the resolution of the measuring instrumentation. A more detailed examination of the uncertainties associated with the primary measurements, *i.e.*, P_{max}, E_{tm}, ΔT_{max}, and period, are considered in the following sections. Both the sources and type of error are identified where possible.

It should be noted that it was common practice that tests were repeated numerous

times to check the reproducibility (Ref. 3-16).

The error estimates made herein are applicable to data measured in the Borax and Spert HEU Al-clad plate-fuel cores. Data from other test cores may be associated with different degrees of uncertainty.

3.3.3.2 Power

The sources of error which are considered with regards to the power measurements are specifically those due to:

(i) the measurement instrumentation electronics,
(ii) calibration,
(iii) data reduction, and
(iv) the presence of steam voids in the core.

The power data must be considered separately for the Borax and Spert projects due to the different normalization used for this quantity and the different method of calibration of the measurements.

3.3.3.2.1 Borax

As mentioned previously (Sec. 3.3.1), in Borax I, the power (and energy) is derived from the prompt fission energy deposited in the fuel plates, based on calibration of the three ion chambers to the measured thermocouple temperature rise of an insulated fuel plate in the instrumented assembly. The total power of the core is then found from:

$$P_m = \left(\frac{N}{PPF} \right) P_i$$

$$P = \left(\frac{1}{f} \right) P_m$$

where P_m is the power calculated for the Borax tests, N is the number of plates in the core, PPF is the peak-to-average power density ratio, and P_i is the power generated in the insulated fuel plate. P is the total nuclear power generated and is the quantity comparable to the power values measured in the Spert tests, and f is the fraction of

the total nuclear energy appearing promptly in the fuel.

The various uncertainty components associated with the Borax power measurements are estimated as:

(i) A random uncertainty in the calibration data, σ_c/c, is estimated as a 4.1% standard deviation from the average (Ref. 3-12).

(ii) An uncertainty in the heat loss from and the temperature distribution in the insulated fuel plate, σ_h/h, is estimated as ± 7% (Ref. 3-12). The physical situation leading to this source of error is illustrated in Figure 3-38 which shows two different temperature distributions for different heat losses to the coolant as well as indicating the difference in temperature with depth in the cladding.

(iii) An uncertainty on the order of ± 20% exists due to normalization of the power density from the insulated plate to a total reactor power based on a power density distribution estimated from foil and wire irradiation measurements (Ref. 3-12).

(iv) Re-normalization of the Borax power data to total fission power (which is the quantity measured in the Spert tests) is based on the approximation that the Borax measurement accounts for 85% of the total fission power. Depending on the absorption of radiation in other fuel plates this value is thought to have a maximum uncertainty of +5%.

(v) There is no uncertainty on the number of fuel plates, N, in the calculation.

These various sources of error combine, using standard error propagation analysis, to give estimates of the total random error, and the total systematic error associated with the power data.

The relative uncertainties in the calibration, σ_c/c, and the heat loss/temperature gradient of the insulated plate, σ_h/h, combine using standard error propagation to give an estimate of the uncertainty on P_i:

$$\frac{\sigma_{P_i}}{P_i} = \sqrt{\left(\frac{\sigma_c}{c}\right)^2 + \left(\frac{\sigma_h}{h}\right)^2}$$

Additional uncertainty associated with the instrumentation electronics is assumed to be negligible compared to these two components. This is thought to be a realistic assumption given the similarity of the Borax and Spert instrumentation (see below). This calibration error represents the random error on the data:

$$\frac{\sigma_P}{P}\Big|_{random} = \frac{\sigma_{P_i}}{P_i} \approx 8.1\%$$

The remainder of the error components are considered systematic due to the re-normalization factor and the power distribution estimates. In other words, the normalization of the measurements will have a common systematic error for all data pairs as the same normalization constants are used. The total systematic uncertainty is therefore estimated as:

$$\frac{\sigma_P}{P}\Big|_{systematic} = \sqrt{\left(\frac{\sigma_{PPF}}{PPF}\right)^2 + \left(\frac{\sigma_f}{f}\right)^2} \approx 21\%$$

Considering these two error components together leads to a total error estimate:

$$\frac{\sigma_P}{P} = \sqrt{\left(\frac{\sigma_{P_i}}{P_i}\right)^2 + \left(\frac{\sigma_{PPF}}{PPF}\right)^2 + \left(\frac{\sigma_f}{f}\right)^2} \approx 22\%$$

3.3.3.2.2 Spert I & IV

In comparison to the Borax calibration, the Spert power measuring equipment was calibrated using a calorimetric approach (see Section 3.3.1) shown pictorially in Figure 3-39. The result is that the power measured in the Spert tests represents the

total generated nuclear power.

The uncertainty in the Spert power measurements arises from the instrument electronics, the data processing and reduction, and the calibration. In contrast to the Borax power measurements the Spert power data are free of any additional uncertainty due to normalization factors (see above).

The best indication of the precision of the power measurements is quoted as ± 3.4% (Ref. 3-7) as calculated from analysis of data from the Spert I A-core calibration. This number incorporates the uncertainties and variances associated with the linear fit to the calibration data (< 1%), nuclear heating rate (0.8%), and combination of nuclear and electrical heating rate (1.8%). The additional random error arising from the instrumentation electronics is quoted as less than ± 1% and that due to data reduction is insignificant compared to the uncertainty on the calibration constants (Ref. 3-7). A conservative value of ± 5% has also been quoted in the literature. This conservative estimate is adopted herein for all of the power data from the Spert I & IV HEU Al-plate cores, *i.e.*,

$$\frac{\sigma_P}{P} \approx 5\%$$

This is considered a random error. No systematic errors of note have been identified with respect to the Spert I & IV HEU Al-clad power measurements.

3.3.3.2.3 Effect of Voids on the Power Measurements

Potentially, any change in the leakage characteristics of the core may affect the power measurements. During a transient, especially on a short period, significant coolant voiding occurs.

At the time of large scale coolant voiding (*i.e.*, at and beyond the time of peak power) the leakage from the core may significantly increase, giving a false high chamber reading and therefore power measurement. Figure 3-40 shows the idealized power trace for a step insertion into an HEU system and indicates the regions of the transient where the measured power is likely to be least accurate.

Specific studies, carried out as part of the Spert Project show that the voiding effect does not have a significant effect on the power measurements until about two periods after peak power when a significant fraction of the core moderator is voided (Ref. 3-

10). This is applicable to short period transients which result in this magnitude of voiding. This conclusion is supported by experimental analysis of tests conducted in Spert IV showing that ion chamber response is relatively insensitive to the presence of central voids (Ref. 3-11).

In addition, in both the Borax and Spert projects calibration curves for the ion chambers were developed as functions of system temperature and void content in the core. Also, flux wires were commonly included in the core during static and transient tests, which allowed for checks of the normalization of the power records to match the total energy generated.

Within the scope of step insertion transients the following conclusions with respect to the accuracy of the power measurements are reported (Ref. 3-7):

- power measurements in the vicinity of the initial power peak are subject to negligible error due to voiding,
- power measurements for equilibrium power behaviour are also subject to negligible error due to voiding,
- near the power minima following the initial power peak, the power measurements may overestimate the actual power by as much as a factor of four, and
- the power rise following the power minima is real but the measurement may be distorted due to void effects.

Overall, the frequency requirements of the power measuring equipment, based on the ion collection time of the chambers, is reported to be accurate (Ref. 3-7).

The uncertainty estimates related to the presence of voids have been made with respect to the initial burst of step or ramp power excursions. These uncertainties may be further amplified in the case of oscillatory/chugging data which involve more complex voiding dynamics. The power measurements between oscillation power peaks are subject to the same uncertainties as the post- power peak region of the step insertion power trace. Peak powers on the oscillations may still be measured with the same relative uncertainty as the P_{max} values of step insertion tests.

3.3.3.2.4 Translation to Power Densities

The average and maximum power density are also quantities of interest. These are given by the relations:

$$PD_{avg} \equiv \frac{P}{V_f}$$

$$PD_{max} = \frac{P}{V_f} \times PPF$$

Where V_f is the volume of fuel in the core, and is assumed to be known precisely, and *PPF* is the power peaking factor which is a ratio of the peak to average power density.

Once again the Borax and Spert measurements must be treated separately. For the Borax data the power densities are related to the measured power in the insulated fuel plate by:

$$PD_{avg} = \frac{P}{V_f} = \left(\frac{1}{V_f}\right)\left(\frac{1}{f}\right)\left(\frac{N}{PPF}\right)P_i$$

$$PD_{max} = \frac{P}{V_f} \times PPF = \left(\frac{1}{V_f}\right)\left(\frac{1}{f}\right)(N)P_i$$

For the Borax data, the relation for PD_{avg} shows that the uncertainty on PD_{avg} is the same as that on the total power, P. The PD_{max} quantity is known more precisely as the uncertainty from the measured power distribution (*PPF*) is removed. This assumes that the insulated plate used for the power calibrations was in fact the hottest plate in the core. As it was located in the peak thermal flux power assembly this is a reasonable approximation. The relative uncertainties on the maximum power density are therefore:

$$\frac{\sigma_{PD_{max}}}{PD_{max}}\Big|_{random} = \frac{\sigma_{P_i}}{P_i}$$
$$\approx 8.1\%$$

$$\frac{\sigma_{PD_{max}}}{PD_{max}}\Big|_{systematic} = \frac{\sigma_f}{f}$$
$$\approx 5\%$$

$$\frac{\sigma_{PD_{max}}}{PD_{max}}\Big|_{total} = \sqrt{\left(\frac{\sigma_{P_i}}{P_i}\right)^2 + \left(\frac{\sigma_f}{f}\right)^2}$$
$$\approx 9.5\%$$

For the Spert data PD_{avg} is associated with the same uncertainty as the total power. For PD_{max}, the uncertainty in the power distribution contributes an additional uncertainty component. This uncertainty in the power distribution is considered a systematic error in the data for each core (from each set of flux wire irradiations). The relative uncertainty on the flux wire based power density distribution is reported as 20% for the Spert I D-core (Ref. 3-32). The relative uncertainties on the maximum power density are therefore:

$$\frac{\sigma_{PD_{max}}}{PD_{max}}\Big|_{random} = \frac{\sigma_{P_i}}{P_i}$$
$$\approx 8.1\%$$

$$\frac{\sigma_{PD_{max}}}{PD_{max}}\Big|_{systematic} = \frac{\sigma_{PPF}}{PPF}$$
$$\approx 20\%$$

$$\frac{\sigma_{PD_{max}}}{PD_{max}}\Big|_{total} = \sqrt{\left(\frac{\sigma_{P_i}}{P_i}\right)^2 + \left(\frac{\sigma_{PPF}}{PPF}\right)^2}$$
$$\approx 21\%$$

Noted that the systematic error with respect to the foil/wire flux distribution may have a common component for all the cores. In this case the relative values of the maximum power densities between Spert cores may be somewhat free of this error.

3.3.3.3 Period

Little information exists regarding the uncertainties related to the period measurements. In the Borax tests useful power readings were usually obtained from all three ion chambers. In such cases the period measured by the three chambers

agreed within ± 10% (Ref. 3-8). This is interpreted as an estimate of the 95% confidence interval. Therefore, the relative standard deviation is:

$$10\% \approx 2 \times \frac{\sigma_\tau}{\tau}$$

$$\frac{\sigma_\tau}{\tau} \approx 5\%$$

Two other reported uncertainties for the period measurements have been located in the literature. The first is a total random uncertainty of ± 3.5% quoted in relation to the period measurement used in void worth measurements in the Spert III C-19/52 core (Ref. 3-51), and the second is ± 2% quoted for the range of periods for the Spert III E-core for ambient-temperature transient tests (Ref. 3-52).

For the analysis herein, the relative error on the period is estimated as ± 5%, common to all data from the Borax I and Spert I & IV HEU Al-clad test cores, *i.e.*,

$$\frac{\sigma_\tau}{\tau} \approx 5\%$$

Given that for the Spert I reactor more ion chambers (up to 12 compared to three for Borax I) were available (Ref. 3-7) and the quality of the electronics and data processing was relatively higher than that used in the Borax I tests, adopting the same level of uncertainty for the Spert data as for the Borax data is a conservative approach.

The uncertainty in the reciprocal period is related to the uncertainty in the period measurement by error propagation:

$$\alpha_o = \frac{1}{\tau}$$

$$\sigma_{\alpha_o}{}^2 = \sigma_\tau{}^2 \left(\frac{d\alpha_o}{d\tau} \right)^2$$

$$= \sigma_\tau{}^2 \left(-\frac{1}{\tau^2} \right)^2$$

$$= \left(\frac{\sigma_\tau}{\tau} \right)^2 \alpha_o{}^2$$

Showing that the relative uncertainty in the reciprocal period is the same as the relative uncertainty in the period, *i.e.*,

$$\frac{\sigma_{\alpha_o}}{\alpha_o} = \frac{\sigma_\tau}{\tau}$$

3.3.3.4 Energy

Two energy quantities are commonly reported in the data:

(i) energy to time of peak power, E_{tm}, and
(ii) total energy, E_{tot}.

Given the considerations of the errors associated with the post-peak power measurements, the former is likely the more accurate of the two. The E_{tm} quantity was not reported for the Borax tests.

The energy data are associated with the same sources of error as the power measurements as it is determined primarily from an integration of the power time traces. Additional methods or measurement for the total energy are based on flux wire/foil irradiation and temperature rise calorimeter measurements. These latter two methods have been used to check the consistency of calibration curves and to estimate the uncertainty on the E_{tot} data.

For the integration-based energy measurements, the total random error due to data

processing is estimated as less than ± 5% for the B-core measurements (Ref. 3-22). Given that the measuring equipment and procedures were common throughout the Spert Project this random uncertainty is adopted for all E_{tm} data from all Spert cores:

$$\frac{\sigma_{E_{tm}}}{E_{tm}} \approx 5\%$$

With respect to the total energy, results using the integration- and calorimetric-based methods are found to agree within 10% for the Spert I A-, B- and P-cores (Ref. 3-14). The integration-based total energy data for the P-core are estimated as accurate within 5% while the estimated accuracy of the calorimetric-based results is 10%. As both agree within the experimental error, the estimated error of ± 5% on the integration-based results appears valid (Ref. 3-40). It is not clear whether these numbers are rough estimates based on the uncertainty of the power data or are derived from a more fundamental error analysis. The self-consistency of the E_{tm} data is expected to be even better than ± 5% given that these readings are free from the uncertainty in the post-peak power measurements, therefore the above uncertainty estimate is likely conservative.

No sources of systematic error are identified for either the E_{tm} or the E_{tot} data from the Spert Project. For the Borax tests the total energy was calculated from calibrated cobalt wire irradiations. This different measurement methodology and the larger uncertainties on the total core power require that a separate uncertainty should be estimated for the Borax E_{tot} data.

Reference 3-52 suggests that the uncertainty in the time of peak power may add a significant component to the random uncertainty. This additional source of error is not incorporated herein.

With reference to energy density (*ED*) values at the time of peak power, the uncertainty in these values are related to the E_{tm} data in the same manner that the uncertainties in the power density values are related to the P_{max} data. For the Spert data, the average energy density (ED_{avg}) values contain the same uncertainty as the E_{tm} data:

$$\left.\frac{\sigma_{ED_{avg}}}{ED_{avg}}\right|_{random} = \left.\frac{\sigma_{E_{tm}}}{E_{tm}}\right|_{random}$$
$$\approx 5\%$$
$$\left.\frac{\sigma_{ED_{avg}}}{ED_{avg}}\right|_{systematic} = \left.\frac{\sigma_{E_{tm}}}{E_{tm}}\right|_{systematic}$$
$$\approx 0\%$$

As for the power density values (see above), additional systematic uncertainty due to the uncertainty on the power density distribution estimates applies to the maximum energy density (ED_{max}) values:

$$\left.\frac{\sigma_{ED_{max}}}{ED_{max}}\right|_{random} = \left.\frac{\sigma_{E_{tm}}}{E_{tm}}\right|_{random}$$
$$\approx 5\%$$
$$\left.\frac{\sigma_{ED_{max}}}{ED_{max}}\right|_{systematic} = \left.\frac{\sigma_{E_{tm}}}{E_{tm}}\right|_{systematic}$$
$$\approx 20\%$$

Like for the power data, it should be noted that the systematic error with respect to the foil/wire flux distribution may have a common component for all the cores in which case the relative values of the maximum energy densities between Spert cores may be somewhat free of this error.

3.3.3.5 Temperature

3.3.3.5.1 Random Sources of Uncertainty

The temperature measurements are associated with the same sources of random error from the electronics and data reduction as the power measurements. In addition, the following sources of random uncertainty are specific to the temperature measurements:

(i) inherent uncertainty in thermocouples, and
(ii) physical changes to the materials over the range of temperature increase (*e.g.*, Ref. 3-33) including melting.

The Spert temperature data were obtained by adding the temperature change as measured by the thermocouples to the initial bulk temperature as measured by the thermopile consisting of an array of thermocouples in and about the core (Ref. 3-7). The same procedure is assumed for the Borax I data.

The uncertainty in the bulk initial reactor temperature is less than ± 1EC. As a result this uncertainty contribution to the T_{tm} and T_{max} data is negligible, especially in the short period range where changes in temperature are large. For some of the Borax I tests and the Spert I D-12/25 tests the initial temperature is not reported accurately for all tests. This leads to an uncertainty of a few degrees (likely no greater than ± 5 EC) in conversion of the reported T_{max} data to ΔT_{max} values.

The most probable error in absolute temperature attributed to the thermocouple response is reported as less than ± 1 EC (Ref. 3-53) for thermocouples used in the Spert I and IV D-cores. Factory calibration for chromel-alumel thermocouples used in the Spert I OC are reported as ± 2.2EC from 0EC to 270EC and ± 3/4% from 270EC to the upper limit of the thermocouple (Ref. 3-20). That due to the transfer of the signal from the detector to the recorder (*i.e.*, the electronics of the system) is reported as approximately 3% (Ref. 3-51).

Reference 3-7 reports that the data reduction process and the uncertainty in the initial reactor temperature contribute a gross random error of up to only ± 2EC on all temperature measurements. This translate to less than 1% random error on the largest temperature changes measured. For the Spert I D-12/25 measurements the uncertainty for the data conversion process is reported as less than 2% for most reported data (Ref. 3-53). A more conservative estimate of "less than 5%" is reported in Reference 3-22 with reference to the Spert I B-core data. This latter reference reports the components contributing to the data processing uncertainty in greater detail than the former reference, and is assumed applicable to all of the Spert data as well as similar to the data processing errors in the Borax data.

Peened thermocouples were introduced in the earlier Spert cores to solve a frequency response problem which resulted in lags in the temperature time traces for true surface thermocouples. This problem was minimized in the latter Spert cores (I & IV D-cores) by flattening the thermocouple junctions. The maximum time lag for a 2 msec transient in the Spert I D-core is estimated as less than 5% (Ref. 3-10). While of interest, the time lag does not necessarily impact on the change in temperature results. Any uncertainty in the T_{tm} and T_{max} data due to time lag is assumed negligible

in the reported temperature change data. The time-lag issue is more relevant to surface thermocouples on stainless-steel clad cores which experience a longer time lag (*e.g.*, Ref. 3-41, 3-54, 3-55).

The signals from peened thermocouples used in the Spert I A- and B-cores suffered from noise on the order of a few degrees centigrade (Ref. 3-27). While also contributing an insignificant uncertainty on temperature changes of a few hundred degrees, this noise did likely mask any fine structure in the temperature time traces from these thermocouples. The surface attached thermocouples used in the Spert I and IV D-cores are apparently free of this noise. For all test data this component of uncertainty is assumed negligible.

Some concern is also expressed over the reliability of the temperature measurements above 400EC due to invalidity of the standard calibration curves used in the data processing (Ref. 3-33). This is not elaborated on in the literature and is not obvious from the data so is not included as additional uncertainty in the temperature measurements. It is also not mentioned in reference to uncertainties in the temperatures measured in the Spert I OC destructive test series which were well above 400EC (Ref. 3-20).

The information available in the literature suggests that the maximum random uncertainty associated with temperature measurements is less than five percent. Most of this uncertainty is seemingly from the data processing. An overall total random uncertainty of ± 5% is adopted as a conservative estimate for the T_{max} (and ΔT_{max}) measurements, *i.e.*:

$$\frac{\sigma_{\Delta T_{max}}}{\Delta T_{max}}\Big|_{random} \approx 5\%$$

Corrections due to differences in subcooling are left as future work. These may help account for the larger variance in the Spert I A-core data compared to the other data sets. Systematic errors are discussed in the following section.

3.3.3.5.2 Systematic Sources of Uncertainty

Some important sources of systematic error exist in the measured temperature data. In relation to the peak surface temperature in the core, the systematic errors are due to the thermocouple location relative to the hottest position in the core. Potentially,

the following components all contribute to this systematic error:

(i) axial position,
(ii) radial position,
(iii) peening depth, and
(iv) peening *vs.* surface

The magnitude of these systematic errors are specific to the exact thermocouple and therefore treatment of these uncertainties is best done for each specific data set individually. In a general sense each of these components are discussed below.

An example of the variation of the measurement with thermocouple location in the axial temperature gradient is reported in Reference 3-7 for tests on the Spert I A-17/28 core. The presence of the control rods/blades near the top of the reactor result in the axial flux peak being offset slightly below the axial centerline of the fuel. Typically the thermal flux peak is on the order of 3" below the centerline for standard height (24" = 60 cm) MTR-type fuel. As a result, many of the "maximum" temperatures recorded for some of the data sets (*e.g.*, Borax I, Spert I A- and B-cores) from thermocouples located at the axial centerline of the fuel represent slightly lower temperatures than the true maximum. The difference is likely within 10% of the true maximum fuel surface temperature on the specific plate. Later in the Spert project, thermocouples were located at 3" and 4" below the axial centerline (Spert I and IV D-cores). These temperature measurements are closer to the true maximum temperature in the core of the test in question.

Temperature in the core also varies with radial position, both in different assemblies in the core grid, and within any given assembly. The location of a thermocouple relative to the radial and local power density peak results in systematic error with respect to maximum core temperature measurements. All of the test fuel assembly designs have uniform plate spacing within an assembly and roughly between adjacent assemblies. In this sense the local variation in power density is minimized. Some local differences may exist due to position relative to control and transient rod/blade gaps and simply from core flux/power-density shape. This systematic error should be assessed on an individual thermocouple basis but radial uncertainties due to local variations are expected to be within 10%.

The thermocouple location is defined in terms of assembly, plate and axial location so systematic errors can be estimated for both the axial and radial positions.

A third source of systematic error exists due to the attachment method of the thermocouples due to the temperature gradient existing within a fuel plate. Measurements from deeply buried thermocouples (located near the centre of the fuel plate) in the Spert I D-12/25 destructive test series are consistently 10-25% higher than measurements from surface welded thermocouples (Ref. 3-33). An example of the effect is shown in Figure 3-41. The difference between deeply-buried and shallow-depth thermocouples was investigated as part of the Spert Project (Ref. 3-51). For periods down to 14 msec the peened thermocouples of different depth agreed within experimental error (3%). In comparison to surface thermocouples, the peened thermocouples consistently read higher. The systematic error between peened and surface thermocouple measurements is therefore between 10-25%.

One further systematic error exists when comparing data from tests conducted with "approximately" the same initial core temperature. One example of this is the "ambient" temperature data set. The variation of T_i introduces a further variation due to the initial degree of subcooling. In all cases the variations in T_i do represent small changes in subcooling for each test which can be considered as contributing to differences in the ΔT_{max} data (see Chapter 4). The range or uncertainty in the various ambient temperature tests data sets are (see experimental data):

- Borax: T_i between 27 and 28EC
- Spert I A-17/28: T_i between 15 and 31EC
- Spert I B-16/40: T_i between 19 and 22EC
- Spert I B-24/32: T_i between 20 and 27EC
- Spert I B-12/64: T_i between 20 and 21EC
- Spert I D-12/25: T_i stated as ~ 15EC but not explicitly reported.
- Spert IV D-12/25: T_i between 19.8 and 22.4EC

The variation in T_i for the Spert I A-17/28 data is broad (16EC) representing a notable change in subcooling. Variation due to changes in subcooling also apply to the power and energy data and have not been included in the uncertainty estimates herein but can be added to the parametric analysis (see Chapter 4) as further work.

3.3.3.6 Reactivity

Although not considered as a primary quantity, reactivity is included in some of the transient summary data tables. As reactivity values are more directly applicable to reactor operation the uncertainty in the reported values are considered herein.

The inserted reactivity is estimated either from a change in position of the calibrated control and transient rods, or calculated from the measured asymptotic reactor period using the Inhour relation. In the former case uncertainties in the rod position and the rod worth contribute to the uncertainty in the reactivity value while in the latter case uncertainties in the period and the various kinetic parameters used in the Inhour relation must be considered.

The uncertainty in the control and transient rod positions prior to ejection/withdrawal (see Fig. 3-35) have been reported: within 0.01 inch for Spert I A (Ref. 3-7) and Spert III C, and within 0.02 inches for Spert I D (Ref. 3-8). Typically, the transient rod was worth on the order of about 30 mk and had a length comparable to that of the fuel, *i.e.*, 24". Considering a maximum differential worth of 2 mk/inch this translates into an uncertainty of no more than 0.04 mk which is less than 1% of a reactivity insertion of 7 mk or more (the range of primary interest in this work).

The total and compensating reactivity during a transient was often calculated from the power history data. While the accuracy of the total net reactivity is related to that of the power data, care should be taken in using the reported reactivity once separated into components since this assumes accurate knowledge of all feedback mechanisms, the associated feedback coefficients, and flux, temperature and density distributions. All of these factors may contribute some degree of uncertainty to the results. It is therefore the author's recommendation that the reported compensating reactivity results, when broken into components, are only used in a qualitative manner.

3.3.3.7 Pressure

The measured pressure is subject to variation due to position of the transducers in relation to the core. Since this is not standardized the pressure results should be primarily treated as qualitative.

3.3.4 Tests *vs.* Event Scenarios

A couple of points are worth making when putting the test data into the context of safety analysis scenarios.

The step test data are applicable to fast reactivity insertion situations such as rapid removal or insertion of samples, rapid removal of control devices, or the fuel loading accident in which a fuel assembly is dropped into a vacant core position. What should be considered when applying the test data is the rate of insertion in the event

under consideration. Simulation work (Ref. 3-56) indicates that reactivity limits are sensitive to insertion times greater than about 250 msec for HEU fuel and about 150 msec for LEU fuel, increasing significantly with insertion duration. This is shown in Figure 3-42.

To put this into context of the reactor tests, the total transient rod ejection times for some of the test cores are reported below:

- Borax I: < 250 msec (Ref. 3-12)
- Spert I A-17/28: 80 to 100 msec (Ref. 3-57)
- Spert I B-cores: 150 msec (average) (Ref. 3-57)

As a result, safety limits derived from the step data may be conservative with respect to specific fast scenarios.

This is illustrated by consideration of the MNR January 1994 fuelling incident (Ref. 3-58) which resulted in an estimated +7.87 mk excess reactivity. Considered as a step insertion this magnitude insertion would produce a minimum (asymptotic) period of about 50 msec ($\alpha_o = 20$ sec^{-1}). However, in the actual event the reactivity insertion of 24.8 mk (into a subcritical core) is estimated to have taken 20 seconds which produces a longer minimum period. In this case a step insertion is conservative with respect to the actual insertion.

It should be noted that the MNR January 1994 fuelling incident was a protected transient so the generated power, energy, and temperatures are significantly below those which would have occurred in an unprotected situation (compare $P_{max} = 8.61$ MW, E_{tot} ($> E_{tm}$) = 1.23 MW-sec, $\Delta T_{max} \sim 60$EC to the test data plotted in Chapter 4 and Appendix C for $\alpha_o = 20$ msec). It should also be noted that this conservative step insertion period is longer than those considered in the short period range of the test data and therefore the methodology presented in Chapter 7 is not directly applicable.

The ramp insertion test data are directly applicable to slower insertion safety analysis scenarios such as flooding of a void space by leakage or the common startup transient in which the shim rods are motor withdrawn from the core beyond limits.

While ramp insertion rates may be comparable to the specific safety analysis scenario what does need considering is the longer term stability of the system. This is often not included in event analysis. Experience with the test reactors shows that longer term power and temperature oscillations are typical when a large amount of

compensating reactivity is held in voids. Chugging type response may prove to be the limiting stage of a transient rather than the initial power pulse (small or non-existent for slow ramps). This means that scenarios initially assessed as benign based on the initial power pulse may in fact turn out to be of serious consequence due to longer term instabilities or oscillatory behaviour.

In summary, when examining and applying the results of the reactor tests to specific SAR scenarios, physical limitations of the system should be considered in comparison to the test data and physics of self-limiting behaviour. For example, in the fuel loading accident, the total worth and terminal velocity of a free-falling fuel assembly in light water put limits on the reactivity insertion size and speed. For the startup accident, the excess reactivity of the core and the motor speed of the control rods similarly limits the initiating ramp and the amount of reactivity available to be returned to the system *via* chugging.

3.3.5 Limitations

Overall the reactor test data set is extensive, provides a wealth of information on characteristic behaviour and parameter sensitivities, and has been impressively collected and reported. Some limitations, however, have become evident while compiling and working with the data set. These are briefly outlined below.

For some of the test series there has been a failure to report the specific initial conditions of each test. For example, the initial temperature for the majority of the Borax I subcooled step tests is only available as "between 19-28EC". Given the sensitivity to the degree of subcooling, this introduces notable uncertainty in the data. Similarly, the initial temperature for the Spert I D-core step test series is only known approximately. While reported, the initial temperature for the Spert I A-core step tests from subcooled conditions was not tightly controlled and was allowed to vary from 13-39EC over the series. In addition, the height of the hydrostatic head is not explicitly stated for most of the test series but is assumed herein to be kept consistent for each core.

Another limitation has to do with the temperature data. These data are noted as being the maximum recorded temperatures for each transient test. It is found that commonly this maximum temperature is recorded from a number of different thermocouples for different tests in the same test series, varying not only by axially location in some cases but also by individual plate and even assembly in other cases. It is unclear whether this is the result of a real physical characteristic of the void

shutdown process, possibly related to the nature of local boiling and dryout fluctuations, or whether this is simply due to the loss of data during the recording or data processing stages, or as a result of thermocouple failure during certain tests. The work herein assumes that the variation in thermocouple position associated with the maximum recorded temperatures is due to the loss of data and that the temperature distribution is proportional to the thermal flux distribution, *i.e.*, hottest at the flux peak. Consideration of data from a single thermocouple significantly reduces the size of the data subset available for quantitative analysis. In comparison, consideration of the entire temperature data subset from various thermocouples would introduce a much larger apparent uncertainty in the measurements. In any event, it is also difficult to compare different thermocouples attached by the peening method due to the significant systematic error associated with the peening depth.

In addition to these points, the temperature data are also limited in some cases by incomplete or ambiguous thermocouple location notation. This is the case for the Spert I A-core step data from ambient conditions where the plate associated with the thermocouple was not recorded for the first part of the test series. This introduces an uncertainty in the data related to local plate-to-plate power/temperature distribution. Similarly, the plate number designation for the Type-B removable plate fuel is unclear as to whether it is based on the plate location with respect to the side plate groove or the total number of plates in the specific B-fuel configuration.

Further limitations are related to incomplete or missing data subsets. Specifically, the subcooling subset from the Spert I B-cores is limited in that only a few data points (if that) exist over the entire short period range for each of the different temperatures investigated. The Borax subcooling data set is also limited in that it is for two discrete periods only.

Incomplete testing also hampers the stability data subset. In general, from a research standpoint tests were terminated too soon, prior to the development of long term behaviour, be it steady state boiling, steady non-boiling, or chugging oscillations. The chugging data set is mainly for the onset of chugging stage while fully developed chugging was not typically investigated. In the cases in which chugging was observed in the Spert I A-core tests, the accompanying temperature data have not been reported (or at least has not been located). The dependence of the power/temperature oscillations on magnitude of reactivity and other initial conditions was not fully studied. It is also of note, and has already been stated, that the nature of some of the stability tests (particularly the Spert I A-core tests) was such that reproducibility was questionable and as a result the data should be used mainly in a

qualitative manner.

Finally, gaps do exist in the data set with respect to LEU plate fuel testing, and testing from high initial power and under forced downward coolant flow conditions. All of these variables are relevant to modern MTR-type core operation.

3.4 References

3-1. J. E. Grund, "Self-Limiting Excursion Tests of a Highly Enriched, Plate-Type D_2O-Moderated Reactor: Part I. Initial Test Series", US AEC Technical Report IDO-16891, Phillips Petroleum Co., July 1963.

3-2. R. L. Johnson, J. E. Grund, "Self-Limiting Excursion Tests of a Highly Enriched, Plate-Type D_2O-Moderated Reactor: Part II. Effect of System Pressure", US AEC Technical Report IDO-16974, Phillips Petroleum Co., May 1964.

3-3. J. A. McClure, R. L. Johnson, "Critical Loading and Initial Static Experiments in the Spert II Reactor with a Close-Packed D_2O-Moderated Core", US AEC Technical Report IDO-16996, Phillips Petroleum Co., June 1964.

3-4. R. L. Johnson, *et al.*, "An Analysis of the Excursion Behavior of a Highly Enriched Plate-Type D_2O-Moderated Core in Spert II", US AEC Technical Report IDO-17109, Phillips Petroleum Co., September 1965.

3-5. G. O. Bright, editor, "Quarterly Progress Report - July, August, September, 1957 - Reactor Projects Branch", US AEC Technical Report IDO-16416, Phillips Petroleum Co., October 1, 1957.

3-6. A. P. Wing, "Transient Tests of the Fully Enriched, Stainless Steel Plate-Type, P Core in the Spert I Reactor: Data Summary Report", US AEC Technical Report IDO-17011, Phillips Petroleum Co., December 1964.

3-7. J. C. Haire, "Subcooled Transient Tests in the Spert I Reactor - Experimental Data", US AEC Technical Report IDO-16342, Phillips Petroleum Co., July 1, 1958.

3-8. J. R. Dietrich, D. C. Layman, "Transient and Steady State Characteristics of a Boiling Reactor. The Borax Experiments, 1953", ANL-5211 (also listed as AECD-3840), Argonne National Laboratory, USA, February 1954.

3-9. F. L. Bentzen, "Spert-I Instrumentation", US AEC Technical Report IDO-16316, Phillips Petroleum Co., March 15, 1957.

3-10. A. H. Spano, R. W. Miller, "Spert I Destructive Test Program Safety Analysis Report", US AEC Technical Report IDO-16790, Phillips Petroleum Co., June 15, 1962.

3-11. F. Schroeder, editor, "Quarterly Technical Report - Spert Project - October, November, December, 1962", US AEC Technical Report IDO-16890, Phillips Petroleum Co., May 17, 1963.

3-12. J. R. Dietrich, "Experimental Investigation of the Self-Limitation of Power During Reactivity Transients in a Subcooled, Water-Moderated Reactor. Borax-I Experiments, 1954", ANL-5323, (also listed as AECD-3668), Argonne National Laboratory, USA, 1954.

3-13. G. F. Brockett, E. Feinauer, "Summary Data Report for Spert Transient Pressure Measurements in the Interval 1955-1961", US AEC Technical Report IDO-16930, Phillips Petroleum Co., April 15, 1964.

3-14. S. G. Forbes, F. L. Bentzen, P. French, J. E. Grund, J. C. Haire, W. E. Nyer, and R. F. Walker, "Analysis of Self-Shutdown Behavior in the Spert I Reactor", US AEC Technical Report IDO-16528, Phillips Petroleum Co., July 23, 1959.

3-15. L. A. Stephan, "Transient Tests of the BSR-II Core in the Spert I Facility", US AEC Technical Report IDO-16768, Phillips Petroleum Co., April 1963.

3-16. W. E. Nyer, S. G. Forbes, F. L. Bentzen, G. O. Bright, F. Schroeder, T. R. Wilson, "Experimental Investigations of Reactor Transients", US AEC Technical Report IDO-16285, Phillips Petroleum Co., April 20, 1956.

3-17. G. O. Bright, editor, "Quarterly Progress Report - April, May, June, 1958 - Reactor Projects Branch", US AEC Technical Report IDO-16489, Phillips Petroleum Co., January 19, 1959.

3-18. F. Schroeder, editor, "Quarterly Technical Report - Spert Project - January, February, March, 1961", US AEC Technical Report IDO-16693, Phillips Petroleum Co., June 30, 1961.

3-19. A. H. Spano, J. E. Barry, L. A. Stephan, J. C. Young, "Self-Limiting Power Excursion Tests of a Water-Moderated Low-Enrichment UO_2 Core in Spert I", US AEC Technical Report IDO-16751, Phillips Petroleum Co., February

28, 1962.

3-20. J. E. Grund, editor, "Experimental Results of Potentially Destructive Reactivity Additions to an Oxide Core", US AEC Technical Report IDO-17028, Phillips Petroleum Co., December 1964.

3-21. W. J. Neal, C. R. Toole, "Ramp Induced Power Excursion Tests in Spert III at Room Temperature", Transactions of the ANS, v.4, n.1, pp.72-73, June 1961.

3-22. A. P. Wing, "Transient Tests of the Fully Enriched, Aluminum Plate-Type B Cores in the Spert I Reactor: Data Summary Report", US AEC Technical Report IDO-16964, Phillips Petroleum Co., June 1964.

3-23. W. E. Nyer, S. G. Forbes, "SPERT I Reactor Safety Studies," Paper P/2428, Proceedings of the Second United Nations International Conference on the Peaceful Uses of Atomic Energy, v. 11, pp. 470-480, Geneva, September 1958.

3-24. F. Schroeder, "Stability Tests with the Spert-I Reactor", US AEC Technical Report IDO-16383, Phillips Petroleum Co., July 1, 1957.

3-25. J. R. Dietrich, "Experimental Determinations of the Self-Regulation and Safety of Operating Water-Moderated Reactors", in the Proceedings from the First International Conference on the Peaceful Uses of Atomic Energy, Geneva, 1955, Argonne National Laboratory, v. 13, pp. 88-101.

3-26. W. E. Nyer, S. G. Forbes, "Spert Program Review", US AEC Technical Report IDO-16634, Phillips Petroleum Co., October 19, 1960.

3-27. G. O. Bright, editor, "Quarterly Progress Report - January, February, March, 1958 - Reactor Projects Branch", US AEC Technical Report IDO-16452, Phillips Petroleum Co., September 10, 1958.

3-28. J. Dugone, D. D. Weiland, "Fuel Plate Experience During the Spert I Destructive Test Series with an Aluminum-Clad, Plate-Type Core", US AEC Technical Report IDO-16885, Phillips Petroleum Co., July 1963.

3-29. F. Schroeder, editor, "Quarterly Technical Report - Spert Project - April, May, June, 1962", US AEC Technical Report IDO-16806, Phillips Petroleum

Co., September 21, 1962.

3-30. F. Schroeder, editor, "Quarterly Technical Report - Spert Project - July, August, September, 1962", US AEC Technical Report IDO-16829, Phillips Petroleum Co., February 28, 1963.

3-31. F. Schroeder, editor, "Quarterly Technical Report - Spert Project - January, February, March, 1963", US AEC Technical Report IDO-16893, Phillips Petroleum Co., May 20, 1963.

3-32. R. W. Miller, Alain Sola, R. K. McCardell, "Report of the Spert I Destructive Test Program on an Aluminum, Plate-Type, Water-Moderated Reactor", US AEC Technical Report IDO-16883, Phillips Petroleum Co., June 1964.

3-33. J. E. Houghtaling, Alain Sola, A. H. Spano, "Transient Temperature Distributions in the Spert I D-12/25 Fuel Plates During Short-Period Power Excursions", US AEC Technical Report IDO-16884, Phillips Petroleum Co., June 1964.

3-34. F. Schroeder, editor, "Quarterly Technical Report - Spert Project - April, May, June, 1963", US AEC Technical Report IDO-16920, Phillips Petroleum Co., September 20, 1963.

3-35. A. H. Spano, editor, "Quarterly Technical Report - Spert Project - July, August, September, 1963", US AEC Technical Report IDO-16931, Phillips Petroleum Co., April 1964.

3-36. J. G. Crocker, L. A. Stephan, "Reactor Power Excursion Tests in the Spert IV Facility", US AEC Technical Report IDO-17000, Phillips Petroleum Co., August 1964.

3-37. SL-1 Project, "Final Report of SL-1 Recovery Operation", US AEC Technical Report IDO-19311, General Electric Company, July 27, 1962.

3-38. Flight Propulsion Laboratory Department, "Additional Analysis of the SL-1 Excursion", US AEC Technical Report IDO-19313, General Electric Company, November 21, 1962.

3-39. R. E. Heffner, "Damage to Stainless Steel Fuel in Spert Reactors", US AEC Technical Report IDO-16729, Phillips Petroleum Co., November 21, 1961.

3-40. F. L. Bentzen, editor, "Quarterly Progress Report - October, November, December, 1958 - Reactor Projects Branch", US AEC Technical Report IDO-16537, Phillips Petroleum Co., September 1, 1959.

3-41. J. A. Norberg, editor, "Quarterly Progress Report - January, February, March, 1959 - Reactor Projects Branch", US AEC Technical Report IDO-16539, Phillips Petroleum Co., November 20, 1959.

3-42. A. H. Spano, editor, "Quarterly Technical Report - Spert Project - July, August, September, 1959", US AEC Technical Report IDO-16606, Phillips Petroleum Co., July 11, 1960.

3-43. F. Schroeder, editor, "Quarterly Technical Report - Spert Project - October, November, December, 1960", US AEC Technical Report IDO-16687, Phillips Petroleum Co., June 1, 1961.

3-44. F. Schroeder, editor, "Quarterly Technical Report - Spert Project - July, August, September, 1961", US AEC Technical Report IDO-16729, Phillips Petroleum Co., December 15, 1961.

3-45. J. Dugone, D. D. Weiland, "Fuel Plate Experience During the Spert I Destructive Test Series with a Stainless Steel Clad, Rod-Type Core", US AEC Technical Report IDO-17048, Phillips Petroleum Co., March 1965.

3-46. Capt. A. Nelson Tardiff, "Some Aspects of the WTR and SL-1 Accidents", US AEC Technical Report IDO-19308, April 9, 1962.

3-47. F. R. Keller, "Fuel Element Flow Blockage in the Engineering Test Reactor", US AEC Technical Report IDO-16780, Phillips Petroleum Co., May 10, 1962.

3-48. S. E. Day, "Power-Peaking Factors in MNR", McMaster Nuclear Reactor Technical Note MNR-TN-010705, McMaster University, Hamilton, Ontario, Canada, July 5, 2001.

3-49. H. L. McMurray, "Temperature Distribution in a Fuel Plate with Exponentially Rising Power - Part I - Theoretical", US AEC Technical Report IDO-16214, Phillips Petroleum Co., March 25, 1955.

3-50. H. L. McMurray, A. V. Grimaud, “Temperature Distribution in a Fuel Plate with Exponentially Rising Power - Part II - Results Based on Asymptotic Solutions”, US AEC Technical Report IDO-16311, Phillips Petroleum Co., January 5, 1955.

3-51. F. Schroeder, editor, “Quarterly Technical Report - Spert Project - October, November, December, 1959", US AEC Technical Report IDO-16616, Phillips Petroleum Co., August 24, 1960.

3-52. T. G. Taxelius, editor, “Quarterly Technical Report - Spert Project - April, May, June, 1967", US AEC Technical Report IDO-17270, Phillips Petroleum Co., June 1968.

3-53. M. R. Zeissler, “Non-Dectructive and Destructive Transient Tests of the Spert I-D, Fully Enriched, Aluminum-Plate-Type Core: Data Summary Report”, US AEC Technical Report IDO-16886, Phillips Petroleum Co., November 1963.

3-54. J. G. Crocker, editor, “Quarterly Technical Report - Spert Project - January, February, March, 1965", US AEC Technical Report IDO-17097, Phillips Petroleum Co., July 1965.

3-55. R. Scott, Jr., C. L. Hale, R. N. Hagen, “Transient Tests of the Fully Enriched Uranium-Oxide Stainless Steel Plate-Type C-Core in the Spert III Reactor: Data Summary Report”, US AEC Technical Report IDO-17223, Phillips Petroleum Co., February 1967.

3-56. W. L. Woodruff, “The PARET Code and the Analysis of the SPERT I Transients”, Argonne National Laboratory Technical Report ANL/RERTR/TM-4, pp. 560-579, from the Proceedings of the International Meeting on Research and Test Reactor Core Conversion from HEU to LEU Fuels, 1982.

3-57. T. R. Wilson, “An Engineering Description of the Spert-I Reactor Facility”, US AEC Technical Report IDO-16318, Phillips Petroleum Co., June 14, 1957.

3-58. M. P. Butler, “Final Report on the January 1994 Fuelling Incident”, McMaster Nuclear Reactor Technical Report MNR-TR-1997-03, McMaster University, Hamilton, Canada, April 28, 1997.

3.5 Tables

Table 3-1: Listing of Test Cores

System	Fuel Type	Enrichment	Cladding Material	Main Objective in Test Program
Borax I	plate	HEU	Al	general characteristics
Spert I A	plate	HEU	Al	general characteristics
Spert I B	plate	HEU	Al	void reactivity
Spert I P	plate	HEU	SS	cladding material
Spert I BSR-II	plate	HEU	SS	inherent v mechanical shutdown
Spert I SA	rod	LEU	SS	power reactor fuel
Spert I D	plate	HEU	Al	destructive testing
Spert I OC	rod	LEU	SS	destructive testing
Spert III C	plate	HEU	SS	power reactor conditions
Spert III E	rod	LEU	SS	power reactor conditions
Spert IV D	plate	HEU	Al	stability & coolant flow
SL-1	plate	HEU	Al	operating reactor
IAEA benchmark	plate	HEU/LEU	Al	simulation problem

2/20/04, 2:43 PM Test Core List PhD_SE-Day_reactor-expt-summary.xls

Table 3-2: Aluminum-Clad Plate-Type Cores Step Test Summary

System	Test Series	Varied Parameters	Reference
Borax I	from saturation	period = 70 msec to 5 msec	ANL-5211
	variation of subcooling	Tsub = 69C to 0C	
	from ambient temperatures (including D-test)	period = 134 msec to 2.6 msec	ANL-5323
Spert I A-17/28	from subcooled temperatures	period = 10 sec to 7 msec Ti = 39C to 12C	IDO-16342 IDO-16551
	from saturation	period = 2.2 sec to 5.2 msec	IDO-16537
	miscellaneous	hydrostatic head = 2' and 9' additives in moderator initial power level	IDO-16551
Spert I B-24/32	from ambient temperatures	period = 13.2 sec to 10.8 msec	IDO-16964
	intermediate subcooling	period = 11.1 sec to 9.2 msec Ti = 40C, 60C, 80C	
	from saturation	period = 10.6 sec to 22.4 msec	
	low flow tests	variation of period with low flow	IDO-16512
Spert I B-16/40	from ambient temperatures	period = 9.6 sec to 13.6 msec	IDO-16964
	intermediate subcooling	period = 8.5 sec to 17.5 msec Ti = 50C, 80C	
	from saturation	period = 3.04 sec to 15.0 msec	
Spert I B-12/64	from ambient temperatures	period = 9.2 sec to 9.4 msec	IDO-16964
	intermediate subcooling	Ti = 40C, 60C, 80C; period ~ 15 msec	
	from saturation	period = 9.07 sec to 11.4 msec	
Spert I D-12/25	from ambient temperatures	period = 1.3 sec to 6.5 msec	IDO-16883,
	damage tests (including D-test)	period = 5.0, 4.6, 3.2 msec	IDO-16886
Spert IV D-12/25	from ambient temperatures	period = 980 msec to 7.0 msec hydrostatic head = 18'	IDO-17000
	from ambient temperatures with reduced hydrostatic head	period = 21.3, 12.0, 8.8 msec hydrostatic head = 2'	
	from ambient temperatures with forced upward coolant flow	period = 560 msec to 9.7 msec flow = 5000 gpm to 500 gpm	

Note: all tests are performed from low power, atmospheric pressure and under natural circulation flow only unless otherwise indicated

2/20/04, 10:34 AM PhD_SE-Day_reactor-expt-summary.xls Step Insertions Al Cores

Table 3-3: Stainless-Steel-Clad Plate-Type Cores Step Test Summary

System	Test Series	Varied Parameters	Reference
Spert I P-18/19	from ambient temperatures	period = 6 sec to 5.0 msec	IDO-17011
	capsule tests	period = 61 msec to 6.2 msec	
	from saturation	period = 76 msec to 4.0 msec	
	refuelling accident	period = 415 msec to 7 msec (reactivity insertion = 0.89$ to 1.35$)	IDO-16606
Spert I BSR-II	from ambient temperatures (self-limiting)	period = 544 msec to 15 msec	IDO-16768
	from ambient temperatures (scram protected)	period = 3 msec various rod combinations and trips	
	from ambient temperatures (reverse protected)	period = 40 msec to 14 msec various trips	
Spert III C-19/52	from ambient conditions	period = 10 sec to 10 msec	IDO-17223
	subcooling	period = 20, 40, 150 msec	
	elevated temperature and pressure	pressure = atm to 2500 psig Ti = ambient to 324C flow = 0 to 20,000 gpm	
	high power tests	Pi = 10 W to 28 MW elevated Ti, Pressure and Flow	IDO-17138

Note: all tests are performed from low power, atmospheric pressure and under natural circulation flow only unless otherwise indicated

2/20/04, 10:28 AM PhD_SE-Day_reactor-expt-summary.xls Step Insertions SS Cores 1 / 1

Table 3-4: LEU Oxide Rod-Type Cores Step Test Summary

System	Test Series	Varied Parameters	Reference
Spert I SA	unconstrained	period = 15 sec to 3.2 msec	IDO-16751 IDO-16752
	constrained	period = 31 sec to 3.2 msec	Nucl. Sci. Eng., v.15, p.37, 1963
Spert I OC	check out test series (some tests ramp-step)	period = 1.3 sec to 9.8 msec	IDO-17028 IDO-16931
	potentially destructive tests (1.6 msec test ramp-step)	period = 2.2 msec, 1.6 msec	
Spert III E	check out	period = 1.9 sec to 10 msec	IDO-17260 IDO-17270
	elevated temperature & pressure, with forced flow	period = 600 msec to 10 msec temperature = 250, 400, 500 C pressure = 1500 psi flow (up) = 2.3 to 23 ft/sec	

Note: all tests are performed from low power, atmospheric pressure and under natural circulation flow only unless otherwise indicated

5/11/2004, 9:53 PM PhD_SE-Day_reactor-expt-summary.xls Step Insertions LEU Rod Cores 1 / 1

Table 3-5: Summary of Ramp Insertion Tests

Core	Test Series	Varied Parameters	Ref.	Notes
Spert I A-17/28	exploratory	ramp rate: 0.011% dk/sec, 0.1% dk/sec, 0.36% dk/sec Pi: 100 micro-W - 200 kW Ti = ambient, boiling	IDO-16285 IDO-16416	seven (7) transients power/period data is reported, results in figures summary of parameter ranges all tests from Ti=20C, atm pressure, nat. circ. flow only
Spert I B-12/64	exploratory	ramp rate: 0.01% dk/sec, 0.5 mW < Pi < 10 W ramp rate: 0.10% dk/sec, 5 mW < Pi < 10 kW ramp rate: 0.27% dk/sec, 1 mW < Pi < 10 kW	IDO-16489 IDO-16528	three (3) transients reported (only power, period data reported, in figure) Same qualitative results as from Spert I A tests Ti = 20C, hydro head 2' for all tests
Spert I BSR-II	startup transient	one test, scram protected	IDO-16640 IDO-16768	
Spert I SA	unconstrained constrained	ramp rate: 0.16, 1.4, 5.1, 13, 18, 21 c/sec ramp rate: 13.3, 18.3 c/sec	IDO-16751 IDO-16716 IDO-16726	reports all SA (6) and SA-C (2) ramp tests, no temperature or energy given six (6) tests from ambient, low power conditions, Pmax v a included (w step curve) two (2) tests from ambient, low power conditions, only minimum periods reported eight (8) tests in total reported
Spert I OC	part of d-test series	period: 970 to 57.8 msec	IDO-17028 IDO-17010	ten (10) tests, from ambient, low power, atm pressure, nat. circ. flow conditions data in summary table and correlated figures
Spert III C-19/52	ambient high temp/press/flow high power	ramp rate: 18c, 35c, 53c/sec 0.1W < Pi < 100 kW pressure: atm, 2500 psi flow: 0, 20 000 gpm (20 ft/sec) period: 180, 45 msec Pi: 0.85, 0.91, 24.5 MW	IDO-16693 IDO-17030 IDO-17138 IDO-17084	includes power, temperature trace comparisons to steps (no data table) two (2) tests from Ti=260C, pr=2500 psi, flow=20 ft/sec summary data reported three (3) tests from Ti=260C, pr=2500 psi, flow= 20 ft/sec, rho=$0.27 @ 5.3 c/sec summary data and time traces of P, T given

Note: all tests are from ambient, low power, atmospheric pressure conditions with natural circulation flow only, unless otherwise stated
Note: apparently there were no ramp tests conducted in Spert I B-24/32, B-16/40 (IDO-16528), P-18/19 (IDO-17011), D-12/25; Spert III E cores
Note: reactivity was added as ramps in Spert IV D-core stability tests,but reported data is on post-power peak behaviour
4:56 PM, 5/16/2004 PhD_SE-Day_reactor-expt-summary.xls Ramp Test Summary 1 / 1

Table 3-6: Summary of Stability Tests

System	flow	water head (feet)	pool temp (Celsius)	reactivity (mk) unless noted initial	reactivity (mk) unless noted refill	power (MW) max	power (MW) avg	min. period (msec)	frequency (cps)	duration of test	Notes
Borax-I	nat.	3 to 4.5	sat.	26	~ 12	57	2	17	~ 1	5 to 20 sec	boiling test, long duration of reactivity addition, Fig. 56 ANL-5211, more extreme step insertion tests with duration of 20 sec had Pmax > 60 MW
	nat.	3 to 4.5	sat.	--	--	11	--	--	~ 1	~ 20 sec	from step tests for period < 30 msec chugging peaks smaller than Pmax on initial pulse (34 Mw), ANL-5211 Fig. 31 (best), and also Fig. 10 Geneva 1955 paper
Spert I A	nat.	2	amb.	27.5	--	<= 200	--	--	2	sustained oscillations	negative reactivity added ramp style @ ~ 0.9 mk/sec, water permanently lost from system during tests
	nat.	2	sat.	15	--	<= 50	--	--	1	~ 75 sec	Fig. 2 IDO-16383 (test no. 4304)
	nat.	9	~ 26	27.5	--	<= 2300	--	3	2		this test not allowed to fully develop into envelope, Figs. 4 & 5 IDO-16383 (test no. 4739)
	nat.	9	sat.	15	--	<= 150	--	--	1	~ 50 sec	Fig. 3 IDO-16383 (test no. 4300)
	nat.	2	sub.	25		38	6				reported in IDO-16489, p.20
Spert I B-12/64	nat.	2	sub.	15	--	85	19	--	1.79	> 40 sec	ramp insertions of 0.7 mk/sec from low power, oscillations lasted for 30 seconds before test ended, see IDO-16489, p.20
	nat.	2	sat.			1.1	boil			10 sec	post peak chugging in step tests from 5W power, see IDO-16964, App. C, Fig. 23, both temperature data and power plotted
	nat.	2	sat.			1	small			20 sec	noise to oscillation transition, IDO-16964, Fig. 24
	nat.	2	sat.			1.5	1.7		1	10 sec	small oscillations, IDO-16964, Fig. 25
	nat.	2	sat.			4	8		1	10 sec	developing oscillations at time of scram, IDO-16964, Fig. 26
	nat.	2	sat.			10	20		1	15 sec	chugging, IDO-16964, Fig. 27
Spert IV D	nat.	18	amb.	$4.2	~ $2.1	onset	~ 7.5	--	~ 3	min to hours	threshold tests, reactivity insertion very slow as series of steps with
											of mean power, plate temp not permitted to exceed 300C, system bulk temperature increased during tests to ~ 35C, Ref. IDO-16992, p.28
	nat.	2	amb.	$4.1	~ $2.1	onset	3 to 5	--	~ 2	min to hours	Ref. IDO-16992, bulk temperature had risen to ~ 70C during test
	upward	18	amb.	$4.1	--	small		--		min to hours	test scrammed as plate temperature > 300C for narrow channels, Ref. IDO-16992
	nat.	18	amb.	$5.0	--	small		--		short	chugging tests, reactivity inserted via ramp insertion ~ 0.9 mk/sec, faster than threshold tests, Ref. IDO-17055
	nat.	2	amb.	$5.0	--	small		--		short	ref. IDO-17055
	nat.	2	~ 70	$4.0	--	onset		48 to 24	~ 2	12.5 min	Test SS89, system allowed to heat up gradually from initially 22C, onset of chugging observed once bulk temp reached ~ 70C, Figs. 27 & 28 IDO-17055

2:25 PM, 2/20/04 PhD_SE-Day_reactor-expt-summary.xls Stability Tests Summary

Table 3-7: Instrumentation Summary for Test Cores

System	Power Detectors	Fuel Temperature Detectors	Other Instrumentation	Reference
Borax I	B-10 ion chambers 3 log for transients 1 lin. for operation	3-mil chromel-alumel TCs welded to clad surface 3-mil chromel-alumel TCs welded to meat and plug filled	pressure transducers in- and out-of-core wires photographic microphone TCs in reflector radiation monitors	ANL-5211, ANL-5323
Spert I A-17/28	B-10 ion chambers log for short period tests lin. for long period tests	10-mil chromel-alumel TCs peened into clad	pressure transducers photographic copper-constantan TCs in reflector radiation monitors	IDO-16342
Spert I B-Cores	Same as Spert I A	same as Spert I A but improved contact via aluminization of wires	same as Spert I A	IDO-16437, IDO-16964
Spert I P-18/19	B-10 ion chambers lin. for all transient data	10-mil chromel-alumel TCs spot welded to clad surface	same as Spert I A general instrument overhaul	IDO-17011, IDO-16489
Spert I BSR-II	assumed same as P-core	assumed same as P-core	assumed same as P-core	IDO-16768
Spert I SA	B-10 ion chambers lin. for all transient data	5-mil chromel-alumel welded to pin surface internal TC's gave erratic readings	same as Spert I A good results from in-core high-speed motion pictures	IDO-16752
Spert I D-12/25	B-10 ion chambers lin. for all transient data mini-ion chambers semirad chambers	5-mil chromel-alumel TCs flattened to 0.5-mil multi-junction welded to clad surface 5-mil chromel-alumel TCs peened into clad to depth of 30-mils	same as Spert I A plus: flow meters in-core wires strain gages accelerometers	IDO-16790, IDO-16886
Spert I OC	B-10 ion chambers lin. for all transient data semi-rad chambers	10-mil chromel-alumel TCs flattened to 3-mil welded to clad surface fuel cell TCs in development stage	same as Spert I A plus: strain gauges accelerometers air pressure microphone	IDO-17028
Spert III C	B-10 ion chambers (assume lin. Amplification for all transient data)	5-mil chromel-alumel TCs welded to clad surface 3-mil chromel-alumel TCs SS-sheathed welded to clad surface (used in high Temp. tests)	similar to Spert I including: pressure transducers in-core Co-wires TCs embedded in vessel wall flow meters	IDO-17223
Spert III E	assume same as Spert III C	assume same as Spert I SA/OC	assume same as Spert III C	
Spert IV D-12/25	B-10 ion chambers mini-B-10 ion chambers mini-fission chambers semi-rad chambers	10-mil chromel-alumel TCs flattened to 3-mil multi-junction welded to clad surface water-channel TCs chromel-alumel single-junction	similar to Spert I including: pressure transducers flow meters photographic equipment radiation monitors	IDO-17000, IDO-17088

Notes: TC stands for thermocouple
lin./log refers to linear/logarithmic amplification of signal

2/20/04, 1:10 PM Instrumentation Summary PhD_SE-Day_reactor-expt-summary.xls

Table 3-8: Uncertainty Estimates for the Experimental Test Data

	Borax I	Spert I A-17/28	Spert I B-24/32	Spert I B-16/40	Spert I B-12/64	Spert I D-12/25	Spert IV D-12/25
RANDOM ERROR							
Pmax							
total random	8%	5%	5%	5%	5%	5%	5%
Pmax/Vf							
total random	8%	5%	5%	5%	5%	5%	5%
Pmax/Vf x PPF							
total random	8%	5%	5%	5%	5%	5%	5%
Asymptotic Period							
total random	5%	5%	5%	5%	5%	5%	5%
Reciprocal Period							
total random	5%	5%	5%	5%	5%	5%	5%
Etm							
total random	-	5%	5%	5%	5%	5%	5%
Etm/Vf							
total random	-	5%	5%	5%	5%	5%	5%
Etm/Vf x PPF							
total random	-	5%	5%	5%	5%	5%	5%
DTm & DTmax							
total random	5%	5%	5%	5%	5%	5%	5%
SYSTEMATIC ERROR							
Pmax							
total systematic	21%	0%	0%	0%	0%	0%	0%
Pmax/Vf							
total systematic	21%	0%	0%	0%	0%	0%	0%
Pmax/Vf x PPF							
total systematic	5%	20%	20%	20%	20%	20%	20%
Asymptotic Period							
total systematic	0%	0%	0%	0%	0%	0%	0%
Reciprocal Period							
total systematic	0%	0%	0%	0%	0%	0%	0%
Etm							
total systematic	-	0%	0%	0%	0%	0%	0%
Etm/Vf							
total systematic	-	0%	0%	0%	0%	0%	0%
Etm/Vf x PPF							
total systematic	-	20%	20%	20%	20%	20%	20%
DTm & DTmax							
total systematic	-10%	0%	0%	0%	0%	-5%	-5%
TC location	21-4-s	55+0; 55-172+0	55 01B +0	55 03B +0	55 01B +0	E5 7W -3	E5 7W -3
peening	-	10%	10%	10%	10%	-	-
axial location	-5%	-5%	-5%	-5%	-5%	-5%	-5%
radial location	-5%	-5%	-5%	-5%	-5%	0%	0%

Note: Error estimates are given as the standard deviation of the reading unless otherwise noted.
Note: systematic error estimates for temperature measurements are related to specific thermocouple locations. Values in table are approximate maximum errors

2/7/2005, 11:56 AM Error Summary PhD_SE-Day_data-uncertainty-estimates.xls 1 / 1

3.6 Figures

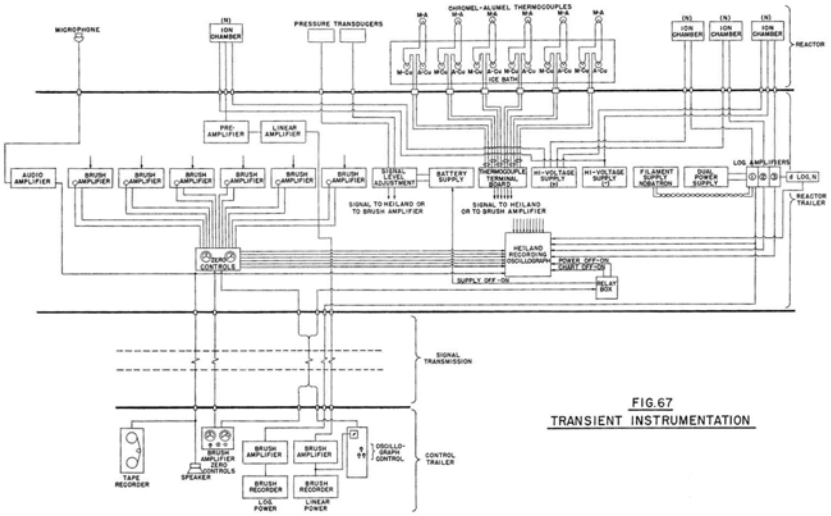

Figure 3-1: Borax I Transient Instrumentation Block Diagram (Ref. 3-8)

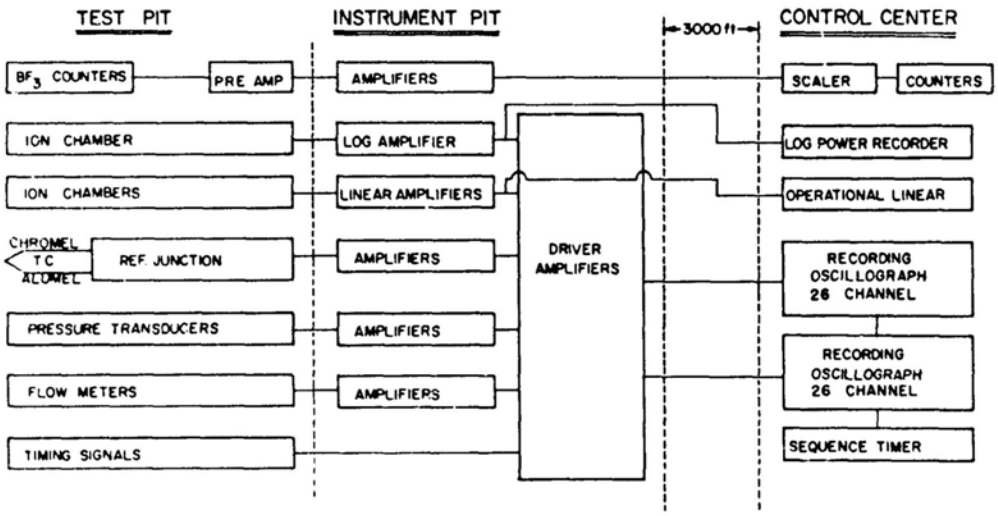

Figure 3-2: Spert I Transient Instrumentation Block Diagram (Ref. 3-6)

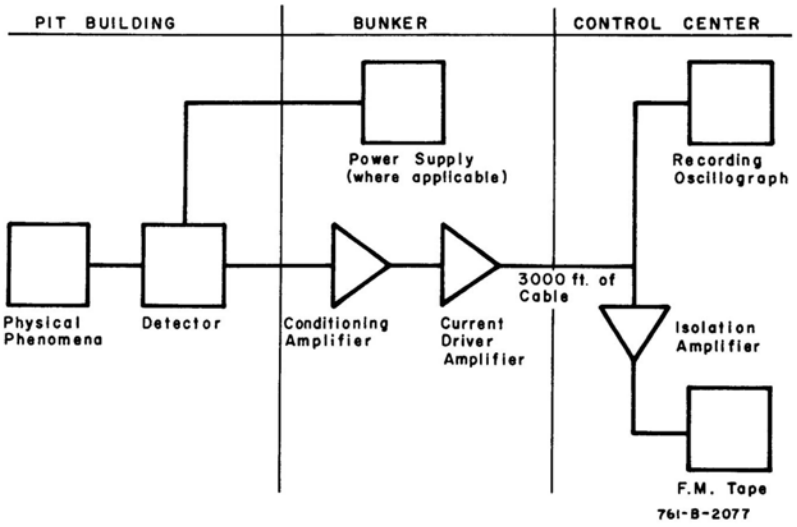

Figure 3-3: Block Diagram of a Typical Data Channel Used in the Reactor Tests (Ref. 3-20)

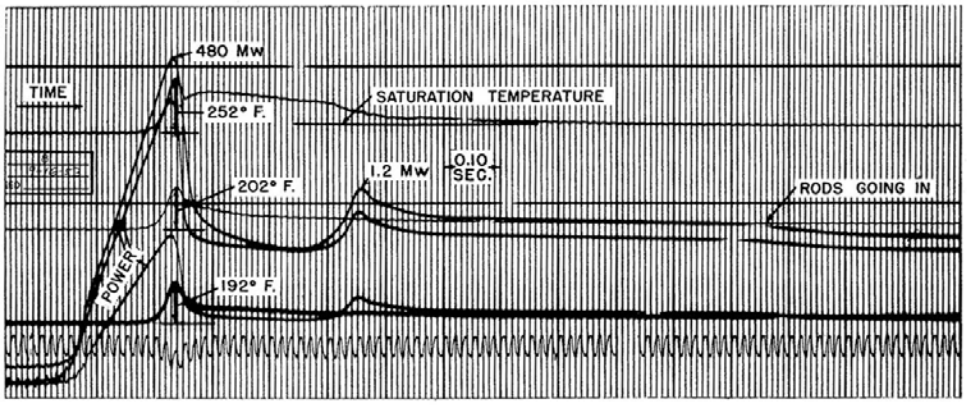

This record is from an excursion of 0.013 second period, with 43F subcooling. The top temperature trace is from the center of fuel Plate 4. The middle trace is from the center of Plate 1, and the bottom trace is from the surface of Plate 1. The three power traces on each record are from ion chambers of three different sensitivities, on logarithmic scales.

Figure 3-4: Data Record for a Typical Subcooled Step-Initiated Transient in Borax I (modified from Ref. 3-8)

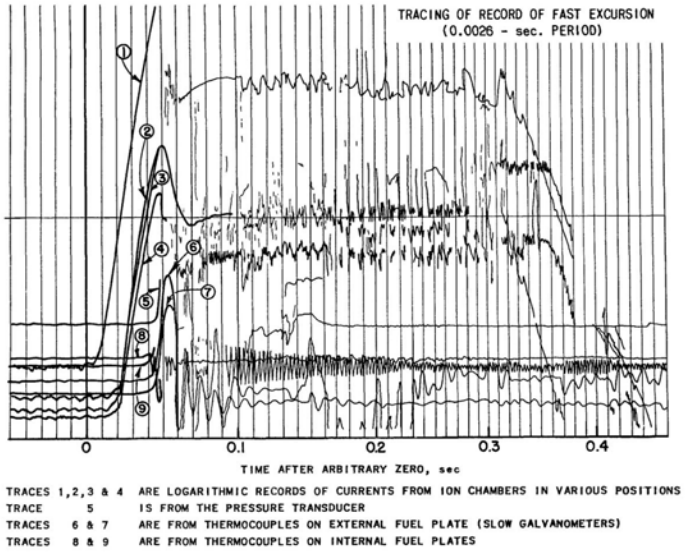

Figure 3-5: Data Record from the Borax I Destructive Test (Ref. 3-12)

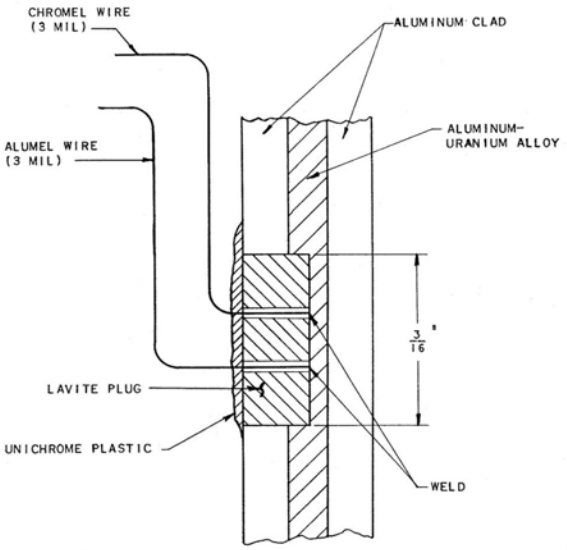

Figure 3-6: Centre Thermocouple Installation in Borax I Fuel Plate *via* "Plug" Method (Ref. 3-8)

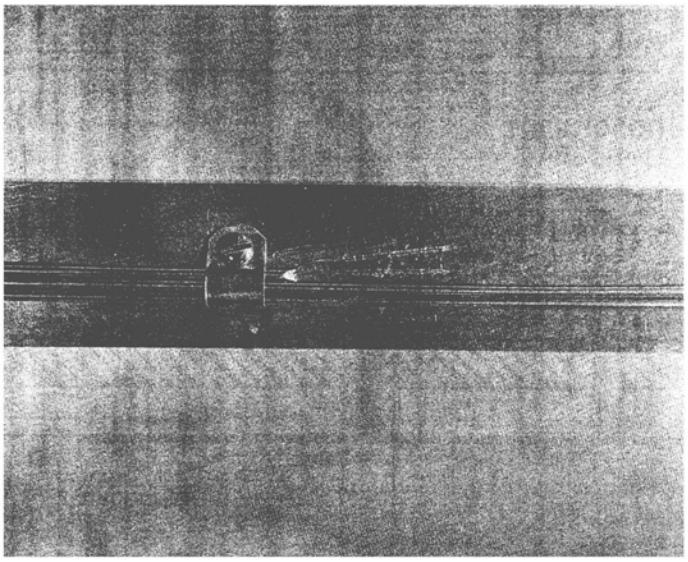

Figure 3-7: Spert I A Peened Thermocouple (Ref. 3-9)

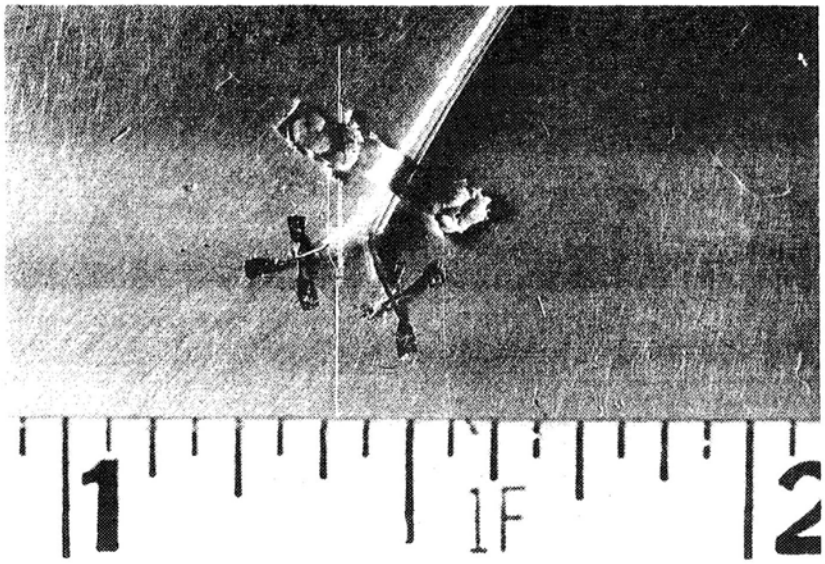

Figure 3-8: Spert I D-Core Surface Thermocouple (Ref. 3-32)

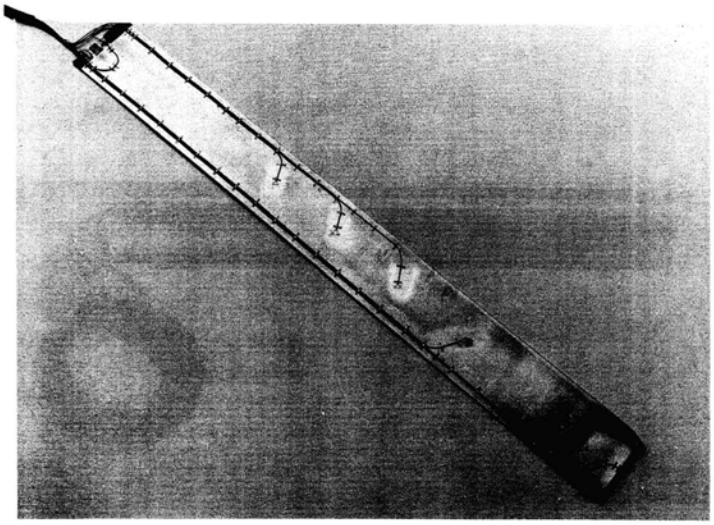

Figure 3-9: Fuel plate instrumented with surface thermocouples (Ref. 3-33)

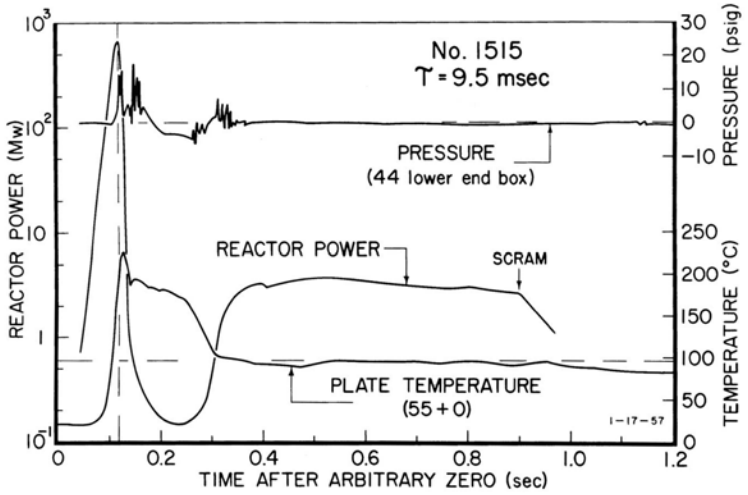

Figure 3-10: Spert I A Power, Fuel Plate Temperature and Pressure Time Trace (Ref. 3-7)

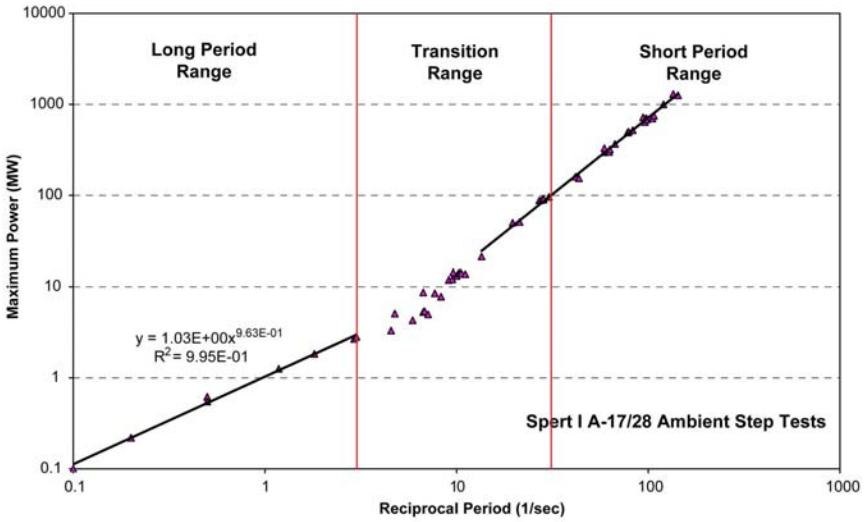

Figure 3-11: Spert I A Correlated Data Plot of Peak Power *vs.* Reciprocal Period for Step Tests from Ambient, Low Power Conditions with Natural Circulation Flow Only

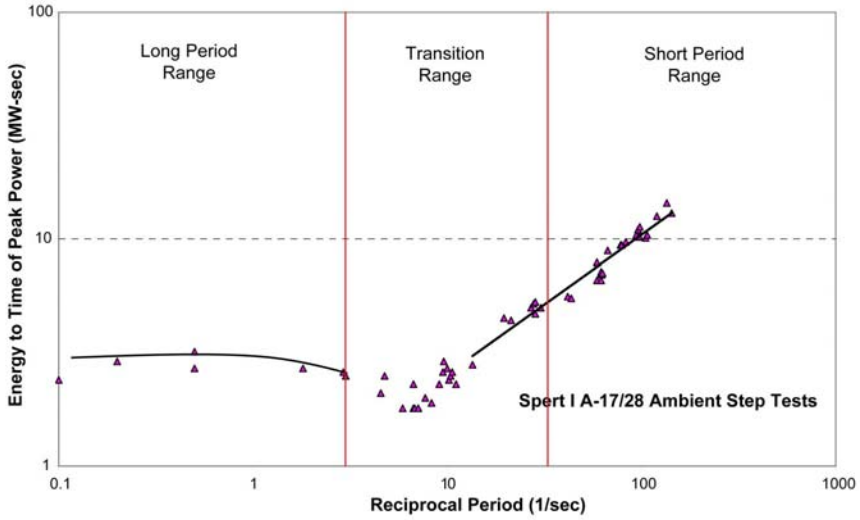

Figure 3-12: Spert I A Correlated Data Plot of Energy Release to Time of Peak Power *vs.* Reciprocal Period for Step Tests from Ambient, Low Power Conditions with Natural Circulation Flow Only

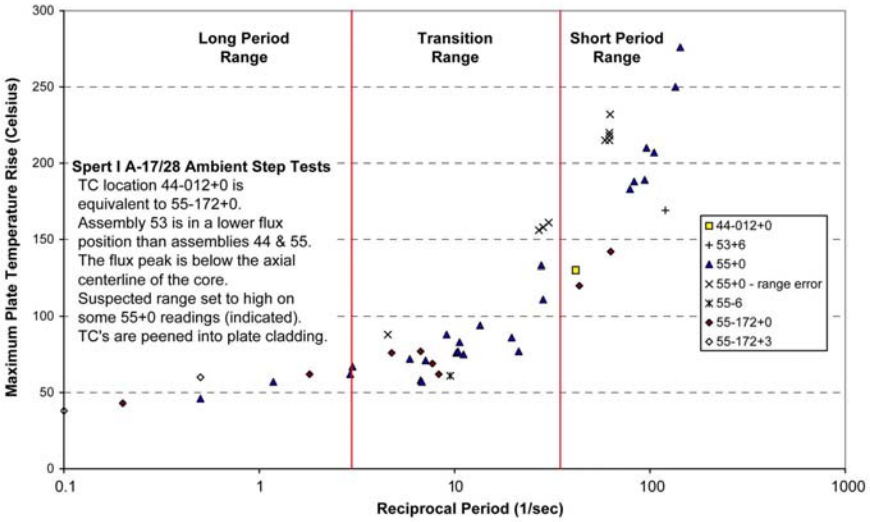

Figure 3-13: Spert I A Correlated Data Plot of Maximum Fuel Plate Surface Temperature *vs.* Reciprocal Period for Step Tests from Ambient, Low Power Conditions with Natural Circulation Flow Only

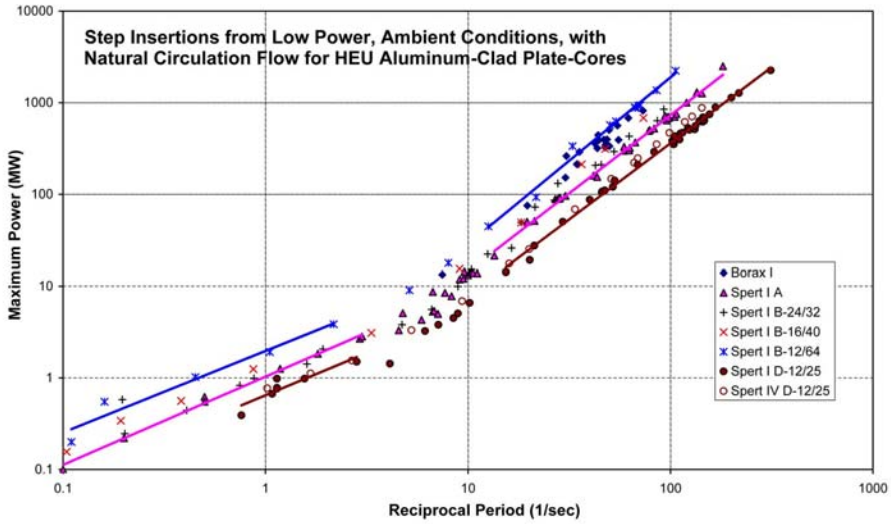

Figure 3-14: Peak Power *vs.* Reciprocal Period for Step Tests from Ambient Conditions for all of the HEU Al-Clad Plate Cores

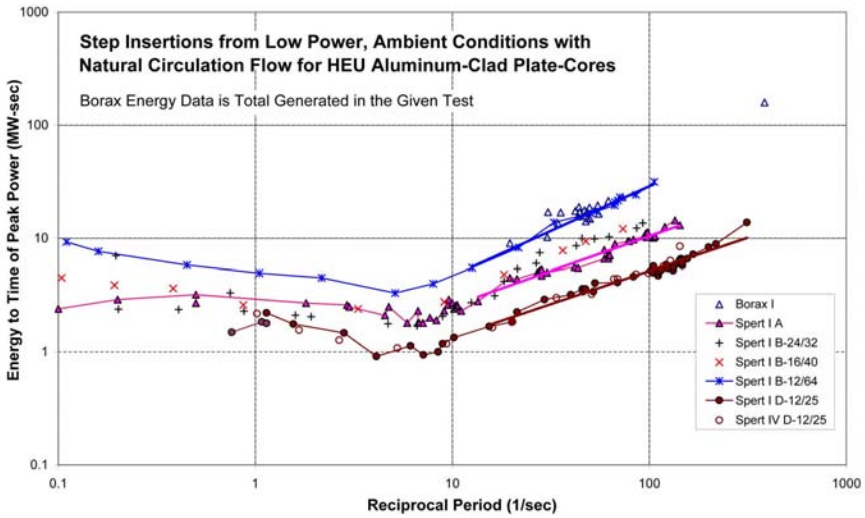

Figure 3-15: Energy Release to Time of Peak Power *vs.* Reciprocal Period for Step Tests from Ambient Conditions for all of the HEU Al-Clad Plate Cores

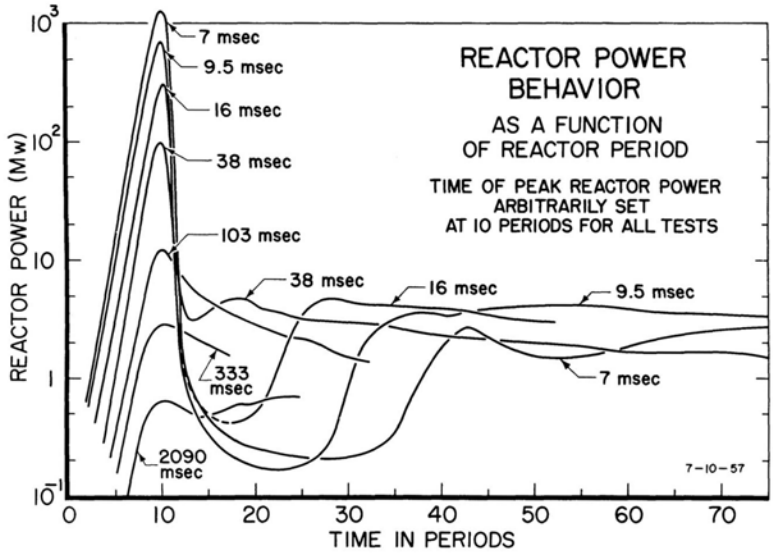

Figure 3-16: Reactor Power Behaviour for Various Reactor Periods for Step Insertion Transients in Spert I A-17/28 (Ref. 3-7)

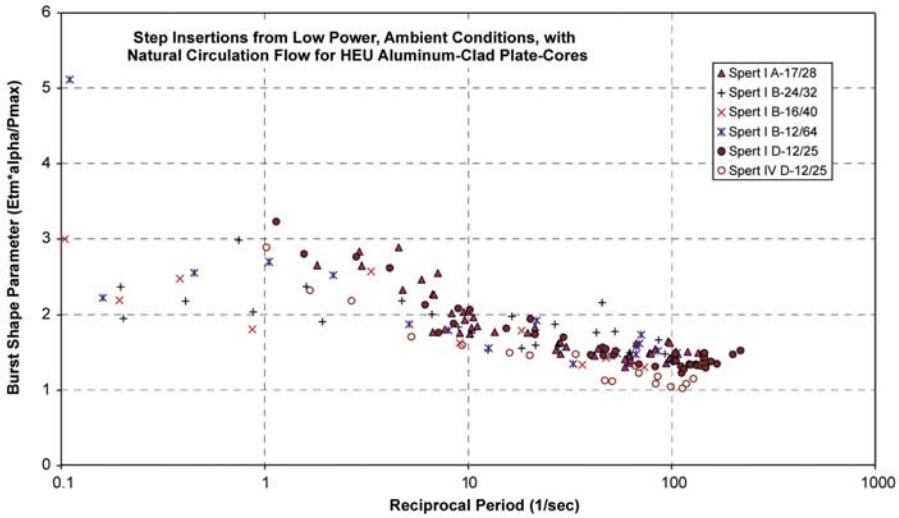

Figure 3-17: Burst Shape Parameter *vs.* Reciprocal Period for Step Tests from Ambient Conditions for all of the HEU Al-Clad Plate Cores

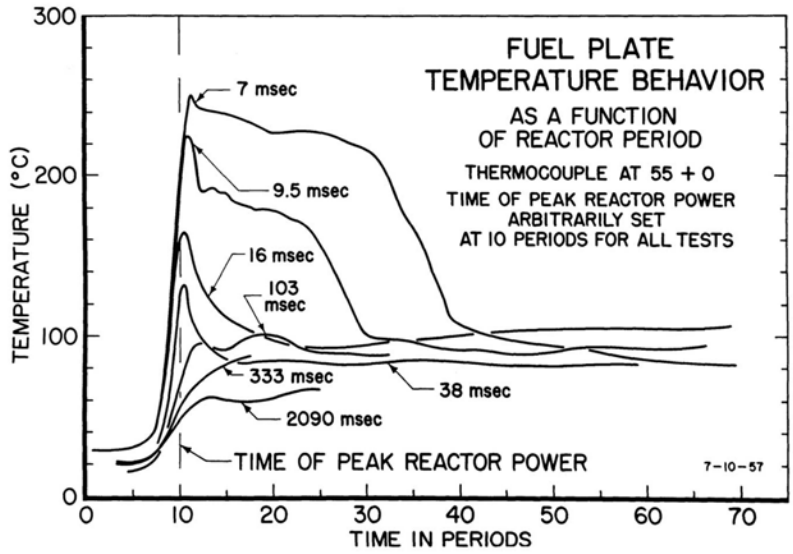

Figure 3-18: Fuel Plate Temperature Behaviour for Various Reactor Periods for Step Insertion Transients in Spert I A-17/28 (Ref. 3-7)

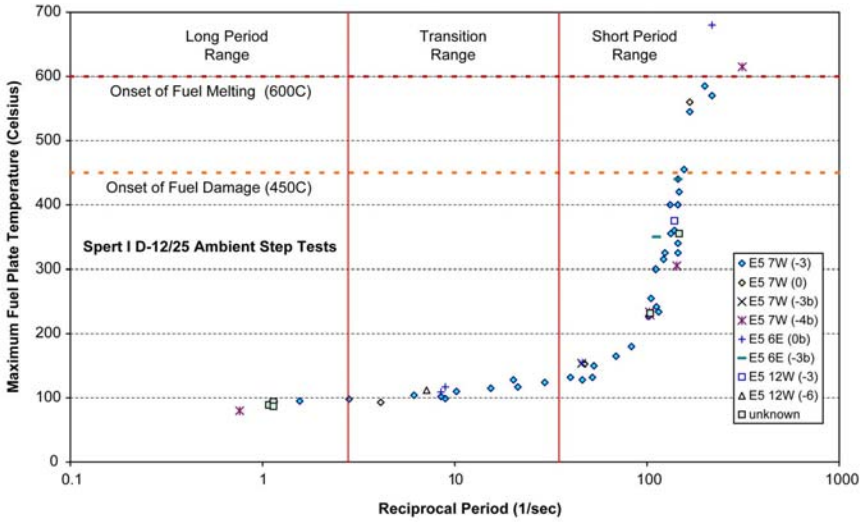

Figure 3-19: Spert I D Correlated Data Plot of Maximum Fuel Plate Surface Temperature *vs.* Reciprocal Period for Step Tests from Ambient, Low Power Conditions with Natural Circulation Flow Only

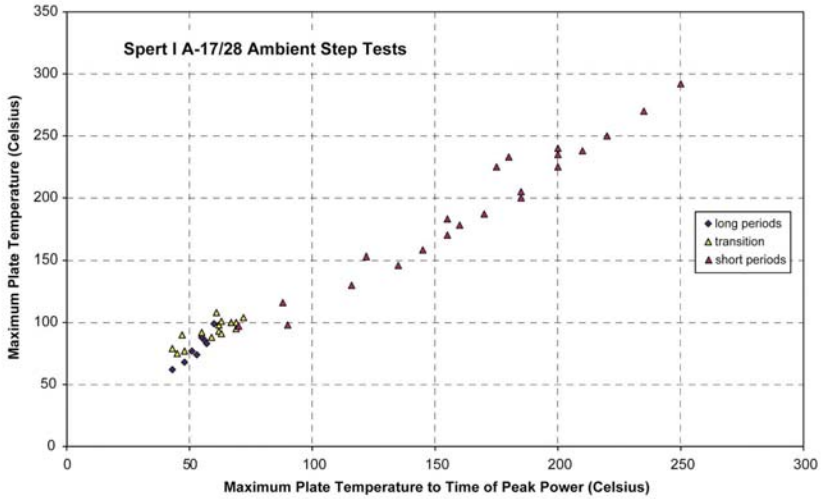

Figure 3-20: Spert I A Correlated Data Plot of Maximum Fuel Plate Surface Temperature *vs.* Maximum Fuel Plate Surface Temperature at the Time of Peak Power for Step Tests from Ambient, Low Power Conditions with Natural Circulation Flow Only

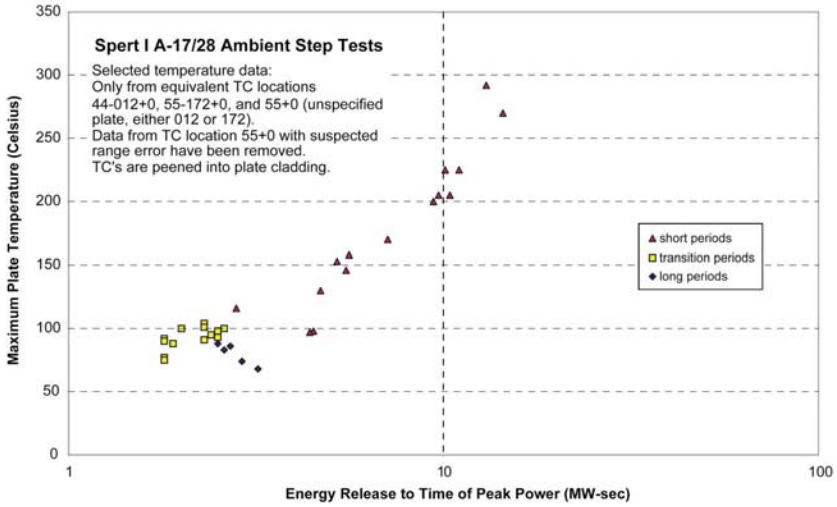

Figure 3-21: Spert I A Correlated Data Plot of Maximum Fuel Plate Surface Temperature *vs.* Energy Release to Time of Peak Power for Step Tests from Ambient, Low Power Conditions with Natural Circulation Flow Only

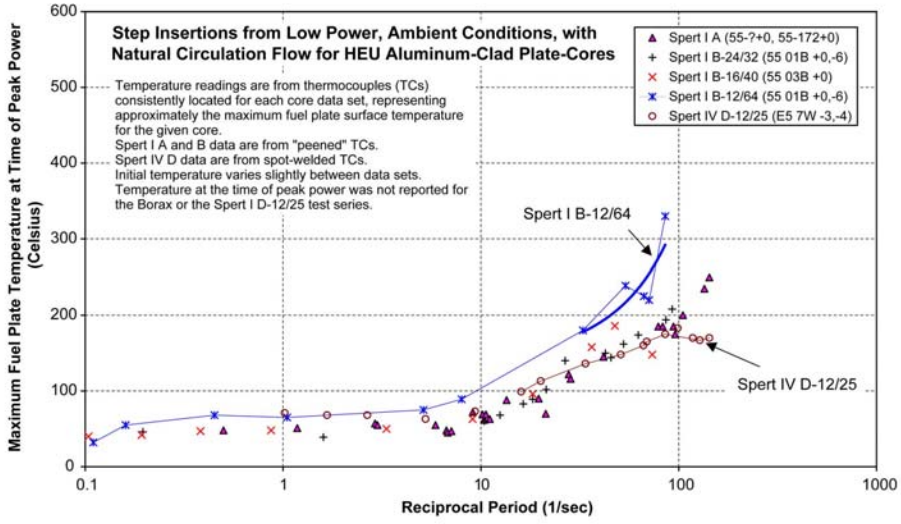

Figure 3-22: Maximum Fuel Plate Surface Temperature at the Time of Peak Power *vs.* Reciprocal Period for Step Tests from Ambient Conditions for all of the HEU Al-Clad Plate Cores

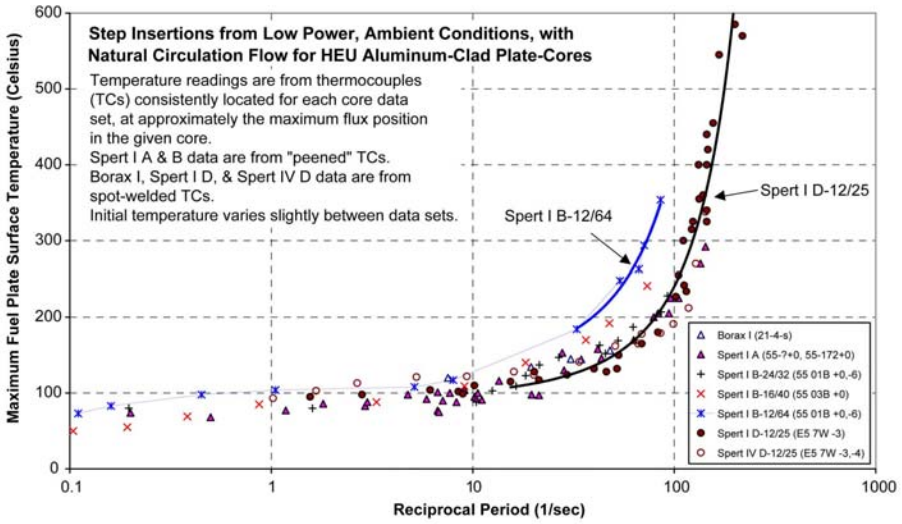

Figure 3-23: Maximum Fuel Plate Surface Temperature *vs.* Reciprocal Period for Step Tests from Ambient Conditions for all of the HEU Al-Clad Plate Cores

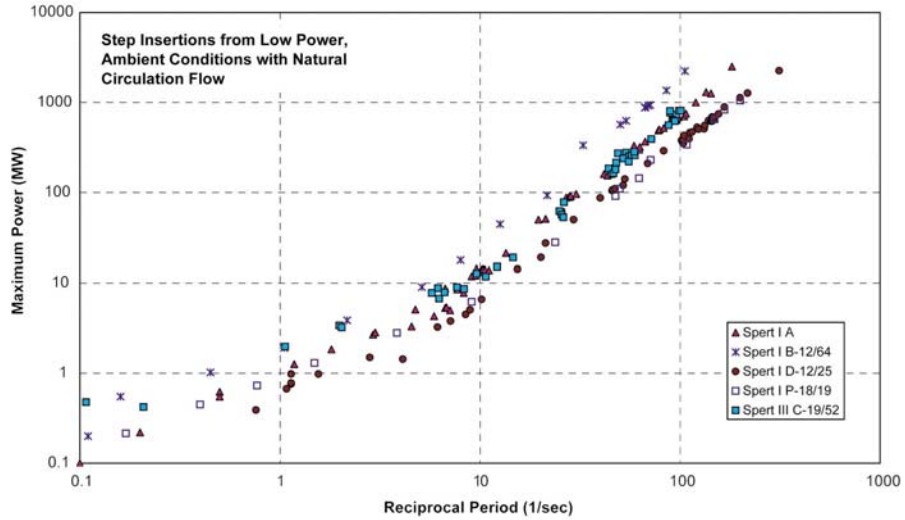

Figure 3-24: Peak Power *vs.* Reciprocal Period for Step Tests from Ambient Conditions for HEU Al- and SS-Clad Plate Cores

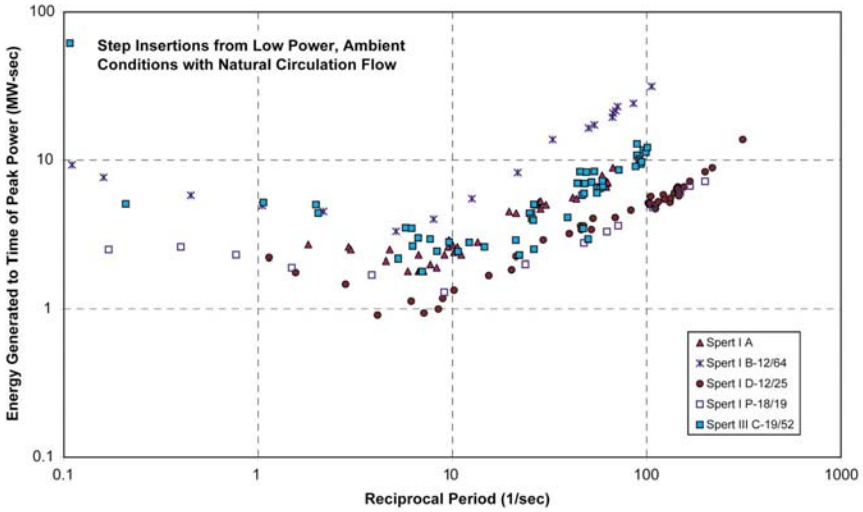

Figure 3-25: Energy to Time of Peak Power *vs.* Reciprocal Period for Step Tests from Ambient Conditions for HEU Al- and SS-Clad Plate Cores

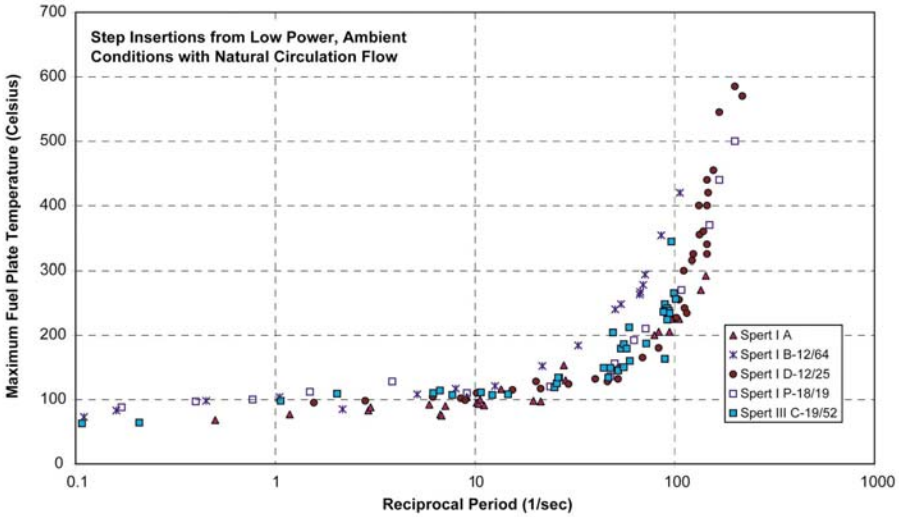

Figure 3-26: Maximum Fuel Plate Surface Temperature *vs.* Reciprocal Period for Step Tests from Ambient Conditions for HEU Al- and SS-Clad Plate Cores

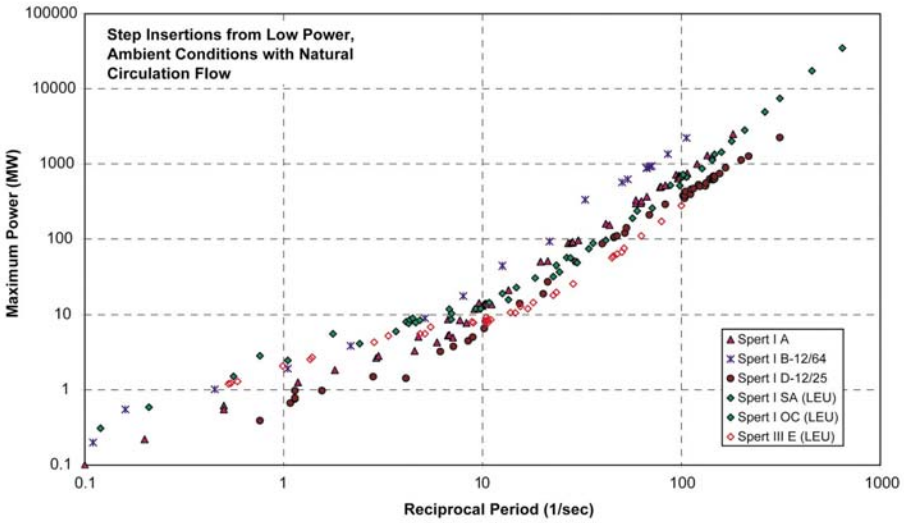

Figure 3-27: Peak Power *vs.* Reciprocal Period for Step Tests from Ambient Conditions for HEU Al-Plate and LEU Oxide-Rod Cores

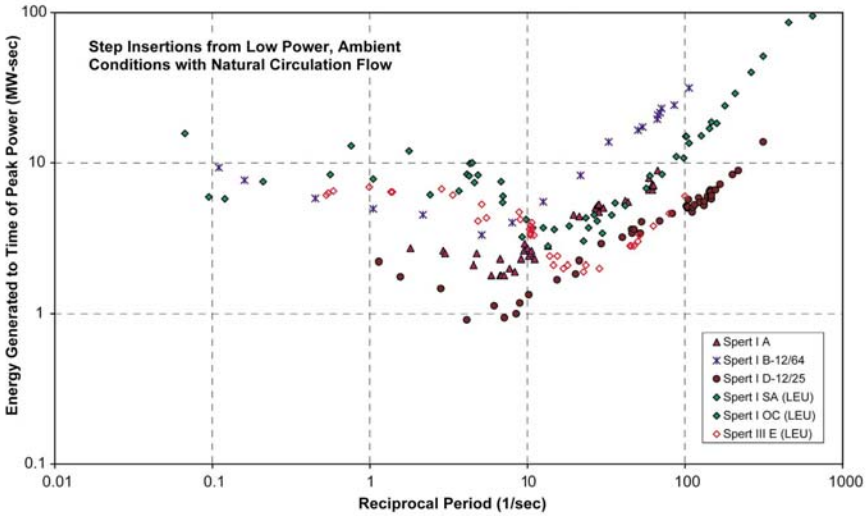

Figure 3-28: Energy to Time of Peak Power *vs.* Reciprocal Period for Step Tests from Ambient Conditions for HEU Al-Plate and LEU Oxide-Rod Cores

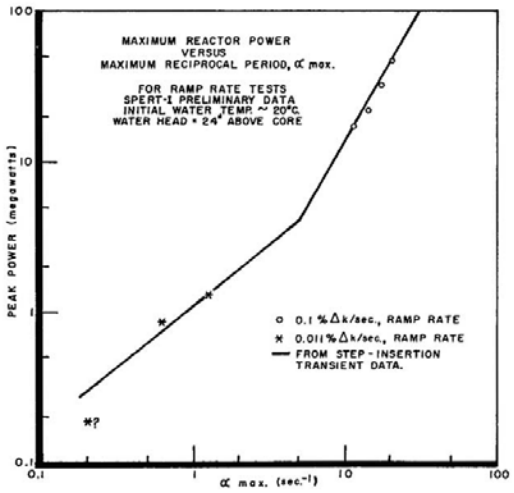

Figure 3-29: A Comparison of Peak Power *vs.* Reciprocal Period for Spert I A Step and Ramp Initiated Transients (Ref. 3-16)

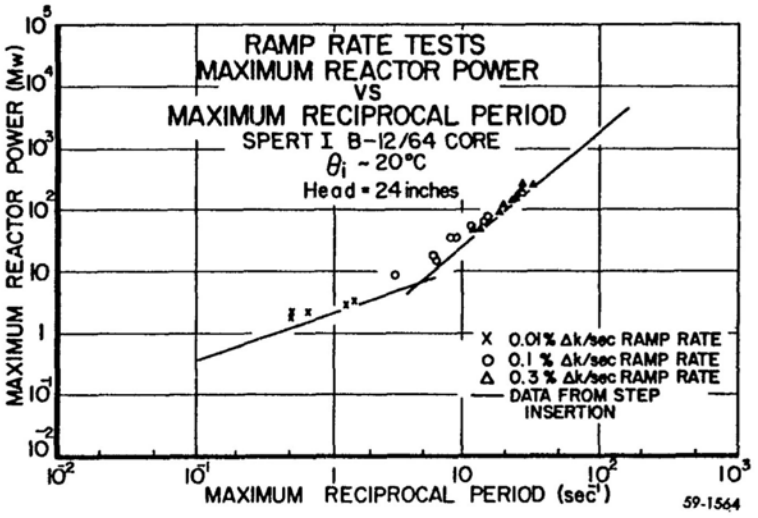

Figure 3-30: A Comparison of Peak Power *vs.* Reciprocal Period for Spert I B-12/64 Step and Ramp Initiated Transients (Ref. 3-14)

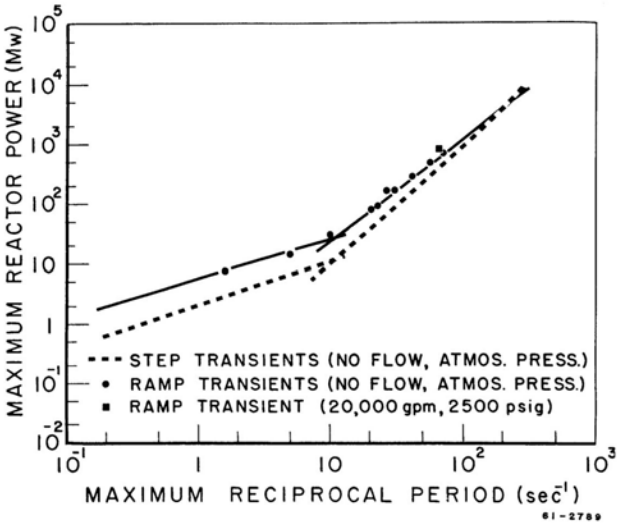

Figure 3-31: A Comparison of Peak Power *vs.* Reciprocal Period for Spert III C-19/52 Step and Ramp Initiated Transients (Ref. 3-18)

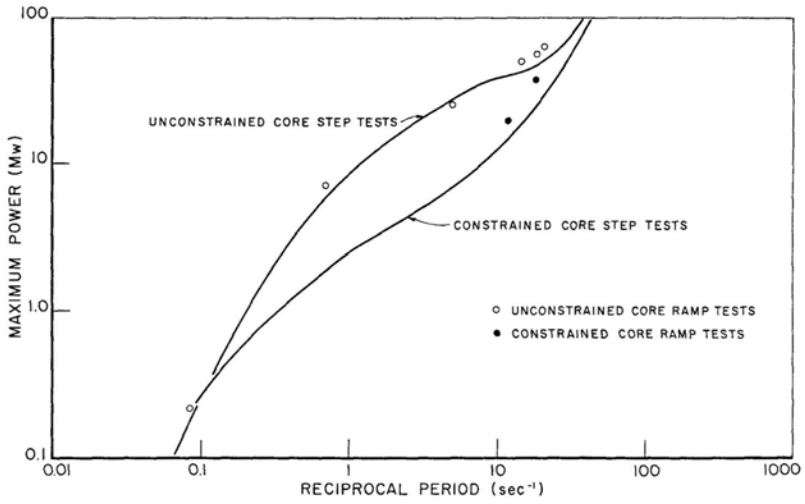

Figure 3-32: A Comparison of Peak Power *vs.* Reciprocal Period for Spert I SA Step and Ramp Initiated Transients (Ref. 3-19)

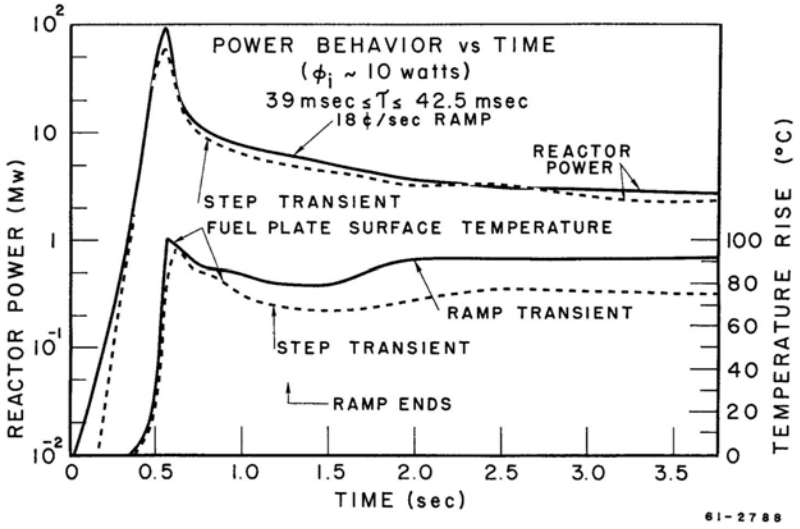

Figure 3-33: Reactor Power and Fuel Plate Surface Temperature for 18c/sec Ramp Test and 40 msec-Period Step Test in Spert III C (Ref. 3-18)

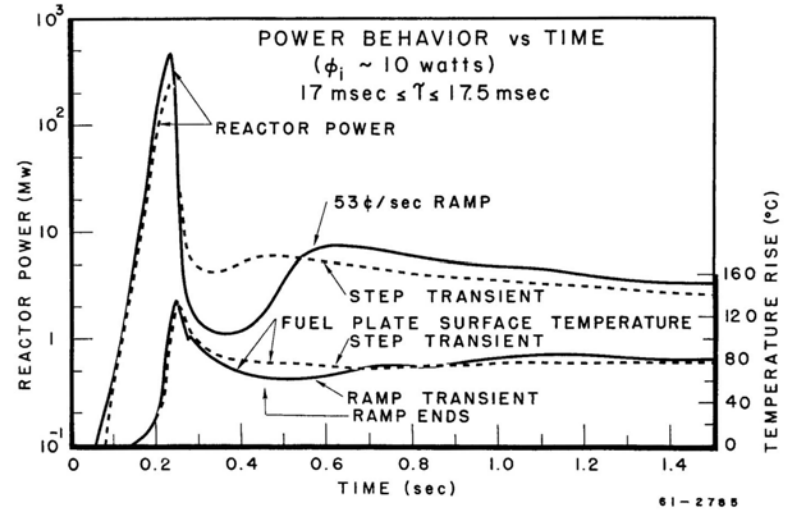

Figure 3-34: Reactor Power and Fuel Plate Surface Temperature for 53c/sec Ramp Test and 17 msec-Period Step Test in Spert III C (Ref. 3-18)

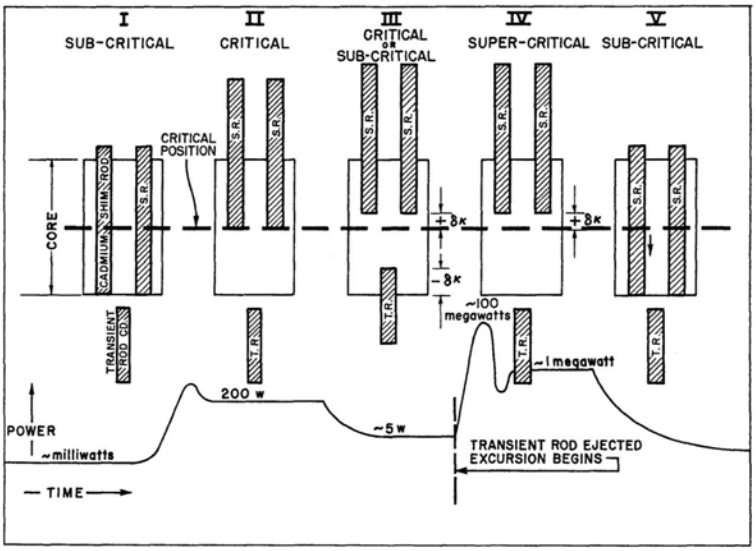

Figure 3-35: Spert I A Step Insertion Test Sequence (Ref. 3-16)

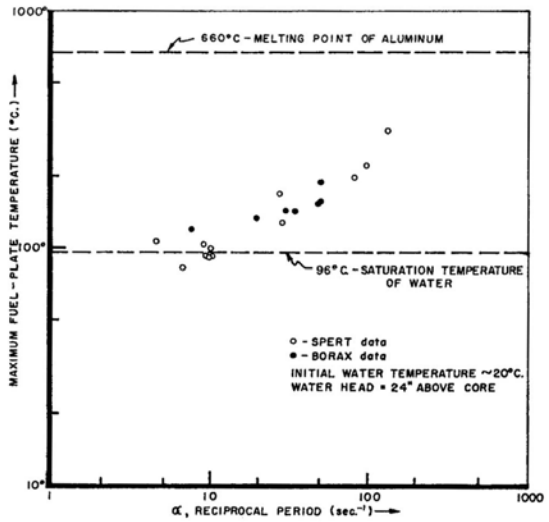

Figure 3-36: Borax I and Spert I A Fuel Plate Temperature Data from Ambient Step Tests (Ref. 3-16)

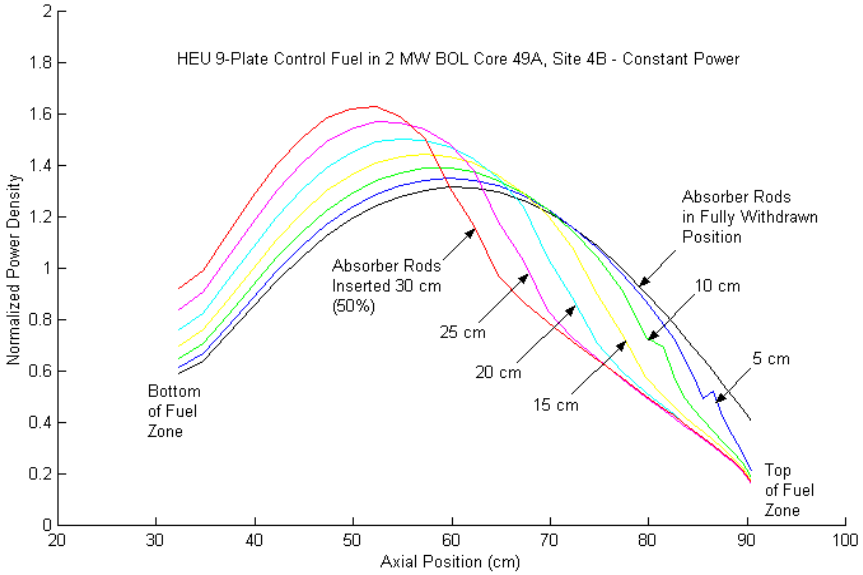

Figure 3-37: Change in Axial Power Peaking Factor with Control Rod Bank Position in MNR (uniform axial burnup)

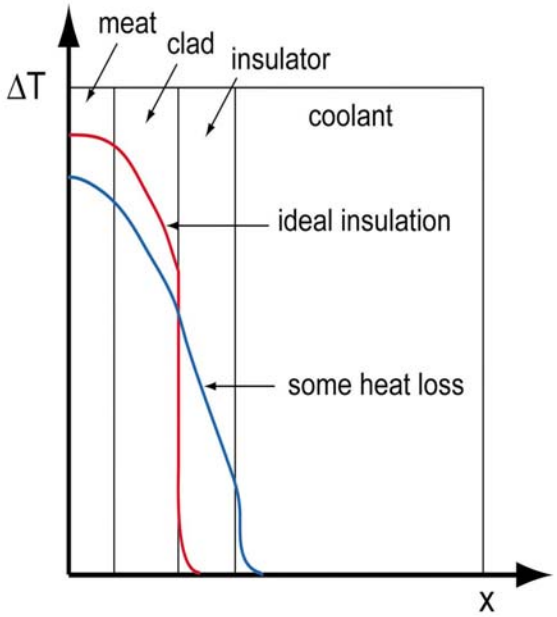

Figure 3-38: Plate to Coolant Temperature Distributions for an Insulated Fuel Plate

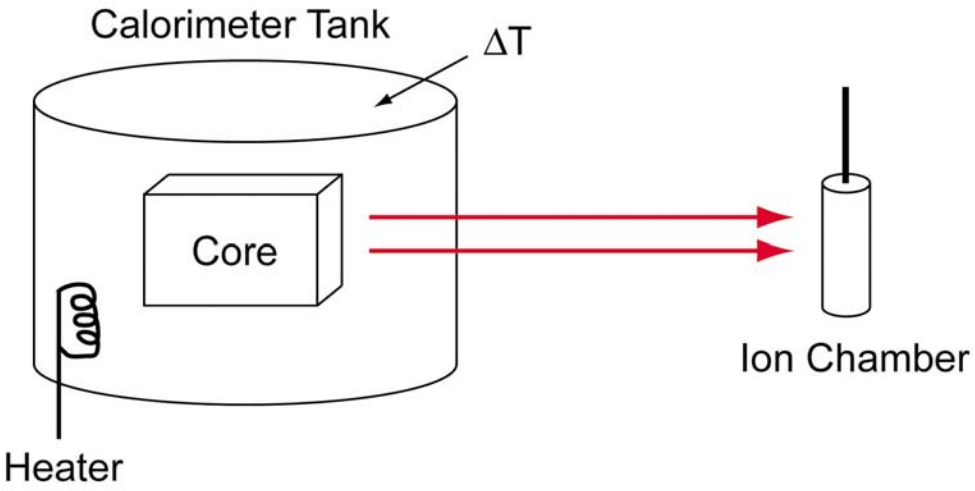

Figure 3-39: Calorimeter Based Power Measurement Calibration

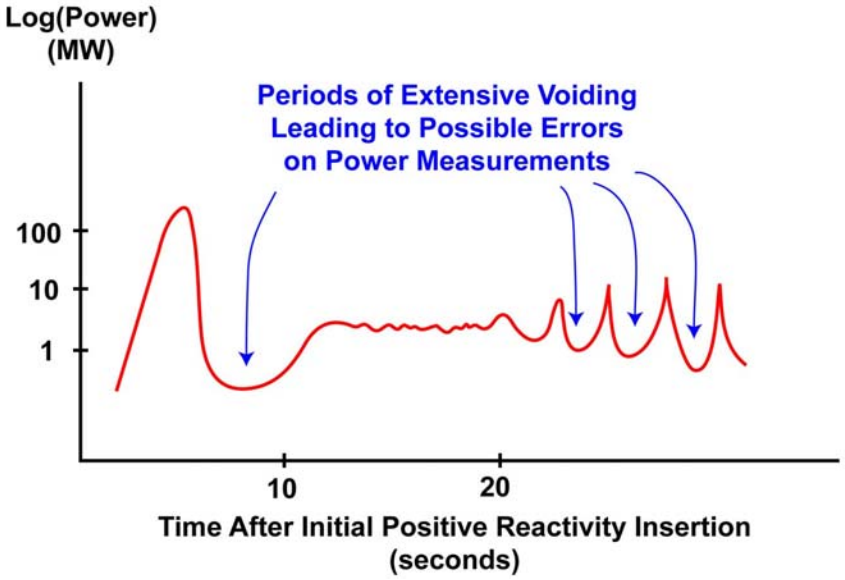

Figure 3-40: Phases of Stylized Self-Limiting Power Response Involving Significant Core Voiding

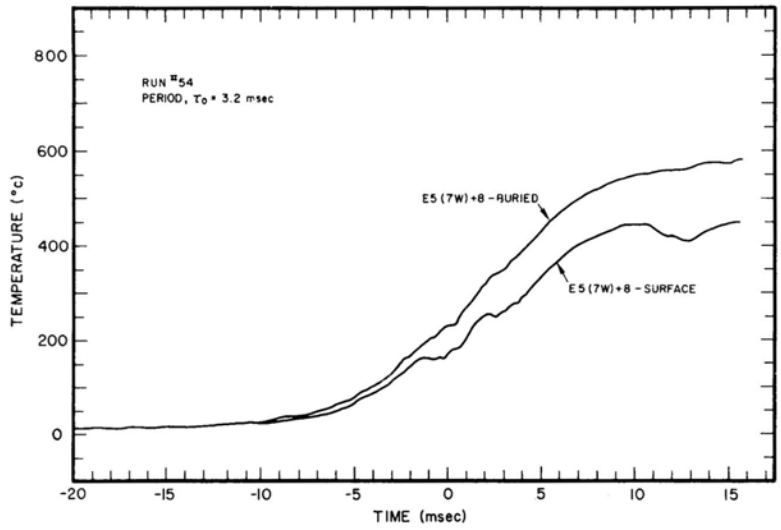

Figure 3-41: Transient temperature data obtained with buried and surface thermocouples during the 3.2-msec period test in the Spert I D-12/25 core (Ref. 3-33)

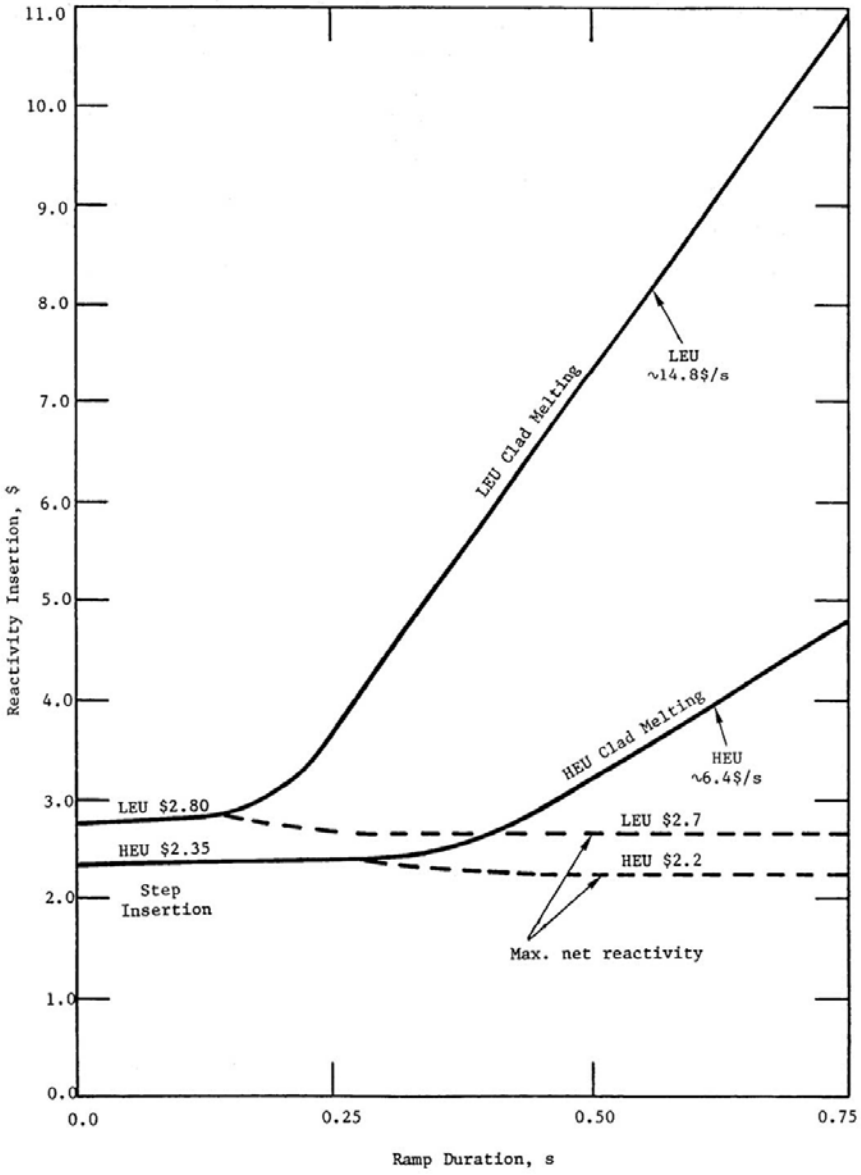

Figure 3-42: Reactivity Limits as a Function of Insertion Time (Ref. 3-56)

(this page is intentionally left blank)

CHAPTER 4 - HEU STEP DATA ANALYSIS

TABLE OF CONTENTS

LIST OF TABLES

LIST OF FIGURES

(this page is intentionally left blank)

4 HEU STEP DATA ANALYSIS

In order to apply the experimental data from the full scale reactor tests to a different MTR-core, the parametric dependencies of the self-limiting response must be accounted for and explained. In this way, the proper adjustments to the experimental data can be made to account for differences in system parameters between the core of interest and the test cores, and the transient response of the former may be predicted.

This chapter addresses trends in the experimental step test data from the HEU Al-clad plate-type cores studied in the Borax and Spert tests, with the objective of explaining differences in the individual data sets (from different cores) in terms of differences in specific system parameters. Herein, a parametric analysis is reported of the transient summary data, *i.e.*, P_{max}, E_{tm}, and T_{max} *vs.* α_0, from the HEU Al-clad MTR-type test cores.

Section 4.1 outlines (i) the formal curve fitting approach used to quantify the trends found in the data and, (ii) the relationships between the summary data quantities upon which the rest of the analysis is based.

The differences in the data from the different test cores are quantified through curve fitting regression analysis over the short period range ($\alpha_o > 29$ sec^{-1}) and the results are used throughout the remainder of the chapter.

An underlying assumption in the analysis as a whole is that parametric dependencies in the temperature test data are fundamentally tied to the same dependencies in the power and energy test data. The physical relationship between these three quantities is put in terms of proportionality relations and examined in terms of the test core results. This relation incorporates core size and power distribution into the analysis.

The remaining system parameters under consideration are those related to void reactivity feedback response (Section 4.2), the degree of subcooling (Section 4.3), and forced *vs.* natural circulation coolant flow (Section 4.4). Suitable scaling factors are derived for the former two variations and a conservative argument is presented for the latter. Additional system parameters are discussed in Section 4.5.

The identification and quantification of trends in the data helps confirm the generic applicability of the test data to MTR-type systems for safety analysis purposes. In addition, equivalence of the transient test data is valuable in the sense that a given

test series on one particular test core, investigating specific aspects of the self-limiting behaviour of MTR-type systems, can be used to complement the entire test data set and round out the big picture of reactor behaviour under unprotected transient conditions.

4.1 Data Preliminaries

4.1.1 Curve Fitting the Summary Test Data

This section explains the curve fitting analysis used to quantify trends in the summary test data, *i.e.*, P_{max}, E_{tm}, and ΔT_{max} with respect to the reciprocal period, α_o, for the short period range (α_o $ 29 sec^{-1}). The following functional relationships are used:

$$\begin{aligned} P_{max} &= b_1 \, \alpha_o^{\,m_1} \\ E_{tm} &= b_2 \, \alpha_o^{\,m_2} \\ \Delta T_{max} &= b_3 \, e^{\alpha_o m_3} \end{aligned}$$

The P_{max} and E_{tm} functions are those suggested by the Shutdown Model (see Section 4.2.1). The functional form applied to the temperature rise data is chosen as it (i) looks reasonable for the data, and (ii) can be linearised by taking logarithms of both sides of the equation. Note: use of a power law fitting function for the temperature (as used for the P_{max} and E_{tm} data) did not capture the additional curvature in the dependence on the reciprocal period, α_o. The validity of these functions for the curve fitting is reflected in the goodness of fit and standard error results of the analysis.

The curve fitting uses standard weighted linear least squares analysis of the linearised forms of the equations, *i.e.*:

$$\begin{aligned} \ln\left(P_{max}\right) &= m_1 \ln\left(\alpha_o\right) + \ln\left(b_1\right) \\ \ln\left(E_{tm}\right) &= m_2 \ln\left(\alpha_o\right) + \ln\left(b_2\right) \\ \ln\left(\Delta T_{max}\right) &= m_3 \, \alpha_o + \ln\left(b_3\right) \end{aligned}$$

Uncertainty in the α_o measurements are incorporated as increased uncertainty on the ordinate (y-axis) values (Ref. 4-1).

Only the step insertion initiated tests from initially ambient (*i.e.*, ~ 20EC) temperature, low power, atmospheric pressure, no flow test conditions are considered in this section.

For each data quantity a reference slope (*i.e.*, m_1, m_2, and m_3) is used for the fitting based on the least squares fitting to the Spert I D-12/25 data set - defined as the "reference data set". This is consistent with theory and the hypothesis of the consistent self-limiting behaviour of the different test cores.

The Spert I D-12/25 data are used as the reference data set as the test series covers the widest range of periods up to and including the damage range. It is also felt that the quality of the Spert I D-12/25 data is highest of all the cores, given: (a) the largest number of data points, and (b) the refined measurement techniques and equipment used in this latter stage of the Spert Project. Both of these factors are assumed to lead to the most meaningful statistics associated with the curve fitting analysis.

The curve fits to the individual data sets from the different test cores are shown in Figures 4-1, 4-2, and 4-3 for the entire range of periods and Figures 4-4, 4-5, and 4-6 over the short period range of transients. The curve fitting results are summarized in Tables 4-1, 4-2, and 4-3.

It is found that the goodness of fit of the individual core data sets is not compromised by using a common slope from the reference data set. Results for both full regression analysis (*i.e.*, where the slope is determined from the least squares regression) and the curve fitting using the pre-defined reference slope are compared in Tables 4-4, 4-5, and 4-6. Further details of the curve fitting analysis are included in Appendix C.

It should be noted that the very shortest period tests conducted on the Spert I D-12/25 core (indicated on the correlated data plots) resulted in various degrees of fuel melting. As a result these tests were not included in the temperature rise regression analysis since the change in phase affects the relation between period and temperature rise. These data points are, however, included in the P_{max} and E_{tm} analysis.

Differences in the ln(b) parameters (*i.e.*, the y-intercepts of the linearised equations) quantifies the differences in the summary data. These y-intercept differences are used in the subsequent parametric analysis.

4.1.2 Proportionality of Power, Energy and Temperature Data

This section investigates the relationship between the power, energy and maximum temperature rise data with the inclusion of parameters representing the core size and the core power distribution.

The nuclear response of the core to the reactivity insertion is described by the power and energy generation with respect to time represented by the P_{max} and E_{tm} summary data. The corresponding thermal response is described by the fuel plate surface temperature rise which lags the power and energy generation with the maximum temperature occurring after the peak power. These quantities appear correlated.

The temperature at any given point in the fuel is a local quantity and is related to the associated power and energy density. For an adiabatic situation, which is approximately the case for a short period transient,

$$\frac{E}{V_f} = \int \frac{P}{V_f} dt = m\, C_p\, \Delta T$$

where m is the mass density of the fuel meat, C_p is the heat capacity of the volume and ΔT is the average temperature rise associated with the energy generation. It follows that:

$$P_{max}, E_{tm} \propto \Delta T_{avg}$$

where ΔT_{avg} is the average fuel temperature rise. Assuming the point reactor representation, constant heat capacity, and uniform heat transfer/removal characteristics throughout the core, the asymptotic fuel temperature distribution is proportional to the power density distribution which is described by the power peaking factor (*PPF*), *i.e.*, the peak to average power density ratio, of the core. In this case the average fuel temperature rise is related to the maximum fuel temperature rise by:

$$\Delta T_{max} = \Delta T_{avg} \times PPF$$

and the summary data quantities are related by:

$$\begin{aligned} \Delta T_{max} &\propto P_{max}/V_f \times PPF \\ &\propto E_{tm}/V_f \times PPF \end{aligned}$$

where V_f is the volume of the fuel meat in the core and *PPF* is the overall power peaking factor. If the above relations hold then the same relative behaviour of the P_{max} and E_{tm} data should also be seen in the ΔT_{max} data when scaled to core size (V_f) and power density distribution (*PPF*). This is expressed as:

$$\Delta T_{max(a),i} = \Delta T_{max,i} \times \frac{V_{f,i}}{V_{f,r}} \times \frac{PPF_r}{PPF_i}$$

where the scaling is normalized to some "reference" core, with the subscripts *i* and *r* denoting the specific core of interest and the reference core respectively. This normalised or "adjusted" temperature rise is denoted herein by the subscript "(*a*)".

Given the relationship between P_{max}, E_{tm}, and ΔT_{max} (outlined above), it is hypothesized that the relative differences found in the P_{max} and E_{tm} data may also be reflected in the suitably normalised temperature data, $\Delta T_{max(a)}$.

This hypothesis is supported by the data as shown in Figures 4-7 and 4-8 where the relative changes in magnitude of $\Delta T_{max(a)}$ are correlated and comparable in magnitude to those for P_{max} and E_{tm} for the different test cores. These figures show the relative changes in magnitude of the summary data quantities as the differences in the *y*-intercepts of the $\ln(\Delta T_{max(a)})$ *vs.* α_o, $\ln(P_{max})$ *vs.* $\ln(\alpha_o)$, and $\ln(E_{tm})$ *vs.* $\ln(\alpha_o)$ plots. The differences are computed relative to the Spert I D-core data as a point of reference. The one-to-one relationships between the power and energy relative to the temperature data changes verify the proportionality relationships hypothesized above.

This then allows for corrections based on the power and energy data to be applied to the temperature rise data given the proper scaling factors for core size and power density distribution. This is used in the remainder of the analysis of the thesis and in the SAR methodology presented in Chapter 7.

4.2 The Effect of Void Reactivity

The analysis herein investigates the parametric dependence of the transient summary data quantities maximum power (P_{max}), energy generated to the time of peak power (E_{tm}), and maximum fuel plate surface temperature rise (ΔT_{max}), on the void reactivity feedback characteristics of an HEU Al-clad plate-fuel core.

4.2.1 The Shutdown Model

It is evident from Figures 4-1, 4-2, and 4-3 that the behaviour of these three related parameters (P_{max}, E_{tm}, and ΔT_{max}) with respect to the size of the reactivity insertion (indexed by the parameter α_o) from the different test cores can be represented by a series of parallel curves. Formalizing this curve fitting by following linear least squares regression analysis both supports this claim and allows for quantification of the differences between the curves in terms of magnitude, *i.e.*, in terms of differences in the *y*-intercept parameter of the linearised form of the equations (see Section 4.1.1). A parametric analysis of these differences in the data is suggested from theory.

Various simple analytical models were developed both prior to and during the Spert Project as tools for describing the self-limiting response of an MTR-type system. The general idea behind these models is to lump the feedback effects of the system into a semi-empirical parameter called the shutdown coefficient where the feedback in the system is a function of generated energy. As such, the complexities of the reactor behaviour are compressed into this single factor. Various functional forms of the shutdown term have been presented in the literature and despite the simplicity, these models can be made to agree reasonably well with experimental data.

The model is based on a point system with only the prompt neutrons considered. This approach is applicable to a small reactor core for which point kinetics theory applies and for short period transients, *i.e.*, large reactivity insertions in excess of prompt critical. The point-prompt model takes the form:

$$\frac{P'(t)}{P(t)} = \frac{\left(k(t)\left(1-\beta\right)-1\right)}{\ell} = \frac{\left(\rho(t)-\beta\right)}{\Lambda(t)}$$

where P is the reactor power (P' is the time derivative), $k(t)$ is the multiplication factor, β is the effective delayed neutron fraction, ℓ is the prompt neutron lifetime, ρ

is the reactivity, and $\Lambda(t)$ is the prompt neutron generation time. The numerator is the reactivity in excess of prompt critical. Additional definitions are:

$$\rho(t) \equiv \frac{k(t)-1}{k(t)} \quad ,$$

$$\Lambda(t) \equiv \frac{\ell}{k(t)}$$

For the case of no feedback, *i.e.*, the reactivity is constant, $\rho = \rho_{in}$, where ρ_{in} is the initially inserted reactivity and the subscript "o" designates the initial value, the solution to this equation has the form:

$$P\left(t\right) = P_o e^{(\alpha_o t)}$$

where,

$$\alpha_o = \frac{\left(k_o\left(1-\beta\right)-1\right)}{\ell} = \frac{\left(\rho_{in}-\beta\right)}{\Lambda_o}$$

The quantity α_o represents the reciprocal asymptotic reactor period, the same quantity measured in the reactor experiments. The point-prompt approximation, for the case of no feedback, can therefore be rewritten as:

$$\frac{P'(t)}{P(t)} = \alpha_o$$

And in the case of feedback,

$$\frac{P'(t)}{P(t)} = \alpha(t)$$

Feedback is incorporated into the point-prompt model in the expression for $\alpha(t)$. The first development was by Fuchs' which was applied to fast assemblies, where the feedback is expressed as a linear function of the energy generation. Further development of the shutdown model incorporated a non-linear dependence on the energy and a delay time to account for the time for the energy deposited in the fuel

meat to be transported to the coolant to be manifested as temperature and density feedback.

These models were compared to the experimental results by examining the calculated *vs.* experimental power burst time trace, compensating reactivity, and P_{max} and E_{tm} values. For an HEU MTR-type system the non-linear $n > 1$, long delay time, $t_d > 1/\alpha_o$, features are found to be most realistic, *i.e.*,

$$\frac{P'(t)}{P(t)} = \alpha_o - w\left[E\left(t - t_d\right)\right]^n$$

where w is the lumped feedback parameter, $E(t\text{-}t_d)$ is the energy generated up to time $(t\text{-}t_d)$ where t_d is the delay time, and n is the exponent of the energy dependence. This is known as the non-linear, long-delay model and is referred to herein simply as the Shutdown Model. The lumped parameter w is referred to as the "shutdown coefficient of reactivity".

Solving the above equation gives expressions for P_{max} and E_{tm}:

$$P_{max} = \frac{\alpha_o^{(n+1)/n}}{w^{1/n}} \mathrm{e}^{(\alpha_o t_d - 1/n)}$$

$$E_{tm} = \frac{\alpha_o^{1/n}}{w^{1/n}} \mathrm{e}^{(\alpha_o t_d - 1/n)}\, q\left(n, 0\right)$$

where $q(n,0)$ is an analytical function of n only, based on the Gamma Function. The product $(\alpha_o t_d)$ is found to be approximately constant (*i.e.*, the delay time in terms of periods is roughly fixed at a value of approximately two) over the short period range (Ref. 4-2) and is taken as fixed in the analysis herein. Further details regarding the Shutdown Model are given in References 4-3 and 4-4.

The Shutdown Model suggests dependencies of the P_{max} and E_{tm} *vs.* α_o data (and therefore also the ΔT_{max} *vs.* α_o *via* the proportionality shown on the previous section) on the shutdown reactivity of the system through the term, $w^{1/n}$. Application of the model therefore depends on the ability to determine both the shutdown coefficient, w, and the characteristic exponent, n. There are two approaches to this problem, both of which are outlined below.

The first approach is to determine the value of n from the slopes of the linearised forms of the above equations for P_{max} and E_{tm}, *i.e.*,

$$\ln\left(P_{max}\right) = \left(\frac{n+1}{n}\right)\ln\left(\alpha_o\right) + b_P$$

$$\ln\left(E_{tm}\right) = \left(\frac{1}{n}\right)\ln\left(\alpha_o\right) + b_E$$

The slopes, *i.e.*, $(n+1)/n$ and $1/n$, can be found from curve fitting the $\ln(P_{max})$ and $\ln(E_{tm})$ *vs.* $\ln(\alpha_o)$ data (see Section 4.1.1).

The y-intercepts of these two equations, b_P and b_E, are functions of the shutdown coefficient, w, the exponent, n, the product $\alpha_o t_d$ which is constant, and in the case of the energy equation, the function $q(n,0)$. Therefore, once n is determined (as above), the value of w can be estimated for the given core from the values of b_P and b_E. This approach has limited practicality as P_{max}, E_{tm}, and α_o data are necessary to calculate w. These are not available for reactors other than the test cores.

The second approach to determining w and n and therefore the term, $w^{1/n}$, does have practical application for any MTR-core of interest. In this approach the shutdown coefficient, w, is estimated from static measurements (which can be performed on any core of interest) and the exponent, n, is subsequently estimated from a correlation of the estimated w and the transient test data (specifically the y-intercepts of the linearised equations above). By letting the exponent, n, remain a free variable, an added degree of empiricism is included, allowing the analyst to work with estimates of the shutdown coefficient.

This approach has application for other reactor cores since the test data are only used to determine the exponent n, which is a common parameter for this type of core. The only information needed for the additional core is the same type of estimate of w. The result is a working model. This approach is formalised and further explained in Section 4.2.3.

4.2.2 Estimates of the Shutdown Coefficient

Application of the theory outlined in the previous section depends on the ability to quantify the shutdown coefficient, w. Estimation of w is possible with some insight into the shutdown characteristics of MTR-type cores.

Given that the primary shutdown mechanism for HEU MTR-type cores in the short period range is coolant voiding *via* boiling (Ref. 4-5), it therefore follows that the shutdown coefficient for HEU MTR-type systems is related to the coolant void reactivity coefficient and voiding characteristics of the core. Work in this area has previously been reported by J. A. Thie (Ref. 4-6), where the shutdown coefficient is defined as:

$$w = K_u \left(\frac{-C_{void}}{\ell} \right)$$

where K_u is a constant of proportionality, and C_{void} is the average void coefficient of reactivity in units of reactivity change per unit void volume produced in the core. The prompt neutron lifetime, ℓ, appears in the denominator as a result of the form of the Shutdown Model, expressed in terms of reactor period. The negative sign appears due to the signing convention used in the shutdown model. This results in a positive value of w for a negative void coefficient of reactivity. This expression is herein referred to as the "unit-volume-based shutdown coefficient" reflecting the units on the void coefficient numerator.

Thie's analysis examined the power and energy test data and was taken to the point of determining the coefficient K and the exponent $1/n$ where n was allowed to vary from the value on the energy term to allow for an added degree of empiricism. This work was applied at MIT as part of the maximum step reactivity insertion analysis for the MITR-II reactor and is reported in their 1970 SAR (Ref. 4-7). The MIT work revisited the Spert I B-core data and determined their own correlations on the above shutdown coefficient using curve fitting and (apparently) the measured values of the void coefficient and the prompt neutron lifetime. The 1970 SAR results are also used in the latest SAR update for MIT (Ref. 4-8) where it was found that the 1970 correlation results did not match particularly well with simulation work.

Although the B-core test series was designed specifically to investigate the effect of varying the void feedback coefficient in the core (by changing the plate number and water channel thickness), the shutdown model suggestions are applicable to all of the Al-clad plate-fuelled test cores given the short period range of transients considered and the almost identical plate dimensions.

Examination of the unit-volume based shutdown coefficient with respect to differences in the test core P_{max} and E_{tm} data show that although the B-core data are

self-consistent, the correlation is not as good with the rest of the test core data taken into account. Results are similar for the $\Delta T_{max(a)}$ data.

Revisiting the physics of the void shutdown mechanism suggests a modification to the expression for the shutdown coefficient. The following modification is based on the evidence that the onset of voiding during a short period transient is a surface area phenomenon.

This is in turn based on the fact that the primary mode of heat transfer during a short period transient, up to the time of peak power, is *via* conduction through the fuel plate and conduction into the boundary layer of coolant next to the fuel plate surface (Ref. 4-9). This is true when the speed of the transient is fast compared to the velocity of the coolant flow, *i.e.*,

$$\frac{U}{\alpha_o} \ll H$$

where U is the velocity of the coolant flow, α_o is the reciprocal period of the transient, and H is the axial height of the fuel. For natural circulation coolant flow and the short period range of transients this condition is fulfilled. Results showing that the effect of forced coolant flow are minor are presented in Section 4.4.

This is also supported by the absence of significant coolant temperature feedback prior to the onset of coolant voiding and by good agreement between calculated surface temperatures (using this conduction model) and measured values (Ref. 4-10).

Calculation shows that the temperature rise in the coolant is mainly within a thin boundary layer adjacent to the fuel plate surface (see for example Figure 4-9, and Ref. 4-11). Large thermal gradients exist over this boundary layer and the bulk coolant temperature is not significantly raised prior to voiding (Fig. 4-10).

The other physical characteristic of importance is that the extent of voiding is determined by the size of the coolant channels. This conclusion is drawn considering the volume/density difference between water and steam (on the order of 900 times). Once boiling begins in the coolant boundary layer the pressure generated by the water to vapour phase change drives the rest of the water from the coolant channel (Fig. 4-11). The voiding in a given channel is expected to extend the entirety of the channel.

With these physical considerations in mind, it is postulated that reactor cores with

similar fuel plate geometry will respond in the same way up to onset of voiding. For the same geometry fuel plates voiding will occur at the same power density of a transient, regardless of coolant channel size (*i.e.*, plate spacing). However, once voiding commences the nuclear response will vary depending on the void reactivity generated. This in turn depends on both the size of the void coefficient of reactivity and the size of the void generated (channel size). The varying void reactivity generation leads to variation in the nuclear response (P_{max}, E_{tm}) and associated temperature rise (ΔT_{max}). The different fuel types used in the reactor tests are almost identical in fuel plate geometry but vary widely in fuel plate spacing (coolant channel thickness) and core size leading to varying void feedback reactivity coefficients.

The result of the physical considerations above is an expression for the shutdown coefficient for HEU MTR-type systems. The reactivity response, represented by the shutdown coefficient, w, is therefore proportional to the reactivity produced by complete voiding of a representative coolant channel, and can be written as:

$$w = K_c \left(\frac{- C_{void} V_c}{\ell} \right)$$

where K_c again is a constant of proportionality, C_{void} is the void coefficient of reactivity (in units of reactivity per unit void volume) and V_c is the volume of a representative coolant channel within the void distribution. This expression is herein referred to as the "channel-based shutdown coefficient."

Given estimates of the void coefficient of reactivity, the coolant channel dimensions and the prompt neutron lifetime allows estimation of a shutdown coefficient (due to voiding) for relative comparisons. Differences in the summary test data, quantified by curve fitting, can subsequently be compared to relative differences in the calculated shutdown coefficient parameter. The exponent on the shutdown coefficient may be found from relations in the summary test data. It is then possible to apply this shutdown coefficient scaling factor to compare the data from the different test cores. This is described in detail in the following sections.

Both the central and the uniform void coefficients of reactivity were considered as candidates for the representative parameter of the shutdown coefficient reactivity expression. However, given that the B-12/64 core is characterized by a small but positive central void coefficient, this quantity is not consistent for representing the self-limiting behaviour of all of the test cores. Preliminary results also indicated that

the variations in the test data were not well correlated to the central coefficient, even without taking into account the B-12/64 data point. As a result, only the average void coefficient of reactivity is considered in the rest of this analysis.

Correlations of the power and energy data variation to the relative unit-volume-based and channel-based shutdown coefficients are shown in Figures 4-12, 4-13, 4-14, and 4-15. Use of the channel-based shutdown coefficient results in a correlation suitable to all of the test data compared to the unit-volume-based correlation which is only representative of the B-core data and does not fit the entire set of all test cores. The channel-based coefficient is used for the remainder of the analysis.

4.2.3 Correlation of Data Differences to the Shutdown Coefficient

It remains to estimate the value of the exponent on the shutdown coefficient term in the Shutdown Model expression. This is done herein by correlating the estimated shutdown coefficient values for each of the test cores against the previously determined core-to-core variation of the summary test data.

Estimates of the "central" and "uniform" void coefficients of reactivity for the test cores are available in the literature. Experimental measurements of these two void coefficients were part of the standard nuclear characterisation of the Spert cores and simulation based values for the Borax core have been reported. These values along with other relevant dimensions and nuclear data are summarized in Table 4-7. The void coefficient values included in Table 4-7 are from a variety of technical reports and have been assessed as consistent.

Using the expression derived in Section 4.2.1, estimates of the shutdown coefficient, w, are calculated in terms of (i) published values of the void coefficient of reactivity, (ii) the dimensions of the coolant channels, and (iii) the prompt neutron lifetime. These are summarized in Table 4-8. Note that the sign of the shutdown coefficient is opposite to that of the void coefficients presented in Table 4-7 given the signing convention followed in the Shutdown Model expression.

Expressions for P_{max} and E_{tm} in terms of α_o and the shutdown coefficient, w, are derived from the Shutdown Model (see Section 4.2.1). Linearising these relations by taking natural logarithms gives:

$$\ln\left(P_{max}\right) = \frac{(n+1)}{n}\ln\left(\alpha_o\right) + \frac{1}{n}\ln\left(w\right) + \left(\alpha_o t_d - 1/n\right)$$
$$\ln\left(E_{tm}\right) = \frac{1}{n}\ln\left(\alpha_o\right) + \frac{1}{n}\ln\left(w\right) + \left(\alpha_o t_d - 1/n\right) + \ln\left(q\left(n,0\right)\right)$$

Additionally, from the data regression analysis:

$$\ln\left(P_{max}\right) = m_1 \ln\left(\alpha_o\right) + \ln\left(b_1\right)$$
$$\ln\left(E_{tm}\right) = m_2 \ln\left(\alpha_o\right) + \ln\left(b_2\right)$$

Combining these expressions gives a relationship between the vertical position (magnitude) of the test data ($\ln(b_1)$ and $\ln(b_2)$), and the shutdown coefficient (w):

$$\ln\left(b_1\right) = m \ln\left(w\right) + C_1$$
$$\ln\left(b_2\right) = m \ln\left(w\right) + C_2$$

where m is a common slope value and corresponds theoretically to:

$$m = 1/n = m_2 = m_1 - 1$$

Considering the relative differences between each core data set and the reference data set (*i.e.*, the Spert I D-12/25 data) leads to:

$$\Delta\ln\left(b_1\right) = m\,\Delta\ln\left(w\right)$$
$$\Delta\ln\left(b_2\right) = m\,\Delta\ln\left(w\right)$$

Part of the hypothesis is that the same relation exists for differences in the normalised temperature rise data ($\Delta T_{max(a)}$). This gives a third relation similar to the preceding two:

$$\ln\left(\Delta T_{max(a)}\right) = m_3\ \alpha_o + \ln\left(b_{3(a)}\right)$$
$$\Delta\ln\left(b_{3(a)}\right) = m\,\Delta\ln\left(w\right)$$

Considering the channel-based shutdown coefficient, these three relations are re-plotted in Figures 4-16, 4-17, and 4-18 complete with regression fits, confidence, and prediction lines. The fitting lines on these plots are from weighted linear least squares analysis to the Spert core data points. The regression results are summarized in Table 4-9.

Three correlations are considered:

- to the complete data set,
- to the Spert-core data only (*i.e.*, all except the Borax I data), and
- to the Spert I B-core data only.

In the power-data $\Delta\ln(b)$ *vs.* $\Delta\ln(w)$ plot the Borax data pair appears to be noticeably removed from the rest of the data. This may be due to the fact that the void coefficient estimates for the Borax I core are from simulation, not necessarily consistent with the measurement-based values for the Spert cores. This is justification for excluding the Borax data point. Although inclusion of the Borax I data pair has little effect on the regression value for the slope of the plot as seen in the results (Tab. 4-9).

There is no Borax data point for the energy data as the E_{tm} quantity was not measured in the Borax tests. The effect of removing this data point from the temperature rise correlation is not as significant as for the power data. However, further analysis taking into account the systematic error correction for the temperature rise data puts this more into line with the power data results (see Section 4.2.4). These results are included in Table 4-9 and indicated by the "corrected" designation.

The B-core correlation is examined since the B-core test series were designed specifically to study the effect of void coefficient on the transient response. Physically the same fuel plates and assemblies were used in the three B-cores (some plates were removable) so arguably other system parameters were better controlled (kept fixed) in these tests. The previously mentioned MIT SAR work using the unit-volume-based shutdown coefficient is based on analysis of the B-core data only.

The statistics on the regression analysis show a strong correlation with reasonable R^2 values for all three of the data quantities (P_{max}, E_{tm}, ΔT_{max}). Standard errors of 7%, 8%, and 16% on the slopes are reasonable considering the uncertainty associated with the transient data and the measured nuclear parameters. The standard errors on the

B-core fits are high as a result of only three data points being used for these correlations. The R^2 values, especially for the P_{max} and $\Delta T_{max(a)}$ correlations, indicate the good fits despite the relatively large standard error values.

The average value for the slope <*m*> is found based on inverse uncertainty weighting. Inclusion or exclusion of the Borax data point with the rest of the Spert core data points makes little difference to the final result. It was decided to omit the Borax I data point from the calculation given that it may be subject to significant systematic error relative to the measured Spert coefficients for the reason cited above. It should however be noted that the Borax data falls within the 95% prediction bands about the fitting line and that the inclusion of the Borax I data does not significantly affect the final average slope (exponent <*m*>) result (Tab. 4-9).

The B-core correlation results in a more gradual slope compared to the All-Spert-cores correlation, indicating a weaker dependence on the shutdown coefficient.

The All-Spert-cores and B-core shutdown coefficient scaling factors and their associated ratios to the Spert I D-12/25 core values are summarized in Table 4-10. These values are based on the uniform void coefficient of reactivity. The average values for *m*, inversely weighted by the standard errors are:

$$\begin{aligned} m &= 0.726 \pm 0.063 \quad \left(all\ Spert-core\ data\right) \\ m &= 0.490 \pm 0.089 \quad \left(B-core\ data\ only\right) \end{aligned}$$

where the average is taken for the P_{max}, E_{tm}, and ΔT_{max} results.

For interest sake the exponent on the scaling factor, *m*, is predicted by the Shutdown Model to be:

$$m = 1/n$$

where *n* is characteristic of the slope of the curve through $\ln(P_{max})$ *vs.* $\ln(\alpha_o)$, and $\ln(E_{tm})$ *vs.* $\ln(\alpha_o)$. From the $\ln(P_{max})$ *vs.* $\ln(\alpha_o)$ and $\ln(E_{tm})$ *vs.* $\ln(\alpha_o)$ correlations for the Spert I D-12/25 reference data set we find:

$$\begin{aligned} P_{max}: &\quad (n+1)/n = 1.597 \pm 0.029 \quad \rightarrow \quad 1/n = 0.597 \pm 0.029 \\ E_{tm}: &\quad 1/n = 0.574 \pm 0.017 \end{aligned}$$

Qualitatively the results agree as the power and energy data behaviour are in agreement. The regression-based values for the exponent on the shutdown coefficient term differ from that suggested solely by the Shutdown Model (*i.e.*, the slopes from the $\ln(P_{max})$ and $\ln(E_{tm})$ vs. $\ln(a_o)$ plots). This is due to the fact that the regression-based values are associated with the working approximation of the uniform void coefficient of reactivity. In this sense the discrepancy in exponent values is not unexpected. The regression-based values, m, and associated estimates for w should be considered the working model values as opposed to the Shutdown Model predictions.

The values of m determined from the $\Delta\ln(b)$ *vs.* $\Delta\ln(w)$ correlations are used herein as it is associated directly with the shutdown coefficient of reactivity based on the uniform void coefficient estimations.

4.2.4 Systematic Error Correction for the Temperature Rise Data

With respect to the temperature rise data, a further correction was investigated to account for systematic error introduced by position and attachment style of the specific thermocouples.

The sources of systematic error correction are approximated as follows (see Chapter 3 for more details on uncertainty estimates):

- **Peening** thermocouple attachment is estimated to result in +10% to +25% on the surface temperature measurements.
- **Axial centerline location** of the thermocouple is estimated to result in -10% on the maximum temperature rise at the axial peak, which occurs at roughly 3" to 4" below the axial centerline due to the presence of the shim rods in the top of the core.
- **Radial location** of the thermocouple in relation to the hot plate in the core. This is assessed on a case by case basis with consideration to factors affecting the local power peaking such as proximity to water-filled control blade gaps. Off-peak radial location is estimated to result in systematic errors typically on the order of -5% to -10% on the ΔT_{max} data.

Both the axial and radial location adjustments are based on simulation experience,

reported in Reference 4-12. Totalling these components the following corrections are made to the data:

- Borax ΔT_{max} data are **increased** by 15% to account for off-peak axial (-10%) and radial (-5%) location of the surface thermocouples in assembly position 21.
- Spert I A- and B-core ΔT_{max} data are **decreased** by 10% to account for higher temperature measurements from the peened thermocouples (+25%) partially offset by off-peak axial (-10%) and radial (-5%) placement.
- The Spert I and IV D-12/25 ΔT_{max} data are **not adjusted** given that the surface thermocouples are located at approximately the axial flux peak on what is assessed as the hottest plate in the core.

These additional corrections to the temperature data improve the correlation with the power data behaviour. This is shown in both the correlation of the relative magnitudes of the temperature rise data with the relative magnitudes of the power data (Fig. 4-19), as well as in the correlation of the relative magnitudes of the temperature data with the relative shutdown coefficient (Fig. 4-20). The regression analysis results for the temperature rise data as a function of the shutdown coefficient are included in Table 4-9 and designated by the "corrected" notation. These results however are not included in the average exponent calculation given their preliminary nature.

In terms of the correlation statistics, no improvement is noted in the corrected $\Delta T_{max(a)}$ data with respect to the E_{tm} data behaviour. This is due to the absence of the Borax I data pair which has the most influence on the temperature and power correlation.

The "corrected" temperature rise data are also discussed in the following section regarding the scaled data. Refinement of the systematic error correction is left as future work.

4.2.5 Scaling of the Test Data

To show the effectiveness of the void correction model the channel-based shutdown coefficient scaling is applied to the summary test data from the various test cores. The previously derived expressions suggest that the P_{max}, E_{tm} and ΔT_{max} data scale inversely with:

$$w^m = \left(K_c \left(\frac{-C_{void} V_c}{\ell} \right) \right)^m$$

where m has been empirically determined parameter from the preceding $\Delta\ln(b)$ *vs.* $\Delta\ln(w)$ correlation analysis:

$$m = 0.726 \pm 0.063 \quad (all\ Spert\text{–}core\ data)$$
$$m = 0.490 \pm 0.089 \quad (B\text{–}core\ data\ only)$$

and w is the channel-based shutdown coefficient based on the uniform void coefficient of reactivity as defined previously (see Section 4.2.1).

Using the scaling factor and the Shutdown Model theory, P_{max}, E_{tm} and ΔT_{max} values from one core, i, can be compared to those from a second core, j, as:

$$w_i^{1/n} P_{max,i} = \alpha_o^{(n+1)/n} e^{(\alpha_o t_d)} = w_j^{1/n} P_{max,j}$$

Similar expressions can be formed for E_{tm} and $\Delta T_{max(a)}$. Replacing $w^{1/n}$ with w^m as determined from the $\Delta\ln(b)$ *vs.* $\Delta\ln(w)$ regression, these relations can be written as:

$$P_{max,j} = \left(w_i / w_j \right)^m P_{max,i}$$
$$E_{tm,j} = \left(w_i / w_j \right)^m E_{tm,i}$$
$$\Delta T_{max,j} = \left(w_i / w_j \right)^m \left[\Delta T_{max,i} \times V_{f,i} / V_{f,j} \times PPF_j / PPF_i \right]$$

Using these relations, the summary data over the short period range, originally presented in Figures 4-4, 4-5, and 4-6, are replotted having been scaled by the above factors relative to the Spert I D-12/25 data (an arbitrary choice). Scaling using both values for the exponent m (from the All-Spert-cores and B-core correlations) are considered. The scaled data are shown in Figures 4-21, 4-23, and 4-25 for the scaling using the all-Spert-cores derived exponent, and in Figures 4-22, 4-24, and 4-26 for the scaling using the B-core derived exponent. The reference slopes from the Spert I D-12/25 data are retained for the curve fits shown on these figures. The results of curve fitting to the scaled data are summarized in Tables 4-11, 4-12, and 4-13.

The relative differences between data from the various cores has been significantly reduced by the void factor scaling. Originally the P_{max}, E_{tm}, and $\Delta T_{max(a)}$ data varied by a factor of about five. This has been reduced by the void correction scaling by at least a factor of two.

It is clear upon examination of the scaled data (Figures 4-21 through 4-26) that, although the core-to-core variation is reduced, some core-to-core dependence still remains after scaling. This explains the relatively poor (*i.e.*, low) R^2 parameter values for the common curve fitting, especially for the energy and temperature rise data. It should be noted that the regression results are based on a regression treating each data point individually rather than by grouping the data by core and performing the analysis based on variation of each data sub-set from the predicted value. This results in disproportionate weight of the results being placed on the core test series with more data points. In hindsight, this latter approach would be more appropriate. As such the regression results for this final result should be considered illustrative only.

Using the all-Spert-cores based scaling factor, the two extremes of the data, *i.e.*, the Spert I B-12/64 (upper bound) and the Spert I D-12/25 (lower bound) data sets collapse approximately onto each other. The results are also quite good for all but the Spert I B-24/32 and Spert I B-16/40 cores. The B-24/32 data remain offset (higher) than the rest of the scaled data and accounts for most of the variance in the scaled data set. The order of the B-core data sets is reversed upon application of this scaling factor, indicating that the channel-based shutdown scaling (using the reported experimental void coefficient and prompt neutron lifetime values) over-corrects the differences in the B-core data. While the B-12/64 data are scaled sufficiently, the B-24/32 data are under-corrected with the B-16/40 data intermediate. The core-to-core variation is reduced by a factor of approximately two. In the case of the P_{max} data, the scaled Borax I results are even further removed from the curve fit than the B-24/32 data. This is not seen for the scaled $\Delta T_{max(a)}$ data suggesting it is an artifact of the Borax power data calibration compared to the Spert power data.

The second scaling, *i.e.*, that using the B-core derived exponent in the scaling factor, removes the inter-core variation between the B-core data sets. However, these three data sets remain offset from the rest of the test data (higher values) after the scaling is applied. Overall there also remains some noticeable offset between the A-core and D-core data sets. The overall "spread" of the data, similarly bounded by the B-24/32 data set (upper bound) and the D-12/25 data sets (lower bound), is slightly greater than found when using the all-Spert-cores derived exponent in the scaling factor.

The remaining core-to-core variation may also be seen *via* plotting of the residuals to the common fitting curves. The $\Delta T_{max(a)}$ residual plots for the data scaled using the all-Spert-cores and B-core scaling factors are shown in Figures 4-27 and 4-28, respectively.

A model capturing all of the trends in the data will show only a random pattern in the residuals. The pattern in the residuals indicates that some of the differences in the data are not accounted for within this model. This may either be due to limitations in the model, other secondary parametric dependencies, or systematic uncertainties in the data which have not been corrected for. The patterns in the residuals are consistent between the P_{max}, E_{tm}, and $\Delta T_{max(a)}$ scaled data.

Assuming that the variation in void reactivity characteristics is the primary and only major parametric dependence, then the all-Spert-cores derived exponent and associated scaling factor is the most applicable of the two scaling factors studied herein. The remaining offset in the data may be attributable to limitations in the model and uncertainties in the Shutdown Coefficient, the latter likely due to the uncertainty in the void coefficient measurements and prompt neutron lifetime estimates. The results suggest an under-estimation of the Spert I B-24/32 core shutdown coefficient. This is supported by the location of the B-24/32 data point on the $\Delta\ln(b)$ *vs.* $\Delta\ln(w)$ plots for the power, energy and temperature rise correlations (Figs. 4-16, 4-17, and 4-18).

The B-core derived exponent and associated scaling factor may prove more valid than the corresponding All-Spert-cores derived factor if a secondary parametric dependence is identified. The validity of this scaling factor is not supported by the remainder of the data points in Figures 4-16, 4-17, and 4-18. Refinement of the model is left as future work. Both scaling factors, and the resulting residuals should however be considered as part of any future refinement.

The tabulated scaled regression fits are associated with scaling relative to the Spert I D-12/25 data and thus are related to the Spert I D-core nuclear parameters.

It is the author's suggestion that the void scaling based on the all-Spert-core derived exponent and associated scaling factor be adopted as the working model. As it stands, the working model provides single fitting curves to the test core data as a whole with standard deviations and 95% prediction bands of:

	Standard Deviation	95% Prediction Band Width
P_{max}	25%	49%
(P_{max}, *no Borax*)	(13%)	(26%)
E_{tm}	16%	32%
$\Delta T_{max(a)}$	23%	46%

The upper 95% prediction band may be used in analysis as a conservative upper bound of the P_{max}, E_{tm}, and $\Delta T_{max(a)}$ data as a function of reciprocal period.

The standard deviation and 95% prediction bands for the P_{max} data are significantly reduced if the Borax data are left out of the curve fitting. Justification for this revolves around the different measurement technique used in the Borax tests, basing P_{max} values on insulated thermocouple calibrations rather than calorimetric methods using the entire reactor core. The Borax I P_{max} data are subject to systematic uncertainty on the order of 21% (Chapter 3). The data scaling results suggest that the Borax I power data are systematically over-estimated.

Marginal improvement is seen in the $\Delta T_{max(a)}$ statistics based on corrections for estimated systematic errors from the thermocouple specifics (these results are included in Table 4-13).

The uncertainty estimates (from error propagation) for the scaled P_{max}, E_{tm}, and $\Delta T_{max(a)}$ data are on the order of 12% to18% varying with each specific core. These estimated uncertainties are on the same order as the standard deviations of the scaled data fits.

Overall, the relative scaling of the Borax and Spert test data has reduced variability between data from different test cores from a factor of five to a factor of two. This can be represented by single curve fits with 95% prediction bands on the order of less than 50% variance (significantly less for the P_{max} and E_{tm} data only considering the Spert experiments) but there is recognized remaining variance between core data sets.

These remaining differences in the data from the different cores may be due in part to uncertainties in the measured values used to estimate the shutdown coefficient or to deficiencies in the model itself. Refinement and extension to the model is left as future work.

4.2.6 A Remark on Shutdown Voiding Dynamics

The experimental results also provide some evidence regarding the voiding dynamics of the MTR-type core under these RIA conditions. The onset of voiding first occurs at the hot point in the core, corresponding to the location of peak power density. As the temperature of the core increases, additional voiding commences at different locations in the core when the surface temperature in these locations reaches the voiding onset temperature. The temperature increase up to the onset of boiling/voiding is governed by the asymptotic reactor period.

The actual void distribution within the core at different stages of the transient may be a complex function of heat transfer and hydraulics. This has not been measured experimentally and given the lack of fundamental understanding of transient heat transfer and voiding dynamics it is not currently predictable using simulation techniques. However, the correlation between P_{max}, E_{tm}, and ΔT_{max} and the shutdown coefficient, as presented herein, indicates that the void distribution at the time of self shutdown is amply represented by a uniform distribution.

This result suggests that the speed of the transient (period) which governs the temperature rise is much shorter than the time required to void a typical coolant channel. Suggesting that expelling the water coolant from the coolant channels is the limiting step in the shutdown mechanism rather than the heat transfer to the coolant from the fuel plate. This is likely a consequence of the inertia of moving the water from the coolant channel. Physically, while the steam generated in the boundary layer of the first coolant channel is expanding to expel the water from the rest of the channel, the rest of the core has "caught up" in terms of temperature and similarly started the voiding process. The overall effect is that, despite the non-uniform temperature distribution, the core voids almost uniformly to provide the shutdown reactivity.

With this in mind, the channel thickness, rather than the total channel volume, may be a more suitable factor in the channel-based shutdown coefficient expression. This is inconsequential in the current analysis given the similar width and height of the different test core coolant channels (and typical nature of these dimensions with respect to modern MTR-type design). Physically, given thickness to height ratios on the order of 1/200, it is not hard to imagine that voiding may extend the thickness of the coolant channel long before expanding the axial extent of the channel.

The above further suggests that parametric dependence on fuel meat and clad

thickness may be minor for typical MTR-type fuel dimensions.

4.3 The Effect of Subcooling

The analysis in this section investigates the parametric dependence of the transient summary data quantities P_{max}, E_{tm}, ΔT_{max}, on the initial subcooling of an HEU Al-clad plate-fuel core.

This effect was studied in both the Borax and Spert Projects. Quantification of this effect allows for application of the experimental data, to a given reactor core operating at a subcooling intermediary to or beyond the range of the values investigated experimentally. Consideration of the Spert subcooling tests builds on existing analysis based solely on the Borax data (Refs. 4-13, 4-14). The analysis herein also studies the 1954 Borax data set which was not available at the time of the analysis in the aforementioned reference.

4.3.1 Theory

A review of the physics behind the self-shutdown behaviour of an MTR-type core indicates that voiding of the coolant *via* boiling is the primary shutdown mechanism in HEU cores and is one of two primary mechanisms in LEU cores (the other being fuel temperature, *i.e.*, Doppler, feedback). The onset of coolant voiding depends on the initial temperature of the coolant, or more specifically the subcooling of the system. Subcooling is defined as the saturation temperature of the coolant minus the initial temperature of the coolant, *i.e.*,

$$T_{sub} \equiv T_{saturation}^{coolant} - T_{initial}^{coolant}$$

where T_{sub} is referred to as the degree of subcooling. A lower initial temperature, or higher degree of subcooling, will delay the onset of boiling as the coolant will require more energy to reach saturation. In other words, more energy (and time) is required to heat the coolant prior to the onset of boiling. This causes a delay in the production of negative void feedback. The delay is increased as the subcooling is increased. A delay in the onset of boiling during an RIA will result in higher peak power, energy generation and fuel temperature rises. This is the effect of subcooling and is shown schematically in Figure 4-29.

This effect was investigated in both the Borax and Spert Projects. This subcooling

data subset is described in Chapter 3. It is comprised of a test series conducted in 1953 with the Borax I core and test series performed with the Spert I B-cores. Tesets from both ambient and saturation initial conditions were conducted in the Spert I A-core and an additional subcooling test series linked to high temperature and pressure operation (although one test series was made under atmospheric pressure conditions) was conducted in the Spert III C-core. Additionally tests with varied hydrostatic head with the Spert IV D-core are also applicable to the subcooling effect.

The 1953 Borax I subcooling data are in terms of total energy generated and maximum fuel plate temperature for various degrees of subcooling. The energy data are shown in Figure 4-30 (Ref. 4-15) while the temperature data have been replotted in degrees centigrade and is shown in Figure 4-31. This data set has been used in SAR reports for two MTR-type reactors, the Michigan (Ford) Nuclear Reactor (FNR, Ref. 4-13) and the McMaster Nuclear Reactor (MNR, Ref. 4-14). The latter simply involves extrapolating the maximum fuel temperature data for the two transient periods investigated to subcooling typical of MNR operation. The former assumes that the transient response in terms of temperature of the fuel is a function of period (τ) and subcooling (s) only and that the two dependencies are separable, *i.e.*,

$$\Delta T_{max}(s,\tau) = S(s)R(\tau)$$

Given this assumption, the response for a transient of a specific period for two different subcoolings, expressed as a ratio, is a function of the subcooling only,

$$\frac{\Delta T_{max}(s_1,\tau)}{\Delta T_{max}(s_2,\tau)} = \frac{S(s_1)R(\tau)}{S(s_2)R(\tau)} = \frac{S(s_1)}{S(s_1)}$$

This allows for application of the subcooling effect to any given period rather than limiting the analysis to the two periods investigated experimentally. When one of the subcoolings is zero, *i.e.*, the initial temperature is saturation, this is expressed as:

$$\frac{\Delta T_{max}(s,\tau)}{\Delta T_{max}(0,\tau)} = \frac{S(s)}{S(0)} = constant \times S(s)$$

Quantification of this effect simply entails evaluation of the constant in the above expression. This allows the differences in the transient response (*e.g.*, P_{max}, E_{tm}, ΔT_{max}) to be evaluated in terms of differences in the initial subcooling.

This approach was used to determine the maximum credible accident reactivity insertion limit for FNR in their 1957 SAR (Ref. 4-16) and is also used in their 1984 SAR update (Ref. 4-17).

Herein, the separability argument is considered with respect to extended experimental data base (*i.e.*, the original 1953 Borax data and the subsequent 1954 Borax data as well as the applicable Spert B-core data with varying subcooling which were not available at the time of the original analysis). The Borax data are also re-analysed rigorously with least squares regression to determine the multiplicative constant.

4.3.2 Separability of Subcooling and Period Dependence

The functional curve fits applied to the ambient test data from the various test cores are considered with respect to the data from the same test core but from different initial temperature conditions. This investigates the separability of the subcooling and period dependencies in the data.

In analysis of the parametric dependence on void shutdown coefficient, curve fitting is used to quantify of differences in the data from the different test cores (see Section 4.2). Curve fitting to the transient summary data quantities P_{max}, E_{tm}, and ΔT_{max} is performed for step insertion tests from ambient initial conditions (see Appendix C). From this analysis, describing functions for the three quantities are identified as:

$$\begin{aligned} P_{max} &= b_1 \alpha_o^{\,m_1} \\ E_{tm} &= b_2 \alpha_o^{\,m_2} \\ \Delta T_{max} &= b_3 e^{m_3 \alpha_o} \end{aligned}$$

where m_1, m_2, and m_3 are common for the type of data (*i.e.*, power, energy, or temperature) and the coefficients b_1, b_2, and b_3 vary between cores.

The hypothesis of separability of period and subcooling dependence means that the period dependence of the describing functions for P_{max}, E_{tm}, and ΔT_{max}, based on the ambient test data, should be applicable to test data from different initial temperatures. The subcooling data subset is considered with respect to this hypothesis.

The Borax tests included step insertion transients conducted from both saturation and ambient (~25EC) initial temperatures. The P_{max} and ΔT_{max} results are shown in

Figures 4-32 and 4-33 for these two data sets. The slope of the trendlines shown in these figures is that of the Reference Data Set from the ambient step data (see Appendix C). The multiple trendlines for $T_i = T_{sat}$ on the temperature rise plot represent fits to the data from different thermocouples.

The dependence on period derived from the ambient test data looks a reasonable representation for the test data from saturation conditions, especially over the period range from 35 msec to 10 msec ($29\ sec^{-1} < \alpha_o < 100\ sec^{-1}$). The shortest period data point (5 msec period, $\alpha_o = 200\ sec^{-1}$) does deviate noticeably from the curve fit but does so in a positive sense for the P_{max} data and a negative sense for the ΔT_{max} data. Unfortunately the size of the saturation test data set is small so definitive quantitative conclusions are difficult to make. The Borax I destructive test point (2.6 msec period) in the ambient data set is not included given the approximate nature of the estimated power (between 13,000 and 20,000 MW) and the lack of temperature data (plus melting phase change differences).

The separability of period and subcooling dependence is further investigated by consideration of the Spert I B-core data. These results are shown in Figures 4-34 to 4-42 for the three summary data quantities from the three B-cores. The Spert I B-core test data set illustrates the effect of subcooling over a wider range of periods than the Borax I 1953 subcooling tests. Much of this data are in the longer period range, *i.e.*, periods > 35 msec. The trendlines in these figures also adopt the slope of the ambient data reference fit. The trends in the data do not contradict the ambient data fitting although some deviations are noted, especially in the test data from initially saturation temperature.

It is also noted that differences in the data due to changes in subcooling on the order of 20EC to 40EC are often on the same order as the uncertainty (or variance) in data from a fixed initial temperature. For example, see the overlap of data points for tests from T_i = 20EC, 40EC, and 60EC for the B-24/32 core and the overlap of the T_i = 80EC and saturation points in the P_{max} *vs.* α_o plot for the B-16/40 core. However, some of the plots do show well spaced data for different subcoolings, see for example the E_{tm} *vs.* α_o plots for the B-16/40 and B-12/64 cores. The former also includes more than one data point for the highest initial temperature tests (T_i = 80EC and saturation), lending more weight to the curve fitting.

Additionally, it is shown that the three quantities are strongly correlated, *i.e.*, the same behaviour of the data with subcooling being evident in the P_{max}, E_{tm}, and ΔT_{max} plots for a given core. In this sense trends in one quantity illustrate the behaviour of

the other two quantities. This is consistent with behaviour noted in the ambient data set with varying void characteristics between the different test cores (see Section 4.2).

This correlation between the summary data quantities is particularly useful when studying this subcooling data subset where the amount of data is sparse, particularly the temperature rise data set which is further reduced in size upon consideration of data from the same thermocouple (given that large systematic variation exists between different thermocouples). In this sense placing a fitting line through a single temperature data point is given more credence when the associated energy and/or power data, for which multiple data points exist in some cases, are considered.

A preliminary assessment of the Spert IV D-core step tests with varying hydrostatic head (and therefore saturation temperature and subcooling) indicates that this data set is also consistent with the effect of subcooling observed in the Borax and Spert I B-core tests. The increase in hydrostatic head from two feet to 18 feet of light water above the core increases the subcooling by about 11EC. The test data are included in Appendix B.

Given the scarcity of data at elevated initial temperatures it is difficult to draw quantitative conclusions with respect to the curve fitting. For now, application of the ambient data functional dependence with period is considered reasonable for the saturation and intermediate data sets and the argument of separability of the subcooling and period dependencies is accepted. A further consideration with regards to this functional separability argument is included in the closing remarks in Section 4.3.4.

4.3.3 Subcooling Effect Model

The subcooling model treated herein is based on the Borax 1953 test data with support of the underlying assumptions from the Borax I 1954 subcooled tests, and the Spert I B-core tests. The Borax I subcooling temperature data (Fig. 4-31) are replotted as functions of transient reciprocal period in Figures 4-43, 4-44, and 4-45 for the three different thermocouples (21-4-c, 21-1-c, 21-1-s, where "c" and "s" designate "center" and "surface" type thermocouple attachments). This style of data plot is typical of the Spert Project results and shows the consistent behaviour of the two tested periods (13 msec and 22 msec). The two fitting curves (*i.e.*, lines on the semi-log scale) use the reference slope value from the curve fitting to the ambient data set and are through the "ambient" and "saturation" initial temperature data points. The curves indicate the bounds of the Borax subcooling tests in terms of

degrees of subcooling. These plots suggest that increasing the subcooling by a given amount simply shifts the fitting curve upwards from the saturation tests curve. This is exactly the postulate of period/subcooling separability.

To investigate the amount and relationship of the "shift" with increasing subcooling, the data from the 21-1-c thermocouple is replotted in Figure 4-46 in terms of the ratio of the temperature rise from the given degree of subcooling to the temperature rise from initially saturated conditions (*i.e.*, zero subcooling). The temperature rise ratio is defined as:

$$\Delta T_{max}\, ratio \quad \equiv \quad \frac{\Delta T_{max}\left(T_{sub}\right)}{\Delta T_{max}\left(T_{sat}\right)}$$

Expressed in this way the data from the 13 msec tests falls on top of the data from the 22 msec tests. Linear least squares regression to the data shows that fitting to the 13 msec data and fitting to the 22 msec data agrees within standard error with fitting to the entire data set. The 95% confidence bands (within which the fitting slope may vary) and the 95% prediction bands (within which 95% of the data are expected to fall) are indicated for the fit to the combined 13 msec and 22 msec data. Similar results were found for the data from the other two thermocouples.

The regression results for the Borax I temperature data are summarized in Table 4-14. The average value for the slope, +*m*,, indicated in the table is the average of the regression results inversely weighted by the standard errors. The average slope is:

$$\left\langle m \right\rangle \quad = \quad \left\langle \frac{\Delta\left(\Delta T_{max}\, ratio\right)}{\Delta T_{sub}} \right\rangle \quad = \quad 0.0424 \pm 0.0071\ per\ °C$$

In other words, the ratio of the response (*i.e.*, temperature rise) to that produced from saturation conditions increases by a value of 0.0424 for every increase of a degree in subcooling.

The curve fitting to the Spert I B-core data allows for similar relationships to be plotted in terms of the *y*-intercept ratios for various degrees of subcooling for all of the P_{max}, E_{tm}, and ΔT_{max} data. The Spert I B-core data are plotted in Figure 4-47 as a ratio to the saturation curve fitting. There is considerable scatter in the data. This is thought to be mainly due to the lack of available data and uncertainty in the saturation data curve fitting *y*-intercept values upon which all of the ratios are based.

Replotting the Spert I B-core data (Fig. 4-48) as ratios to the ambient data fits (which are better determined given the larger amount of data) reduces the scatter in the data and shows agreement between the P_{max}, E_{tm}, and ΔT_{max} data and also between the data from the different cores.

An example of the subcooling effect, using the Borax I regression result, is shown in Figure 4-49. Two different subcoolings are considered: 97EC (conservative MNR estimate) and 73EC (Borax I maximum), giving a difference in the degree of subcooling of 24EC. The corresponding ratios of the ΔT_{max} response of the system from these subcoolings to that from initially saturation conditions are indicated, *i.e.*,

$$\Delta T_{max}\, ratio\left(97°C\right) \equiv \frac{\Delta T_{max}\left(T_{sub} = 97°C\right)}{\Delta T_{max}\left(T_{sub} = 0°C\right)} = 5.11$$

$$\Delta T_{max}\, ratio\left(73°C\right) \equiv \frac{\Delta T_{max}\left(T_{sub} = 73°C\right)}{\Delta T_{max}\left(T_{sub} = 0°C\right)} = 4.10$$

To compare the maximum temperature rise for the two degrees of subcooling these two values are considered as a ratio (*i.e.*, a ratio of the ratios):

$$\begin{aligned} Subcooling\ Factor\ (T_{sub}\text{–}Factor) &\equiv \frac{\Delta T_{max}\, ratio\left(97°C\right)}{\Delta T_{max}\, ratio\left(73°C\right)} = \frac{\Delta T_{max}\left(T_{sub} = 97°C\right)}{\Delta T_{max}\left(T_{sub} = 73°C\right)} \\ &= \frac{5.11}{4.10} = 1.25 \end{aligned}$$

In other words, for this example, the maximum temperature rise for a subcooling of 97EC will be a factor of 1.25 higher than that for a subcooling of 73EC. In general the effect of subcooling can be expressed as:

$$\Delta T_{max}\left(T_{sub,i}\right) = T_{sub}\text{–}Factor \times \Delta T_{max}\left(T_{sub,j}\right)$$

where,

$$T_{sub}\text{–}Factor \equiv \frac{\Delta T_{max}\, ratio\left(T_{sub,i}\right)}{\Delta T_{max}\, ratio\left(T_{sub,j}\right)} = \frac{\left(1 + 0.0424\, T_{sub,i}\right)}{\left(1 + 0.0424\, T_{sub,j}\right)} \quad , \quad subcooling\ in\ °C$$

This scaling factor is applicable to the temperature rise as well as the maximum power and generated energy and is also applicable to transients of any given period in the short period range (35 msec $ τ). Application of this factor as part of a full parametric variation analysis is discussed in Chapter 7.

4.3.4 Additional Remarks

There is some suggestion that the saturation and ambient data sets may converge at very short periods (see for example the B-12/64 P_{max} and E_{tm} *vs.* α_o plots in Figures 4-40 and 4-41). This would also be consistent if the "short period range" was extended to longer periods for the saturation tests. An argument can be made for extending this period range given that the short period range is defined based on it being the range of periods where shutdown is by voiding from boiling rather than slower mechanisms. For initial temperature at coolant saturation it physically makes sense that the onset of boiling is sooner for longer periods. Boiling shutdown can be confirmed from the individual test temperature time traces.

The limited amount of data in the Spert I B-core sets is prohibitive to further quantification of the subcooling effect, at least to the same degree of accuracy as available in the Borax I data. However, the effect of convergence of ambient and saturation test data at very short periods is also suggested by the data from the Spert I A-core tests from varying initial temperature (Ref. 4-18). These data were located post-analysis and has not been subject to rigorous curve fitting. Use of the presented methodology therefore may represent a conservative treatment of the subcooling effect, over-estimating any penalties to a reactivity margin at short periods.

Given that a change in subcooling physically translates to a change in the time to onset of boiling shutdown, one avenue of further work is to consider the subcooling effect as appearing in the "delay time" factor in the Shutdown Model (see Section 4.2.1).

Further investigation into the functional dependence on period and the subcooling

effect at elevated initial temperatures is left as future work.

4.4 The Effect of Coolant Flow

In modern day MTR-type reactors, operation at power levels on the order of MWs requires degrees of cooling only available with forced coolant flow. As a result, an operating state with forced coolant flow must be added to the sets of conditions considered in a safety analysis of reactivity insertion accidents. It is therefore of interest to consider the effect of coolant flow on the self-limiting transient response of an MTR-type system.

4.4.1 Experimental Data Investigating Coolant Flow Effects

The Spert IV facility was designed to include the capability of forced coolant flow. Step initiated transient test series were conducted with forced upward coolant flow up to 5000 US gpm (12 ft/sec) in this test series. The relationships of P_{max} and ΔT_{max} *vs.* α_o results are shown in Figures 4-50 and 4-51, respectively, for both natural circulation and forced upward flow.

A coolant flow of 1600 US gpm in the downward direction is typical for 2 MW operation of MNR. Typically flow is downward in present day operating pool reactors. Differences due to flow direction are considered herein.

4.4.2 Data Trends

Forced flow delays the onset of voiding and thus the appearance of void feedback by removing energy from the core. As a result the maximum power for a transient of a given period is increased with the addition of forced flow relative to natural circulation coolant conditions. This is illustrated in Figure 4-50.

The effect on temperature rise is also small but is opposite to that for maximum power. The addition of forced flow increases the cooling during the transient. During the power rise the heat removal is improved and following the power peak the channel refilling is faster also leading to improved cooling. The decrease in ΔT_{max} with upward forced flow is shown in Figure 4-51.

The effect becomes small for transients in the short period range (τ_o # 35 msec, α_o $ 29 sec^{-1}). For periods of 10 msec and less the effect on maximum temperature rise

was found to be insignificant (Ref. 4-19). These results are for tests with forced upward flow.

No reactor tests were performed under forced downward flow conditions. In the case of forced downward flow the buoyancy force acts opposite to the flow direction. As a result any trends found for forced upward flow are slightly reduced. Maximum powers and temperature rises for forced downward flow conditions are enveloped by the natural circulation and forced upward flow results.

For a transient with a given period, the maximum power with a given forced downward flow will be no higher than that for the same forced flow in the upward direction (*i.e.*, forced downward flow P_{max} data are bounded by a maximum of the forced upward flow data). The maximum temperature rise for a transient with a given period under forced downward flow conditions will be no higher than that for the same period transient under natural circulation conditions (*i.e.*, the forced downward flow ΔT_{max} is bounded by a maximum of the natural circulation data).

Note that for fuel with non-uniform channel spacing the limiting plate surface temperature in narrow channels may not necessarily govern the self-limiting process. As a result limited local fuel damage may occur in situations where the core otherwise successfully self-limits a transient. This situation was found in the Spert IV D-12/25 core for very short period transients precluding widespread core damage (Ref. 4-19).

4.4.3 Assessment with Respect to Safety Limit

The transient test data from the Spert Project show that variation of coolant flow has little to no effect on the self-limiting response of an MTR-type system. The effect is further reduced as the period is shortened (*i.e.*, the size of the reactivity insertion and the subsequent speed of the transient are increased). Therefore the reactor test data collected for natural circulation conditions for uniformly spaced plates are conservative relative to forced upward or downward flow with respect to the maximum temperature rise resulting from the initial power peak.

This conclusion is in agreement with similar work reported by Thie (Ref. 4-6) based on the Spert III C-core test data from ambient initial conditions. This latter work was used to justify a conservative approach in the MIT 1970 SAR (Ref. 4-7).

Note that flow direction may affect longer term stability characteristics of a core

under unprotected transient conditions. This is discussed in Chapter 5.

In addition, localized fuel damage may be of concern for fuel with non-uniform coolant channel thickness as discussed previously in Section 4.4.2.

4.5 Additional Factors

The preceding sections have addressed the parametric dependence of the self-limiting response of an MTR-type core on void reactivity feedback characteristics, subcooling, and coolant flow.

Additional factors worth considering include:

- operating history,
- reflector characteristics,
- clad and meat geometry,
- hydrostatic head/pressure, and
- initial power.

The test core data are from clean, cold, HEU cores. Exposure of the fuel (*i.e.*, burnup/depletion) was insignificant during the transient testing. This is in contrast to existing working reactors such as MNR which operate with an equilibrium core. Differences due to operating history are however implicitly accounted for in the nuclear parameters used in the methodology, *i.e.*, the void coefficient of reactivity, the prompt neutron lifetime, and the power peaking factors describing the core. Both the void coefficient of reactivity and the prompt neutron lifetime appear in the expression derived for the shutdown coefficient of reactivity scaling term. The prompt neutron lifetime differences are also taken into account explicitly when translating limiting reactor period to the associated reactivity insertion value (and *vice versa*). The same is true for any differences in fuel material affecting the delayed neutron characteristics of the core. Operating history is explicitly accounted for in the definition of safety limits applicable to irradiated fuel. This is discussed in more detail in Chapter 7.

Similarly, other differences between the system of interest and the test cores, such as reflector materials and geometry, and fuel plate geometry are also accounted for in terms of the nuclear parameters of interest at the time of nuclear characterisation of the core.

Differences in clad and meat geometry will also alter the internal plate temperature distribution with the centerline temperature of a thicker plate being hotter than that of a thin plate with the same internal energy generation. This is the result of it taking longer to "get the heat out" of a thicker plate as the energy is deposited preferentially in the fuel meat and must be conducted through the clad. The reactivity limit has been shown to be fairly insensitive to changes in thermal conductivity of the plate (Fig. 4-52, Ref. 4-20) suggesting that small differences in meat and clad thickness are likely second order effects.

In the case that the fuel plates are thicker than those used in the test cores the centerline temperature for very short period transients should be considered with respect to cladding-temperature-based safety limits to confirm that other limits are not exceeded (*i.e.*, vapourization temperature as hypothesized for the SL-1 reactor accident).

Pressure differences resulting from differences in hydrostatic head associated with open pool operation are implicitly taken into account in the subcooling correction given the change in saturation temperature. For higher pressure operation, typical of pressure vessel systems, the test data may be revisited as test series at elevated temperature and pressure were performed but are not included in the analysis herein. Information on these tests is included in Appendix B.

Finally, the applicability of the test data to events occurring at elevated initial power has not explicitly been studied herein. Indications are however, that low initial power data are conservative with respect to higher power conditions from the standpoint of the initial power pulse. This is illustrated in the testing of this parameter with respect to ramp insertion transients (Fig. 4-53, Ref. 4-21). Higher initial power allows for earlier influence of feedback mechanisms and likely reduces the subcooling of the system. It should also be considered that high initial power also reduces the remaining temperature defect associated with the change from initial to saturation coolant conditions. This is relevant to longer term stability margins (see Chapter 5).

4.6 References

4-1. P. R. Bevington, D. K. Robinson, Data Reduction and Error Analysis for the Physical Sciences, Second Edition, McGraw-Hill Companies Inc., 1992, ISBN 0-07-911243-9.

4-2. G. O. Bright, editor, "Quarterly Progress Report - January, February, March, 1958 - Reactor Projects Branch", US AEC Technical Report IDO-16452, Phillips Petroleum Co., September 10, 1958.

4-3. S. G. Forbes, F. L. Bentzen, P. French, J. E. Grund, J. C. Haire, W. E. Nyer, R. F. Walker, "Analysis of Self-Shutdown Behavior in the Spert I Reactor", US AEC Technical Report IDO-16528, Phillips Petroleum Co., July 23, 1959.

4-4. T. J. Thompson, J. G. Beckerly, editors, The Technology of Nuclear Reactor Safety, Vol. 1, "Reactor Physics and Control", Chapter 7, W. E. Nyer, "Mathematical Models of Fast Transients", The MIT Press, 1964.

4-5. F. Schroeder, editor, "Quarterly Technical Report - Spert Project - April, May, June, 1960", US AEC Technical Report IDO-16640, Phillips Petroleum Co., April 7, 1961.

4-6. T. J. Thompson, J. G. Beckerly, editors, The Technology of Nuclear Reactor Safety, Vol. 1, "Reactor Physics and Control", Chapter 8, J. A. Thie, "Water Reactor Kinetics", The MIT Press, 1964.

4-7. Safety Analysis Report for the MIT Research Reactor (MITR-II), MITNE-115, October 1970.

4-8. Safety Analysis Report for the MIT Research Reactor, draft version of Chapter 13, *circa* November 2002.

4-9. R. J. Wagner, "HEAT 1 - A One Dimensional Time Dependent or Steady State Heat Conduction Code for the IBM-650", US AEC Technical Report IDO-16867, Phillips Petroleum Co., April 1963.

4-10. J. E. Houghtaling, Alain Sola, A. H. Spano, "Transient Temperature Distributions in the Spert I D-12/25 Fuel Plates During Short-Period Power Excursions", US AEC Technical Report IDO-16884, Phillips Petroleum Co., June 1964.

4-11. H. L. McMurry, A. V. Grimaud, "Temperature Distribution in a Fuel Plate with Exponentially Rising Power, Part II - Results Based on Asymptotic Solutions", US AEC Technical Report IDO-16311, Phillips Petroleum Co., Januray 5, 1955.

4-12. S.E.Day, "Power-Peaking Factors in MNR", McMaster Nuclear Reactor Technical Note MNR-TN-1999-07-r1, Hamilton, Canada, Feb. 17, 2002.

4-13. W. K. Luckow, L. C. Widdoes, "Predicting Reactor Temperature Excursions by Extrapolating Borax Data", Nucleonics, Vol.14, No.1, January 1956.

4-14. McMaster Nuclear Reactor - Safety Analysis Report, McMaster University, Hamilton, Canada, February 2002.

4-15. J. R. Dietrich, D. C. Layman, "Transient and Steady State Characteristics of a Boiling Reactor. The Borax Experiments, 1953", ANL-5211 (also listed as AECD-3840), Argonne National Laboratory, USA, February 1954.

4-16. Michigan Memorial-Phoenix Project, Ford Nuclear Reactor - Description and Operation, The University of Michigan, Ann Arbor, Michigan, June 1957.

4-17. Michigan Memorial-Phoenix Project, The University of Michigan, Safety Analysis, Ford Nuclear Reactor, The University of Michigan, Docket 50-2, License R-28, Ann Arbor, Michigan, November 1984.

4-18. W. E. Nyer, S. G. Forbes, "SPERT I Reactor Safety Studies," Paper P/2428, Proceedings of the Second United Nations International Conference on the Peaceful Uses of Atomic Energy, v. 11, pp. 470-480, Geneva, September 1958.

4-19. J. G. Crocker, L. A. Stephan, "Reactor Power Excursion Tests in the Spert IV Facility", US AEC Technical Report IDO-17000, Phillips Petroleum Co., August 1964.

4-20. J. E. Matos, K. E. Freese, "Safety Analyses for HEU and LEU Equilibrium Cores and HEU-LEU Transition Core for the IAEA Generic 10 MW Reactor", ANL, IAEA-TECDOC-643, v.2, Appendix A-2, 1992.

4-21. W. E. Nyer, S. G. Forbes, F. L. Bentzen, G. O. Bright, F. Schroeder, T. R. Wilson, "Experimental Investigations of Reactor Transients", US AEC Technical Report IDO-16285, Phillips Petroleum Co., April 20, 1956.

4.7 Tables

Table 4-1: Regression Results for Ambient Temperature Tests Power Data

Core	N	Reference Data Set m	sig(m)	Pmax (MW) ln(b1)	sig(ln(b1))	standard error s	R2
Borax I	19	1.597	0.029	-0.194	0.170	0.170	0.803
Spert I A-17/28	27	1.597	0.029	-0.806	0.097	0.097	0.986
Spert I B-24/32	6	1.597	0.029	-0.627	0.094	0.094	0.974
Spert I B-16/40	3	1.597	0.029	-0.384	0.041	0.041	0.995
Spert I B-12/64	9	1.597	0.029	0.110	0.082	0.082	0.977
Spert I D-12/25	41	1.597	0.029	-1.456	0.049	0.049	0.997
Spert IV D-12/25	9	1.597	0.029	-1.248	0.075	0.075	0.992

note: fitting uses reference slope from full linear regression on reference data set
note: the Spert I D-12/25 data set is considered as the reference data set
Working Equations 1 Pmax = b1 alpha^m

Table 4-2: Regression Results for Ambient Temperature Tests Energy Data

Core	N	Reference Data Set m2	sig(m2)	Etm (MW-sec) ln(b2)	sig(ln(b2))	standard error s	R2
Borax I	-	-	-	-	-	-	-
Spert I A-17/28	26	0.574	0.017	-0.321	0.09082	0.091	0.916
Spert I B-24/32	6	0.574	0.017	0.008	0.05665	0.057	0.883
Spert I B-16/40	3	0.574	0.017	0.015	0.01987	0.020	0.992
Spert I B-12/64	9	0.574	0.017	0.629	0.07025	0.070	0.915
Spert I D-12/25	41	0.574	0.017	-0.998	0.08794	0.088	0.923
Spert IV D-12/25	9	0.574	0.017	-0.949	0.10595	0.106	0.891

note: fitting uses reference slope from full linear regression on reference data set
note: the Spert I D-12/25 data set is considered as the reference data set
Working Equation 1 Etm = b2 alpha^m2

Table 4-3: Regression Results for Ambient Temperature Tests Temperature Rise Data

Core	N	Reference Data Set m3	sig(m3)	DTmax (deg C) ln(b3)	sig(ln(b3))	standard error s	R2
Borax I	3	0.0114	0.000359	4.376	0.080	0.080	-0.443
Spert I A-17/28	10	0.0114	0.000359	4.247	0.149	0.149	0.803
Spert I B-24/32	6	0.0114	0.000359	4.371	0.086	0.086	0.819
Spert I B-16/40	3	0.0114	0.000359	4.591	0.033	0.033	0.986
Spert I B-12/64	4	0.0114	0.000359	4.767	0.061	0.061	0.952
Spert I D-12/25	25	0.0114	0.000359	4.261	0.105	0.105	0.963
Spert IV D-12/25	7	0.0114	0.000359	4.255	0.149	0.149	0.868

note: fitting uses reference slope from linear regression on reference data set
note: the Spert I D-12/25 data set is considered as the reference data set
Working Equation 1 ΔTmax = b3 exp(m3*alpha)

Table 4-4: Comparison of Regression Results for Ambient Temperature Tests Power Data using Reference Slope with Independent Slope Fitting

Core	N	Standard Deviation in Fitted Data		R2	
		Ref. Slope	Indiv. Fit	Ref. Slope	Indiv. Fit
Borax I	19	0.170	0.175	0.803	0.804
Spert I A-17/28	27	0.097	0.078	0.986	0.991
Spert I B-24/32	6	0.094	0.081	0.974	0.985
Spert I B-16/40	3	0.041	0.045	0.995	0.997
Spert I B-12/64	9	0.082	0.087	0.977	0.977
Spert I D-12/25	41	0.049	0.049	0.997	0.997
Spert IV D-12/25	9	0.075	0.021	0.992	0.999

note: the Spert I D-12/25 data set is considered as the reference data set

Table 4-5: Comparison of Regression Results for Ambient Temperature Tests Energy Data using Reference Slope with Independent Slope Fitting

Core	N	Standard Deviation in Fitted Data		R2	
		Ref. Slope	Indiv. Fit	Ref. Slope	Indiv. Fit
Borax I	-	-	-	-	-
Spert I A-17/28	26	0.091	0.081	0.916	0.935
Spert I B-24/32	6	0.057	0.055	0.883	0.913
Spert I B-16/40	3	0.020	0.015	0.992	0.998
Spert I B-12/64	9	0.070	0.060	0.915	0.945
Spert I D-12/25	41	0.088	0.088	0.923	0.923
Spert IV D-12/25	9	0.106	0.106	0.891	0.904

note: the Spert I D-12/25 data set is considered as the reference data set

Table 4-6: Comparison of Regression Results for Ambient Temperature Tests Temperature Rise Data using Reference Slope with Independent Slope Fitting

Core	N	Standard Deviation in Fitted Data		R2	
		Ref. Slope	Indiv. Fit	Ref. Slope	Indiv. Fit
Borax I	3	0.080	0.004	-0.443	0.997
Spert I A-17/28	10	0.149	0.061	0.803	0.967
Spert I B-24/32	6	0.086	0.041	0.819	0.959
Spert I B-16/40	3	0.033	0.016	0.986	0.997
Spert I B-12/64	4	0.061	0.053	0.952	0.963
Spert I D-12/25	25	0.105	0.105	0.963	0.963
Spert IV D-12/25	7	0.149	0.081	0.868	0.961

note: the Spert I D-12/25 data set is considered as the reference data set

Table 4-7: Nuclear Characteristics and Dimensions of the Test Cores

HEU Al-Clad Plate Cores	Borax I	Sperl I A-17/28	Sperl I B-24/32	Sperl I B-16/40	Sperl I B-12/64	Sperl I D-12/25	Sperl IV D-12/25	MNR RC-16/28-9/6
Temperature Defect								
20C to 95C (mk)	-8.17	-10.9	-12.4	-11.6	-10.2	N/A	N/A	N/A
Void Coefficient								
Metal/Water Ratio - central	0.687	0.782	1.128	0.635	0.465	0.704	0.703	-
Metal/Water Ratio - std assembly	0.687	0.782	1.128	0.635	0.465	0.525	0.522	0.576
Metal/Water Ratio - core	0.687	0.782	1.128	0.635	0.465	0.629	0.627	-
Average (Uniform)								
(mk/%-void)	-2.4	-1.9	-2.8	-1.8	-1.1	-2.4	-2.3	-2.1
(mk/cc-void)	-3.4E-03	-3.5E-03	-5.1E-03	-2.0E-03	-6.9E-04	-4.6E-03	-4.5E-03	-3.3E-03
(mk/channel)	-0.41	-0.39	-0.36	-0.28	-0.14	-0.87	-0.85	-0.39
Central								
(mk/%-void)	-4.5	-3.9	-6.5	-2.9	0.9	-3.4	-3.1	-4.5
(mk/cc-void)	-6.6E-03	-7.2E-03	-1.2E-02	-3.3E-03	6.0E-04	-6.3E-03	-6.0E-03	-7.1E-03
(mk/channel)	-0.78	-0.80	-0.83	-0.45	0.12	-1.20	-1.14	-0.84
Prompt Neutron Lifetime								
(micro-sec)	65	50	50	70	77	60	57	N/A
Power Peaking Factor								
Overall	2.0	2.0	2.5	2.1	2.2	2.4	2.4	4.2
Dimensions								
Fuel meat thickness (cm)	0.053	0.051	0.051	0.051	0.051	0.051	0.051	0.051
Clad thickness (cm)	0.050	0.051	0.051	0.051	0.051	0.051	0.051	0.038
Fuel surface area (cm2)	4.31E+05	3.55E+05	6.47E+05	5.39E+05	6.47E+05	2.26E+05	2.26E+05	4.00E+05
Fuel meat volume (cc)	1.10E+04	7.57E+03	1.51E+04	1.26E+04	1.51E+04	5.20E+03	5.20E+03	9.57E+03
SA/Vol Ratio	39	47	43	43	43	43	43	42
Volume Coolant/Channel (cc)	119	111	69	136	203	190	190	119

note: fuel surface area and coolant volume are based on active height of the fuel

Table 4-8: Scaling Parameters and Ratios

Core	Core Size Vf (cc)	ratio to Spert I D-12/25 value	Power Peaking PPF	ratio to Spert I D-12/25 value
Borax I	10976	2.109	1.96	0.817
Spert I A-17/28	7571	1.455	2.0	0.833
Spert I B-24/32	15133	2.908	2.5	1.042
Spert I B-16/40	12610	2.424	2.1	0.875
Spert I B-12/64	15133	2.908	2.2	0.917
Spert I D-12/25	5203	1.000	2.4	1.000
Spert IV D-12/25	5203	1.000	2.35	0.979
Core	**Shutdown Coefficient w (uniform)**	**ratio to Spert I D-12/25 value**	**Shutdown Coefficient w (central)**	**ratio to Spert I D-12/25 value**
Borax I	6.30E-03	0.436	1.21E-02	0.603
Spert I A-17/28	7.75E-03	0.537	1.59E-02	0.798
Spert I B-24/32	7.10E-03	0.492	1.65E-02	0.828
Spert I B-16/40	3.95E-03	0.274	6.41E-03	0.321
Spert I B-12/64	1.83E-03	0.127	-1.58E-03	-0.079
Spert I D-12/25	1.44E-02	1.000	2.00E-02	1.000
Spert IV D-12/25	1.50E-02	1.039	2.01E-02	1.004

Table 4-9: Regression Results for Correlation of Relative Data Magnitudes to Relative Shutdown Coefficient

Data	Slope mi	Error sig(mi)	Error sig(mi)/mi	Fit R^2
All Cores				
Pmax	-0.7204	0.0530	-7.4%	0.8333
Etm	-	-	-	-
ΔTmax(a)	-0.8136	0.1277	-15.7%	0.8782
ΔTmax(a) (corrected)	-0.7654	0.1277	-16.7%	0.8339
All Except Borax I				
Pmax	-0.7188	0.0530	-7.4%	0.9592
Etm	-0.7175	0.0559	-7.8%	0.9220
ΔTmax(a)	-0.8148	0.1277	-15.7%	0.8944
ΔTmax(a) (corrected)	-0.7678	0.1277	-16.6%	0.8991
Spert B-cores Only				
Pmax	-0.5559	0.1124	-20.2%	0.9853
Etm	-0.4619	0.0925	-20.0%	0.8214
ΔTmax(a)	-0.3874	0.2313	-59.7%	0.9990
ΔTmax(a) (corrected)	-0.3874	0.2313	-59.7%	0.9990

Regression is weighted linear least squares on Δ ln(b) vs. Δ ln(w), where w is the shutdown coefficient (Cvoid * Vc/PNL)
Note: Etm was not measured in the Borax tests so this data point is not available

	Average, <m>	N	Standard Deviation (N-1) sig(<m>)	sig(<m>)/<m>
All Cores	-0.734	2	0.081	11.0%
All Except Borax I (A)	**-0.726**	3	**0.063**	8.7%
Spert B-cores Only (B)	**-0.490**	3	**0.089**	18.1%

Note: only Pmax, Etm, and ΔTmax results are averaged for the above

Table 4-10: Uniform Void Shutdown Coefficient Scaling Factors and Ratios

Core	Scaling Factor (Spert Core m) s = w^m	ratio to Spert I D-12/25 value	Scaling Factor (B-Core m) s = w^m	ratio to Spert I D-12/25 value
Borax I	2.52E-02	0.548	8.34E-02	0.666
Spert I A-17/28	2.93E-02	0.637	9.24E-02	0.737
Spert I B-24/32	2.75E-02	0.598	8.85E-02	0.707
Spert I B-16/40	1.80E-02	0.390	6.64E-02	0.530
Spert I B-12/64	1.03E-02	0.223	4.55E-02	0.364
Spert I D-12/25	4.60E-02	1.000	1.25E-01	1.000
Spert IV D-12/25	4.73E-02	1.028	1.28E-01	1.019

Note: the shutdown coefficient, w, is based on the uniform void coefficient of reactivity
Note: the exponent, -m, is the negative of the slope of the $\Delta\ln(b)$ vs. $\Delta\ln(w)$ correlation

Table 4-11: Regression Results for Scaled Power Data

Using Scaling Factor based on All Cores Except Borax I Data

Data	Data Points N	Slope n	Intercept ln(b)	stnd dev s	95% band width	Fit R^2
Spert I D-12/25 *	41	1.597	-1.456	0.049	0.125	0.997
All Cores	114	1.597	-1.271	0.248	0.491	0.901
All Spert Cores	95	1.597	-1.348	0.130	0.259	0.975
Spert I B-Cores	18	1.597	-1.271	0.140	0.296	0.935

Using Scaling Factor based on Spert I B-Core Data only

Data	Data Points N	Slope n	Intercept ln(b)	stnd dev s	95% band width	Fit R^2
Spert I D-12/25 *	41	1.597	-1.456	0.049	0.125	0.997
All Cores	114	1.597	-1.197	0.325	0.643	0.813
All Spert Cores	95	1.597	-1.281	0.221	0.440	0.922
Spert I B-Cores	18	1.597	-0.954	0.091	0.192	0.973

Note: the above is for the working Equation: $\ln(P_{max}(s)) = n \ln(\alpha) + \ln(b)$
Note: the curve fitting is to the Pmax data scaled for the effect of void reactivity, relative to the Spert I D-12/25 data set
Note: the curve fitting adopts the previously determined reference slope parameters from fitting to the Spert I D-12/25 data set
Note: * the 95% band width for the full regression fit is taken as W*s, where W = SQRT(2 F(0.95, 2, N-2))
Note: the standard deviation and 95% prediction band values represent relative errors on the linear Pmax vs. alpha data

Table 4-12: Regression Results for Scaled Energy Data

Using Scaling Factor based on All Cores Except Borax I Data

Data	Data Points N	Slope n	Intercept ln(b)	stnd dev s	95% band width	Fit R^2
Spert I D-12/25 *	41	0.574	-0.998	0.088	0.224	0.923
All Spert Cores	94	0.574	-0.889	0.160	0.318	0.726
Spert I B-Cores	18	0.574	-0.715	0.198	0.418	0.514

Using Scaling Factor based on Spert I B-Core Data only

Data	Data Points N	Slope n	Intercept ln(b)	stnd dev s	95% band width	Fit R^2
Spert I D-12/25 *	41	0.574	-0.998	0.088	0.224	0.923
All Spert Cores	94	0.574	-0.839	0.264	0.523	0.311
Spert I B-Cores	18	0.574	-0.397	0.116	0.244	0.786

Note: the above is for the working Equation: $\ln(E_{tm}(s)) = n \ln(\alpha) + \ln(b)$
Note: the curve fitting is to the Etm data scaled for the effect of void reactivity, relative to the Spert I D-12/25 data set
Note: the curve fitting adopts the previously determined reference slope parameters from fitting to the Spert I D-12/25 data set
Note: * the 95% band width for the full regression fit is taken as W*s, where W = SQRT(2 F(0.95, 2, N-2)
Note: the standard deviation and 95% prediction band values represent relative errors on the linear Etm vs. alpha data

Table 4-13: Regression Results for Scaled Temperature Rise Data

Using Scaling Factor based on All Cores Except Borax I Data

Data	Data Points N	Slope n	Intercept ln(b)	stnd dev s	95% band width	Fit R^2
Spert I D-12/25 *	25	0.01138	4.261	0.105	0.274	0.963
All Cores	58	0.01138	4.392	0.232	0.465	0.664
Spert I B-Cores	13	0.01138	4.734	0.213	0.464	0.504
All Cores (corrected)	58	0.01138	4.361	0.228	0.456	0.689

Using Scaling Factor based on Spert I B-Core Data only

Data	Data Points N	Slope n	Intercept ln(b)	stnd dev s	95% band width	Fit R^2
Spert I D-12/25 *	25	0.01138	4.261	0.105	0.274	0.963
All Cores	58	0.01138	4.447	0.328	0.656	0.299
Spert I B-Cores	13	0.01138	5.010	0.084	0.183	0.837
All Cores (corrected)	58	0.01138	4.420	0.308	0.616	0.364

Note: the above is for the working Equation: $\ln(\Delta Tmax(a)(s)) = n \ (alpha) + \ln(b)$
Note: the curve fitting is to the ΔTmax data scaled for the effect of void reactivity, relative to the Spert I D-12/25 data set
Note: the curve fitting adopts the previously determined reference slope parameters from fitting to the Spert I D-12/25 data set
Note: * the 95% band width for the full regression fit is taken as W*s, where W = SQRT(2 F(0.95, 2, N-2))
Note: the standard deviation and 95% prediction band values represent relative errors on the linear (ΔTmax x Vf/PPF) vs. alpha data
Note: "corrected" data is adjusted for estimated systematic error

Table 4-14: Regression Results for the Temperature Rise Ratio *vs.* the Degree of Subcooling for the Borax I data

TC	N	m	sig(m)	b	sig(b)	s	R2
21-4-c	12	0.0434	0.0038	1.026	0.057	0.086	0.992
21-1-c	12	0.0406	0.0038	1.000	0.058	0.084	0.992
21-1-s	12	0.0485	0.0047	1.079	0.066	0.239	0.963

	<m>	sig(<m>)
Average	0.0424	0.0071

note: working equaiton is ΔTmax-ratio = m * Tsub + b; where ΔTmax-ratio is the ratio of ΔTmax at the given subcooling to that at zero subcooling.
note: Average slope value, <m>, is weighted by the inverse square of the standard errors
note: sig(<m>) is linear combination of uncertainties on contributing values, mi

4.8 Figures

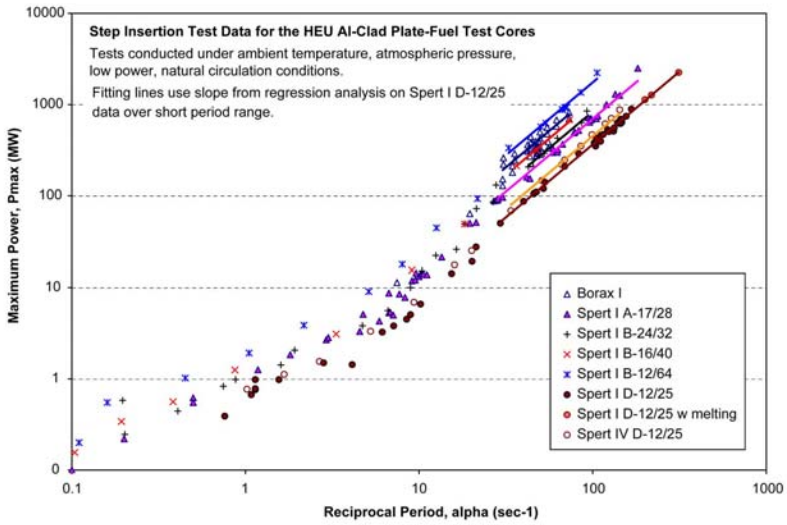

Figure 4-1: Maximum power as a function of reciprocal period

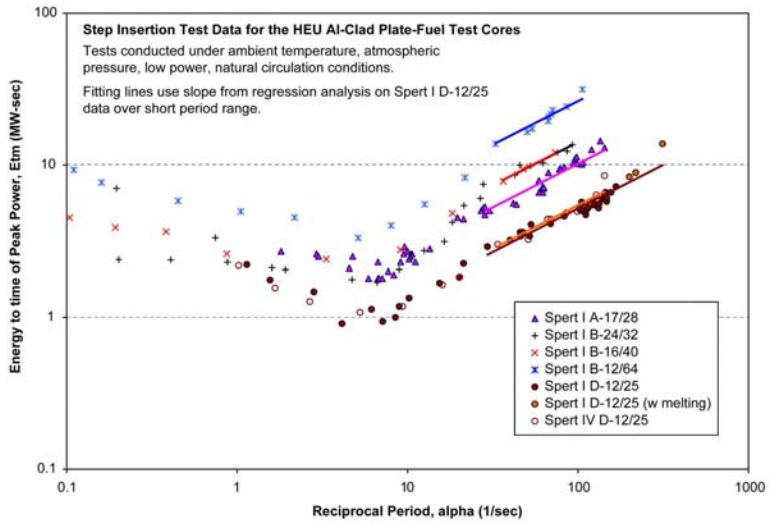

Figure 4-2: Energy generated to time of peak power as a function of reciprocal period

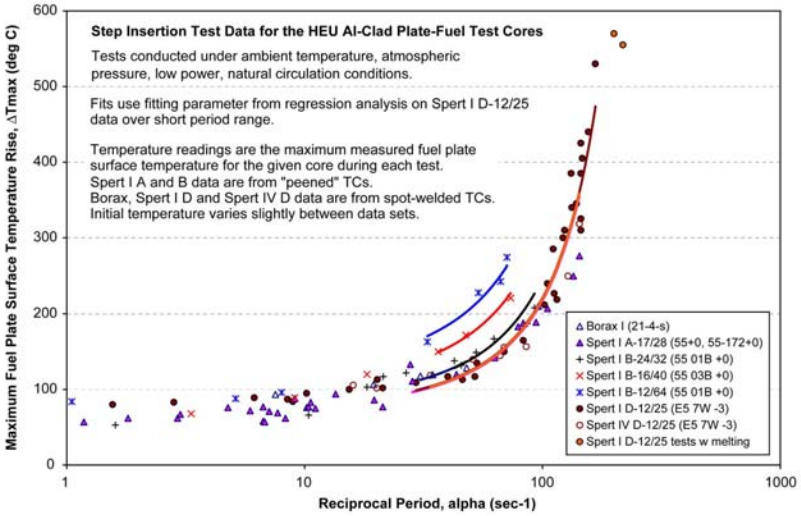

Figure 4-3: Maximum fuel plate surface temperature rise as a function of reciprocal period

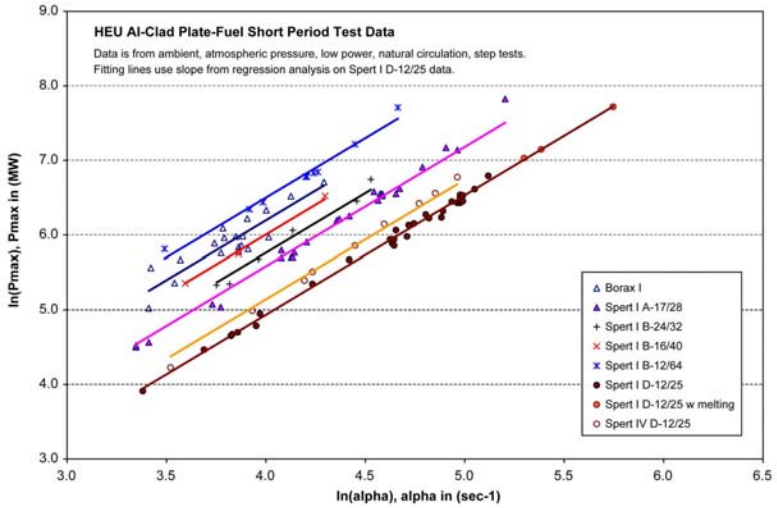

Figure 4-4: Curve Fits to P_{max} Data over the Short Period Range

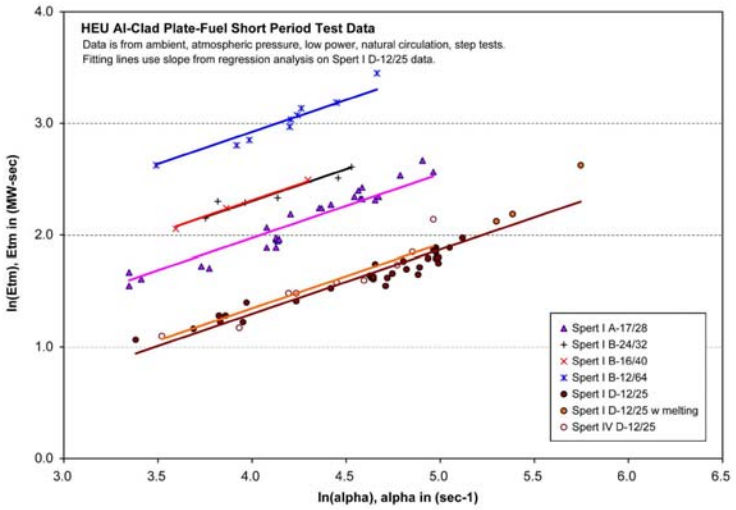

Figure 4-5: Curve Fits to E_{tm} Data over the Short Period Range

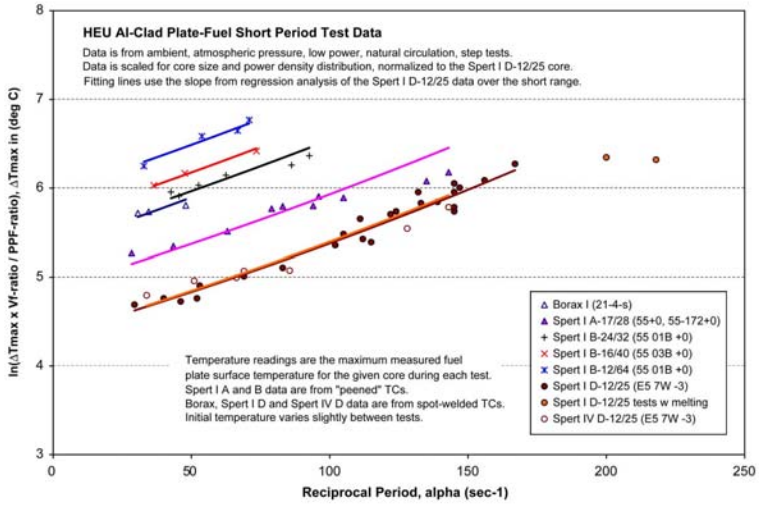

Figure 4-6: Curve Fits to the Normalized ΔT_{max} Data over the Short Period Range

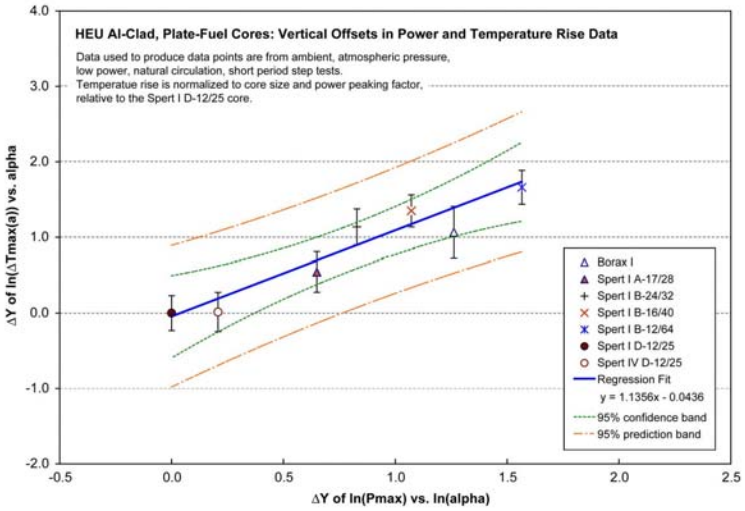

Figure 4-7: Correlation of Relative Magnitude for Normalized Temperature Rise Data to Power Data

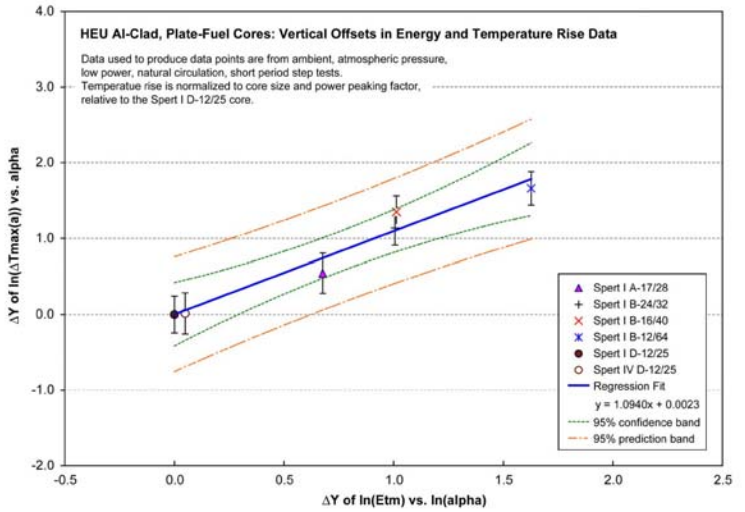

Figure 4-8: Correlation of Relative Magnitude for Normalized Temperature Rise Data to Energy Data

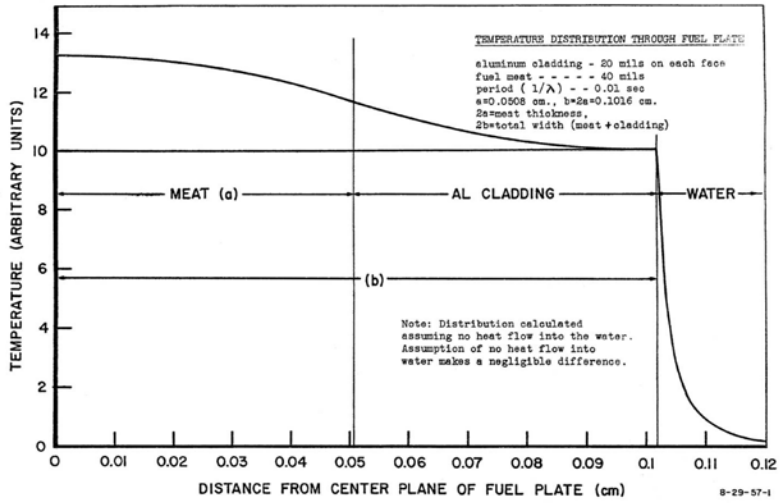

Figure 4-9: Asymptotic Temperature Distribution within a Fuel Plate as Calculated by the Conduction Model for a Short Period Transient (Ref. 4-11)

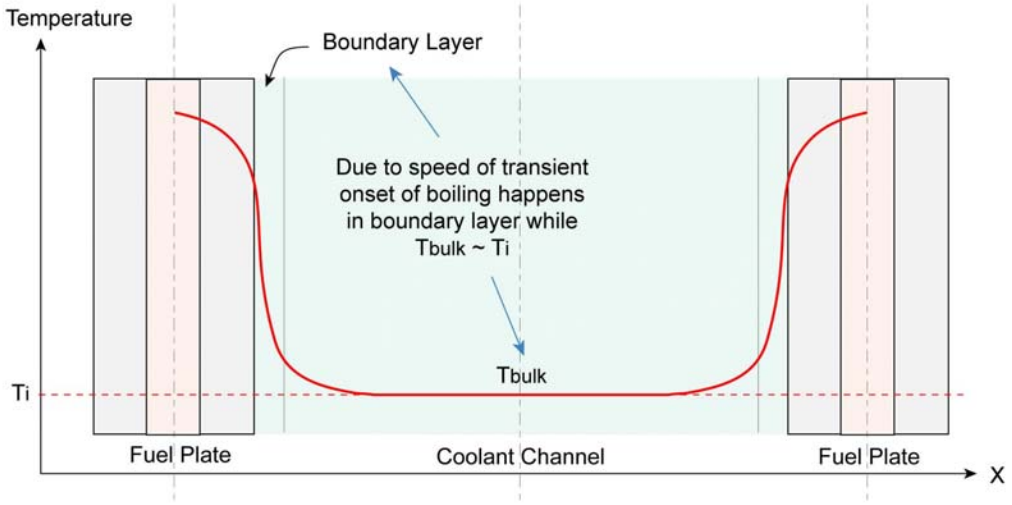

Figure 4-10: Stylized Temperature Distribution Prior to Onset of Boiling During a Short Period Transient

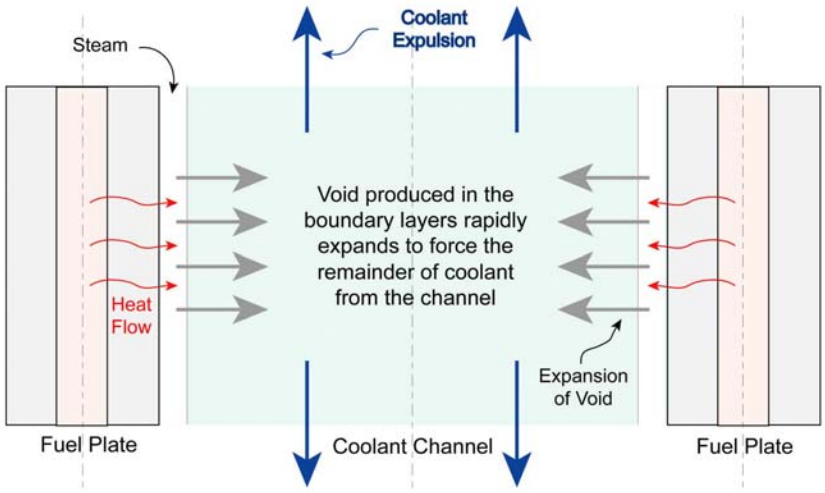

Figure 4-11: Voiding Mechanism During a Short Period Transient

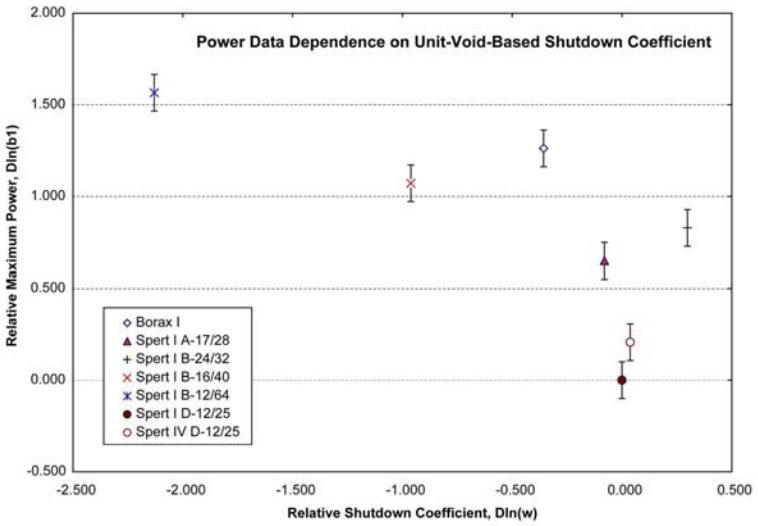

Figure 4-12: Unit-Void-Based Shutdown Coefficient Correlation to the Power Test Data

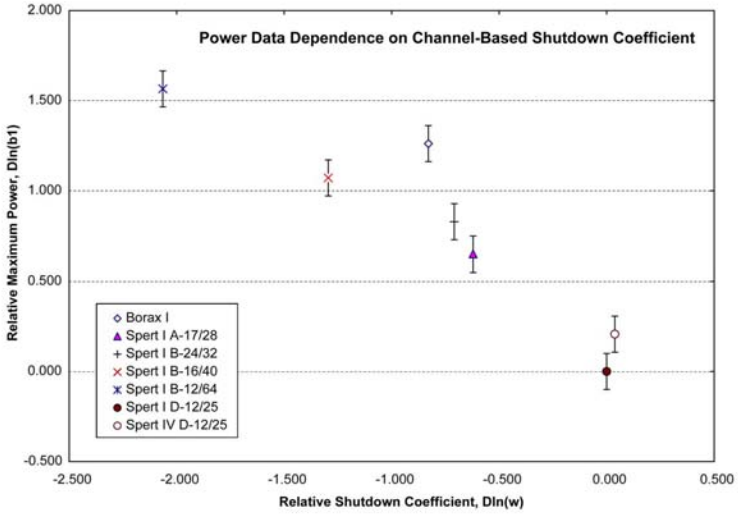

Figure 4-13: Channel-Based Shutdown Coefficient Correlation to the Power Test Data

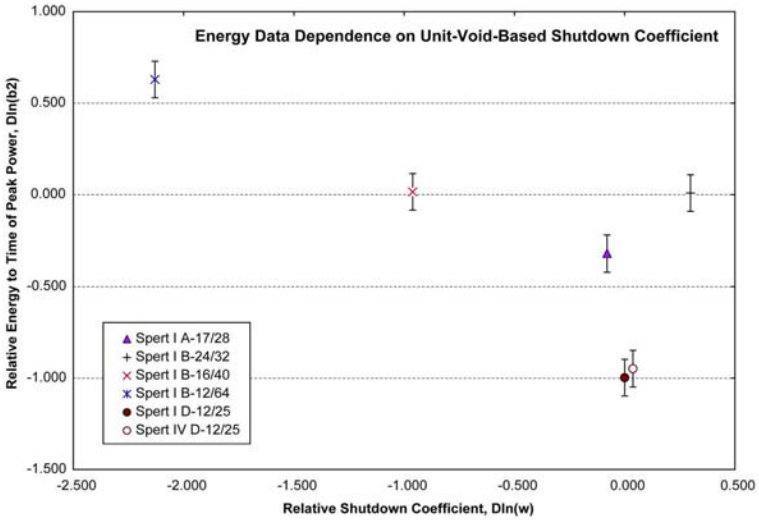

Figure 4-14: Unit-Void-Based Shutdown Coefficient Correlation to the Energy Test Data

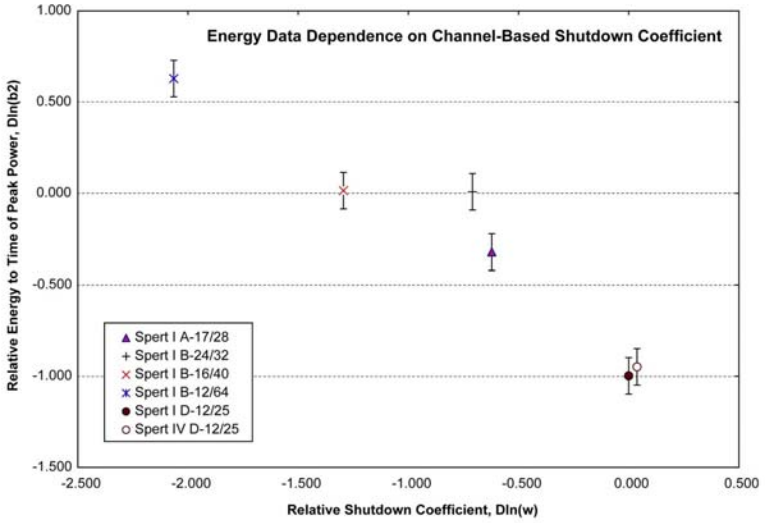

Figure 4-15: Channel-Based Shutdown Coefficient Correlation to the Energy Test Data

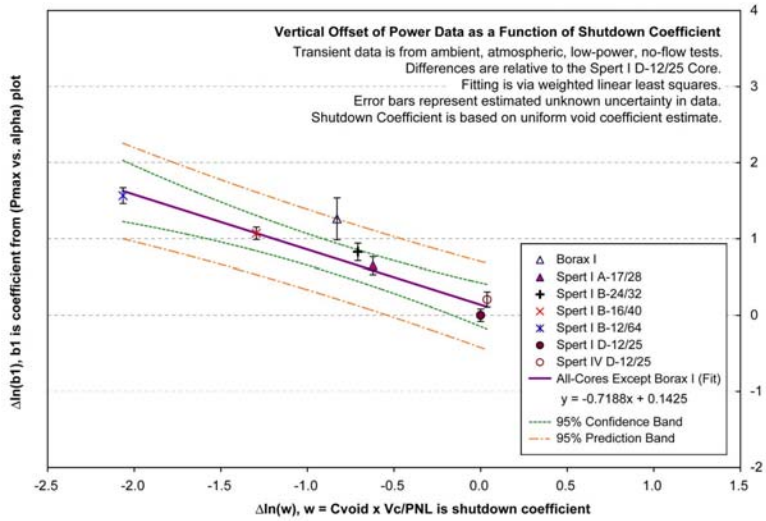

Figure 4-16: Correlation of Power Data to Shutdown Coefficient

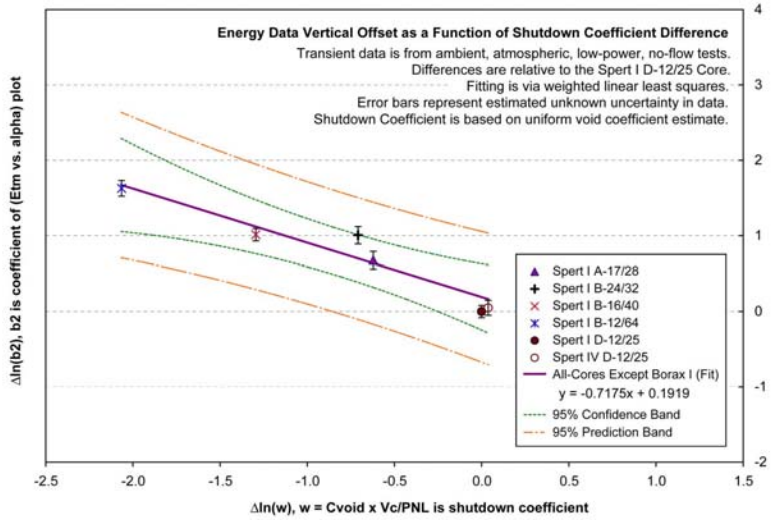

Figure 4-17: Correlation of Energy Data to Shutdown Coefficient

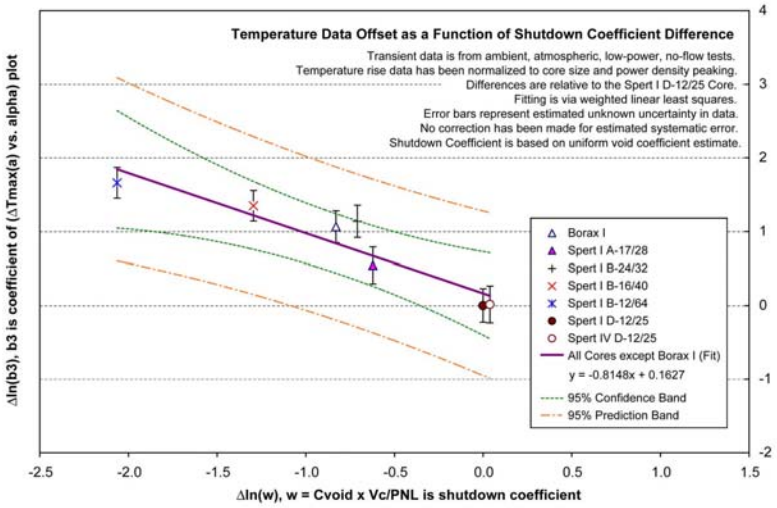

Figure 4-18: Correlation of Normalized Temperature Rise Data to Shutdown Coefficient

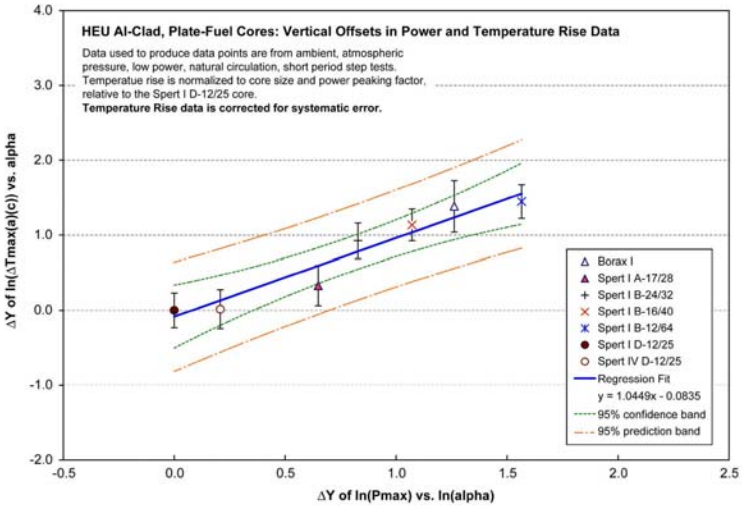

Figure 4-19: Correlation of Relative Magnitude for Normalized and Corrected Temperature Rise Data to Power Data

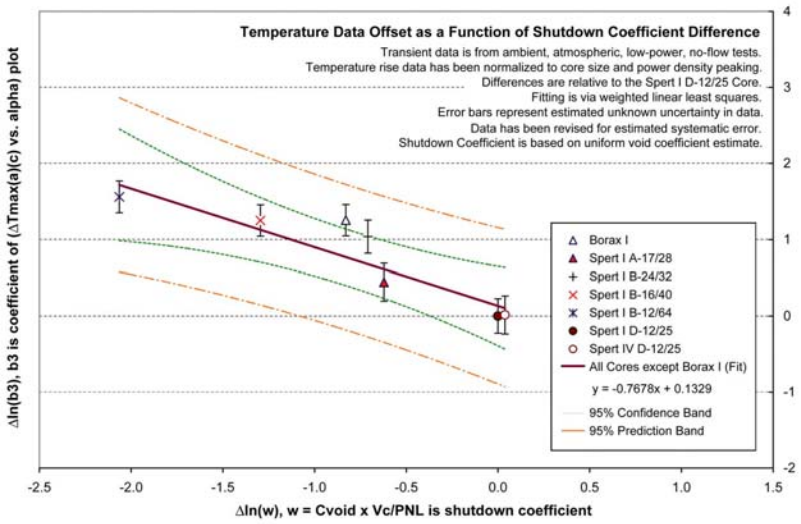

Figure 4-20: Correlation of Normalized and Corrected Temperature Rise Data to Shutdown Coefficient

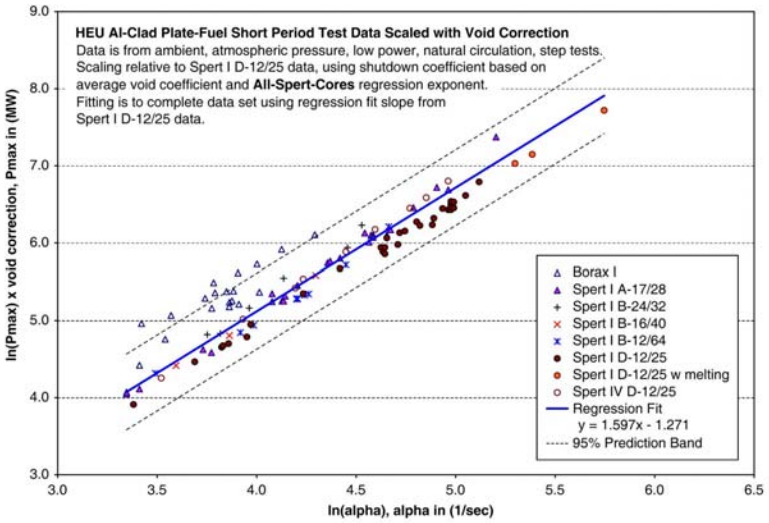

Figure 4-21: Scaled P_{max} Data over the Short Period Range, using All-Spert-cores derived scaling exponent

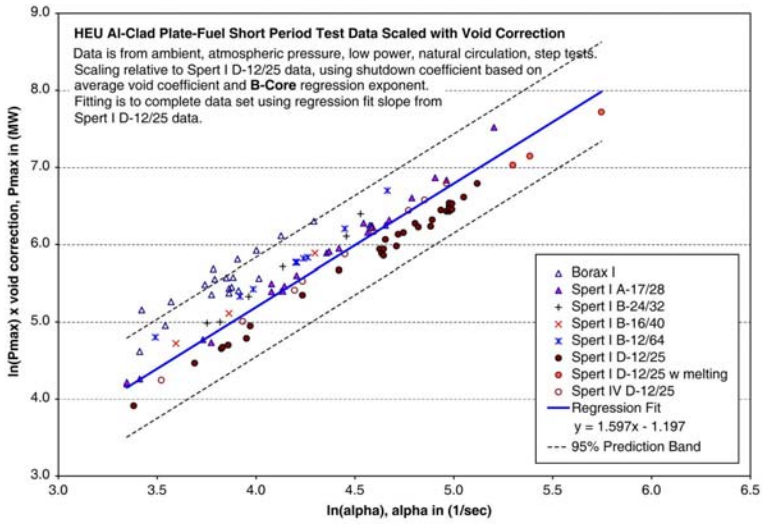

Figure 4-22: Scaled P_{max} Data over the Short Period Range, using B-core derived scaling exponent

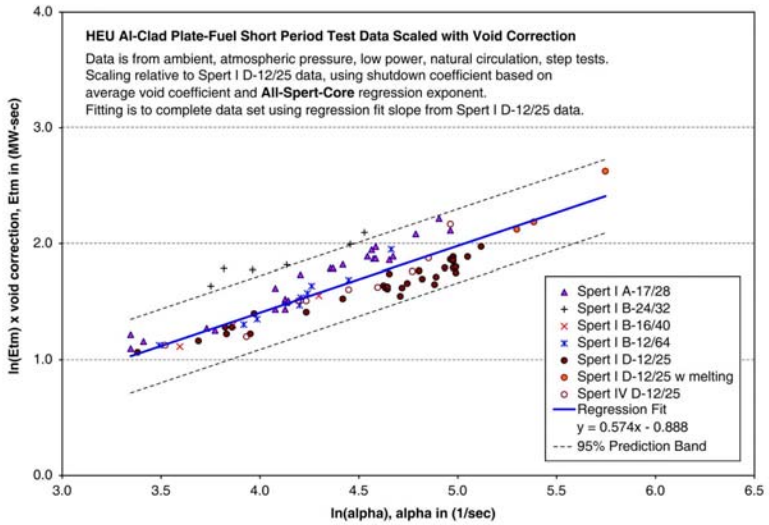

Figure 4-23: Scaled E_{tm} Data over the Short Period Range, using All-Spert-cores derived scaling exponent

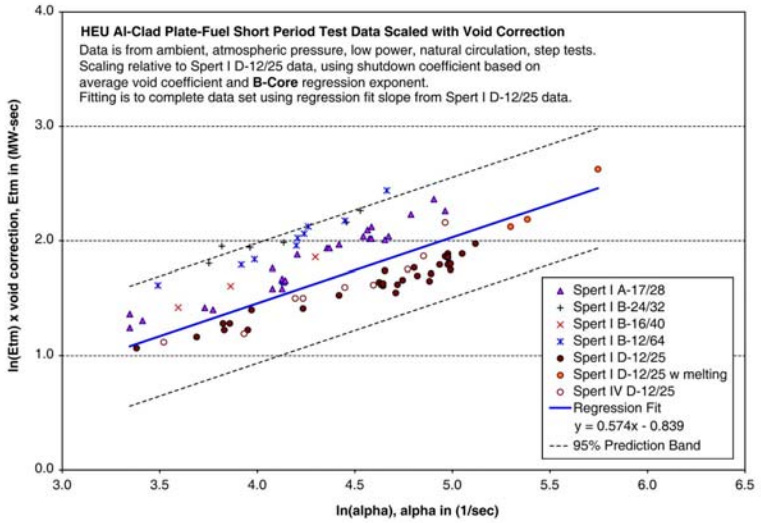

Figure 4-24: Scaled E_{tm} Data over the Short Period Range, using B-core derived scaling exponent

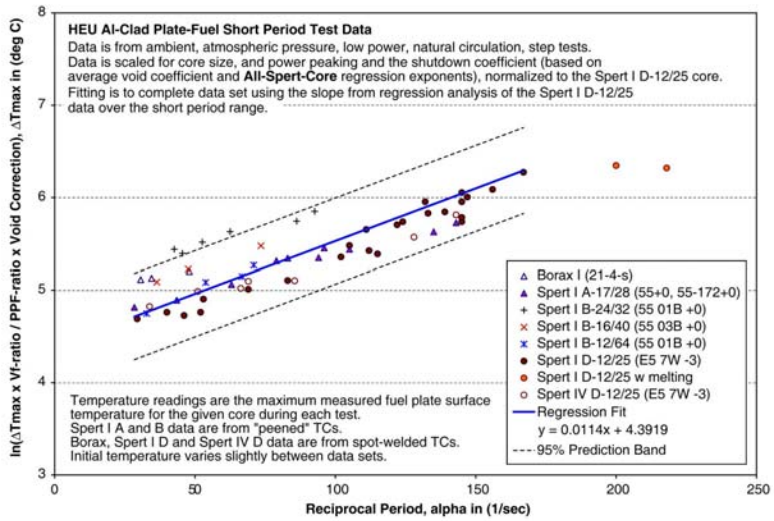

Figure 4-25: Scaled and Normalized ΔT_{max} Data over the Short Period Range, using All-Spert-cores derived scaling exponent

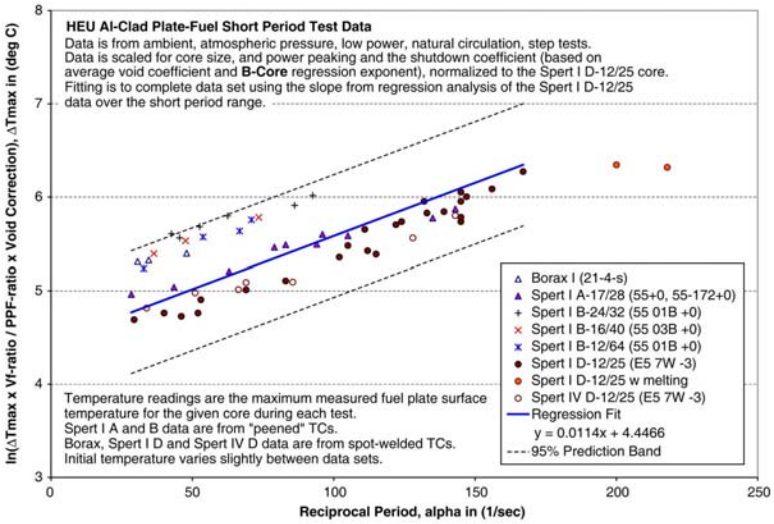

Figure 4-26: Scaled and Normalized ΔT_{max} Data over the Short Period Range, using B-core derived scaling exponent

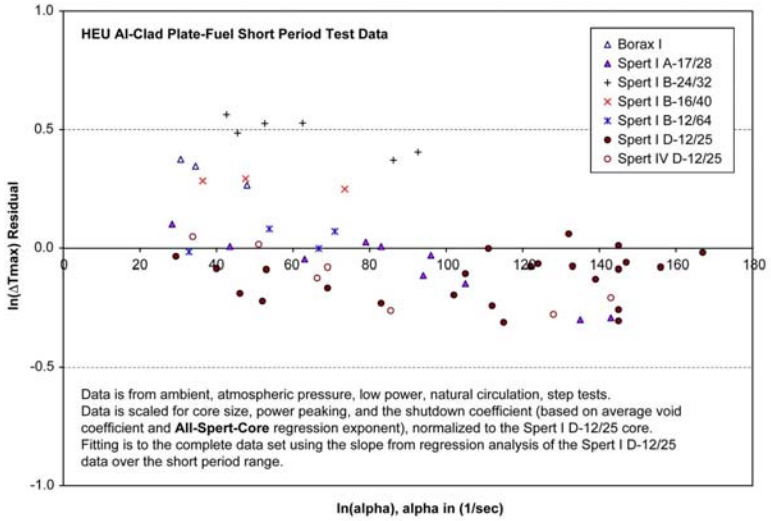

Figure 4-27: Residuals from Fit to Scaled and Normalized ΔT_{max} Data over the Short Period Range, Scaling using the All-Spert-cores derived scaling exponent

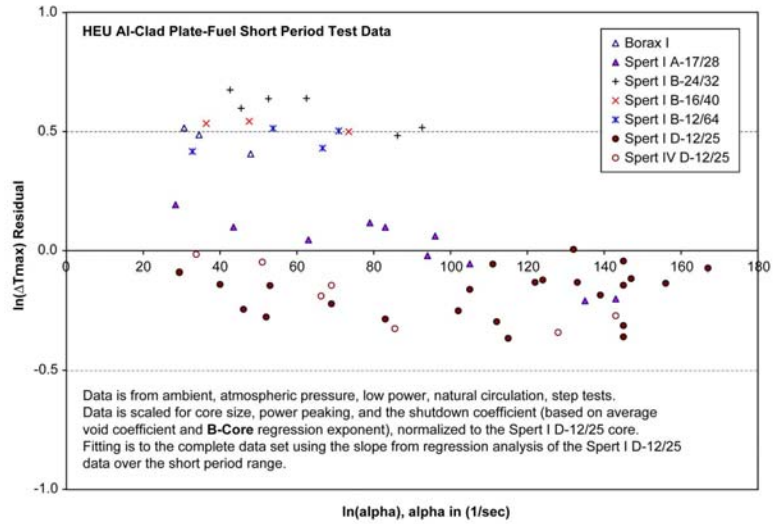

Figure 4-28: Residuals from Fit to Scaled and Normalized ΔT_{max} Data over the Short Period Range, Scaling using the B-core derived scaling exponent

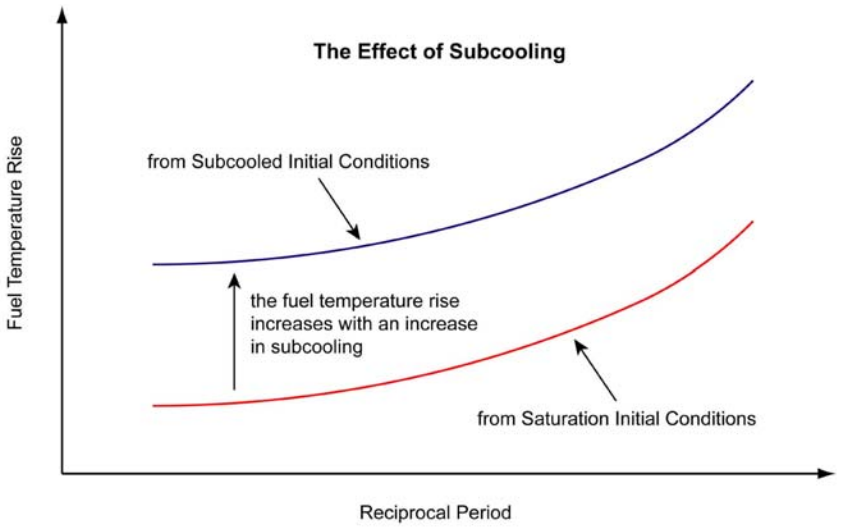

Figure 4-29: Schematic representation of the Effect of Subcooling

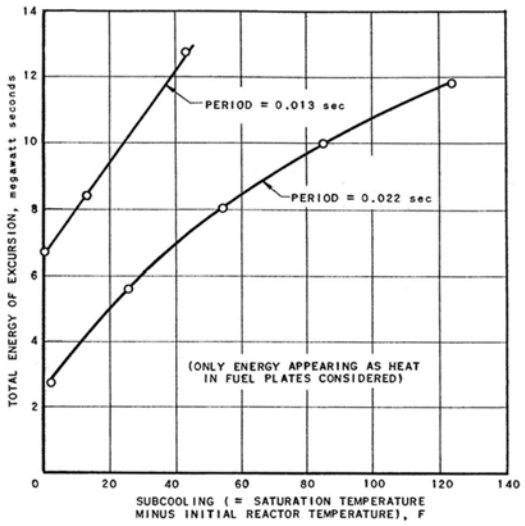

Figure 4-30: Borax I 1953 Energy Data from the Subcooling Test Series (Ref. 4-15)

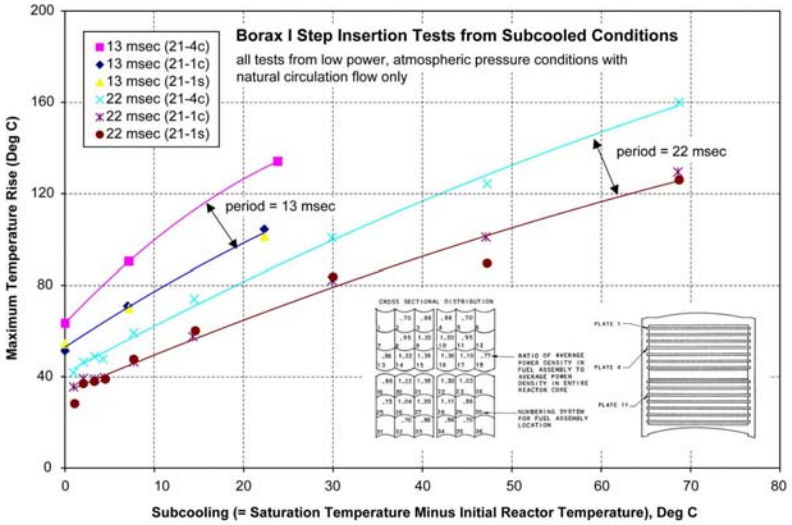

Figure 4-31: Borax I 1953 Temperature Data from the Subcooling Test Series

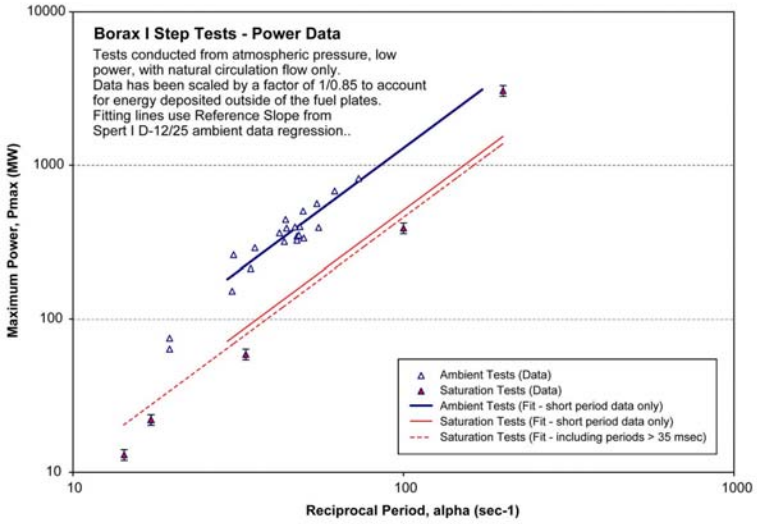

Figure 4-32: Borax I Power Data for Tests from Ambient and Saturation Initial Temperatures

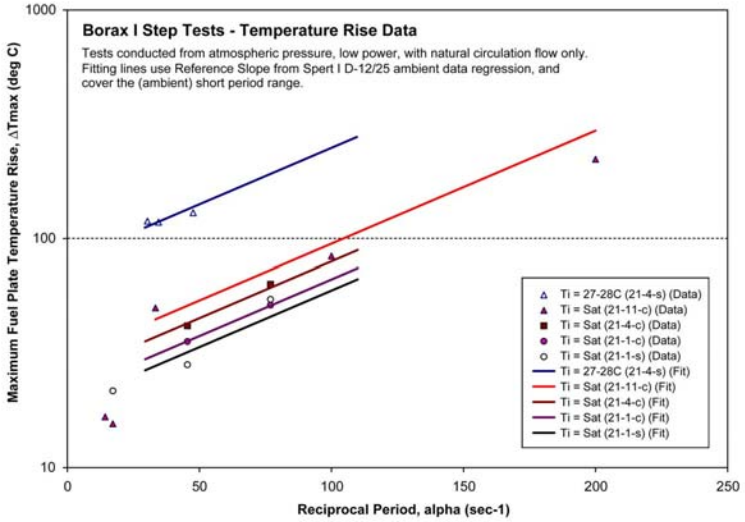

Figure 4-33: Borax I Temperature Data for Tests from Ambient and Saturation Initial Temperatures

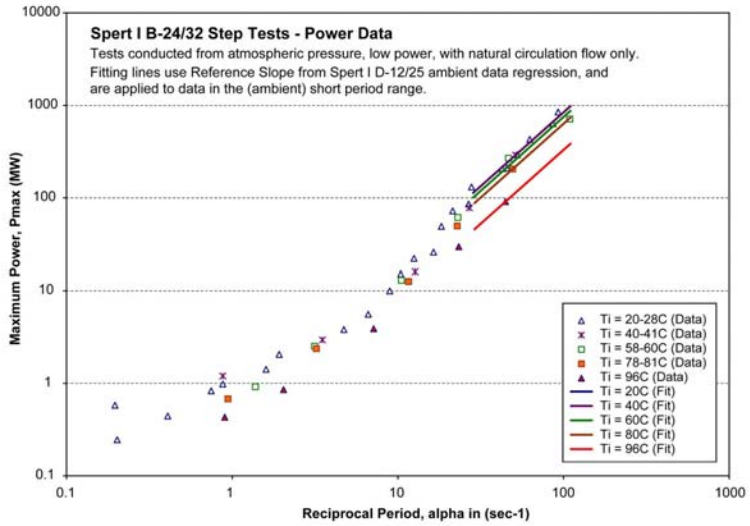

Figure 4-34: Spert I B-24/32 Power Data for the Subcooling Test Series

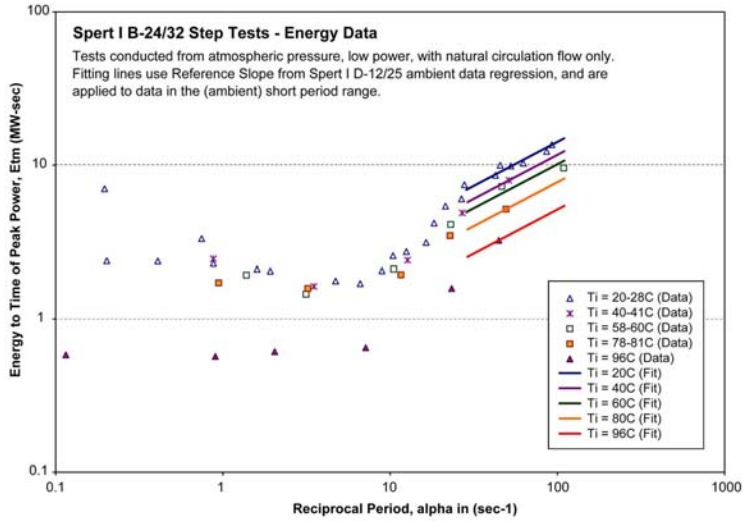

Figure 4-35: Spert I B-24/32 Energy Data for the Subcooling Test Series

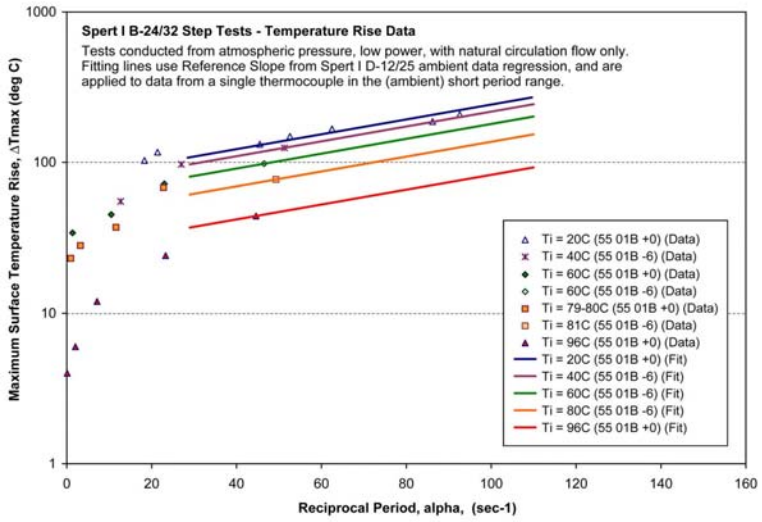

Figure 4-36: Spert I B-24/32 Temperature Data for the Subcooling Test Series

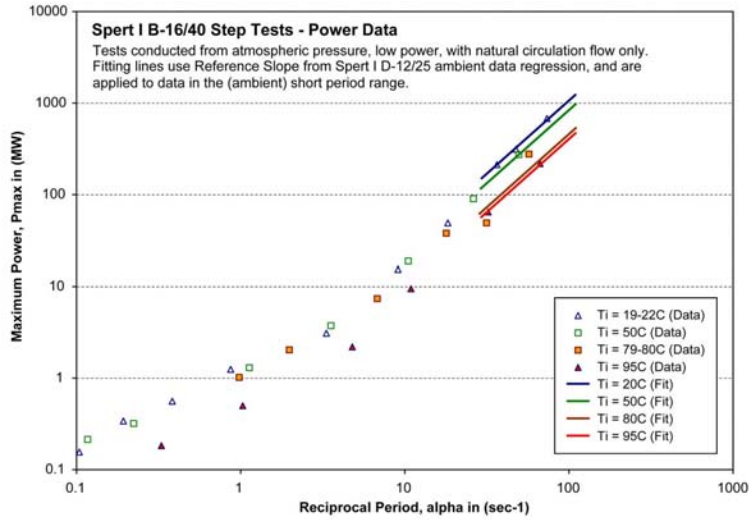

Figure 4-37: Spert I B-16/40 Power Data for the Subcooling Test Series

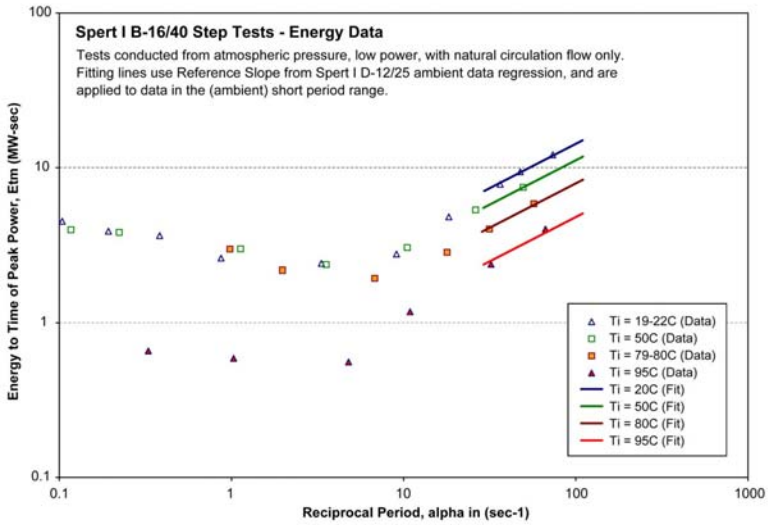

Figure 4-38: Spert I B-16/40 Energy Data for the Subcooling Test Series

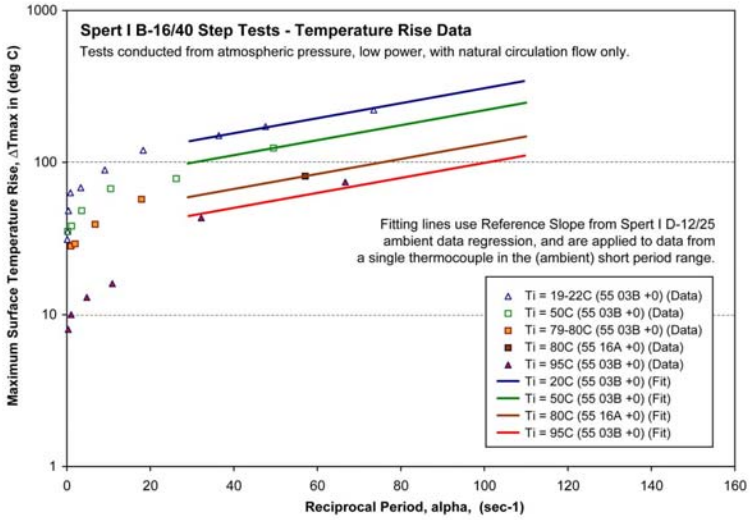

Figure 4-39: Spert I B-16/40 Temperature Data for the Subcooling Test Series

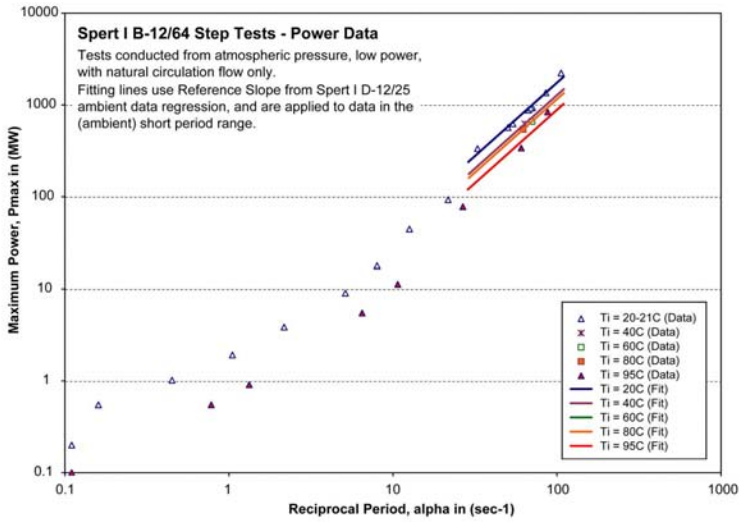

Figure 4-40: Spert I B-12/64 Power Data for the Subcooling Test Series

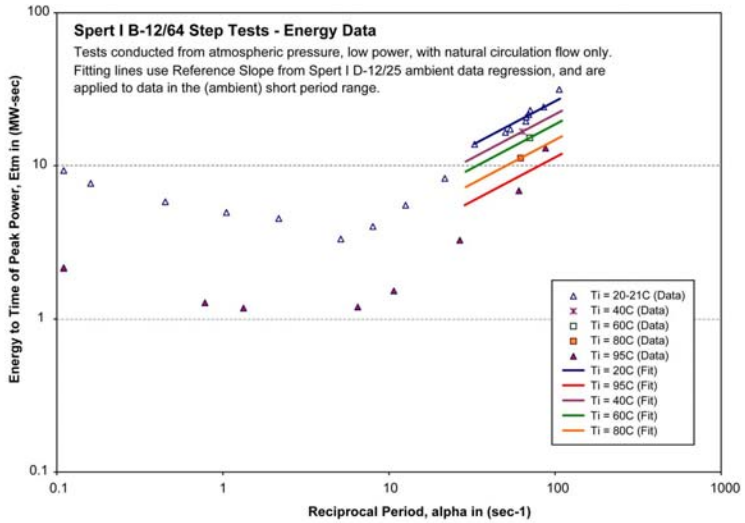

Figure 4-41: Spert I B-12/64 Energy Data for the Subcooling Test Series

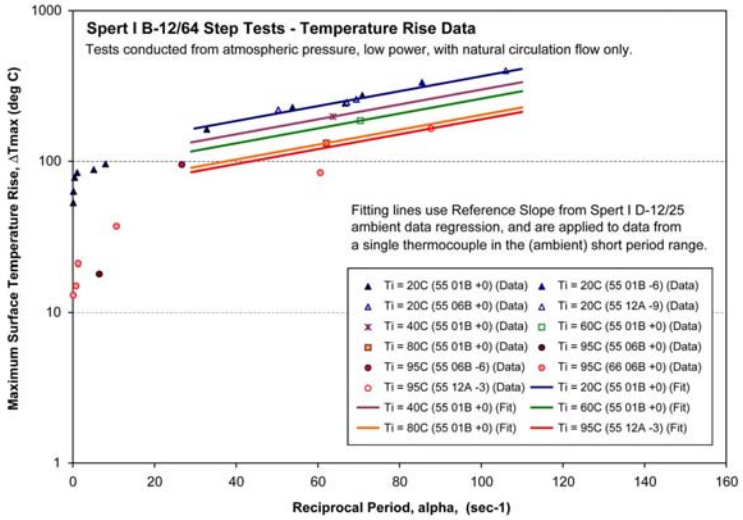

Figure 4-42: Spert I B-12/64 Temperature Data for the Subcooling Test Series

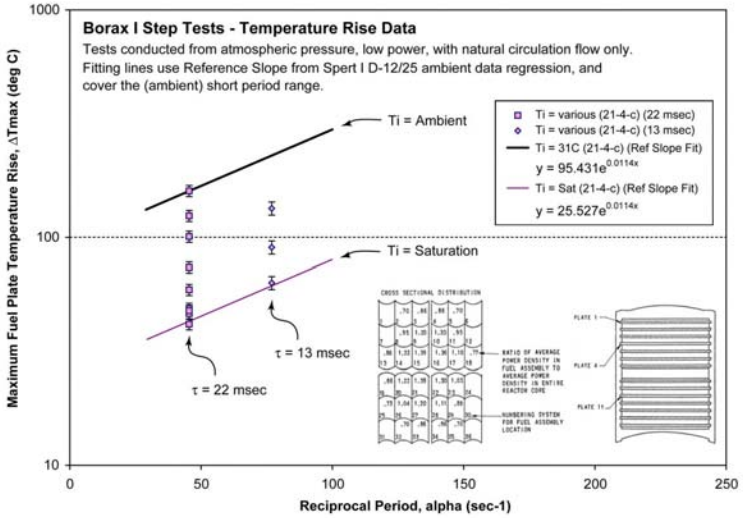

Figure 4-43: Borax I Subcooling Temperature Data from the 21-4-c Thermocouple

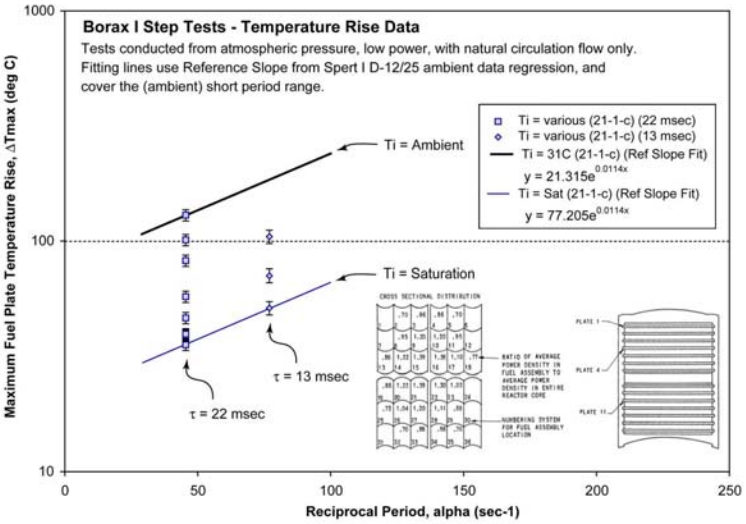

Figure 4-44: Borax I Subcooling Temperature Data from the 21-1-c Thermocouple

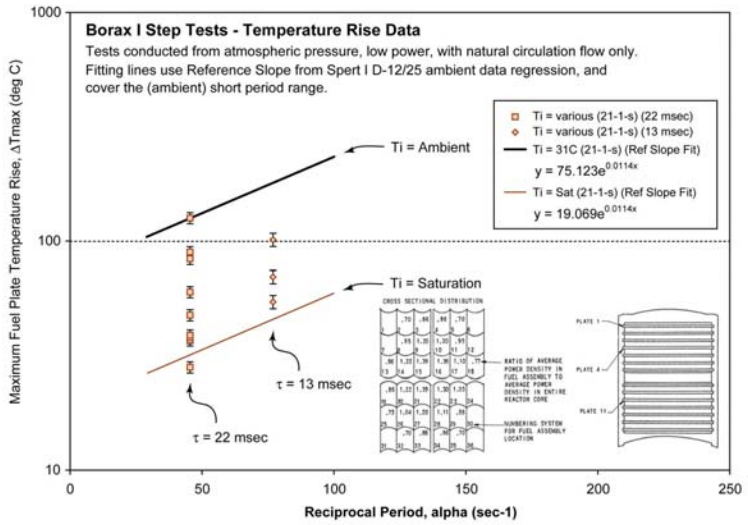

Figure 4-45: Borax I Subcooling Temperature Data from the 21-1-s Thermocouple

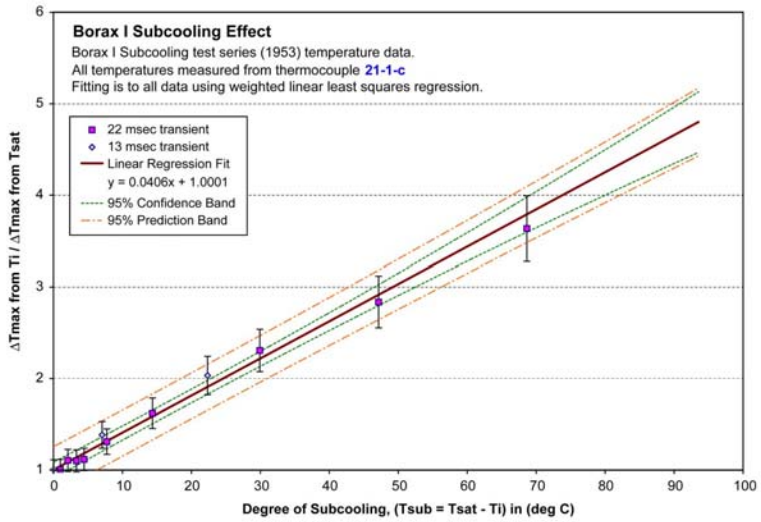

Figure 4-46: Borax I Subcooling Temperature Rise Ratio 21-1-c Thermocouple

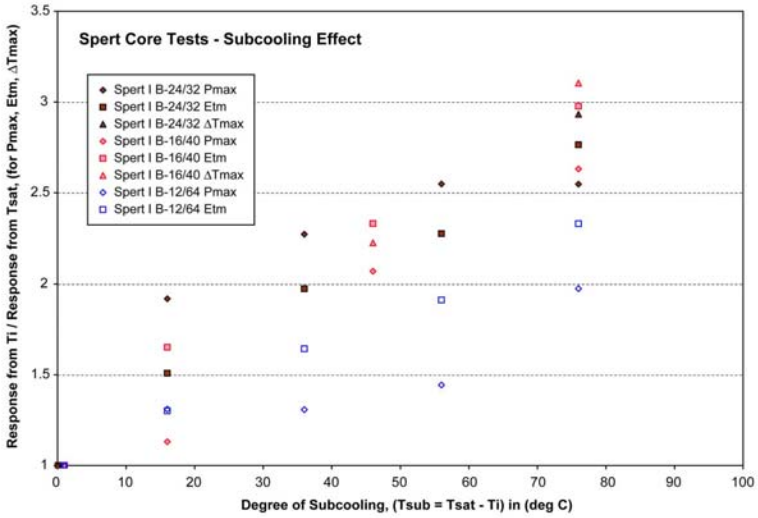

Figure 4-47: Spert I B-Core Subcooling Temperature Rise Ratio with Respect to Saturation Initial Temperature

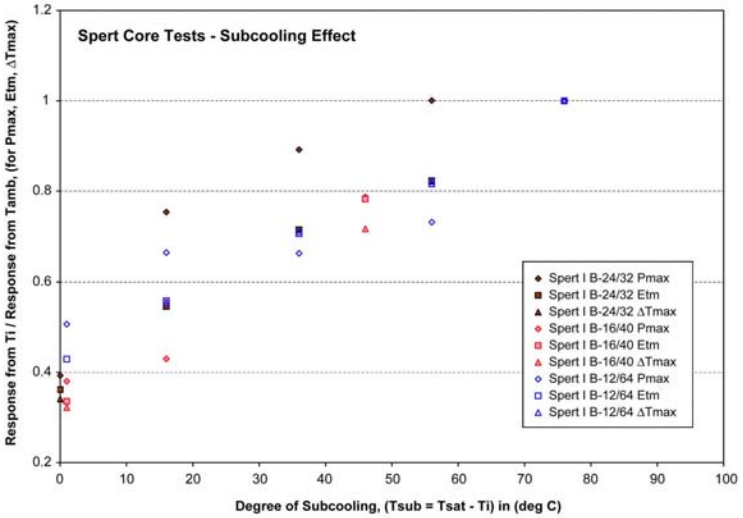

Figure 4-48: Spert I B-Core Subcooling Temperature Rise Ratio with Respect to Ambient Initial Temperature

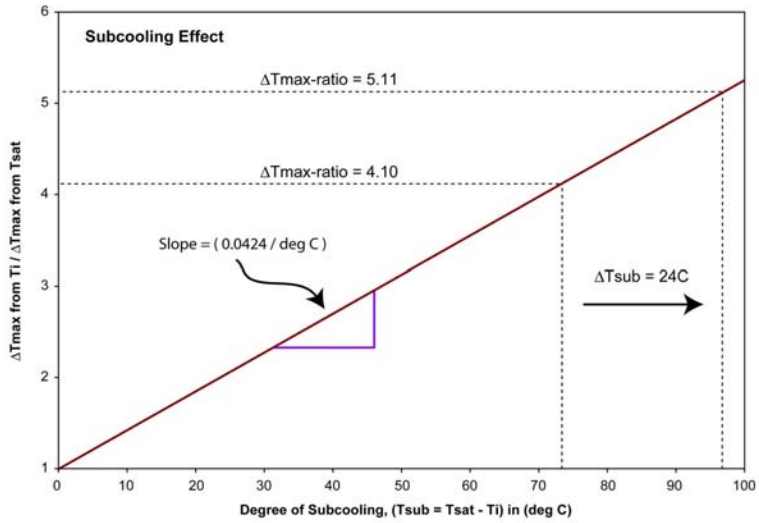

Figure 4-49: Example of the Subcooling Correction

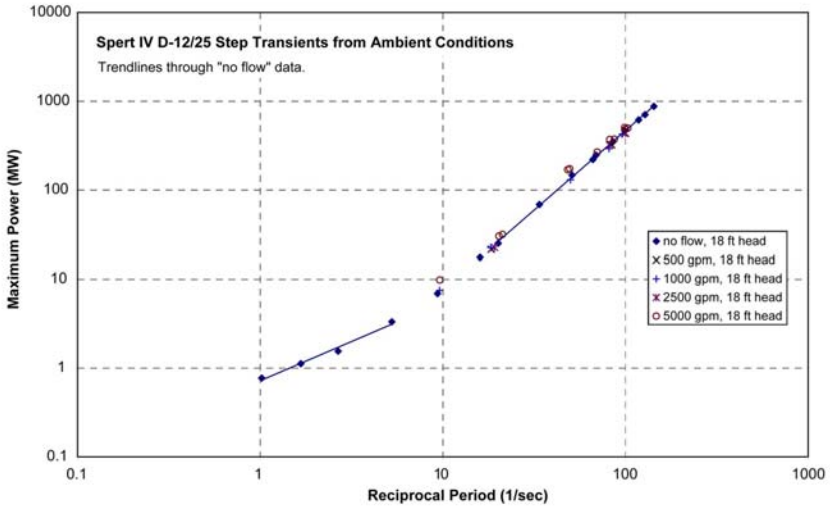

Figure 4-50: Spert IV D-12/25 Power Data for Varying Coolant Flow Rate

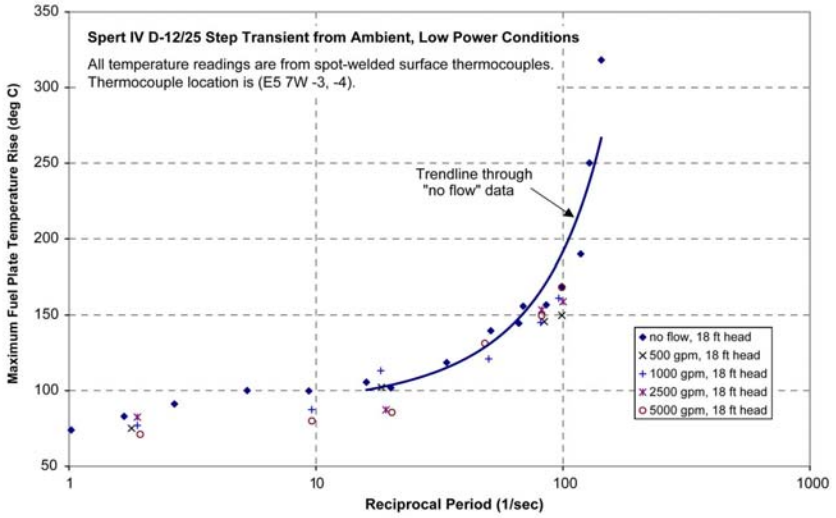

Figure 4-51: Spert IV D-12/25 Temperature Rise Data for Varying Coolant Flow Rate

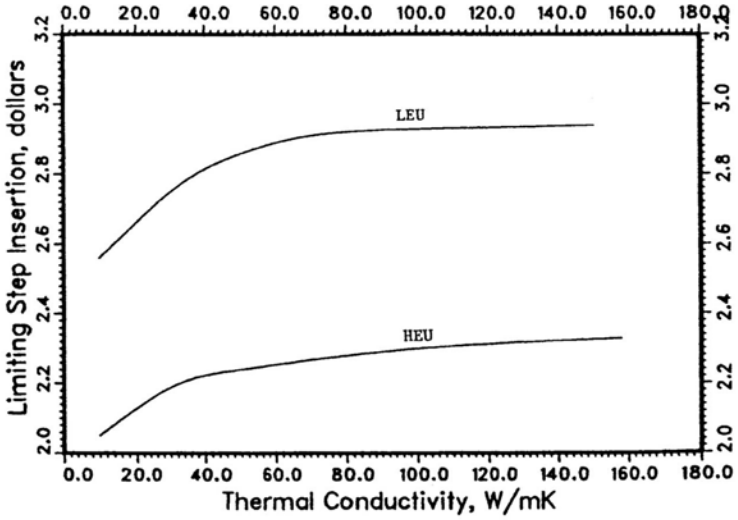

Figure 4-52: Variation of Limiting Step Insertion with Thermal Conductivity of Fuel Meat (Ref. 4-20)

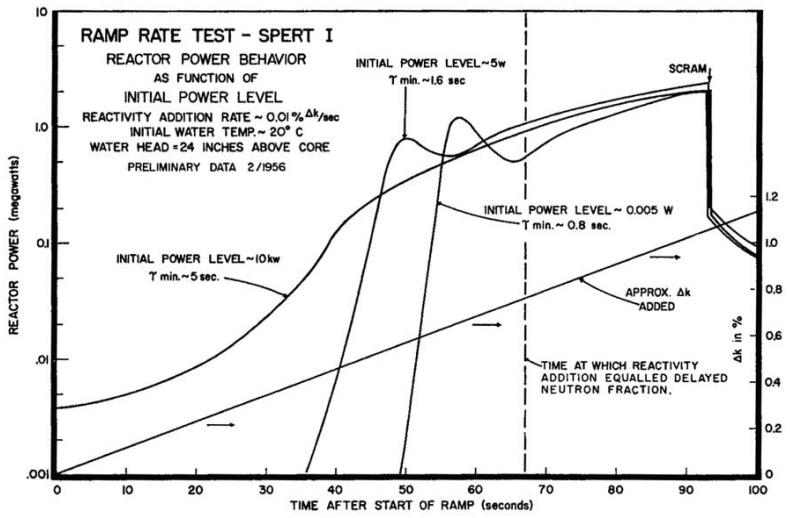

Figure 4-53: Power Behaviour of Ramp Insertion Transients with Varying Initial Power Level (Ref. 4-21)

CHAPTER 5 - STABILITY AND CHUGGING

TABLE OF CONTENTS

LIST OF TABLES

LIST OF FIGURES

5 STABILITY & CHUGGING

This chapter extends the preceding analysis of Chapter 4 to consider the behaviour with regards to stability of the system after the initial power pulse, *i.e.*, on a longer time scale. In some cases, in particular for slow reactivity insertion situations, this part of the self-limiting behaviour is found to be the stage of the transient associated with the safety limit. The phenomenon of "chugging" is discussed with reference to the experimental data in which this behaviour is observed and a safety analysis methodology is suggested.

This analysis is based on the stability subset of the test data as summarized in Chapter 3. This data are also described in more detail in Appendix B. The chugging tests are summarized in Table 5-1.

Ideally an analysis of chugging should be able to predict the inception point, frequency and amplitude of the power oscillations, and the associated temperature response of the system as well as the dependence on system parameters. Previous work has involved noise analysis of steady boiling and small amplitude oscillatory operation (Ref. 5-1). Most of the focus of these approaches is on the onset threshold for chugging and lend little information to the chugging behaviour itself. Herein, two analysis approaches are presented with respect to chugging behaviour of an MTR-type core as a result of reactivity being held in voids.

The first is a stylized approach explicitly treating the void, reactivity, power, and temperature oscillations. This approach is useful in the development of a physical picture of the processes involved in this mode of operation but the quantitative value is limited by the uncertainties resulting from (a) the sparsity of experimental data, and (b) the lack of first principles knowledge of transient heat transfer and boiling dynamics.

The second analysis approach is built on empirically correlating the experimental data based on the postulate that chugging void/power/temperature oscillations are equivalent to repeated step insertion responses by the system. This allows use of the much larger step insertion transient data set and derivation of reactivity damage thresholds analogous to those derived for step insertion transients. Reactivity limits are determined from a reactivity balance argument.

The critical question with respect to chugging operation is regarding the temperature stability of the limiting fuel plate. The lesser question of mechanical stress on the

system as a result of pressure generated during the voiding may be of concern but this is not included in the analysis.

5.1 Stylized Chugging Analysis

5.1.1 Void Response of the System

The similarity between test loop flow instability traces and reactor power instabilities and the agreement in exit void fractions between maximum power assemblies and test loop results points to a hydrodynamic basis for reactor instability (Ref. 5-2).

The driving force for large amplitude voiding *via* steam generation is related to the power generation in the fuel plates and the flow characteristics of the system. The fission power provides the energy which changes the water in the coolant channels to steam, thus voiding the channel. The direction of flow determines the exact transition from single phase (liquid coolant) to large amplitude voiding and whether a stable boiling state is possible (described in Chapter 2).

For forced downward flow the creation of steam in the coolant channel causes a decrease in flow due to the upwardly directed buoyancy force on the steam and the increased friction or pressure drop in the channel due to the presence of two phases (Figure 5-1). Note that the gravitational force on the steam voids is negligible. The resulting reduction in flow further compounds the power/flow mismatch. Unless a compensating drop in power occurs, due to negative reactivity feedback and/or manual intervention, this situation can only develop into large scale voiding (see Fig. 5-2). Examination of step insertion power pulse shape for fast transients in an HEU system indicates that power increases until voiding becomes significant, therefore the heat source can be assumed increasing, thus compounding the voiding, until large amplitude voiding is generated.

For upward flow, including natural circulation, the physics is slightly different in that the buoyancy force on the steam is in the same direction as the flow. The increased friction due to the change from single to two phase flow will still increase the pressure drop (Fig. 5-1). As a result the system may steady state boil (see Fig. 5-3) or develop into large scale voiding (see Fig. 5-4). The latter will occur when the increases in friction outweigh the gains in flow due to the buoyancy effects. This threshold is related to a certain void fraction in the coolant channel. For steady boiling the void fraction will be axially dependent with the maximum at the channel

outlet and has been measured to be as high as 0.75 at the outlet of a Spert I A coolant channel (Ref. 5-3).

Irrespective of any ability to operate with void precluding large amplitude voiding, once the system enters into the mode of large amplitude voiding the volume of void increases rapidly.

The pressure associated with the steam generation is a result of the specific volume change between water and steam which is greater than 900 times at atmospheric pressure (Ref. 5-4). The pressure increases exponentially as the steam volume, due to the feedback property of the void production.

Coolant temperature measurements at multiple axial locations in Spert IV D-12/25 coolant channels (Figs. 5-5, 5-6) indicate that the voiding is between 50% and 100% of the channel volume for small amplitude oscillatory behaviour (*i.e.*, less severe than chugging oscillations). Projecting this information to more severe chugging operation, and considering the violent water ejection associated with chugging in Spert I A, suggests that voiding extent is certainly likely to reach 100% of the channel volume (Ref. 5-5).

The refill/condensation time is postulated as the limiting stage of the oscillation cycle and the rate of escape of steam is postulated as the limiting time constant for channel voiding rather than the rate of formation of steam (Ref. 5-6). In subcooled systems, steam can dissipate *via* condensation which makes the system more stable.

The speed of the voiding process is fast compared to the cycle length of the chugging oscillations with the rate at which water is driven out of the core by steam formation largely limited by the mechanical inertia of the water (Ref. 5-7). If the time required to heat the refilling water to saturation is included in the voiding time, systems with more highly subcooled bulk water (*i.e.*, colder relative to the saturation temperature) will have longer times associated with voiding. However, these increases in voiding time will only be on the order of a few periods which is small compared to refill time. Increasing the system pressure, such as *via* an increase in hydrostatic head, will effect the voiding time in this way by raising the saturation temperature.

Once the coolant channel has been fully voided there is no longer any pressure generation and the pressure drop of the primary system (*e.g.*, driven by the pump, hydrostatic head, or density differences) is re-established. This provides the driving force, in addition to buoyancy driven escape of the steam, for refill of the core and

determines the speed of refill. The primary system flow also determines the direction of refill; from the top of the core down for downward forced flow and from the bottom of the core up for upward forced flow and natural circulation conditions. During refill, the channel inlet is re-wetted first and is not dry for long while the outlet of the channel is dry until complete refill is achieved. In addition to flow driven refill, steam can also be removed from the system *via* condensation (*i.e.*, void collapse).

Examination of the axial coolant temperature measurements from the Spert IV D-12/25 chugging tests under natural circulation conditions (Figs. 5-5, 5-6) indicates that refill of the coolant channels is roughly linear with time. Also shown is that under natural circulation conditions, the direction of refill is from the bottom of the channel upwards. The linearity with respect to time is shown as the timing of the temperature drop from saturation for the inlet, centre, and outlet thermocouples. As expected, the coolant temperature oscillations were found to be in phase with the fuel plate surface temperature oscillations. Refill from the top of the core driven by downward flow will be inhibited by the buoyancy of the steam in the channel.

From the above reasoning, systems with more subcooled (lower temperature) bulk reactor temperature and higher primary flow rates should demonstrate faster core refill and therefore shorter chugging cycle lengths. This is observed in the experimental data.

Refill times for full channel voiding in Spert IV D-12/25 core under natural circulation and subcooled conditions are estimated as between 0.6 and 0.7 seconds (Fig. 5-7). Other estimates suggest a faster refilling time on the order of 0.1 sec (Refs. 5-5, 5-8).

The frequency of the voiding/refilling cycle is determined by the sum of the voiding and refilling times. The frequency of the chugging oscillations varies between one and four cycles per second for the Borax I, Spert I A-17/28, Spert I B-12/64, and Spert IV D-12/25 cores under natural circulation coolant conditions. Some dependence of the cycle length is observed for variations in the size of the hydrostatic head for systems operating under natural circulations conditions, with shorter cycle lengths for the case of an 18 foot hydrostatic head as compared to cases with nine and two foot hydrostatic heads. Additionally, there does seem to be a dependence on the initial pool temperature with frequencies near one cycle per second associated with saturated pool temperature and two cycles per second with ambient pool temperature (Tab. 5-1). These results are consistent between all four cores for which results are

reported. This latter dependence indicates that the process of steam dissipation by condensation is a dominant factor. As it seems that the refill (*i.e.*, steam removal) is the limiting process it is expected that systems with a larger pressure drop in the primary (due to forced flow) and a more subcooled bulk temperature will have higher frequency oscillations.

The stylized voiding response of the system is shown in Figure 5-8.

Although the preceding discussion has been concerned mainly with a single coolant channel, the experimental data show that for chugging operation the voiding/refilling of the parallel coolant channels are in phase with one another and with the power oscillations (Fig. 5-9).

The Type-D assemblies are characterized by non-uniform channel width with narrow outer channels. The results from these tests also show that while the narrow and wider standard coolant channels are voiding/refilling on different frequencies the system power oscillations are limited and showed no tendency to increase beyond ± 50% of a mean power level. The narrow channel voiding behaviour (shown as temperature data) is found to be strongly linked to the power oscillations of the system as shown in Figure 5-10 while the wider channel voiding oscillated on a longer cycle length. As more reactivity is added to the system the wider channels begin to void/refill in sync with the narrower channels at which point the power oscillations are observed to grow in amplitude as shown in Figure 5-9 (Ref. 5-9). The constructive interference of the narrow and wide channel voiding is associated with a larger net reactivity insertion. This illustrates that separate flow channels are coupled in their hydrodynamic behaviour during chugging.

Further evidence of this relationship between the power and the temperature oscillations is seen in the data for the Spert IV D-12/25 chugging test in which the bulk reactor temperature was allowed to increase until the onset of chugging was reached. At the point where the power oscillations begin to increase to large amplitude, all measured fuel plate surface temperatures increase and decrease with the power showing the direct relationship (Ref. 5-1). This is shown in Figure 5-11. This evidence indicates that the local voiding and refilling mechanisms for a single channel can be applied to the core as a whole with some fraction of the core voiding and refilling. Thus the complexities of parallel channel flow are avoided as they are not relevant.

Systems with larger void coefficient of reactivity will be more stable under given

initial reactivity insertion conditions since less void fraction is needed for the same compensating reactivity

Also, systems with flatter power/flow profiles will be more stable as the void volume related to a given compensating reactivity will be more spread out over the core and therefore less void fraction in a given channel for the same compensating reactivity.

5.1.2 Reactivity Response of the System

The phenomenon of chugging indicates that MTR-type systems have the inherent ability to return large amounts of reactivity to the system, *via* coolant channel refilling.

Voiding of the coolant provides the negative reactivity required to self-limit unprotected power excursions. This "compensating" reactivity is then available to be returned to the system as a positive reactivity insertion upon void collapse. The amount of reactivity held in or required to be held in voids for self-limitation of a reactivity initiated transient determines the maximum reactivity which can be inserted upon void collapse.

The void reactivity is associated with the void volume by the system's void reactivity coefficient. This quantity depends upon the metal to water ratio of the fuel (*i.e.*, coolant channel size) and also on the location of the voiding within the core. It also may be non-linear in nature with respect to void volume for the range of zero to full channel voiding throughout an assembly or group of assemblies. In other words the void reactivity feedback is a function of the void distribution throughout the core which cannot easily be described by considering the behaviour of a single coolant channel. Rather, this void distribution is dependent on the power, flow, and temperature distributions. Thus, this quantity is difficult to derive from a deterministic analysis. Via the stylized approach used in the previous section on void response the general trends associated with the reactivity response can be described. There is some indication that despite the complexities of the voiding dynamics, that the resulting void distribution may be represented by a uniform void coefficient value (for more details see Chapter 4).

Negative reactivity *via* void production is produced to compensate for the initial reactivity insertion. The energy required to produce this void is created within the fuel plate from the fission process. As a result this energy is not instantaneously available to change water to steam but rather must be transferred from the fuel plate

to the coolant. The resulting time delay associated with this heat transfer process and also with the development of the void volume allows more energy to be produced in the fuel plate before the power excursion can be self limited. The result is that more energy and subsequently more void is produced than required to compensate for the excess reactivity in the system. The longer the thermal time constant for the system, *i.e.*, the longer it takes to transfer heat from the plates to the coolant and the longer the time to move water from the channel, the more negative void reactivity will be produced and the greater the over-compensation of reactivity (*i.e.*, the more subcritical the system will become upon void production).

Irrespective of the amount of negative reactivity over-compensation *via* void feedback, upon subsequent refill of the core the maximum excess reactivity can only be as much as the original value assuming no other positive source of reactivity. The shutdown depth upon voiding will only affect the timing of when the system returns to critical as the core refills. A stylized representation of the system reactivity due to voiding/refilling during chugging is shown in Figure 5-12.

The voiding process is fast relative to the refilling process so the reduction in reactivity occurs quickly whereas the subsequent rise from subcritical to supercritical is more gradual. Assuming that void reactivity is linear with void volume and that the core refill is linear with time, the reactivity insertion is also linear with time. Evidence indicates that unobstructed coolant channel refill is a rapid process, on a time scale as short as 100 msec which approximates a step reactivity insertion and is also on the order of the rod ejection time for initiation of the step transient tests (Refs. 5-5, 5-8). Longer refill times will result in less severe oscillations.

Since the process of refilling the core introduces positive reactivity to the system and initiates the subsequent power increase, full channel refill is conservative with respect to the amount of excess reactivity and the resulting power pulse.

Incomplete refill will occur if the plate surface temperature is high enough so that the refilling water is converted to steam before the channel is completely re-wet. This partial refill only returns a fraction of the excess reactivity to the system and therefore results in a smaller subsequent power pulse and reduced plate temperature. This may account for some of the fluctuation in height of the chugging power pulses, however the sustained oscillation envelope (see for example Fig. 5-13) indicates that the same extent of refill and void is maintained on average. Along a similar line of argument systems with saturated bulk water temperatures may be more likely to only partially refill as the required energy to “re-void” the coolant is decreased.

Despite the difficulties associated with relating the voiding and refilling behaviour of a single channel to that of the whole core (except that the timing is in phase), an estimate of the excess reactivity available for return to the system upon void collapse can be obtained by conducting a reactivity balance calculation for the system. This approach avoids the reliance upon accurate knowledge of the void coefficient and void distribution within the core.

Prior to the initiation of the transient the system is at some steady state, either critical or shutdown in a subcritical state. Considering the latter case, the transient is initiated by a positive reactivity insertion, where the mode of reactivity insertion is irrelevant to the chugging analysis (Ref. 5-5). The resulting initial excess reactivity is found from:

$$\rho_{ex}(0) = \rho_{in} + \rho_{sd}$$

where $\rho_{ex}(0)$ is the resulting initial reactivity of the system, ρ_{in} is the initially inserted reactivity and ρ_{sd} is the shutdown depth of the system (therefore a negative value). For an initially critical system (*e.g.*, at-power initial conditions) ρ_{sd} is simply zero. Between the initiation of the transient and the onset of chugging the system conditions will change as the fuel, moderator, and coolant increase in temperature. This provides various sources of feedback reactivity, namely fuel temperature, coolant temperature and density, and reflector temperature contributions. In a self-limiting situation, *i.e.*, the net reactivity of the system is less than or equal to zero, the remainder of the excess reactivity must be compensated by steam voids. Therefore:

$$0 = \rho_{ex}(0) + \rho_f + \rho_c + \rho_r + \rho_v$$
$$\rho_v = -\left[\rho_{ex}(0) + \rho_f + \rho_c + \rho_r\right]$$

where ρ_f, ρ_c, and ρ_r, are the reactivity contributions due to temperature and density changes in the fuel, coolant, and reflector, respectively, and ρ_v is the reactivity contribution from coolant voiding. These feedback terms can be written in terms of the applicable temperature change, ΔT, and reactivity coefficient, α, *i.e.*,

$$\rho_v = -\left[\rho_{ex}(0) + \alpha_f \Delta T_f + \alpha_c \Delta T_c + \alpha_r \Delta T_r\right]$$

where the subscripts *f*, *c*, and *r* refer to fuel, coolant, and reflector respectively. For an MTR-type system the fuel and coolant temperature reactivity coefficients are

negative. Indications from previously published work are that the reflector coefficient of reactivity for this type of reactor is positive (Ref. 5-10).

Consider Figure 5-14 which is a stylized runout of a power transient which develops into chugging oscillations. The onset of chugging may occur at various times of the runout and depends on the specific system and reactivity balance. The reactivity balance is considered at three different times:

Directly following the initiating reactivity insertion, in order to self-limit the power excursion the system need only compensate for the prompt supercritical portion of the inserted reactivity plus the initial delayed neutron source, since the delayed neutron source is still based on the prior initial power level. This is indicated as time, t_1, in Figure 5-14. The minimum compensating void reactivity can be written as:

$$\rho_v(t_1) = -\left[\left((\rho_{in} - \beta) + \rho_{sd}\right) + \alpha_f \Delta T_f + \alpha_c \Delta T_c\right]$$

where the excess reactivity, ρ_{ex}, has been written in terms of the prompt supercritical portion of the initially inserted reactivity, (ρ_{in} - β), and the shutdown depth. Also note for this case the reflector will not have had time to increase in temperature so the corresponding reactivity feedback term has been dropped.

On a longer time frame the delayed neutron source will build up due to the cumulative fissions to correspond to the new average power level. If the system is not in chugging mode it may develop into chugging as the excess reactivity of the system increases as the delayed neutron source increases. With the increased reactivity of the system more compensating reactivity must be generated *via* steam formation leading to higher void fractions and possibly the onset of chugging. This is arguably what drives the transition from steady power to the onset of oscillations and the growth of the oscillation envelope between 10 sec and 20 sec for the Spert I A-core stability test shown in Figure 13. The delayed neutron source build up is indicated over time interval t_1 to t_2 on Figure 5-14. Time t_2 in Figure 14 corresponds to $t \sim 15$ sec for the test shown in Figure 13. The associated minimum void reactivity can be written as:

$$\rho_v(t_2) = -\left[\left(\rho_{in} + \rho_{sd}\right) + \alpha_f \Delta T_f + \alpha_c \Delta T_c\right]$$

It is still assumed that by time t_2 the reflector temperature has not changed appreciably from the initial conditions. This is a realistic assumption for subcooled

systems with either very large water inventories, as in a swimming pool, or those in which heat removal is credited to keep the reflector temperature constant. It should be noted that $|\rho_v(t_2)| > |\rho_v(t_1)|$.

On a still longer time frame in a situation where heat removal is not keeping the reflector at a constant temperature below coolant saturation, there is an additional reactivity feedback effect from temperature increase of the reflector. This is indicated as time, t_3, in Figure 5-14. In the Spert IV D-core stability tests the pool temperature increased on a time frame of many minutes (Ref. 5-1). The reactivity required to be held in voids can be written as:

$$\rho_v(t_3) = -\left[\left(\rho_{in} + \rho_{sd}\right) + \alpha_f \Delta T_f + \alpha_c \Delta T_c + \alpha_r \Delta T_r\right]$$

In the case of the Spert U-Al H_2O reflected cores the reflector coefficient of reactivity has been calculated to be positive (Ref. 5-10). As a result $|\rho_v(t_3)| > |\rho_v(t_2)|$. If the system is not in chugging mode it may develop into chugging as the reflector increases in temperature. This scenario was observed in the Spert IV D-core stability tests (Ref. 5-1) in which a test in which about 28 mk ($4) of reactivity was inserted did not develop into chugging until the bulk reactor temperature increased from about 20EC to about 70EC. The time trace of power and fuel surface temperature for this test is shown in Figure 5-11 where $t \sim 747$ sec corresponds to t_3 in Figure 5-14. Considering the calculated reflector temperature coefficients for Spert I D-12/25 core (Ref. 5-10),

$$\alpha_r = +10.0 \times 10^{-5}\ \Delta k / °C$$

and assuming these can be applied to the similar Spert IV D-12/25 core, a change in reflector temperature of 50EC leads to an increase in reactivity of the system on the order of 5 mk.

For situations where the system enters into chugging mode by times t_1 or t_2 in Figure 5-14, the increase in system reactivity due to the delayed neutron fraction and the increase in temperature of the reflector serves to increase the magnitude of the oscillation envelope.

Note that for systems with a positive reflector coefficient of reactivity the maximum compensating void reactivity is associated with the longest time frame, *i.e.*, t_3. Therefore, the reactivity estimate $p_v(t_3)$ should be used as a conservative limiting

value for predicting the maximum chugging power and temperature response of the system.

Also note that the reactivity balance calculations rely on *a priori* knowledge of the system feedback coefficients which is part of the problem previously discussed with respect to directly calculating the void reactivity feedback. However, since the reactivity swing during chugging can be calculated from the difference in reactivity between system equilibrium or average states precluding chugging this calculational approach can be expected to be reasonably accurate based on steady state calculations and measurements.

Part of the nuclear characterization of the Borax I and Spert I A- and B-cores included measuring the reactivity change for uniform heating of the system from ambient to saturation temperatures. The reactivity changes were calculated from the change in critical position of the control rods as system temperature was increased. This "temperature defect" provides an estimate of the reactivity change in the system from initial shutdown conditions to those associated with time, t_3, in Figure 5-14, which is the conservative case under consideration.

As an illustrative exercise the excess reactivity held in voids can be estimated for the Borax I and Spert I A cores for the conditions applicable to the transient tests which showed chugging behaviour. The temperature defects for the Borax I and Spert I A- and B-cores, summarized in Table 5-2, have been estimated from Figures 5-15 and 5-16 (Refs. 5-11, 5-12) by digitizing the curves and fitting them with polynomials *via* a least squares method. The temperature defect values range between -8.2 mk for Borax I to -12.4 mk for Spert I B-24/32. Similar temperature defect values have not been reported for the Spert IV D-12/25 core. However, the system is similar to Borax I and the other Spert HEU U-Al plate-type cores so a similar temperature defect can be expected.

Therefore, from initial low power and temperature, *i.e.*, 20EC, conditions the amount of inserted reactivity which must be compensated by void and therefore the amount available to be returned to the system is estimated as:

$$\rho_v \quad = \quad \rho_{ex} \quad + \quad \rho_{T-defect}$$

Reported estimates of the initial (ρ_{in}) and void compensated (*i.e.*, refill, ρ_v) reactivity are about 29 mk ($4.1) and about 15 mk ($2.1), respectively for a threshold test in

Spert IV D-12/25 from initially ambient conditions with a two-foot hydrostatic head (the same conditions under which the temperature defects for the Spert I A- and B-cores were measured). The difference between these two reactivity values is the temperature defect from ambient to chugging conditions. Assuming a β value of 7 mk,

$$\begin{aligned} \text{Spert IV D} - 12/25, \quad \rho_{T-defect} &= -\rho_{in} - \rho_{v} \\ &= -\$4.1 - (-\$2.1) \\ &= -\$2.0 = -14\ mk \end{aligned}$$

This result is close to the range of the Borax I and Spert I A- and B-core measurements.

Further evidence supporting this reactivity balance argument is shown in a pair of figures from Reference 5-13. The first, Figure 5-17, shows 14 msec step transient responses in Borax I and Spert I A, initiated from ambient temperature. The post initial power peak behaviour of the two systems differs in that the Borax I power runout shows oscillatory features while the Spert I A power runout is stable. Table 5-2 shows the magnitude of the temperature defect of Borax I is less (-8.2 mk) than that for Spert I A (-10.9 mk). As a result, in order to compensate the same initial reactivity insertion more reactivity must be compensated by void generation in Borax I when compared to Spert I A. Assuming similar void reactivity feedback coefficients and void distribution for the two systems, this is equivalent to a larger void volume in Borax I, which in this case is evidently near the threshold for the onset of chugging. The amount of void in the Spert I A system for this initial reactivity insertion is shown to be below the threshold for the onset of chugging immediately after the initial power pulse.

The second, Figure 5-18, shows the power runout for 18 msec-period transients in Spert I A from different initial system temperatures. As the degree of subcooling is decreased, *i.e.*, as the initial temperature is increased, the resulting stability of the system is decreased, moving from a stable power runout for an initial temperature of 20EC to runouts which show oscillatory tendencies for initial temperatures of 60EC and 96EC. The degree of subcooling is proportional to the available temperature defect for the system and as it is reduced the amount of compensating reactivity required in voids is increased. This amount of void reactivity which is associated with a given void volume approaches the threshold for the onset of chugging for

transients initiated from some temperature between 20EC and 60EC.

It should be noted that the system temperatures which exist just prior to the onset of chugging and during chugging oscillations are not uniform. Although coolant and reflector temperatures are limited to the saturation temperature of light water, the fuel temperature will exceed the coolant saturation temperature. For steady boiling the fuel surface temperature may be as much as 15EC to 20EC in excess of the saturation temperature of the coolant. This is also typical of the baseline temperature of the fuel during chugging oscillations. Since the fuel temperature (Doppler) feedback coefficient is negative, neglecting this larger fuel temperature rise from initial conditions is a conservative approximation, especially for LEU fuel.

For at-power initial conditions system temperatures are not uniform. A similar enveloping approach may be taken with regards to the temperature defect calculation. Otherwise, knowledge of the various feedback coefficients are needed. These can be estimated from additional measurements or static simulations.

A certain amount of reactivity held in voids is associated with a different void distribution and volume for different systems. This is of no concern for systems operating under forced downward flow conditions which develop into chugging as soon as boiling commences in a reactivity insertion accident, but will affect the reactivity threshold for the onset of chugging for systems operating under natural circulation or forced upward flow conditions.

The distribution of void depends on the power density and flow distributions of the core. The more peaked the power density distribution and the more mismatched with the flow distribution of the core the more concentrated the void volume will be in the hot assemblies. Therefore, a core with a more peaked power density distribution will exceed the onset of chugging threshold for a smaller reactivity insertion compared to a core with a flatter power density / flow distribution. Flux peaking factors for the Borax I and Spert HEU U-Al plate-type cores are given in Table 5-2.

The amount of void also depends on the magnitude of the void reactivity coefficient for the specific system. Systems with smaller void reactivity coefficients require a larger void volume to generate the same compensating void reactivity as a system with a larger void coefficient of reactivity and will therefore exceed the void volume threshold for the onset of chugging for smaller compensated void reactivity. This is reflected in the results for the Spert I B-12/64 core compared to those for the Borax I and Spert I A cores. The Spert I B-12/64 core, which has a smaller void coefficient

of reactivity (and a locally positive central void coefficient) as compared to these other systems, developed into chugging for an initial reactivity insertion of about 15 mk compared to the Borax I and Spert I A cores which did not develop chugging until the inserted reactivity exceeded about 25 mk. Void coefficients for these systems are given in Table 5-2.

With respect to differences due to variation in the size of the hydrostatic head, this sensitivity is hard to determine from the Spert IV D-core threshold tests as the inlet water temperature was different for the 18-foot (~ 35EC) compared to the two-foot (~ 70EC) head tests. It is also hard to determine any sensitivity from the Spert I A tests as water was lost from the system during the chugging.

What information is available suggests that the threshold to chugging for the larger hydrostatic head case occurs at slightly larger total reactivity insertions than the smaller hydrostatic head case. The difference can be attributed to more reactivity being compensated by non-boiling mechanisms for the larger hydrostatic head case due to the increase in saturation temperature. The 18-foot head, natural circulation case conducted in the Spert IV D-core stability test series showed similar divergent, *i.e.*, developing chugging, behaviour for a $4.2 total initial reactivity insertion as that shown for the two-foot head case (Fig. 5-9) which required $4.1 of reactivity.

5.1.3 Power Response of the System

The hydraulic oscillations are associated with reactivity changes which drive the power oscillations observed in chugging.

A stylized power response during chugging is shown in Figure 5-19.

The system is super-critical (*i.e.*, $k > 1$) when the coolant channels are filled with water. While super-critical the power of the core increases. The speed or period depends on the amount of excess reactivity returned to the system. As a conservative approximation, the reactivity insertion can be treated as a step insertion, therefore, the power increase is typical of a step insertion, *i.e.*, exponential in nature for an HEU core. The power increases until enough heat is transferred to the coolant from the fuel plate to produce steam voids in the coolant.

The system is sub-critical when the coolant channels are voided. When subcritical the power of the core drops to a low level. As in the case of a step insertion initial power pulse the power rise has been found to drop more rapidly than the rate of

power rise for the power pulse. This is due to the rapid nature of the voiding process and the apparent significant amount of negative reactivity over-compensation.

The magnitude of the power pulses is dependent on the amount of reactivity being returned to the system when the coolant channels refill. This is related to the initial reactivity insertion with consideration of the initial shutdown depth of the system and the temperature defect as the system reaches chugging conditions. This is explained previously in Section 5.1.2. The larger the amount of reactivity returned upon void collapse the shorter the period of the power rise and the larger the magnitude of the power oscillations. This is analogous to the dependence of a step insertion power pulse on inserted reactivity.

Similarly, analogous to a step insertion transient response, the chugging power oscillations are expected to increase in magnitude with increased subcooling of the refill coolant for the same reactivity oscillations.

As the processes and time frames involved are the same as those for a step transient so the same difficulties exist in simulating and calculating the power response for chugging operation. A conservative estimate on the power rise portion of each peak can be obtained by assuming no feedback until the time of voiding (determined from the hydraulic cycle). The period of the power rise can be found from the period to reactivity relation for the system. The minimum period of the power rise is associated with the maximum excess reactivity.

An alternative semi-empirical correlative method, as used in step insertion analysis is discussed in Section 5.2.

5.1.4 Temperature Response of the System

The temperature rise in the fuel over an oscillation cycle depends on the amount of energy deposited during the power pulse and the heat transfer from the plate to the coolant and reactor structure.

An estimate of the temperature rise over an oscillation cycle may be made if an energy balance can be constructed. The energy source is simply the fission energy integrated over the chugging power pulse, suitably distributed according to the power distribution throughout the core. Roughly 85% of the fission energy is deposited in the fuel plate (Ref. 5-11) with the remainder distributed in the coolant, core structure and reflector. The energy loss from the plate is that required to raise the coolant

temperature to saturation and that required to change the liquid coolant to steam.

To formulate a realistic estimate of the energy loss term an idea of the refilling water temperature and the amount of water converted to steam is required. These quantities depend on rather complex hydraulics of steam removal and voiding dynamics.

If an energy balance can be formulated then the temperature distribution within the fuel plate should also be estimated and needs the definition of a source distribution and heat transfer to the coolant. Indications from step insertion analysis are that losses from the fuel plate are negligible up to the time of onset of voiding (Ref. 5-14).

Stylized temperature oscillations are shown in Figure 5-20. During chugging the temperature oscillations are strongly linked to the power oscillations, lagging the power oscillations as a result of the delay in heat transfer out of the fuel plate. The exact temperature response is difficult to model as it depends upon the transient heat transfer.

As in the case of the stylized power response of the system, an alternative semi-empirical correlative method based on step transient data is suggested. This is presented in Sections 5.2 and 5.3.

5.2 Step Transient Equivalence

Chugging can be analysed in the context of the much more complete step insertion transient data set on the premise that the initiating reactivity insertion and the physical processes involved in self-limitation are equivalent in the two cases. In this way the chugging response is considered as a repeating set of step reactivity insertion responses.

The coolant channel refill returns positive reactivity to the system in a prompt fashion, on a timescale similar to that for the rod ejection used to initiate step transient tests (Ref. 5-5). For refill times slower than the rod ejection times the comparison to step insertion transient data is conservative since faster insertion times result in more severe power and temperature excursions.

Heat transfer from the fuel plate to the coolant, producing large amplitude steam voids in the coolant channels is the self-limiting mechanism during chugging operation. These are the same processes which are responsible for the self-limiting

characteristics in response to step reactivity insertion situations. The power pulses in chugging have been found to be qualitatively similar to a step insertion transient initial power pulse. The associated temperature "pulse" in chugging lags the power pulse and is also qualitatively similar to the step transient initial temperature response.

Considering the reactivity insertion and self-limiting characteristics involved in chugging it is therefore concluded that chugging can be considered as a cyclic set of step insertions and is similarly expected to be safely self-limiting up to some reactivity limit associated with the onset of fuel damage. As such, the correlated data from step insertion tests are applicable to chugging analysis.

In order to check this premise the rather sparse chugging data subset is compared to relevant step transient data. For the Borax I chugging test shown in Figure 5-21, peak power and change in temperature are compared to step test data from saturated conditions (Fig. 5-22). This comparison is summarized in Table 5-3. Data from other tests show that the centre thermocouple in plate 1 reads higher than the centre thermocouple in plate 11 so the temperature rise comparison is far from exact.

A similar comparison between chugging power and temperature peaks and step insertion initial peaks is available for some Spert I B-12/64 data. The chugging data are extracted from Figure 5-23 (Ref. 5-15). For equivalent peak powers the fuel plate surface temperature rise from the step initial pulse data are larger than that measured during the chugging. This indicates that the use of step pulse data from chugging analysis is conservative. This discrepancy may be attributed to the elevated fuel temperature which is the "initial condition" for the chugging pulses providing a pre-established temperature gradient between the fuel and coolant. A more direct comparison may be expected between the chugging data and step transient data from at-power conditions but this is not available. The present comparison is conservative with respect to fuel temperature rise.

Unfortunately step transient data for the Spert I A-17/28 and Spert IV D-12/25 cores for elevated initial temperatures are not available so a direct comparison between chugging and step data is not possible. However, comparison of the data gives differences qualitatively consistent with the effect of subcooling on peak power and temperature.

There are important factors to consider when comparing step insertion and chugging behaviour limits. Firstly, chugging occurs on a longer time frame than the initial

power peak of a step insertion initiated test. As a result, the conditions at the time of the initial reactivity insertion are not necessarily the same as the conditions at the onset of, or the average conditions during chugging. These differences are important to consider in order to reference the proper step data set and must be taken into account with respect to sensitivities in system parameters, *e.g.*, degree of subcooling.

Additionally, the change in conditions from the start of the initial reactivity insertion to developed chugging must also be factored into the calculation of the reactivity balance of the system (Sec. 5.1.2) in order to determine the amount of reactivity inserted during chugging. Most MTR-type systems will have a negative temperature defect and therefore the reactivity available to be inserted by chugging refill will be less than the initially inserted reactivity. As a result, the initially inserted reactivity can be used as an enveloping value but this is an overly conservative approach for determining the reactivity limit for chugging.

Other environment conditions that may affect chugging behaviour compared to step transient behaviour include the state of the refilling water. After multiple voiding and refilling cycles the refilling water may be of higher temperature and have a "frothy" consistency (*i.e.*, contains some suspended steam voids). This was observed in the Spert I A-core tests (Ref. 5-5). Ignoring each of these factors represents a conservative approach due to subcooling and partial refill reduced reactivity, respectively.

The other major difference between step transient and chugging response is that the chugging behaviour is, by definition, cyclic whereas the step transient is considered as an isolated single pulse response. As a result the "recovery" time of the system is markedly different and is of concern with regards to temperature stability during chugging. This question is addressed in the following section.

5.3 Temperature Stability

Chugging operation may produce dramatic power oscillations and hydraulic conditions in the core but the underlying safety question remains the same; does the fuel remain cooled below a temperature associated with the onset of fuel damage? This statement is qualified in that mechanical damage as a result of pressures produced during voiding and refilling is not addressed and that mechanical damage, *e.g.*, resulting in flow blockage, can lead to local fuel melting.

As long as fuel temperatures remain below the damage threshold (and mechanical damage is avoided) an MTR-type system can safely operate in a chugging mode indefinitely.

A temperature crisis may occur as a result of a single pulse from initial conditions as in the case of a step insertion power pulse. This scenario is shown in Figure 5-24 and is of concern for gradual reactivity insertion situations where the most severe power/temperature increase is during chugging.

Assuming that a single power oscillation is not enough to drive the fuel plate surface temperature from saturation to damage levels, a temperature crisis may also occur as a result of the average fuel temperature increasing with time over many oscillations. The maximum temperature may therefore exceed the damage threshold for a given chugging pulse which in isolation would not normally cause fuel damage temperatures. This scenario is shown in Figure 5-25 and is applicable to any manner of reactivity insertion which results in chugging operation.

In summary, chugging remains a safe operating mode under the following conditions related to fuel plate temperature:

$$T_{f,base} + \Delta T_f \Big|_{\max} \quad < \quad T_{f,damage} \quad ,$$

$$\frac{dT_{f,base}}{dt} \quad \leq \quad 0$$

where $T_{f,base}$ is the baseline temperature of the fuel during chugging, $\Delta T_f|_{max}$ is the maximum fuel temperature increase for a single chugging oscillation, and $T_{f,damage}$ is the onset of damage temperature threshold.

From the reported data the fuel plate temperature during chugging does not show a tendency to either increase or decrease on average over many oscillations once chugging has been developed. In other words, the temperature of the fuel plate returns to a baseline value by the end of each oscillation. Examples are shown in Figures 5-21, 5-22 (second trace from the top), and 5-23. Admittedly the duration of these tests is relatively short.

More evidence for the stability of the temperature during chugging can be inferred from the lack of temperature information reported in conjunction with the power data

for chugging tests in both the Spert I A-core and Spert I B-12/64. The Spert I A-core tests in question are reported in Reference 5-5. Oscillation envelopes, of greater than 50 MW and greater than 150 MW, were maintained for 50 to 70 seconds in these tests. An example is shown in Figure 5-13.

A temperature crisis would surely have been reported if it had occurred and no fuel melting was reported. Similarly, the Spert I B-12/64 chugging test maintained oscillations of up to 85 MW for about 30 seconds (Ref. 5-16). Again, no temperature crisis or fuel melting is reported.

Thus, this experimental data set is evidence in support of stable temperature behaviour during chugging. Additionally, examination of step insertion transient data set suggests temperature stability during chugging in that the duration of the initial temperature pulse is on the order of 200 to 400 milliseconds showing that the fuel plate temperature returns to a stable baseline value on a time frame consistent with the cycle length of chugging oscillations. Examples of this temperature behaviour are shown for relatively short period transients in Figures 5-22 (top three traces), 5-26, 5-27, and 5-28. All of the Borax I and Spert HEU UAl plate-type cores share these characteristics.

This stable or quasi-stable temperature behaviour has been observed for chugging operation with oscillation frequencies ranging between about one and four cycles per second, *i.e.*, cycle lengths between 250 msec and one second. Because the experimental data set is sparse, no trend in temperature stability is recognizable with respect to cycle length. In fact there may not be any dependence on the chugging frequency. The factor of primary importance with respect to temperature stability may be the availability and size of the heat sink, *i.e.*, the speed of the channel refill may not be of prime importance but rather the extent of refill and ability to re-wet the fuel plate surface.

The fuel plate temperature will remain high when the plates remain steam blanketed upon coolant channel refill. This is a function of peak power, total energy deposition of the power pulse, and the associated heat flux from the plate to the coolant. Examples of this behaviour are seen in Figures 5-29, and 5-30 (Ref. 5-17). The two cases shown in these figures are for transients with periods of 6.9 and 4.6 msec respectively, the latter resulting in fuel melting. This maintained elevated fuel plate temperature behaviour is also seen in Figure 5-22 (bottom trace) for the Borax I reactor. Under these conditions chugging is expected to result in fuel melting.

This steam blanketing effect was also noticed during the stability test series on the Spert IV D-12/25 core. The situation arose prior to the onset of chugging in the outer fuel plates adjacent to narrow coolant channels during tests with forced flow. The flow distribution accentuated the power/heat-removal mismatch and resulted in sustained elevated fuel plate temperatures (Fig. 5-31). The test was terminated as the fuel plate surface temperature exceeded 300EC which was an arbitrarily defined safety limit.

This "narrow channel effect" may lead to localized fuel melting but not to a core destructive situation as the remainder of the core is still cool and therefore not in a weakened state (see Chapter 2). This effect is also an artifact of the specific fuel design and is unlikely to occur in a fuel design with equal coolant channel thicknesses across the assembly and a reasonably flat flow distribution between fuel channels.

For less severe temperature drift increases during chugging fuel temperature reactivity may be able to self-limit the situation returning it to a quasi-stable state. This is likely more applicable for LEU fuel due to the much larger Doppler feedback effect.

5.4 Closing Remarks

Many unresolved issues remain which limit the quantitative value of a stylized analysis approach to chugging. These include:

- the amount of water converted to steam in a given coolant channel,
- the amount of negative reactivity over-compensation created by the large amplitude voiding, and
- the voiding, temperature, and void coefficient distribution over the core during chugging.

In this way, an energy balance calculation and the reactivity as a function of time are not readily available.

However, information which can be quantified from a stylized analysis includes the maximum available excess reactivity to be inserted to the system during core refill. This, along with the evidence that both chugging and step reactivity insertion power

excursions are both similar in initiating reactivity insertion type and are both self-limited by the same processes allows for use of step reactivity insertion transient data to provide the link between the reactivity returned to the system in chugging and the maximum power and fuel plate temperatures experienced during the chugging oscillations. The use of the step insertion data thus allows the determination of reactivity limits with respect to the onset of fuel damage, similar to the methodology used for analysis of step reactivity insertion situations.

The chugging reactivity limits are associated with two scenarios:

- the maximum temperature generated as a result of the first chugging power pulse exceeds the damage threshold, or
- the temperature does not return to the baseline value by the end of the chugging oscillation and so the average fuel plate temperature increases over many oscillation cycles until it exceeds the damage threshold.

Mechanical damage as a result of pressures generated in chugging was not considered in this analysis. Deformation of fuel plates was reported during the Spert I A-17/28 stability tests but fuel melting was not observed (Ref. 5-5).

5.5 References

5-1. J. G. Crocker, Z. R. Martinson, R. M. Potenza, L. A. Stephan, "Reactor Stability Tests in the Spert IV Facility", US AEC Technical Report IDO-17088, Phillips Petroleum Co., July 1965.

5-2. P. A. Lottes, R. P. Anderson, B. M. Hoglund, J. F. Marchaterre, M. Petrick, G. F. Popper, and R. J. Weatherhead, "Boiling Water Reactor Technology Status of the Art Report. Volume I. Heat Transfer and Hydraulics", US AEC Technical Report ANL-6561, Argonne National Laboratory, February 1962.

5-3. S. M. Zivi, A. L. Morse, R. W. Wright, "Constant Power Steam Distribution for Boiling in a Simulated Spert IA Water Channel", Transactions of the American Nuclear Society, v.3, n., 1960, pp.112-114.

5-4. McMaster Nuclear Reactor Safety Analysis Report, McMaster University, Hamilton, Ontario, Canada, February 2002.

5-5. F. Schroeder, "Stability Tests with the Spert-I Reactor", US AEC Technical Report IDO-16383, Phillips Petroleum Co., July 1, 1957.

5-6. J. R. Dietrich, "Experimental Determinations of the Self-Regulation and Safety of Operating Water-Moderated Reactors", in the Proceedings from the First International Conference on the Peaceful Uses of Atomic Energy, Geneva, 1955, Argonne National Laboratory, v. 13, pp. 88-101.

5-7. W. A. Horning, H. C. Corben, "Theory of Power Transients in the Spert I Reactor", US AEC Technical Report IDO-16446, Ramo-Wooldridge Corporation for Phillips Petroleum Co., August 20, 1957.

5-8. R. W. Wright, "Large Amplitude Steam Oscillations under Forced Flow", Transactions of the American Nuclear Society, v.5, n.1, p.170, June 1962.

5-9. A. H. Spano, editor, "Quarterly Technical Report - Spert Project - October, November, December, 1963", US AEC Technical Report IDO-16992, Phillips Petroleum Co., June 1964.

5-10. B. E. Clancy, J. W. Connolly, B. V. Harrington, "An Analysis of Power Transients Observed in Spert I Reactors. Part 1. Transients in Aluminum Plate-Type Reactors Initiated at Ambient Temperature", Australian Atomic

Energy Commission Technical Report AAEC/E345, Lucas Heights, March 1975.

5-11. J. R. Dietrich, D. C. Layman, "Transient and Steady State Characteristics of a Boiling Reactor. The Borax Experiments, 1953", ANL-5211 (also listed as AECD-3840), Argonne National Laboratory, USA, February 1954.

5-12. G. O. Bright, editor, "Quarterly Progress Report - October, November, December, 1957 - Reactor Projects Branch", US AEC Technical Report IDO-16437, Phillips Petroleum Co., March 21, 1958.

5-13. W. E. Nyer, S. G. Forbes, F. L. Bentzen, G. O. Bright, F. Schroeder, T. R. Wilson, "Experimental Investigations of Reactor Transients", US AEC Technical Report IDO-16285, Phillips Petroleum Co., April 20, 1956.

5-14. H. L. McMurray, A. V. Grimaud, "Temperature Distribution in a Fuel Plate with Exponentially Rising Power, Part II - Results Based on Asymptotic Solutions", US AEC Technical Report IDO-16311, Phillips Petroleum Co., January 5, 1955.

5-15. A. P. Wing, "Transient Tests on the Fully Enriched, Aluminum Plate-Type, B Cores in the Spert I Reactor: Data Summary Report", US AEC Technical Report IDO-16964, Phillips Petroleum Co., June 1964.

5-16. G. O. Bright, editor, "Quarterly Progress Report - April, May, June, 1958 - Reactor Projects Branch", US AEC Technical Report IDO-16489, Phillips Petroleum Co., January 19, 1959.

5-17. M. R. Zeissler, "Non-Destructive and Destructive Transient Tests of the Spert I-D, Fully Enriched, Aluminum-Plate-Type Core: Data Summary Report", US AEC Technical Report IDO-16886, Phillips Petroleum Co., November 1963.

5.6 Tables

Table 5-1: Summary of Chugging Data from the Full-Scale Reactor Experiments

System	flow	water head (feet)	pool temp (Celsius)	reactivity (mk) unless noted initial	reactivity (mk) unless noted refill	power (MW) max	power (MW) avg	min. period (msec)	frequency (cps)	duration of test	Notes
Borax-I	nat.	3 to 4.5	sat.	26	~ 12	57	2	17	~ 1	5 to 20 sec	boiling test, long duration of reactivity addition, Fig. 56 ANL-5211, more extreme step insertion tests with duration of 20 sec had Pmax > 60 MW
	nat.	3 to 4.5	sat.	--	--	11	--	--	~ 1	~ 20 sec	from step tests for period < 30 msec chugging peaks smaller than Pmax on initial pulse (34 Mw), ANL-5211 Fig. 31 (best), and also Fig. 10 Geneva 1955 paper
Spert I A	nat.	2	amb.	27.5	--	<= 200	--	--	2	sustained oscillations	negative reactivity added ramp style @ ~ 0.9 mk/sec, water permanently lost from system during tests
	nat.	2	sat.	15	--	<= 50	--	--	1	~ 75 sec	Fig. 2 IDO-16383 (test no. 4304)
	nat.	9	~ 26	27.5	--	<= 2300	--	3	2		this test not allowed to fully develop into envelope, Figs. 4 & 5 IDO-16383 (test no. 4759)
	nat.	9	sat.	15	--	<= 150	--	--	1	~ 50 sec	Fig. 3 IDO-16383 (test no. 4300)
	nat.	2	sub.	25		38	6				reported in IDO-16489, p.20
Spert I B-12/64	nat.	2	sub.	15	--	85	19	--	1.79	> 40 sec	ramp insertions of 0.7 mk/sec from low power, oscillations lasted for 30 seconds before test ended, see IDO-16489, p.20
	nat.	2	sat.			1.1	boil			10 sec	post peak chugging in step tests from 5W power, see IDO-16964, App. C, Fig. 23, both temperature data and power plotted
	nat.	2	sat.			1	small			20 sec	noise to oscillation transition, IDO-16964, Fig. 24
	nat.	2	sat.			1.5	1.7		1	10 sec	small oscillations, IDO-16964, Fig. 25
	nat.	2	sat.			4	8		1	10 sec	developing oscillations at time of scram, IDO-16964, Fig. 26
	nat.	2	sat.			10	20		1	15 sec	chugging, IDO-16964, Fig. 27
Spert IV D	nat.	18	amb.	$4.2	~ $2.1	onset	~ 7.5	--	~ 3	min to hours	threshold tests, reactivity insertion very slow as series of steps with
											of mean power, plate temp not permitted to exceed 300C, system bulk temperature increased during tests to ~ 35C, Ref. IDO-16992, p.28
	nat.	2	amb.	$4.1	~ $2.1	onset	3 to 5	--	~ 2	min to hours	Ref. IDO-16992, bulk temperature had risen to ~ 70C during test
	upward	18	amb.	$4.1	--	small		--		min to hours	test scrammed as plate temperature > 300C for narrow channels, Ref. IDO-16992
	nat.	18	amb.	$5.0	--	small		--		short	chugging tests, reactivity inserted via ramp insertion ~ 0.9 mk/sec, faster than threshold tests, Ref. IDO-17055
	nat.	2	amb.	$5.0	--	small		--		short	ref. IDO-17055
	nat.	2	~ 70	$4.0	--	onset		48 to 24	~ 2	12.5 min	Test SS89, system allowed to heat up gradually from initially 22C, onset of chugging observed once bulk temp reached ~ 70C, Figs. 27 & 28 IDO-17055

2:25 PM, 2/20/04 PhD_SE-Day_reactor-expt-summary.xls Stability Tests Summary

Table 5-2: Nuclear Characteristics and Dimensions of the Test Cores

HEU Al-Clad Plate Cores	Borax I	Spert I A-17/28	Spert I B-24/32	Spert I B-16/40	Spert I B-12/64	Spert I D-12/25	Spert IV D-12/25	MNR RC-16/28-9/6
Temperature Defect								
20C to 95C (mk)	-8.17	-10.9	-12.4	-11.6	-10.2	N/A	N/A	N/A
Void Coefficient								
Metal/Water Ratio - central	0.687	0.782	1.128	0.635	0.465	0.704	0.703	-
Metal/Water Ratio - std assembly	0.687	0.782	1.128	0.635	0.465	0.525	0.522	0.576
Metal/Water Ratio - core	0.687	0.782	1.128	0.635	0.465	0.629	0.627	-
Average (Uniform)								
(mk/%-void)	-2.4	-1.9	-2.8	-1.8	-1.1	-2.4	-2.3	-2.1
(mk/cc-void)	-3.4E-03	-3.5E-03	-5.1E-03	-2.0E-03	-6.9E-04	-4.6E-03	-4.5E-03	-3.3E-03
(mk/channel)	-0.41	-0.39	-0.36	-0.28	-0.14	-0.87	-0.85	-0.39
Central								
(mk/%-void)	-4.5	-3.9	-6.5	-2.9	0.9	-3.4	-3.1	-4.5
(mk/cc-void)	-6.6E-03	-7.2E-03	-1.2E-02	-3.3E-03	6.0E-04	-6.3E-03	-6.0E-03	-7.1E-03
(mk/channel)	-0.78	-0.80	-0.83	-0.45	0.12	-1.20	-1.14	-0.84
Prompt Neutron Lifetime								
(micro-sec)	65	50	50	70	77	60	57	N/A
Power Peaking Factor								
Overall	2.0	2.0	2.5	2.1	2.2	2.4	2.4	4.2
Dimensions								
Fuel meat thickness (cm)	0.053	0.051	0.051	0.051	0.051	0.051	0.051	0.051
Clad thickness (cm)	0.050	0.051	0.051	0.051	0.051	0.051	0.051	0.038
Fuel surface area (cm2)	4.31E+05	3.55E+05	6.47E+05	5.39E+05	6.47E+05	2.26E+05	2.26E+05	4.00E+05
Fuel meat volume (cc)	1.10E+04	7.57E+03	1.51E+04	1.26E+04	1.51E+04	5.20E+03	5.20E+03	9.57E+03
SA/Vol Ratio	39	47	43	43	43	43	43	42
Volume Coolant/Channel (cc)	119	111	69	136	203	190	190	119

note: fuel surface area and coolant volume are based on active height of the fuel

Table 5-3: Comparison of Step Insertion Test and Chugging Test Data

Core	Test Type	Pmax (MW)	ΔTmax (EC)	Conditions	Reference
Borax I	Chugging	55	36 (1-c)	system bulk temperature at saturation	ANL-5211, Fig.56
	Step	50	50 (11-c)	system bulk temperature at saturation	ANL-5211, Fig.31
Spert I B-12/64	Chugging	15.9	19.3	system bulk temperature at saturation, natural circulation, two foot hydrostatic head, chugging follows initial step response	IDO-16964, Fig. C27
		14.5	18.3		
		16.5	16.1		
		18.1	16.9		
		18.4	25.2		
		22.4	26.0		
		24.8	31.8		
	Step	5.5	18	system bulk temperature at saturation, initially low power (5 W), natural circulation, two foot hydrostatic head	IDO-16964, Figs. C25, C26, C27
		11.3	37		
		78.0	95		

5.7 Figures

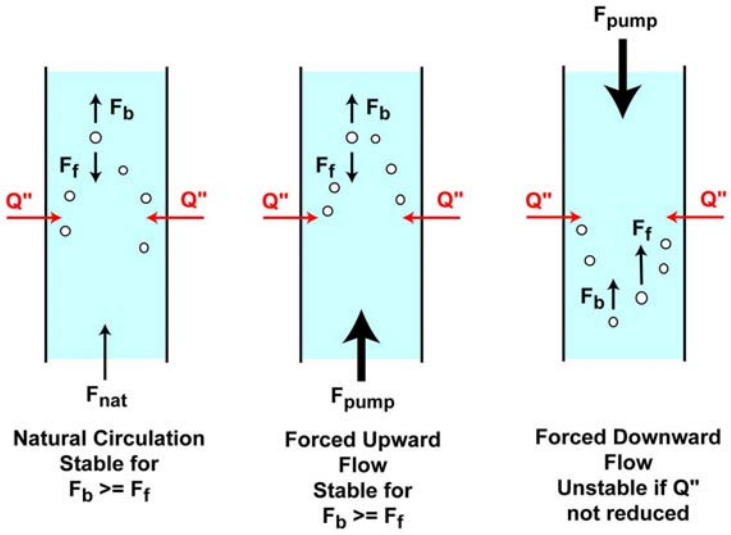

Figure 5-1: Force and Heat Diagram for Possible Flow Modes in an MTR-Type Fuel Channel

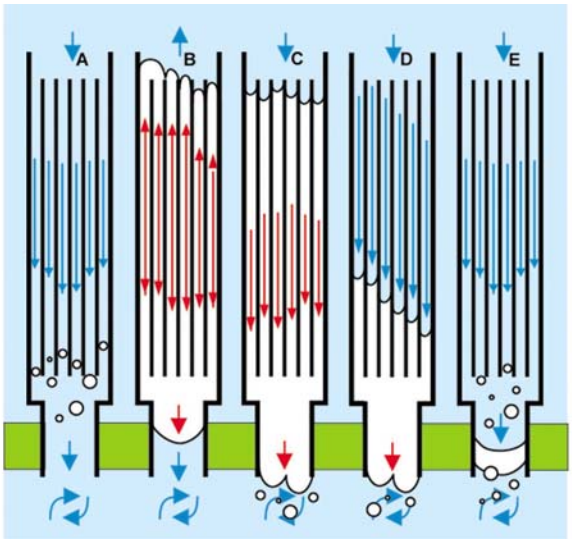

Figure 5-2: Hydraulic Stages of Boiling and Chugging Behaviour in a System with Downward Flow

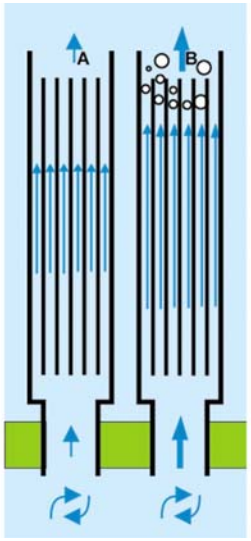

Figure 5-3: Hydraulic Stages of Steady Boiling in a System with Upward Flow

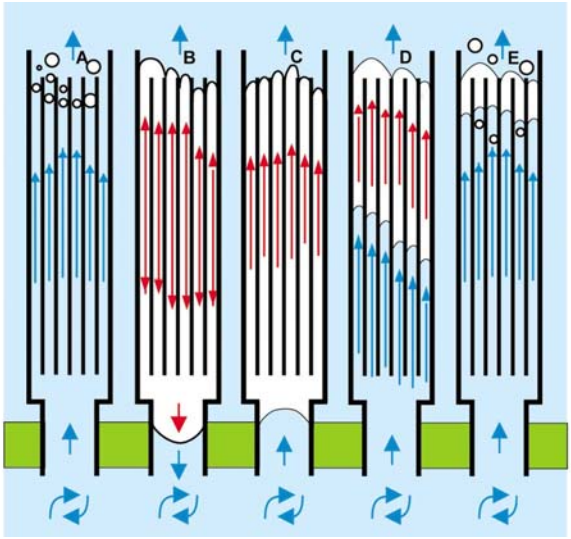

Figure 5-4: Hydraulic Stages of Boiling and Chugging Behaviour in a System with Upward Flow

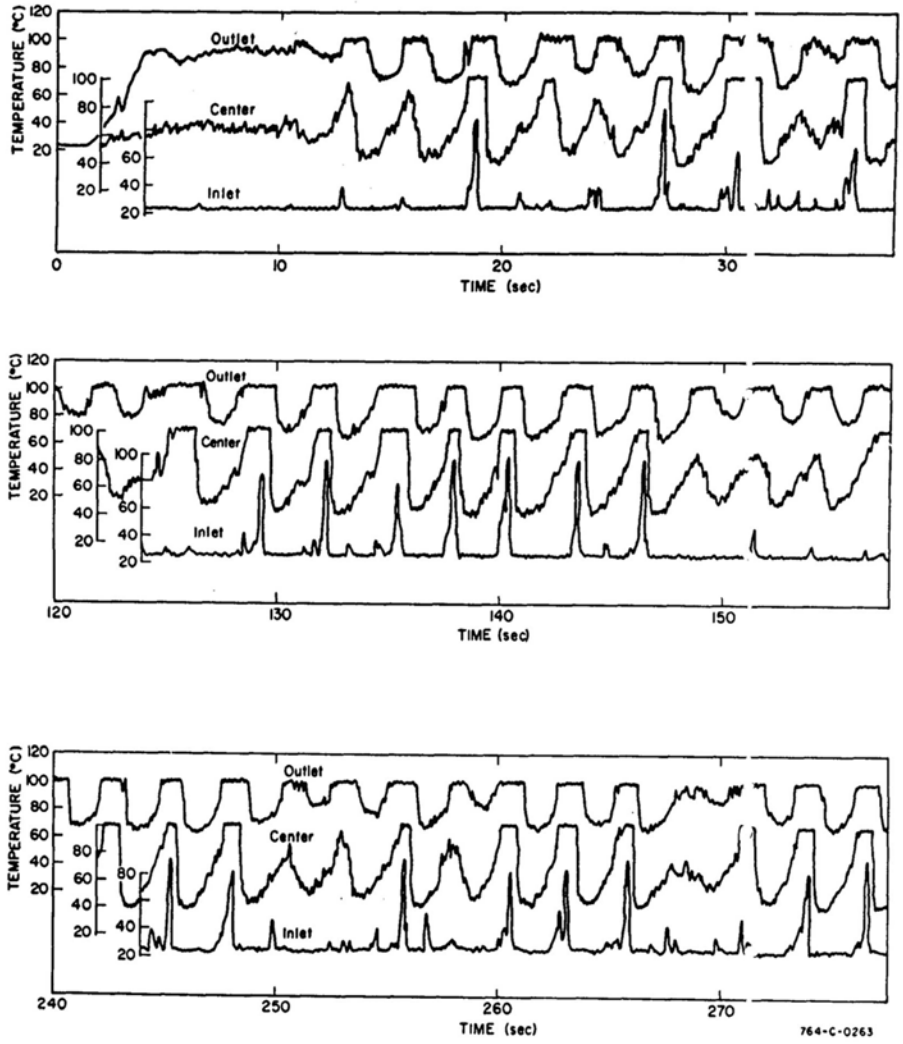

Fig. 31 Inlet, center, and outlet water channel temperature behavior for selected times during first half of test No. SS 89.

Figure 5-5: Inlet, Centre, and Outlet Water Channel Temperature Behaviour for Selected Times During Spert IV D-12/25 Chugging Test (Ref. 5-1)

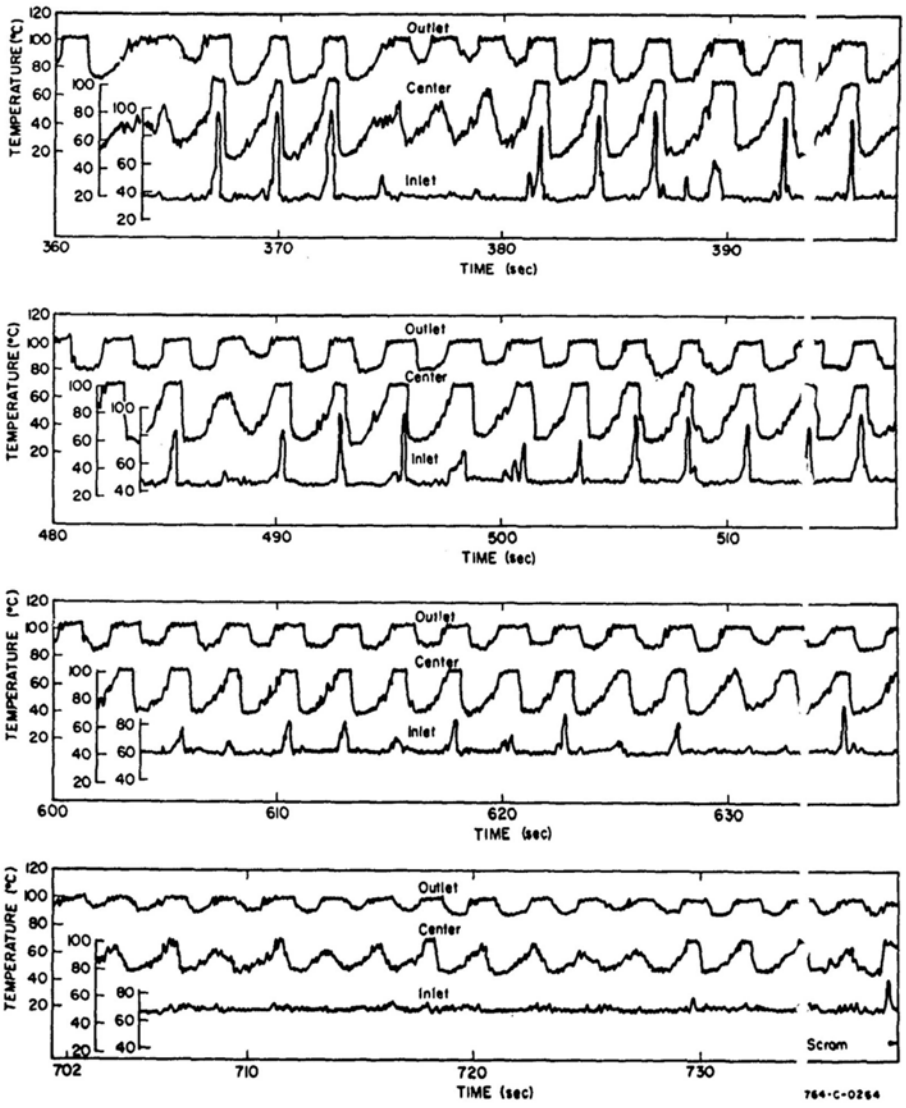

Fig. 32 Inlet, center, and outlet water channel temperature behavior for selected tir ss during last half of test No. SS 89.

Figure 5-6: Inlet, Centre, and Outlet Water Channel Temperature Behaviour for Selected Times During Spert IV D-12/25 Chugging Test (Ref. 5-1)

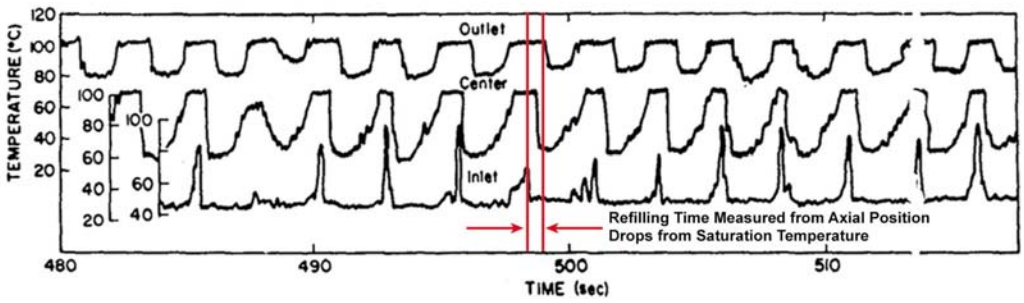

Figure 5-7: Example of Refill Time Measurement Based on Coolant Temperature Oscillations During a Spert IV Chugging Test (modified from Ref. 5-1)

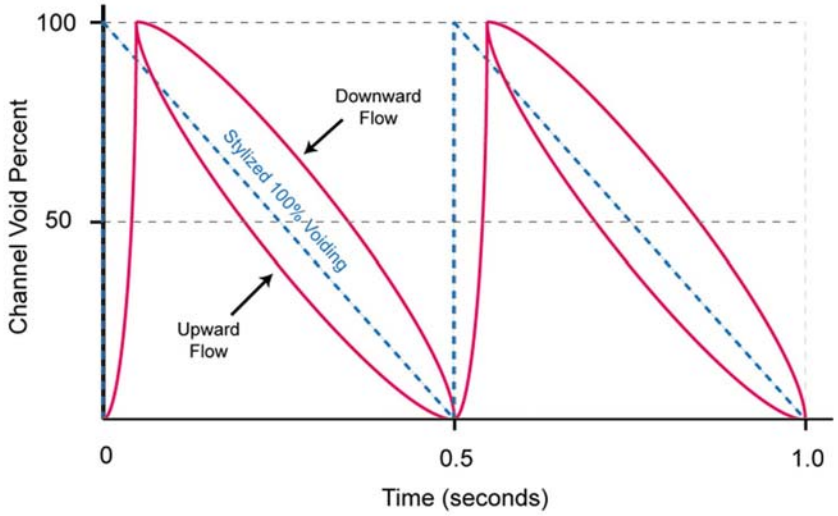

Figure 5-8: Stylized Voiding Oscillations During Chugging

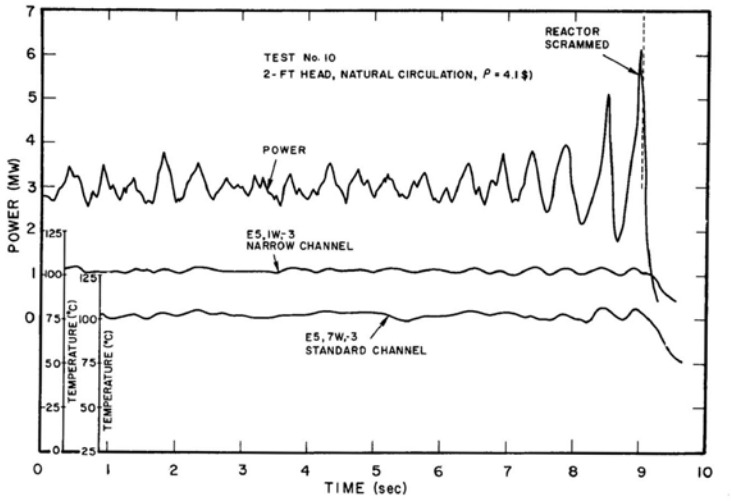

Figure 5-9: Reactor Power and Cladding Surface Temperature Behaviour in a Narrow and a Standard Coolant Channel During an 2-Foot Head, Natural-Circulation Stability Test in Spert IV D-12/25 (Ref. 5-9)

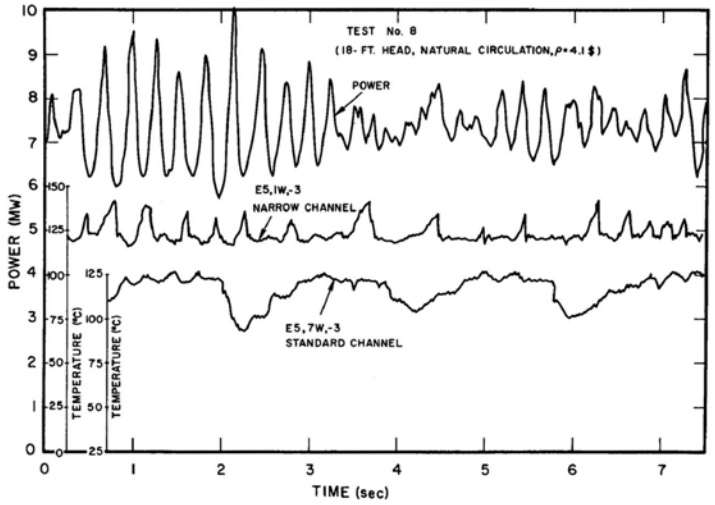

Figure 5-10: Reactor Power and Cladding Surface Temperature Behaviour in a Narrow and a Standard Coolant Channel During an 18-Foot Head, Natural-Circulation Stability Test in Spert IV D-12/25 (Ref. 5-9)

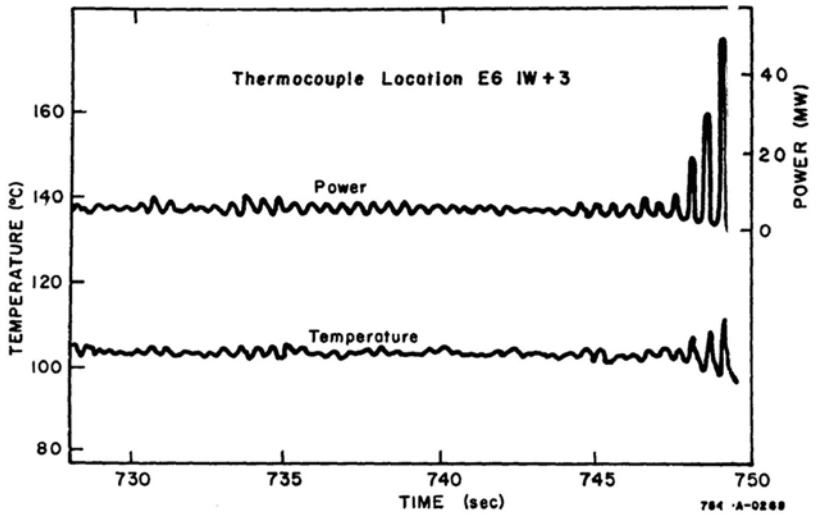

Figure 5-11: Reactor Power and Cladding Surface Temperature Behaviour at the Time of Onset of Chugging from Spert IV D-12/25 Chugging Test (Ref. 5-1)

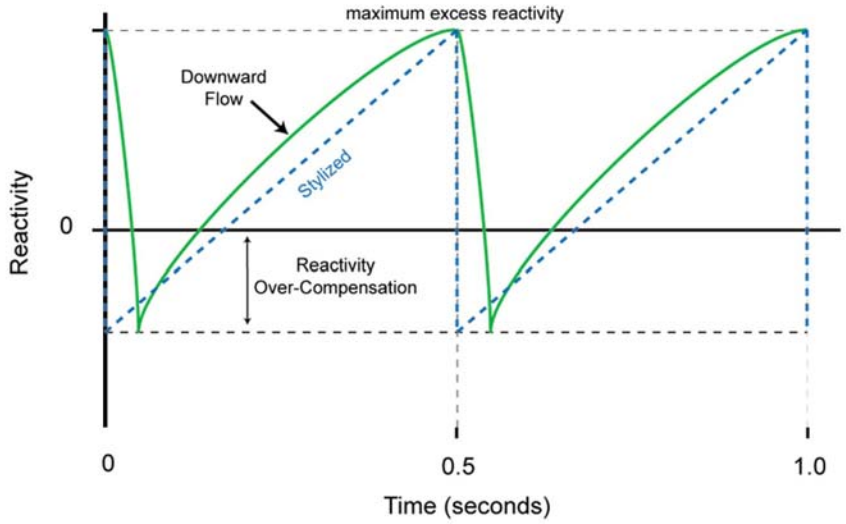

Figure 5-12: Stylized Reactivity Oscillations During Chugging

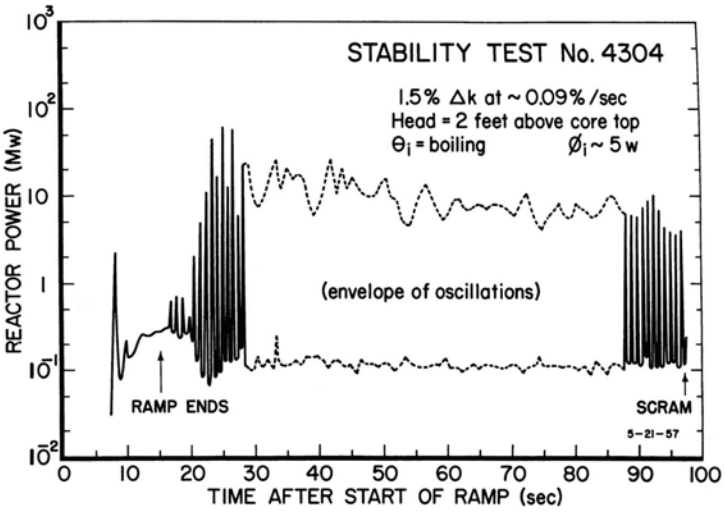

Figure 5-13: Power Trace for Spert I A-17/28 Stability Test, 2-Foot Hydrostatic Head, Saturation Conditions (Ref. 5-5)

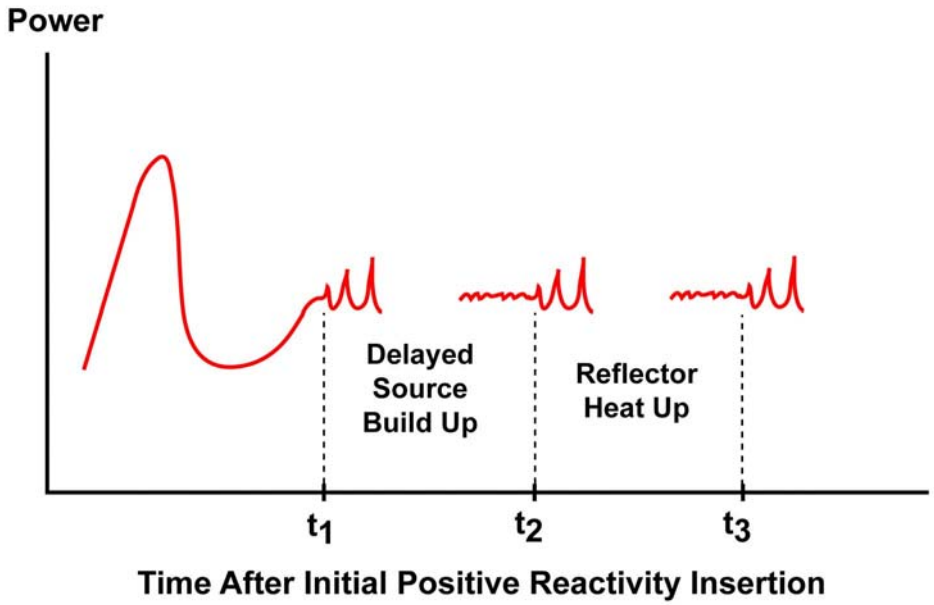

Figure 5-14: Stylized Runout of a Self-Limiting Power Transient Showing Time Frames Relevant to Chugging Reactivity Insertion

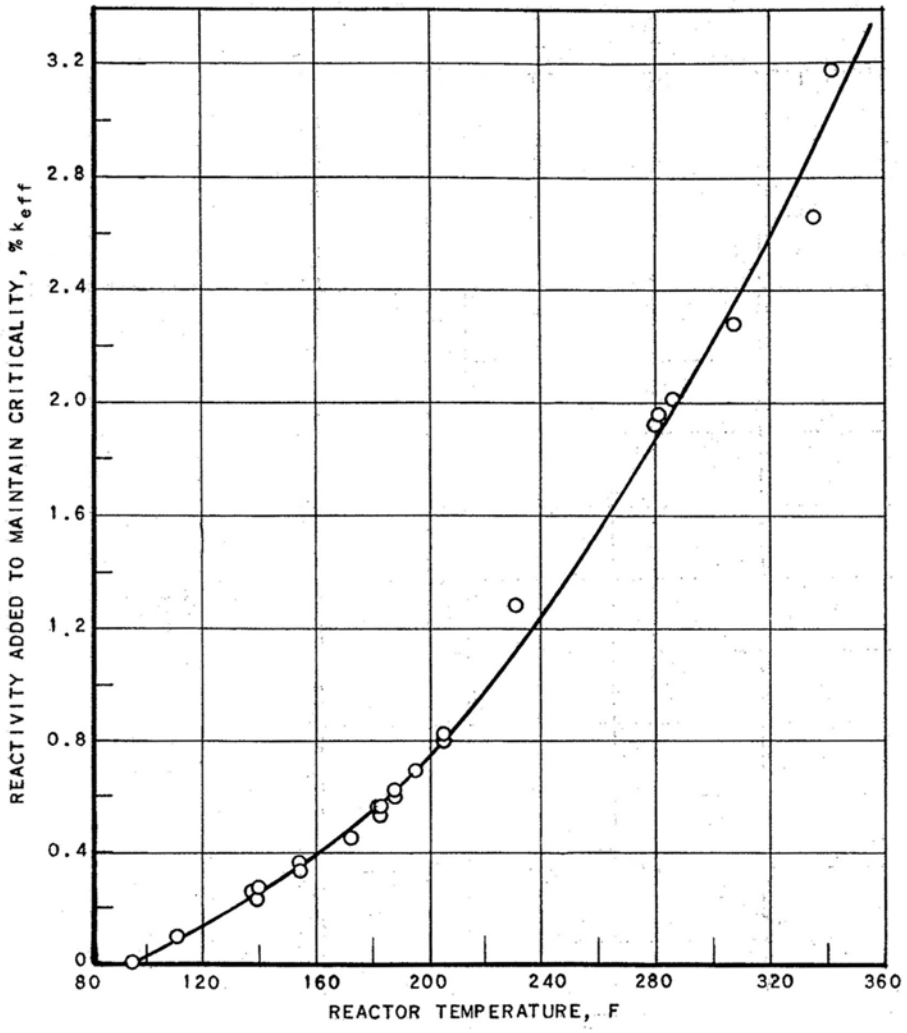

Figure 5-15: Reactivity Loss due to Uniform System Temperature Rise in Borax I (Ref. 5-11)

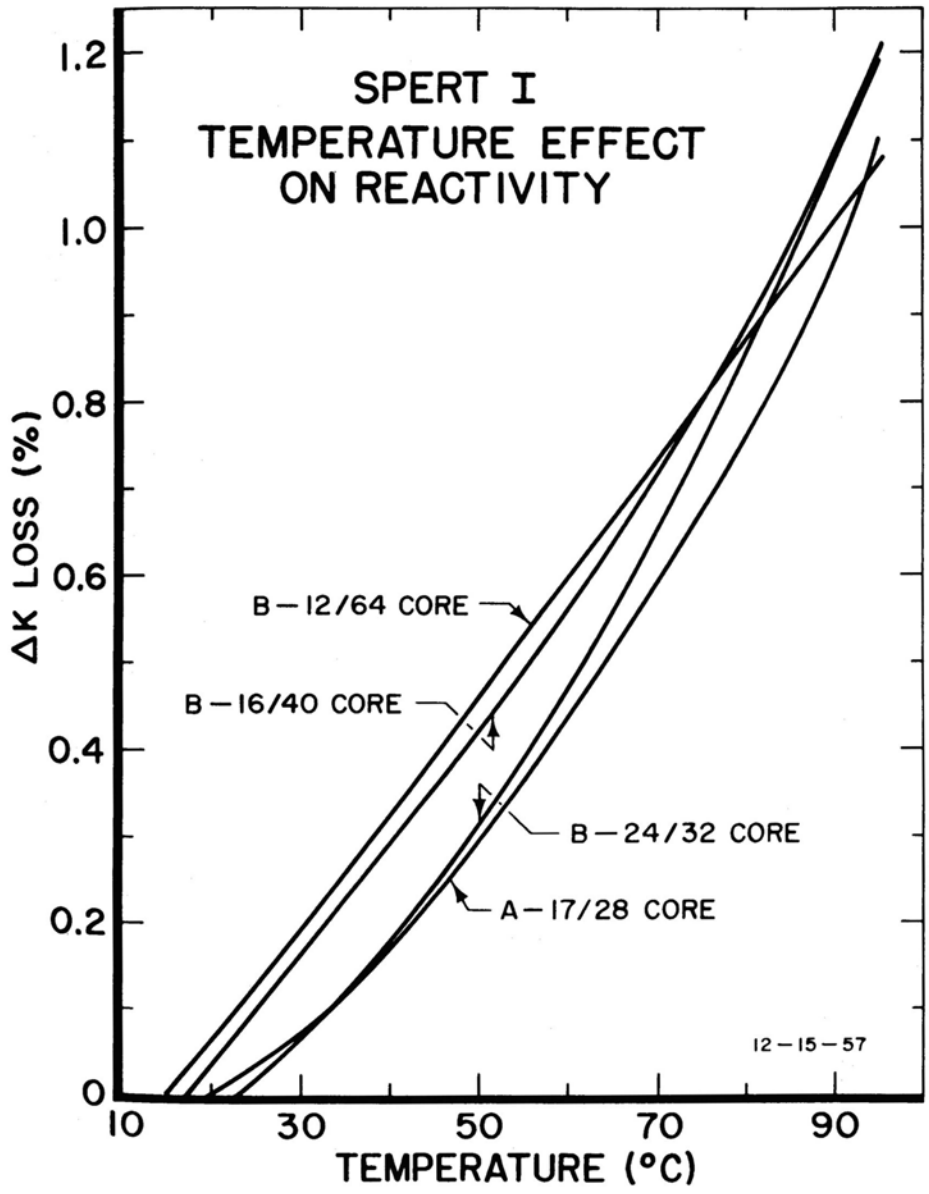

Figure 5-16: Reactivity Loss due to Uniform System Temperature Rise in Spert I A & B Cores (Ref. 5-12)

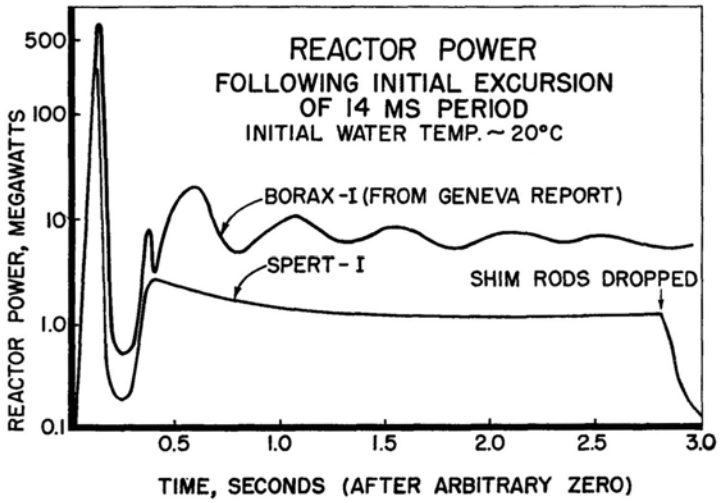

Figure 5-17: Comparison of Stability of Borax I and Spert I A Following a Step Insertion of Reactivity (Ref. 5-13).

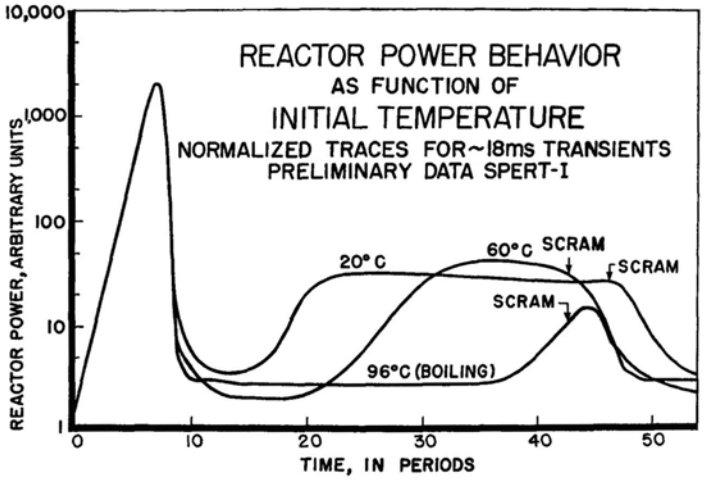

Figure 5-18: Comparison of Stability of Spert I A for Different Degrees of Subcooling (Ref. 5-13).

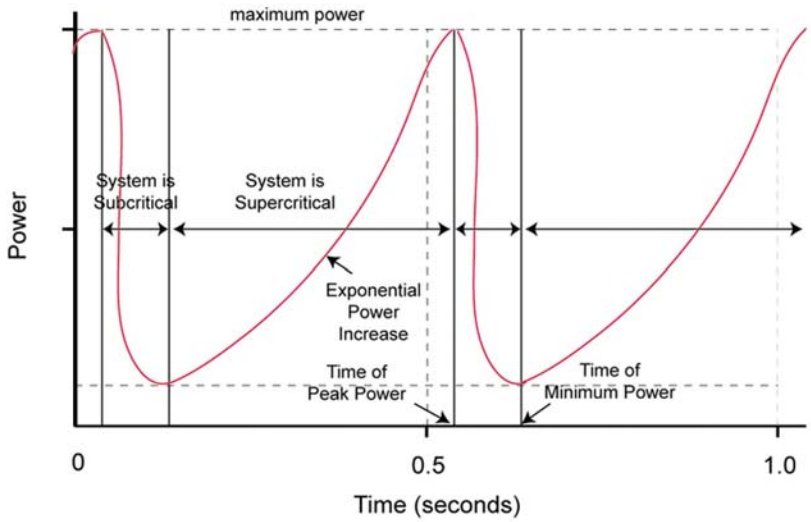

Figure 5-19: Stylized Power Oscillations During Chugging Operation

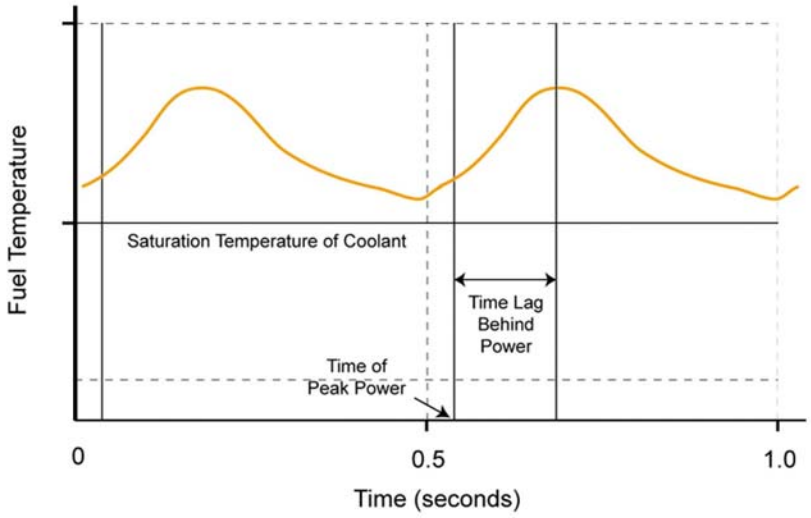

Figure 5-20: Stylized Temperature Oscillations During Chugging Operation

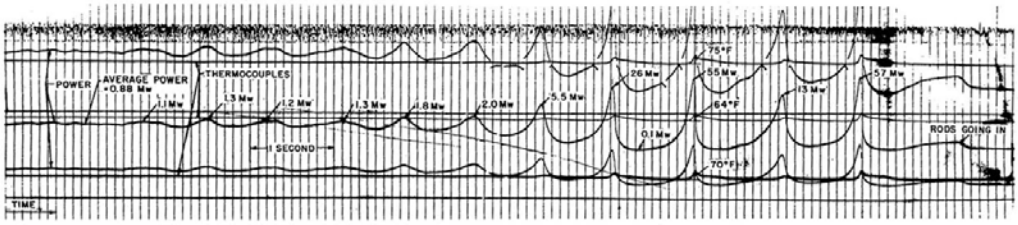

FAST GALVANOMETER RECORDS SHOWING TRANSITION FROM OSCILLATORY BOILING TO "CHUGGING" AT ATMOSPHERIC PRESSURE. 2.6% k_{eff} COMPENSATED BY STEAM (END OF RUN 2, 9/18/53)

THE THREE POWER RECORDS ARE FROM ION CHAMBERS OF DIFFERENT SENSITIVITIES, ON LOGARITHMIC SCALE. THE UPPERMOST TRACE IS UNRELIABLE BECAUSE OF A STICKING GALVANOMETER. THE TOP TEMPERATURE TRACE IS FROM THE CENTER OF FUEL PLATE 4. THE MIDDLE TRACE IS FROM THE CENTER OF PLATE 1, AND THE LOWEST TRACE FROM THE SURFACE OF PLATE 1.

Figure 5-21: Saturated Chugging Record from Borax I Boiling Tests (Ref. 5-11)

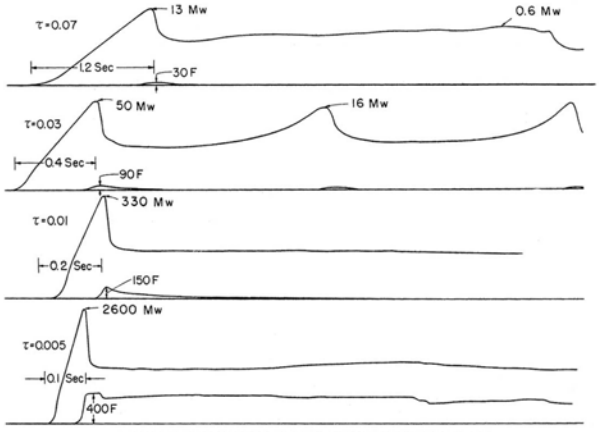

REPRESENTATIVE RECORDS OF EXCURSIONS AT SATURATION TEMPERATURE WITH VARIOUS EXCESS REACTIVITIES

THESE WERE TRACED DIRECTLY FROM THE GALVANOMETER RECORDS.
NOTE THAT THE TIME SCALE CHANGES FROM RUN TO RUN.
THE PERIOD (τ) OF THE EXCURSION IS MARKED ON EACH RUN IN SECONDS. THE TEMPERATURE RECORD IS FROM THE CENTER OF FUEL PLATE 11

Figure 5-22: Borax I Step Insertion Transients from Saturation Temperature (Ref. 5-11)

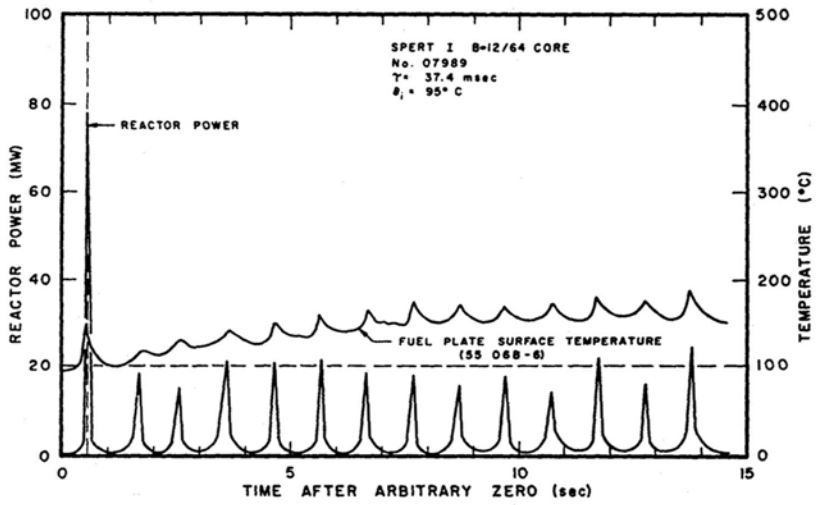

Figure 5-23: Spert I B-12/64 Step Insertion Transient Power and Temperature Trace Showing Chugging Behaviour (Ref. 5-15)

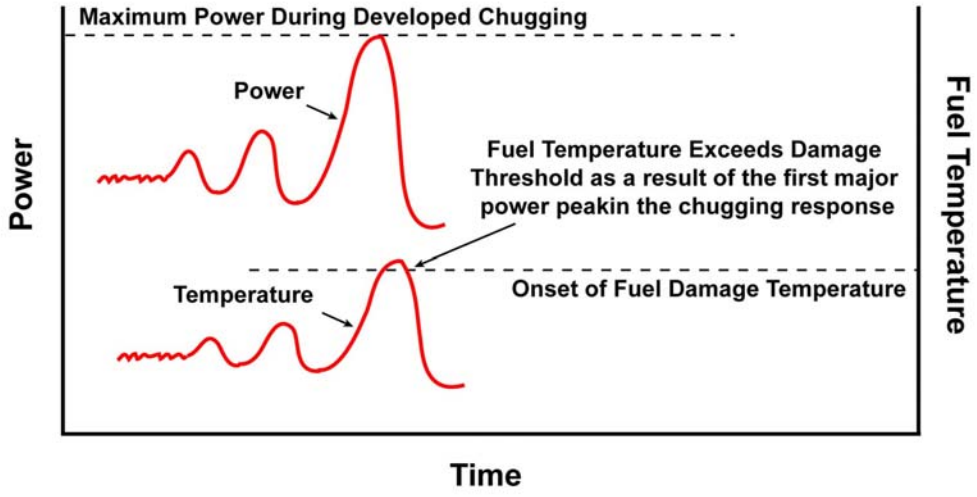

Figure 5-24: Possible Damage Scenario During Chugging Operation as a Result of a Single Power Pulse

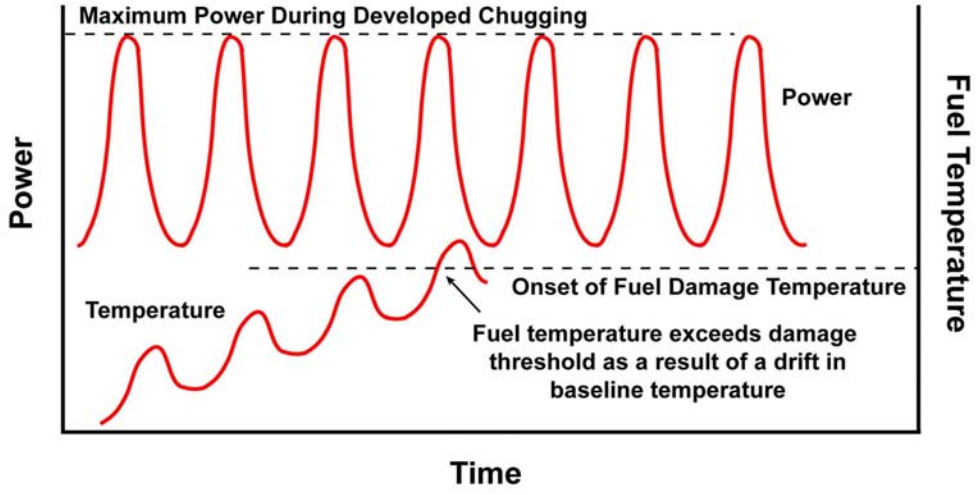

Figure 5-25: Possible Damage Scenario During Chugging Operation as a Result of an Increasing Temperature Drift over Many Power Pulses

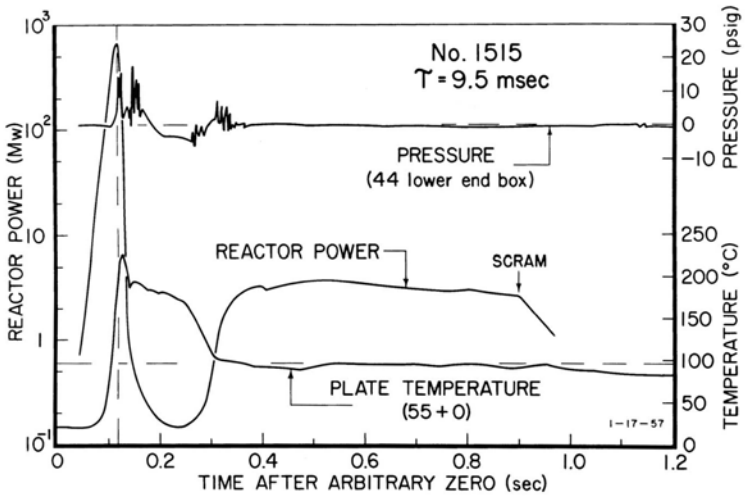

Figure 5-26: Spert I A-17/28 9.5 msec Period Step Reactivity Insertion Transient Trace (Ref. 5-5)

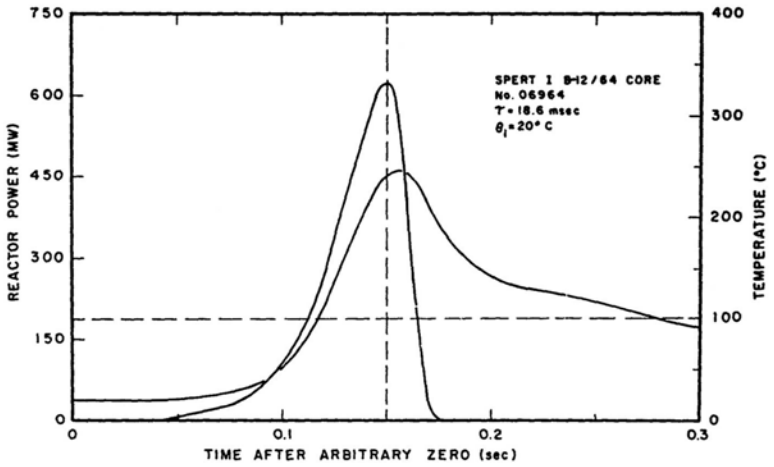

Figure 5-27: Spert I B-12/64 18.6 msec Period Step Reactivity Insertion Transient Trace (Ref. 5-15)

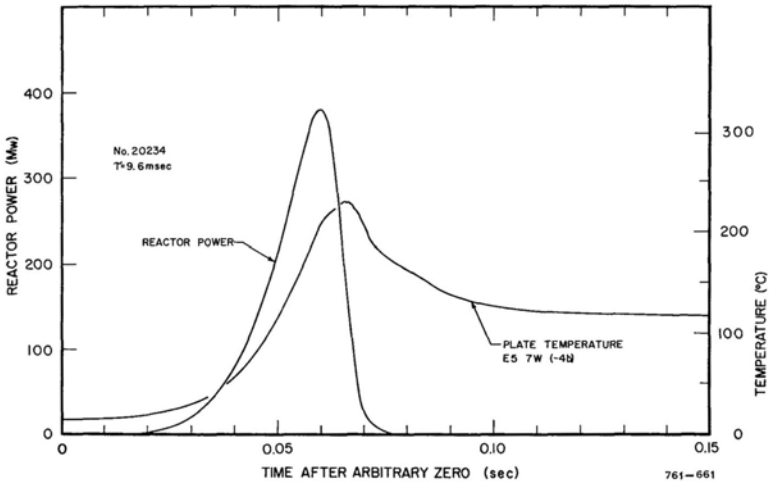

Figure 5-28: Spert I D-12/25 9.6 msec Period Step Reactivity Insertion Transient Trace (Ref. 5-17)

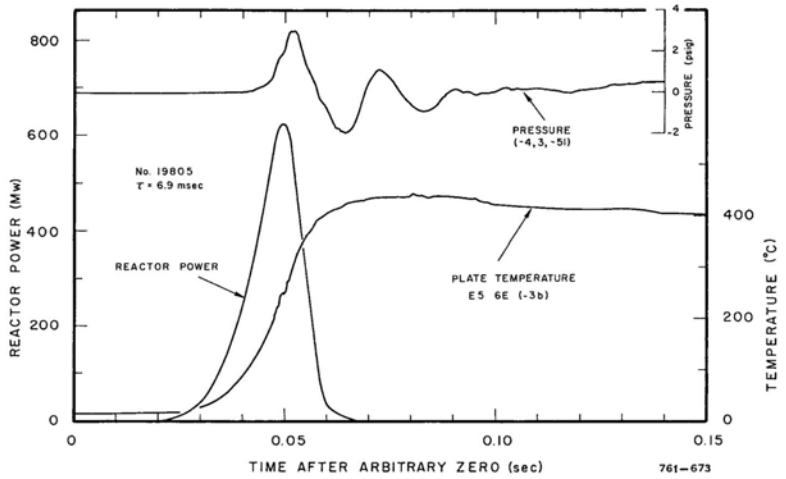

Figure 5-29: Spert I D-12/25 6.9 msec Period Step Reactivity Insertion Transient Trace Showing a Maintained Elevated Fuel Plate Surface Temperature (Ref. 5-17)

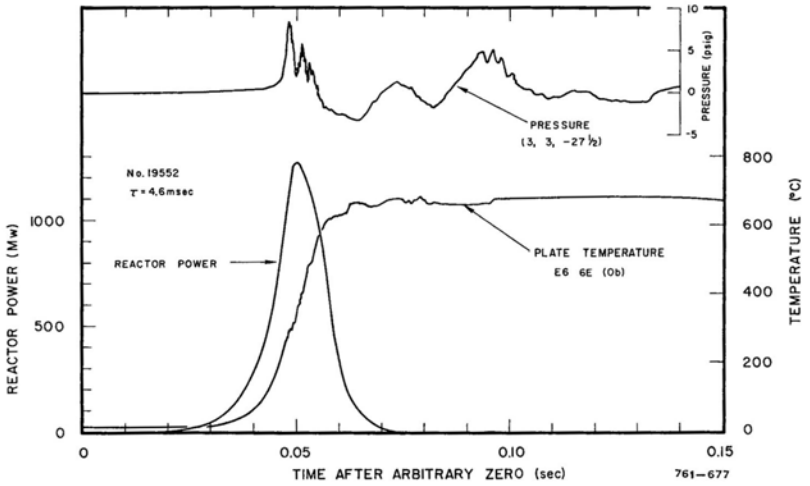

Figure 5-30: Spert I D-12/25 4.6 msec Period Step Reactivity Insertion Transient Trace Showing a Maintained Elevated Fuel Plate Surface Temperature (Ref. 5-17)

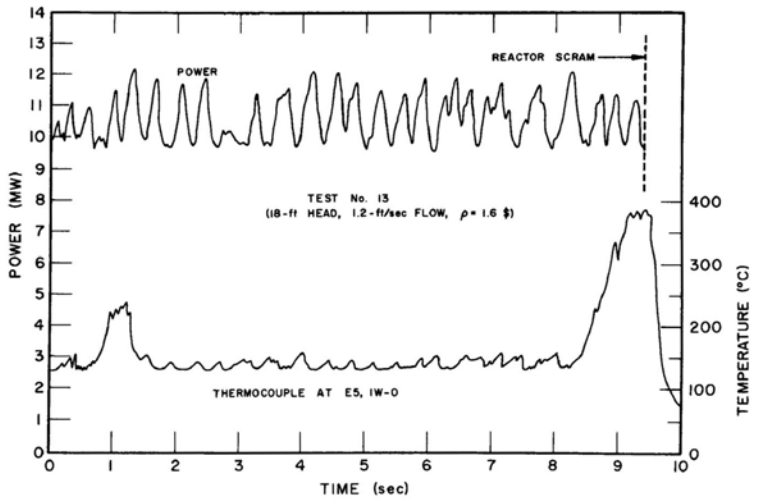

Figure 5-31: Spert IV D-12/25 Stability Test Trace Showing Elevated Fuel Plate Surface Temperatures Adjacent to a Narrow Coolant Channel Prior to Chugging (Ref. 5-9)

(this page is intentionally left blank)

CHAPTER 6 - EXTENSION TO THE LEU FUEL CYCLE

TABLE OF CONTENTS

LIST OF TABLES

LIST OF FIGURES

(this page is intentionally left blank)

6 EXTENSION TO THE LEU FUEL CYCLE

This chapter discusses the differences between the highly-enriched uranium (HEU) and low-enrichment uranium (LEU) fuel cycles in the context of self-limiting transient behaviour. The extension of the safety analysis methodology to LEU fuel cycles is relevant to modern day MTR-type reactors worldwide under the mandate of the Reduced Enrichment for Research and Test Reactors (RERTR) program.

The experimental and simulation-based results relevant to the self-limiting behaviour of the LEU fuel cycle in MTR-type reactors are summarized and discussed herein.

Given the lack of LEU MTR-type test data, simulation-based results from the literature are used to develop an extension to the previously determined HEU reactivity limit methodology for LEU fuel. The limitations of a simulation-based approach for unprotected short-period transients, as discussed in Chapter 1, are recognized and discussed in the context of the results.

Conclusions are drawn from the literature and suggested extensions to the existing information are outlined.

6.1 Specifics of the LEU Fuel Cycle

The relevance of LEU plate-type fuel is clear as operating reactors continue to convert and new facilities are designed to use an LEU fuel cycle under the mandate of the RERTR program. Currently (2005), the McMaster Nuclear Reactor is replacing HEU with LEU assemblies as part of the normal refuelling process. This conversion is expected to be complete in 2006.

The analysis in Chapters 4 and 5 is based on the results from the HEU plate-type core experiments. The HEU fuel cycle associated with MTR-type reactors is 93 wt% U-235 whereas the LEU fuel cycle is typically just under 20 wt%, *e.g.*, 19.75 wt% U-235.

The increased relative uranium loading necessary for the LEU fuel cycle results in differences in the thermal properties of the fuel meat, namely:

- decreased thermal conductivity, and
- slightly decreased heat capacity.

In addition, the switch to an LEU fuel cycle is accompanied by changes to some of the nuclear characteristics of the core; namely:

- larger negative Doppler (fuel temperature) coefficient,
- larger negative coolant void reactivity feedback coefficient,
- shortened prompt neutron lifetime, and
- different delayed neutron characteristics.

For illustrative purposes, these parameters for the IAEA 10 MW reactor benchmark problem are summarized in Table 6-1 for the HEU and LEU fuel. In order to extend this analysis to LEU plate-fuel systems in general, the impact of each of these changes must be considered.

Unlike the void reactivity feedback mechanism governing the self-limiting behaviour of HEU systems, which is dependent on the heat transfer from the fuel to the coolant, the fuel temperature feedback mechanism is prompt in nature. Identified as resulting almost entirely from the broadening of the U-238 absorption cross section resonances with increasing fuel temperature (Ref. 6-1 and App. E), this factor is often referred to simply as the Doppler effect. It is negligible in HEU fuel but is significant for LEU fuel.

The large magnitude and prompt nature of the Doppler effect in LEU fuel results in it being the most important difference between the two fuel cycles. This has been demonstrated by related experiments during the Spert Project (see Section 6.2) and investigated as part of simulation based analysis reported in the literature (see Section 6.3).

The other differences between the two fuel cycles can be considered secondary, including those in the void reactivity feedback coefficient of the core (the variation in the void feedback of the system for HEU fuelled cores was investigated in Chapter 4). For an LEU core the variation in void reactivity feedback is expected to be less important due to the added feedback due to the Doppler effect. The void mechanism still plays a role in the self-limiting behaviour of an LEU core and was examined in the simulation analysis reported in the literature. This is discussed in Section 6.3.

With respect to the thermal properties of the fuel, differences in heat capacity are very small and can be considered negligible (see Table 6-1 for example). From the point of view of the Doppler effect, the lower thermal conductivity of the LEU fuel meat increases the magnitude of the prompt fuel temperature feedback (heat is kept

in the fuel meat), whereas differences in the thermal conductivity account for only a small part of the delay time associated with the void feedback mechanism. A parametric study with respect to the thermal conductivity of the fuel meat is reported in the literature and is included in the discussion of Section 6.3.

Other differences in the nuclear characteristics of the system are also secondary to those of the Doppler coefficient. In the short period range of transients any differences in the effective delayed neutron characteristics are negligible with respect to the initial power burst. The delayed neutron fraction only affects the longer term stability of the system but even so the differences due to the fuel cycles are small. The prompt neutron lifetime for an LEU core is shorter than for the comparable HEU core meaning that the nuclear response is faster for a given reactivity insertion. The comparisons reported in the literature are based on reactivity rather than period so any differences due to the neutron lifetime are taken into account. In addition, a parametric study with respect to the prompt neutron lifetime is reported in the literature and is included in the discussion in Section 6.3.

Overall, experimental results and analysis based on simulation have shown that reactivity insertion safety limits derived for an HEU system are conservative with respect to the corresponding LEU system. In this sense, any reactivity limits derived for an HEU core are applicable to, and conservative with respect to, the associated mixed HEU/LEU or complete LEU core. Removal or reduction in the degree of conservatism of the HEU-data-derived reactivity limits requires a quantitative extension of the analysis. This is addressed in the following sections.

Due to the strength and timing of the self-limiting Doppler feedback, LEU cores are less reliant on delayed moderator voiding shutdown mechanisms. This should lead to a reduced penalty with respect to subcooling, however, application of the full penalty as derived from HEU data is a conservative approach.

6.2 Experimental Data

The experimental data relevant to LEU fuel cycles are discussed in Chapter 3. Although the latter stages of the Spert Project investigated the transient behaviour of LEU cores, this fuel was UO_2 rod-type, clad in stainless steel. The enrichment was between 3% and 5%, typical of power reactors, compared to 20% which is common for research reactors. As such, a gap in the Borax and Spert experimental data set exists with respect to LEU plate-type fuel.

The Spert oxide core program did, however, demonstrate the **prompt nature** and **large magnitude** of the fuel temperature effect in LEU fuel; an effect not present in a heterogeneous HEU core. This is due principally to the increased Doppler effect, *i.e.*, feedback resulting from the broadening of the U-238 resonances, and subsequent increased absorption rate, upon an increase in fuel temperature.

Due to the relatively long thermal time constant of the LEU oxide rod-type fuel (cited as on the order of one second in Reference 6-2), the Doppler shutdown mechanism was effectively isolated in the short-period oxide rod-core Spert tests. This is illustrated in the test data by the measured clad surface temperature rise which is on the order of only a few degrees Celsius at the time of peak power (*i.e.*, at the time of self-limitation of the transient), well below the saturation temperature of the coolant for the short period tests. An example of this is shown in the time trace of power and temperature in Figure 6-1 (taken from Ref. 6-3). These tests showed that, for an oxide ceramic core, transients with periods as short as 3.0 msec can be self-limited *via* the Doppler effect alone.

Importantly, the Spert LEU oxide core test data set has also been used to benchmark transient simulation tools applicable to MTR-type system kinetic analysis. In addition these tests have been analytically modelled with good success (Refs. 6-4, 6-5), the results of which may be useful in a similar parametric analysis to that used for the HEU experimental data in Chapter 4.

With the shorter thermal time constant characteristic of the plate fuel, the behaviour of the LEU MTR-type fuel under unprotected transient conditions is expected to be governed by a combination of the prompt Doppler effect and the delayed moderator expulsion (from boiling) mechanism. Simulation results examining the case of LEU MTR-type fuel are discussed in the following section.

6.3 Existing Simulation Results

As part of the RERTR program, Argonne National Laboratory (ANL) has reported simulation-based analysis of HEU and LEU fuelled cores under unprotected reactivity insertion transient conditions. The purpose of this work is to bridge the gap in the experimental data left between the tests on the HEU plate-type cores and those on the LEU rod-type cores. The simulation results represent the main quantitative information on the behaviour of LEU plate-fuel MTR-type fuel relative to the HEU counterpart.

6.3.1 The PARET Code

The simulation work discussed herein uses the PARET code (Ref. 6-6), which is considered the Industry Standard tool for research reactor kinetics analysis.

PARET is a coupled reactor physics, heat transfer and hydraulics code. The reactor physics portion of the code uses a point kinetics model with feedback coefficients volume-weighted between up to four "channels" representing different regions of the core. The geometry of the model is specified both radially and axially. Heat transfer is *via* conduction through the fuel meat and cladding to the coolant in one-dimension and *via* various empirical single- and two-phase correlations at the clad/coolant boundary. The hydraulics modelling is based on a momentum equation. Output from the code includes power, total reactivity, material temperatures, and coolant flow rates as a function of time.

This code was developed during the Spert Project, and was initially used to investigate transients under elevated temperature and pressure conditions, typical of a PWR system, studied in the Spert III reactor. It was used to analyse the Spert III E-core (LEU SS-clad rod fuel) experimental results and also to project these results to more severe reactivity insertions. The agreement between the code and the experimental results was found to be adequate (Ref. 6-7). This is the primary LEU benchmark study for the PARET code. The code and associated coolant properties library have since been expanded to include data for use in studying transients under conditions more typical of research reactor operation, *i.e.*, ambient temperature and atmospheric pressure.

6.3.2 PARET Benchmarking

The ANL analysis as part of the RERTR program extends the use of the code to MTR-type cores. Models of the Spert I B-24/32, Spert I B-12/64, and Spert I D-12/25 cores were used to benchmark the code to the HEU experimental data (Refs. 6-1, 6-8, 6-9). Cases were considered spanning the same wide range of reactor periods covered by the Spert Project experimental work. Similar in format to the measurements taken in the reactor tests, time traces of the power and temperatures were generated in the simulation cases. Peak power, energy to the time of peak power, and maximum cladding surface temperature at the time of peak power were extracted from the results and compared to the experimental data. These results are shown in correlated data plots of P_{max}, E_{tm}, and ΔT_{tm}, *vs.* α_o (Figs. 6-2, 6-3, 6-4).

With respect to details of the modelling approach, the analysis shows that for plate-fuel systems the transient results are relatively insensitive to the number of specified "channels" in the model (Ref. 6-1).

As a result the most common model includes two channels, one representing the "average" fuel plate and coolant channel and the second representing the "hot channel", *i.e.*, the hot plate and associated coolant channel. This two-channel approach was used in the ANL benchmarking models. The choice of a different number of channels for a model simply requires different breakdowns of the associated feedback coefficients for the different core regions represented by the individual channels. Appropriate feedback coefficient choice will result in the same core average transient response.

Similarly, it is found that the PARET results are relatively insensitive to the feedback weighting (radially and axially) scheme to calculate core-averaged values of the feedback coefficients. A uniform (axial and radial) weighting scheme is found to yield slightly conservative results compared to axially and radially weighted values (Ref. 6-1). This uniform reactivity feedback coefficient weighting is adopted in the ANL models. Linear feedback coefficients, with respect to temperature, and uniform axial weighting of such coefficients, are used in the analysis.

In contrast, the simulation results are found to be relatively sensitive to the choice of void model parameters and strongly dependent on the choice heat transfer correlations for both single- and two-phase flow (Ref. 6-9). These parameters and correlations are tuned to give good agreement between the experimental and simulation results, while at the same time staying conservative to the safety limit of maximum temperature. Agreement is found to be best in the short period range of transients.

Sample PARET input files for the Spert I D-12/25 core and both the HEU and LEU IAEA 10 MW Benchmark problems (see the following section) are included in Appendix F along with a description of the input. Agreement between simulation and experiment is closest for the Spert I B-24/32 core but this input file, and that for the Spert I B-12/64 core have not been located.

6.3.3 The IAEA Benchmark Problem

The ANL analysis also includes modelling of the IAEA 10MW Benchmark Reactor. This theoretical benchmark problem is designed to be typical of modern day

MTR-type reactors. The fuel geometry and materials are similar to the Borax I and Spert Al-clad plate fuel. Both an HEU and an LEU fuel have been defined.

The modelling options and fitting parameters, including the void model parameters and heat transfer correlations, identified in the Spert core modelling are used directly in the models of the IAEA 10 MW Benchmark reactor problem. Both the HEU and LEU IAEA cores are included in the analysis with appropriate feedback coefficients and nuclear parameters determined from static simulation.

The analysis on the IAEA benchmark HEU and LEU cores is summarized in the following section. The results are discussed in the context of the methodology for determining reactivity limits for an MTR-type reactor.

6.3.4 Results from PARET Simulation Analysis

There are two main objectives of the ANL PARET analysis. The first is to show qualitatively how an LEU MTR-type core behaves relative to the associated HEU core. The second is to quantitatively express this with respect to a safety limit. The results of the analysis are reported in References 6-1, 6-8, 6-9.

6.3.4.1 General Behaviour

Results for a reactivity insertion of $1.50/0.5 sec are reported for the HEU and LEU IAEA cores, both self-limited and with overpower scram protection, and also for the LEU core self-limited but with no credit to Doppler feedback. The results are reproduced in Table 6-2. Both the literature values and the results from re-running the cases at MNR using the current version of PARET (PARET-ANL v.5.0, 03/2001) on the Windows XP computing platform at MNR are included.

The results for the self-limited HEU case are included in Figure 6-4 overlaid on the experimental data and simulation results for the Spert I D-12/25 core.

For the self-limiting cases, all of the maximum power, energy generated to time of peak power, and maximum clad temperature values are substantially lower for the LEU core. For this specific transient the HEU and LEU margins to clad melting are 275EC and 320EC, respectively.

It should also be noted that this comparison is on the basis of the same reactivity insertion rather than period which is typically used as an index of the transient for the

HEU experimental data. The same reactivity insertion produces a shorter asymptotic period in the LEU core relative to the HEU core. This is the result of the LEU core having a shorter prompt neutron lifetime (or prompt neutron generation time) compared to the HEU core.

6.3.4.2 Reactivity Limits

In addition to this comparison of the \$1.50/0.5 sec transient, the limiting reactivity insertions for both the HEU and LEU cores were determined for reactivity insertions varying in insertion time from instantaneous steps to 0.75 second ramps. The safety limit used in this analysis is based on fuel clad melting.

A plot of the limiting reactivity insertion for both LEU and HEU cores as a function of time of insertion of the initial positive reactivity is shown in Figure 6-5. For instantaneous step insertions of reactivity the ratio of LEU to HEU reactivity limits is:

$$\frac{\$2.80}{\$2.35} = 1.19$$

indicating that the IAEA LEU core can self-limit an instantaneous initial reactivity insertion 19% larger than the IAEA HEU core (where \$ is a unit of reactivity, *i.e.*, \$1 = $\beta \sim 7$ mk, as defined in Chapter 2). The Doppler coefficient used in the model is assumed linear with temperature over the fuel meat temperature range associated with the clad surface temperature between ambient (~20EC) and melting (582EC) and is included in Table 6-1. Similar analysis (Ref. 6-10) reports a slightly larger ratio, *i.e.*, \$2.9/\$2.3 = 1.26. This is likely rounding approximation.

The simulation results indicate that for ramp insertions up to about 0.125 seconds (for the LEU core) and 0.35 seconds (for the HEU core) in duration the systems have the same response as for an instantaneous step insertion. Power and temperature changes and associated feedback effects are apparently not significant before the entire reactivity insertion is complete up to these times.

For longer duration (slower) reactivity insertions, the amount of reactivity the system can compensate for precluding fuel clad melting increases significantly. For the LEU and HEU fuel cycles the limiting reactivity increases with insertion time by approximately:

- $14.8/sec for LEU
- $6.4/sec for HEU

These are the slopes of the curves shown in Figure 6-5. For large total reactivity insertions the initial power burst may not represent the limiting part of the transient and consideration should be given to the longer term stability of the system which is discussed in Chapter 5. In these cases the reactivity limit may be specified by the post-initial-power peak response of the system

The ratio of the two curves presented in Figure 6-5 is plotted in Figure 6-6. For ramps shorter than about 0.125 seconds in duration the ratio of the limiting reactivity for the LEU and HEU cores is constant at about 1.19. This ratio then increases up to a value of 2.29 for ramps of duration longer than about 0.475 seconds. Thus the ratio value 1.19 represents a conservative minimum.

In actual safety analysis scenarios the insertion time duration should be considered when determining the reactivity limit. Representative values of the ratio of LEU to HEU limiting reactivity, as extracted from Figure 6-6 are given below:

Duration of Insertion (seconds)	LEU/HEU Reactivity Ratio
0.000	1.19
0.125	1.18
0.250	1.56
0.350	2.06
0.475	2.29

Insertion times for the reactor step transients are the rod ejection times. These are reported as:

- Borax I: < .25 sec for complete rod ejection (Ref. 6-11)
- Spert I A & B cores: 0.080 to 0.120 sec for complete ejection (Refs. 6-12, 6-13)

The test core step insertions are therefore associated with the horizontal part of the reactivity insertion limit curve for the HEU fuel cycle (*i.e.*, < 0.35 sec ramp

durations) (Fig. 5).

No indication of the behaviour of this LEU:HEU reactivity ratio is given for other temperatures leading up to the limit associated with fuel clad melting temperature. For the purposes of this analysis the published ratio of 1.19 is used in the application of the safety analysis methodology reported herein.

6.3.4.3 Feedback Components

An indication of the contributing feedback mechanisms is found upon comparison of the limiting ramp of duration 0.5 sec in the IAEA core (consider the limiting reactivity values for 0.5 sec from Figure 6-5). These results are shown in Table 6-3, and indicate that about two thirds of the difference between the HEU and LEU core response is due to the Doppler effect. Most of the remaining difference is due to the larger negative void coefficient associated with the LEU core.

6.3.4.4 Parametric Analysis

Finally, sensitivity analysis of the limiting reactivity insertion with respect to variation of the prompt neutron generation time and the thermal conductivity of the fuel meat is reported as part of the ANL simulation analysis. These results are shown graphically in Figures 6-7 and 6-8. Values of these parameters for the IAEA 10 MW benchmark problem are given in Table 6-1.

6.3.4.5 Limitations & Remarks

As discussed in Chapter 1, use of empirical fitting parameters from one core model for use in a model for a different core represents a limitation in the simulation approach. Specifically, the physical meaning of the empirical fitting parameters may not be apparent and the sensitivity with respect to changes in various system parameters may not be available.

With respect to the simulation based analysis presented in the literature, these limitations are recognized. Herein, the published results are not used in an absolute sense but rather as a relative comparison between HEU and LEU fuel. Since the boiling and heat transfer properties at the clad/coolant interface are not expected to be affected by the fuel cycle enrichment, and since these results are used in a relative sense, they are considered reasonable.

The maximum fuel plate surface temperature is used directly to identify limiting reactivity values in the published work. This quantity was not compared to experimental results in the benchmark calculations. Simulation of short period transients is expected to be least accurate in the post-power peak range of the transient when complex boiling and voiding patterns are created.

However, examination of the HEU reactor test data shows that maximum fuel temperature is proportional to maximum power, energy generation up to the time of peak power, and temperature at the time of peak power, all of which have been benchmarked. Given these relations in the test data and the approach of using the simulation results for T_{max} in a comparative manner, the relative results are considered reasonable. Given the relative nature of the analysis systematic errors in the results may be expected to cancel.

6.4 Extensions to the Simulation Analysis

The published analysis by ANL based on the IAEA 10 MW Benchmark reactor problem gives a good indication of the behaviour of an LEU MTR-type core relative to an HEU MTR-type core under self-protected transient conditions. The IAEA 10 MW benchmark reactor is defined to be typical of a large class of modern day research reactors.

Two extensions to the ANL PARET-based simulation work are suggested herein. Both of these are intended to compliment the existing analysis and produce reactivity limit results which are more generically applicable to MTR-type reactor safety analysis.

The planned extensions to this work continues to adopt the approach of a relative comparison of HEU and LEU response to step insertions of reactivity of varying magnitude. Details of the extension are given in the following sections.

6.4.1 Suggested Parametric Analysis

6.4.1.1 Variation of the Doppler Coefficient of Reactivity

The ANL PARET simulation reported in the literature is based on the specific nuclear parameters associated with the IAEA 10 MW Benchmark reactor problem. This includes a single value for the Doppler feedback coefficient of reactivity

determined from static simulation calculations.

The first extension to the this work is to include a parametric analysis of the safety limit with variation of the Doppler coefficient of reactivity. Not only is this of general use for LEU cores but is also of specific interest for partially converted cores which contain a mixture of HEU and LEU fuel.

With respect to the Doppler coefficient of reactivity, this feedback parameter may vary with fuel assembly design (metal/water ratio), loading/depletion, and certainly with mixed HEU/LEU core configurations which are relevant to partially converted reactor cores. Unit-cell-based simulation suggests that the Doppler coefficient of reactivity may vary by 50% and 70% over ranges of metal to water ratios and fuel loadings enveloping realistic MTR-type reactor values and encompassing the values used for the IAEA 10MW Benchmark Reactor work by ANL (see Appendix E). Mixed HEU/LEU core Doppler coefficients may be expected to vary from the negligible HEU level to the range of LEU values depending on the relative number of HEU and LEU assemblies.

In addition, the ANL PARET simulation used a linear Doppler feedback coefficient which was derived from static calculations over the range of fuel temperature from 38EC to 200EC (Fig. 6-9). For self-limited short period transients the fuel meat temperature is expected to exceed 200EC and may reach temperatures on the order of 1000EC or more. Preliminary calculations of the fuel temperature reactivity suggest a non-linear Doppler coefficient may be more realistic (App. E). As a result the ANL analysis may be over-estimating the Doppler feedback effect.

It is therefore suggested that a non-linear form of the Doppler coefficient of reactivity, determined from a wider range of fuel temperatures, be considered for any extension of the existing simulation analysis.

6.4.1.2 Consideration of a More Conservative Safety Limit

The second analysis extension involves the safety limit criterion related to the limiting reactivity insertion. The published results are based on a safety limit of fuel clad melting at a temperature of 582EC (Ref. 6-9). A more conservative safety limit for the fuel clad temperature, is associated with the onset of clad blistering for irradiated fuel (Ref. 6-14). This is discussed in more detail in Chapter 7.

In the ANL analysis, the progression from cooler temperatures to the safety limit of

fuel clad surface melting for increasing size of the reactivity insertions is not reported. As a result, the relationship between the LEU and HEU reactivity limits for a lower maximum fuel clad temperature is uncertain.

The extension to the reported analysis is therefore to determine the LEU to HEU reactivity limit ratio for a range of limiting maximum fuel clad temperatures enveloping the onset of blistering temperature.

6.4.1.3 Proposed Parametric Analysis Methodology

These two extensions to the simulation-based analysis can be approached in the same way as the calculations for the existing analysis reported in the literature. The suggested methodology for the parametric study is shown pictorially in Figure 6-10.

A series of cases can be run with incrementally increasing reactivity insertions. The range of reactivity insertions should be large enough to produce maximum fuel clad surface temperatures up to and even beyond the limit for onset of clad melting. These cases should also envelope the lower temperature limit for onset of clad blistering. The asymptotic period and maximum temperature (as well as power and energy for further data comparisons) can be extracted from the code output and used to create maximum temperature *vs.* inserted reactivity curves for each value of the Doppler coefficient. A separate curve should be produced for each value of the Doppler coefficient covering the expected possible range of this parameter from the negligible HEU-fuel value to the maximum expected value for the LEU-fuel cycle.

In this way the reactivity, representing the maximum limiting value, associated with a maximum temperature can be read directly from each ρ_{in} *vs.* temperature curve and the ratios of these reactivity limits to the reference HEU-fuel value can be found.

This parametric analysis can be coupled with a parametric analysis of the Doppler coefficient with variations in system parameters such as fuel plate geometry, core depletion and loading patterns, such as started in Appendix E but ideally being extended to full-core static simulation to take into account core effects not seen on the unit cell scale.

In the absence of a rigorous parametric analysis a linear scaling the reactivity limit ratio with a relative comparison of the Doppler coefficient of reactivity for the system of interest to that used for the IAEA LEU analysis, *i.e.*,

$$\frac{\rho_{\text{limit}}^{\text{LEU}}}{\rho_{\text{limit}}^{\text{HEU}}} \times \frac{\alpha_{\text{Doppler}}^{i}}{\alpha_{\text{Doppler}}^{\text{IAEA LEU}}}$$

can serve as a first approximation, where ρ_{limit} is the limiting reactivity insertion based on fuel melting, α_{Doppler} is the Doppler coefficient of reactivity, and i is an index for the system of interest.

6.4.2 Problems with the PARET Code

Originally, the additional simulation using the PARET code outlined in the previous section was planned as part of this thesis.

To prepare for this analysis samples of the benchmark cases used in the ANL RERTR analysis, were obtained from ANL and re-run using the current version of the code (PARET-ANL v.5.0, 03/2001) on the WinXP computing platform. The input model details were checked against those reported in the literature (Refs. 6-1, 6-8, 6-9).

The various IAEA \$1.50/0.5 sec cases discussed in the previous section on PARET benchmarking were re-run as was the Spert I D-12/25 core model with a \$1.50/0.07 sec reactivity insertion. The results are included in Table 6-2 where they are compared to the results from the literature.

During the running of these reference cases an instability in the PARET code was identified. The problem occurs in the post-power peak stage of the unprotected transient, showing up only in the unprotected HEU cases at times of extensive voiding of the coolant. The problem appears related to the stability of the numerical solution scheme causing the run to terminate prematurely just after the code output indicates a negative coolant enthalpy value in the hot channel at times of steam production *via* boiling.

An example of the output from a case experiencing the code instability is shown in Figure 6-11. The case terminates at the last temperature point on the plot. It is unclear whether the maximum temperature has been attained or not, although the results for the reference cases compare well to those reported in the literature.

The problem was also noted in the Spert I D-12/25 \$1.50/0.07 sec case at a time significantly before the peak cladding temperature was reached. The case ran to completion for a different specification of time step intervals.

It is also unclear whether this problem existed in previous releases of the PARET code, in particular the versions used for the unprotected transient scenario simulation of the Spert and IAEA models. The results reported in the literature are assumed to be reliable in the context of any numerical problems experienced in running the PARET code.

The code developer and holder (ANL) has been contacted about this problem (Ref. 6-15). The instability is common to both Windows PC and Linux/UNIX computing platforms, although a case experiencing the problem on the WinXP platform ran to completion on the Linux and Unix platforms. Further investigation is ongoing and upgrades to the code in multiple areas are planned.

Without a full understanding of the code problem it can not be said with certainty that the post-power peak data, in particular the maximum temperature results, generated by this version of the code are reliable. Therefore, for the remainder of this research project the PARET code is considered unavailable. As a result the planned extension to the existing simulation analysis is left as future work.

It is also unclear at this time why the MNR-run energy results in Table 6-2 For the unprotected cases are noticeably different than the previously published results although period and maximum power are consistently reproduced. It is the author's impression that the input files are consistent.

6.5 Incorporation into an SAR Methodology

The ratio of reactivity insertion limits for LEU to HEU cores can be used directly with HEU-based reactivity limits derived from the reactor test data (see Chapters 4 and 5) to determine reactivity insertion limits for an LEU core, *i.e.*,

$$\rho_{\text{limit}}^{\text{LEU}} = \rho_{\text{limit}}^{\text{HEU}} \times \frac{\rho_{\text{limit}}^{\text{LEU}}}{\rho_{\text{limit}}^{\text{HEU}}}$$

The limiting reactivity insertion ratio can be determined from simulation analysis as summarized earlier in this chapter. A value for this ratio has been determined in the ANL analysis of the IAEA 10 MW Benchmark problem is typical of a large class of operating research reactors and is based on a safety limit of clad melting.

A parametric analysis with respect to the magnitude of the Doppler feedback coefficient and a more conservative safety limit of onset of clad blistering, applicable to irradiated fuel, has been suggested to compliment the ANL simulation results. In addition, a non-linear form of the Doppler coefficient of reactivity with respect to temperature may be more realistic than the linear relation used in the ANL PARET analysis.

Since the simulation work derives a ratio based on the inserted reactivity rather than the period of the transient, this adjustment must be applied to the derived HEU reactivity insertion limit following the calculation of the reactivity insertion limit from a limiting period.

6.6 References

6-1. J. E. Matos, E. M. Pennington, K. E. Freese, W. L. Woodruff, "Safety-Related Benchmark Calculations for MTR-Type Reactors with HEU, MEU and LEU Fuels", ANL, IAEA-TECDOC-643, v.3, Appendix G-1, 1992.

6-2. A. H. Spano, J. E. Barry, L. A. Stephan, J. C. Young, "Self-Limiting Power Excursion Tests of a Water-Moderated Low-Enrichment UO_2 Core in Spert I", US AEC Technical Report IDO-16751, Phillips Petroleum Co., February 28, 1962.

6-3. R. Scott Jr., A. A. Wasserman, R. C. Schmitt, "Transient Tests of the Spert I Low-Enrichment UO_2 Core: Data Summary Report", US AEC Technical Report IDO-16752, Phillips Petroleum Co., September 1963.

6-4. A. H. Spano, "Analysis of Doppler-Limited Power Excursions in a Water-Moderated Oxide Core", Nuclear Science and Engineering, v.19, n.2, 1964, pp.172-186.

6-5. J. E. Houghtaling, "A Model for Analysis of Fast Transient Reactivity Effects in Low-Enriched Oxide-Fueled Reactors", US AEC Technical Report IDO-17224, Phillips Petroleum Co., January 1967, (originally issued June 1966 as a Masters Thesis for the University of Idaho).

6-6. C. F. Obenchain, "PARET - A Program for the Analysis of Reactor Transients", US AEC Technical Report IDO-17282, Phillips Petroleum Co., January 1969.

6-7. T. G. Taxelius, editor, "Quarterly Technical Report - Spert Project - July, August, September 1967", US AEC Technical Report IDO-17271, Phillips Petroleum Co., July 1968.

6-8. W. L. Woodruff, "The PARET Code and the Analysis of the SPERT I Transients", Argonne National Laboratory Technical Report ANL/RERTR/TM-4, pp. 560-579, from the Proceedings of the International Meeting on Research and Test Reactor Core Conversion from HEU to LEU Fuels, 1982.

6-9. W. L. Woodruff, "A Kinetics and Thermal-Hydraulics Capability for the Analysis of Research Reactors", Nuclear Technology, v. 64, pp. 196-206,

February 1984.

6-10. J. E. Matos, K. E. Freese, "Safety Analyses for HEU and LEU Equilibrium Cores and HEU-LEU Transition Core for the IAEA Generic 10 MW Reactor", ANL, IAEA-TECDOC-643, v.2, Appendix A-2, 1992.

6-11. J. R. Dietrich, "Experimental Investigation of the Self-Limitation of Power During Reactivity Transients in a Subcooled, Water-Moderated Reactor. Borax-I Experiments, 1954", ANL-5323, (also listed as AECD-3668), Argonne National Laboratory, USA, 1954.

6-12. W. E. Nyer, S. G. Forbes, F. L. Bentzen, G. O. Bright, F. Schroeder, T. R. Wilson, "Experimental Investigations of Reactor Transients", US AEC Technical Report IDO-16285, Phillips Petroleum Co., April 20, 1956.

6-13. T. R. Wilson, "An Engineering Description of the Spert-I Reactor Facility", US AEC Technical Report IDO-16318, Phillips Petroleum Co., June 14, 1957.

6-14. J. M. Beeston, R. R. Hobbins, G. W. Gibson, W. C. Francis, "Development and Irradiation Performance of Uranium Aluminide Fuels in Test Reactors," Nuclear Technology, v.49, June 1980, p.136.

6-15. Personal communication with A. P. Olson, Argonne National Laboratory, email, May 5, 2004.

6.7 Tables

Table 6-1: Fuel specifications and thermal and kinetic parameters for the HEU and LEU IAEA 10 MW Reactor Fuel

	HEU	**LEU**	**Clad**
fuel type	UAl_x-Al	U_3Si_2-Al	Al
enrichment, w% U-235	93	19.75	-
loading, g U-235 / plate	12.2	17.0	-
thermal properties			
k, W/m-DegC	158	50	180
Cp, J/cm^3-DegC (1), * J/g-DegC (2)	1.985 + 0.0010 T 0.728	1.929 + 0.0007 T 0.340	2.069 + 0.0012 T 0.892
kinetics parameters			
Λ, μsec	55.96	43.74	-
β_{eff}	7.607E-3	7.275E-3	-
α coolant temp., mk/Deg-C **	-0.1169	-0.0787	-
α void, mk/v%-void	-2.48	-2.94	-
α Doppler, mk/Deg-C	-0.00027	-0.0241	-

(1) from Reference 6-10
(2) from Reference 6-1
* T in K
** spectrum component only, *i.e.*, density effects not included

Table 6-2: PARET Results for a $1.50 / 0.5 sec reactivity insertion into the IAEA 10 MW Benchmark Reactor (also Spert I D-12/25 step insertion results).

Case	Period (msec)	Max Power (MW)	Energy at Max Power (MW-sec)	Clad Surface Temp at Max Power (EC)	Max Clad Surface Temp (EC)
HEU (w scram)					
Nucl Tech 1984	14.5	132 (0.656)	3.29	131	156 (0.672)
MNR WinXP	14.5	133 (0.656)	3.25	132	160 (0.672)
HEU (w/o scram)					
Nucl Tech 1984	14.5	371 (0.667)	7.30	220	308 (0.685)
MNR WinXP	14.5	371 (0.666)	7.21	214	315 (0.685)[1]
LEU (w scram)					
Nucl Tech 1984	11.9	146 (0.613)	2.94	126	157 (0.628)
MNR WinXP	11.9	148 (0.613)	2.96	129	160 (0.627)
LEU (w/o scram)					
Nucl Tech 1984	11.9	283 (0.622)	5.56	181	263 (0.642)
MNR WinXP	11.9	279 (0.621)	5.31	177	249 (0.641)
LEU (w/o scram and no Doppler)					
Nucl Tech 1984	11.9	445 (0.621)	6.87	220	314 (0.636)
MNR WinXP	11.9	441 (0.620)	6.59	210	316 (0.635)
Spert I D-12/25 ($1.50/0.07sec)					
MNR WinXP	16.8	220 (0.334)	4.82	216	328 (0.353)

The following modifications were made to the IAEA 10MW Benchmark Reactor input files supplied by ANL (Dec/04) and rerun on the MNR WinXP platform with PARET-ANL v5.0 (03/2001):

Original single phase heat transfer subroutine selected
Seider-Tate single phase correlation was selected (as specified in Ref. 6-9)
Heat source in moderator included
Time increments were shortened during power and temperature pulse portions of transient for those supplied
Inlet coolant temperature was changed to 38EC (as specified in Ref. 6-1)

[1] Problem did not finish gracefully. Stopped immediately after peak clad temperature is reached (negative coolant enthalpy)

Table 6-3: Feedback Components with 0.5-sec Limiting Ramp for the IAEA 10 MW Benchmark Problem

Case	Limiting Ramp ($)	Relative Change (% of total)
LEU Base	7.4	---
LEU without Doppler	4.6	-2.80 (67)
LEU without Doppler and with HEU void coefficient	3.4	-4.00 (95)
HEU	3.2	-4.20 (100)

Data reproduced from Reference 6-9

6.8 Figures

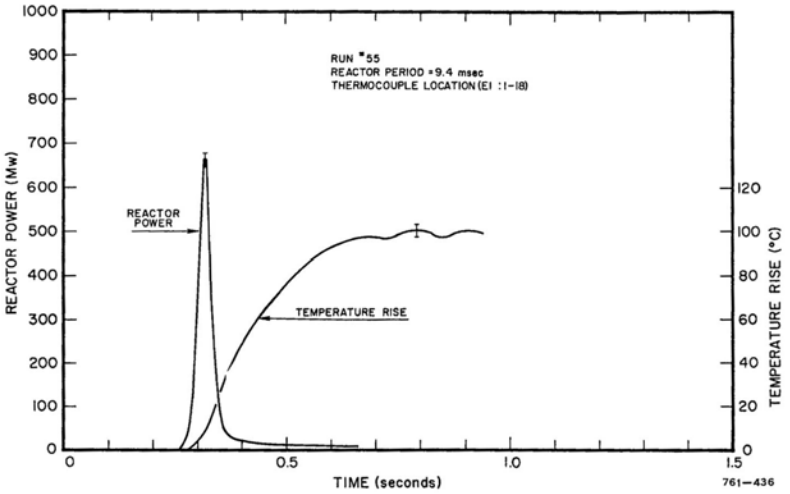

Figure 6-1: Typical Power and Clad Surface Temperature Time Trace from a Short Period Transient Test in the Spert I OC-592 Low-Enrichment UO_2 Rod-Fuel Core (Ref.3)

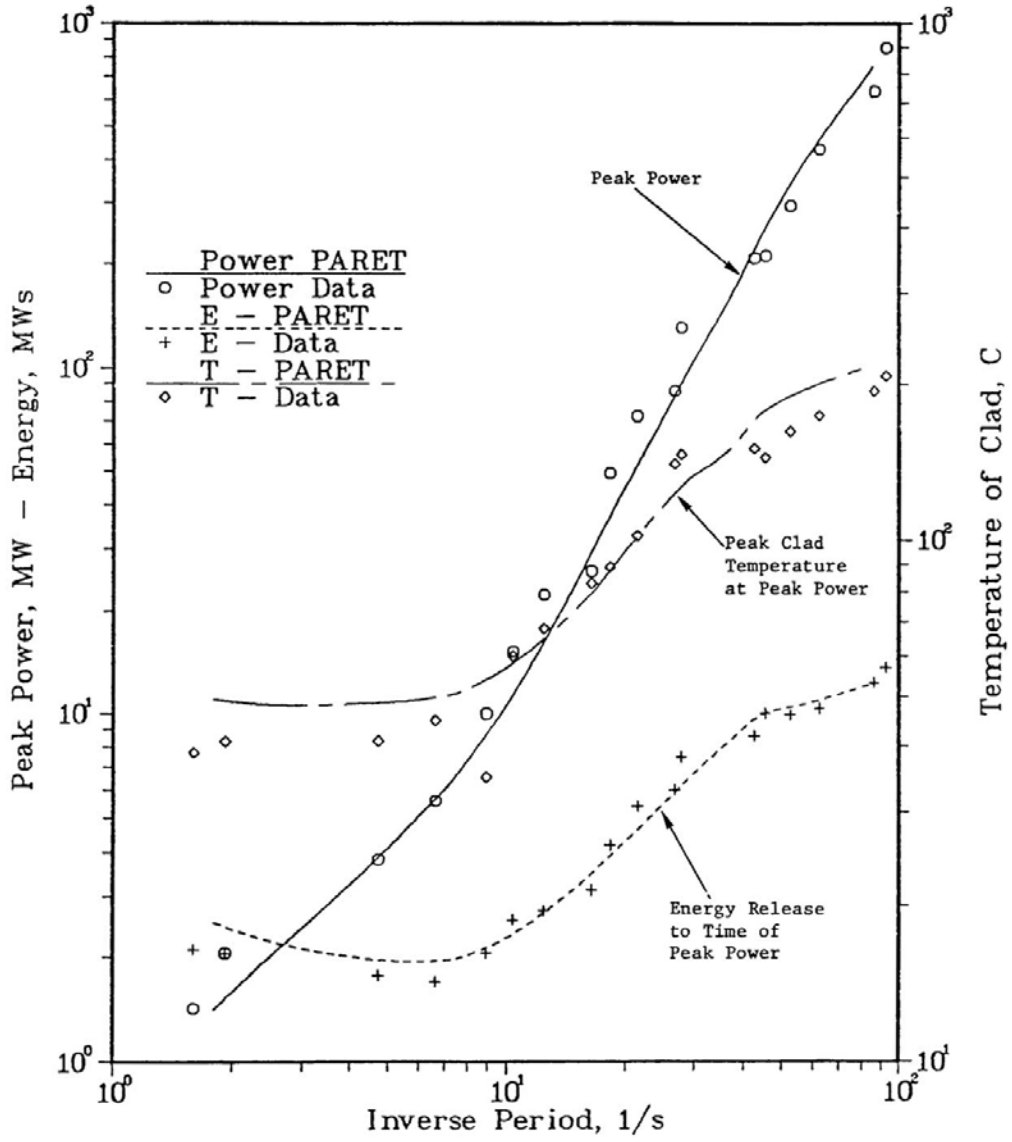

Figure 6-2: Spert I B-24/32 Data and PARET Comparison (Ref. 6-8)

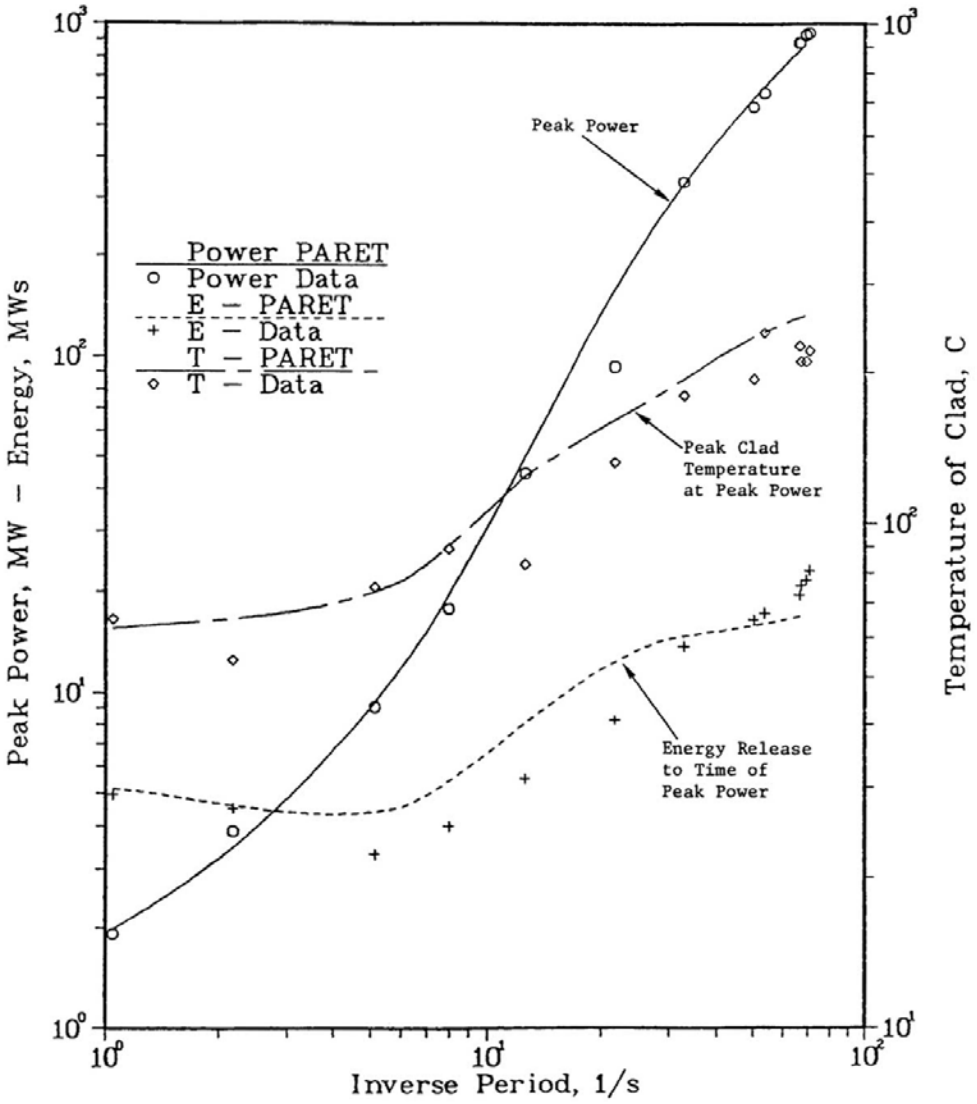

Figure 6-3: Spert I B-12/64 Data and PARET Comparison (Ref. 6-8)

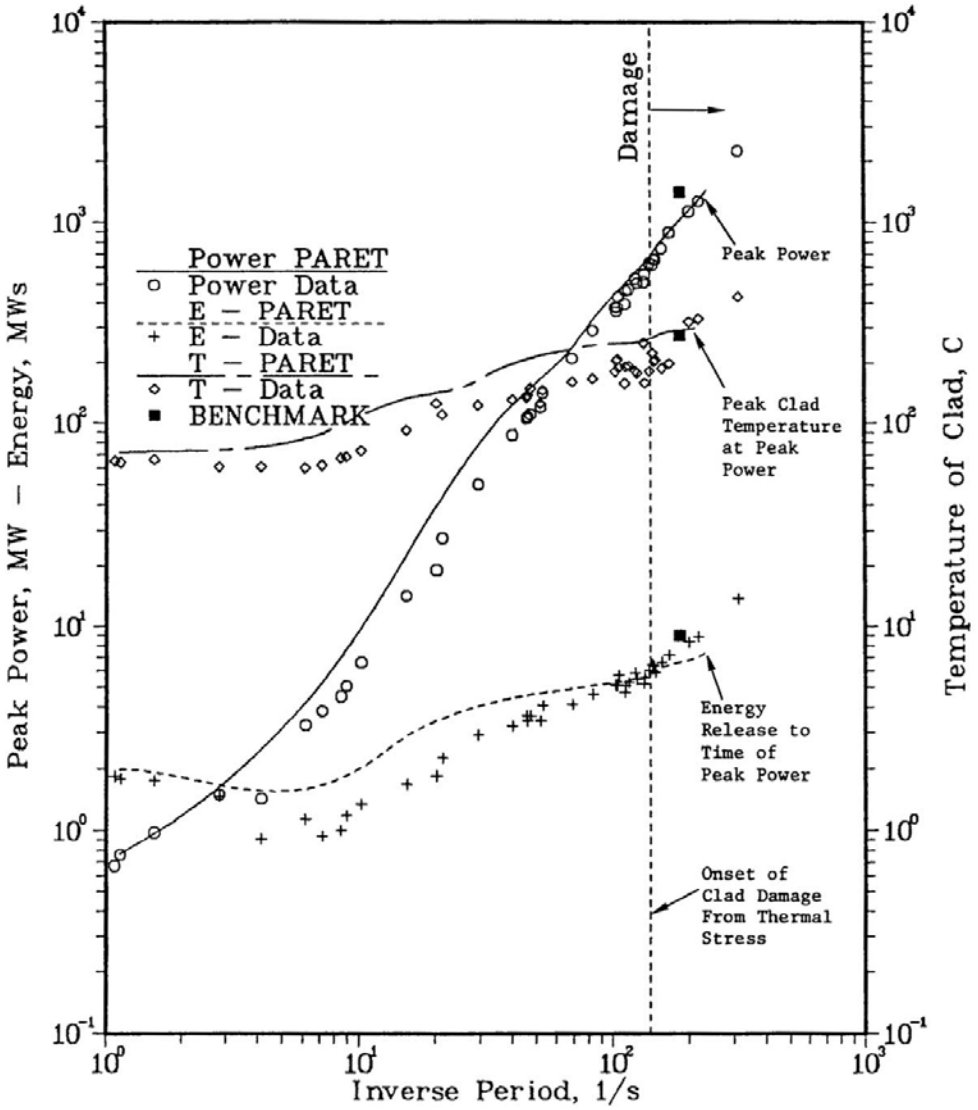

Figure 6-4: Spert I D-12/25 Data and PARET Comparison (Ref. 6-8)

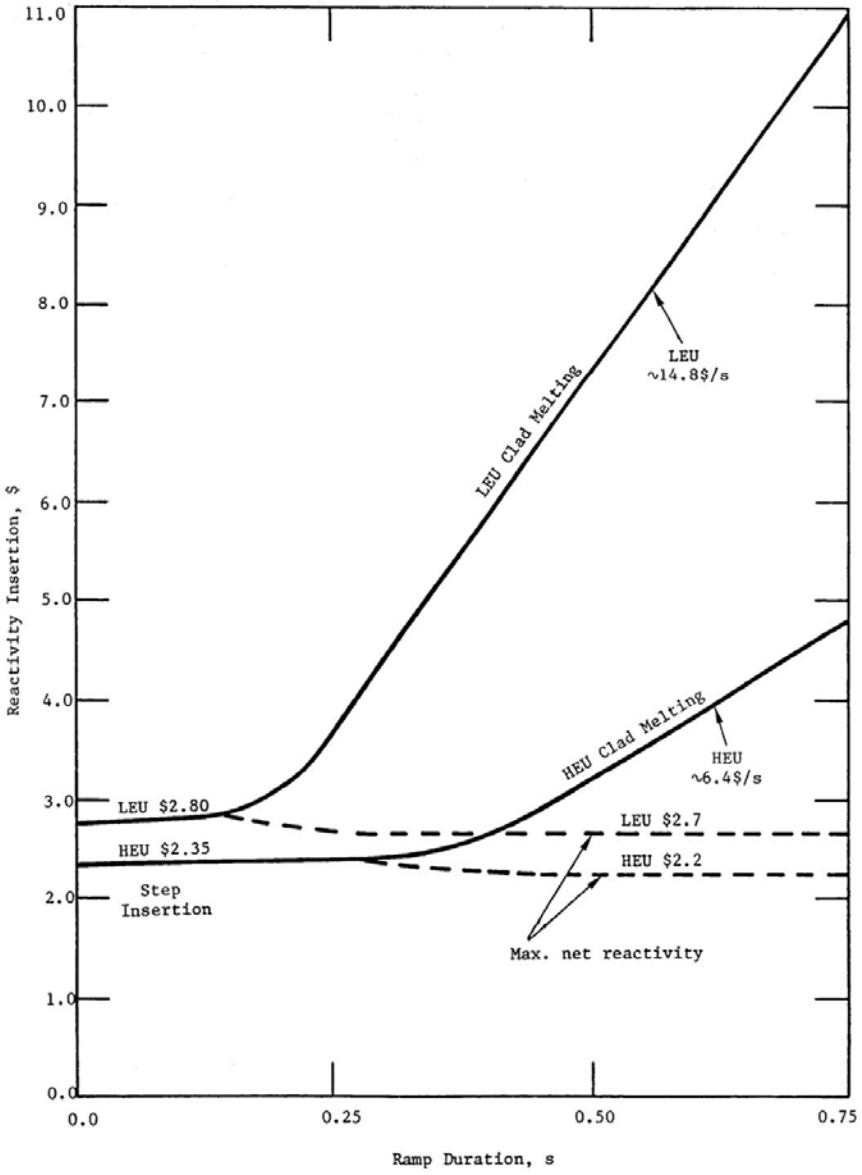

Figure 6-5: Reactivity Insertion Limits precluding Clad Melting for the IAEA 10 MW Benchmark Reactor Problem (Ref. 6-8)

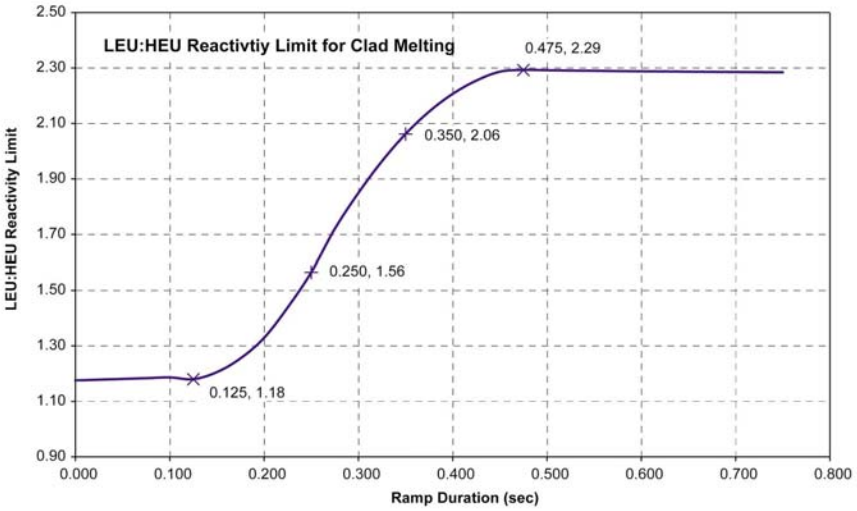

Figure 6-6: Ratio of Reactivity Limits precluding Clad Melting for the IAEA 10 MW Benchmark Reactor Problem

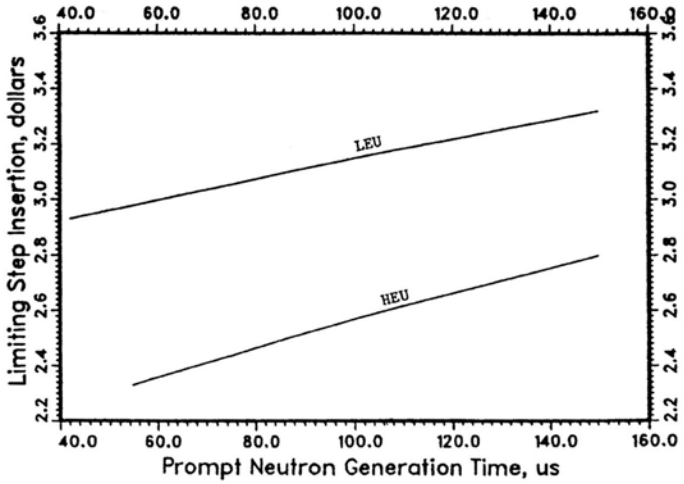

Figure 6-7: Step Reactivity Insertion to Initiate Clad Melting *vs.* Prompt Neutron Generation Time (Ref. 6-10)

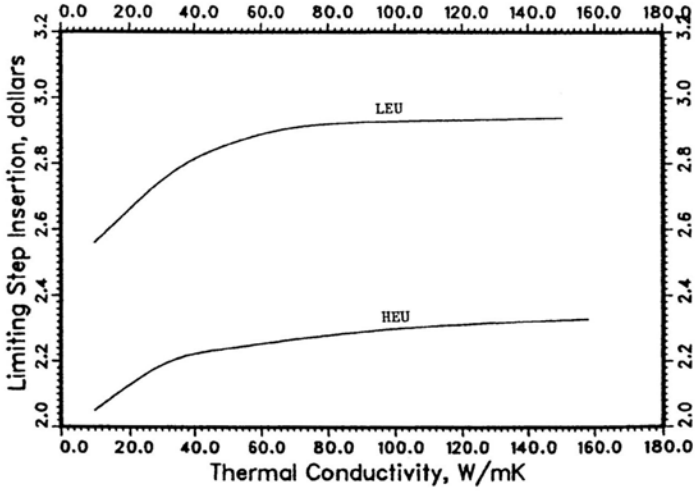

Figure 6-8: Step Reactivity Insertion to Initiate Clad Melting *vs.* Thermal Conductivity of the Fuel Meat (Ref. 6-10)

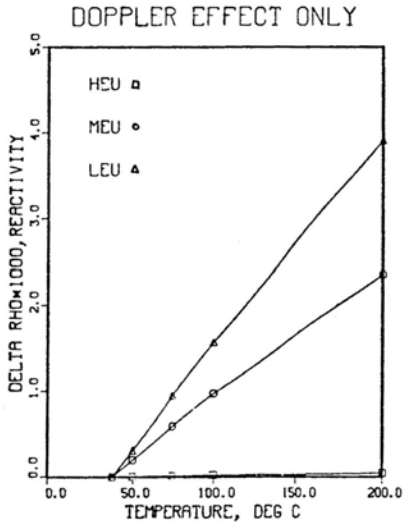

Figure 6-9: Doppler Feedback Data from Static Calculations for the IAEA 10 MW Benchmark Reactor Problem (Ref. 6-1)

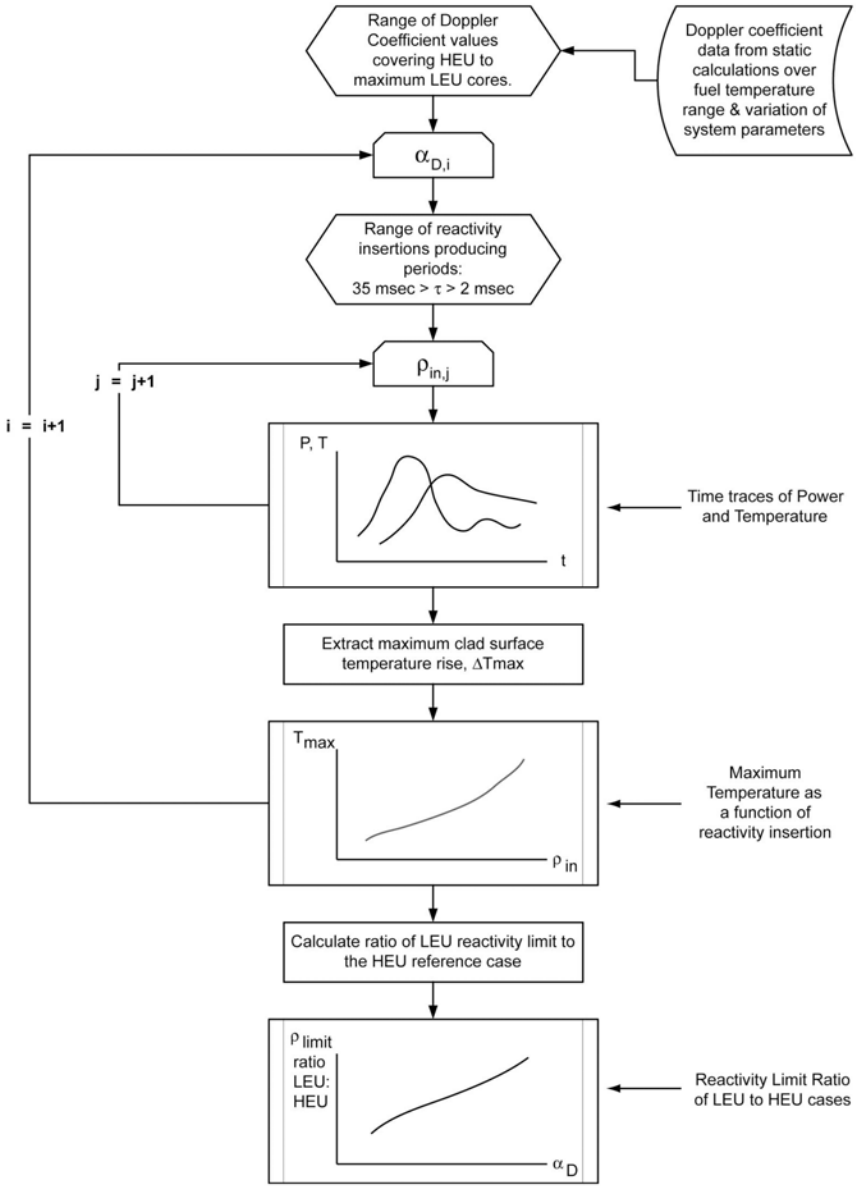

Figure 6-10: Flowchart for Parametric Analysis of Doppler Coefficient

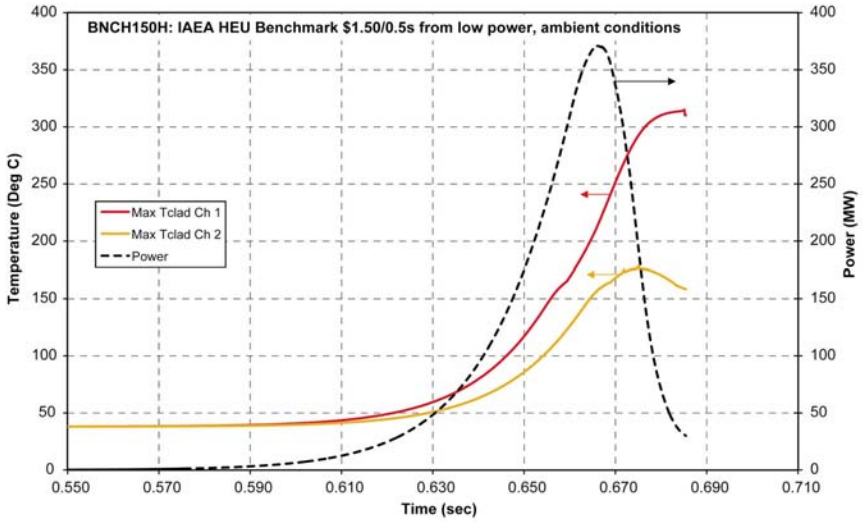

Figure 6-11: Time Traces of Power and Clad Surface Temperatures for a PARET HEU IAEA 10 MW Benchmark Case which Terminates Early on Negative Enthalpy

CHAPTER 7 - SAR METHODOLOGY

TABLE OF CONTENTS

LIST OF TABLES

LIST OF FIGURES

(this page is intentionally left blank)

7 SAR METHODOLOGY

This chapter describes a safety analysis methodology for estimating reactivity limits and transient response of an MTR-type reactor based on the general characteristics and the parametric dependencies derived from the reactor test data.

The behaviour of an MTR-type core under RIA conditions is described in Chapter 2. A working methodology is created by combining this physical understanding of the self-limiting characteristics of such systems with the trends in the test data (Chapter 3, and Appendix C) and the quantification of parametric dependencies (Chapters 4, 5, and 6).

Section 7.1 discusses the framework for the methodology, specifically the input data which is needed in the various steps of the calculation. This includes safety limits appropriate for MTR-type fuel, comparisons with the test cores in terms of system parameters, and determination of these parameters for the system of interest.

Section 7.2 outlines the methodology. This is considered from two starting points: (i) the derivation of a maximum reactivity limit from a given temperature-based safety limit, and (ii) the derivation of a transient response in terms of P_{max}, E_{tm}, and ΔT_{max} for a given reactivity insertion. Both step and ramp reactivity insertions are considered as is the longer term stability of the core in terms of chugging limitations.

Section 7.3 details a walk-through of the methodology for the case of the maximum step and stability limits for the McMaster Nuclear Reactor (MNR) based on the current nuclear characterisation of the core.

Section 7.4 contains some final remarks on the use of the experimental data for MTR-type core safety analysis calculations. The extent and limitations of the methodology are discussed and areas for future work are suggested.

7.1 Methodology Framework

7.1.1 Safety Limit

The information pertaining to the various stages of fuel damage (see Chapter 2) suggest a set of temperature related safety limits for MTR-type cores. These safety limits are relevant to unprotected RIAs in which the temperature increase in the fuel

plates is both large and rapid.

The various stages of fuel damage are categorized in the following list from lowest to highest temperature of occurrence. The approximate onset temperatures of each are indicated in parentheses:

- minor mechanical damage (T_{max} > 210EC)
- blistering of irradiated fuel (T_{max} > 400EC, depends on fuel material)
- clad melting (typical Al-clad solidus temperature, T_{max} > 582EC)
- core disassembly (just beyond melting onset if global core heating)

Onset of mechanical fuel damage represents a damage threshold, more conservative than the onset of clad melting, and applicable to both fresh and irradiated fuel. Observations from the reactor tests suggest that fuel plate deformation occurred during transients in which maximum fuel plate clad surface temperatures reached 210EC to 438EC. This range of temperatures associated with onset of plate deformation is derived from least squares fitting to the transient data for tests from ambient initial temperatures (see Appendix C) and transient periods suggested in the literature (see Chapter 2). This is a wide range of temperature and reflects both the uncertainty related to the temperature data fitting and the qualitative and approximate nature of "onset" period reporting in the literature.

Resistance of a fuel plate to blistering (caused by gas bubble agglomeration) is a standard test of fuel plate stability used in the research reactor community (Ref. 7-1). Testing indicates that fuel irradiated to burnup typical of research reactor exit levels and beyond experience blistering at temperatures in the range of 400EC to 600EC depending on the fuel type.

Experimental data based on mini-plates and full-sized plates indicate the onset of blistering for the following standard dispersion fuels (Refs. 7-1, 7-2, 7-3):

- HEU UAl_x-Al: 480EC to > 565EC
- HEU U_3O_8-Al: 400EC to > 550EC
- LEU U_3Si_2-Al: 515EC and 575EC

The LEU dispersion fuels appear to be at least as stable if not more so as the

associated HEU fuels. Blister threshold ranges for other research reactor fuels are reported in Reference 7-1.

Onset of fuel plate surface melting is the next in the progressively increasing temperature limits applicable to fuel damage. The clad "melting temperature" is somewhat ambiguous, defined by a range of temperatures between the solidus temperature (at which the material is 100% solid) and the liquidus temperature (at which the material is 100% liquid). The common reactor grade aluminum alloy Al-6061 T6 melting "point" is 582EC (solidus) to 652EC (liquidus) (Ref. 7-4). The solidus temperature is identified as being associated with the next stage of fission product release after fuel plate blistering (Ref. 7-3). The reactor transient tests in which fuel plate melting was observed are associated with maximum fuel plate surface temperatures > 570EC as recorded by spot-welded thermocouples (Ref. 7-5).

The final safety limit for MTR-type cores may be considered as the onset of core disassembly. As discussed in Chapter 2, the clad surface temperature related to the core disassembly threshold varies in relation to the onset of fuel clad surface melting depending on the thermal resistance (conductivity and plate thickness) of the specific fuel.

For typical fuel plate dimensions of operating MTR-type reactors, *i.e.*, fuel meat thickness # 0.051 cm and clad thickness # 0.051 cm, the onset clad surface temperature for core disassembly is higher than the onset of clad surface melting temperature. In this sense, the onset of fuel clad surface melting (solidus temperature) is a conservative estimate for the core disassembly temperature threshold for typical MTR-type fuel. Of course this is assuming that the temperature rise is core-wide and that the maximum clad surface temperature is taken as the governing temperature. Identification of a more precise temperature threshold is left as future work.

Temperature increases and limits are predictable in terms of the asymptotic reactor period which in turn is generated by the initial positive reactivity insertion. The exact period and reactivity are specific to the individual MTR-type core and depend on certain system parameters. These can be determined from the test data with reference to any of the safety limits.

7.1.2 Comparison to Test Systems

With the safety limits defined (see Section 7.1.1) the next required step is to compare

the system of interest to the Borax and Spert test cores. This is done by determining the relevant system parameters for the system of interest.

The preceding analysis has identified the following system parameters as important in characterising an MTR-type core:

- overall power peaking factor (product of local, radial and axial factors),
- fuel meat volume,
- prompt neutron lifetime,
- delayed neutron fraction, relative yields and associated decay constants,
- average void coefficient of reactivity,
- initial temperature and saturation temperature,
- temperature defect from initial to saturation conditions,
- coolant flow direction,
- fuel enrichment, and
- fuel plate geometry including meat and clad thicknesses and heat transfer surface area.

These parameters can be compared to the ranges studied in the test core experiments and are subsequently used in adjustments for core size, power distribution, shutdown feedback, and subcooling, as well as to calculate stability limits and to convert limiting reactor period to reactivity and *vice versa*.

In addition, reactivity-related specifics of the system, such as maximum available reactivity (*e.g.*, shutdown depth, rod worth, assembly worth, excess reactivity of the core), maximum rate of reactivity addition (*e.g.*, motor-driven or manual withdrawal of the control rods, terminal velocity of falling fuel assembly in light water), and other reactivity magnitude and insertion rate characteristics and limits, should be considered. This puts the scenario under consideration in context compared to the step insertion predictions from the test data.

7.1.3 Characterisation of the System

In order to compare the core under consideration to the test cores and the range of parameters that they represent it is necessary to characterise the system of interest. This can be done by a combination of simulation analysis, experiments and even assessment of existing literature and fundamental physics. Ideally, the MTR-type

core under consideration should be characterised in the same manner as the test cores or conversely the test cores can be re-assessed using updated characterisation methods. The important aspect is that nuclear and material parameters used for comparison are consistent.

Initial conditions should be assessed from relevant operating limits and conditions as well as in terms of the specific scenario under consideration when conditions are decidedly off-normal (compared to normal operation). A conservative bound can be considered when necessary. One example is the initial temperature of the system. Given that transient response becomes more severe in terms of a step reactivity insertion when subcooling is increased, lower bound initial temperature and upper bound saturation temperature represent the conservative subcooling condition.

The following set of nuclear parameters needs to be determined in order to use the methodology:

- total plate dimensions, geometry and materials,
- fuel meat volume,
- coolant material and circulation information,
- overall power peaking factor,
- average void coefficient of reactivity,
- temperature defect (*i.e.*, reactivity change) for the system going from cold to saturation conditions,
- prompt neutron lifetime, and
- delayed neutron fractions and decay constants.

If not explicitly determined then bounding values should be adopted, maintaining a conservative envelope on the analysis.

The fuel plate dimensions, geometry, and materials should be compared to the test cores in order to either conclude equivalent heat transfer characteristics or supplement this methodology with an adjustment with respect to variations in these characteristics. The methodology herein is conservatively applicable to aluminum clad MTR-type plate-cores with meat and cladding thicknesses of 0.051 cm or less.

The core should be completely characterised in terms of power density distribution and void reactivity feedback coefficient. This can be done by adopting similar experimental methods as used to characterise the test cores, *i.e.*, flux wire activation and simulated-void-material reactivity changes. Reference can be made to

Appendices B and D which contain information on the static testing of the test cores and the MNR core, respectively. Further details can be found in the cited references.

The temperature defect can be measured for the system in question by experimental methods, as done for the test cores (see Appendix B), or from code simulation calculations. A combination of experiment and simulation is recommended. This value and the overall moderator/reflector feedback temperature coefficient is used in the stability analysis of the system.

The prompt neutron lifetime can be found either from kinetic experiments or simulation or a combination of both. This parameter is used in the shutdown coefficient analysis as well as in the conversion of reactor period to reactivity which is the final step in the methodology. The delayed neutron fractions and decay constants are similarly used at this stage of the methodology.

The test data collected under natural circulation coolant conditions have been shown to be conservative with respect to forced flow situations when considering maximum temperature from the initial power pulse (see Chapter 4). However, coolant flow direction must be considered with respect to the longer term stability of the system.

An additional factor for consideration in the characterisation of a core is the Doppler coefficient of reactivity. A parametric analysis of this factor is not included in this work but a framework of such an analysis has been suggested in Chapter 6.

The experimental measurements can be supplemented with simulation code analysis. It is possible that a more detailed characterisation of the cores can be found through code analysis, although it is the author's suggestion that code analysis not be used exclusively in order to avoid systematic errors on comparison to the test system experimental measurements. Improvements in characterisation may lead to further refinements in the data application such as scaling of the experimental temperature data with thermocouple location, and a more advanced treatment of the void coefficient values used in the shutdown coefficient analysis. If this approach is taken the simulation models of the test cores must likely be developed which relies on confirmation of some technical specifications such as lattice pitch, and side plate dimensions which were not always forthcoming from the literature.

7.2 Summary of the Methodology

The methodology includes all of: step reactivity insertions, ramp reactivity insertions, and the associated stability limit for post-power-peak response. The step methodology is shown in the context of the experimental data and complimentary information (such as the LEU simulation work available in the literature) in Figure 7-1. The knowledge flow in this figure is from left to right and shows the information derived from the test data and how it relates to the derivation of a reactivity limit associated with a temperature-based safety limit.

The methodology can be used in two different forms. The first, which fits the information flow in Figure 7-1, is designed for determining reactivity limits associated with pre-defined safety limits on temperature (or power or energy if desired). The second use of the methodology involves the reverse sequence and is designed for the purpose of determining the reactor response in terms of P_{max}, E_{tm}, and ΔT_{max} given a defined reactivity insertion. These two forms of the methodology are illustrated in more detail in Figures 7-2 and 7-3, respectively.

7.2.1 Step Insertions of Reactivity

The step insertion methodology is shown as part of the full methodology presented in Figures 7-2 and 7-3. In fact the steps in the methodology related to a step reactivity insertion are shared by that for ramp insertion and stability limit analyses. The steps in the step insertion methodology are described below.

Considering Figure 7-2, the input quantity is a maximum temperature rise (ΔT_{max}) which is associated with a safety limit for the system of interest. Following the flowchart from top to bottom, the first steps translate the maximum temperature rise for the system of interest into the equivalent maximum temperature rise for a specific test core. The Spert I D-12/25 core can be chosen as the reference test core as done in the void reactivity parametric analysis of Chapter 4. Since all scaling for system parameters is relative it is not required to scale to the Spert I D-12/25 core but this data set is the most complete of any core for subcooled step transients and thus the curve fitting is well defined.

The first four blocks of the methodology represent scaling for differences in:

- subcooling,
- core size,

- power distribution, and
- void reactivity feedback characteristics.

The required input data for these scaling steps are:

- the initial subcooling,
- the fuel meat volume,
- the overall power peaking factor, and
- the average void coefficient, prompt neutron lifetime and coolant channel volume.

for both the core of interest and the reference test core (*e.g.*, Spert I D-12/25). The shutdown coefficient can be constructed from this data as can the required subcooling ratio factor (as described in Chapter 4). The input maximum temperature rise can then be scaled by the series of relative factors to produce the equivalent maximum temperature rise for the test core, *i.e.*

$$\Delta T_{max}^{Test\,Core} = \Delta T_{max}^{i} \times \frac{\Delta T_{max}\text{–}ratio^{Test\,Core}}{\Delta T_{max}\text{–}ratio^{i}} \times \frac{PPF^{Test\,Core}}{PPF^{i}} \times \frac{V_f^{i}}{V_f^{Test\,Core}} \times \left(\frac{w^{i}}{w^{Test\,Core}} \right)^{m}$$

where the superscript *i* denotes the system of interest (*e.g.*, MNR). These scaling factors account for differences between the system of interest and the reference test core in terms of subcooling (ΔT_{max}-*ratio*), power distribution (*PPF*), core size (V_f), and void reactivity feedback (w^m). Details are given in Chapter 4.

Once the equivalent test core maximum temperature rise has been determined the associated step insertion initial asymptotic reactor period can be determined from the curve fitting relations of the maximum temperature rise to reciprocal period (α_o), *i.e.*,

$$\Delta T_{max}^{Test\,Core} = b_{Test\,Core} e^{m_3 \alpha_o}, \quad \textit{rearranged to give}$$

$$\alpha_o = \frac{1}{m_3} \ln \left(\frac{\Delta T_{max}^{Test\,Core}}{b_{Test\,Core}} \right)$$

where m_3 is the characteristic exponent for the maximum temperature rise relation to asymptotic reciprocal period. The fitting parameters *m* and *b* are included in Chapter 4 and the curve fitting is described in Appendix C.

After determining the related asymptotic reactor period the related step reactivity insertion can be determined using the Inhour Equation. Input data needed for this step of the methodology is the prompt neutron lifetime and delayed neutron fractions and decay constants for the system of interest (HEU fuel values). The period to reactivity conversion is described in more detail in Section 7.2.4. At this point the limiting step reactivity insertion for an HEU core has been determined.

The remaining step, if relevant, is to credit the improved self-limiting ability associated with the LEU fuel cycle. This is done by applying the ratio of limiting reactivity insertions as found from the simulation work reported by ANL (see Chapter 6), *i.e.*,

$$\rho_{limit}^{LEU} = \rho_{limit}^{HEU} \times \left(\frac{\rho_{limit}^{LEU}}{\rho_{limit}^{HEU}} \right)$$

For a step reactivity insertion this is the limiting amount of reactivity associated with the temperature rise limit originally used as input. Chugging oscillations, if they occur, will be enveloped by this result for the initial power peak response.

To use the methodology in the other form (Figure 7-3), *i.e.*, to determine the reactor response to a given step reactivity insertion, the steps of the methodology are reversed. The reactivity insertion is adjusted to an HEU value if necessary by applying the HEU to LEU ratio, *i.e.*, the inverse of the ratio used in the previous application of the methodology. The reactivity insertion can then be translated to the associated asymptotic period using the Inhour Equation with the system of interest input data (for HEU fuel).

Once the period has been determined the associated P_{max}, E_{tm}, and ΔT_{max} values can be read from the desired test core fit. The test core response must then be translated to the equivalent response for the system of interest by applying the scaling for shutdown (void) coefficient, power peaking, core size, and subcooling as outlined previously, but once again by using the inverse of the ratios used in the companion application of the methodology. It should be noted that the PPF and V_f scaling factors need only be applied to the temperature data and should not be applied to the power and energy data. The calculated system-of-interest transient data (P_{max}, E_{tm}, and ΔT_{max}) may then be compared to relevant safety limits.

7.2.2 Ramp Insertions of Reactivity

Much of the same methodology as applied for analysis of a step insertion of reactivity is common to the analysis of a ramp insertion of reactivity. This is based on the evidence that the initial power pulse behaviour due to a ramp reactivity addition can be represented by an "equivalent" step reactivity addition. The equivalence is in terms of the reactor period. The reactivity addition of the "equivalent" step insertion is always smaller than the reactivity associated with the ramp reactivity insertion at the point of the initial power pulse.

With respect to the methodology of ramp insertions of reactivity extra steps are required in addition to the step methodology sequence. Considering the case of an input temperature limit (ΔT_{max}) and the desired associated reactivity limit (Fig. 7-2) the methodology is common to the step insertion case. Once the step insertion limit of reactivity is determined, it must be converted back into the asymptotic period for a step insertion *via* the Inhour Equation. Once converted, the associated minimum period can be determined by using simulation tools such as a point kinetics code.

For a ramp reactivity insertion both the maximum reactivity to be inserted and the duration of the ramp are free parameters. Either of these can be determined from physical characteristics of the system, *e.g.*, the duration of the ramp is determined by the motor speed of the rod drives for a rod withdrawal event, and the maximum reactivity is the total available worth of the rods to be withdrawn. Knowing either the reactivity addition rate or the total insertion, the limit on the other parameter can then be identified.

It should be noted that the second conversion of the step limiting reactivity back into a period can be avoided if the analysis is for an HEU system. For this case the asymptotic period found directly from the test core data curve fitting relations can be equated directly to the equivalent minimum period for use in simulation of the ramp response.

The other form of the methodology, for determining reactor response from an input ramp reactivity insertion (Fig. 7-3) is similar in extension from the step reactivity methodology. In this case the ramp parameters (duration and size) are pre-defined and can be used in a simulation model to determine the minimum reactor period associated with the initial power pulse. Once found, the minimum period is equated to an asymptotic period for the equivalent step reactivity insertion. This period is converted to a reactivity value if an adjustment for the LEU fuel cycle is desired or

can be used directly in the test data curve fitting relations for P_{max}, E_{tm}, and ΔT_{max} if an HEU core is being analysed. The methodology then follows the same sequence as for the step reactivity insertion case.

This use of the methodology is relevant to the initial power pulse stage of a ramp reactivity insertion transient only. Examination of the post-initial-pulse behaviour of a ramp insertion transient is necessary for proper safety limit coverage of the event. The methodology associated with this "stability limit" is described in the following section.

7.2.3 Stability/Chugging

Depending on the ability of the system of interest to operate with a certain void fraction the limiting stage of a ramp transient may very well be associated with the post-initial-power-pulse. Reactivity may be returned to the system in cases where boiling causes hydraulic chugging oscillations. These drive power and subsequent temperature oscillations. Chugging is discussed in more detail in Chapter 5.

It is common that post-initial-power-burst stability is not considered for ramp insertion events in safety analysis work. To extend the methodology to incorporate stability limits the step reactivity insertion methodology is followed with a simple additional step of crediting any temperature defect associated with a change in reactor conditions from the time of the initial reactivity insertion to the time at which chugging may be applicable.

For example, for the startup transient, or any other ramp insertion from cold, clean conditions, the core is initially at a certain subcooled condition and the fuel temperature is commonly in thermal equilibrium with the coolant. Following the initial power rise the system increases in temperature to the point where boiling of the coolant begins. This will be the saturation temperature of the coolant. There is a negative reactivity contribution associated with this increase in coolant and fuel temperature which is referred to as the temperature defect. This may also be somewhat offset by a positive reactivity term from increased temperature of the reflector material (*e.g.*, reactor pool). Details are given in Chapter 5.

This temperature defect can be credited, either by adding it to the limiting reactivity insertion determined from following the step insertion methodology for an input ΔT_{max} (Fig. 7-2), or subtracted from an input reactivity when determining the reactor response (Fig. 7-3).

7.2.4 Conversion of Period and Reactivity Limits

Part of the analysis methodology involves converting the reactor period to the associated reactivity insertion and *vice versa*. This is the result of the transient test data relations being developed based on a reactor period scale while the LEU scaling factor and the final working numbers applicable to reactor operation and safety limits are in units of reactivity.

The conversion requires use of the relation between the prompt neutron lifetime, the delayed neutron characteristics, the reactivity, and the resulting reactor period. This has been previously mentioned in Chapter 2 as derived from the governing time dependent neutron equations. By assuming spatial and temporal separability, this relation is described by the Inhour Equation (Ref. 7-6),

$$\rho_{in} = \frac{\omega\ell}{1+\omega\ell} + \frac{1}{1+\omega\ell}\sum_i \frac{\omega\beta_i}{\omega+\lambda_i}, \quad \textit{where the largest } \omega = \frac{1}{\tau_0}$$

where λ_i and β_i are the average decay constants and delayed fission neutron yields associated with the delayed neutron precursors. It is conventional to represent the delayed neutron data in six groups, representing the range of half-lives of the precursors. The fundamental mode solution is associated with the "stable" or "asymptotic" reactor period (where the fundamental mode $\omega = \alpha$, the reciprocal period). Delayed neutron data for U-235 are summarized in Table 7-1 (Ref. 7-6). The asymptotic period as a function of reactivity insertion is shown for varying prompt neutron lifetimes corresponding to both MNR and a few of the test cores in Figures 7-4 and 7-5. The Spert I B-12/64 and A-17/28 cores are characterised by the longest and shortest prompt neutron lifetimes, respectively, of any of the test cores.

7.3 Application of the Methodology

This section provides a walk-through of the safety analysis methodology for the case of the McMaster Nuclear Reactor (MNR). The calculations are based on current best estimates for the required nuclear parameters and on conservative bounds for relevant operating conditions. Only the step insertion and the stability limits of reactivity are considered.

MNR is a typical MTR-type facility, *i.e.*, swimming-pool type, light-water cooled and

moderated facility. It currently uses a mixture of HEU U_3O_8-Al and LEU U_3Si_2-Al dispersion fuel, clad in aluminum. The core includes both 18-plate "standard" fuel assemblies and 9-plate "control" fuel assemblies. The inner sixteen fuel plates in the standard fuel assemblies contain fuel material while the outer plates are solid aluminum (*i.e.*, "dummy" plates). The control fuel assemblies are similar to the standard fuel assemblies with the central plates removed and replaced with an aluminum guide structure which houses oval cross section control rods. All nine plates in the control fuel assemblies contain fuel material. Five of the six rods are highly absorbing Ag-In-Cd alloy while the sixth rod is stainless steel and used for regulation. The HEU standard fuel plates contain a nominal 12.25 grams of U-235 at an enrichment of 93% whereas the LEU standard fuel plates contain 14.06 grams of U-235 at an enrichment of 19.75%. The plate and assembly dimensions are close to those of the test fuel, specifically the fuel meat thickness and axial extent is practically identical to the test core dimensions and the clad thickness is slightly less, 0.038 cm compared to 0.051 cm in the test core Al-clad fuel. MNR dimensions are included in Table 7-2.

The MNR Reference Core (Ref. 7-7) contains 28 standard fuel assemblies plus the six control fuel assemblies arranged in a six by seven array within the six by nine grid plate. It is reflected on one side by a row of graphite assemblies and on all sides by light water. The core also contains a single beryllium reflector assembly and houses multiple in-core irradiation sites. Both mixed HEU:LEU and complete LEU fuel loading patterns are defined.

With regards to event initial conditions, MNR typically operates under a hydrostatic head of eight metres resulting in a saturation temperature of approximately 117EC. Coolant flow varies with operating state and is typically on the order of 1900 USG per minute downwards (driven by gravity and made up by a pump) for 3 MW_{th} operation, and is natural circulation for low power (< 110 kW_{th}) operation or during core shutdown. The pool temperature typically ranges with weather conditions between 20EC and 30EC with a core outlet temperature on the order of 50EC for power operation (depending on operating power). Choosing 20EC is therefore a conservative approach for subcooling.

MNR has been characterised from void substitution experiments which involved determining the reactivity worth of aluminum "void" plates in the coolant channels of various fuel assemblies. These results have been used to estimate both central and average void coefficients of reactivity for MNR. A report on the experiments is included as Appendix D. The nuclear parameters of MNR are included in Table 7-2.

The aluminum-clad cores tested in the full-scale reactor experiments are:

- Borax I (18/26-32)
- Spert I A-17/28
- Spert I B-24/32
- Spert I B-16/40
- Spert I B-12/64
- Spert I D-12/25
- Spert II B-12/64 (H_2O)
- Spert IV D-12/25

The number of plates and assemblies in MNR Reference Core (MNR RC) are enveloped by the range used in the test cores. This is also the case for the void coefficient for MNR relative to the range covered by the test cores. The system for which the parameters are closest to those of MNR is Borax I. The relevant system parameters for each of the test cores and the MNR RC for use in the methodology are summarized in Table 7-3.

7.3.1 Maximum Step Reactivity Insertion in MNR

Considering a safety limit of 400EC, associated with blistering of irradiated U_3O_8-Al_x HEU fuel, the maximum step insertion of reactivity for MNR can be calculated by following the methodology outlined in Section 7.2.1 and illustrated in Figure 7-2.

The MNR core is compared to the Spert I D-12/25 core. The input data for these two cores are included in Table 7-3. The initial and saturation temperatures for the two cores are taken as:

$$\begin{aligned} &MNR: && T_i = 20°C, \quad T_{sat} = 117°C \quad \rightarrow \quad T_{sub} = 97°C \\ &Spert\ I\ D: && T_i = 20°C, \quad T_{sat} = 96°C \quad \rightarrow \quad T_{sub} = 76°C \end{aligned}$$

The MNR safety limit of 400EC translates to a maximum temperature rise of 380EC for these initial conditions. Using this data the following quantities are determined:

$$\begin{aligned} \Delta T_{max}\text{–}ratio^{MNR}\left(97°C\right) &= 1 + 0.0424\left(97\right) = 5.11 \\ \Delta T_{max}\text{–}ratio^{Spert\ I\ D}\left(76°C\right) &= 1 + 0.0424\left(76\right) = 4.22 \end{aligned}$$

and using the average void coefficients, prompt neutron lifetime, and coolant channel

volumes from Table 7-2 the shutdown coefficients for the two cores are (with the prompt neutron lifetime of 56 Fsec for the IAEA HEU 10MW Reactor used for MNR):

$$w^{MNR} = = 7.03\times10^{-3}\, mk/\mu sec$$
$$w^{Spert\,I\,D} = = 14.4\times10^{-3}\, mk/\mu sec$$

These factors plus the power peaking factors and fuel meat volumes are then used to construct the associated scaling factors. These ratios for the MNR HEU RC relative to the Spert I D-core are:

$$\begin{aligned}
&\textit{Subcooling}: && 5.11/4.22 && = 0.83 \rightarrow \textit{lose margin}\\
&\textit{Power Distribution}: && 4.2/2.4 && = 0.57 \rightarrow \textit{lose margin}\\
&\textit{Core Size}: && 9570/5200 && = 1.84 \rightarrow \textit{gain margin}\\
&\textit{Void Feedback}: && (7.03/14.4)^{0.726} && = 0.59 \rightarrow \textit{lose margin}
\end{aligned}$$

As indicated the higher degree of subcooling, the more peaked power distribution, and the weaker void reactivity feedback in MNR (relative to the Spert I D-core) all take away from the safety margin. The larger core size acts in the opposite direction, improving the margin.

Using these scaling parameters the equivalent ΔT_{max} in the Spert I D-core for a MNR ΔT_{max} of 380EC is found to be equal to:

$$\begin{aligned}
\Delta T_{max}^{Spert\,I\,D} &= \Delta T_{max}^{MNR} \times \frac{\Delta T_{max}\text{–}ratio^{Spert\,I\,D}}{\Delta T_{max}\text{–}ratio^{MNR}} \times \frac{PPF^{Spert\,I\,D}}{PPF^{MNR}} \times \frac{V_f^{MNR}}{V_f^{Spert\,I\,D}} \times \left(\frac{w^{MNR}}{w^{Spert\,I\,D}}\right)^m\\
&= 194°C
\end{aligned}$$

This temperature can then be converted to the corresponding asymptotic initial period using the temperature rise curve fit for the Spert I D-12/25 data, *i.e.*,

$$\alpha_o = \frac{1}{m_3}\ln\left(\frac{\Delta T_{max}^{Spert\,I\,D}}{b_{Spert\,I\,D}}\right), \quad m_3 = 0.0114\,sec, \quad b_{Spert\,I\,D} = 70.88°C$$
$$= 88.3\,sec^{-1}$$
$$\tau_o = \frac{1}{\alpha_o} = 11.3\,msec$$

Using the Inhour Equation with the previously used value of the prompt neutron lifetime for MNR and the delayed neutron data in Table 7-1, the corresponding HEU fuel step reactivity insertion limit is:

$$\rho_{limit}^{HEU} = 11.7\,mk \quad (Spert\ I\ D - core\ estimate)$$

This compares to an asymptotic period and limiting reactivity for ΔT_{max} = 380EC in Spert I D-12/25 of 6.8 msec and 15.5 mk.

The scaling factors for MNR relative to the other test cores are included in Table 7-3. The resulting equivalent temperature rises and associated reactivity limits for this example and the same calculations using the other test cores as the reference test core are summarized in Table 7-4.

The spread of the reactivity values in Table 7-4 (~ 3 mk) is an indication of the uncertainty attached to this final result and reflects the remaining variance in the void scaling of Chapter 4. The most conservative estimate of an HEU limit for MNR is therefore:

$$\rho_{limit}^{HEU} = 8.6\,mk \quad (most\ conservative\ estimate)$$

Table 7-4 also includes the results based on a slightly less conservative blistering onset temperature (450EC) and a clad melting onset temperature (562EC) used in the MNR 2002 SAR (Ref. 7-8). A similar spread of limiting reactivity values are found for these safety limits.

Taking the most conservative HEU reactivity limits, an idea of the associated MNR LEU RC limits can be determined by applying the LEU:HEU scaling factor of 1.19 for a step insertion of reactivity (Chapter 6). For example, for the 450EC blistering limit used in Reference 7-8 (400EC is not associated with LEU fuel), the most

conservative LEU reactivity limit estimate is:

$$\rho_{limit}^{LEU} = 11.1\,mk \quad \left(most\,conservative\,estimate\right)$$

A slightly higher limit is applicable given a less conservative estimation of the LEU U_3Si_2-Al blister limit of 515EC (sec. 7.1.1).

7.3.2 Stability Limit in MNR

The stability limit for MNR can be found by taking the previously determined step insertion reactivity limits and crediting the temperature defect associated with the change in conditions from the initial reactivity insertion to onset of chugging.

For illustrative purposes the MNR temperature defect is assumed to be similar to those associated with a 20EC to 97EC temperature change in the test cores. Taking this estimate as 10 mk the stability limits for the MNR RC are found to be:

$$\rho_{stability\,limit}^{HEU} = 18.6\,mk$$
$$\rho_{stability\,limit}^{LEU} = 21.1\,mk$$

7.4 Closing Remarks

7.4.1 Extent of Application

The safety analysis methodology developed herein is based on fresh HEU core step insertion transient data. It is designed for analysis of step insertion transients in MTR-type cores. The methodology explicitly accounts for differences in subcooling, power distribution, core size, void reactivity feedback, and coolant flow in HEU fuel. It is applicable to equilibrium cores *via* proper nuclear characterisation of the core of interest and by suitable choice of irradiated fuel safety limits, and has been extended to both ramp insertion transient situations as well as the LEU fuel cycle

Reactivity limits derived using this methodology have direct application in setting operational limits on minimum shutdown depth and maximum excess reactivity. The former is relevant to fast reactivity insertion situations such as the fuel drop event while the latter is relevant to stability considerations related to slower reactivity

insertions such as in the startup accident event.

As an example, the MNR January 1994 Fuelling Incident (Ref. 7-9) resulted in an estimated 7.87 mk of excess reactivity. This magnitude insertion is below the most conservative HEU limit derived from the test data for onset of blistering in an unprotected situation. In the actual incident the transient was terminated by the trip shutdown mechanism. Generated power (P_{max} = 8.61 MW), energy (E_{tm} = 1.23 MW-sec), and temperature (ΔT_{max} ~ 80EC) were well below the range represented by the test data. The fuelling incident was also a ramp insertion situation which adds a further degree of conservatism to the step insertion comparison above.

7.4.2 Uncertainty and Conservatism in the Analysis

Uncertainties in the final results arise from uncertainties in the test data, curve fitting and those related to the scaling factors based on the system parameters.

The relative approach of the scaling factors is expected to reduce uncertainty given the likely correlated error on the values for the compared cores. This relies on consistent nuclear characterization. The same is true for uncertainties in the subcooling scaling where an over- or under-estimation of the subcooling correction will affect both the numerator and denominator of the subcooling scaling factor. Given consistent nuclear characterization the majority of the uncertainty may be attributed to that remaining in the void reactivity scaling approach.

The overall uncertainty is reflected in the spread of the limiting reactivity values as calculated from the methodology. For the range associated with the fuel damage safety limits (~10 to 15 mk), this uncertainty is on the order of 3 mk (which represents the total spread of the results).

In the absence of more rigorous error propagation analysis, a conservative approach may be adopted. In the example for MNR this was done by selecting the lowest estimate of the limiting reactivity from the range of values calculated from the different test cores. In addition the power peaking factor used for MNR is associated with a fresh LEU fuel assembly whereas the safety limit is based on irradiated HEU fuel.

The analysis is also conservative with respect to forced coolant flow conditions and the application of step limits to real life events in which the reactivity is inserted over a measurable time (a fast ramp).

A final note is with regards to the step/ramp equivalence argument. Further analysis of the test data is recommended to investigate the conservative nature of this approximation. An additional margin may be needed if this is not the case.

7.4.3 Non-RIA Scenarios

Non-RIA scenarios are a class of event required in safety analysis for MTR-type cores. These include flow blockage, and loss of flow accidents. While these scenarios, like RIA's, constitute power/flow or power/cooling mismatch situations, the absence of an initiating reactivity insertion makes them significantly different from RIA's. Relevant characteristics, as identified from the reactor tests are outlined below as are critical differences which must be kept in mind when analysing such events.

In any situation of a power/cooling mismatch certain characteristics will be similar to those found during the reactivity insertion reactor test behaviour. With eroded or removed cooling, fuel will increase in temperature and, if severe enough, increase the temperature of the coolant to the point of boiling. If the power/cooling mismatch is global, *i.e.*, over the entire extent of the core, then the temperature rise of the fuel and coolant will also be global as will boiling, which will also depend on the power density distribution in the core. Voiding will produce a negative reactivity insertion (in all but isolated local situations), inserting negative reactivity into the system. Operation may continue with a certain void volume, depending on the coolant flow conditions, or may develop into hydraulic instabilities, *i.e.*, chugging.

Critical differences between this type of situation and an RIA event is that initially there is no insertion of positive reactivity. Production of void produces negative reactivity as does increases in temperature of the core materials. Even given a positive reflector temperature coefficient of reactivity and any local positive void coefficients, the overall reactivity change due to a global temperature increase and void *via* boiling in the coolant channels, will be negative. In the case of local positive voiding, any generated positive reactivity will only serve to temporarily raise the power until enough negative reactivity from voiding in other parts of the core is created to not only compensate this local positive reactivity but also generate a net negative reactivity from the initial power/cooling mismatch conditions. Any positive reactivity generated from refill of coolant channels in a chugging situation will only result in bringing the core back to a critical multiplication (at most). The result will be a decay of the average power level until a lower equilibrium power level is reached.

In the absence of an initiating positive reactivity insertion, internal temperature gradients within and maximum temperature rises of the fuel are expected to be mild in comparison to the those experienced for short period RIA transients.

Flow blockage represents situations of degraded coolant circulation, the degree of degradation proportional to the degree of the blockage. In these situations a characteristic necessary of consideration is the potentially inhibited refill of voided coolant channels. Voiding will preferentially occur out of the end of the assembly which is not blocked. Pressure generated by coolant voiding may or may not result in clearing of the blockage. Mild examples of flow blockage events have occurred in MNR and have been benign in terms of fuel damage. However, the potential does exist for fuel damage and radiation release within these events. An example of such an event is the Engineering Test Reactor (ETR) blockage accident which occurred in 1961 (Ref. 7-10). In this accident fuel fission breaks resulted from blockage of multiple assemblies by a melted plastic viewing plate unintentionally left in the core. A total of six fuel assemblies experienced melting in one to eight fuel plates. Additionally, post-event examination of the damaged fuel assemblies provided evidence of a partial refill chugging response.

While fuel damage is possible in these situations, the lack of a positive reactivity insertion and the associated large temperature rises in the interior of the fuel plates means that it is unlikely that even a core with extensive blockage will be placed into a degraded state of tensile strength such as that necessary for a core disassembly event. As such, damage may occur but will be limited to local in extent, confined to the blockage areas and limited in magnitude to clad melting. Loss of coolant accidents may share similar characteristics to full blockage situations where refill of coolant channels is completely prevented.

For events such as flow blockage there is an increased onus on detection of such events by mechanical safety systems based on power and rate fluctuations.

In summary, the reactor tests provide general information with respect to system temperature, power, hydraulic and reactivity response relevant to non-RIA scenarios as well as relevant information regarding fuel damage and safety limits. Non-RIA events are however significantly different than RIA situations.

7.5 References

7-1. "Safety Evaluation Report related to the Evaluation of Low-Enriched Uranium Silicide-Aluminum Dispersion Fuel for Use in Non-Power Reactors", U.S. Nuclear Regulatory Commission Technical Report NUREG-1313, July 1988.

7-2. J. M. Beeston, R. R. Hobbins, G. W. Gibson, W. C. Francis, "Development and Irradiation Performance of Uranium Aluminide Fuels in Test Reactors", Nuclear Technology, v.49, June 1980, p.136.

7-3. R. P. Taleyarkhan, "Analysis and Modelling of Fission Product Release from Various Uranium-Aluminum Plate-Type Reactor Fuels", Nuclear Safety, v.33, n.1, pp.6-22, January-March 1992.

7-4. "Aluminum 6061-T6; 6061-T651", Matweb: Material Property Data - Online Material Data Sheet, internet address: http://www.matls.com/, November 11, 2003.

7-5. M. R. Zeissler, "Non-Destructive and Destructive Transient Tests of the Spert I-D, Fully Enriched, Aluminum-Plate-Type Core: Data Summary Report", US AEC Technical Report IDO-16886, Phillips Petroleum Co., November 1963.

7-6. J. J. Duderstadt, L. J. Hamilton, Nuclear Reactor Analysis, John Wiley & Sons, 1976.

7-7. S. E. Day, "MNR Reference Core for SAR", MNR Technical Report MNR-TR-2000-06, Rev. 0, McMaster University, Hamilton, Ontario, Canada, October 3, 2001.

7-8. McMaster Nuclear Reactor Safety Analysis Report, McMaster University, Hamilton, Ontario, Canada, February 2002.

7-9. M. P. Butler, "Final Report on the January 1994 Fuelling Incident", McMaster Nuclear Reactor Technical Report MNR-TR-1997-03, McMaster University, Hamilton, Canada, April 28, 1997.

7-10. F. R. Keller, "Fuel Element Flow Blockage in the Engineering Test Reactor", US AEC Technical Report IDO-16780, Phillips Petroleum Co., May 10, 1962.

7.6 Tables

Table 7-1: Delayed Neutron Data for U-235

Isotope	U-235			
νd	0.01668	+/-	0.0007	delayed neutrons yield = ν β
E	192.9	+/-	0.5	MeV/fission
ν	2.432	+/-	0.066	average neutrons per fission
β	0.00686	+/-	0.00034	

Group	**τ 1/2 (sec)**	**λ (sec-1)**	**βi/β**	**sig(βi/β) +/-**	**βi**
1	54.51	0.01272	0.038	0.004	0.00026
2	21.84	0.03174	0.213	0.007	0.00146
3	6.00	0.116	0.188	0.024	0.00129
4	2.23	0.311	0.407	0.010	0.00279
5	0.496	1.397	0.128	0.012	0.00088
6	0.179	3.872	0.026	0.004	0.00018
Total			1.000		0.00686

Ref. Duderstadt & Hamilton, Nuclear Reactor Analysis, 1976, Fig. 2.20, p.61 & Tab. 2-3, p.64

Table 7-2: Aluminum-Clad Plate-Fuel Core Nuclear Characteristics

HEU Al-Clad Plate Cores	Borax I	Spert I A-17/28	Spert I B-24/32	Spert I B-16/40	Spert I B-12/64	Spert I D-12/25	Spert IV D-12/25	MNR RC-16/28-9/6
Temperature Defect								
20C to 95C (mk)	-8.17	-10.9	-12.4	-11.6	-10.2	N/A	N/A	N/A
Void Coefficient								
Metal/Water Ratio - central	0.687	0.782	1.128	0.635	0.465	0.704	0.703	-
Metal/Water Ratio - std assembly	0.687	0.782	1.128	0.635	0.465	0.525	0.522	0.576
Metal/Water Ratio - core	0.687	0.782	1.128	0.635	0.465	0.629	0.627	-
Average (Uniform)								
(mk/%-void)	-2.4	-1.9	-2.8	-1.8	-1.1	-2.4	-2.3	-2.1
(mk/cc-void)	-3.4E-03	-3.5E-03	-5.1E-03	-2.0E-03	-6.9E-04	-4.6E-03	-4.5E-03	-3.3E-03
(mk/channel)	-0.41	-0.39	-0.36	-0.28	-0.14	-0.87	-0.85	-0.39
Central								
(mk/%-void)	-4.5	-3.9	-6.5	-2.9	0.9	-3.4	-3.1	-4.5
(mk/cc-void)	-6.6E-03	-7.2E-03	-1.2E-02	-3.3E-03	6.0E-04	-6.3E-03	-6.0E-03	-7.1E-03
(mk/channel)	-0.78	-0.80	-0.83	-0.45	0.12	-1.20	-1.14	-0.84
Prompt Neutron Lifetime								
(micro-sec)	65	50	50	70	77	60	57	N/A
Power Peaking Factor								
Overall	2.0	2.0	2.5	2.1	2.2	2.4	2.4	4.2
Dimensions								
Fuel meat thickness (cm)	0.053	0.051	0.051	0.051	0.051	0.051	0.051	0.051
Clad thickness (cm)	0.050	0.051	0.051	0.051	0.051	0.051	0.051	0.038
Fuel surface area (cm2)	4.31E+05	3.55E+05	6.47E+05	5.39E+05	6.47E+05	2.26E+05	2.26E+05	4.00E+05
Fuel meat volume (cc)	1.10E+04	7.57E+03	1.51E+04	1.26E+04	1.51E+04	5.20E+03	5.20E+03	9.57E+03
SA/Vol Ratio	39	47	43	43	43	43	43	42
Volume Coolant/Channel (cc)	119	111	69	136	203	190	190	119

note: fuel surface area and coolant volume are based on active height of the fuel

Table 7-3: Core Parameters and Scaling Factors

Core Parameters relevant for ΔTmax scaling

Shutdown coeff exponent 0.726 +/- 0.063

Subcooling slope, m 0.0424 +/- 0.0071 deg C

Core	Ti (deg C)	Tsat (deg C)	Tsub (deg C)	PPF	Vf (cc)	Cv(avg) (mk/cc)	Vchan (cc)	ℓ (usec)	w (mk/usec)	ΔTmax-ratio
Borax I	28	96	68	2.0	1.10E+04	-3.4E-03	119	65	6.30E-03	3.88
Spert I A-17/28	25	96	71	2.0	7.57E+03	-3.5E-03	111	50	7.75E-03	4.01
Spert I B-24/32	20	96	76	2.5	1.51E+04	-5.1E-03	69	50	7.10E-03	4.22
Spert I B-16/40	20	96	76	2.1	1.26E+04	-2.0E-03	136	70	3.95E-03	4.22
Spert I B-12/64	20	96	76	2.2	1.51E+04	-6.9E-04	203	77	1.83E-03	4.22
Spert I D-12/25	20	96	76	2.4	5.20E+03	-4.6E-03	190	60	1.44E-02	4.22
Spert IV D-12/25	20	96	76	2.4	5.20E+03	-3.3E-03	190	57	1.11E-02	4.22
MNR HEU RC	20	117	97	4.2	9.57E+03	-3.3E-03	119	56	7.03E-03	5.11

note: IAEA HEU 10 MW Core prompt neutron lifetime is used for MNR HEU RFC

note: shutdown void coefficient defined as, w=(-Cv(avg) Vchan / ℓ)

note: subcooling correction is based on ratio of ΔTmax-ratio(Tsub) = 1+m*Tsub, where m is subcooling trend coefficient

Scaling Factors for translating MNR ΔTmax to Test Core ΔTmax

Core	Tsub-factor (1)	PPF-factor (2)	Vf-factor (3)	Void-factor (4)	Product (1)(2)(3)(4)	b3 (ΔTmax v αo)	sig(b3)/b3
Borax I	0.760	0.462	0.872	1.084	0.332	83.10	0.04
Spert I A-17/28	0.784	0.472	1.264	0.932	0.436	69.87	0.15
Spert I B-24/32	0.826	0.590	0.632	0.993	0.306	79.15	0.09
Spert I B-16/40	0.826	0.495	0.759	1.520	0.472	98.57	0.03
Spert I B-12/64	0.826	0.519	0.632	2.657	0.720	117.52	0.06
Spert I D-12/25	0.826	0.566	1.839	0.594	0.510	70.88	0.10
Spert IV D-12/25	0.826	0.554	1.839	0.719	0.605	70.45	0.15

note: fitting coefficient (b3) and uncertainty are from ΔTmax v αo regression analysis using reference fit

Table 7-4: Equivalent Maximum Temperature Rise and Limiting Reactivity (MNR HEU)

ΔTmax v αo exp 0.0114 +/- 0.000359 sec

MNR ΔTmax 380 deg C (Onset of Blistering U3O8-Al conservative estimate)

Test Core	ΔTmax (deg C)	αo (sec-1)	period (msec)	reactivity (mk)
Borax I	126	36.6	27.3	8.8
Spert I A-17/28	166	75.7	13.2	11.0
Spert I B-24/32	116	33.7	29.7	8.6
Spert I B-16/40	179	52.5	19.1	9.7
Spert I B-12/64	274	74.1	13.5	10.9
Spert I D-12/25	194	88.3	11.3	11.7
Spert IV D-12/25	230	103.8	9.6	12.6

MNR ΔTmax 430 deg C (Onset of Blistering MNR SAR 2002)

Test Core	ΔTmax (deg C)	αo (sec-1)	period (msec)	reactivity (mk)
Borax I	143	47.4	21.1	9.4
Spert I A-17/28	187	86.6	11.6	11.6
Spert I B-24/32	132	44.5	22.5	9.3
Spert I B-16/40	203	63.3	15.8	10.3
Spert I B-12/64	310	85.0	11.8	11.5
Spert I D-12/25	219	99.2	10.1	12.3
Spert IV D-12/25	260	114.7	8.7	13.2

MNR ΔTmax 542 deg C (Onset of Clad Melting MNR SAR 2002)

Test Core	ΔTmax (deg C)	αo (sec-1)	period (msec)	reactivity (mk)
Borax I	180	67.7	14.8	10.6
Spert I A-17/28	236	106.9	9.4	12.7
Spert I B-24/32	166	64.8	15.4	10.4
Spert I B-16/40	256	83.6	12.0	11.5
Spert I B-12/64	390	105.3	9.5	12.7
Spert I D-12/25	277	119.5	8.4	13.4
Spert IV D-12/25	328	135.0	7.4	14.3

7.7 Figures

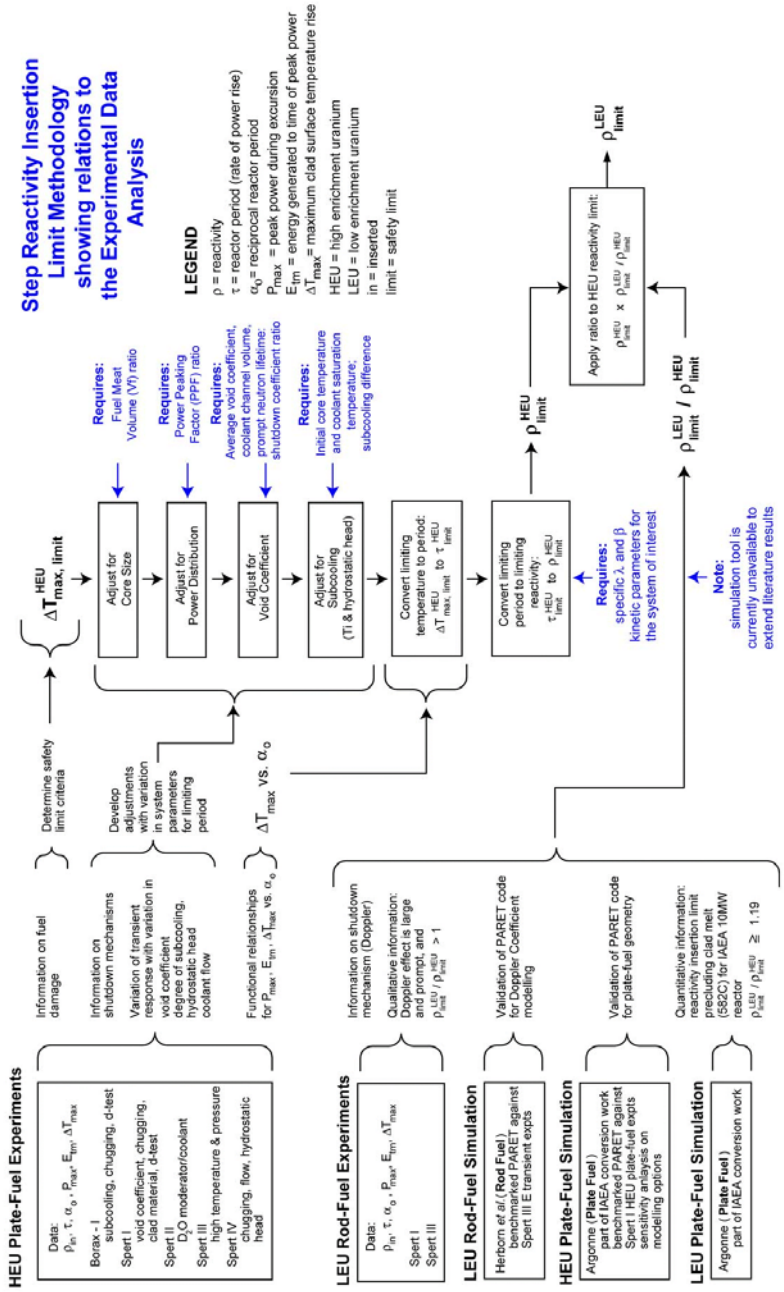

Figure 7-1: The Relation of the Step Insertion Methodology to the Test Data

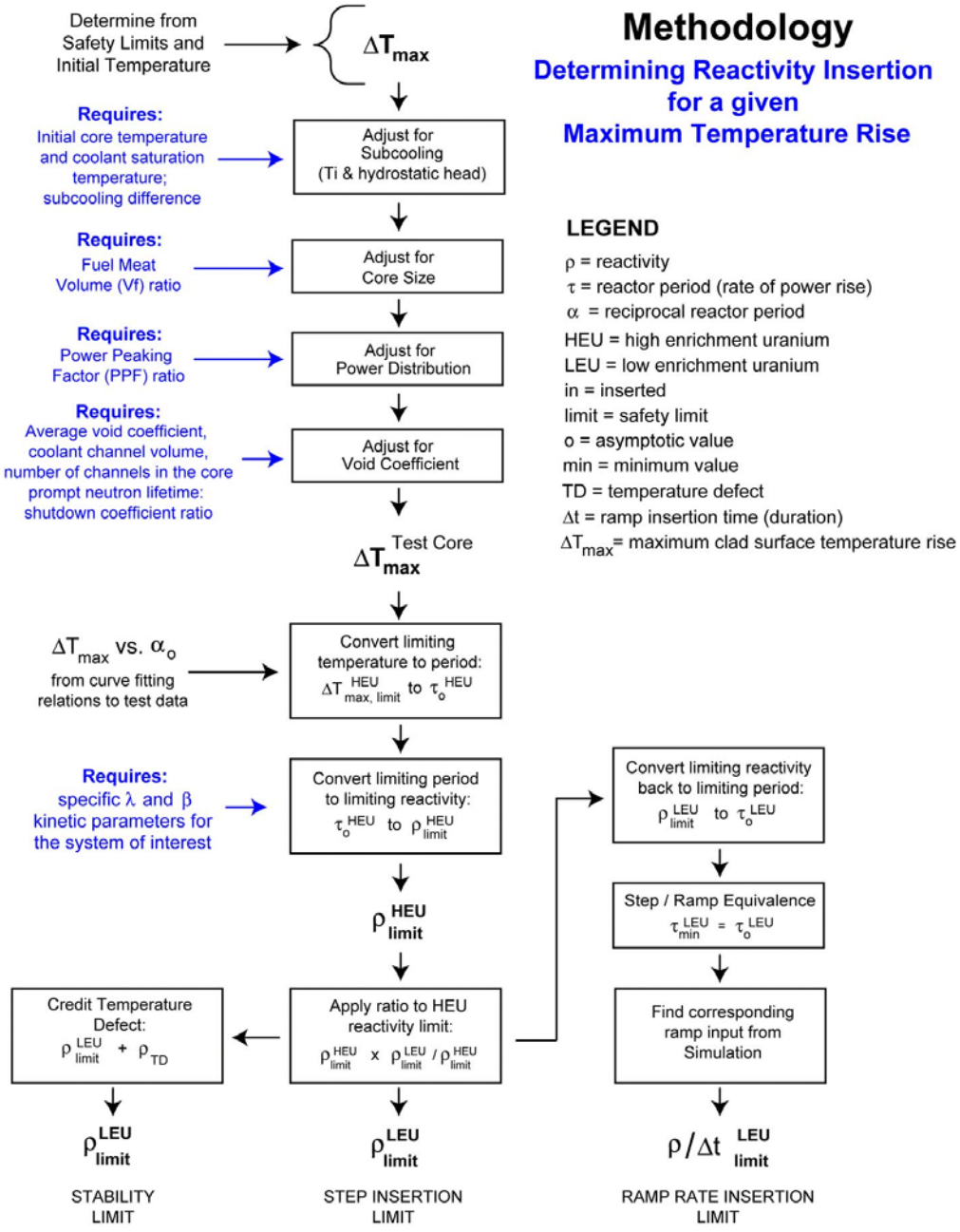

Figure 7-2: Methodology Flowchart for Input Temperature Rise Limit

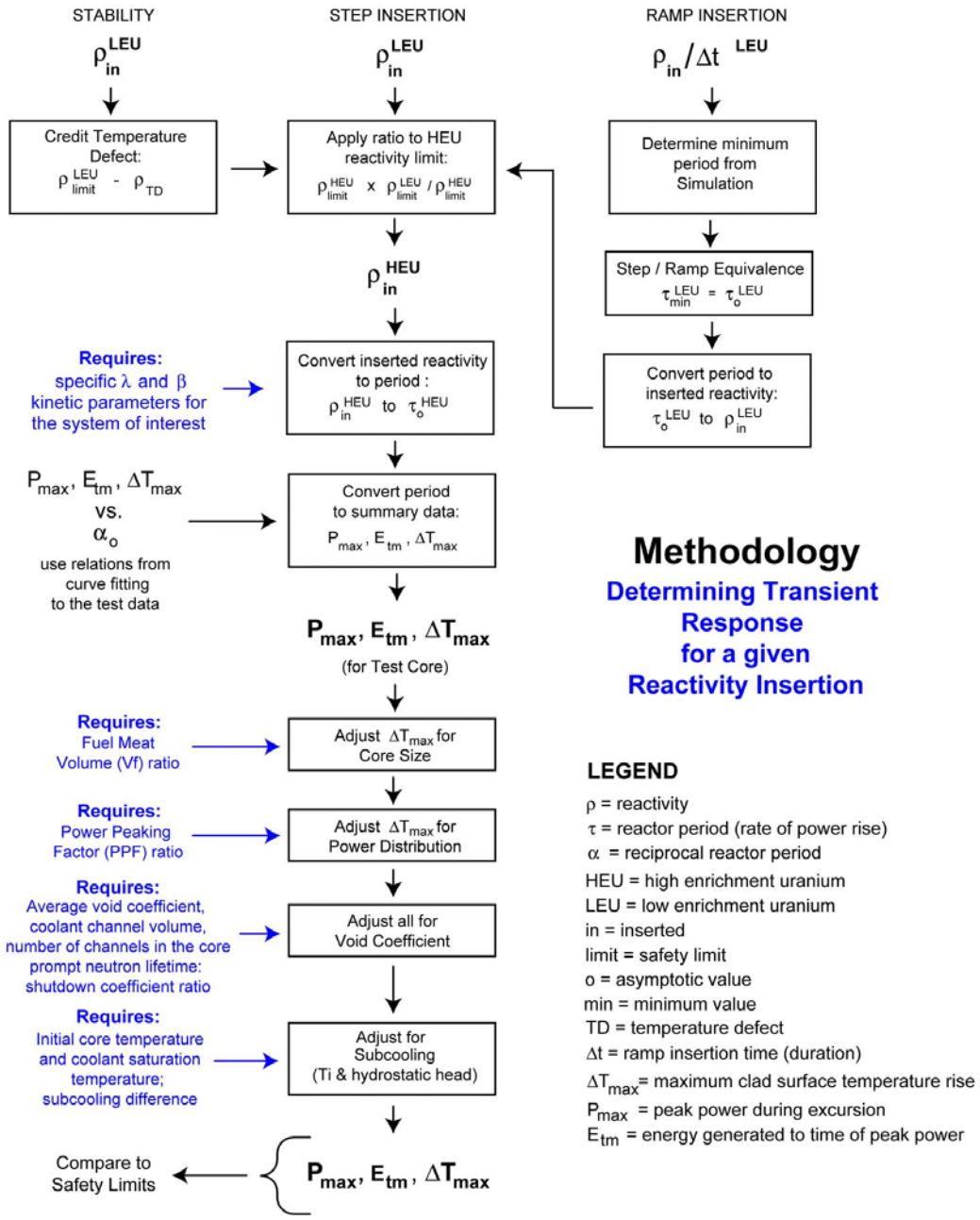

Figure 7-3: Methodology Flowchart for Input Reactivity Insertion

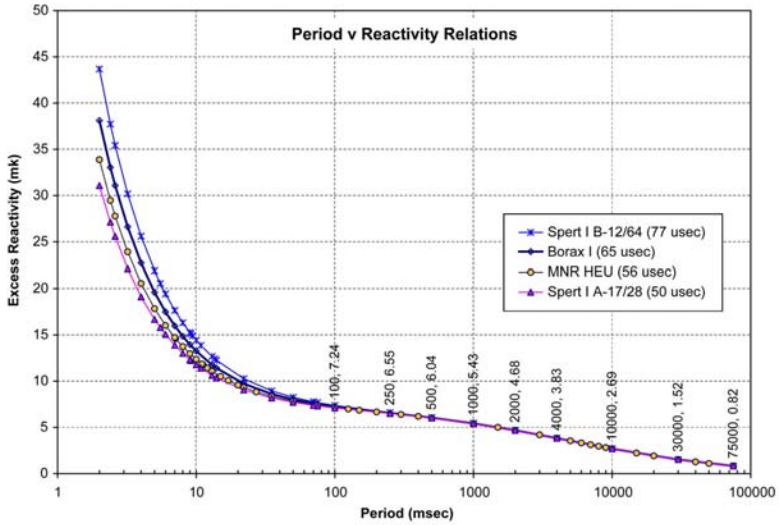

Figure 7-4: Reactivity as a Function of Period for Varying Prompt Neutron Lifetimes

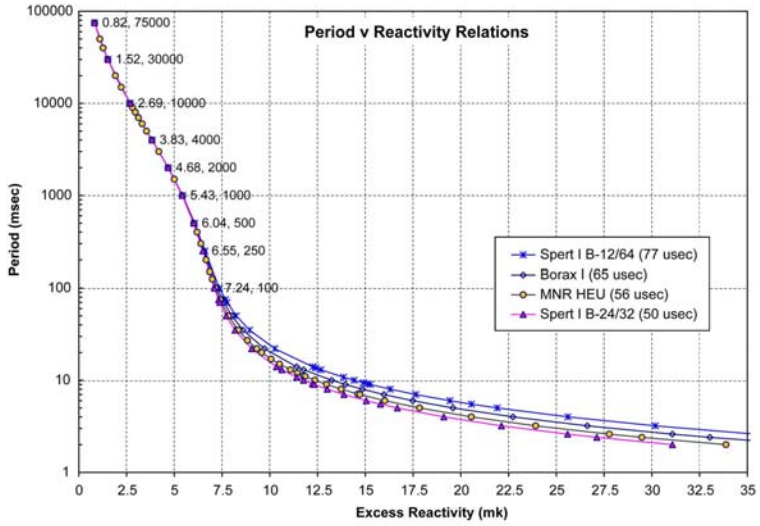

Figure 7-5: Period as a Function of Reactivity for Varying Prompt Neutron Lifetimes

CHAPTER 8 - CONCLUSIONS

TABLE OF CONTENTS

(this page is intentionally left blank)

8 CONCLUSIONS

This chapter contains a summary of conclusions. These take the form of answers to the original objectives of the project, contributions to the knowledge base, and directions for future work.

8.1 Hypothesis/Objective Assessment

The objective of this study has been to assess the experimental data set from the full-scale reactor transient experiments of the Borax and Spert projects to create a working safety analysis methodology for an MTR-type reactor. Specifically two hypotheses were presented in Chapter 1 and are repeated here:

- the existing experimental data set can be interpolated and extrapolated using physical judgement of the self-limiting characteristics of plate-fuel water-moderated reactor systems, to derive reactivity limits precluding the onset of fuel damage in an unprotected accident situation, and
- current kinetic simulation codes, previously benchmarked against experimental transient data for these types of reactors can be used to provide a bridge in the experimental data between different uranium-enrichment fuel, thus making the derived reactivity limits applicable to fuel-cycle converted or converting facilities.

These two hypotheses are assessed with respect to the analysis results in the following sections.

8.1.1 Reactivity Limit Derivation

This study has shown the first hypothesis regarding the idea of deriving reactivity limits from the experimental data to be feasible. Trends in the data have been quantified using rigorous curve fitting, statistics, and error assessment. These data trends coupled with a physical understanding of the processes involved in the self-limiting behaviour of these reactor cores under transient conditions, has allowed for quantification of dependencies in the transient response related to the important system parameters: namely void reactivity feedback, degree of subcooling, core size, and power density distribution. Other system parameters have also been assessed as

either encompassed by these quantities (operating history, reflector materials, hydrostatic head) or of secondary importance (thermal conductivity of the fuel). Initial conditions for a transient have also been examined and conservative use of the data has been outlined (*i.e.*, with respect to coolant flow and initial power). Understanding and quantification of these parametric dependencies allows for generic application of the experimental data.

The quality of the various subsets of the experimental data has been found to vary which dictates the use in, and the approach to, various parts of the parametric analysis. In some cases the data can only be used qualitatively while in others quantitative results can be extracted. Limitations in the data are noted throughout the text of the thesis and particularly in Chapter 3.

Temperature based safety limits have been identified from the fuel damage test data and from supplemental information available in the literature. By examining the fuel damage mechanism the appropriate safety limits have been defined for MTR-type fuel under reactivity initiated accident situations. For an equilibrium MTR-type core, *i.e.*, one with partially burnt fuel, the temperature-based safety limit adopted herein is related to the onset of fuel clad blistering. Other limits for consideration relate to the onset of fuel plate deformation, fuel clad melting, and fuel vapourisation.

The safety limit can be expressed in terms of the limiting size of a step reactivity insertion where this reactivity value can be found by adjusting maximum temperature rise data from the test cores for the various differences in system parameters between the test cores and the system (core) of interest, *e.g.*, considering MNR relative to the test cores. The temperature (and associated power and energy generation) test data are indexed in terms of reciprocal reactor period, *i.e.*, the speed of the transient. Therefore the limiting temperature can be translated to a limiting period which in turn can be translated into a limiting reactivity using standard methods. The accuracy of the method is a function of the uncertainty in the test data and is reflected in the uncertainty estimates on the curve fitting to the experimental data as well as the range of reactivity limit values for the example problem presented in Chapter 7.

The analysis has been used to develop a practical step-by-step methodology for use in safety analysis for a generic MTR-type reactor core. Reactivity limits related to the initial power pulse as well as those related to the longer term stability of a transient have been considered. The physics discussion (see Chapter 2), data collection and assessment (see Chapter 3), analysis details (see Chapters 4, 5, and 6), and the methodology, including an example calculation (see Chapter 7) are included

in the body of this thesis.

8.1.2 LEU Extension Using Simulation

LEU plate-fuel represents a gap in the experimental data set. The second hypothesis, stated above, was geared towards addressing this gap by combining what experimental information that does exist with the use of current industry standard simulation tools (computer programs).

The idea behind the proposed analysis was to simulate reactivity initiated transients with LEU plate-fuel to generate additional data and explore the parametric dependence of this enrichment fuel on related system parameters (***e.g.***, loading, burnup, fuel assembly geometry, ***etc.***). Unfortunately it was found that current simulation tools are limited in their ability to model the stages of these transients after the initial power burst, specifically those involving large scale and complex voiding of the light water coolant.

As a result the LEU-related analysis is limited to an assessment of the Doppler reactivity feedback mechanism as seen in some LEU rod-type oxide fuel transient tests conducted in the Spert Project, and the existing simulation results available in the literature using the PARET code (see Chapter 6). The nature of the LEU fuel response is evident and the conservative nature of the HEU-derived reactivity limits is recognized. A relative treatment of existing simulation results is suggested and an adjustment based on these results is presented as part of the methodology herein. Suggested extensions to this work are presented in Chapter 6. As it stands, the parametric analysis on the size of the Doppler coefficient of reactivity is outstanding.

Progress in this area may depend somewhat on the future availability of simulation codes. Additional possibilities may exist given the relationship of the maximum power rise to the initial power burst data, which can be modelled. Suggestions for future work direction in this area, not restricted to simulation studies, are included in Section 8.3.

8.2 Summary of Contributions

The contributions to the knowledge base of this area of study can be classified into two broad categories: improvements, and novel aspects. These are summarized in the following sections. In addition, significance of the work is outlined.

8.2.1 Improvements

One of the contributions of this work is in the sum of the collected parts. This thesis brings together many of the different pieces which make up the transient behaviour of an MTR-type core under reactivity initiated transient conditions. Some of this represents integration of existing work. Specific improvements in the field are:

- the extensive data collection and assessment (Ch. 3, App. A, App. B),
- the detailed physical explanation of self-limiting behaviour (Ch. 2),
- the error assessment of the experimental data (Ch. 3),
- the identification and treatment of the differences in the power and energy normalisation between the Borax and Spert data (Ch. 3),
- the identification of systematic errors introduced by thermocouple specifics (Ch. 3),
- the curve fitting results and statistics (Ch. 4, App. C),
- the confirmation of some parametric dependencies (Ch. 4), and
- the review of existing analysis (Ch. 4, Ch. 6).

These are described briefly below. Overall, the improvements listed may also be considered a novel aspect of the work given that understanding of the subject may have been improved.

As far as the author knows, this thesis certainly contains the largest single collection of the experimental data. Data subsets, relating to specific parametric dependencies and aspects of the self-limiting response have been collected and are described and assessed.

The detailed treatment of the physics behind the reactor transient response leads to an improved ability to assess and analyse the experimental data and the transient

behaviour of MTR-type cores in general.

The data assessment includes a complete error assessment from uncertainties documented in the literature and additional consideration of the measurement equipment and techniques behind each of the test data series. Differences in the power/energy calibration, thermocouple attachment technique, and thermocouple location are found to be important in comparing the various data sets. These points have been overlooked in previous studies of the test data, and therefore allow for correction of slightly mis-interpreted (or mis-represented) data such as the comparison of Borax and Spert power data and the association of Borax damage observations with a limiting period (for more details see Chapter 3).

The curve fitting analysis represents an improvement in the quantification of the data and can be refined and used in future analysis.

Certain parts of the analysis are not entirely new. The associated references to the literature are indicated throughout the text. In these cases the present analysis serves as a confirmation of previously drawn conclusions, *e.g.*, the coolant flow and the subcooling parametric dependencies. Improvements in these areas come from the consideration of additional test data and the increased detail of the analysis. This can also be said of the LEU extension as incorporated in the SAR methodology. This is based on existing results but the assessment and application of these are thought to be an improvement and advancement of the knowledge base.

8.2.2 Novel Aspects

In addition to the various improvements described in the previous section this work also contributes a number of novel aspects to the study of the self-limiting behaviour of MTR-type reactors. These include:

- an expanded breadth and depth of general understanding,
- the proportionality and scaling of ΔT_{max} with respect to P_{max} and E_{tm} (Ch. 4),
- the parametric dependence on core size and power distribution (Ch. 4),
- the practical model for void reactivity dependence (Ch. 4),
- the longer term stability-based reactivity limit (Ch. 5),
- the application of LEU simulation results and suggested future direction (Ch. 6)

- the construction of practical working SAR methodology for reactivity limits (Ch. 7), and
- the future directions for additional research and development.

Each of these points is discussed briefly below.

This thesis represents new work in terms of the breadth and depth of understanding and analysis of the unprotected transient behaviour of MTR-type reactor cores under reactivity initiated transient conditions. The depth of the data assessment and error analysis appears to be new material as does the collection, assessment, and analysis of the entire data set as a whole.

The phenomenological approach used to detail the physics behind the shutdown mechanisms and the experimental data was not only paramount in this study but is suggested for future analysts. Although some of the points made in this discussion already exist in the literature, advances have been made, mainly in the overall understanding of the relation of the various summary data quantities (*e.g.*, power, energy, and temperature) to the hydraulics and reactivity behaviour of the core.

Also coming from this approach is the derivation of the safety limits based on first principles and an assessment of the fuel damage observations from the transient tests. These safety limits are also assessed with respect to a hypothesized core disassembly mechanism which puts the onset of local fuel damage into the perspective of the maximum hazard associated with an MTR-type reactor (see Chapters 2 and 7).

More specific examples of novel aspects in this work include the identification and quantification of the relationship of the maximum temperature rise generated during a transient to the initial power burst quantities of maximum power and energy generation. This relationship is outlined from first principles based on an understanding of the physics of the situation and is shown by correlations in the data from the various test cores. Involved in this correlation are the system parameters describing core size and the power density distribution. Adjustments associated with these parameters are incorporated into the SAR methodology.

The analysis also includes the development of a practical model for void reactivity dependence. The derived void reactivity shutdown coefficient (channel based) is new and compared to a previously used expression (unit-volume based). It is practical in the sense that the necessary information is measureable on any given MTR-type core using static experiments and/or simulation models (see Chapter 4 and Appendix D).

With respect to the post-power-peak behaviour of an MTR-type core under Reactivity Initiated Accident (RIA) conditions, the chugging/stability analysis contains many new aspects. Firstly the chugging oscillations are treated in a stylized manner which equates each oscillation to an isolated initial power burst. Improved understanding of the mechanisms behind the chugging phenomenon has been developed from an assessment of the experimental data and careful consideration of the various test conditions. This leads to a reactivity balance argument for the associated reactivity limit in which temperature defect and reflector temperature reactivity are contributing factors. Previously no reactivity limit has been associated with the chugging stability issue. This is relevant to any ramp (*i.e.*, slow) insertion event including the common startup accident for MTR-type core safety analysis. More details are given in Chapters 5 and 7.

The analysis with respect to the LEU fuel extension also represents a novel contribution despite the use of existing simulation. The application of these results in the framework of the methodology and the relation to the test data results represents new work.

Additionally the preliminary simulation work regarding parametric variation of the Doppler coefficient with various unit-cell parameters (*i.e.*, fuel loading, plate spacing) and the suggested extensions to the core-based-simulation parametric study are novel contributions (see Chapter 6 and Appendix E).

The presented core disassembly mechanism is of use for interpreting safety limits in relation to the maximum hazard of an MTR-type core, and indicates what system parameters must be considered prior to the selection of a particular temperature related safety limit (*i.e.*, the analyst should determine the internal maximum temperature in relation to the maximum clad temperature for the specific fuel plate material and geometry). Also underlined is the point that dryout (or critical heat flux) should not be necessarily used as a safety limit, certainly not one related to the onset of fuel damage (the test core data show that dryout does not necessarily lead to fuel temperatures associated with onset of fuel damage - see Chapter 2 for more details).

The result of the above improvements and novel aspects of this thesis is the construction of a methodology to use the experimental data to derive safety-based reactivity limits for this kind of reactor. This has been identified (Ref. 8-1) as missing from or under-developed in current safety analysis approaches for research and test reactors.

An example of the usefulness of this process has been the identification of at least one misinterpretation of the test data (Ref. 8-2) and significant extensions to other previous uses of the test data which have incorporated only parts of this work (***e.g.***, Refs. 8-3, 8-4, 8-5, 8-6, 8-7).

8.2.3 Significance

The work herein has indicated the availability and applicability of experimental data for safety analysis in general, also serving as a thorough reference for the full-scale reactor transient tests. This information is a valuable addition to the safety analysis toolbox for MTR-type cores and should be considered to compliment any simulation- or PSA-based approaches.

The study of RIAs is required in research reactor safety analysis. The methodology enables the determination of reactivity limits for both step and ramp insertions of reactivity and complements existing PSA and simulation-based analysis. Importantly, the experimental data analysis is suitable for situations in which simulation tools are limited. The extent of application of the methodology is summarized in Chapter 7.

Reactivity limits derived using this methodology have direct application in setting operational limits on minimum shutdown depth and maximum excess reactivity. The former is relevant to fast reactivity insertion situations such as the fuel drop event while the latter is relevant to stability considerations related to slower reactivity insertions such as in the startup accident event.

The methodology is currently being adopted by MNR and is being reviewed by the Canadian Nuclear Safety Commission.

8.3 Future Work Direction

As is common in any research project, questions and areas for future work have arisen during the course of this thesis. Some of these ideas for future work, including refinements to the existing analysis, are:

- a full uncertainty analysis on the final reactivity limit result,
- additional assessment of the subcooling effect,
- additional parametric studies including plate dimensions,

- revisiting the void coefficient and prompt neutron lifetime data for the test cores,
- investigation of voiding dynamics,
- development of the step/ramp equivalence approach,
- continuation with the investigation into the LEU fuel response, and
- further assessment of mechanical deformation as related to safety limits.

These are discussed briefly below.

The first three listed topics are simply extensions to the presented work. The first suggestion is a full uncertainty analysis on the estimated reactivity limit. Uncertainty analysis has been performed on the separate stages of the methodology and a conservative approach has been adopted throughout. A more rigorous approach to the final reactivity value uncertainty may remove some extra margin introduced by the conservative approximations.

With respect to the subcooling analysis, additional data have been located from the Spert I A-core tests which may prove useful in further study of the period/subcooling separability hypothesis. The analysis as it stands suffers slightly from a lack of test data, although it does appear reasonable. The additional data are available in Reference 8-8. The Spert III C-core subcooling data set should also be added to the extended analysis as should the Spert IV D-core hydrostatic head variation test results.

Additional parametric analysis may be of interest on factors assessed to be of secondary importance to the specific fuel used in the test cores and in typical modern day designs. One example is the fuel plate geometry variation, in particular the thickness of fuel plates. This dependence should be examined with reference to the maximum internal plate temperature, hypothesized to be of importance in the SL-1 accident destructive mechanism.

Refinement of the void reactivity dependence model may prove useful given the remaining variance in the scaled data (see Chapter 4). A starting point may be to revisit the experimentally measured void coefficients and the reported prompt neutron lifetime estimates, both of which are used to estimate the void shutdown coefficient in the model. Further insight into this may come from a study of the void dynamics of an MTR-type core.

A different approach to the study of the subcooling effect may be to consider the subcooling effect as a contribution to a delay time term in the Shutdown Model (see Chapter 4).

Perhaps one of the most useful areas of future work would be in the area of void dynamics, in particular related to the dynamics of water expulsion from the coolant channels, channel refill, and void distribution over the core during the transient. Further information, particularly from experiment would be of use with respect to the following aspects of the analysis:

- confirmation of the assumptions of full channel and entire core voiding in the void shutdown reactivity model,
- refinement of the existing void shutdown reactivity model,
- investigation of the possible dependence of void distribution on power density distribution,
- confirmation of the limiting mechanism (bottleneck) being voiding rather than heat transfer for the self-limiting void production,
- confirmation of the stylized chugging model,
- confirmation of suggested chugging behaviour during forced downward flow circulation,
- determination of chugging channel refill time to assess the conservative nature of the step insertion equivalence, and
- further investigation of temperature drift and stability during chugging.

In addition to the voiding dynamics, any advancement on the topic of transient heat transfer would be extremely useful, for example, in simulation studies.

The extension to ramp insertion transients is outlined but requires further work to quantify the step/ramp equivalence for a generic situation. Free parameters for this study are the reactivity insertion rate as well as the total reactivity to be inserted. The equivalence is based on the asymptotic period for a step transient and the minimum period in a ramp transient. This involves the stage of the transient prior to boiling which is more conducive to simulation techniques. Indications from the test data are that an additional margin may be warranted with respect to the equivalent step for a given ramp insertion of reactivity (see Chapter 3).

The LEU analysis should be extended to include a parametric dependence on the

magnitude of the Doppler feedback coefficient of reactivity. In addition, the LEU:HEU reactivity limit ratio should be considered for other temperature safety limits besides the onset of clad melting, such as the onset of irradiated fuel blistering. These may be investigated using simulation or other analysis approaches.

Additional information relevant to the use of simulation models is the relationship between the peak power and energy to time of peak power data and the post-power-peak maximum temperature generated in the transient.

Not only is relationship between the post-peak maximum temperature and the burst power and energy important to the reactivity limit determination from the data but it also may provide valuable information for future simulation-based studies. Currently simulation tools are limited in their ability to model the post power peak stage of a transient in the cases of large scale coolant voiding. Basing parametric studies on the maximum power and energy generation instead may alleviate this problem (with attention to proper scaling for core size and power density distribution).

Another suggestion for future LEU-fuel analysis related to the Doppler reactivity feedback contribution is to make use of an analytical model as was done with the Shutdown Model for the parametric analysis performed for the void reactivity feedback (see Chapter 4). A similar lumped parameter energy feedback expression for an LEU core may take a form with two separate feedback terms, one representing the delayed feedback effects of coolant density change (voiding), and the other representing the prompt feedback effects (Doppler). This could take a form similar to:

$$\frac{P'(t)}{P(t)} = \alpha_o - w\left[E\left(t-t_d\right)\right]^n - c\left[E\left(t\right)\right]^m$$

where *c* would represent the Doppler shutdown coefficient and *m* is not necessarily equal to *n*. The form of the prompt term has been suggested by Spano (Refs. 8-9, 8-10) in the analytical modelling of the LEU rod-fuel experimental results. An extension to this work on LEU fuel may include a comparison of such an analytical model functional dependence to experimental data and simulation based results. For this work the Spert LEU rod-type oxide fuel tests may provide useful data given that the Doppler feedback was practically isolated from the void feedback characteristic of plate fuel.

Finally, the area of mechanical deformation fuel damage may prove relevant to safety limit definition and the core disassembly mechanism. This type of damage was not incorporated into the methodology.

8.4 References

8-1. Wm. J. Garland, C. Heysel, "McMaster Nuclear Reactor Safety Analysis Methodology Overview", presented at the IAEA Technical Meeting on Safety Analysis for Research Reactors, Vienna, Austria, June 3-7, 2002.

8-2. Safety Analysis Report for the MIT Research Reactor (MITR-II), MITNE-115, October 1970.

8-3. Ford Nuclear Reactor - Description and Operation, Michigan Memorial Phoenix Project, University of Michigan, June 1957.

8-4. Safety Analysis, Ford Nuclear Reactor, Michigan Memorial Project, University of Michigan, Docket 50-2, License R-28, 1984.

8-5. Safety Analysis Report for the MIT Research Reactor (MITR-II), MITNE-115, October 1970.

8-6. Safety Analysis Report for the MIT Research Reactor, draft version of Chapter 13, *circa* November 2002.

8-7. McMaster Nuclear Reactor Safety Analysis Report, McMaster University, Hamilton, Ontario, Canada, February 2002.

8-8. W. E. Nyer, S. G. Forbes, "SPERT I Reactor Safety Studies", Paper P/2428, Proceedings of the Second United Nations International Conference on the Peaceful Uses of Atomic Energy, v.11, pp.470-480, Geneva, September 1958.

8-9. A. H. Spano, "Self-Limiting Power Excursion Tests of a Water-Moderated Low-Enrichment UO_2 Core", Nuclear Science and Engineering, v.15, 1963, pp.37-51.

8-10. A. H. Spano, "Analysis of Doppler-Limited Power Excursions in a Water-Moderated Oxide Core", Nuclear Science and Engineering, v.19, n.2, 1964, pp.172-186.

(this page is intentionally left blank)

APPENDIX A - DESCRIPTION OF THE SYSTEMS

TABLE OF CONTENTS

LIST OF TABLES

LIST OF FIGURES

A DESCRIPTION OF THE SYSTEMS

This appendix presents a brief description of each test reactor system. The technical specifications of the different fuel-types and core arrangements, along with core coordinate systems for referencing the location of instrumentation are included. The nuclear parameters of each core arrangement are also summarized. Additional detail can be found in the cited references.

Prior to the commencement of transient testing, each test core was characterised by a series of static and checkout tests. These included measuring the control and transient rod worth, the flux distribution and the temperature and void coefficients of reactivity.

The period method was typically used in conjunction with a soluble poison for rod calibration. Gold foils were commonly used for thermal flux distribution measurement. The temperature coefficient was typically measured by uniformly heating the reactor while the void coefficient was measured using simulated voids made of most commonly aluminum but also magnesium strips. Other nuclear parameters, such as the neutron lifetime and delayed neutron fraction were either derived from the transient data or calculated from simulation.

The specifics of these experiments are found in the cited references listed in the descriptions of each reactor.

A.1 Aluminum-Clad Plate Cores

A.1.1 Borax I

The Borax Project was conducted at the National Reactor Testing Station (NRTS) in Idaho (Fig. A-1) in the 1950s by Argonne National Laboratory (ANL). Borax I was the first of four Borax reactors. The facility was built partially underground so as to provide external support for the shield tank and extra shielding during the experiments (Figs. A-2, A-3). A vertical schematic of the Borax I facility is shown in Figure A-4.

The core was contained in a reactor tank within a larger shield tank and could be operated with an open top or closed and under pressurized conditions. The tests considered herein were conducted in the open top configuration with a hydrostatic

head of three to four-and-a-half feet above the top of the reactor core. There were no provisions for forced coolant circulation and as such all tests were performed with natural circulation coolant flow.

The core consisted mainly of standard fuel assemblies but also included a special instrumented fuel assembly of slightly different design. Each standard fuel assembly consisted of 18 curved plates, shown in Figure A-5. These comprised most of the fuel in the core. In each core loading a special instrumented assembly (Fig. A-6) was included. The design varied slightly from the standard fuel in that the plates were flat and removable and the assembly only contained 15 plates. The plate and fuel meat dimensions remained the same as did the coolant water gap relative to the standard fuel design. The instrumented fuel assembly used standard plate loading for the 1953 tests but for the 1954 tests a 20% more highly loaded fuel plate was used in the plate number four position. A third type of fuel assembly was incorporated in the 1954 tests. This assembly contained 10 plates rather than the standard 18 plates.

The fuel assemblies were supported by a six by six aluminum grid plate. Control was maintained by a set of four control blades, which inserted in a cross arrangement between rows of the fuel assemblies effectively dividing the core into quadrants, and a central transient rod, which was varied between a flat and cruciform style. The control rods were raised out of the core to bring the reactor to power and the transient rod was driven out of the bottom of the core to initiate a transient. The spring loaded transient rod could be completely ejected in less than 0.25 seconds (Ref. A-1).

The core loading varied between 26 and 32 fuel assemblies during the 1953-1954 test program. The instrumented fuel assembly occupied position 21 in the grid plate, which is the measured “hot assembly” as indicated by the flux wire results, for the majority of the transient tests but was moved to a lower power density location (position 26) for the 1954 destructive testing. These loading patterns along with the location of the instrumented fuel assembly and the instrumented plates within the assembly for which data are reported are shown in Figure A-7. Fuel and core specifications are given in detail in References A-1 and A-2 and summarized in Table A-1.

Power measurements were from out-of-core ion chambers. Temperature measurements were from both interior-type and spot-welded surface thermocouples. Two plates at a time in the special assembly were instrumented with two thermocouples on each plate, located approximately on the axial centerline of the active fuel. Only three of the four thermocouple readings were recorded for a given

transient due to limits on the number of recording channels. The plate numbering, used to locate thermocouples is shown in Figure A-8. The assembly orientation is shown in Figure A-7 from which the individual plate location can be deduced. A summary of the instrumentation for the Borax core is given in Table A-2.

The Borax I core was characterized *via* a series of static tests. Flux mapping measurements used gold foils at low power in the 26-assembly critical loading and cobalt foils during steady state operation (about 600 kW) in the 28-assembly core loading pattern (see Fig. A-7). No local power peaking values are reported for variation of the power distribution over the different plates of an assembly. Rod worth and the temperature coefficient of reactivity were measured while reactivity changes for a uniform distributions of void were calculated. A summary of the Borax I nuclear characteristics is given in Table A-3. Further details on instrumentation and nuclear characterisation are available in Reference A-1.

A.1.2 Spert I A

The Spert I facility was similar to the Borax I facility in many respects. Like Borax, Spert was also located at the NRTS (Fig. A-1). The facility remained the same for the testing of the various cores with the exception of altering the core support structure, rod drives, the height of the reactor tank and the core itself.

Spert I was a light water tank system, shown pictorially in Figure A-9 and as an elevation cutaway in Figure A-10. The facility was housed in an open building (Fig. A-11) and operated remotely from ½ a mile away (Fig. A-12). The core was contained in a four foot inner diameter by 10.5 foot high reactor tank of light water, open to the atmosphere, which in turn was contained in a larger shield (pit) tank. The core was located and supported by an aluminum grid structure with a top "hold down" plate to keep the assemblies in place. There were no provisions for pressurization, forced coolant flow, or heat removal.

The A-core, designated A-17/28, was the first core tested in Spert I. It was comprised of 28 standard Type-A fuel assemblies in a symmetrical approximate cylindrical configuration (Fig. A-13). The Type-A fuel (Fig. A-14) was similar to the Borax I fuel in that it was aluminum-clad, plate-type rectangular style, but differed in that each assembly contained 17 straight plates, reinforced by two plate stiffeners running the length of the fuel assembly and dividing each plate into three "sub-plates." As well, the loading of the Type-A fuel was heavier than the standard Borax I fuel. Disregarding the plate stiffeners, the Type-A fuel plates were almost identical

in dimension to the Borax I fuel plates, as was the coolant channel thickness. The fuel plates were brazed, *i.e.*, permanently fixed, into the aluminum side-plates except for the outer two plates on selected assemblies to allow removal and instrumentation.

The core was controlled by a set of gang-operated cadmium control blades, travelling inside a guide space dividing the core into quadrants, again, similar to the arrangement in the Borax I reactor. The control blades were raised out of the core to bring the system to critical. An air- and motor-driven transient blade was located in the geometrical centre of the core and ejected out of the bottom of the core to initiate a transient. Travel time for the transient rod was on the order of 100 msec (Ref. A-3). More detailed descriptions of the Spert I facility, A-core and Type-A fuel are given in References A-3 and A-4. Technical specifications are summarized in Table A-1.

For Spert I A power measurements were from out-of-core ion chambers, much like those used in the Borax I facility. Temperature measurements were from peened thermocouples. The fuel-plate thermocouple position is indicated by a numbering scheme for the assemblies, fuel plates, and vertical position shown in Figure A-15. The removable/instrumented plates were the middle sub-plates of the outer plates of an assembly corresponding to position 012 and 172. Three to six thermocouples were attached to a given plate at various vertical positions. Up to 24 thermocouples were included in the Spert I A core for a given transient test. A summary of the Spert I A-core instrumentation is included in Table A-2. More information on instrumentation for the Spert facility and in particular the A-core can be found in References A-5 and A-6.

The Spert I A core was characterised *via* a series of experiments, reported in References A-4, A-7, A-8, and A-9. A summary of the Spert I A-core nuclear characteristics is given in Table A-1.

A.1.3 Spert I B

Following the conclusion of the A-core tests, the B-cores were installed in the Spert I facility. The B-cores used the same reactor structure as used for the A-core, *i.e.*, grid plate and rod guides, with only minor modifications, including removal of the upper hold-down grid in favour of a bottom locking mechanism for the assemblies (Ref. A-10). Apart from this, the facility was as described in the previous section.

The Type-B fuel (Fig. A-16) was similar to the previously used Borax and Spert

Type-A fuel in that the fuel and plate dimensions, materials and enrichment were practically identical. Characteristics of note of the Type-B fuel are a nominal loading of 7.0 g U-235/plate (lighter than the Borax and Type-A fuel), and that all but four of the plates were removable allowing for instrumentation. Four plates were brazed into the aluminum side plates and the assembly had space for 20 more removable fuel plates. In addition, the plate stiffeners, used in the Type-A fuel were not included in the Type-B design.

The ability to remove fuel plates allowed for the construction of cores with varying number of fuel plates per assembly, and consequently varying size of the coolant channels. Three different B-cores were studied, the B-24/32, B-16/40, and B-12/64 configurations. The 24- and 12-plate assemblies had uniform coolant channel spacing but the 16-plate assemblies had alternate wide and thin coolant channels due to the position of the four fixed plates (Fig. A-17). All of the cores were assembled in an approximate cylindrical pattern and are shown in Figure A-18. The assembly orientation in the cores was uniform with the fuel plates running from east to west. The varying fuel plate spacing facilitated one of the primary objectives of the B-core tests which was to investigate the effect of varying void reactivity characteristics on the transient behaviour of such cores. The Type-B fuel and B-core technical specifications are summarized in Table A-1 and in References A-10 and A-11.

The B-cores were characterised in the same manner as the Spert I A-core, using the standard static tests. Gold flux wires were used to measure the flux distribution, the temperature coefficient of reactivity was measured for uniform heating of the core and reflector, and the void coefficient was measuring using simulated voids; aluminum and lead strips in the B-24/32 core, aluminum strips in the B-16/40 core, and styrofoam in the B-12/64 core. The central void coefficient of the "watery" B-12/64 core was found to be slightly positive. The reader should also note that results from void simulation on the B-12/64 core using magnesium strips were found to be in error (Ref. A-12). Also of note is that both experiment and calculation have shown that the temperature defect of the reflector is positive (Refs. A-13, A-14), in contrast with that of the core only. The static tests measured a combination of these two effects. The static test results are reported in References A-7, A-10, A-11, A-12, and A-13. A summary of the Spert I B-core nuclear characteristics is given in Table A-3.

Various instrument upgrades were made upon conclusion of the Spert I A-core tests for use with the B-cores (Ref. A-10). However, the measurement methods and instrumentation essentially remained the same as that used in the A-core testing (*i.e.*,

out-of-core ion chambers and peened thermocouples). Spert I B-core instrumentation is summarized in Table A-2. The coordinate system for locating the thermocouples is shown in Figure A-19. The nomenclature is such that the assembly position, plate number, side of the plate and vertical position relative to the axial centerline of the active fuel is indicated. For example, 55 01B +3 indicates a position on the assembly in grid position 55, on the South (B) side of plate 01 (plates are numbered north to south), three inches above the centerline of the fuel.

A.1.4 Spert I D

Following completion of testing on the LEU oxide core, the D-core was installed in Spert I. First criticality was in March of 1962 and testing continued until the final destructive test on November 5, 1962. The facility was modified to accommodate the plate-fuel D-core but this only constituted changes to the support structure and rod drives.

The D-core, designated D-12/25, was composed of 25 fuel assemblies (20 standard and five control fuel) in a rectangular five by five array (Fig. A-20). The standard fuel (Fig. A-21) contained 12 removable fuel plates per assembly. The dimensions of the Type-D fuel plates and the outer dimensions of the Type-D assembly were similar to the Borax and Spert types A and B fuels. The main differences between the Type-D and previously used aluminum-clad fuels were the coolant channel size due to the number of plates and the higher loading of the Type-D fuel. Also of note is that the outer coolant channels on the Type-D fuel were reduced in thickness due to the presence of the outer aluminum can on the assembly.

Four gang-operated boron-alloy double-blade control rods, located symmetrically on the core periphery and the same style transient rod, located in the centre of the core, were accommodated in modified six-plate fuel assemblies (Fig. A-22).

Specifications for the Type-D fuel and the D-core are summarized in Table A-1 and available in References A-15, A-16, A-17, and A-18.

Nuclear characterisation of the D-core was accomplished *via* the standard set of static and kinetic tests. These are described in detail in References A-15, A-16, and A-19, and the results are summarized in Table A-3.

The D-core was instrumented in much the same fashion as previous Spert I cores. Additional instrumentation, to provide a higher degree of redundancy and coverage

for aspects of the planned destructive testing, was added to the D-core. Specifically, in addition to the standard out-of-core ion chambers, power was measured by three in-core miniature ion-chambers and in-core Cobalt wires. Both surface and buried thermocouples were installed to measure the fuel plate temperature. The surface thermocouples were multiple-junction style, spot welded to the plate surfaces. The buried thermocouples were peened into the fuel meat to a depth of 0.076 cm from the plate surface (the cladding and meat thickness of the Type-D fuel were each 0.051 cm). Thermocouple location is specified as indicated in Figure A-20 by designating the assembly grid position, plate number from east to west, the east or west side of the plate and the axial distance in inches from the axial centerline of the fuel region. Buried thermocouples are indicated by a letter "B" in the data table. For the Destructive Test Series, fuel capsule thermocouples were also used. The core was also instrumented with pressure gages, flow metres, strain gages, accelerometers, air pressure sensors, photographic equipment, and radiation measurement equipment. The instrumentation of the D-core is described in detail in References A-15, A-16, and A-17 and is summarized in Table A-2.

A.1.5 Spert IV D

The final aluminum plate-type core studied as part of the Spert Project was the Spert IV D-12/25 core. This core was almost identical to that used in the Spert I facility save for a different control fuel/rod arrangement. Conditions for the tests were also changed from those of Spert I in that a larger hydrostatic head and forced flow were available.

The Spert IV facility was a pool type system with provisions both for forced coolant flow up to 5000 gpm and 1 MW-capacity heat removal. Like all other Spert reactors, Spert IV was designed to be operated and controlled remotely from about ½-mile away (Fig. A-12).

The pool structure consisted of two 20-ft-diameter by 25-ft-deep tanks, connected by a 6-ft by 6-ft gate at the top of the tanks (Fig. A-23). The core was operated in the north pool which contained the coolant flow inlet, and was suspended from a bridge which spanned the pool and could be moved on rails the entire length of both pools.

The D-12/25 core was the first core installed in Spert IV. It was composed of 25 fuel assemblies in a square five by five section of the nine by nine supporting grid (Fig. A-24). Apart from the positions of the four control rods (which were moved to more central grid positions), the D-core was identical to the D-12/25 core used in the

destructive test series in Spert I. This core and the Type-D fuel, control, and transient rods have been described previously. A flow skirt was added to the core structure to direct the coolant flow through the core. The Spert IV D-core and components are described in References A-20 and A-21 and technical specifications are summarized in Table A-1.

As done for previous Spert cores, the Spert IV D-core was characterised by a series of static tests and preliminary kinetic tests. The tests and their results are summarized in Reference A-21 and also reported in References A-19, A-22, and A-23. A summary of the Spert IV D-core nuclear characteristics is given in Table A-3.

Thermocouple location is specified by the same nomenclature as used in the Spert I D-core with the plate coordinate indicating either the plate to which the thermocouple was welded or the plate adjacent to the coolant channel containing the thermocouple. Coolant channel thermocouples were placed in the assemblies in grid positions E3 and E6 at various vertical positions. Instrumentation for the Spert IV D-core is described in References A-23 and A-24 and is summarized in Table A-2.

A.2 Stainless-Steel-Clad Plate Cores

A.2.1 Spert I P

The Spert I P-18/19 core, also referred to as the Army Package Power Reactor or APPR core (October 1958 to August 1959) was the first stainless-steel core tested in the Spert Project. Compared to the A- and B-cores it was a more highly under-moderated core characterized by a smaller negative moderator temperature coefficient of reactivity and a larger negative void coefficient of reactivity.

Minor modifications were made to the Spert I facility on the changeover from the B-cores to the P-core (Refs. A-8, A-12). The main modification was that concerned with switching from blade-type control rods to control-fuel assemblies. The transient rod was initially aluminum-clad cadmium but was altered to Boron-10 doped stainless steel to provide sufficient reactivity.

A cutaway picture of the Spert I facility housing the P-core is shown in Figure A-25 and the core configuration is shown in Figure A-26. The stainless-steel clad fuel (Fig. A-27) contained 18-plates per assembly and despite the difference in cladding material is similar in geometry to the aluminum-clad fuel used in Borax and the

previous Spert I cores, with the exception that the cladding itself on the fuel plates was thinner than the aluminum-clad fuels. The loading of the Type-P fuel was significantly higher than the aluminum-clad fuel and in fact was the highest loading stainless-steel plate-fuel used in the Spert Project. Technical specifications for the P-core and Type-P fuel are given in Table A-4.

Ion-chambers and other out-of-core instrumentation presumably stayed the same as that used in the B-core test series. All power data reported in the main data summary (Ref. A-25) for the P-core tests were taken from the ion chambers connected to linear amplifies as opposed to logarithmic amplifiers. The P-core 0.010" diameter chromel-alumel thermocouples were spot welded to the outer cladding surface of the two outer fuel plates (numbers 1 and 18) of selected fuel assemblies. The thermocouple location is noted according to the P-core coordinate system shown in Figure A-28. The P-core instrumentation is summarized in Table A-2. More information is available in References A-13, A-25, and A-26.

Nuclear characterisation of the P-core was similar to that for the Al-clad plate cores. Static test results on the P-core are reported in References A-8, A-9, and A-27.

A.2.2 Spert I BSR-II

The Bulk Shielding Reactor II (BSR-II) core was loaned to the Spert Project from Oak Ridge National Laboratory (ORNL) for testing from October 1959 to April 1960. The core was designed for experimental purposes at ORNL in the area of shielding development.

Installation in Spert I was almost identical to that at ORNL except for modification of the central and two of the adjacent assemblies to accommodate the Spert I transient rod (Ref. A-28). The core loading pattern consisted of 25 assemblies and is shown in Figure A-29. Two slightly different core loadings were used with the BSR-II fuel. The first is shown in Figure A-29 and is referred to as the “6068 g U-235 loading”, in which the four corner assemblies were only ¼ loaded compared to the standard fuel. The second loading, the “6140 g U-235 loading” also contained 25 assemblies with one of the quarter-loaded assemblies replaced with an assembly with half the loading of the standard fuel. This makes little difference to the static and transient testing. The reader should take note of the difference in plate orientation between the three central assemblies and the rest of the core (indicated by the lines within the assemblies in Figure A-29).

The BSR-II fuel (shown in Figure A-30) was stainless steel with each fuel assembly containing 20 plates. The fuel meat was thinner and the active height was shorter than the previously used aluminum-clad and Type-P stainless-steel clad fuels. Like the Type-P fuel, the cladding was also thinner than the aluminum-clad fuels. The loading of the BSR-II fuel was about half of that of the Type-P fuel. Two assemblies, in positions 32 and 34 (Fig. A-29), adjacent to the central position, were modified by having two plates removed in each to make room for the transient rod. The control fuel assemblies also contained 20 plates but of a reduced width to accommodate the absorbers. The absorbers themselves were fork style and included fuel follower sections so that when the absorber was removed from the core fuel plates filled the control slots. The BSR-II core and fuel technical specifications are summarized in Table A-4 and described in References A-28, and A-29. Static test results for the BSR-II core are reported in References A-28, A-29, and A-30.

Information regarding the transient instrumentation for the BSR-II core is limited but there is no reason to believe that the out-of-core instrumentation, other than the addition of the BSR-II control system, differed from that used for the previous B-cores and P-core. Chromel-alumel thermocouples were resistance welded (like those on the Type-P fuel) to the fuel plate surfaces (Ref. A-28). No plate coordinate system is given for the BSR-II core to describe the thermocouple locations.

A.2.3 Spert III C

The Spert III facility was constructed primarily to provide transient testing capabilities under elevated pressure, temperature, and forced flow conditions typical of Pressurized Water Reactor (PWR) systems. Spert III consisted of a four foot diameter by 19 foot high reactor vessel inside a pressurizing tank (Fig. A-31), designed for operation up to pressures of 2500 psig and bulk coolant temperatures up to about 350EC, and able to accommodate cores of various shapes and sizes. Two primary coolant loops and a secondary system provided primary coolant flow up to 20,000 gpm and heat removal capabilities for short term (around 30 minutes) operation at 60 MW.

The C-core was the first core loaded into Spert III. First criticality was on December 18, 1958 (Ref. A- 27). The Type-C fuel was stainless-steel, rectangular plate-type, with each standard fuel assembly, referred to as Type-1S, contained 19 fuel plates (Fig. A-32). The fuel plate dimensions were similar to the Type-P fuel used in Spert I except for an axial height almost double the Type-P fuel and the inclusion of a plate-stiffener, similar to that used in the Type-A fuel, which divided each plate into

two sub-plates. The per-plate U-235 loading was higher than the BSR-II fuel but not as heavy as the Type-P fuel. The four central fuel assemblies (referred to as Type-2S) were modified to a slightly smaller size to accommodate the central cruciform transient rod. Control was *via* eight fuel-style control assemblies, connected in pairs to the drive mechanisms. Each control fuel assembly was composed of a top poison section of a hollow-box design and a bottom fuel section similar to the standard fuel assemblies but of slightly lighter U-235 loading. Each pair of assemblies constituted a "rod" (Fig. A-33).

The operational loading contained 52 assemblies; 40 Type-1S, four Type-2S, and eight control-fuel) configured symmetrically into quadrants (Fig. A-34). The assembly orientation was consistent over but varied between quadrants as shown in the figure. The remainder of the lattice positions housed stainless-steel "filler" pieces. The Spert III Facility and C-core are described in detail in References A-31, and A-32 and summarized in Table A-4. The reader should note that specifications published prior to Reference A-31 are based on design data and may not represent the facility as built.

Instrumentation used in Spert III was similar to that previously used in the Borax I and Spert I facilities. Transient power measurements were from a series of out-of-core ion chambers and pressure measurements were from transducers located around the core and in the end boxes on the bottoms of the fuel assemblies. The temperature of the tank water was measured by thermocouples above the core and embedded in the reactor vessel wall.

Two types of thermocouples were attached to the fuel plate surfaces by spot (resistance) welding. The 0.005" diameter chromel-alumel thermocouples, standard by this stage of the Spert Project for testing of the Al-clad fuel, were found to have problems holding up under the high temperature and forced flow conditions under which some of the testing was conducted (Ref. A-33). As a result, stainless-steel-sheathed thermocouples were used for some test series in conjunction with the original thermocouples. On average about 24 thermocouples were in the core for a given test. The thermocouple location is specified by the core coordinate system shown in Figure A-34 and the assembly coordinate system shown in Figure A-35 where the lowest numbered plate is nearest the interior of the core (note: this is quadrant dependent due to the plate orientation). The Spert III C-core instrumentation is described in more detail in Reference A-32 and summarized in Table A-2.

The Spert III C-core was characterised through a series of standard experiments as done for previous cores. These are summarized and the results are reported in References A-32, and A-34, and originally reported in a series of quarterly reports (Refs. A-13, A-27, A-29, A-35, A-36) and a report on the nuclear startup of the facility (Ref. A-37).

A.3 LEU Oxide Rod Cores

A total of four low enrichment cores were involved in testing as part of the Spert Project. All of these cores were composed of LEU oxide stainless-steel clad rod-type fuel. Three of the four LEU cores were tested to investigate the self-limiting behaviour of LEU fuel. These are described in the following sections.

The fourth, the Capsule Driver Core (CDC) was installed in both the Spert I (the last core in Spert I) and Spert IV facilities as part of the subassembly test program. The main purpose of the CDC core test program was to test fuel samples with the rod-type LEU core used as a driver. Test data from the CDC (in both Spert I and Spert IV) lend information to fuel behaviour and shutdown mechanisms but the nature of the tests was designed to operate the core within previously established transient ranges (the concept of a “driver” core) so these tests contribute little to the data set on core response. The CDC core is not considered further in this report.

A.3.1 Spert I SA & OC

Two cores were studied as part of the Spert I Oxide-Core Experimental Program investigating water-moderated, heterogeneous, slightly-enriched oxide cores relating to power reactors. Although comprising two separate installations, these two cores were almost identical and therefore it is convenient to consider them together.

The fuel rods (or pins) used in the Spert I oxide cores were originally used in the Babcock & Wilcox N.S. Savannah Critical Assembly. Each rod was a roughly 72 cm (six foot) long stainless steel welded-seam tube of half-inch outer diameter. The fuel material was 4% enriched UO_2 powder, compressed to 85% of the maximum density. In terms of research reactor fuel cycles, this enrichment fuel is more properly referred to as Slightly Enriched Uranium (SEU) rather than LEU which is more typically on the order of 20% enrichment. The fuel rods were assembled in a grid with a lattice pitch (centre-to-centre distance) of 1.68 cm. Fuel specifications are summarized in Table A-5 and can be found in References A-38 and A-39.

The SA configuration (often referred to simply as the "oxide core" in the technical reports as it was the first LEU oxide core tested in the Spert Project) was installed in Spert I following the conclusion of the testing on the BSR-II core. It was tested from February to October 1961. Critical loading was estimated to occur with 500 fuel rods (SA-500 loading). Additional rods were added to provide the desired excess reactivity for the transient tests with the transients tests conducted on the SA-592 loading. During the short period testing, fuel rod bowing was observed, producing a positive reactivity effect. As a result, a constraining grid, located near the axial flux peak, was added to the core to limit the rod movement. The same loading pattern was maintained and the self-limited response of the system was affected as predicted. The presence of the grid was also found to influence some of the static parameters of the system. The core with and without the constraining grid is referred to as the "unconstrained" and "constrained" cores and can be designated as SA-592 and SA-592C respectively.

A top view of the SA-core is shown in Figure A-36 and a quarter section of the SA-592 loading pattern is shown in Figure A-37. The core is divided into quadrants by an aluminum rod-guide cross which housed four control blades and a central cruciform transient rod. The poison sections of the blades and transient rod were made of "Binal", an aluminum-boron alloy.

The OC (or Destructive Core) was installed in Spert I following testing on the D-12/25 Core for the purpose of investigating destructive effects in an oxide core. The core was almost identical to the SA-core with a slightly different constraining grid. Two loadings, OC-590C and OC-599C were used in the transient testing. The SA-592 and OC loading patterns are shown in Figure A-38.

The Spert I oxide cores were instrumented in a similar fashion to previous Spert cores. The instrumentation for both the SA and OC cores is summarized in Table A-2 and described in References A-39, and A-40, respectively. Power measurements were made using out-of-core ion chambers, pressure transducers were located within the core region, and thermocouples were used for both bulk system and fuel plate temperature measurements. The fuel thermocouples were spot welded to the outer surface of the rods. The core coordinate scheme, primarily used for thermocouple location reference is shown in Figure A-39.

The two cores were characterized by the standard series of static and transient experiments and associated calculations as for previous cores. The results are summarized in detail in References A-38 and A-39 having previously been reported

in a series of quarterly reports (Refs. A-41, A-42, A-43) and Reference A-44. It should be noted that the static measurements varied slightly between the cores, notably with and without the constraining grid, but in general the results from the different sets of measurements compliment each other.

A.3.2 Spert III E

The Spert oxide core experimental program was continued with testing using the Spert III E-core for the purpose of extending the testing conditions to those more typical of power reactors (*i.e.*, elevated pressure and temperature, and forced coolant flow). The E-core was operated from January 1965 until midway through 1968.

The Type-E fuel is different from that used in the Spert I oxide cores in a number of aspects. The enrichment is slightly higher at 4.8%, the fuel is in the form of sintered fuel pellets in the stainless steel tubes rather than compressed powder. The UO_2 density is higher, and the fuel rods themselves are significantly shorter. The Type-E rods are also contained in square stainless steel fuel cans (*i.e*, rectangular fuel assembly boxes), resembling the outer appearance of MTR-type assemblies. Each fuel assembly typically contained 25 rods. Modified central assemblies only contained 16 rods each as did the fuel follower sections of the control rod/fuel. The Type-E 25-rod fuel assembly is shown in Figure A-40.

The E-core was assembled on a square grid in a symmetrical loading pattern (Fig. A-41). The operational loading contained 60 fuel assemblies, eight of which were associated with the fuel follow sections of the yoked control-rod pairs, while four central assemblies were modified to make room for the central cruciform transient rod. Specifications for the E-core are summarized in Table A-5 and are given along with further details in References A-45 and A-46.

The E-core was characterised in much the same way as previous Spert cores by a series of static experiments. These are reported in Reference A-47. Instrumentation information on the E-core was not located. It seems reasonable to assume that the E-core was instrumented in much the same way as the Spert III C-core and Spert I SA- and OC-cores (Tab. A-2).

A.4 Other Systems of Interest

Although neither of the following reactors were part of the Borax or Spert Projects,

both are relevant to analysis of MTR-type system self-limiting power excursion behaviour. The destructive accident at SL-1 provides additional information on fuel damage and the core destructive mechanism and data from the accident can be compared to the Borax I and Spert I D-core destructive test data. The IAEA 10 MW Benchmark Reactor is an analysis definition which has been used in conjunction with the Spert data for simulation of self-limiting power excursions. As such both are included herein and described below.

A.4.1 SL-1

The Stationary Low Power Reactor No. 1 (SL-1, originally called the Argonne Low Power Reactor or ALPR) was a 3 MW direct-cycle boiling water reactor designed by Argonne National Laboratory (ANL) and built at the NRTS (Fig. A-1) for demonstration and training purposes. The SL-1 was light water moderated and cooled and operated under natural circulation coolant conditions. It was designed to operate at pressures up to 400 psi and steam temperatures of 230EC (450EF). A cutaway drawing of the SL-1 facility is shown in Figure A-42. The SL-1 first went critical on August 11, 1958 and had been in operation for over two years before being destroyed by a reactivity initiated accident on January 3, 1961.

The SL-1 core was supported by an eight by eight grid plate within a 4 ½" diameter by 14 ½" high pressure vessel. The pressure vessel was surrounded by a biological shield with the entire facility was enclosed in a steel building. A vertical section of the reactor vessel is shown in Figure A-43 and a perspective drawing is shown in Figure A-44.

The SL-1 fuel was similar in style to the fuel used in the Borax and Spert projects in that it was plate fuel with each assembly containing nine fuel plates (Fig. A-45). Significant differences between the SL-1 and Borax and Spert fuel was the much heavier U-235 loading per plate in SL-1 and the substantially thicker fuel meat, clad and coolant channels. The core also contained burnable poison in the form of boron strips attached to the fuel assembly side plates.

At the time of the accident the system was depressurized with a hydrostatic water head of seven feet above the core. The loading consisted of 40 fuel assemblies shown in Figure A-46. The design data for SL-1 are given in Reference A-48 and further description is given in References A-49, A-50, and A-51 . The technical specifications for the SL-1 fuel and core are summarized in Table A-1.

Nuclear design data for SL-1 are given in Reference A-48. At the time of the accident no power recording equipment was operating, however flux wires were present in the core. The core characteristics at the time of the accident are reported in Reference A-51.

A.4.2 IAEA 10 MW Benchmark Reactor

The IAEA 10MW Benchmark Reactor is a benchmark problem, existing only on paper, defined by an IAEA working group as part of the Reduced Enrichment for Research and Test Reactor (RERTR) program. The problem has been specified primarily for use in both static and kinetic calculations in support of converting MTR-type cores from the use of HEU to LEU fuel, and is designed to be typical of MTR-type systems in general. Specifications for the problem, with both HEU and LEU fuel, are given in two IAEA technical documents (Refs. A-52, A-53).

The IAEA Benchmark Reactor has been used in safety analysis simulation for both scram-protected and self-limiting reactivity insertion transients. Validation of the model was done using experimental data from the Spert I B- and D-core tests as well as for the stainless-steel Spert III C-core and the LEU-oxide Spert III E-core.

Each standard fuel assemblies contains 23 straight fuel plates, while the fork-type absorbers move within control-fuel assemblies which are similar to the standard fuel assemblies but with six fuel plates replaced by four aluminum plates and gaps for the absorbers. A schematic of the fuel assembly cross section is shown in Figure A-47.

The IAEA Benchmark Reactor is based on a five-by-six assembly core containing 21 standard fuel assemblies and four control fuel assemblies. The core contains a central flux trap and is reflected on two opposite sides by graphite and in all directions by light water. Burnup of the assemblies varies between 5% and 50% U-235 depletion, representative of an operating MTR-type system. The core loading pattern is shown in Figure A-48.

The specifications for the fuel and core are summarized in Tables A-6 and A-7, respectively, and material properties and nuclear parameters are summarized in Table A-8. The nuclear parameters are those calculated by the ANL group as part of their PARET simulation analysis (taken from Ref. A-54).

A.5 References

A-1. J. R. Dietrich, D. C. Layman, “Transient and Steady State Characteristics of a Boiling Reactor. The Borax Experiments, 1953", ANL-5211 (also listed as AECD-3840), Argonne National Laboratory, USA, February 1954.

A-2. J. R. Dietrich, “Experimental Investigation of the Self-Limitation of Power During Reactivity Transients in a Subcooled, Water-Moderated Reactor. Borax-I Experiments, 1954", ANL-5323, (also listed as AECD-3668), Argonne National Laboratory, USA, 1954.

A-3. T. R. Wilson, “An Engineering Description of the Spert-I Reactor Facility”, US AEC Technical Report IDO-16318, Phillips Petroleum Co., June 14, 1957.

A-4. W. E. Nyer, S. G. Forbes, F. L. Bentzen, G. O. Bright, F. Schroeder, T. R. Wilson, “Experimental Investigations of Reactor Transients”, US AEC Technical Report IDO-16285, Phillips Petroleum Co., April 20, 1956.

A-5. F. L. Bentzen, “Spert-I Instrumentation”, US AEC Technical Report IDO-16316, Phillips Petroleum Co., March 15, 1957.

A-6. J. C. Haire, “Subcooled Transient Tests in the Spert I Reactor - Experimental Data”, US AEC Technical Report IDO-16342, Phillips Petroleum Co., July 1, 1958.

A-7. G. O. Bright, editor, “Quarterly Progress Report - October, November, December, 1957 - Reactor Projects Branch”, US AEC Technical Report IDO-16437, Phillips Petroleum Co., March 21, 1958.

A-8. G. O. Bright, editor, “Quarterly Progress Report - July, August, September, 1958 - Reactor Projects Branch”, US AEC Technical Report IDO-16512, Phillips Petroleum Co., May 6, 1959.

A-9. S. G. Forbes, F. L. Bentzen, P. French, J. E. Grund, J. C. Haire, W. E. Nyer, R. F. Walker, “Analysis of Self-Shutdown Behavior in the Spert I Reactor”, US AEC Technical Report IDO-16528, Phillips Petroleum Co., July 23, 1959.

A-10. G. O. Bright, editor, “Quarterly Progress Report - July, August, September, 1957 - Reactor Projects Branch”, US AEC Technical Report IDO-16416, Phillips Petroleum Co., October 1, 1957.

A-11. A. P. Wing, “Transient Tests of the Fully Enriched, Aluminum Plate-Type, B Cores in the Spert I Reactor: Data Summary Report”, US AEC Technical Report IDO-16964, Phillips Petroleum Co., June 1964.

A-12. G. O. Bright, editor, “Quarterly Progress Report - January, February, March, 1958 - Reactor Projects Branch”, US AEC Technical Report IDO-16452, Phillips Petroleum Co., September 10, 1958.

A-13. J. A. Norberg, editor, “Quarterly Progress Report - January, February, March, 1959 - Reactor Projects Branch", US AEC Technical Report IDO-16539, Phillips Petroleum Co., November 20, 1959.

A-14. B. E. Clancy, J. W. Connelly, B. V. Harrington, “An Analysis of Power Transients Observed in Spert I Reactors: Transients in Aluminum-Plate-Type Reactors Initiated at Ambient Temperatures”, Australian Atomic Energy Commission Technical Report AAEC/E345, March 1975.

A-15. A. H. Spano, R. W. Miller, “Spert I Destructive Test Program Safety Analysis Report”, US AEC Technical Report IDO-16790, Phillips Petroleum Co., June 15, 1962.

A-16. R. W. Miller, A. Sola, R. K. McCardell, “Report of the Spert I Destructive Test Program on an Aluminum, Plate-Type, Water-Moderated Reactor”, US AEC Technical Report IDO-16883, Phillips Petroleum Co., June 1964.

A-17. J. E. Houghtaling, Alain Sola, A. H. Spano, “Transient Temperature Distributions in the Spert I D-12/25 Fuel Plates During Short-Period Power Excursions”, US AEC Technical Report IDO-16884, Phillips Petroleum Co., June 1964.

A-18. J. Dugone, D. D. Wieland, “Fuel Plate Experience During the Spert I Destructive Test Series with an Aluminum-Clad, Plate-Type Core”, US AEC Technical Report IDO-16885, Phillips Petroleum Co., July 24, 1963.

A-19. F. Schroeder, editor, “Quarterly Technical Report - Spert Project - July, August, September, 1962", US AEC Technical Report IDO-16829, Phillips

Petroleum Co., February 28, 1963.

A-20. R. E. Heffner, E. L. Morris, D. T. Jones, D. R. Seaman, M. K. Shane, “Spert IV Facility”, US AEC Technical Report IDO-16745, Phillips Petroleum Co., February 22, 1962.

A-21. J. G. Crocker, J. E. Koch, Z. R. Martinson, A. M. McGlinsky, L. A. Stephan, “Nuclear Start-Up of the Spert IV Reactor”, US AEC Technical Report IDO-16905, Phillips Petroleum Co., July 24, 1963.

A-22. F. Schroeder, editor, “Quarterly Technical Report - Spert Project - October, November, December, 1962", US AEC Technical Report IDO-16890, Phillips Petroleum Co., May 17, 1963.

A-23. J. G. Crocker, L. A. Stephan, “Reactor Power Excursion Tests in the Spert IV Facility”, US AEC Technical Report IDO-17000, Phillips Petroleum Co., August 1964.

A-24. J. G. Crocker, Z. R. Martinson, R. M. Potenza, L. A. Stephan, “Reactor Stability Tests in the Spert IV Facility”, US AEC Technical Report IDO-17088, Phillips Petroleum Co., July 1965.

A-25. A. P. Wing, “Transient Tests of the Fully Enriched, Stainless Steel Plate-Type, P Core in the Spert I Reactor: Data Summary Report”, US AEC Technical Report IDO-17011, Phillips Petroleum Co., December 1964.

A-26. R. E. Heffner, “Damage to Stainless Steel Fuel in Spert Reactors”, US AEC Technical Report IDO-16729, Phillips Petroleum Co., November 22, 1961.

A-27. F. L. Bentzen, editor, “Quarterly Progress Report - October, November, December, 1958 - Reactor Projects Branch”, US AEC Technical Report IDO-16537, Phillips Petroleum Co., September 1, 1959.

A-28. L. A. Stephan, “Transient Tests of the BSR-II Core in the Spert I Facility”, US AEC Technical Report IDO-16768, Phillips Petroleum Co., April 5, 1963.

A-29. F. Schroeder, editor, “Quarterly Technical Report - Spert Project - October, November, December, 1959", US AEC Technical Report IDO-16616, Phillips Petroleum Co., August 24, 1960.

A-30. F. Schroeder, editor, “Quarterly Technical Report - Spert Project - April, May, June, 1960", US AEC Technical Report IDO-16640, Phillips Petroleum Co., April 7, 1961.

A-31. R. E. Heffner, T. R. Wilson, “Spert III Reactor Facility”, US AEC Technical Report IDO-16721, Phillips Petroleum Co., October 25, 1961.

A-32. R. Scott, Jr., C. L. Hale, R. N. Hagen, “Transient Tests of the Fully Enriched Uranium-Oxide Stainless Steel Plate-Type C-Core in the Spert III Reactor: Data Summary Report”, US AEC Technical Report IDO-17223, Phillips Petroleum Co., February 1967.

A-33. A. H. Spano, editor, “Quarterly Technical Report - Spert Project - January, February, March, 1964", US AEC Technical Report IDO-17010, Phillips Petroleum Co., July 1964.

A-34. C. M. Condit, J. F. Scott, R. L. Johnson, “The Effects of Coolant Temperature and Initial Power Level on the Excursion Behavior of a Highly Enriched Plate Core in Spert III – Experiment and Analysis”, US AEC Technical Report IDO-17138, Phillips Petroleum Co., March 1967.

A-35. T. R. Wilson, editor, “Quarterly Technical Report - Spert Project - January, February, March, 1960", US AEC Technical Report IDO-16617, Phillips Petroleum Co., March 31, 1961.

A-36. A. H. Spano, editor, “Quarterly Technical Report - Spert Project - July, August, September 1959", US AEC Technical Report IDO-16606, Phillips Petroleum Co., July 11, 1960.

A-37. F. Schroeder, W. J. Neal, C. R. Toole, R. A. Zahn, “The Spert III Reactor Nuclear Startup”, US AEC Technical Report IDO-16586, Phillips Petroleum Co., March 18, 1960.

A-38. A. H. Spano, J. E. Barry, L. A. Stephan, J. C. Young, “Self-Limiting Power Excursion Tests of a Water-Moderated Low-Enrichment UO_2 Core in Spert I”, US AEC Technical Report IDO-16751, Phillips Petroleum Co., February 28, 1962.

A-39. J. E. Grund, editor, “Experimental Results of Potentially Destructive Reactivity Additions to an Oxide Core”, US AEC Technical Report IDO-

17028, Phillips Petroleum Co., December 1964.

A-40. R. Scott, Jr., A. A. Wasserman, R. C. Schmitt, “Transient Tests of the Spert I Low-Enrichment UO_2 Core: Data Summary Report”, US AEC Technical Report IDO-16752, Phillips Petroleum Co., September 1963.

A-41. F. Schroeder, editor, “Quarterly Technical Report - Spert Project - April, May, June, 1961", US AEC Technical Report IDO-16716, Phillips Petroleum Co., September 15, 1961.

A-42. F. Schroeder, editor, “Quarterly Technical Report - Spert Project - April, May, June, 1963", US AEC Technical Report IDO-16920, Phillips Petroleum Co., September 20, 1963.

A-43. A. H. Spano, editor, “Quarterly Technical Report - Spert Project - July, August, September, 1963", US AEC Technical Report IDO-16931, Phillips Petroleum Co., April 1964.

A-44. A. H. Spano, “Self-Limiting Power Excursion Tests of a Water-Moderated Low-Enrichment UO_2 Core”, Nuclear Science and Engineering, v.15, pp.37-51, 1963

A-45. R. M. Potenza, editor, “Quarterly Technical Report - Spert Project - January, February, March, 1966", US AEC Technical Report IDO-17206, Phillips Petroleum Co., September 1966.

A-46. J. C. Crocker, editor, “Quarterly Technical Report - Spert Project - October, November, December, 1964", US AEC Technical Report IDO-17084, Phillips Petroleum Co., April 1965.

A-47. T. G. Taxelius, R. M. Potenza, editors, “Quarterly Technical Report - Spert Project - April, May, June, 1966", US AEC Technical Report IDO-17207, Phillips Petroleum Co., January 1967.

A-48. SL-1 Report Task Force, “IDO Report on the Nuclear Incident at the SL-1 Reactor on January 3, 1961 at the National Reactor Testing Station”, US AEC Technical Report IDO-19302, January 1962.

A-49. Capt. A. Nelson Tardiff, “Some Aspects of the WTR and SL-1 Accidents”, US AEC Technical Report IDO-19308, April 9, 1962.

A-50. SL-1 Project, "Final Report of SL-1 Recovery Operation", US AEC Technical Report IDO-19311, General Electric Company, July 27, 1962.

A-51. Flight Propulsion Laboratory Department, "Additional Analysis of the SL-1 Excursion", US AEC Technical Report IDO-19313, General Electric Company, November 21, 1962.

A-52. "Research Reactor Core Conversion from the use of Highly Enriched Uranium to the use of Low Enriched Uranium Fuels Guidebook", International Atomic Energy Agency Technical Document IAEA-TECDOC-233, Vienna, Austria, 1980.

A-53. "Research Reactor Core Conversion Guidebook", International Atomic Energy Agency Technical Document IAEA-TECDOC-643, Vienna, Austria, April 1992.

A-54. W. L. Woodruff, "A Kinetics and Thermal-Hydraulics Capability for the Analysis of Research Reactors", Nuclear Technology, v. 64, pp. 196-206, February 1984.

A.6 Tables

Table A-1: Aluminum-Clad Plate-Fuel Core Technical Specifications

	Borax I	Spert I A-17/28	Spert I B-24/32	Spert I B-16/40	Spert I B-12/64	Spert I D-12/25	Spert IV D-12/25	SL-1
Fuel	(standard)	93.5	93.5	93.5	93.5	(standard)	(standard)	93
Enrichment (wt% U-235)	93	9.88	7.0	7.0	7.0	93	93	38.9
U-235/plate (g)	7.70	U-Al alloy	U-Al alloy	U-Al alloy	U-Al alloy	14.0	14.0	U-Ni-Al alloy
Meat Material	U-Al alloy	17	24	16	12	U-Al alloy	U-Al alloy	9
Plates per Assembly	18	straight, w stiffeners	straight	straight	straight	12	12	straight
Plate style	curved	0.051	0.051	0.051	0.051	straight	straight	0.127
Meat Dimensions	0.053	3 x 1.73	6.36	6.36	6.36	0.051	0.051	8.89
thickness (cm)	6.35	60.3	61.0	61.0	61.0	6.22	6.22	65.5
width (cm)	60.0					61.0	61.0	
height (cm)								
Clad								
Clad Material	Al, 99.75% pure	Al type 1100	Al type 6061	Al type 6061	Al type 6061	Al type 6061	Al type 6061	Al-Ni X-8100
Clad thickness (cm)	0.050	0.051	0.051	0.051	0.051	0.051	0.051	0.089
Plate								
Plate Dimensions								
thickness (cm)	0.152	0.152	0.152	0.152	0.152	0.152	0.152	0.305
width (cm)	7.23	5.19 (estimated)	6.92	6.92	6.92	6.87	6.87	8.89 (estimated)
height (cm)	62.5	62.6	63.8	63.8	63.8	61.3	61.3	70.6
Coolant								
Channel Thickness								
nominal (cm)	0.297	0.297	0.165	0.483	0.483	0.455	0.455	0.787
other (cm)	-	-	-	0.165 (alternating)	-	0.231 (outer)	0.231 (outer)	-
Other								
Metal/Water Ratio (assembly)	0.69	0.78	1.14	0.63	0.46	0.66	0.66	-
Core								
Number of Assemblies	26 - 32	28	32	40	64	25	25	40
Number of Plates	540 (30 strd assmb)	476	768	640	768	270	270	360
Control Rod Type	blades btw assemblies	blades btw assemblies	blades btw assemblies	blades btw assemblies	blades btw assemblies	blades in assemblies	blades in assemblies	blades btw assemblies
Transient Rod Type	central blade / cross	central cruciform	central cruciform	central cruciform	central cruciform	central double blade	central double blade	central cruciform
U-235 loading (kg) calc	4.16 (30 strd assmb)	4.70	5.38	4.48	5.38	3.78	3.78	14.00
Coolant material	H2O	H2O	H2O	H2O	H2O	H2O	H2O	H2O
Reflector material	H2O	H2O	H2O	H2O	H2O	H2O	H2O	H2O
hydrostatic head (ft)	3 to 4.5	2	2	2	2	2	2 to 18	7
meat volume (cc)	1.10E+04	7.57E+03	1.51E+04	1.26E+04	1.51E+04	5.20E+03	5.20E+03	2.66E+04
total plate area (cm2) calc	5.00E+05	3.19E+05	6.95E+05	5.79E+05	6.95E+05	2.33E+05	2.33E+05	4.70E+05
Facility								
Vessel type	open tank	open tank	open tank	open tank	open tank	open tank	pool	sealed tank
Pressure	atm.	atm.	atm.	atm.	atm.	atm.	atm.	pressurized
Flow Direction	nat. circ.	nat. circ.	nat. circ.	nat. circ.	nat. circ.	nat. circ.	nat. circ. / up	nat. circ.
References	ANL-5211	IDO-16318	IDO-16790	IDO-16964	IDO-16790	IDO-16788	IDO-16745	IDO-19302
	ANL-5323	IDO-16790	IDO-16964		IDO-16964	IDO-16790		IDO-19308
	IDO-16790					IDO-16883		IDO-19313
						IDO-16886		

2/20/04, 9:55 PM PhD_SE-Day_core-data-summary.xls Tech Specs Al-Cores

Table A-2: Borax and Spert Core Instrumentation

System	Power Detectors	Fuel Temperature Detectors	Other Instrumentation	Reference
Borax I	B-10 ion chambers 3 log for transients 1 lin. for operation	3-mil chromel-alumel TCs welded to clad surface 3-mil chromel-alumel TCs welded to meat and plug filled	pressure transducers in- and out-of-core wires photographic microphone TCs in reflector radiation monitors	ANL-5211, ANL-5323
Spert I A-17/28	B-10 ion chambers log for short period tests lin. for long period tests	10-mil chromel-alumel TCs peened into clad	pressure transducers photographic copper-constantan TCs in reflector radiation monitors	IDO-16342
Spert I B-Cores	Same as Spert I A	same as Spert I A but improved contact via aluminization of wires	same as Spert I A	IDO-16437, IDO-16964
Spert I P-18/19	B-10 ion chambers lin. for all transient data	10-mil chromel-alumel TCs spot welded to clad surface	same as Spert I A general instrument overhaul	IDO-17011, IDO-16489
Spert I BSR-II	assumed same as P-core	assumed same as P-core	assumed same as P-core	IDO-16768
Spert I SA	B-10 ion chambers lin. for all transient data	5-mil chromel-alumel welded to pin surface internal TC's gave erratic readings	same as Spert I A good results from in-core high-speed motion pictures	IDO-16752
Spert I D-12/25	B-10 ion chambers lin. for all transient data mini-ion chambers semirad chambers	5-mil chromel-alumel TCs flattened to 0.5-mil multi-junction welded to clad surface 5-mil chromel-alumel TCs peened into clad to depth of 30-mils	same as Spert I A plus: flow meters in-core wires strain gages accelerometers	IDO-16790, IDO-16886
Spert I OC	B-10 ion chambers lin. for all transient data semi-rad chambers	10-mil chromel-alumel TCs flattened to 3-mil welded to clad surface fuel cell TCs in development stage	same as Spert I A plus: strain gauges accelerometers air pressure microphone	IDO-17028
Spert III C	B-10 ion chambers (assume lin. Amplification for all transient data)	5-mil chromel-alumel TCs welded to clad surface 3-mil chromel-alumel TCs SS-sheathed welded to clad surface (used in high Temp. tests)	similar to Spert I including: pressure transducers in-core Co-wires TCs embedded in vessel wall flow meters	IDO-17223
Spert III E	assume same as Spert III C	assume same as Spert I SA/OC	assume same as Spert III C	
Spert IV D-12/25	B-10 ion chambers mini-B-10 ion chambers mini-fission chambers semi-rad chambers	10-mil chromel-alumel TCs flattened to 3-mil multi-junction welded to clad surface water-channel TCs chromel-alumel single-junction	similar to Spert I including: pressure transducers flow meters photographic equipment radiation monitors	IDO-17000, IDO-17088

Notes: TC stands for thermocouple
lin./log refers to linear/logarithmic amplification of signal

2/20/04, 1:10 PM Instrumentation Summary PhD_SE-Day_reactor-expt-summary.xls

Table A-3: Aluminum-Clad Plate-Fuel Core Nuclear Characteristics

HEU Al-Clad Plate Cores	Borax I	Spert I A-17/28	Spert I B-24/32	Spert I B-16/40	Spert I B-12/64	Spert I D-12/25	Spert IV D-12/25	MNR RC-16/28-9/6
Temperature Defect								
20C to 95C (mk)	-8.17	-10.9	-12.4	-11.6	-10.2	N/A	N/A	N/A
Void Coefficient								
Metal/Water Ratio - central	0.687	0.782	1.128	0.635	0.465	0.704	0.703	-
Metal/Water Ratio - std assembly	0.687	0.782	1.128	0.635	0.465	0.525	0.522	0.576
Metal/Water Ratio - core	0.687	0.782	1.128	0.635	0.465	0.629	0.627	-
Average (Uniform)								
(mk/%-void)	-2.4	-1.9	-2.8	-1.8	-1.1	-2.4	-2.3	-2.1
(mk/cc-void)	-3.4E-03	-3.5E-03	-5.1E-03	-2.0E-03	-6.9E-04	-4.6E-03	-4.5E-03	-3.3E-03
(mk/channel)	-0.41	-0.39	-0.36	-0.28	-0.14	-0.87	-0.85	-0.39
Central								
(mk/%-void)	-4.5	-3.9	-6.5	-2.9	0.9	-3.4	-3.1	-4.5
(mk/cc-void)	-6.6E-03	-7.2E-03	-1.2E-02	-3.3E-03	6.0E-04	-6.3E-03	-6.0E-03	-7.1E-03
(mk/channel)	-0.78	-0.80	-0.83	-0.45	0.12	-1.20	-1.14	-0.84
Prompt Neutron Lifetime								
(micro-sec)	65	50	50	70	77	60	57	N/A
Power Peaking Factor								
Overall	2.0	2.0	2.5	2.1	2.2	2.4	2.4	4.2
Dimensions								
Fuel meat thickness (cm)	0.053	0.051	0.051	0.051	0.051	0.051	0.051	0.051
Clad thickness (cm)	0.050	0.051	0.051	0.051	0.051	0.051	0.051	0.038
Fuel surface area (cm2)	4.31E+05	3.55E+05	6.47E+05	5.39E+05	6.47E+05	2.26E+05	2.26E+05	4.00E+05
Fuel meat volume (cc)	1.10E+04	7.57E+03	1.51E+04	1.26E+04	1.51E+04	5.20E+03	5.20E+03	9.57E+03
SA/Vol Ratio	39	47	43	43	43	43	43	42
Volume Coolant/Channel (cc)	119	111	69	136	203	190	190	119

note: fuel surface area and coolant volume are based on active height of the fuel

Table A-4: Stainless-Steel-Clad Plate-Fuel Core Technical Specifications

	Spert I P-18/19	**Spert I BSR-II**	**Spert III C-19/52**
Fuel	(standard)	(standard)	(standard 1S)
Enrichment (wt% U-235)	93.2	93	93.2
U-235/plate (g)	28.65	14.5	33.6
Meat Material	UO2 SS cermet	UO2 in SS	UO2 in SS 304 mod.
Plates per Assembly	18	20	19
Plate style	straight	straight	straight w stiffener
Meat Dimensions			
thickness (cm)	0.051	0.036	0.051
width (cm)	6.35	6.53	2 x 2.93
height (cm)	55.9	38.1	91.4
Clad			
Clad Material	SS type 304L	SS type 347	SS type 304L
Clad thickness (cm)	0.0127	0.0203	0.0127
Plate			
Plate Dimensions			
thickness (cm)	0.076	0.076	0.076
width (cm)	7.06	7.34	2 x 3.67
height (cm)	58.4	40.0	94.0
Coolant			
Channel Thickness			
nominal (cm)	0.323	0.305	0.325
other (cm)	-	-	-
Other			
Metal/Water Ratio (assembly)	0.258	0.291	0.298
Core			
Number of Assemblies	19	25	52
Number of Plates	332	502	952
Control Rod Type	assembly w fuel follower	blades in assemblies	assembly w fuel follower
Transient Rod Type	blade in assembly	blades in assemblies	central cruciform
U-235 loading (kg) calc	9.80	6.07	30.8
Coolant material	H2O	H2O	H2O
Reflector material	H2O	H2O	H2O
hydrostatic head (ft)	2	2	varied
meat volume (cc)	5.88E+03	4.22E+03	2.48E+04
total plate area (cm2) calc	2.73E+05	2.87E+05	1.28E+06
Facility			
Vessel type	open tank	open tank	pressure
Pressure	atm.	atm.	varied
Flow Direction	nat. circ.	nat. circ.	upwards
References	IDO-16729	IDO-16729 IDO-16722	IDO-16721 IDO-16729

2/20/04, 9:58 PM PhD_SE-Day_core-data-summary.xls Tech Specs SS-Cores

Table A-5: Spert Rod-Type Oxide Fuel and Core Technical Specifications

	Spert I SA	Spert I OC	Spert III E
Fuel			
Type	Rods	Rods	Rods in Assemblies
Enrichment (wt% U-235)	4.02	4.02	4.8
Meat Material	compressed UO2 powder	compressed UO2 powder	sintered UO2 pellets
UO2 density, (g/cc)	9.45	9.45	10.5
UO2/rod, (g)	1600	1600	913.5
U-235/rod (g)	56.7	56.7	38.6
U-238/rod (g)	1353	1353	766.4
Rods per Assembly	-	-	25 (16 ctrl + central)
Rod Dimensions (cm)			
outer diameter	1.27	1.27	1.18
total height	181.6	181.6	103.6
active height	169.9	169.9	97.3
Pellet Dimensions (cm)			
outer diameter	-	-	1.07
length (short)	-	-	1.30
length (long)	-	-	1.95
Gas gap (cm)	-	-	0.00762
Clad Material	SS type 304	SS type 304	SS type 348
Clad thickness (cm)	0.0711	0.0711	0.0508
Lattice Pitch (cm)	1.68	1.68	1.49
Core			
Number of Assemblies	-	-	48 + 4 central + 8 ctrl
Number of Rods	592	590, 599	1264 (128 ctrl)
Control Rod Type	blades in channels	blades in channels	assembly w follower
Transient Rod Type	central cruciform	central cruciform	central cruciform
U-235 loading (kg)	33.57	33.45, 33.96	48.8 (4.9 ctrl)
Coolant material	H2O	H2O	H2O
Reflector material	H2O	H2O	H2O
hydrostatic head (ft)	2	2	varied
fuel material volume (cc)	1.00E+05	1.00E+05, 1.02E+05	4.12E+05 (4.17E+04 ctrl)
total rod surface area (cm2)	4.29E+05	4.28E+05, 4.34E+05	4.87E+05 (4.93E+04 ctrl)
Facility			
Vessel type	open tank	open tank	pressurized tank
Pressure	atm.	atm.	varied
Flow Direction	nat. circ.	nat. circ.	upwards
References	IDO-16751	IDO-17028 IDO-16751	IDO-17206 IDO-17084

5/7/2004, 12:21 PM PhD_SE-Day_core-data-summary.xls Tech Specs Oxide-Cores 1 / 1

Table A-6: IAEA 10MW Benchmark Reactor Fuel Technical Specifications

Fuel Element Design Description

	HEU	LEU
Fuel Material	UAlx-Al	U3Si2-Al
Enrichment, w% U-235	93	20
Clad Material	Al 6061	Al 6061
Plate Style	straight	straight
Assembly Dimensions, cm3	7.6 x 8.0 x 60.0	7.6 x 8.0 x 60.0
Plates/Assembly		
Standard	23	23
Control	17 + 4 Al Plates	17 + 4 Al Plates
Plate Dimensions, cm		
Thickness (inner plates)	0.127	0.127
Thickness (outer plates)	0.150	0.150
Width between Side Plates	6.64	6.64
Coolant Channel Thickness, cm	0.2188	0.2188
Fuel Meat Dimensions, cm		
Thickness	0.051	0.051
Width between Side Plates	6.30	6.30
Height	60.0	60.0
Side Plate Dimensions, cm	0.48 x 8.0	0.48 x 8.0
Uranium Density in Meat, g/cm3	0.68	4.45
U-235/Assembly, g		
Standard	280	390
Control	207	288
Assembly Volume Fractions		
Standard (Control)		
Fuel Meat	0.1185 (0.0876)	0.1185 (0.0876)
Aluminum	0.3205 (0.3244)	0.3205 (0.3244)
Water (+)	0.5610 (0.5880)	0.5610 (0.5880)

from IAEA-TECDOC-233, App.F, Tab.2-15 & Fig.A36; IAEA-TECDOC-643, App.G-0

(+) includes a 5 mm water channel surrounding each assembly

5/7/2004, 12:45 PM Tech Specs IAEA-10MW PhD_SE-Day_core-data-summary.xls

Table A-7: IAEA 10MW Benchmark Reactor Core Technical Specifications

Reactor Design Description

Reactor Type	Pool-Type MTR
Steady-State Power Level, MW	10
Assemblies in Core	
Standard	21
Control	4
Fuel Plates in Core	3519
Total Fuel Volume, cc	6.784E+04
Irradiation Channels	1 at Core Center
Active Core Geometry	5 x 6 Positions
Grid Plate	8 x 9 Positions
Lattice Pitch, cm2	7.7 x 8.1
Moderator, Coolant	H2O
Reflectors	C, H2O
Control Rod Style	fork in assembly
Coolant Flow	Nat. Circ. or Forced Upward
Coolant Flow Rate, m3/h	1000
Coolant Inlet Temperature, C	
for static calculations	20
for transient calculations	38
Pressure at core height, bar	1.7

from IAEA-TECDOC-233, App.F, Tab.2-15; IAEA-TECDOC-643, App.G-0

5/7/2004, 12:45 PM Tech Specs IAEA-10MW PhD_SE-Day_core-data-summary.xls

Table A-8: IAEA 10MW Benchmark Reactor Core Material and Nuclear Properties

Material and Nuclear Data

	HEU	LEU	Clad
Thermal Conductivity, W/m-C	158	50	180
Specific Heat			
J/cm3-K (1) *	1.985 + 0.0010*T	1.929 + 0.0007*T	2.069 + 0.0012*T
J/g-K (3)	0.728	0.340	0.892
Neutron Generation Time, msec	55.96	43.74	-
Beff	7.61E-03	7.28E-03	-
Coolant Temperature, mk/C **	0.1169	0.07872	-
Coolant Void, mk/%-void	2.478	2.944	-
Doppler, mk/C	2.70E-04	2.41E-02	-
Hot Channel Factors (2)			
Radial x Local PPF	1.4	1.4	-
Axial PPF	1.5	1.5	-
Engineering Factor	1.2	1.2	-
Overpower Factor	1.2	1.2	-
Peak/Average Power	2.52	2.52	-

from IAEA-TECDOC-643, App.A-2 (1), IAEA-TECDOC-643, App.G-0 (2), App.G-1 (3)

Kinetics parameters taken from Nucl. Tech., v.64, p.196, 1984

* T in K; ** spectrum component only, i.e., density effects not included

5/7/2004, 12:46 PM Tech Specs IAEA-10MW PhD_SE-Day_core-data-summary.xls

A.7 Figures

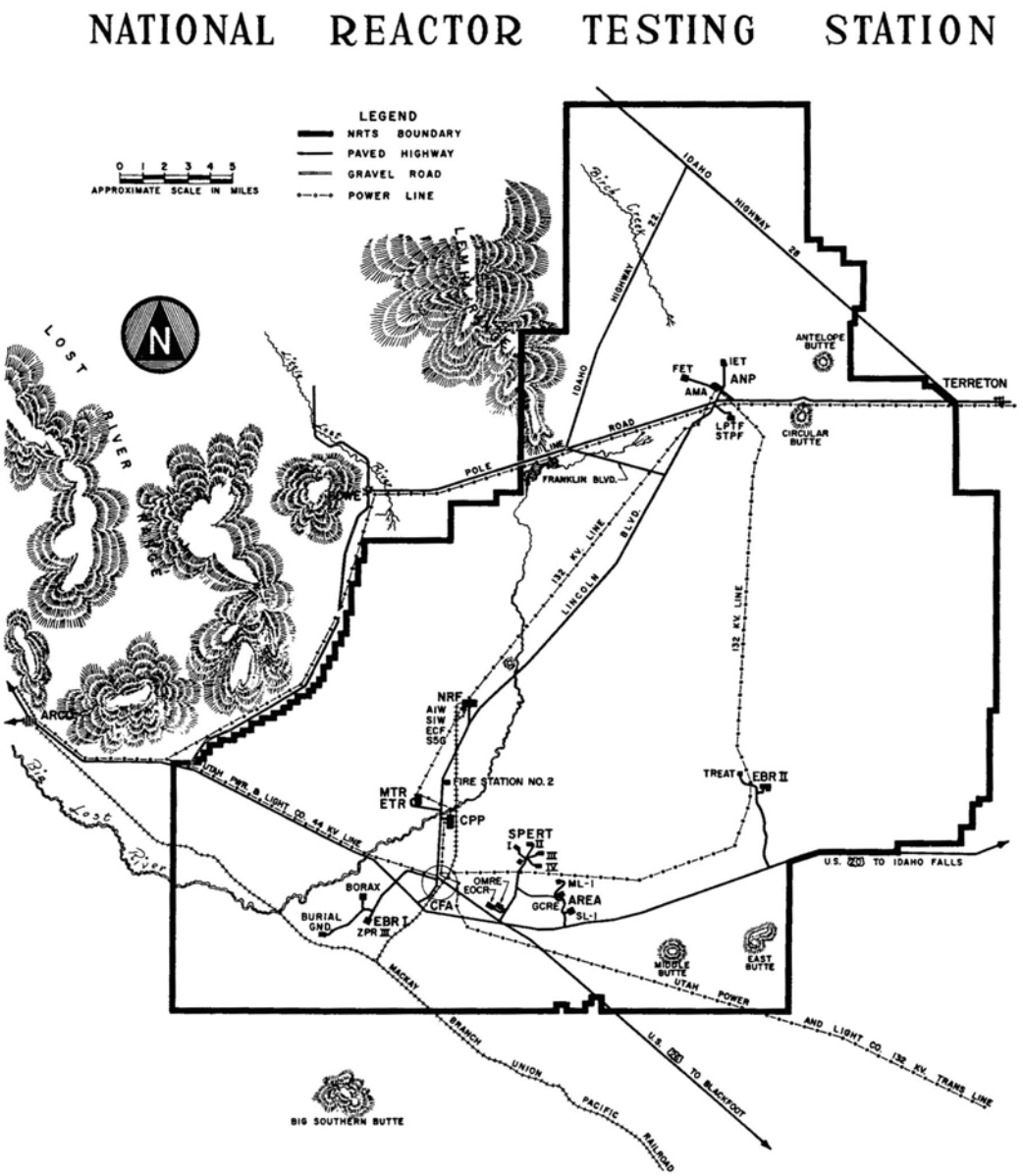

Figure A-1: Map of the National Reactor Testing Station (Ref. A-15).

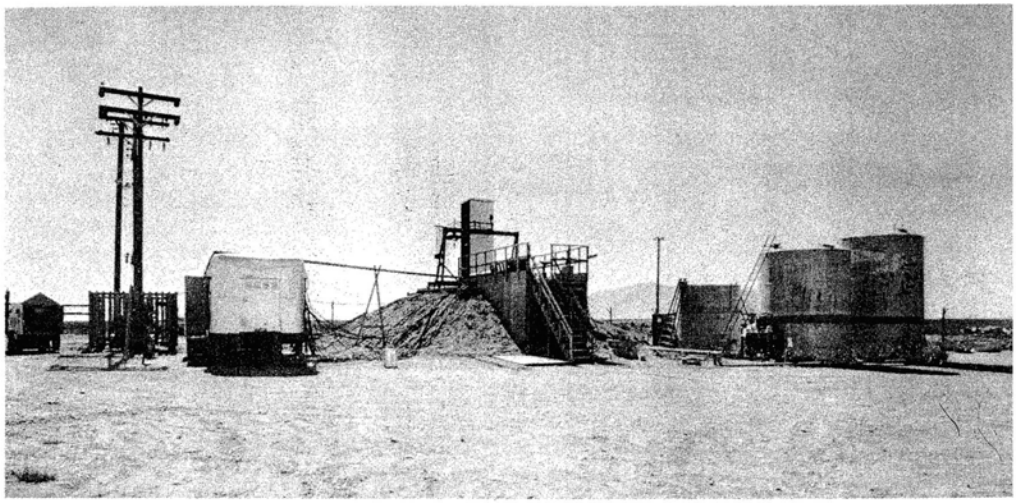

The view is toward the reactor through the pump pit. The trailer on the left contains the recording instruments. Tanks on the right hold a supply of shield water and deionized reactor water.

Figure A-2: The Borax I Site at the NRTS (modified from Ref. A-1)

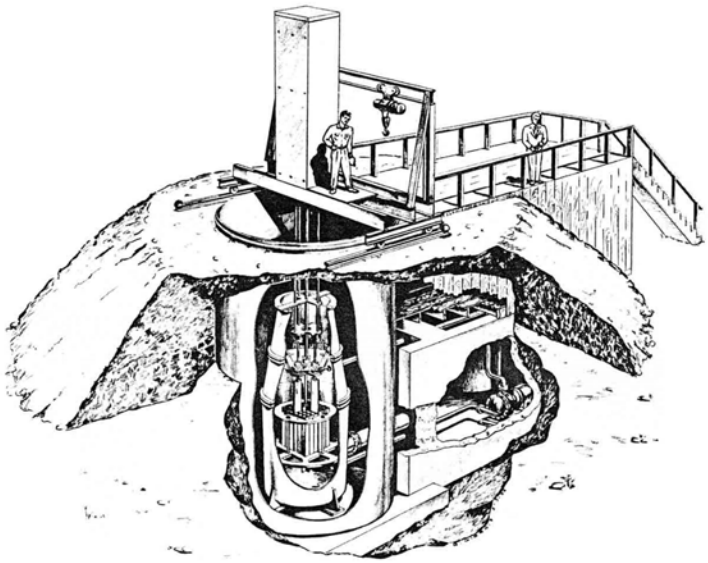

Figure A-3: Cutaway Drawing of the Borax I Reactor Showing Partial Underground Location. (Ref. A-2)

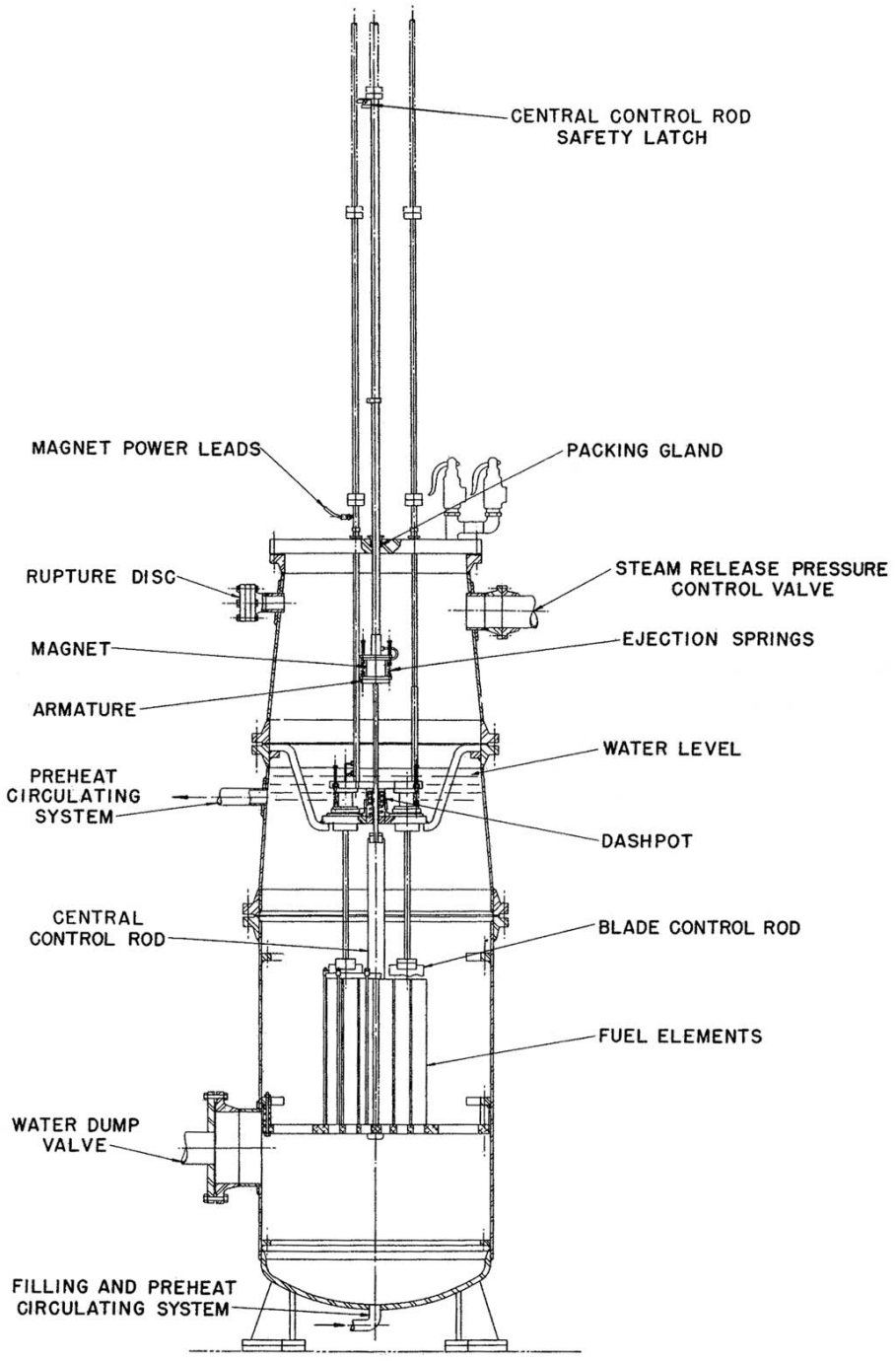

Figure A-4: Borax I Vertical Section (Ref. A-1).

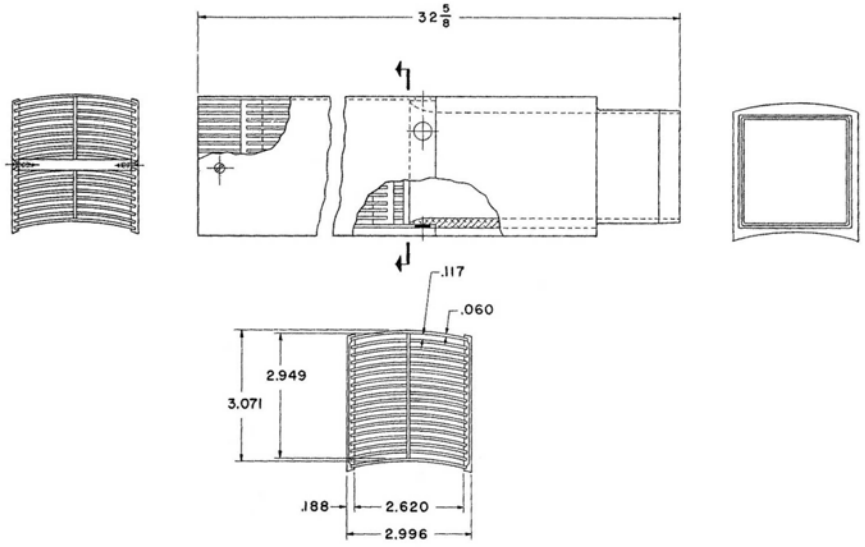

Figure A-5: Borax I Standard Fuel Assembly (modified from Ref. A-1)

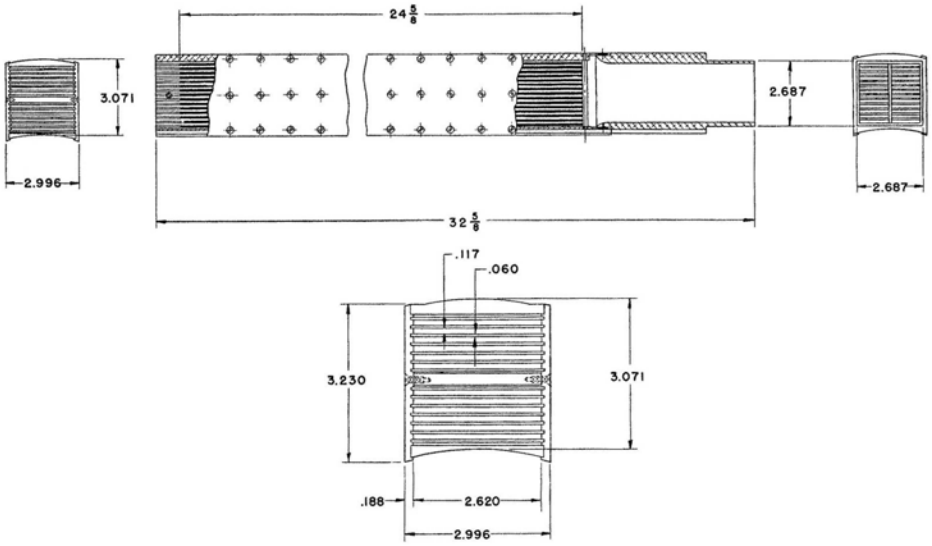

Figure A-6: Borax I Removable Plate Fuel Assembly (modified from Ref. A-1)

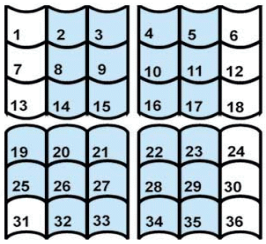

Critical Loading, 1953

26 Assemblies

Instrumented Assembly in position 21
all other assemblies standard

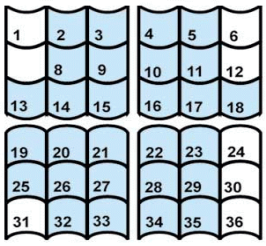

Flux Mapping Loading, 1953

28 Assemblies

Instrumented Assembly in position 21
all other assemblies standard

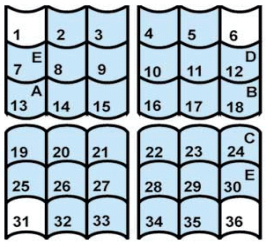

Transient Test Loadings, 1953

27 to 30 Assemblies
added according to letters A to E, to provide sufficient excess reactivity

Instrumented Assembly in position 21
plate 1: surface and center thermocouple
plate 4: center thermocouple
plate 11: surface and center thermocouple
all other assemblies standard

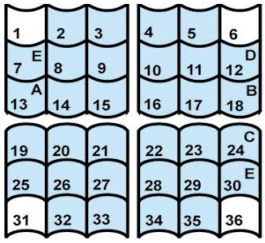

Transient Test Loadings, 1954

27 to 30 Assemblies
added according to letters A to E, to provide sufficient excess reactivity
power and energy results normalized to 30 assembly core

Instrumented Assembly in position 21
plate 1: ?
plate 4 (plate loading 20% higher than standard plate): two surface thermocouples
plate 11: ?
10-plate assembly (higher loading than standard assembly) in position 20
all other assemblies standard

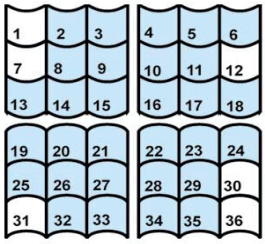

Destructive-Test Loading, 1954

30 Assemblies

Instrumented Assembly in position 26
plate 4 (loading 20% higher than standard plate): two surface thermocouples
10-plate assembly (higher loading than standard assembly) in position 20 (assumed)
all other assemblies standard

out-of-core thermocouples on a plate 6" from the core
higher worth transient rod

Figure A-7: Core loading patterns and Thermocouple Locations for Borax I Test Program

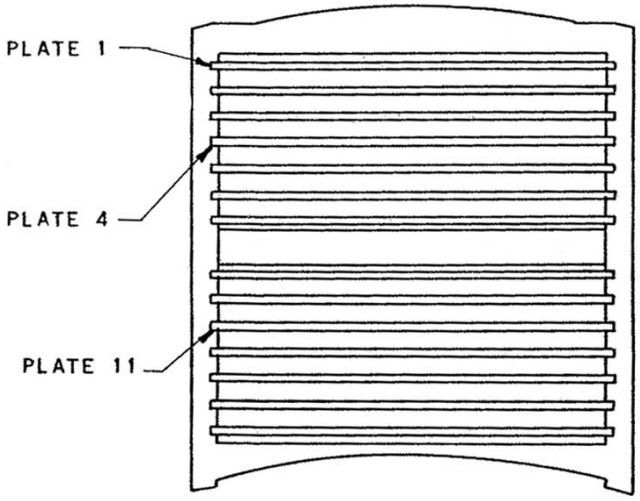

Figure A-8: Borax I Instrumented Fuel Plate Numbering Scheme (adapted from Ref. A-1)

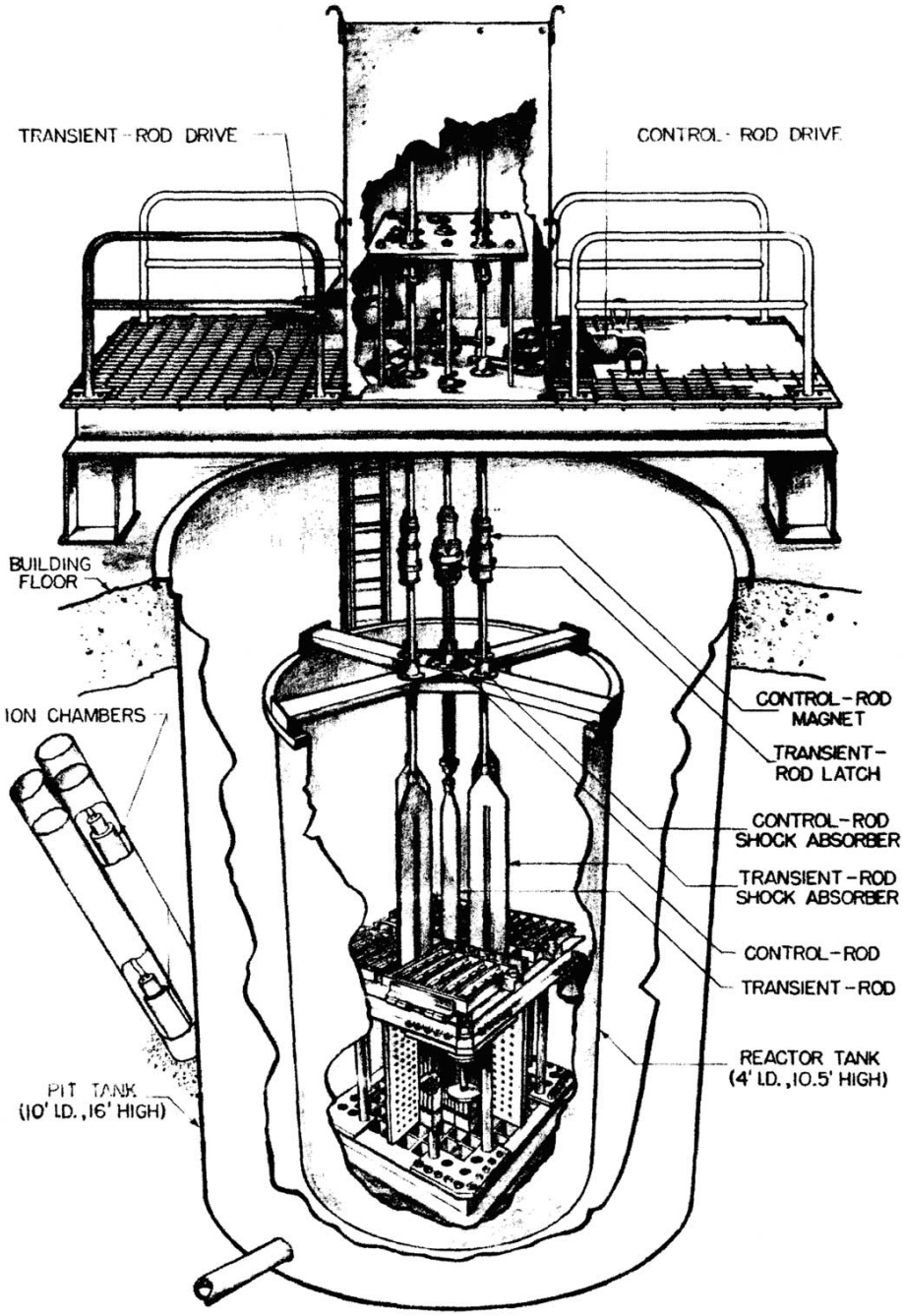

Figure A-9: Spert I A Cutaway Drawing Showing A-Core Structure (Ref. A-5)

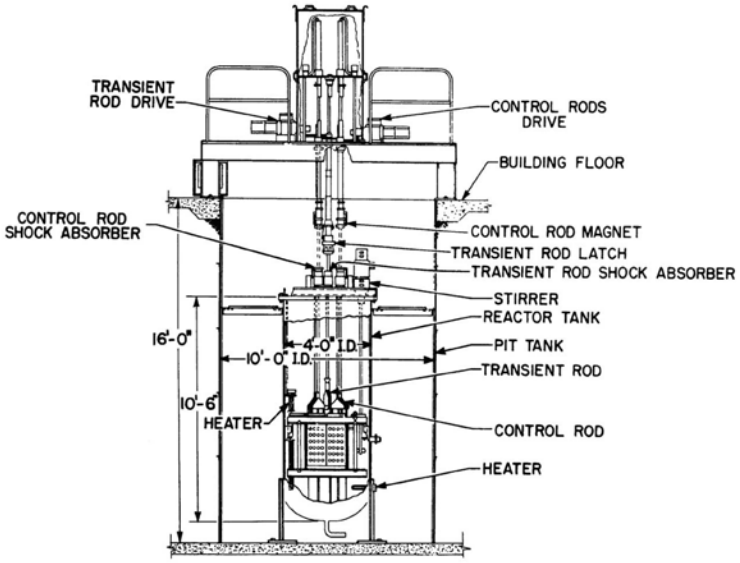

Figure A-10: Spert I Facility Elevation Cutaway Showing A-Core Structure (Ref. A-3)

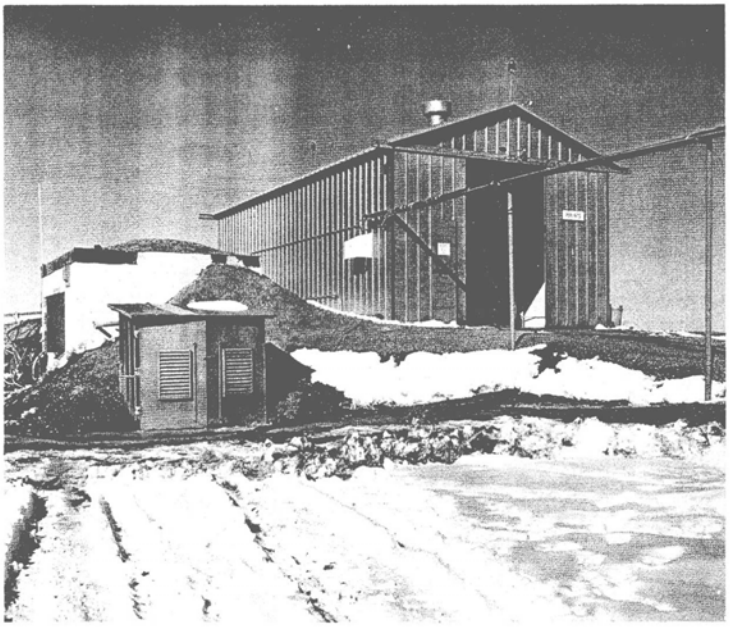

Figure A-11: Spert I Reactor Building at the NRTS (Ref. A-15)

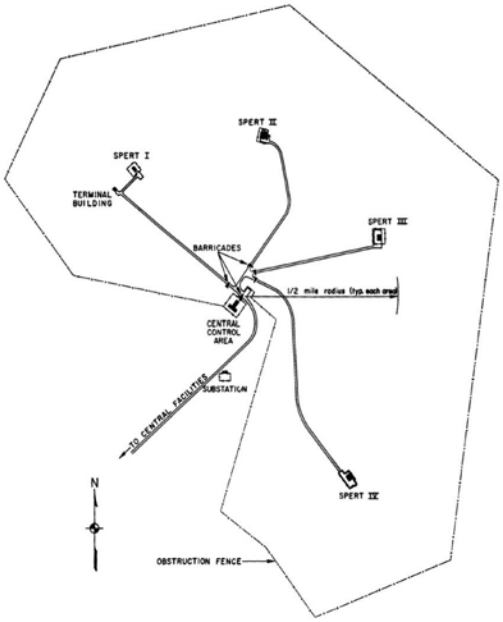

Figure A-12: Spert Project Site Map (Ref. A-15)

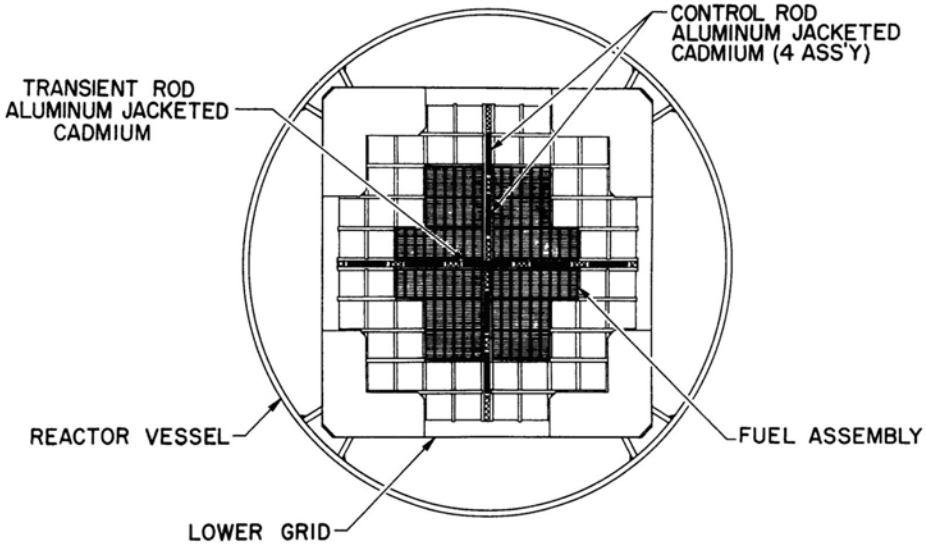

Figure A-13: Spert I A Core Configuration (Ref. A-3)

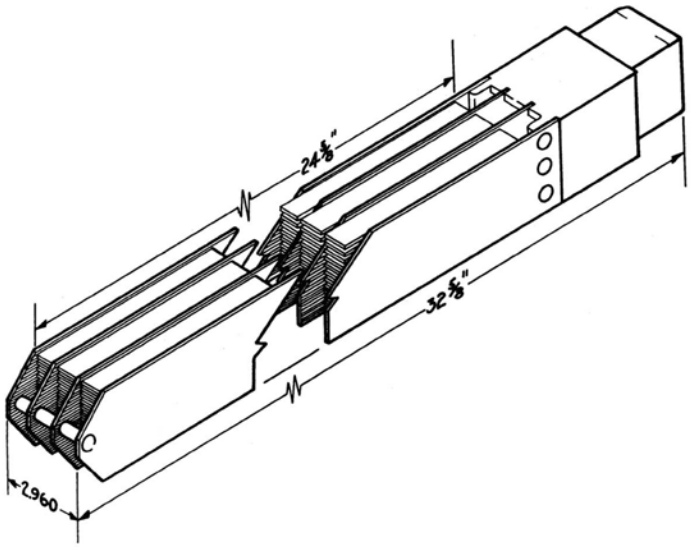

Figure A-14: Spert I Type-A Fuel Assembly (Ref. A-3)

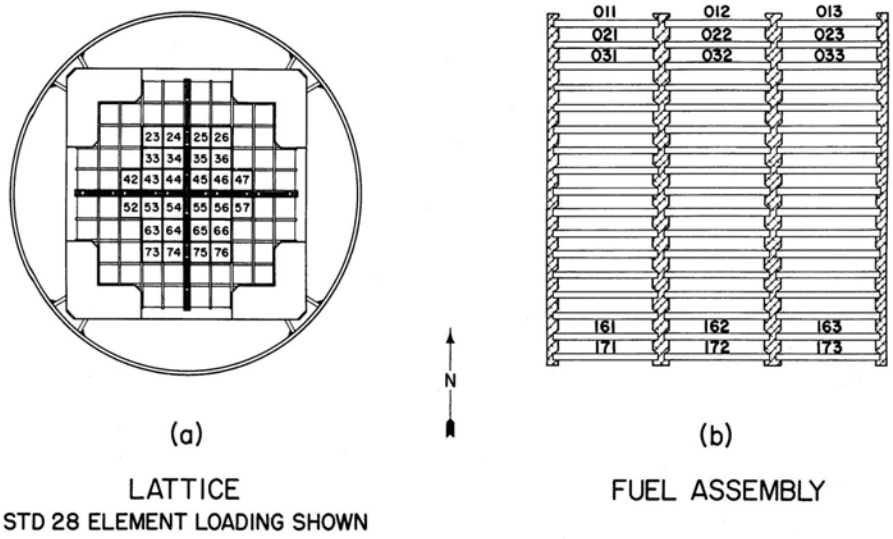

Figure A-15: Spert I A Assembly and Fuel Plate Numbering Scheme (Ref. A-6)

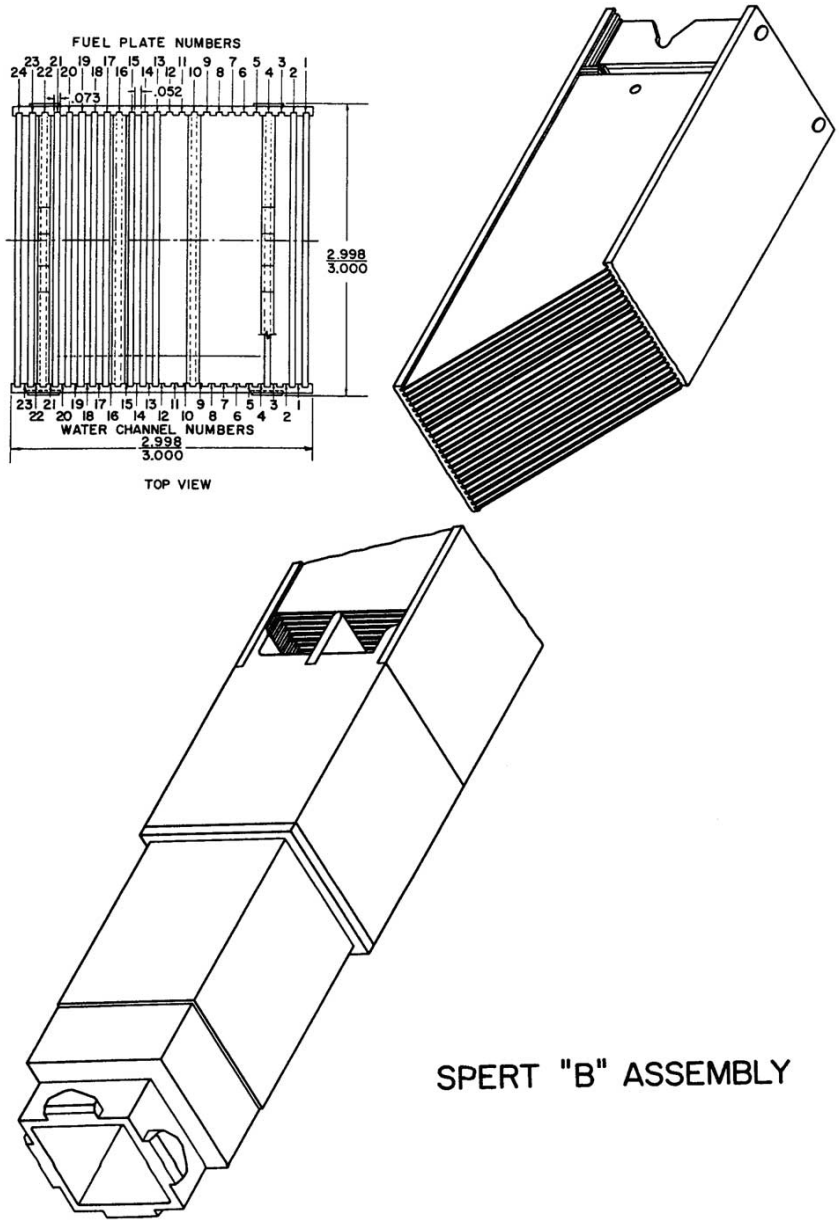

Figure A-16: Spert Type-B Fuel Assembly (Ref. A-10)

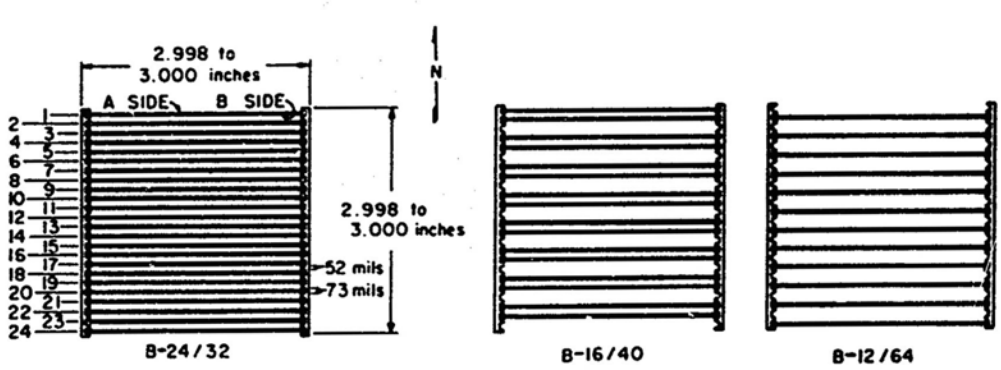

Figure A-17: Top View of Type-B Fuel Assemblies with 24-, 16-, and 12-plate Loadings (Ref. A-11)

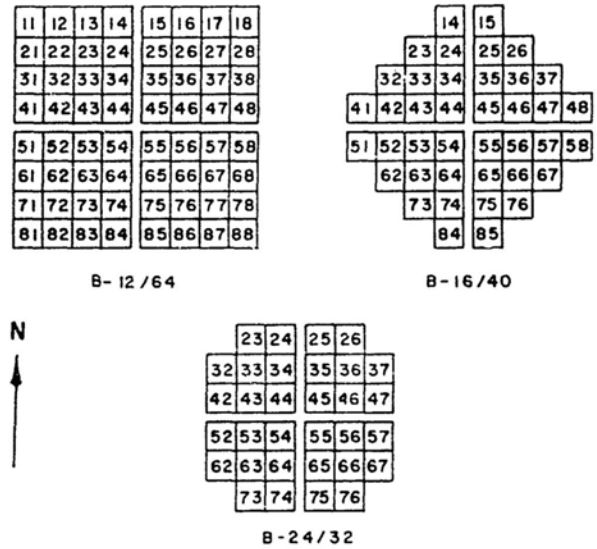

Figure A-18: Spert I B-Core Configurations (Ref. A-11)

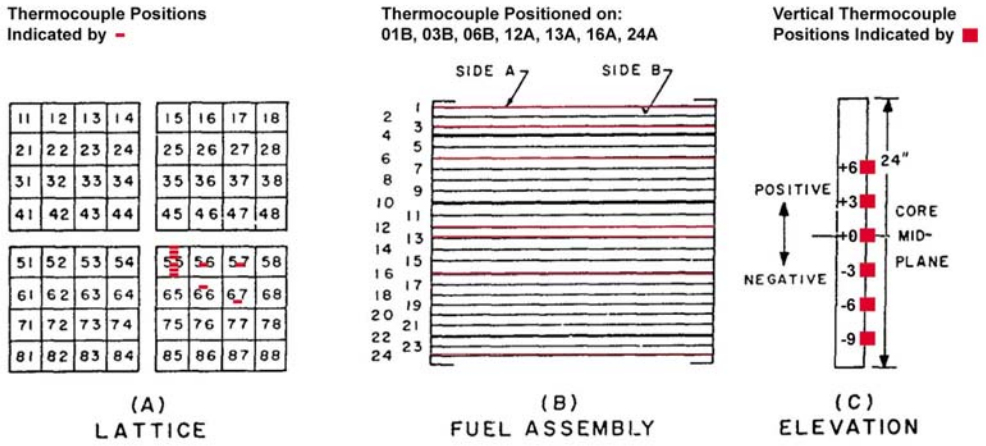

Figure A-19: Spert I B-Core Coordinate System and Thermocouple Locations (modified from Ref. A-11)

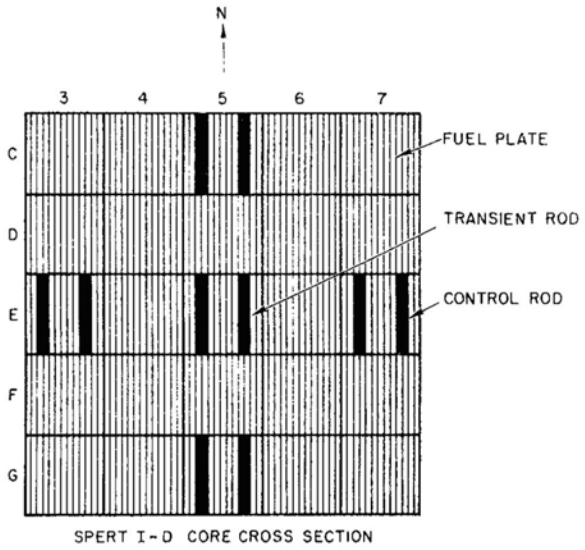

Figure A-20: Spert I D-12/25 Core Configuration (Ref. A-17)

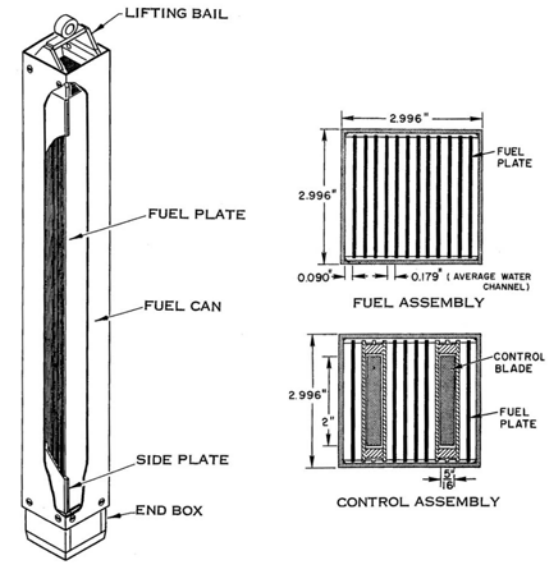

Figure A-21: Spert Type-D Fuel and Control-Fuel Assemblies (modified from Ref. A-21)

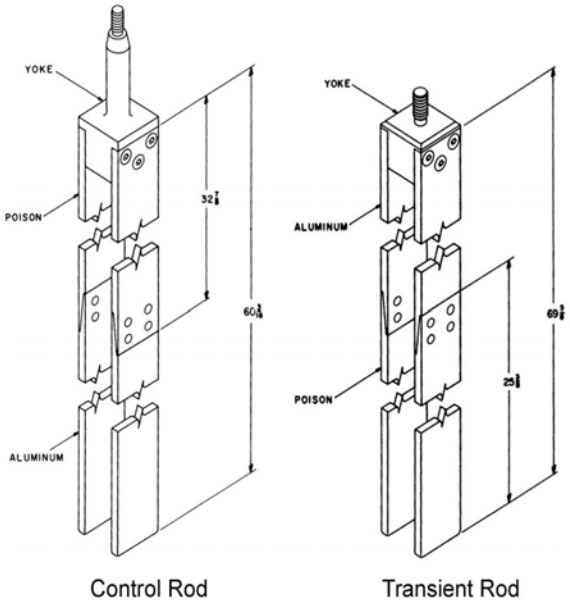

Figure A-22: Spert I D-Core Control and Transient Rods (modified from Ref. A-15)

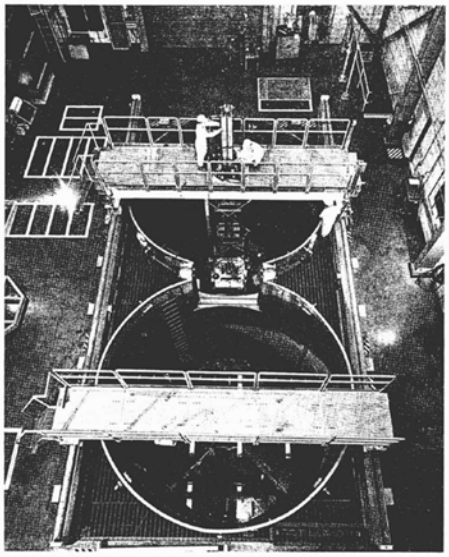

Figure A-23: Overhead Photograph of the Spert IV Reactor (Ref. A-21)

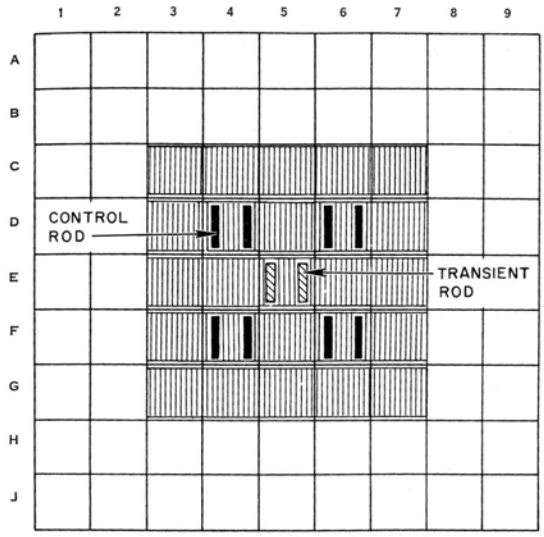

Figure A-24: Spert IV D-12/25 Core Configuration (Ref. A-21)

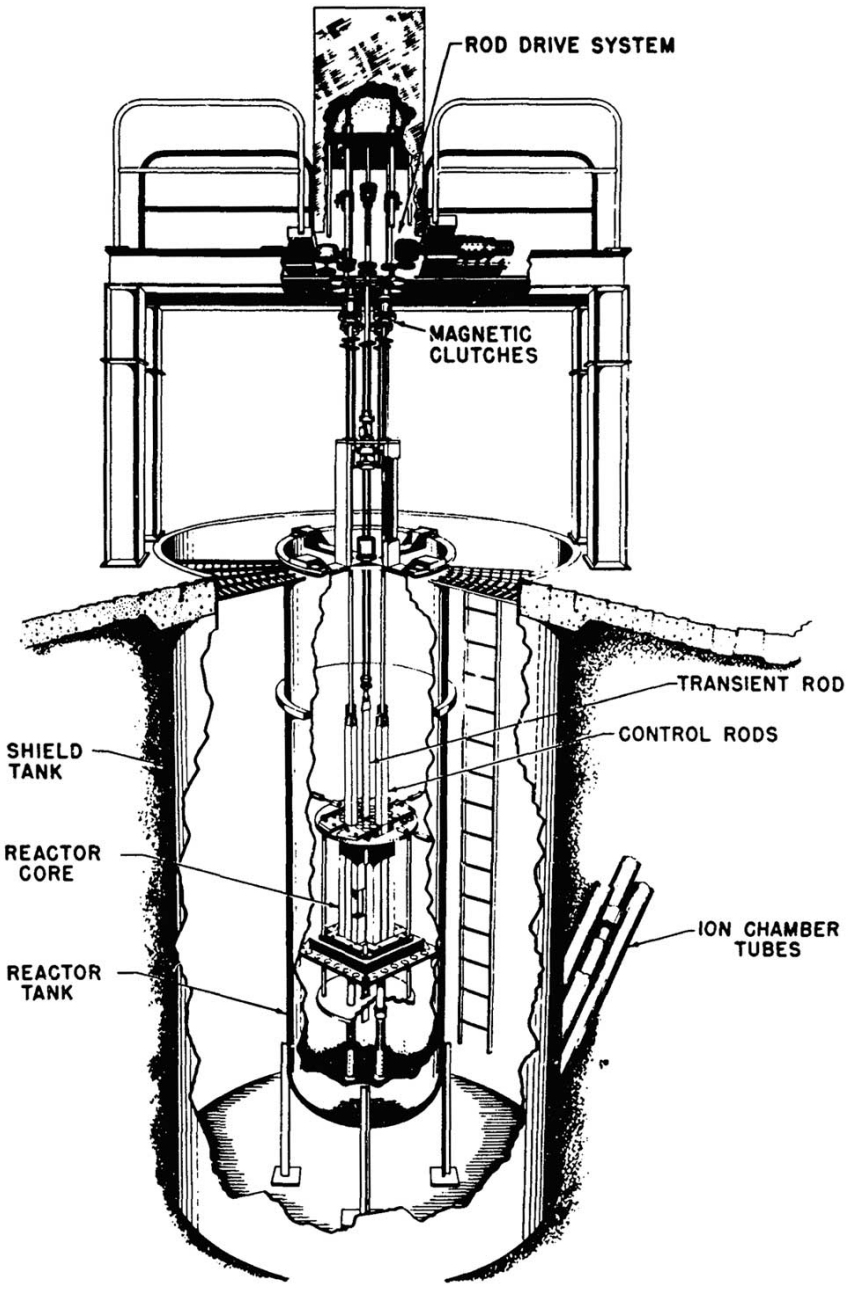

Figure A-25: Cutaway Drawing of Spert I with the P-Core Installed (Ref. A-25)

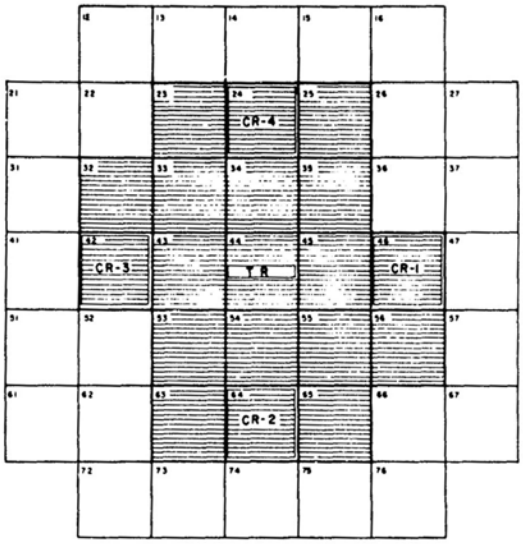

Figure A-26: Spert I P-18/19 Core Configuration (Ref. A-25)

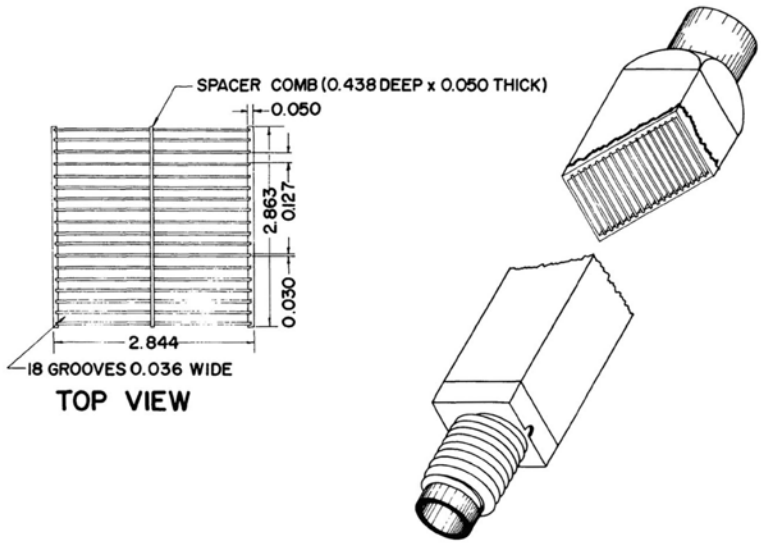

Figure A-27: Spert Type-P Fuel Assembly (modified from Ref. A-26)

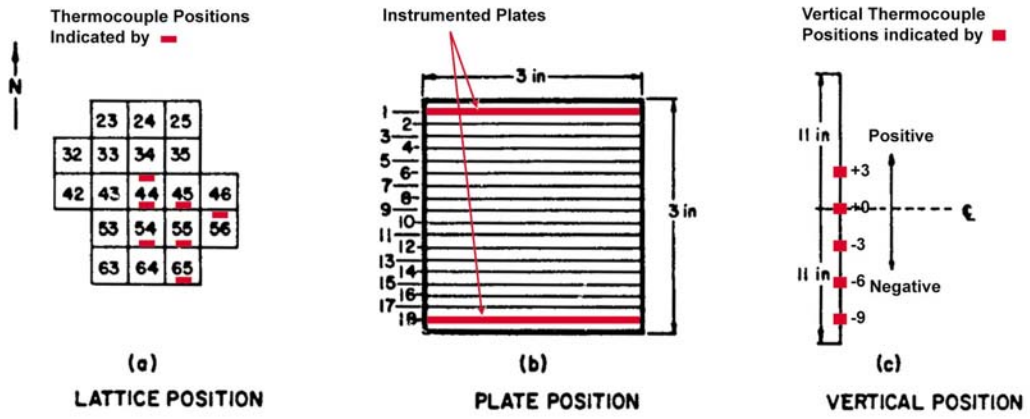

Figure A-28: Spert I P-Core Coordinate System and Thermocouple Locations (modified from Ref. A-25)

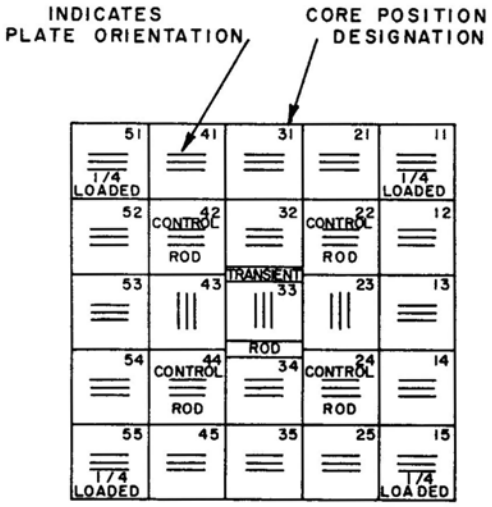

Figure A-29: Spert I BSR-II (6070-g Loading) Core Configuration (Ref. A-28)

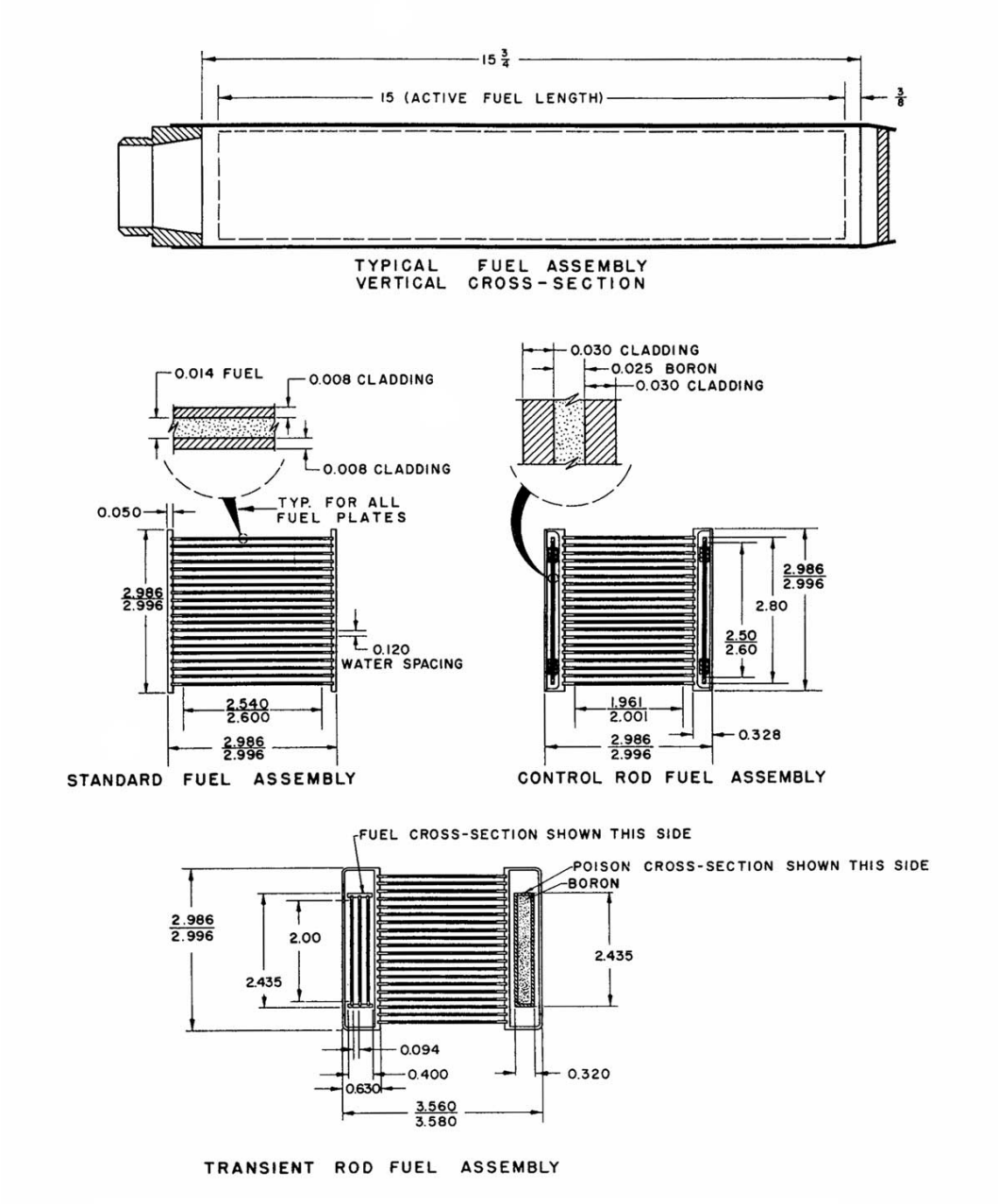

Figure A-30: Spert I BSR-II Standard Fuel, Control Rod, and Transient Rod Fuel Assemblies (Ref. A-28)

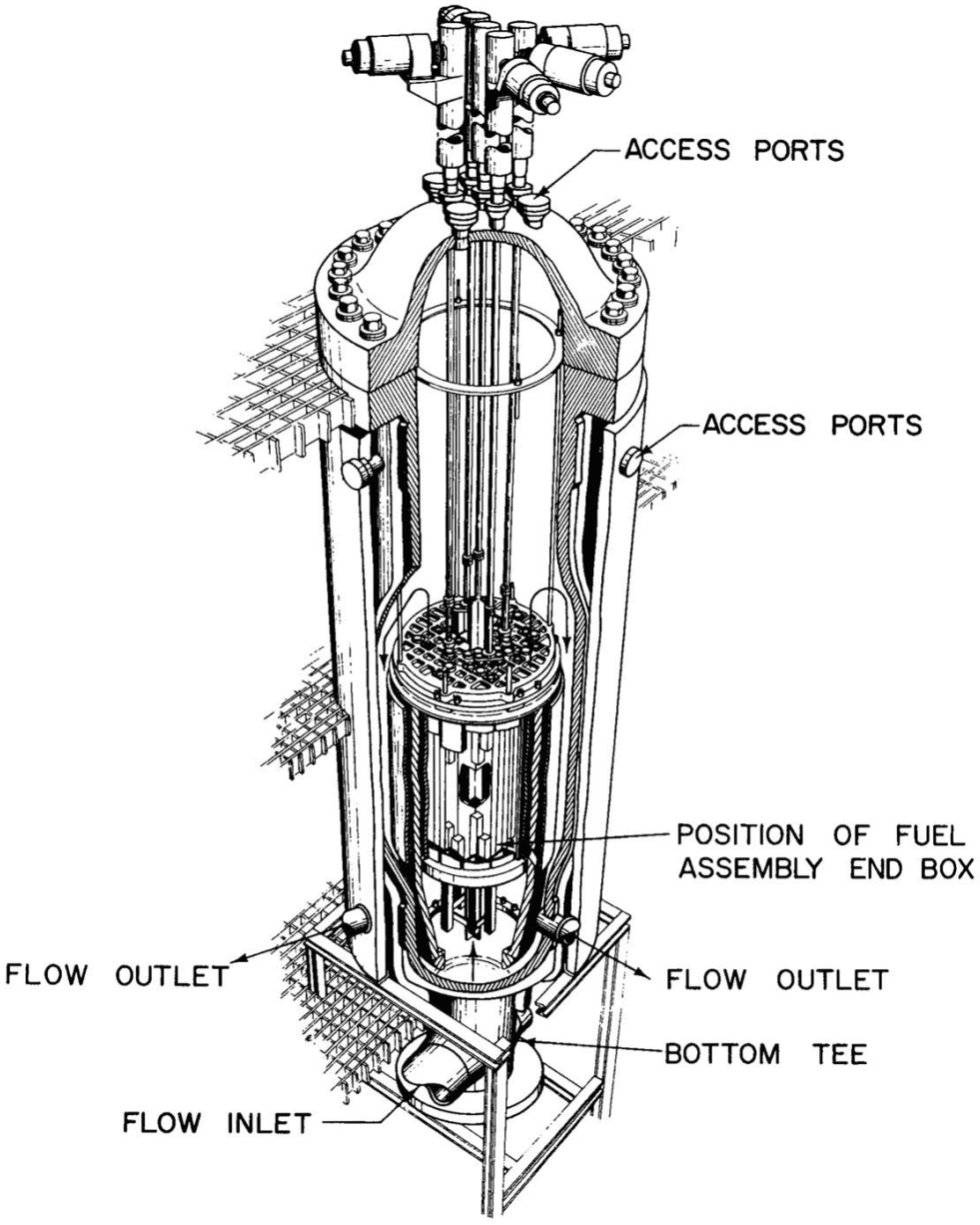

Figure A-31: Cutaway Drawing of the Spert III Facility with the C-Core Installed (Ref. A-32)

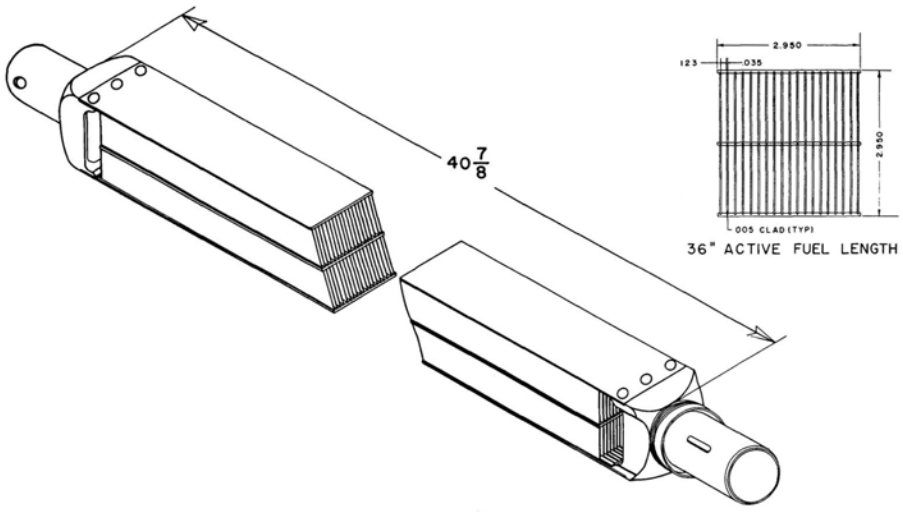

Figure A-32: Spert Type-C Fuel Assembly (Ref. A-26)

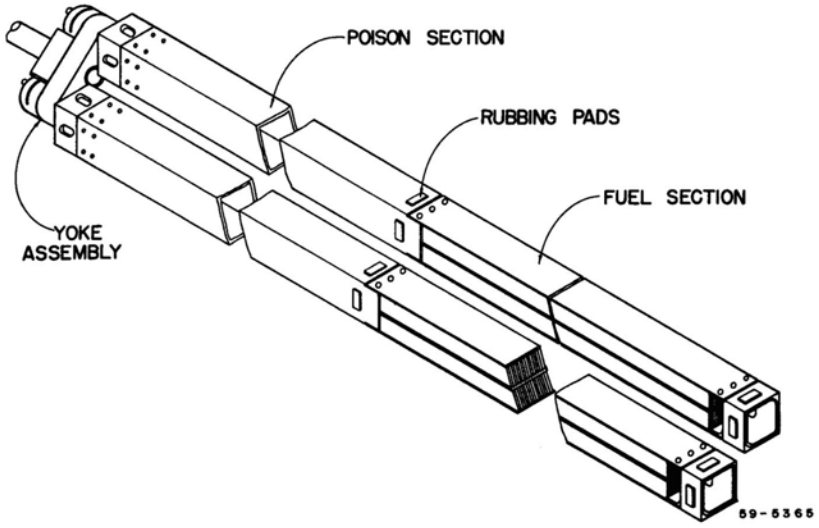

Figure A-33: Spert C-Core Control-Fuel Assembly (Ref. A-37)

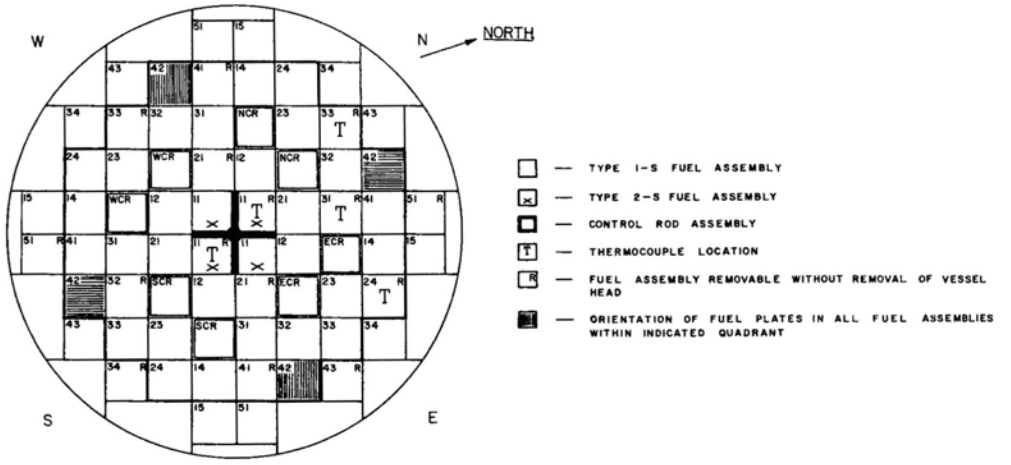

Figure A-34: Spert III C-19/52 Core Configuration (modified from Ref. A-32)

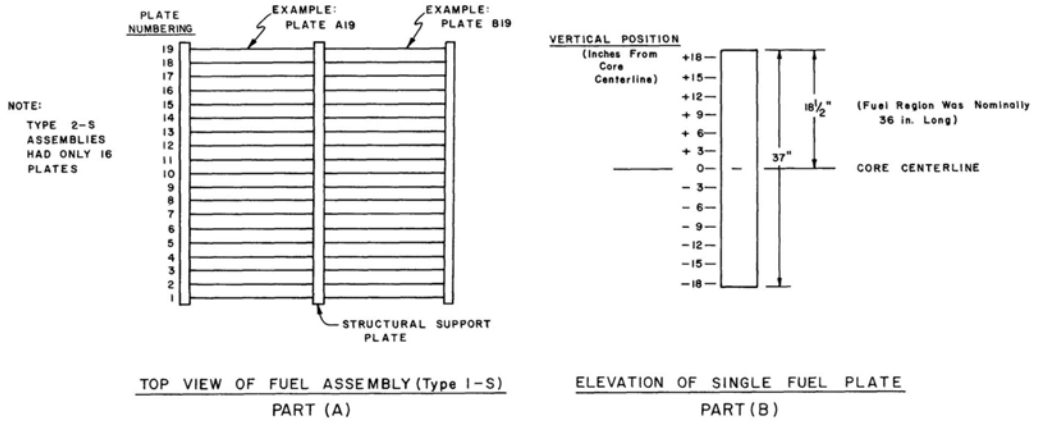

Figure A-35: Spert III C-Core Assembly Coordinate System (modified from Ref. A-32)

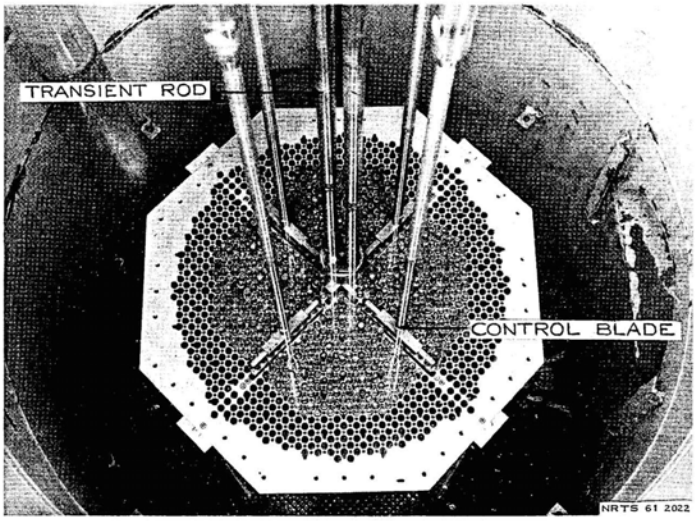

Figure A-36: Top View of Spert I Oxide Core (Ref. A-38)

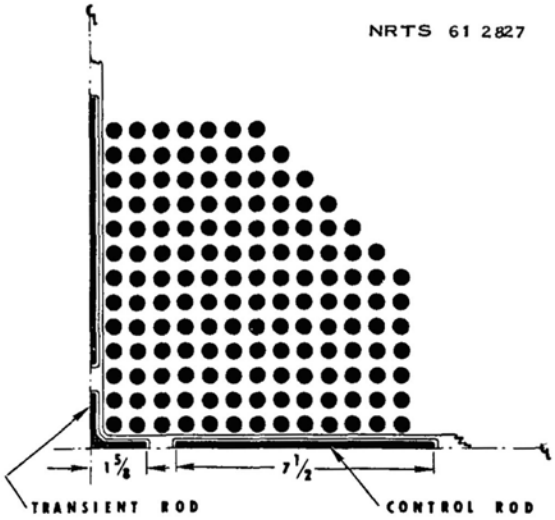

Figure A-37: Quarter Section of the Spert I SA-592 Oxide Core (Ref. A-38)

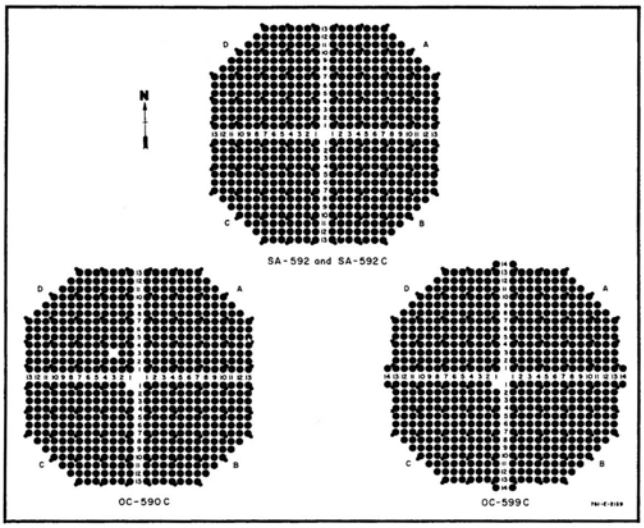

Figure A-38: Loading patterns for the Spert I SA-592, SA-592C, OC-500C and OC-599C Cores (Ref. A-39)

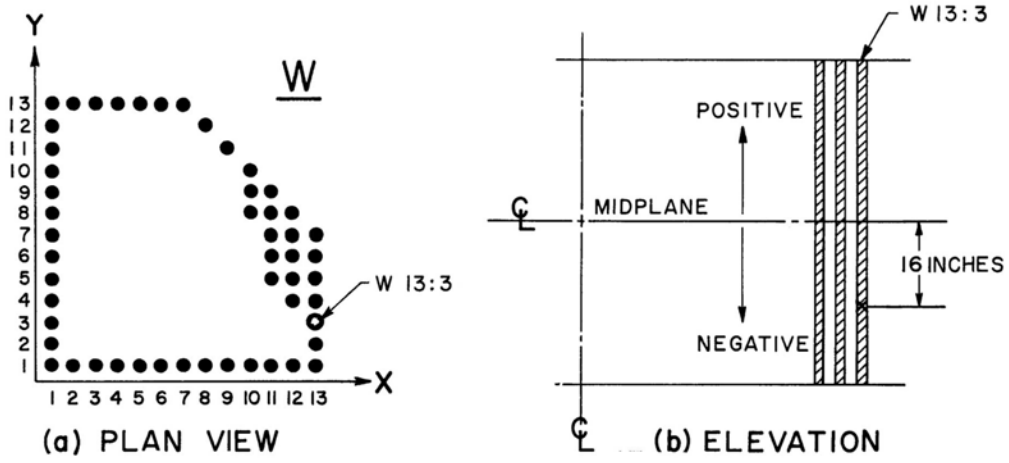

Figure A-39: Scheme for specifying thermocouple location in the Spert I SA-592 core (modified from Ref. A-40)

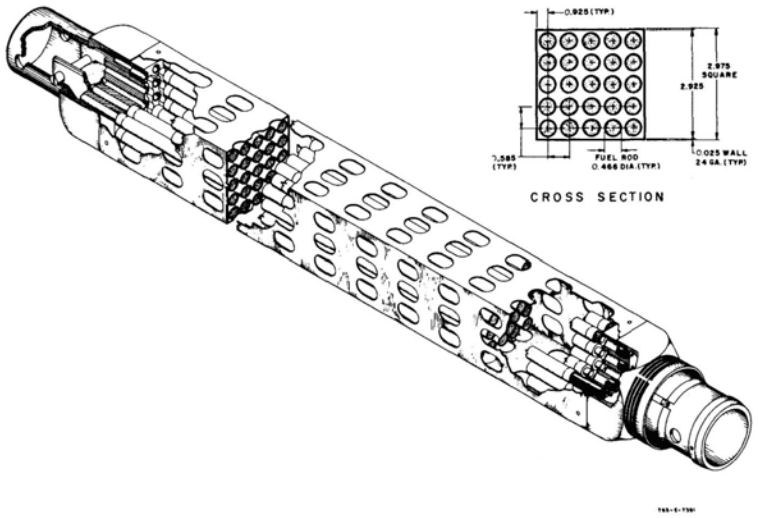

Figure A-40: Spert III Type-E 25-rod Fuel Assembly (Ref. A-45)

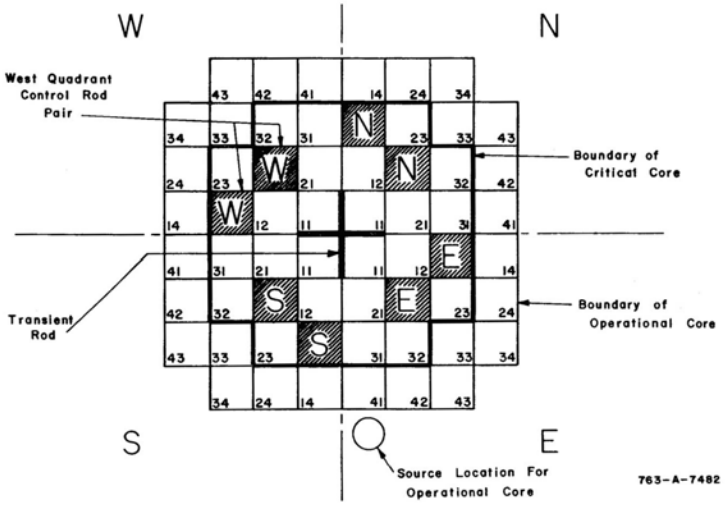

Figure A-41: Spert III E-Core Loading Pattern (Ref. A-45)

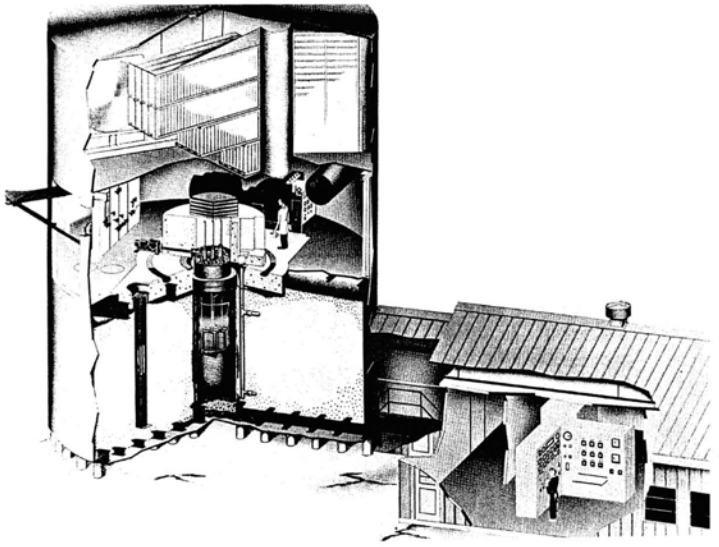

Figure A-42: Cutaway Drawing of the SL-1 Facility (Ref. A-50)

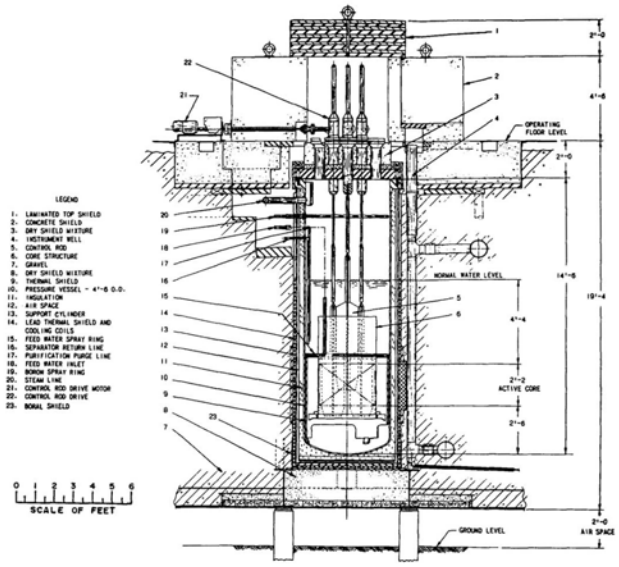

Figure A-43: SL-1 Vertical Section Diagram (modified from Ref. A-48)

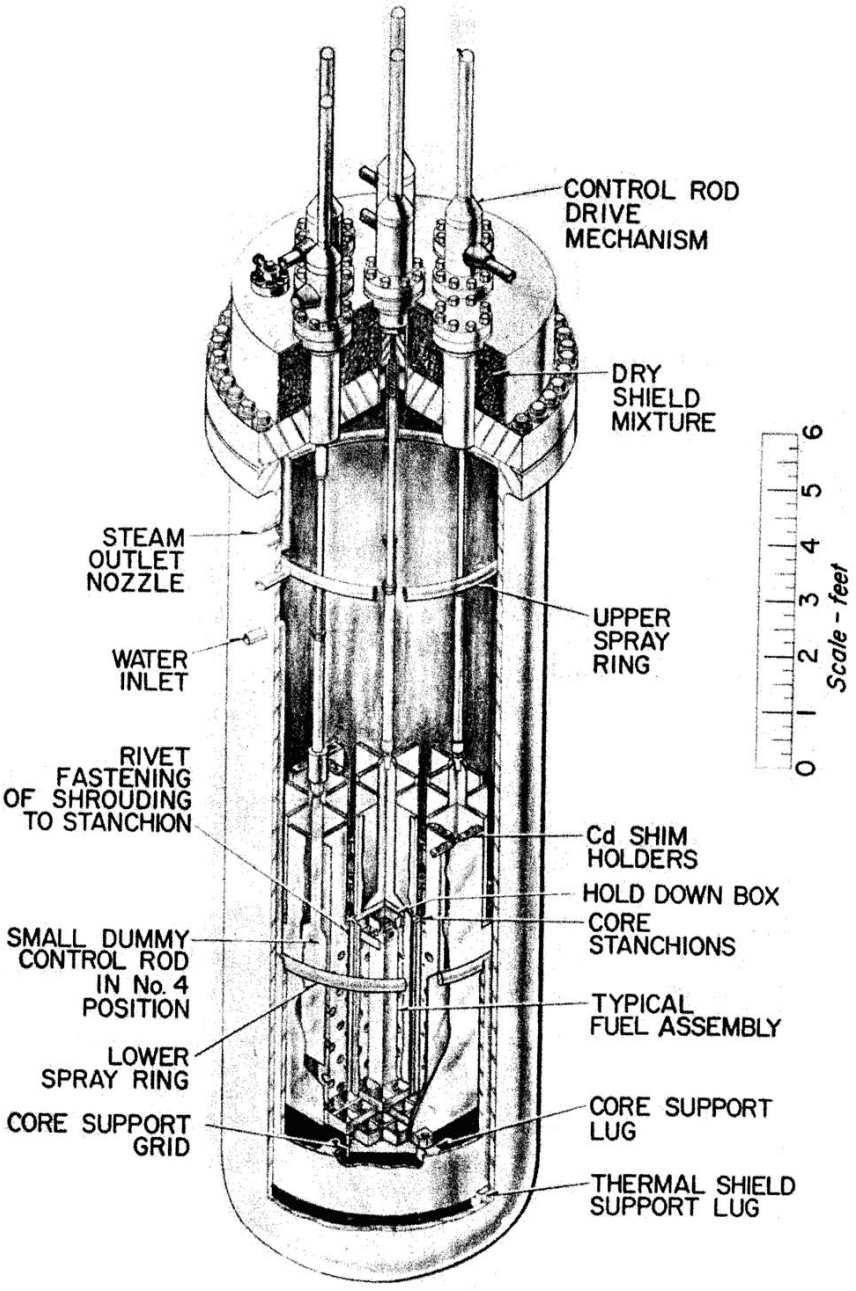

Figure A-44: Cutaway Drawing of the SL-1 Reactor Vessel (Ref. A-49)

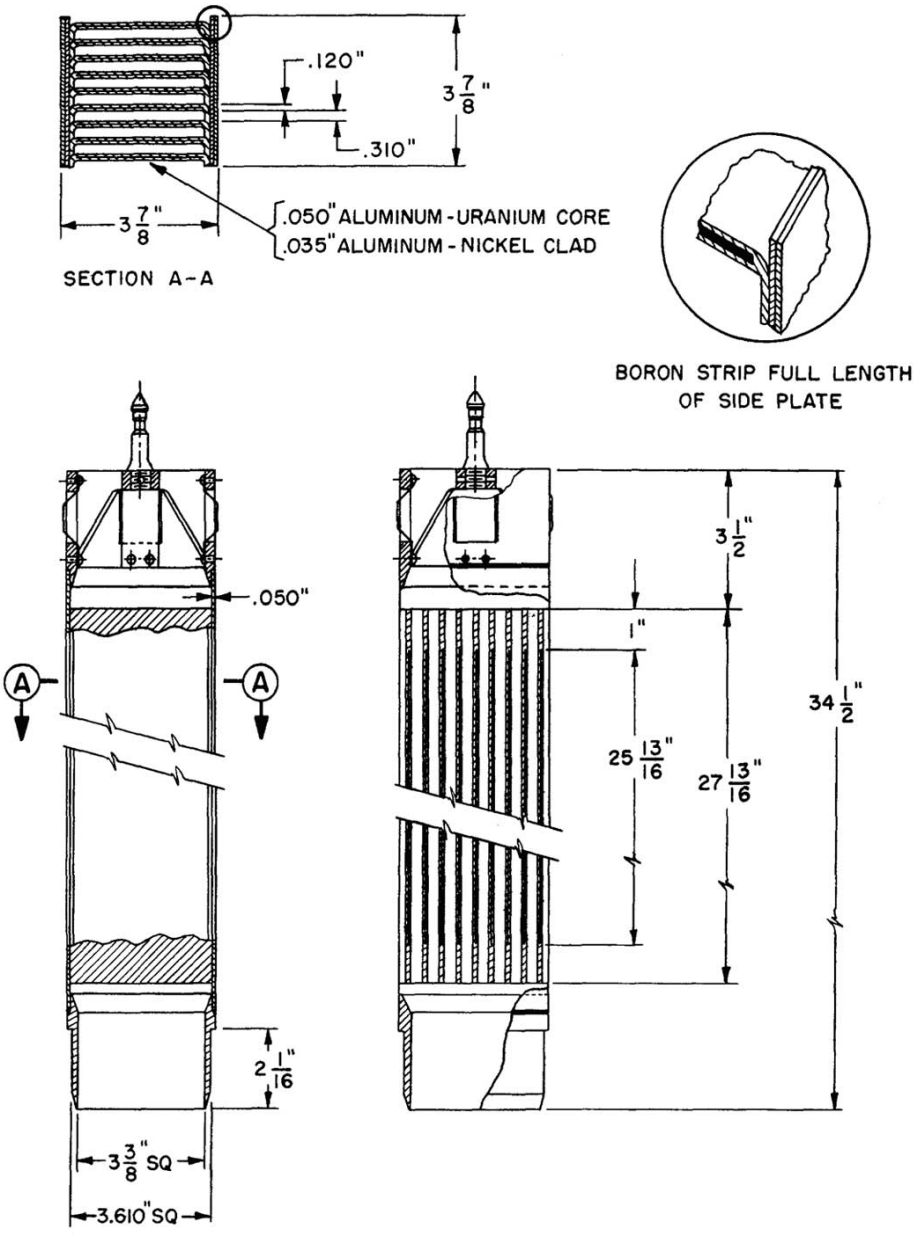

Figure A-45: SL-1 Fuel Assembly Schematic (Ref. A-48)

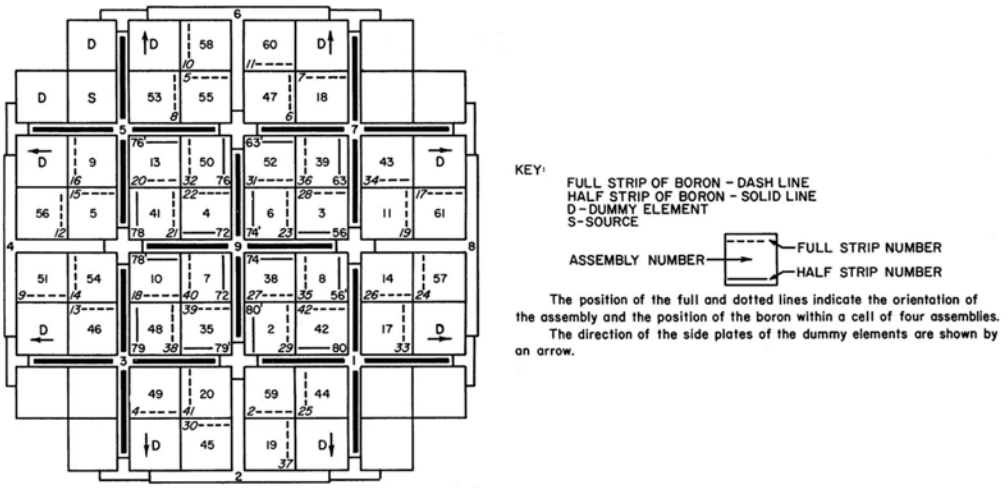

Figure A-46: SL-1 Core Configuration (modified from Ref. A-49)

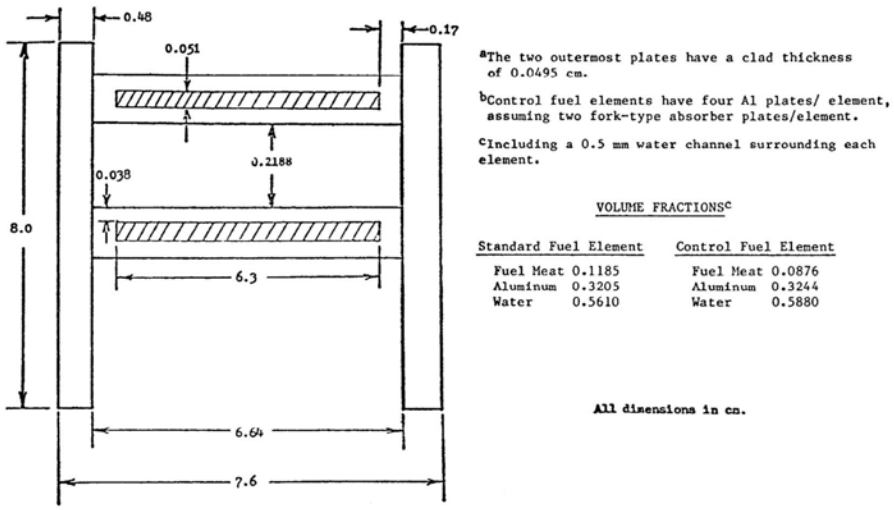

Figure A-47: IAEA 10MW Benchmark Reactor Fuel Assembly (Ref. A-52)

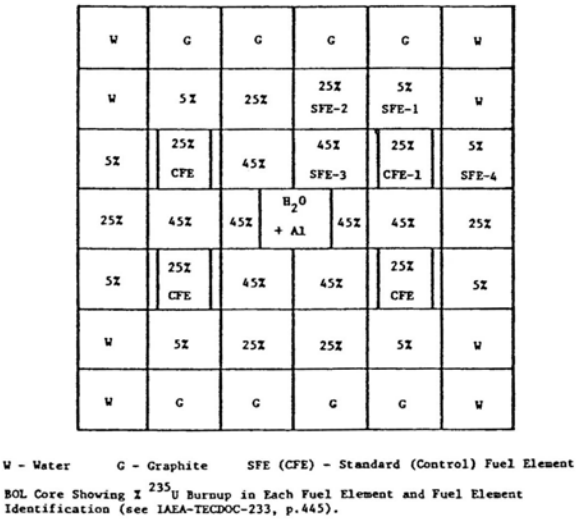

Figure A-48: IAEA 10MW Benchmark Reactor Core Configuration (Ref. A-53)

(this page is intentionally left blank)

APPENDIX B - THE EXPERIMENTAL DATA: SUMMARY

TABLE OF CONTENTS

LIST OF TABLES

LIST OF FIGURES

(this page is intentionally left blank)

B THE EXPERIMENTAL DATA: SUMMARY

This appendix provides a summary of the test data as collected from the literature.

The data presented herein have already been "processed" from the original oscillograph recordings. In this sense multiple sensor readings have been interpreted previously. The state of the data is in the form of tabulated values, processed time traces and correlated figures, mainly extracted from the relevant series of ANL and IDO technical reports published during the Borax and Spert Projects by the US Atomic Energy Commission. The sources are referenced throughout.

Mostly, the data are indexed by the period of the transient rather than the size of the initiating reactivity insertion. To provide additional context for the data the range of reactivities associated with the test series are included. Unless otherwise indicated these have been backed out of the Inhour equation using U-235 delayed neutron data and the reported prompt neutron lifetimes for each of the test cores.

B.1 Step Tests

The following sections summarize the transient data collected for tests initiated by step insertions of reactivity in the following types of cores:

- aluminum-clad HEU plate fuel
- stainless-steel-clad HEU plate fuel
- stainless-steel-clad LEU rod fuel

Both the Borax I and Spert programs are considered.

B.1.1 Aluminum-Clad Plate-Type Cores

Step reactivity insertion tests were carried out in each of the following cores. A brief description of the specific test series follows.

- Borax I
- Spert I A-17/28
- Spert I B-24/32
- Spert I B-16/40
- Spert I B-12/64

- Spert I D-12/25
- Spert IV D-12/25

B.1.1.1 Borax I Step Tests

The Borax step insertion transient tests can be categorized into three groups:

- step insertions of various sizes from saturation coolant conditions,
- variation of the degree of subcooling for two different period transients, and
- step insertions of various sizes from ambient coolant conditions.

All step reactivity insertion tests were initiated from low power conditions with only natural circulation coolant conditions. In Borax I the emphasis of the testing program was initially on boiling conditions. Tests were performed with periods ranging from 70 msec to 5 msec, corresponding to reactivity insertions between roughly 8 mk and 20 mk. These tests show the relation of maximum power, generated energy and fuel plate temperature rise with respect to the period of the transient. The data are presented in a series of plots of in Reference B-1 and is summarized in Table B-1.

The second group of tests is comprised of transients with periods of 22 msec and 13 msec, performed with the reactor initially at temperatures at and below coolant saturation, *i.e.*, subcooled coolant conditions. These periods are generated by reactivity insertions of about 10 and 12 mk respectively. This data set is useful in deriving the functional dependence of the damage indicators (*i.e.*, power, temperature, energy) on the degree of subcooling. Research reactors typically operate under subcooled conditions and this dependence proves critical when applying the test data to other specific reactor systems. The maximum temperature rise of the fuel plates and the associated energy generated as a function of the degree of subcooling are reported in the form of plots in Reference B-1. These are reproduced as Figures B-1 and B-2. These "subcooling" data have been digitized from the figures in Reference B-1 and are given in Table B-2. It should be noted that the Borax energy data reported in Reference B-1 and shown in the two figures represent only that fraction which are deposited as heat in the fuel plate (approximately 85% of the total generated energy). This has been adjusted, using a factor of 0.85 in Table B-2. Maximum power is not reported for these tests.

The first two test series comprise 70 experiments. The maximum fuel temperature in all of these tests, including those with subcooling, never exceeded 340EC (*i.e.*, 640EF). This is below the conservative estimate for the onset of blistering of fuel damage.

The test program was then extended to include a destructive test series. These tests were conducted in the spring, summer and fall of 1954 and comprise the third group of experiments. Step insertions, from ambient coolant conditions were performed with periods ranging from 134 msec to the final destructive test (D-test) which had a period of 2.6 msec, corresponding to a step reactivity insertion of about 31 mk. The 2.6 msec D-test was the only subcooled test with a period shorter than 13 msec.

The time traces of the power and fuel plate surface temperature are given for four of these tests (Figures B-9 to B-12 of Ref. B-2) as well as the maximum temperature for these plus one other test in the series (Figure B-16 of Ref. B-2). For these tests the initial coolant temperature is noted on the plots. For the remainder of the tests in this series, the subcooling is reported as "approximately 80EF" (27EC) but is indicated to range between 66EF and 82EF (19EC to 28EC) on Figure B-41 of Reference B-2. These data are available as energy generated and maximum power *vs.* reciprocal period plots (see Figs. B-3 and B-4). Except for the aforementioned four tests, temperature data are not reported for this group of tests. The data from these figures have been digitized and are summarized in Table B-3. The data in this group of tests are useful to compare to similar test series from the various Spert cores to determine sensitivities to various system parameters. The lack of precise initial temperature conditions may account for some of the scatter in the 1954 energy and maximum power data, which is considerable.

Results for the Borax I destructive test are discussed in Reference B-2. The time traces of the data are reproduced in Figure B-5. Results of this test are only approximate but are useful in extending the range of transients of the step insertions from ambient conditions. Energy generated was calculated from cobalt foil activation with estimates ranging between 125 MW-sec and 181 MW-sec. The value of 135 MW-sec is assessed as the most reliable (Ref. B-2). Power estimates are only approximate as the ion chamber traces were lost in noise which does not allow for normalization to the energy value. The two in-core thermocouples failed before the peak temperature had been reached. One reached 690EC but the maximum temperature is likely higher than this judging by the trend in the data. The two out-of-core thermocouples failed approximately 8 msec after the peak power was reached. The centre temperature of the hot-plate in the core is estimated to have

reached between 1093EC and 1650EC. Pressure generated in the test is estimated to have reached at least 6000 psi based on damage to the diaphragm of a pressure transducer.

B.1.1.2 Spert I A Step Tests

A brief summary of the transient tests conducted with the Spert I A-17/28 core is given in Reference B-3. Of the 606 transient tests with the A-core, the majority were of the step reactivity insertion variety in which the parameters varied were the initial temperature (*i.e.*, subcooling) of the system and the size of the initiating reactivity insertion (*i.e.*, resulting in a specific period). The Spert I A transient step insertion tests can be categorized into two groups:

- step insertions from ambient conditions
- step insertions from saturation conditions

The tests were conducted with a two foot hydrostatic head above the core, from low power (~ 5 W), at atmospheric pressure and with natural circulation coolant flow.

For the ambient condition tests the results for a total of 56 tests are reported spanning the range of periods from 10 sec to 7 msec (step reactivity insertion between 2.6 and 14 mk). The initial temperature varied between 12EC to 39EC, although the majority (46) of the tests had an initial temperature between 15EC and 25EC. The test sequence for the Spert I A step reactivity insertion tests is shown in Figure B-6. It should be noted that the reactor was either just critical or slightly subcritical when the transient rod was ejected to initiate the test. The power had been allowed to decay from a level of about 200 W as the shim rods were positioned, to the initial power level of about 5 W.

The results of this test series are reported as time traces of power, fuel plate temperature, and pressure, as well as in tabular format in Reference B-3 (these data have been previously reported in References B-4 and B-5). Accompanying reactivity calculations for some of these tests are reported in Reference B-6. The data for this test series are summarized in Table B-4.

It is noted in Reference B-3 that for some of the tests it is suspected that the range on the thermocouple was incorrectly set. These tests are indicated in Table B-4. In addition, for the earlier tests, the plate from which the thermocouple readings were taken was not noted. The plate was either 012 or 172 (see Appendix A for coordinate

system). It should be noted that plate 012 in assembly 55 is next to the control blade gap and thus may be associated with a higher power density and subsequent temperature.

A companion "boiling series" was also conducted with the Spert I A-core. The tests were initiated from boiling conditions (~ 96EC). Some data are presented in Reference B-7, but do not include the fuel plate temperature or pressure results. The saturation test results are reported in Reference B-8 in graphical format. Due to the late nature of locating these results, these data are not included in the tabulations of this appendix.

In addition to these two test series, various step insertion tests, exploratory in nature, were conducted in Spert I A which investigated changes in moderator properties by the addition of additives, the variation of the hydrostatic head, and the variation of initial power. A single short period test, extending the range of periods for the ambient step insertion test series was also included in these tests. This test extends the range of the ambient step insertion series down to a period of 5.5 msec (ρ_{in} • 16 mk). The results from these tests are reported in Reference B-9. The data from this short period test are included in Table B-4, however energy and thermocouple location are not reported and the initial temperature was only given as "ambient". The results of the tests with variation of hydrostatic head and initial power are mainly qualitative in nature and informative from a shutdown mechanism standpoint.

B.1.1.3 Spert I B Step Tests

The principle goal of the Spert I B-core tests was to investigate the effect of variation in the void coefficient of reactivity on the self-shutdown characteristics of the system.

Step insertion tests were conducted on the Spert I B-cores (B-24/32, B-16/40 and B-12/64) for various degrees of subcooling but mostly with the system at ambient (~ 20EC) or coolant saturation temperatures from low power (~ 5 W) with a two-foot hydrostatic head. The removable plates in the Type-B assemblies allowed for variable water channel spacing and as a result varying core size and void coefficient of reactivity for the different configurations. The tests cover the range of periods down to about 10 msec only (produced by ρ_{in} of 12 to 14 mk). The data summary for these tests is reported in Reference B-10 and includes tabulated data, time traces of power, temperature and pressure, and summary and correlated data plots. The summary data for these tests for the three B-cores are given in Tables B-5, B-6, and B-7.

The step tests from varying initial temperature (*i.e.*, subcooling) compliment the data reported from the Borax I tests with regards to the sensitivity with subcooling.

In addition to the main test series, an additional test series was conducted using the B-24/32 core to explore step insertion initiated transients with forced coolant flow (using a stirrer system as Spert I had no other forced flow capabilities). The results of these tests are mainly qualitative in nature and are reported in Reference B-11.

B.1.1.4 Spert I D Step Tests

The last aluminum plate core studied in Spert I was the D-12/25 configuration. Following the usual initial testing procedure for a new core, a "fiducial", or check-out test series of 47 step insertion transients was conducted covering the range of periods from 1.3 sec to 6.4 msec (5.2 mk < ρ_{in} < 16 mk). This was followed by an exploratory test series, the Destructive Test Series, consisting of three step insertion tests. These three tests produced periods of 6.0, 5.0, and 4.6 msec (ρ_{in} ~ 20 mk). Fuel plate clad melting was observed in the latter two tests in the central region of the core. Testing was concluded with a destructive test, a step reactivity insertion of about 25 mk from subcooled conditions which produced a period of 3.2 msec. The majority of the test data are reported in References B-12 and B-13. The summary data from these tests are given in Table B-8. For all these tests the initial temperature of the system was ambient and only natural circulation flow was used.

B.1.1.5 Spert IV D Step Tests

The Spert IV facility was designed primarily to investigate stability issues (*i.e.*, chugging) which were observed in both the Borax I and Spert I systems. However, as part of the test program three sets of self-limiting step insertion tests were conducted prior to the stability test program. The test series carried out with the Spert IV D-12/25 core were:

- step insertions with an 18' hydrostatic head
- step insertions with a 2' hydrostatic head
- step insertions under forced upward flow conditions

All of these tests were conducted from low power (about 1 W), ambient temperatures and atmospheric pressure conditions. The first test series (16 tests reported) was performed with natural circulation coolant flow under a hydrostatic head of 18 feet, for a range of periods between 980 msec and 7 msec, corresponding to a range of

initiating reactivity insertions between about 5.6 mk and 15 mk ($0.8 to $2.14). Slight fuel plate bowing was observed for the 7 msec-period test and melting was predicted for periods less than 6 msec. The second test series was comprised of three tests under the same conditions but with a hydrostatic head of 2 feet. The periods associated with these tests were 21.3, 12.0 and 8.8 msec. The third series of tests (27 tests reported) was also conducted from ambient temperatures and atmospheric pressure under an 18 foot hydrostatic head. This test series included forced upward coolant flow ranging between 500 and 5000 gpm. The range of periods studied were 560 msec to 9.7 msec.

The results from these tests are reported in tabular and graphical form in Reference B-14. Time traces of power, energy, temperature and pressure are included in the reported results. The temperature traces generally represent the highest recorded fuel temperature for the specific test. The data from Reference B-14 are also found in a pair of quarterly reports (Refs. B-15, B-16) and tabulated in the primary Spert IV stability report (Ref. B-17). The summary data from these tests are given in Table B-9.

B.1.2 Stainless-Steel-Clad Plate-Type Cores

Step reactivity insertion tests were studied in each of the following cores:

- Spert I P-18/19 (APPR)
- Spert I BSR-II
- Spert III C-19/52

A brief description of the specific test series follows.

B.1.2.1 Spert I P Step Tests

Testing on the Spert I P-core was solely of step transients for periods ranging between 6 sec and 4 msec for the purpose of investigating differences in transient response due to differences in heat transfer characteristics of aluminum and stainless steel. The initial power was approximately 2 W for these tests from either initially ambient (between 14EC and 21EC) or saturated temperature conditions (96EC). Moderator-expulsion (*i.e.*, mechanism) capsule tests were conducted from ambient conditions using this core but the range of periods were enveloped by the initial ambient step transient tests (Refs. B-18, B-19). A final test series which involved a simulation of a fuel-drop accident scenario is associated with a fast reactivity

insertion, close to a step (see Section B.4 "Safety Analysis Scenario Tests").

The power, fuel plate surface temperature and pressure for the step tests are summarized in Reference B-20. The data also include fuel plate surface temperature rise as a function of both axial and radial position in the core. The summary data from these tests are given in Table B-10.

B.1.2.2 Spert I BSR-II Step Tests

Step insertion tests on the BSR-II core were conducted as part of a study on the effectiveness of mechanical shutdown systems, *i.e.*, control rod insertion. Self-limiting tests with periods between 544 msec and 15 msec were included in the test series. Shorter period self-limiting tests were not conducted as to avoid warping and rippling damage as experienced with the stainless steel P-core fuel for periods shorter than 15 msec. During all tests the surface temperature of the fuel did not exceed 200EC.

A total of eight self-limiting step tests are reported (Ref. B-21). These tests were conducted from low power (mW range) and ambient conditions. As these tests were conducted in the Spert I facility there was no additional pressurization or coolant flow beyond natural circulation. The results of the tests are reported in correlated data plots of maximum power (Fig. B-7), energy release to the time of peak power (Fig. B-8), and peak fuel temperature at the time of peak power (Fig. B-9) and overall during the transient (Fig. B-10). The maximum power data are also presented in plots comparing the self-limiting tests with the various types of protected tests (see Section B.4 "Safety Analysis Scenario Tests"). Time traces of the power and temperature for the eight tests are also given in the appendix of Reference B-21). The thermocouple locations associated with the temperature traces are not indicated.

B.1.2.3 Spert III C Step Tests

The Spert III C-19/52 core tests were designed to extend the range of testing of stainless-steel-clad plate-type cores into conditions more typical of power reactors. As a result most tests were conducted from elevated temperatures and under pressurized conditions, both with and without forced coolant flow.

The step tests conducted on the C-19/52 core can be grouped into four sets based on their initial conditions:

- tests from low power, ambient temperature, atmospheric pressure, with natural circulation flow,
- tests from low power, varied subcooling, atmospheric pressure, with natural circulation flow,
- tests from low power, elevated temperature and pressure, with varying forced upward flow, and
- tests from high power, elevated temperature and pressure, with forced upward flow.

The first two groupings are most relevant to research reactor conditions. These two test groups are comprised of 51 tests from initial temperatures between 18EC and 90EC for a range of periods from 9.3 seconds to 10 msec. Periods on the order of 20, 40, and 150 msec were selected for testing in the subcooling series. In the reported analysis of these tests the periods of the individual tests were corrected to these three values using trends from ambient step insertion test results.

Reference B-22 contains the most complete summary of all of the step tests except the high power tests. The reported temperature data and associated thermocouple locations correspond to the hottest temperature recorded for the tests. Time traces of power, temperature, reactivity and energy for a selection of representative tests spanning the range of periods are also included. These results had previously been reported in a series of quarterly reports and two summary reports. The high power tests are reported in References B-23, B-24, and B-25.

The summary data for the tests in the first two groupings, *i.e.*, those conducted under atmospheric pressure and natural circulations conditions, are given in Table B-11.

B.1.3 LEU Oxide Rod-Type Cores

Step reactivity insertion tests were studied in each of the following cores:

- Spert I SA-592
- Spert I OC (Destructive Core)
- Spert III E

A brief description of the specific test series follows.

B.1.3.1 Spert I SA Step Tests

A program of kinetic tests on low enrichment oxide rod-type cores commenced in February 1961 with the 4% enriched UO_2 SA-592 core in the Spert I facility. This program ran until October 1961. An initial series of self-limiting transients were performed covering a range of reactor periods from 15 sec to 3.2 msec. All step insertion tests were conducted from atmospheric pressure, ambient temperature, and low power with no forced flow and a hydrostatic head of approximately two feet above the top of the core.

At short periods it was found that rod-bowing produced an additional positive reactivity effect and resulted in multiple power burst responses. The step transient tests were repeated with a constraining grid holding the rods in place, eliminating the bowing effect. Data for the "unconstrained" and "constrained" core test series, including time traces of surface temperature, power, energy, and compensating reactivity, as well as correlated data plots, are reported in tabular form in Reference B-26. The associated rod position data are reported in the tables given in References B-27 and B-28. The "constrained" core data are reproduced herein in Table B-12.

B.1.3.2 Spert I OC Step Tests

The "Destructive Test Series" was conducted between May 1963 and May 1964 and consisted of 13 check-out step transient tests (of previously explored periods) and two potentially destructive step tests, all conducted from atmospheric pressure, ambient temperature, low initial power and natural circulation only conditions under an approximately two-foot hydrostatic head.

The check out tests were conducted to determine the reproducibility of the results from the SA-592 core and covered the period range from 1.3 sec to 9.8 msec. Results varied noticeably between the SA-592 and OC cores and are attributed to differences in the rod restraining grid and a modified transient rod.

The two potentially destructive tests with periods of 2.2 msec and 1.6 msec both resulted in the rupture of two fuel rods. The rod ruptures occurred just after the peak power in the 2.2-msec period test and just prior to peak power in the 1.6-msec period test, and resulted in negative reactivity *via* coolant voiding produced by dispersion of the hot fuel material. As a result the 2.2-msec period test power burst data are consistent and extrapolatable from longer period data while the burst data from the 1.6-msec period test are not.

The Destructive Test Series data set is reported in Reference B-29, which includes time traces of power, clad surface temperature, energy and compensated reactivity, correlated data plots and a full tabulation of the data. Additional information regarding the two potentially destructive tests is given in References B-30 and B-31. The data are reproduced herein in Table B-13.

B.1.3.3 Spert III E Step Tests

Testing of LEU oxide cores continued with the Spert III E-core. These tests were designed to supplement the Spert I oxide core program results by extending the test conditions to high pressure and temperature and including forced coolant flow. These test conditions are more typical of power reactors rather than research reactors.

A "check out" series of step tests was conducted under ambient temperature, atmospheric pressure, and natural circulation conditions from low initial power. This test series covered the range of periods from 1.9 sec to 10 msec. A second series from elevated temperature and pressure conditions with forced coolant flow was also conducted. Periods ranged from approximately 600 msec to 10 msec for initial temperatures of 250, 400 and 500EC with coolant flow rates of 2.3 to 23 ft/sec at a system pressure of 1500 psi. The data are reported in tabular format (Refs. B-32, B-33) but time traces have not been located. Subsequent problems operating the Spert III E-core resulted in the termination of the LEU oxide core test program. The summary data from these tests are given in Table B-14.

B.2 Ramp Tests

The following sections summarize the transient data reported for tests initiated by ramp insertions of reactivity. Ramp reactivity insertion tests were studied in the following cores:

- Spert I A-17/28
- Spert I B-12/64
- Spert I SA-592, SA-592C
- Spert I OC (Destructive Core)
- Spert III C-19/52

B.2.1 Spert I A Ramp Tests

Two exploratory ramp insertion test series are reported in Reference B-4. Power *vs.* reciprocal period results are reported for two test series (Figs. B-11 and B-12). The first series involved a ramp rate addition of 0.1 %Δk/sec from initial power ranging from 10 micro-watts to 5 W. The second series involved a ramp rate addition of 0.01%Δk/sec from an initial power ranging between 5 mW and 10 kW. The data from these two test series are also shown in a correlated data plot of maximum reciprocal period (minimum period) and maximum power against initial power in Figure B-13, and in a plot of maximum power against reciprocal period (Fig. B-14). The ramp data are not tabulated and consist only of power results (no temperature or pressure has been located).

A broader parameter range for the Spert I A ramp tests is indicated in Reference B-34, *i.e.*, starting power between 100 micro-Watts and 200 kW, initial temperature between ambient and boiling, and reactivity addition rate between 0.011% δk/sec to 0.36% δk/sec. Data for these tests have not been located.

B.2.2 Spert I B-12/64 Ramp Tests

Three ramp insertion test series were conducted on the B-12/64 core. These tests were with a two foot hydrostatic head above the core and from an initial system temperature of 20EC. The ramp reactivity addition rate and the initial reactor power were varied. These test series were similar to those conducted with the A-17/28 core. Ramp rates of 0.01%Δk/sec, 0.10%Δk/sec, and 0.27%Δk/sec were tested and the initial power was varied between 0.5 mW and 10 kW. The power and period results are tabulated and plotted in References B-35 and B-36. The data are plotted along with B-12/64 step insertion test results in Figure B-15. Reference B-35 also contains time trace plots of power for varying addition rate and initial power level.

B.2.3 Spert I SA Ramp Tests

A total of eight ramp tests are reported for the Spert I SA cores. Six of these tests were conducted with the"unconstrained" core, while the other two were with the"constrained" core. All tests were carried out from ambient, low power, atmospheric pressure conditions with natural circulation coolant flow only. The reactivity addition rate was varied between 0.16 cents/sec to 21 cents/sec resulting in minimum periods ranging between 12 seconds and 48 msec. Only the power and period data, *i.e.*, no associated temperature or pressure data, are reported for the tests.

A correlated plot of P_{max} *vs.* α is given in Figure B-16 and a tabulation of the results can also be found in Reference B-27.

B.2.4 Spert I OC Ramp Tests

Ten ramp tests are reported as part of the Destructive Test Series conducted with the Spert I OC core (Ref. B-29) which also included combination ramp-step tests. As in the case of the Spert I SA-core tests, all of the ramp tests were conducted from ambient, low power, atmospheric pressure conditions with natural circulation coolant flow only. The ramp rate addition was varied to generate minimum periods ranging between 0.97 seconds and 58 msec. The data from these tests are more complete than the preceding tests with the Spert I A, B-12/64, and SA cores in that the energy and temperature data are also reported. The data are summarized in Table B-15. These data are also available in a series of correlated data plots of P_{max}, E_{tm}, T_{tm}, and T_{max} against α in Reference B-29.

B.2.5 Spert III C Ramp Tests

Ramp insertion tests were conducted in the HEU stainless steel clad C-19/52 core in the Spert III facility. Test conditions ranged from those typical of research reactors (ambient temperature, atmospheric pressure) to those more typical of power reactors (elevated temperature and pressure). Tests both with and without forced coolant flow were included.

For the ambient temperature tests the ramp addition rate was either 18, 35, or 53 cents/sec and the initial power was varied between 0.1 W and 100 kW. No data tabulation has been located for these tests but power time traces showing the variation with addition rate and initial power are included in Reference B-37. The results show the same dependencies as the HEU Al-plate core ramp tests conducted in Spert I A and B-12/64.

In addition, time traces of power and temperature for two transients (periods ~ 40 msec and ~ 17 msec) are also included as is a correlated plot of P_{max} *vs.* α. These latter three plots are included herein as Figures B-17, B-18, and B-19.

Tests conducted under elevated temperature, pressure and forced coolant flow conditions are reported in Reference B-30, and the tests conducted during the high power test series are reported in Reference B-23.

B.3 Stability Tests

In addition to the short term response of a system to both step and ramp insertions of reactivity the longer term "stability" of such a system has been the subject of experimentation and analysis. Examples of stable and unstable behaviour following a generic impulse to the system are shown in Figure B-20 (Ref. B-38). These definitions are adopted herein.

The systems for which stability characteristics were investigated are:

- Borax I
- Spert I A-17/28
- Spert I B-12/64
- Spert IV D-12/25

Herein, stability is taken to encompass steady boiling operation and the progression to oscillatory behaviour. Large amplitude oscillatory behaviour is termed "chugging".

B.3.1 Borax I Stability Data

Much of the Borax I experimental program was geared towards investigating the behaviour of an MTR-type core under steady boiling conditions. This mode of operation is reported and discussed in terms of stability in References B-1 and B-39.

Chugging was first identified during the 1953 steady state boiling tests with the Borax I reactor (Ref. B-1). These tests were carried out under atmospheric pressure conditions, with natural circulation of coolant, a water head between three and four and a half feet, with the bulk reactor temperature at saturation. The procedure for these tests was to incrementally add reactivity in a gradual fashion by withdrawing control rods. Results are discussed in a general manner in the text of Reference B-1. The power and temperature time traces for a single test are reported and included herein as Figure B-21.

In addition to the boiling tests, chugging was also observed in step reactivity insertion transients from saturation conditions in Borax I (Refs. B-1, B-39). A representative power and temperature record is shown in Figure B-22.

With regards to subcooled conditions, small amplitude power oscillations were

observed as were secondary power peaks following the initial power pulse of step insertion tets. Examples of this behaviour are reported and included herein as Figures B-23 and B-24.

B.3.2 Spert I A-Core Stability Data

Following this identification of the chugging phenomenon, further investigation was incorporated into the Spert Project. A stability test series was conducted in the Spert I reactor using the A-17/28 core. The objectives of these tests were to study the characteristics of the large amplitude oscillatory behaviour as well as to investigate the sensitivity of these oscillations to system parameters including the height of the hydrostatic head above the core, restriction of some flow channels, and the presence of surface tension reducing additives. The results of these tests are reported in References B-40, B-41, and B-42. For these tests, with the core initially at low power (~ 5 W), reactivity was added as a ramp insertion by rod withdrawal at a rate of approximately 0.9 mk/sec to a predetermined amount.

Tests were conducted with the initial bulk temperature of the tank at both ambient and boiling temperatures and for hydrostatic heads of two and nine feet (the maximum for the Spert I system) above the core. The oscillatory behaviour was allowed to continue up to 70 seconds, again showing no tendency to diverge or be damped. Examples of the power data are shown in Figures B-25, B-26, B-27, and B-28. Unfortunately, the accompanying temperature and void fraction data are not reported for these tests.

The voiding and refilling cycles associated with these tests were violent enough in nature to result in mechanical damage to fuel plates including having brazed plates ripped out of the side plates of the assemblies. The Spert I A stability program was concluded at this point as the design limitations of the system did not allow for adequate control over some important system parameters, *i.e.*, bulk system temperature, flow and hydrostatic head. The test program was continued later in the more advanced Spert IV reactor.

Additional tests in Spert I A were conducted to estimate the limits to the amount of reactivity held in voids for this system. These estimates were compared to estimates of the same quantity in the Borax I core (Ref. B-9). The results of these tests are somewhat questionable in that the compensating reactivity held in voids may be in error as other reactivity effects such as that due to bulk pool temperature changes were possibly not taken into account.

B.3.3 Spert I B-12/64 Stability Data

A series of three subcooled stability tests were conducted following the completion of a ramp transient test series in the Spert I B-12/64 core (Ref. B-35, B-43). Reactivity was added as a 0.7 mk/sec ramp. The system remained stable for reactivity additions of 10 mk and 12.5 mk, but oscillations developed for a 15 mk addition 8.4 seconds after the initial power peak. Under these conditions for the 15 mk addition, the mean power was 19 MW and oscillations reached peak powers of 85 MW on an average frequency of ~ 1.7 cps. The oscillations were allowed to continue for 30 seconds before the test was terminated. The degree to which these tests are reported is limited to the description in the text of Reference B-35.

Also in the Spert I B-12/64 core testing, steady boiling, small amplitude oscillations, and chugging were observed in the post initial power pulse run out of a series of step insertion transients from initially almost saturated conditions. Although not discussed in the results the power and fuel plate temperature time traces are included in Reference B-10. The maximum power during the chugging was about 20 MW and this was sustained over a duration of about 15 seconds.

B.3.4 Spert IV D-Core Stability Data

The Spert stability tests were continued in the Spert IV reactor with the D-12/25 core. These are reported in a series of Spert quarterly reports (Refs. B-25, B-31, B-44, B-45) and a summary report (Ref. B-17). The latter contains all the data in tabular form and the most complete analysis. The large pool volume in the Spert IV system allowed for tests with larger hydrostatic heads, up to 18 feet. The system also included heat removal and coolant flow capabilities. The objectives of the Spert IV stability test series were threefold:

- to determine the threshold of oscillations for various hydrostatic heads and flow rates,
- to provide data for evaluating the various analytical methods of predicting the threshold of oscillations, and
- to obtain data on the behaviour of the large amplitude oscillations.

The Spert IV stability tests were broken into three sets:

- threshold tests,

- ringing tests, and
- chugging tests.

The "threshold of instability" was arbitrarily defined as that where the power oscillation magnitude exceeded ± 50% of the mean power level. A more suitable terminology instead of "threshold of instability" is "threshold for the onset of chugging". Most of the work conducted in Spert IV was concerned with investigation of this onset threshold. Large amplitude oscillations were never allowed to develop to the degree of those studied in the Spert I A tests. Power, fuel plate surface temperature, and coolant temperature data are reported for these tests.

For the "threshold" tests, reactivity was added gradually *via* rod withdrawal in small increments from low power critical, ambient temperature initial conditions. This reactivity was added until a desired power level or a total inserted reactivity was achieved. The steady state or oscillatory behaviour of the system was then observed over a time frame of many minutes to sometimes a large fraction of an hour. If the power oscillations exceeded ± 50% of the average power or the fuel plate surface temperature exceeded 300EC then the tests were scrammed.

Tests were conducted under natural circulation coolant conditions for both 18-foot and two-foot hydrostatic heads, and also for forced upward flow with an 18-foot hydrostatic head. Due to the design of the Type-D fuel assemblies, the limiting fuel plate temperatures exceeded the safety cutoff before the threshold to chugging could be reached in the tests with forced flow. This was due to the lower flow rates in the more narrow outer fuel channels of the fuel assemblies. As a result, the stability tests with forced flow were deferred pending a redesign of the fuel assemblies which unfortunately never happened.

The threshold for the onset of chugging was determined for natural circulation conditions for both the 18-foot and two-foot hydrostatic head cases. Representative power and temperature traces for these two cases are shown in Figures B-29 and B-30.

To further investigate the point of onset of chugging, a set of "ringing" tests were conducted on the Spert IV D-12/25 core (Ref. B-17). The procedure for these tests followed that of the threshold tests up to a total reactivity precluding any oscillations above the noise associated with steady boiling. An additional amount of reactivity was then inserted rapidly (step insertion) to bring the system to just below the threshold for the onset of chugging previously determined in the threshold tests. The

ratio of the resulting primary and secondary power pulses provides information on the threshold to the onset of chugging for the system. An example of a ringing test power trace is shown in Figure B- 31 and a complete report of the data from these tests is given in Reference B-31.

The stability test program in Spert IV was concluded with a series of "chugging" tests (Ref. B-17). The same hydrostatic heads as investigated in the threshold tests were studied under natural circulation coolant conditions. The difference between these tests and the threshold tests was the means of the reactivity addition. In the chugging tests the reactivity was inserted as a ramp at a rate of approximately 0.9 mk/sec, *i.e.*, much faster than the reactivity addition in the threshold tests. The ramp insertion was completed within about 30 seconds and the total duration of the tests was generally five to six minutes during which the inlet water temperature remained near ambient.

These tests exhibited the characteristics of typical ramp insertion transients, *i.e.*, the occurrence of an initial power pulse followed by the system approaching a new equilibrium power level. Oscillations about this power level were first induced for significantly higher total reactivity additions when compared to the threshold tests under the same conditions. This difference is attributed to the longer duration of the threshold tests during which the bulk pool temperature could increase to higher temperatures. For some of the chugging tests, the bulk reactor temperature was allowed to rise. For one of these tests chugging was initiated once the bulk pool temperature increased from about 20EC to approximately 70EC. This temperature is consistent with inlet temperatures during the threshold tests which reached the onset of chugging. The power trace record of this test is shown in Figure B-32. Representative fuel plate surface temperatures and coolant temperatures for this test are reported in graphical form in Reference B-17 and are included herein in Figures B-35 and B-36.

B.3.5 Additional Stability Data

In addition to the Borax and Spert in-pile tests, a number of out-of-pile experiments were conducted at the Space Technology Laboratory (STL) to investigate primarily the hydrodynamics of large amplitude voiding. Work by Wright (Ref. B-46) on a Spert I A geometry flow channel studied the void fractions at the axial mid-plane of the channel using x-ray attenuation techniques. Large amplitude voiding was observed for both natural circulation and forced flow conditions. The results indicate that the production of large scale voiding is a rapid process, on the order of a few

msec. These tests were conducted at steady power, rather than simulating the void-power feedback. As a result, the voiding was limited to a fraction of the total channel volume.

Outside of the full scale reactor tests, evidence of chugging was observed during the December 12, 1961 fuel element flow blockage accident in the Engineering Test Reactor (ETR) (Ref. B-47). The ETR was similar to the Borax and Spert reactors in the design of the plate fuel assemblies and core. The accident occurred during 90 MW operation (full power operation was 175 MW) with forced downward flow. The flow blockage accident involved flow obstruction on the top (inlet) of multiple fuel assemblies resulting in partial melting of 18 fuel plates distributed throughout six assemblies. Instrument behaviour and post accident analysis suggest that the voiding during the accident was associated with chugging behaviour. Coolant refill was likely from the bottom (outlet) of the assemblies and only partial in extent judging by the regions of fuel melting.

B.4 Safety Analysis Scenario Tests

Various Safety Analysis Report (SAR) specific tests were conducted as part of the Spert Project, in particular: (a) fuel drop tests with the Spert I P-core, (b) a single start-up transient test with the Spert I BSR-II core, and (c) a study involving inherent *vs.* mechanical shutdown tests, also with the Spert I BSR-II core.

In addition, the SL-1 accident scenario and sequence is directly relevant to MTR-type reactor safety analysis. These tests and events are summarized in the following sections.

B.4.1 Fuel Drop Tests

The last test series conducted in the Spert I P-core was the simulation of a fuel-drop accident (Ref. B-48). The fuel drop scenario was simulated by dropping an assembly from a position just above a vacant peripheral core position with the core slightly subcritical at low power (~ 1 watt) and under ambient conditions. The P-18/18 core configuration and the fuel drop location are shown in Figure B-37. The amount of inserted reactivity was varied by altering the position of the control rods and therefore the shutdown depth prior to the fuel drop. The maximum reactivity inserted in the series of tests was about 9.5 mk ($1.35) at a maximum rate of about 24 mk/sec ($3.4/sec).

Only the maximum power, reactivity, period, and total energy results are reported for these tests. No temperature data have been located. The transient data are summarized in Table B-16.

B.4.2 Startup Accident Tests

A single test designed to simulate the typical "startup transient" was conducted in the Spert I BSR-II core (Refs. B-21, B-49). This test was conducted from ambient temperature, atmospheric pressure, and low power (~ 10-5 W), with only natural circulation coolant flow. All safety settings were in operation including the power level tri p (100 kW), and the period trip (1 second). The control rod bank was motor withdrawn at maximum speed, providing a reactivity insertion rate of about 20 cents/second. The period trip scrammed the test at a trivial power level and a minimum period of about 50 msec.

Since this test series was performed under protected conditions it is not directly applicable to self-limiting behaviour.

B.4.3 Inherent *vs.* Mechanical Shutdown Tests

Mechanical shutdown systems are designed for early detection of potentially hazardous situations and to be fast acting. Part of the Spert Project included comparisons of the shutdown effectiveness of mechanical systems, *i.e.*, absorber rod insertion, to inherent shutdown mechanisms. This testing was performed in Spert I on the stainless-steel plate-type BSR-II core between October 1959 and April 1960 (Refs. B-21, B-50, B-51).

The shutdown system for the BSR-II core consisted of a bank of absorber rods, spring loaded for downward release into the core. These rods achieved an initial acceleration of about 8g upon actuation. The rods could also be motor driven into the core. This system could be activated by both high-power level and short-period scram signals. A block diagram of the safety system as installed in the Spert I facility is shown in Fig B-38.

Tests were conducted on the mechanical shutdown system for both rod reversal (rods motor driven into the core) and rod drop shutdowns. Both high-power level and short-period trip signals were investigated in the testing. The high-power level trip tests were also conducted with different number of rods available. All tests were conducted from initially low power conditions for step reactivity insertion transients.

The period trip scram (period < 1 sec) was found to be more effective under these conditions compared to the high-level power scram (power > 100 kW). Due to the slower action, the rod reversal shutdown was not surprisingly found to be less effective than the scram shutdown response. The results of these tests are in the form of the peak power results only. They are summarized in Figure B-39 along with the power results from the BSR-II self-limiting tests.

B.4.4 SL-1 Accident

The SL-1 accident which resulted in disassembly of the core, was the result of an accidental rapid control rod withdrawal. Details of the SL-1 accident progression and analysis are given in References B-52, B-53, and B-54.

B.5 References

B-1. J. R. Dietrich, D. C. Layman, "Transient and Steady State Characteristics of a Boiling Reactor. The Borax Experiments, 1953", ANL-5211 (also listed as AECD-3840), Argonne National Laboratory, USA, February 1954.

B-2. J. R. Dietrich, "Experimental Investigation of the Self-Limitation of Power During Reactivity Transients in a Subcooled, Water-Moderated Reactor. Borax-I Experiments, 1954", ANL-5323, (also listed as AECD-3668), Argonne National Laboratory, USA, 1954.

B-3. J. C. Haire, "Subcooled Transient Tests in the Spert I Reactor - Experimental Data", US AEC Technical Report IDO-16342, Phillips Petroleum Co., July 1, 1958.

B-4. W. E. Nyer, S. G. Forbes, F. L. Bentzen, G. O. Bright, F. Schroeder, T. R. Wilson, "Experimental Investigations of Reactor Transients", US AEC Technical Report IDO-16285, Phillips Petroleum Co., April 20, 1956.

B-5. F. Schroeder, S. G. Forbes, W. E. Nyer, F. L. Bentzen, G. O. Bright, "Experimental Study of Transient Behavior in a Subcooled Water-Moderated Rector", Nuclear Science and Engineering, v. 2, pp. 96-115, 1957.

B-6. R. W. Miller, "Calculations of Reactivity Behavior During Spert-I Transients", US AEC Technical Report IDO-16317, Phillips Petroleum Co., June 1, 1957.

B-7. F. L. Bentzen, editor, "Quarterly Progress Report - October, November, December, 1958 - Reactor Projects Branch", US AEC Technical Report IDO-16537, Phillips Petroleum Co., September 1, 1959.

B-8. W. E. Nyer, S. G. Forbes, "SPERT I Reactor Safety Studies," Paper P/2428, Proceedings of the Second United Nations International Conference on the Peaceful Uses of Atomic Energy, v. 11, pp. 470-480, Geneva, September 1958.

B-9. G. O. Bright, S. G. Forbes, "Miscellaneous Tests with the Spert I Reactor", US AEC Technical Report IDO-16551, Phillips Petroleum Co., October 23, 1959.

B-10. A. P. Wing, “Transient Tests of the Fully Enriched, Aluminum Plate-Type, B Cores in the Spert I Reactor: Data Summary Report”, US AEC Technical Report IDO-16964, Phillips Petroleum Co., June 1964.

B-11. G. O. Bright, editor, “Quarterly Progress Report - July, August, September, 1958 - Reactor Projects Branch”, US AEC Technical Report IDO-16512, Phillips Petroleum Co., May 6, 1959.

B-12. R. W. Miller, A. Sola, R. K. McCardell, “Report of the Spert I Destructive Test Program on an Aluminum, Plate-Type, Water-Moderated Reactor”, US AEC Technical Report IDO-16883, Phillips Petroleum Co., June 1964.

B-13. M. R. Zeissler, “Non-Destructive and Destructive Transient Tests of the Spert I-D, Fully Enriched, Aluminum-Plate-Type Core: Data Summary Report”, US AEC Technical Report IDO-16886, Phillips Petroleum Co., November 1963.

B-14. J. G. Crocker, L. A. Stephan, “Reactor Power Excursion Tests in the Spert IV Facility”, US AEC Technical Report IDO-17000, Phillips Petroleum Co., August 1964.

B-15. F. Schroeder, editor, “Quarterly Technical Report - Spert Project - January, February, March, 1963", US AEC Technical Report IDO-16893, Phillips Petroleum Co., May 20, 1963.

B-16. F. Schroeder, editor, “Quarterly Technical Report - Spert Project - April, May, June, 1963", US AEC Technical Report IDO-16920, Phillips Petroleum Co., September 20, 1963.

B-17. J. G. Crocker, Z. R. Martinson, R. M. Potenza, L. A. Stephan, “Reactor Stability Tests in the Spert IV Facility”, US AEC Technical Report IDO-17088, Phillips Petroleum Co., July 1965.

B-18. J. A. Norberg, editor, “Quarterly Progress Report - January, February, March, 1959 - Reactor Projects Branch”, US AEC Technical Report IDO-16539, Phillips Petroleum Co., November 20, 1959.

B-19. S. G. Forbes, editor, “Quarterly Technical Report - Spert Project - April, May, June 1959", US AEC Technical Report IDO-16584, Phillips Petroleum Co., April 12, 1960.

B-20. A. P. Wing, "Transient Tests of the Fully Enriched, Stainless Steel Plate-Type, P Core in the Spert I Reactor: Data Summary Report", US AEC Technical Report IDO-17011, Phillips Petroleum Co., December 1964.

B-21. L. A. Stephan, "Transient Tests of the BSR-II Core in the Spert I Facility", US AEC Technical Report IDO-16768, Phillips Petroleum Co., April 5, 1963.

B-22. R. Scott, Jr., C. L. Hale, R. N. Hagen, "Transient Tests of the Fully Enriched Uranium-Oxide Stainless Steel Plate-Type C-Core in the Spert III Reactor: Data Summary Report", US AEC Technical Report IDO-17223, February 1967.

B-23. C. M. Condit, J. F. Scott, R. L. Johnson, "The Effects of Coolant Temperature and Initial Power Level on the Excursion Behaviour of a Highly Enriched Plate Core in Spert III – Experiment and Analysis", US AEC Technical Report IDO-17138, March 1967.

B-24. J. G. Crocker, editor, "Quarterly Technical Report - Spert Project - October, November, December, 1964", US AEC Technical Report IDO-17084, Phillips Petroleum Co., April 1965.

B-25. J. G. Crocker, editor, "Quarterly Technical Report - Spert Project - July, August, September, 1964", US AEC Technical Report IDO-17055, Phillips Petroleum Co., January 1965.

B-26. R. Scott, Jr., A. A. Wasserman, R. C. Schmitt, "Transient Tests of the Spert I Low-Enrichment UO_2 Core: Data Summary Report", US AEC Technical Report IDO-16752, Phillips Petroleum Co., September 1963.

B-27. A. H. Spano, J. E. Barry, L. A. Stephan, J. C. Young, "Self-Limiting Power Excursion Tests of a Water-Moderated Low-Enrichment UO_2 Core in Spert I", US AEC Technical Report IDO-16751, Phillips Petroleum Co., February 28, 1962.

B-28. A. H. Spano, "Self-Limiting Power Excursion Tests of a Water-Moderated Low-Enrichment UO_2 Core", Nuclear Science and Engineering, v.15, pp.37-51, 1963.

B-29. J. E. Grund, editor, "Experimental Results of Potentially Destructive Reactivity Additions to an Oxide Core", US AEC Technical Report IDO-17028, Phillips Petroleum Co., December 1964.

B-30. A. H. Spano, editor, "Quarterly Technical Report - Spert Project - April, May, June, 1964", US AEC Technical Report IDO-17030, Phillips Petroleum Co., September 1964.

B-31. A. H. Spano, editor, "Quarterly Technical Report - Spert Project - January, February, March, 1964", US AEC Technical Report IDO-17010, Phillips Petroleum Co., July 1964.

B-32. T. G. Taxelius, editor, "Quarterly Technical Report - Spert Project - January, February, March, 1967", US AEC Technical Report IDO-17260, Phillips Petroleum Co., February 1968.

B-33. T. G. Taxelius, editor, "Quarterly Technical Report - Spert Project - April, May, June, 1967", US AEC Technical Report IDO-17270, Phillips Petroleum Co., June 1968.

B-34. G. O. Bright, editor, "Quarterly Progress Report - July, August, September, 1957 - Reactor Projects Branch", US AEC Technical Report IDO-16416, Phillips Petroleum Co., October 1, 1957.

B-35. G. O. Bright, editor, "Quarterly Progress Report - April, May, June, 1958 - Reactor Projects Branch", US AEC Technical Report IDO-16489, Phillips Petroleum Co., January 19, 1959.

B-36. S. G. Forbes, F. L. Bentzen, P. French, J. E. Grund, J. C. Haire, W. E. Nyer, and R. F. Walker, "Analysis of Self-Shutdown Behavior in the Spert I Reactor", US AEC Technical Report IDO-16528, Phillips Petroleum Co., July 23, 1959.

B-37. F. Schroeder, editor, "Quarterly Technical Report - Spert Project - January, February, March, 1961", US AEC Technical Report IDO-16693, Phillips Petroleum Co., June 30, 1961.

B-38. L. A. Belblidia, Nodal Analysis of Density-Wave Oscillations In Boiling Water Nuclear Reactors, PhD Dissertation, Georgia Institute of Technology, August 1982.

B-39. J. R. Dietrich, "Experimental Determinations of the Self-Regulation and Safety of Operating Water-Moderated Reactors", in the Proceedings from the First International Conference on the Peaceful Uses of Atomic Energy, Geneva, 1955, Argonne National Laboratory, v. 13, pp. 88-101.

B-40. S. G. Forbes, F. Schroeder, W. E. Nyer, "Instability in the Spert-I Reactor - Preliminary Report", US AEC Technical Report IDO-16309, Phillips Petroleum Co., October 10, 1956.

B-41. S. G. Forbes, F. Schroeder, W. E. Nyer, "First Reports on Instability in Spert-I", Nucleonics, v.15, n.1, June 1957, pp. 41-43.

B-42. F. Schroeder, "Stability Tests with the Spert-I Reactor", US AEC Technical Report IDO-16383, Phillips Petroleum Co., July 1, 1957.

B-43. G. O. Bright, editor, "Quarterly Progress Report - January, February, March, 1958 - Reactor Projects Branch", US AEC Technical Report IDO-16452, Phillips Petroleum Co., September 10, 1958.

B-44. A. H. Spano, editor, "Quarterly Technical Report - Spert Project - July, August, September, 1963", US AEC Technical Report IDO-16931, Phillips Petroleum Co., April 1964.

B-45. A. H. Spano, editor, "Quarterly Technical Report - Spert Project - October, November, December, 1963", US AEC Technical Report IDO-16992, Phillips Petroleum Co., June 1964.

B-46. R. W. Wright, "Large Amplitude Steam Void Oscillations under Forced Flow", Transactions of the American Nuclear Society, v.5, n.1, June 1962, pp.170-172.

B-47. F. R. Keller, "Fuel Element Flow Blockage in the Engineering Test Reactor", US AEC Technical Report IDO-16780, Phillips Petroleum Co., May 10, 1962.

B-48. A. H. Spano, editor, "Quarterly Technical Report - Spert Project - July, August, September 1959", US AEC Technical Report IDO-16606, Phillips Petroleum Co., July 11, 1960.

B-49. T. R. Wilson, editor, "Quarterly Technical Report - Spert Project - January, February, March, 1960", US AEC Technical Report IDO-16617, Phillips Petroleum Co., March 31, 1961.

B-50. F. L. Bentzen, "The Merits of Inherent Shutdown Vs Mechanical Shutdown of a Plate-Type Water-Moderated and -Reflected Reactor In a Runaway Condition", Transactions of the American Nuclear Society, v.3, n.2, 1960, pp.429-430.

B-51. F. L. Bentzen, "The Merits of Inherent Shutdown Vs Mechanical Shutdown of a Plate-Type Water-Moderated and -Reflected Reactor In a Runaway Condition", US AEC Technical Report IDO-16722, Phillips Petroleum Co., November 3, 1961.

B-52. Capt. A. Nelson Tardiff, "Some Aspects of the WTR and SL-1 Accidents", US AEC Technical Report IDO-19308, April 9, 1962.

B-53. SL-1 Project, "Final Report of SL-1 Recovery Operation", US AEC Technical Report IDO-19311, General Electric Company, July 27, 1962.

B-54. Flight Propulsion Laboratory Department, "Additional Analysis of the SL-1 Excursion", US AEC Technical Report IDO-19313, General Electric Company, November 21, 1962.

B.6 Tables

Table B-1: Borax I 1953 Saturation Conditions Step Transient Test Data (extracted from Ref. B-1)

Test No.	Period (msec)	1/Period (sec-1)	Pmax (MW)	ΔTmax (deg F)	ΔTmax (deg C)	TC Location	Figure
1	70	14.3	13	30	17	21-11-c	31
2	58	17.2	22	28	16	21-11-c	43
3	30	33.3	50	90	50	21-11-c	31
8	10	100	330	151	84	21-11-c	30
8 ?	10	100	330	150	83	21-11-avg	31
5	5	200	2600	400	222	21-11-c	31
8	10	100	330	149	83	21-11-s	30
2 ?	58	17.2	22	39	22	21-1-s	43

Notes: regarding the above tests, data taken from ANL-5211
The central thermocouple in plate 1 does not read significantly higher than the surface thermocouple in plate 1
More energy and temperature information is presented as functions of the reciprocal period in Figures 38-41, ANL-5211
code for thermocouple location (X-Y-a): X = core grid location, Y = plate number, a = tc type (c=center, s=surface)

Table B-2: Borax I Subcooling Step Transient Test Data (extracted from Ref. B-1)

Period msec	1/Period sec-1	Etot (MW-sec)	Tsub C	Tmax C	Tsat C	delTmax C	TC Location
13	76.9	7.8	0	163	100	63	21-4-c
13	76.9	9.8	7	183	100	90	21-4-c
13	76.9	15.1	24	210	100	134	21-4-c
13	76.9	7.8	0	151	100	51	21-1-c
13	76.9	9.8	7	164	100	71	21-1-c
13	76.9	-	22	182	100	104	21-1-c
13	76.9	7.8	0	154	100	54	21-1-s
13	76.9	9.8	7	163	100	70	21-1-s
13	76.9	-	22	179	100	101	21-1-s
22	45.5	3.1	1	141	100	42	21-4-c
22	45.5	-	2	144	100	46	21-4-c
22	45.5	-	3	146	100	49	21-4-c
22	45.5	-	4	144	100	48	21-4-c
22	45.5	-	8	151	100	59	21-4-c
22	45.5	6.5	14	159	100	74	21-4-c
22	45.5	9.4	30	171	100	101	21-4-c
22	45.5	11.7	47	177	100	124	21-4-c
22	45.5	13.9	69	191	100	160	21-4-c
22	45.5	3.1	1	135	100	36	21-1-c
22	45.5	-	2	137	100	39	21-1-c
22	45.5	-	3	136	100	39	21-1-c
22	45.5	-	4	135	100	40	21-1-c
22	45.5	-	8	139	100	47	21-1-c
22	45.5	6.5	14	143	100	58	21-1-c
22	45.5	9.4	30	152	100	82	21-1-c
22	45.5	11.7	47	154	100	101	21-1-c
22	45.5	13.9	69	161	100	129	21-1-c
22	45.5	3.1	1	127	100	28	21-1-s
22	45.5	-	2	135	100	37	21-1-s
22	45.5	-	3	135	100	38	21-1-s
22	45.5	-	5	134	100	39	21-1-s
22	45.5	-	8	140	100	48	21-1-s
22	45.5	-	15	146	100	60	21-1-s
22	45.5	9.4	30	154	100	84	21-1-s
22	45.5	11.7	47	142	100	89	21-1-s
22	45.5	13.9	69	157	100	126	21-1-s

Note: Etot data extracted from Fig. 35, ANL-5211
Note: Etot values adjusted with 1/0.85 factor
Note: Temperature data extracted from Fig. 37, ANL-5211
9:53 AM, 11/8/03 Borax I - summary PhD_SE-Day_reactor-experiment-data.xls

Table B-3: Borax I Step Transients from Ambient Conditions (extracted from Ref. B-2)

Test No.	Period msec	alpha sec-1	Pmax Mw	Etot Mw-sec	Ti deg C	Tsub deg C	Tmax deg C	ΔTmax deg C	TC Location	Figure No.	Text page
1	134	7.5	11.4		27	73	120	94	21-4-s	9,14	20,22
2	51	19.6	63.7	7.7	28	72	139	111	21-4-s	10,13,14	20,22
3	33	30.3	129	8.7	27	73	146	119	21-4-s	11,13,14	20,22
4	33	30.6	222	14.4	19 - 28	72-81	-	-	-	13,14	22
5	29	34.5	181	11.4	28	72	144	116	21-4-s	13,14,16	22
6	28	35.5	246	14.3	19 - 28	72-81	-	-	-	13,14	22
7	24	42.1	307	14.8	19 - 28	72-81	-	-	-	13,14	22
8	23	43.6	270	13.2	19 - 28	72-81	-	-	-	13,14	22
9	23	44.0	376	16.1	19 - 28	72-81	-	-	-	13,14	22
10	23	44.3	330	14.5	19 - 28	72-81	-	-	-	13,14	22
11	21	46.9	336	15.0	19 - 28	72-81	-	-	-	13,14	22
12	21	47.6	275	12.0	19 - 28	72-81	-	-	-	13,14	22
13	21	47.6	292	13.4	28	72	157	130	21-4-s	12,13,14	20,22
14	21	48.3	297	14.6	19 - 28	72-81	-	-	-	13,14	22
15	21	48.6	337	12.8	19 - 28	72-81	-	-	-	13,14	22
16	20	49.7	426	15.9	19 - 28	72-81	-	-	-	13,14	22
17	20	49.9	285	12.6	19 - 28	72-81	-	-	-	13,14	22
18	18	54.7	477	16.6	19 - 28	72-81	-	-	-	13,14	22
19	18	55.4	333	14.0	19 - 28	72-81	-	-	-	13,14	22
20	16	61.9	576	18.2	19 - 28	72-81	-	-	-	13,14	22
21	14	73.1	696	19.6	19 - 28	72-81	-	-	-	13,14	22
D-test	2.6	385	950-1400	135	amb	72-81	> 690C	> 660 C	26-?-s	22	26-29,38-39

note: all data is taken from ANL-5323
note: Saturation temperature is assumed to be 100 deg C from which the degree of Subcooling is calculated.
note: data taken in order of weighting from (1) text or figure labels, (2) time trace figure, (3) combined figures [linear], (4) combined figures [log]
note: D-test data besides period incorporate significant estimation, Etot varies in a large range and Tmax is estimated from calculations
note: can also compare period and reciprocal period values taken from Figs. 13 & 14 for the same tests
note: tests 4 through 21 are from an approximate subcooling of 80C but may vary (Ti between 66F [19C) and 82F [28C])

Table B-4: Spert I A-17/28 Step Transient Summary Data

STEP INSERTIONS FROM SUBCOOLED COOLANT CONDITIONS

Index No.	Test No.	period msec	T/period sec-1	rho in mk	Pmax Mw	Etm (i) Mw-sec	Etot (ii) Mw-sec	Ti C	Ttm C	Tmax C	T note	TC loc'n	Tmax-Ti C	Tsat C	Tsub C	pmax psig	BSP Etm^a/Pmax	IDO-16342 Fig.	IDO-16317 Fig.	also in
1	2577	10000	0.1	-	0.10	2.4	-	24	43	62	-	55-172+3	38	96	72	-	2.40	2	-	-
2	2579	5000	0.2	-	0.22	2.9	-	31	53	74	-	55-172+0	43	96	65	-	2.64	3	-	-
3	1850	2000	0.5	4.8	0.62	3.2	-	22	48	68	-	55+0	46	96	74	-	2.58	4	6	c
4	2581	2000	0.5	-	0.55	2.7	-	39	60	99	-	55-172+3	60	96	57	-	2.45	5	-	a
5	1852	850	1.18	-	1.26	-	-	20	51	77	-	55+0	57	96	76	-	-	6	7	c
6	1854	550	1.81	-	1.84	2.7	-	24	56	86	-	55-172+0	62	96	72	-	2.66	7	8	a, c
7	1846	343	2.92	-	2.68	2.6	-	21	57	83	-	55+0	62	96	75	-	2.83	8	-	-
8	1841	333	3.00	-	2.83	2.5	-	21	55	88	-	55+0	67	96	75	-	2.65	9	9	c
9	1442	220	4.55	-	3.31	2.1	8.2	20	61	108	iii	55+0	88	96	76	-	2.89	10	-	-
10	2839	210	4.76	-	5.1	2.5	-	22	62	96	-	55-172+0	76	96	74	-	2.33	11	9	c
11	1838	170	5.9	-	4.3	1.8	-	20	55	92	-	55+0	72	96	76	-	2.47	12	10	c
12	2841	150	6.7	-	8.7	2.3	-	24	63	101	-	55-172+0	77	96	72	-	1.77	13	10	c
13	1423	150	6.7	-	5.3	1.8	7.4	19	48	77	-	55+0	58	96	77	-	2.28	14	11	c
14	1425	148	6.8	-	5.4	1.8	7.2	18	45	75	-	55+0	57	96	78	-	2.27	15	-	-
15	1422	140	7.1	-	5.0	1.8	7.2	19	47	90	-	55+0	71	96	77	-	2.56	16	11	c
16	2847	130	7.7	-	8.5	2.0	-	31	67	100	-	55-172+0	69	96	65	-	1.81	17,18	12	c
17	2506	120	8.3	-	7.8	1.9	-	26	59	88	-	55-172+0	62	96	70	-	2.02	19	12	c
18	1412	110	9.1	-	11.9	2.3	10.5	16	72	104	-	55+0	88	96	80	-	1.76	20	-	a, b
19	1410	105	9.5	-	12.1	2.6	10.9	18	43	79	-	55-0	61	96	78	-	2.04	21	-	-
20	1389	104	9.6	-	14.4	2.9	16.5	13	-	-	-	-	-	96	83	-	1.93	22	-	-
21	1390	100	10.0	-	13.2	2.7	13.2	15	-	-	-	-	-	96	81	-	2.05	23	-	-
22	1417	98	10.2	-	14.0	2.4	8.5	19	69	95	-	55+0	76	96	77	-	1.75	24	-	-
23	1415	96	10.4	-	14.2	2.5	8.5	16	62	93	-	55+0	77	96	80	-	1.83	25	-	-
24	1414	94	10.6	-	14.0	2.6	8.6	17	69	100	-	55+0	83	96	79	-	1.97	26	-	-
25	1418	90	11.1	-	13.8	2.3	8.4	16	63	91	-	55+0	75	96	80	-	1.85	27	13	c
26	1830	74	13.5	-	21.3	2.8	-	22	88	116	-	55+0	94	96	74	0.5	1.77	28	13	c
27	1653	51	19.6	-	50	4.5	-	12	90	96	-	55+0	86	96	84	1.5	1.76	29	-	-
28	1427	47	21.3	-	51	4.4	10.2	20	70	97	-	55+0	77	96	76	1.4	1.84	30	-	-
29	1436	37	27.0	-	88	5.0	8.8	22	160	178	iii	55+0	156	96	74	1.8	1.53	31	-	-
30	1429	36	27.8	-	89	5.2	9.2	20	122	153	-	55+0	133	96	76	2.5	1.62	32	-	-
31	1431	35	28.4	-	90	4.7	7.8	19	116	130	-	55+0	111	96	77	4.4	1.48	33	14	a, c
32	1434	35	28.4	-	92	5.3	8.9	20	160	178	iii	55+0	158	96	76	-	1.64	34	-	-
33	1438	33	30.3	-	96	5.0	8.1	22	155	183	iii	55+0	161	96	74	1.5	1.58	35	-	-
34	2510	24	41.7	-	160	5.6	8.5	28	145	158	-	44-012+0	130	96	68	2.3	1.46	36	-	-
35	2843	23	43.5	-	154	5.5	8.6	26	135	146	iii	55-172+0	120	96	70	4.2	1.55	37,38,39	-	-
36	1466	17	59	-	298	6.6	19.9	18	180	233	iii	55+0	215	96	78	8	1.31	40	-	-
37	1375	17	59	-	330	7.9	11.8	20	-	-	-	-	-	96	76	-	1.41	58	-	-
38	1470	16	62	-	300	7.1	10.0	20	200	235	iii	55+0	215	96	76	12.3	1.47	41	-	-
39	1469	16	62	-	300	6.6	9.6	20	210	238	iii	55+0	218	96	76	11	1.36	42	15	a, c
40	1468	16	62	-	300	7.2	10.4	20	200	240	iii	55+0	220	96	76	9	1.49	43	-	b
41	1464	16	62.5	-	300	7.0	10.2	18	220	250	iii	55+0	232	96	78	5	1.46	44	-	-
42	2845	15.8	63	-	320	7.1	10.9	28	155	170	-	55-172+0	142	96	68	10.5	1.40	45,46,47	-	-
43	1392	15	67	-	367	8.9	12.6	16	-	-	-	-	-	96	80	-	1.62	58	-	-
44	1377	12.8	78	-	490	9.4	13.9	17	-	-	-	-	-	96	79	-	1.50	59	-	-
45	1502	12.7	79	-	500	9.4	13.7	17	185	200	-	55+0	183	96	79	14.7	1.49	48	-	-
46	1500	12.0	83	-	520	9.7	14.5	17	185	205	-	55+0	188	96	79	13	1.55	49	16	c
47	1513	10.6	94	-	720	10.4	17.0	16	195	205	-	55+0	189	96	80	17.3	1.36	50	-	-
48	1496	10.4	96	-	640	11.0	16.4	15	175	225	-	55+0	210	96	81	12	1.65	51	-	-
48	1379	10.3	97	-	700	10.2	15.2	18	-	-	-	-	-	96	78	-	1.41	59	-	-
50	1380	10.2	98	-	700	10.2	15.0	20	-	-	-	-	-	96	76	-	1.43	60	-	-
51	1394	10.2	98	-	680	11.3	16.2	17	-	-	-	-	-	96	79	-	1.63	60	-	-
52	1515	9.5	105	-	700	10.1	14.9	18	200	225	-	55+0	207	96	78	17.3	1.52	52	17	c
53	1396	9.3	107	-	750	10.4	15.8	14	-	-	-	-	-	96	82	-	1.48	53	-	-
54	2232	8.3	120	-	1000	12.6	18.7	18	170	187	-	53+6	169	96	78	23	1.51	54	-	-
55	1529	7.4	135	-	1300	14.4	21.0	20	235	270	-	55+0	250	96	76	29.6	1.50	55	-	-
56	1530	7.0	143	14	1260	13.0	19.4	16	250	292	-	55+0	276	96	80	26.5	1.48	56,57	18	a, c
57	-	5.5	-	-	2500	-	-	amb.	-	590	-	-	-	-	-	~ 50	-	-	-	d

(i) Energy measurements from integration of power trace from 1% of max power to peak power
(ii) Total energy measurements from integration of power trace from 1% of max power to either 1% of max power on decline or time of scram, whichever came first
(iii) range for TC (Ttm & Tmax) suspected to be set too high (300C instead of 200C) for this test series, refer to test. p.21 for tests 1434 through 1470
Thermocouple location (TC Location) is designated as X-Y-Z where: X=assembly position, Y=plate, Z=vertical position in inches wrt centerline, see Fig. 1, IDO-16342
other references: (a) Schroeder et al., Nucl. Sci. Eng., v 2, p 96, (b) Nyer et al, IDO-16285, (c) IDO-16317, (d) IDO-16551
12:26 PM, 11/23/03 PhD_SE-Day_reactor-experiment-data.xls Spert IA - summary

Table B-5: Spert I B-24/32 Step Transient Summary Data

Test No.	Period msec	1/Period sec-1	Ti deg C	Pmax Mw	Etm Mw-sec	Ttm deg C	Tmax deg C	ΔTmax deg C	TC Location	BSP	Note
5485	13200	0.076	22	0.110	2.78	28	50	28	55 24A +6	1.92	
5613	11000	0.091	21	0.540	6.78	44	79	58	55 01B +6	1.14	stirrer on
5618	5110	0.196	22	0.580	7.02	46	80	58	55 01B -6	2.37	stirrer on
5506	4950	0.202	25	0.246	2.38	33	56	31	55 24A +6	1.95	
5487	2450	0.408	26	0.443	2.37	35	65	39	55 24A +6	2.18	
5608	1340	0.746	20	0.830	3.32	43	75	55	55 01B +6	2.98	
5492	1140	0.877	20	0.984	2.29	38	67	47	55 24A +0	2.04	
5490	626	1.60	27	1.42	2.11	39	80	53	55 01B +0	2.38	
5494	522	1.92	28	2.06	2.05	41	80	52	55 24A +3	1.91	
5502	212	4.72	25	3.82	1.77	41	87	62	55 24A +0	2.19	
5496	151	6.62	28	5.60	1.70	45	77	49	55 01B +6	2.01	
5508	112	8.93	24	9.99	2.06	35	88	64	55 24A +0	1.84	
5615	96.7	10.4	22	15.2	2.57	60	88	66	55 01B +0	1.76	
5696	80.0	12.5	20	22.2	2.73	68	103	83	55 01B -6	1.54	
5511	61.1	16.4	24	25.9	3.13	83	109	85	55 01B -6	1.98	
5630	54.6	18.3	20	49.2	4.19	89	123	103	55 01B +0	1.56	
5633	46.7	21.4	20	72.3	5.40	102	137	117	55 01B +0	1.60	
5695	37.4	26.7	25	85.6	6.02	140	147	122	55 01B +0	1.88	
5514	36.0	27.8	25	131	7.46	146	180	155	55 24A +0	1.58	
5517	23.5	42.6	25	207	8.59	150	163	138	55 01B +0	1.77	
5636	22.0	45.5	20	210	9.98	144	152	132	55 01B +0	2.16	
5691	19.0	52.6	20	292	9.88	162	169	149	55 01B +0	1.78	
5693	16.0	62.5	20	429	10.3	174	187	167	55 01B +0	1.50	
5701	11.6	86.2	20	635	12.3	194	207	187	55 01B +0	1.67	
5703	10.8	92.6	20	849	13.6	208	228	208	55 01B +0	1.48	
5819	10300	0.097	40	0.131	2.77	51	64	24	55 24A -6	2.05	
5823	1130	0.877	41	1.20	2.45	61	83	42	55 01B +0	1.79	
5825	286	3.50	40	2.95	1.63	53	86	46	55 01B +6	1.93	
5826	78.9	12.7	40	16.0	2.40	61	95	55	55 01B -6	1.91	
5828	37.0	27.0	40	78.0	4.88	112	137	97	55 01B -6	1.69	
5830	19.5	51.3	40	290	7.96	152	165	125	55 01B -6	1.41	
5832	11100	0.090	60	0.180	2.31	78	82	22	55 24A +3	1.16	
5834	726	1.38	58	0.920	1.93	74	92	34	55 01B +0	2.90	
5837	318	3.14	60	2.52	1.45	75	100	40	55 24A +3	1.81	
5838	95.2	10.5	60	13.0	2.11	80	105	45	55 01B +0	1.70	
5842	43.5	23.0	60	61.3	4.10	117	132	72	55 01B +0	1.54	
5844	21.5	46.5	60	268	7.26	151	158	98	55 01B -6	1.26	
5846	9.15	109	60	710	9.58	192	215	155	56 13A +0	1.47	
6063	10500	0.095	78	0.133	2.74	88	102	24	55 01B +6	1.96	
6065	1060	0.943	79	0.680	1.72	93	102	23	55 01B +0	2.39	
6067	311	3.22	80	2.38	1.58	95	108	28	55 01B +0	2.14	
6069	86.1	11.6	80	12.6	1.94	106	117	37	55 01B +0	1.79	
6072	43.9	22.8	79	49.6	3.47	127	147	68	55 01B +0	1.60	
6074	20.3	49.3	81	205	5.16	150	158	77	55 01B -6	1.24	
6170	10600	0.094	96	0.053	0.546	96	100	4	55 01B -6	0.97	
6172	8650	0.115	96	0.058	0.583	96	100	4	55 01B +0	1.16	
6174	1110	0.901	96	0.430	0.570	101	101	5	55 01B -6	1.19	
6175	491	2.04	96	0.856	0.612	99	102	6	55 01B +0	1.46	
6177	140	7.14	96	3.90	0.649	105	108	12	55 01B +0	1.19	
6179	43.0	23.3	96	29.6	1.58	118	120	24	55 01B +0	1.24	
6181	22.4	44.6	96	91.0	3.23	130	140	44	55 01B +0	1.58	

Note: data from Table IV, IDO-16964, pp. 89-90

Table B-6: Spert I B-16/40 Step Transient Summary Data

Test No.	Period msec	1/Period sec-1	Ti C	Pmax Mw	Etm Mw-sec	Ttm C	Tmax C	Dtmax C	TC Location	BSP	Note
6523	9600	0.104	19	0.156	4.50	40	50	31	55 03B +0	3.00	
6543	5180	0.193	20	0.341	3.88	42	55	35	55 03B +0	2.20	
6541	2610	0.383	21	0.560	3.63	47	69	48	55 03B +0	2.48	
6525	1150	0.870	22	1.25	2.60	48	85	63	55 03B +0	1.81	
6527	300	3.33	20	3.10	2.40	50	88	68	55 03B +0	2.58	
6529	110	9.09	20	15.4	2.76	63	109	89	55 03B +0	1.63	
6531	54.6	18.3	20	49.0	4.80	96	140	120	55 03B +0	1.79	
6533	27.5	36.4	20	212	7.80	158	170	150	55 03B +0	1.34	
6536	21.0	47.6	20	313	9.40	186	192	172	55 03B +0	1.43	
6545	13.6	73.5	20	680	12.1	148	241	221	55 03B +0	1.31	
6632	8540	0.117	50	0.214	3.96	58	76	26	55 16A +0	2.17	
6636	4490	0.223	50	0.320	3.81	65	85	35	55 03B +0	2.66	
6634	886	1.13	50	1.30	2.98	54	88	38	55 03B +0	2.59	
6638	282	3.55	50	3.75	2.36	78	98	48	55 03B +0	2.23	
6640	94.9	10.5	50	18.8	3.04	92	117	67	55 03B +0	1.70	
6641	38.1	26.2	50	90.0	5.32	123	128	78	55 03B +0	1.55	
6643	20.2	49.5	50	273.0	7.45	168	174	124	55 03B +0	1.35	
6644	1020	0.980	79	1.02	2.97	103	107	28	55 03B +0	2.85	stirrer on
6647	505	1.98	80	2.04	2.18	105	109	29	55 03B +0	2.12	stirrer on
6646	147	6.80	80	7.41	1.94	109	119	39	55 03B +0	1.78	
6648	56.0	17.9	80	37.8	2.83	128	137	57	55 03B +0	1.34	
6651	31.7	31.5	80	49.0	4.00	109	127	47	67 16A +0	2.57	
6655	17.5	57.1	80	277	5.84	130	161	81	55 16A +0	1.20	
6666	3040	0.329	95	0.183	0.658	100	103	8	55 03B +0	1.18	
6658	972	1.03	95	0.500	0.589	102	105	10	55 03B +0	1.21	
6660	211	4.79	95	2.20	0.558	102	108	13	55 03B +0	1.21	
6662	91.7	10.9	95	9.50	1.18	105	111	16	55 03B +0	1.35	
6664	31.1	32.2	95	64.6	2.37	112	138	43	55 03B +0	1.18	
6665	15.0	66.7	95	218	4.00	147	169	74	55 03B +0	1.22	

Note: all tests conducted from an initial power ~ 5 W, with a 2' hydrostatic head above the core
Note: data from Table V, IDO-16964, p. 90
10:49 PM, 2/20/04 PhD_SE-Day_reactor-expt-data.xls Spert I B-16|40 steps

Table B-7: Spert I B-12/64 Step Transient Summary Data

Test No.	Period msec	1/Period sec-1	Ti deg C	Pmax Mw	Etm Mw-sec	Ttm deg C	Tmax deg C	ΔTmax deg C	TC Location	BSP	Note
6887	9150	0.110	20	0.200	9.30	32	73	53	55 01B +0	5.12	
6891	6280	0.160	20	0.550	7.66	55	83	63	55 01B +0	2.23	
6978	2200	0.450	20	1.02	5.80	68	98	78	55 01B +0	2.56	
6893	955	1.05	20	1.92	4.94	65	104	84	55 01B +0	2.70	
6895	461	2.17	20	3.87	4.51	54	85	65	57 12A +0	2.53	
6902	195	5.13	20	9.05	3.31	75	108	88	55 01B +0	1.88	
6905	125	8.00	21	17.8	4.00	89	117	96	55 01B +0	1.80	
6906	79.0	12.6	20	44.5	5.51	83	121	101	55 12A -6	1.56	
7936	46.0	21.7	20	93.0	8.26	132	152	132	55 06B -6	1.93	
6908	28.7	32.8	21	335	13.8	180	184	163	55 01B +0	1.35	
7960	19.9	50.3	20	569	16.5	194	240	220	55 06B +0	1.46	
6964	18.6	53.8	20	625	17.3	239	248	228	55 01B +0	1.49	
7945	15.0	66.7	20	880	19.5	225	263	243	55 01B +0	1.48	
7942	14.9	67.1	20	881	20.8	210	267	247	55 06B +0	1.58	
7949	14.4	69.4	20	925	21.6	210	278	258	55 06B +0	1.62	
7940	14.1	70.9	20	938	23.0	220	294	274	55 01B +0	1.74	
6965	11.7	85.5	20	1360	24.2	330	354	334	55 01B -6	1.52	
6976	9.40	106	20	2230	31.5	300	420	400	55 12A -9	1.50	
7964	15.7	63.7	40	622	16.7	196	238	198	55 01B +0	1.71	
7967	14.2	70.4	60	661	15.2	198	246	186	55 01B +0	1.62	
7969	16.1	62.1	80	542	11.2	180	212	132	55 01B +0	1.28	
7980	9070.0	0.110	95	0.100	2.15	98	108	13	66 06B +0	2.37	short duration, no post peak
7981	1280.0	0.780	95	0.550	1.28	103	110	15	66 06B +0	1.82	steady boiling reached
7984	753	1.33	95	0.910	1.18	102	116	21	66 06B +0	1.72	small amp oscillations
7986	154	6.49	95	5.50	1.20	100	113	18	55 06B +0	1.42	small amp oscillations
7976	93.4	10.7	95	11.3	1.53	103	132	37	66 06B +0	1.45	developing oscillations @ scram
7989	37.4	26.7	95	78.0	3.25	149	190	95	55 06B -6	1.11	chugging
7972	16.5	60.6	95	340	6.85	164	179	84	66 06B +0	1.22	short duration, no post peak
7992	11.4	87.7	95	840	13.0	214	260	165	55 12A -3	1.36	short duration, no post peak

Note: all tests conducted from an initial power ~ 5 W, with a 2' hydrostatic head above the core
Note: data from Table VI, IDO-16964, p. 91

Table B-8: Spert I D-12/25 Step Transient Summary Data

Test No.	Period (msec)	1/period (1/sec)	Dko ($)	Pmax (Mw)	Etm (Mw-sec)	Etot (Mw-sec)	Tmax (deg C)	TC location	Pr max (psi)	PT location	tm sec	BSP a*Etm/Pmax
20207	1310	0.760	0.75	0.390	1.49	--	80	E5 7W (-4b)	--	--	24.72	2.90
	930	1.080	0.80	0.670	1.84	--	89	? ? (?)	--	--	--	2.97
16953	880	1.14	0.81	0.760	1.79	--	94	E5 6E (-3b)	--	--	15.38	2.69
	880	1.14	0.81	0.980	--	--	94	? ? (?)	--	--	--	-
	880	1.14	0.81	0.780	2.21	--	87	? ? (?b)	--	--	--	3.23
18887	640	1.56	0.85	0.980	1.76	--	95	E5 7W (-3)	--	--	11.56	2.80
18895	355	2.82	0.92	1.50	1.47	--	98	E5 7W (-3)	--	--	6.407	2.76
20215	243	4.12	0.95	1.43	0.910	--	93	E5 7W (0)	--	--	--	2.62
18899	163	6.14	0.99	3.25	1.13	--	104	E5 7W (-3)	--	--	3.202	2.13
20223	140	7.14	1.02	3.80	0.940	--	112	E5 12W (-6)	--	--	2.593	1.77
19657	118	8.48	1.03	4.50	1.00	--	109	E5 6E (0b)	--	--	2.748	1.88
19657	118	8.48	1.03	4.50	1.00	--	102	E5 7W (-3)	--	--	2.748	1.88
19688	112	8.93	1.03	5.05	1.18	--	117	E5 6E (0b)	--	--	2.198	2.09
19688	112	8.93	1.03	5.05	1.18	--	99	E5 7W (-3)	--	--	2.198	2.09
	98	10.2	1.05	6.60	1.34	--	110	E5 7W (-3)	--	--	--	2.07
18921	65.0	15.4	1.10	14.2	1.68	--	115	E5 7W (-3)	--	--	1.312	1.82
19447	49.5	20.2	1.13	19.1	1.84	3.20	128	E5 7W (-3)	--	--	1.344	1.95
18927	47.0	21.3	1.16	27.5	2.25	3.95	117	E5 7W (-3)	--	--	1.002	1.74
18931	34.0	29.4	1.23	50.0	2.90	4.90	124	E5 7W (-3)	--	--	0.7535	1.71
18942	25.0	40.0	1.32	87.0	3.20	4.90	132	E5 7W (-3)	--	--	0.5905	1.47
19694	22.4	45.8	1.35	105	3.60	5.40	154	E5 7W (-3b)	--	--	0.6612	1.57
19661	21.7	46.1	1.37	107	3.40	5.05	155	E5 6E (0b)	--	--	0.7130	1.46
19661	21.7	46.1	1.37	107	3.40	5.05	128	E5 7W (-3)	--	--	0.7130	1.46
20229	21.1	47.4	1.38	110	3.60	5.40	153	E5 7W (0)	--	--	0.6295	1.55
19183	19.3	52	1.42	120	3.40	4.70	132	E5 7W (-3)	--	--	0.5940	1.47
18946	19.0	53	1.42	141	4.05	5.85	150	E5 7W (-3)	--	--	0.4655	1.52
18950	14.5	69	1.56	210	4.10	5.80	165	E5 7W (-3)	--	--	0.3778	1.35
18954	12.1	83	1.67	290	4.60	6.45	180	E5 7W (-3)	--	--	0.3153	1.32
18958	9.8	102	1.80	380	5.15	7.55	227	E5 7W (-3)	--	--	0.2730	1.38
20332	9.7	103	1.84	360	5.05	7.45	234	E5 7W (-4b)	--	--	0.3627	1.44
	9.6	104	1.85	350	5.00	7.15	232	? ? (?b)	--	--	--	1.49
20234	9.6	104	1.85	380	5.10	7.45	229	E5 7W (-4b)	--	--	0.3595	1.40
18996	9.5	105	1.85	430	5.70	7.25	255	E5 7W (-3)	--	--	0.2605	1.39
19204	9.0	111	1.90	395	4.70	7.85	300	E5 7W (-3)	1.7	(3, 3, 19-1/2)	0.3805	1.32
19666	8.9	112	1.91	460	5.05	7.10	350	E5 6E (-3b)	2	(-4, -3, -51)	0.3820	1.23
19666	8.9	112	1.91	460	5.05	7.10	242	E5 7W (-3)	2	(-4, -3, -51)	0.3820	1.23
19699	8.7	115	1.93	470	5.25	7.65	234	E5 7W (-3)	--	--	0.3855	1.28
19022	8.2	122	1.99	530	5.85	8.20	315	E5 7W (-3)	3.6	(3, 3, -30-1/2)	0.2305	1.35
19342	8.1	124	2.00	505	5.45	8.55	325	E5 7W (-3)	1.6	(3, 3, 19-1/2)	0.3585	1.34
19452	7.6	132	2.03	510	5.20	9.20	400	E5 7W (-3)	2.1	(3, 3, 19-1/2)	0.3590	1.35
19275	7.5	133	2.08	555	5.55	9.40	355	E5 7W (-3)	2.5	(3, 3, 19-1/2)	0.3620	1.33
19026	7.2	139	2.13	630	6.00	8.80	375	E5 12W (-3)	4.2	(3, 3, 19-1/2)	0.2790	1.32
19026	7.2	139	2.13	630	6.00	8.80	360	E5 7W (-3)	4.2	(3, 3, 19-1/2)	0.2790	1.32
20237	7.0	143	2.16	620	6.45	9.32	305	E5 7W (-4b)	3.1	(5, 4-3/4, 23-1/4)	0.2837	1.49
19800	6.9	145	2.18	660	6.35	10.2	340	E5 7W (-3)	2.8	(-4, 3, -51)	0.3539	1.40
19805	6.9	145	2.18	665	6.60	10.4	440	E5 6E (-3b)	3.1	(-4, 3, -51)	0.3535	1.44
19805	6.9	145	2.18	665	6.60	10.4	325	E5 7W (-3)	3.1	(-4, 3, -51)	0.3535	1.44
	6.9	145	2.18	690	6.45	10.2	400	E5 7W (-3)	--	--	--	1.36
	6.9	145	2.14	620	6.40	10.9	440	E5 7W (-3)	--	--	--	1.50
	6.9	145	2.18	640	6.00	9.7	340	E5 7W (-3)	--	--	--	1.36
	6.8	147	2.20	635	5.75	9.2	355	? ? (?b)	--	--	--	1.33
	6.8	147	2.20	685	6.05	10.0	420	E5 7W (-3)	--	--	--	1.30
19046	6.4	156	2.27	745	6.60	10.5	455	E5 7W (-3)	4.3	(3, 3, -30-1/2)	0.3165	1.38
19280	6.0	167	2.36	890	7.20	13.2	560	E5 7W (0)	4.6	(10-1/2, 0, 0)	0.3848	1.35
19280	6.0	167	2.36	890	7.20	13.2	545	E5 7W (-3)	4.6	(10-1/2, 0, 0)	0.3848	1.35
19358	5.0	200	2.63	1130	8.35	17.5	585	E5 7W (-3)	7	(10-1/2, 0, 0)	0.3727	1.48
19552	4.6	218	2.72	1270	8.90	19.0	680	E6 6E (0b)	8.2	(3, 3, -27-1/2)	0.3520	1.53
19552	4.6	218	2.72	1270	8.90	19.0	570	E5 7W (-3)	8.2	(3, 3, -27-1/2)	0.3520	1.53
20461	3.2	313	3.55	2250	13.8	30.7	615	E5 7W (-4b)	35	(3, -3-3/8, -19-7/3)	0.1534	1.92

Note: tests initiated from low power, ambient temperature (~15C), with a 2 ft hydrostatic head, and natural circulation flow only

Note: Data was primarily taken from IDO-16886. This was supplemented with Dko ($) data and additional temperature data from IDO-16883.

Note: A few tests not reported in IDO-16886 which were reported in IDO-16883 were added.

Note: The test series culminated in a destructive test

Note: Melt patterns from the D-test series (see IDO-16883, App. D) indicate that position assembly E5 is the hottest, and plates 1 and 12 are the limiting plates, axially just below the CL is the hot spot ~ -3"

Note: From the above melt patterns the limiting TC position is E5 12W but E5 7W should be close, E5 6E should be close to E5 7W.

2/21/04, 9:02 AM PhD_SE-Day_reactor-expt-data.xls Spert I D-12|25 steps

Table B-9: Spert IV D-12/25 Step Transient Summary Data

Test No.	ρi ($)	Period (msec)	a (1/sec)	Pmax (Mw)	Etm (Mw-sec)	Pr max (psig)	Ti (deg C)	Ttm (deg C)	Tmax (deg C)	ΔTmax (deg C)	TC Location	Head (ft)	Flow (gpm)	BSP	Note
2	0.80	980	1.02	0.77	2.18	0	19.0	71	93	74	E5 7W -4	18	0	2.89	
3	0.88	598	1.67	1.12	1.56	0	20.0	68	103	83	E5 7W -4	18	0	2.33	
5	0.92	374	2.67	1.55	1.27	0	21.8	68	113	91	E5 7W -4	18	0	2.19	
4	0.98	190	5.26	3.32	1.08	0	20.9	63	121	100	E5 7W -4	18	0	1.71	
6	1.04	107	9.35	6.9	1.18	0	22.2	73	122	100	E5 7W -4	18	0	1.60	
9	1.11	62.4	16.0	17.5	1.64	0	22.4	99	128	106	E5 7W -3	18	0	1.50	
7	1.15	49.8	20.1	25.1	1.83	0	22.2	113	124	102	E5 7W -3	18	0	1.47	
8	1.26	29.6	33.8	68.5	3.00	0	22.4	136	141	119	E5 7W -3	18	0	1.48	
10	1.40	19.6	51.0	147	3.23	3.7	22.4	148	162	140	E5 7W -3	18	0	1.12	
49	1.53	15.8	66.3	220	4.40	8	20.5	160	165	145	E5 7W -3	18	0	1.33	
11	1.54	14.5	69.0	247	4.40	-	22.2	165	178	156	E5 7W -3	18	0	1.23	
12	1.68	11.7	85.5	350	4.84	15	22.3	175	179	157	E5 7W -3	18	0	1.18	
13	1.82	10.1	99.0	467	4.94	16	22.2	183	191	169	E5 7W -4	18	0	1.05	
14	1.91	8.48	118	615	5.66	18	22.0	170	212	190	E5 7W -4	18	0	1.09	
52	2.00	7.83	128	705	6.35	19	19.9	167	270	250	E5 7W -3	18	0	1.15	
53	2.14	7.0	143	875	8.50	21	19.8	170	338	318	E5 7W -3	18	0	1.39	
15	1.40	21.3	47.0	145	3.49	3.3	22.0	131	138	116	E5 7W -4	2	0	1.13	
16	1.68	12.0	83.4	340	4.43	12	21.8	155	156	134	E5 7W -4	2	0	1.09	
17	1.91	8.83	113	570	5.18	18	21.7	165	184	162	E5 7W -4	2	0	1.03	
34	0.88	560	1.79	-	-	0	21.9	-	97	75	E5 7W -3	18	500	-	[a]
38	1.14	54.2	18.4	21.5	2.32	0	22.8	103	125	102	E5 7W -3	18	500	1.99	
42	1.66	11.9	84.0	322	5.26	14	23.3	163	169	146	E5 7W -3	18	500	1.37	
46	1.80	10.1	99.0	435	5.97	18	23.2	165	173	150	E5 7W -3	18	500	1.36	
35	0.88	529	1.89	-	-	0	22	-	99	77	E5 7W -3	18	1000	-	[a]
37	1.04	103	9.60	7.5	1.30	0	22.5	64	110	88	E5 7W -3	18	1000	1.66	
39	1.14	54.5	18.3	22.5	2.35	0	22.8	124	136	113	E5 7W -3	18	1000	1.91	
41	1.39	20.0	50.0	130	4.94	3	23	138	144	121	E5 7W -3	18	1000	1.90	
43	1.66	12.3	81.3	292	5.49	14	22.9	160	168	145	E5 7W -3	18	1000	1.53	
45	1.80	10.4	96.1	425	6.05	18	22.9	167	184	161	E5 7W -3	18	1000	1.37	
36	0.88	531	1.89	-	-	0	22.5	-	105	83	E5 7W -3	18	2500	-	[a]
40	1.14	52.1	19.2	22.5	2.51	0	22.7	91	110	87	E5 7W -3	18	2500	2.14	
44	1.66	12.2	82.0	320	5.41	14	22.6	169	176	153	E5 7W -3	18	2500	1.39	
47	1.80	10.0	100	435	6.13	18	23.2	182	182	159	E5 7W -3	18	2500	1.41	[c]
	0.87	554	1.81	-	-	0		-	149	149		18	5000	-	[a],[b]
18	0.88	516	1.94	-	-	0	21.9	-	93	71	E5 7W -4	18	5000	-	[a]
19	1.05	104	9.62	9.8	1.79	0	22.0	58	102	80	E5 7W -4	18	5000	1.76	
20	1.14	49.3	20.3	30.2	2.71	0	22.4	90	108	86	E5 7W -4	18	5000	1.82	
	1.14	47.2	21.2	31.5	-	0		-	129	129		18	5000	-	[b]
21	1.39	20.7	48.3	169	4.78	4.0	20.7	149	152	131	E5 7W -4	18	5000	1.37	[d]
	1.39	20.2	49.5	173	-	4.0		-	167	167		18	5000	-	[b]
	1.53	14.3	70.0	267	-	10		-	177	177		18	5000	-	[b]
22	1.66	12.2	82.0	370	5.26	14	23.4	167	173	150	E5 7W -4	18	5000	1.17	[e]
	1.66	11.5	87.0	373	-	15		-	184	184		18	5000	-	[b]
23	1.80	10.1	99.0	505	6.08	17	23.7	185	192	168	E5 7W -3	18	5000	1.19	[e]
	1.80	10.0	100	481	-	23		-	200	200		18	5000	-	[b]
	1.80	9.7	103	497	-	19		-	270	270		18	5000	-	[b]

[a] = power exhibited no peak
[b] = all maximum temperature data for these tests are for narrow channels
[c] = sustained power oscillations observed during test
[d] = secondary power peak observed during test
[e] = damped power oscillations observed during test
Note: all tests conducted from low initial power and ambient temperatures
Note: data was primarily taken from IDO-17000 (includes all data reported in IDO-16920, is the same as the data reported in IDO-17088)
Note: test numbers and thermocouple locations taken from tme trace figures

Table B-10: Spert I P-18/19 Step Transient Summary Data

Test No.	Period (msec)	1/period (1/sec)	Rho in ($)	D Rod (inches)	Ti (deg C)	Pmax (Mw)	Etm (Mw-sec)	Etot (int) (MW-sec)	Etot (T) (MW-sec)	Ttm (deg C)	Tmax (deg C)	TC Location	Ttm (deg C)	Tmax (deg C)	TC Location	Pr max (psi)
Ambient Step Tests (from IDO-17011, IDO-16537, IDO-16539)																
8522	6000	0.17	0.49	0.52	20	0.215	2.50	42	41	48	88	44-18-3	52	73	44-18-6	0
8527	2500	0.40	0.65	0.68	20	0.450	2.60	12	13	60	97	44-01-6	59	86	44-18-6	0
8531	1300	0.77	0.75	0.81	20	0.730	2.30	11	11	64	100	44-18-3	73	97	44-18-6	0
8535	670	1.49	0.84	0.90	21	1.30	1.90	10	11	81	112	44-01-6	71	95	44-18-6	0
8538	260	3.85	0.92	1.00	19	2.80	1.70	9	9	77	128	44-01-6	67	110	44-18-6	0
8617	110	9.09	0.98	1.05	18	6.20	1.30	12	11	61	110	44-01-3	61	110	44-18-6	0
8621	42	23.8	1.04	1.12	17	28.0	2.00	12	12	98	120	44-01-6	91	120	44-18-6	0
8613	21	47.6	1.11	1.19	17	91.0	2.77	13	13	118	136	44-18+0	110	130	44-18-6	0
8623	20	50.0	1.12	1.21	18	110	2.92	9	8	120	156	44-18-3	120	160	44-18-6	0
8631	16	62.5	1.14	1.24	20	144	3.30	11	11	142	192	44-18-6	120	170	44-18-6	2
8722	14	71.4	1.17	1.29	15	230	3.61	12	16	124	210	44-18-6	130	210	44-18-6	2
8725	9.3	108	1.24	1.37	16	340	4.80	19	19	140	270	44-18-6	140	270	44-18-6	4
8760	6.7	149	1.36	1.49	17	650	6.10	10	12	150	370	44-18-6	160	370	44-18-6	13
8796	6.0	167	1.41	1.58	18	830	6.70	11	12	160	440	44-18-6	160	440	44-18-6	24
8815	5.0	200	1.50	1.66	17	1050	7.20	12	12	190	500	44-18-6	180	500	44-18-6	31
Ambient Step Tests with Capsule in Core (from IDO-17011, IDO-16539)																
9417	61	16.4	1.02	1.16	14	15.0	1.50	7	8.1	70	107	43-01-6	-	-	-	0
9326	38	26.3	1.05	1.15	13	38.0	2.13	5	5.4	83	120	43-01+3	-	-	-	0
9420	26	38.5	1.06	1.34	15	62.0	2.57	6	8.5	109	128	43-01-3	-	-	-	0
9425	10	100	1.24	1.41	-	370	4.7	10	10.5	145	160	-	-	-	-	3
9423	9.6	104	1.25	1.41	-	285	4.2	9	9.4	135	166	-	-	-	-	3
9423	9.1	110	1.27	1.40	-	360	4.2	8	9.9	134	180	-	-	-	-	14
9344	6.2	161	1.40	1.52	-	630	5.8	10	11.4	172	250	-	-	-	-	14
Boiling Step Tests (from IDO-17011, IDO-17584)																
10223	76.0	13.2	-	-	97	2.00	0.190	-	-	101	102	55-01+0	-	-	-	0
10230	23.0	43.5	-	-	97	15.0	0.401	-	-	103	113	55-01-6	-	-	-	0
10233	11.0	90.9	-	-	97	89.0	1.20	-	-	116	126	54-01-3	-	-	-	6
10235	5.0	200	-	-	97	390	2.81	-	-	174	233	54-01-3	-	-	-	21
10241	4.0	250	-	-	97	560	3.45	-	-	195	275	54-01-3	-	-	-	27

Note: data taken from IDO-17011.
Note: Rho in (inserted reactivity), and D Rod (change in rod position) data taken from IDO-16537, p.35, T.4 & IDO-16539, pp.26-27, T.5
Note: Etot data taken from IDO-16539, pp.26-27, T.5
Note: axial and horizontal thermocouple comparisons for some of these transients are given in App. B & C of IDO-17011 (which allows comparison and use of different TC location data)
Note: can supplement this information with rho inserted values from earlier reports, as well as TC: 44-18-6 data for first 15 ambient step tests
Note: Etot (int.) / (T) = Total Energy generated to time of scram, calculated by integrating power curve / temperature balance
2/20/04, 11:32 PM PhD_SE-Day_reactor-expt-data.xls Spert I P-18|19 steps

Table B-11: Spert III C-19/52 Step Transient Summary Data

Test No.	Ti (deg C)	period (msec)	α (1/sec)	ρi ($)	Ptm (Mw)	Etm (Mw-sec)	ρc tm ($)	Pr tm (psi)	Pr max (psi)	ΔTm (deg C)	ΔTmax (deg C)	TC Location	BSP
1	18	504	2.0	0.87	3.39	5.01	-0.18			38	89	N11-A1-10-1/2 g	2.93
2	18	174	5.7	0.96	7.78	3.5	-0.10			55	106	N11-A1-10-1/2 g	2.59
4242	18	22	45.5	1.10	160	8.37	-0.12			134	154	N11-A1-11	2.38
11	19	104	9.6	0.99	12.7	2.81	-0.07			41	94	N11-B1-12-1/2 f	2.13
10	19	39.1	25.6	1.06	60.4	4.38	-0.09			69	89	N11-B1-12-1/2 f	1.85
9	19	20.8	48.1	1.14	215	6.97	-0.17	21 e	21 e	101	106	N11-B1-12-1/2 f	1.56
3570	21	160	6.3	0.96	6.72	2.64	-0.09			45	95	S11-B16-12	2.46
3171	21	120	8.3	1.15	8.61	2.43	-0.07			No TC's connected for this run			2.35
3169	21	93.5	10.7	0.98	11.8	2.42	-0.06			45	90	N11-A16-12	2.19
3568	21	40	25.0	1.05	62	4.39	-0.08			61	98	N11-A16-9	1.77
1859	22	22.7	44.1	1.08	185	7.0	-0.10		7	125	127	S11-A16-12	1.67
3546	22	18.6	53.8	1.11	277	8.39	-0.13			146	157	S11-B16-9	1.63
3548	22	11.2	89.3	1.20	770	12.9	-0.23			205	226	N11-A16-9	1.50
1863	23	11.2	89.3	1.22	802.6	10.8	-0.26		15	127	140	N31-B19-9	1.20
2233	23	10.9	91.7	1.22	650	10.2	-0.26			175	201	S11-A16-12	1.44
1292	24	940	1.1	0.77	1.97	5.19	-0.20			56	74	S11-A16-12	2.80
1422	24	130	7.7	0.97	9.0	2.94	-0.08			41	83	N11-A1-12	2.51
1593	24	39	25.6	1.04	56.6	4.05	-0.07			80	101	S11-A16-12	1.83
3167	24	21.5	46.5	1.09	163	5.80	-0.11			109	110	N11-A16-12	1.66
2221	24	18	55.6	1.13	252	6.59	-0.15			150	162	S11-A16-12	1.45
2124	24	17.4	57.5	1.14	258	6.45	-0.16			138	155	S11-A16-12	1.44
1604	24	13.9	71.9	1.14	392	8.6	-0.16		12	142	163	S11-A16-12	1.58
1425	25	9300	0.1	0.41	0.478 a	61.6 b	-0.40 a,b			38	38	S11-B16-6	13.86
1307	25	490	2.0	0.87	3.23	4.4	-0.17			48	84	N11-A1-9	2.78
4083	25	150	6.7	0.96	7.9	2.99	-0.09			40	89	S11-A16-13	2.52
4136	25	38	26.3	1.05	77.7	5.03	-0.08			97	109	N11-B1-11	1.70
4145	25	20.4	49.0	1.11	272	8.32	-0.13			134	179	N11-A1-11	1.50
1958	25	16.8	59.5	1.14	258	6.66	-0.18			113	135	S11-A16-12	1.54
4226	25	10.4	96.2	1.22	734	11.7	-0.28			207	319	N11-A1-11	1.53
1309	26	162	6.2	0.94	8.8	3.48	-0.07			46	84	N11-A1-12	2.44
1595	26	16.9	59.2	1.13	284	7.25	-0.15	7		56	186	S11-A16-12	1.51
2127	26	10.9	91.7	1.21	638	9.88	-0.28			190	216	S11-A16-12	1.42
1676	26	10.1	99.0	1.24	810	11.3	-0.29	8		201	239	S11-A16-12	1.38
1446	27	81.9	12.2	0.99	15.1	2.79	-0.05			41	80	S11-A16-12	2.26
1470	27	68.3	14.6	1.01	19	2.60	-0.06			41	81	S11-A16-12	2.00
1311	28	4800	0.2	0.49	0.422 a	5.08 b	-0.21 a			36	36	S11-A16-12	2.51
3163	28	19.2	52.1	1.11	238	7.11	-0.12			104	117	N11-A16-12	1.56
2157	28	18	55.6	1.13	220	6.02	-0.15			107	122	S11-A16-12	1.52
2246	28	10.7	93.5	1.23	621.3	9.42	-0.26			180	210	S11-A16-12	1.42
1967	28	10.6	94.3	1.20	620	9.76	-0.23	11		178	206	S11-A16-12	1.49
4695	29	38.3	26.1	1.04	53	3.94	-0.07			75	105	S11-B16-11	1.94
4745	29	21	47.6	1.10	180	5.97	-0.13			119	120	S11-B16-11	1.58
3620	30	9.9	101.0	1.25	810	12.2	-0.29			202	226	N11-A16-9	1.52
1955	34	11.4	87.7	1.21	560	9.09	-0.26	14		172	202	S11-A16-12	1.42
4299	60	190	5.3	0.95	394	2.18	-0.11			31	50	N11-A1-11	0.03
4302	60	47.1	21.2	1.03	32.4	2.89	-0.07			44	67	N11-81-9	1.89
4305	60	25.5	39.2	1.09	119	4.11	-0.11			81	81	N11-A1-11	1.35
4317	82	143	7.0	0.97	5.4	1.79	-0.08			23	31	N11-B1-9	2.32
4320	82	38	26.3	1.05	42.6	2.51	-0.09			31	36	N11-A1-11	1.55
4323	82	21.2	47.2	1.11	114	3.46	-0.15			59	63	N11-A1-9	1.43
4387	90	45.2	22.1	1.04	28.4	2.29	-0.09			41	42	N11-B1-9	1.78
4399	90	20	50.0	1.12	105	2.94	-0.17	6		56	61	N11-A1-11	1.40

[a] Maximum power reached during a test just prior to reactor scram
[b] Total energy measured during the test
[c] There was no definite power peak, therefore, rho c tm is replaced by the compensated reactivity at the time of maximum power
[d] Insufficient deflection of data
[e] Indicate oscillograph records trace deflection between 5 and 10 mm
[f] Measurements from 0.5 mil TC's - all other temperature measurements from 5 mil chromel-alumel TC's
[g] Measurements from stainless steel TC -- all other temperature measurements from 5 mil Chromel Alumel TC's
Note: Test no. = for 1-81 this is the "run number", for all other tests this is the "oscillograph trace number"
Note: data from IDO-17223, Table II

Table B-12: Spert I SA-Core Step Transient Summary Data

Test No.	rod position (in.) Crit.	Trans.	Period (msec)	1/period (1/sec)	Pmax (Mw)	Etm (Mw-sec)	DTmax (deg C)	DTtm (deg C)	TC location	tm - to (sec)	rho in (cents)	rho_c at tm (cents)	BSP a*Etm/Pmax
44	10.36	10.97	3.10E+04	0.032	-	-	-	-	-	-	20.8	-	-
46	10.41	11.18	2.00E+04	0.050	-	-	-	-	-	-	26.3	-	-
47	10.41	11.32	1.50E+04	0.067	0.185	15.7	32.0	31.0	E1:1-20	262.0	30.6	35.5	5.69
41	10.32	11.41	1.05E+04	0.095	0.240	5.93	35.6	24.9	E1:1-20	140.22	36.8	26.0	2.35
56	10.45	11.67	8.10E+03	0.12	0.310	5.76	26.0	20.0	E1:4-23	114.0	40.7	20.0	2.23
45	10.39	11.9	4.80E+03	0.21	0.590	7.51	50.0	30.7	E1:1-20	63.0	50.3	26.4	2.67
48	10.44	12.46	1.80E+03	0.56	1.52	8.36	68.7	43.0	E1:1-20	25.5	65.9	26.5	3.08
42	10.36	12.7	957	1.05	2.48	7.82	82.0	36.0	E1:1-20	17.17	75.5	26.0	3.31
49	10.35	13.02	416	2.41	4.14	6.14	84.0	35.5	E1:1-20	7.53	85.5	22.6	3.57
43	10.44	13.24	273	3.67	6.01	6.50	84.0	23.0	E1:1-20	4.46	89.0	16.0	3.97
40	10.31	13.27	144	6.96	8.70	5.45	88.5	12.0	E1:1-20	2.175	94.5	13.5	4.36
52	10.42	13.46	108	9.26	12.11	3.21	81.0	8.0	E1:1-20	1.395	96.4	9.0	2.45
39	10.29	13.41	73.9	13.5	15.9	2.79	91.0	8.0	E1:1-20	1.14	99.3	8.0	2.37
53	10.37	13.6	44.1	22.7	32.3	3.02	90.5	6.0	E1:1-20	0.900	102.3	9.25	2.12
68	10.36	13.69	33.5	29.9	48.6	3.40	92.5	5.0	E1:1-20	0.615	105.3	12.6	2.09
50	10.45	13.89	29.2	34.2	74.4	4.49	88.0	7.0	E1:1-20	0.607	107.4	14.0	2.06
38	10.2	13.92	17.6	56.8	190.0	6.76	85.0	8.0	E1:1-20	0.407	116.7	20.6	2.02
51	10.49	14.35	14.0	71.4	259.0	8.40	93.0	8.0	E1:1-20	0.468	118.2	24.6	2.32
54	10.45	14.71	10.2	98.1	515.0	10.76	92.0	4.5	E1:1-20	0.337	129.0	36.0	2.05
55	10.43	14.9	9.4	106.0	669.0	13.51	97.8	9.5	E1:1-20	0.316	135.0	43.8	2.14
59	10.49	15.18	7.9	127.0	869.0	15.12	102.0	34.0	E1:1-20	0.275	140.0	45.0	2.21
69	10.38	15.21	7.0	143.0	1126.0	16.93	91.5	9.0	E1:1-20	0.254	145.0	50.0	2.15
61	10.49	15.49	6.8	147.0	1345.0	18.69	93.5	10.0	E7-7-12	0.276	148.0	45.0	2.04
70	10.4	15.5	6.3	159.0	1440.0	18.35	99.5	2.0	E1:1-18	0.241	151.0	60.0	2.03
71	10.42	15.92	5.6	179.0	2010.0	24.0	88.5	6.0	E1:1-20	0.226	161.0	50.0	2.14
72	10.46	16.41	4.8	208.0	2820.0	29.0	87.5	8.0	E1:1-20	0.194	172.0	70.0	2.14
73	10.41	17.06	3.8	263.0	4930.0	40.0	99.0	10.0	E1:1-20	0.185	190.0	102.5	2.13
74	10.47	17.97	3.2	313.0	7480.0	51.3	179.0	16.0	E1:1-20	0.198	210.0	107.5	2.15

Note: data was primarily taken from IDO-16752 but was supplemented with rod position information and a few extra long period runs from IDO-16751

For thermocouple location scheme see IDO-16752, Fig. 1, p.9

2/21/04, 8:24 AM PhD_SE-Day_reactor-expt-data.xls Spert I SA-592 steps **Constrained Core**

Table B-13: Spert I OC-Core Step Transient Summary Data

Test No.	Run Type	Period (msec)	1/period (1/sec)	Pmax (Mw)	Etm (Mw-sec)	Etot (Mw-sec)	Dtmax (Deg C)	DTtm (Deg C)	TC location	rho in (cents)	rho_c @ tm (cents)	BSP a*Etm/Pmax
1	step	1310	0.76	2.85	13	22	72 (a)	46	D4-1 17	73	30	3.47
2	step	565	1.77	5.59	12	54	86	36	C2-2 14	84	25	3.80
33	step	242	4.13	8.07	8.4	36	95	-	C4-1 20	93	-	4.30
31	step	235	4.26	7.69	8.2	36	110	-	C4-1 20	93	-	4.54
3	step	232	4.31	8.60	9.9	48	97	29	C2-2 17	93	21	4.96
4	step	224	4.46	9.02	10	50	94	30	C2-2 17	93	21	4.94
34	step	217	4.61	7.88	7.4	35	84	-	C4-1 20	94	-	4.33
30	step	206	4.85	8.49	8.3	33	85	-	D1-4 23	94	-	4.74
5	step	147	6.80	11.9	7.5	36	93	16	C2-2 17	97	16	4.29
15	step	143	6.99	10.4	6.0	35	103	-	D4-1 23	97	-	4.03
16	step	102	9.80	12.1	4.2	36	107	-	C2-2 21.5	98	-	3.40
36	step	92	10.8	14.5	3.7	19	102	-	C4-1 17	100	-	2.76
6	step	79.6	12.6	19.2	3.7	31	95	5	C2-2 17	101	8.4	2.43
8	step	67.8	14.8	23.1	3.6	36	98	5	C2-2 21.5	102	8.6	2.31
7	step	54.4	18.4	31.0	3.8	38	92	4	C2-2 14	104	8.8	2.26
9	step	42.6	23.5	44.9	4.3	43	99	4	C2-2 26	106	10	2.25
17	step	40.9	24.4	37.2	3.7	37	107	-	C2-2 21.5	107	-	2.43
12	step	37.8	26.5	56.6	4.5	22	86	4	C4-1 14	108	11	2.11
29	ramp-step	36.1	27.7	56.1	4.1	38	92	-	D1-4 26	108	-	2.02
10	step	27.8	36.0	88.2	5.4	50	99	5	C4-1 17	112	14	2.20
18	step	24.0	41.7	96.5	5.2	46	125	-	C1-4 20	114	-	2.25
19	step	16.7	59.9	237	8.2	50	107	-	D4-1 20	121	-	2.07
35	ramp-step	11.3	88.0	520	11	64	109	-	D4-1 26	131	32	1.86
13	step	9.9	101	677	15	61	99	6	C1-4 20	136	37	2.24
11	step	9.8	102	722	15	64	105	5	C2-2 26	136	37	2.12
14	step	2.2	454	17400	86	155	556	13	C2-2 21.5	262	173	2.24
37	ramp-step	1.55	645	35000	95	165	682	22	C4-1 23	330	231	1.75

Note: data was primarily taken from IDO-17028 but was supplemented with extra thermocouple data (hot spot) for some of the checkout tests from IDO-16931

Note: all tests conducted from low power, ambient temperature, atmospheric pressure, under a 2 ft hydrostatic head, with only natural circulation flow

Note: TC location scheme is shown in IDO-17028, Fig. B-1, p.72 for the quadrant and pin XY numbering. Axial location number is assumed to be from bottom of axial fuel region.

2/21/04, 9:24 AM PhD_SE-Day_reactor-expt-data.xls Spert I OC steps

Table B-14: Spert III E-Core Step Transient Summary Data

Run Number	Period (msec)	a (1/sec)	Pmax (Mw)	Etm (Mw-sec)	DTtm (deg C)	DTtm tc location	DTmax (deg C)	DTmax tc location	Rin ($)	Rc tm ($)	BSP	Note
5	1890.0	0.529	1.21	6.1	37.7	S-11-C-7	45.2	S-11-C-7	0.675	0.242	2.67	a
4	1840.0	0.543	1.23	6.3	-	-	-	-	0.680	0.252	2.78	a
2	1710.0	0.586	1.30	6.5	37.8	S-11-C-7	62.8	S-11-C-7	0.688	0.264	2.93	a
22	1010.0	0.991	2.09	6.9	31.1	S-11-C-4	51.1	S-11-C-4	0.768	0.263	3.27	
6	735.0	1.360	2.56	6.4	31.4	S-11-C-4	63.1	S-11-C-7	0.809	0.262	3.40	a
3	718.0	1.39	2.71	6.4	30.8	S-11-C-7	65.7	S-11-C-7	0.816	0.242	3.28	
18	351.0	2.85	4.32	6.7	20.2	S-11-C-4	54.9	S-11-C-7	0.895	0.233	4.42	
7	298.0	3.36	5.24	6.1	17.5	S-11-C-4	83.0	S-11-C-4	0.905	0.199	3.91	a
13	206.0	4.85	5.58	4.1	13.3	S-11-C-4	70.3	S-11-C-4	0.933	0.185	3.56	
14	195.0	5.13	5.61	5.3	13.6	S-11-C-4	48.0	S-11-C-7	0.936	0.196	4.85	
8	182.0	5.49	6.88	4.3	11.7	S-11-C-4	65.1	S-11-C-4	0.943	0.180	3.43	a
39	113.0	8.85	8.06	4.7	8.8	S-11-C-7	79.4	S-11-C-7	0.973	0.167	5.16	
23	111.0	9.01	7.85	4.2	7.8	S-11-C-4	73.0	S-11-C-4	0.974	0.156	4.82	
45	96.8	10.30	8.24	3.6	5.8	S-11-C-7	83.2	S-11-C-13	0.982	0.133	4.50	
15	95.8	10.40	8.02	3.4	5.0	S-11-C-4	69.5	S-11-C-13	0.987	0.131	4.41	
50	95.7	10.45	9.24	3.3	-	-	83.2	-	0.983	0.112	3.73	
44	95.0	10.50	8.32	3.8	7.0	S-11-C-7	73.2	S-11-C-13	0.983	0.141	4.80	
46	94.0	10.64	8.53	4.0	-	-	83.0	-	0.984	0.145	4.99	
71	94.0	10.64	7.88	3.6	-	-	82.0	-	0.984	0.141	4.86	
17	91.0	11.00	8.59	3.3	5.1	S-11-C-4	65.1	S-11-C-4	0.988	0.124	4.23	
51	72.3	13.83	10.7	2.4	-	-	72.3	-	0.999	0.089	3.10	
49	68.4	14.62	10.6	2.1	-	-	79.1	-	1.002	0.081	2.90	
9	64.6	15.50	12.90	2.4	1.9	S-11-C-13	78.8	S-11-C-4	1.000	0.086	2.88	a
16	59.3	16.90	12.10	2.0	0.7	S-11-C-13	65.8	S-11-C-13	1.010	0.075	2.79	
38	55.5	18.00	14.60	2.1	2.2	S-11-C-7	92.1	S-11-C-7	1.015	0.074	2.59	
19	44.0	22.70	18.20	1.9	1.5	S-11-C-13	64.1	S-11-C-13	1.029	0.074	2.37	
10	42.6	23.50	19.90	2.1	1.1	S-11-C-13	74.4	S-11-C-4	1.032	0.075	2.48	
20	35.0	28.60	25.90	2.0	0.7	S-11-C-7	68.6	S-11-C-7	1.033	0.080	2.21	
21	22.3	44.80	56.40	2.8	0.4	S-11-C-7	65.3	S-11-C-13	1.086	0.109	2.22	
40	22.0	45.50	59.40	2.8	0.6	S-11-C-7	87.6	S-11-C-7	1.089	0.109	2.14	
48	21.1	47.39	63.0	2.8	-	-	78.4	-	1.087	0.112	2.11	
47	19.9	50.25	67.3	3.0	-	-	86.4	-	1.093	0.120	2.24	
11	19.4	51.50	75.40	3.3	1.2	S-11-C-4	84.6	S-11-C-4	1.104	0.121	2.25	
41	15.9	62.90	110.00	3.8	2.9	S-11-C-7	81.2	S-11-C-13	1.130	0.144	2.17	
42	12.6	79.40	172.00	4.6	1.8	S-11-C-7	81.8	S-11-C-7	1.167	0.180	2.12	
43	10.0	100.00	279.00	6.0	0.7	S-11-C-7	82.0	S-11-C-7	1.213	0.218	2.15	

Note: all tests conducted from initial power ~ 10W, temperature ~ 70F (~ 21C), under atmospheric pressure, with natural circulation flow only
Note: Runs 2 through 9 were performed prior to correcting defective control rod assembly
Note: data taken from IDO-17260, and IDO-17270
Note: [a] problem with control rod flux suppressor
2/21/04, 2:17 PM PhD_SE-Day_reactor-expt-data.xls Spert III E-Core steps

Table B-15: Spert I OC-Core Ramp Transient Summary Data

Test No.	Period (msec)	1/period (1/sec)	Pmax (Mw)	Etm (Mw-sec)	Etot (Mw-sec)	Dtmax (Deg C)	TC location	rho in (cents)	BSP Etm*a/Pmax
20	970	1.03	3.42	12	37	79	C2-2 17	77	3.61
26	301	3.32	8.12	11	38	85	D10-10 26	91	4.50
32	256	3.91	6.99	9.6	36	110	C1-4 20	92	5.37
25	251	3.98	8.15	8.1	35	84	C2-2 26	92	3.96
22	242	4.13	9.83	11	37	84	D10-10 23	93	4.62
24	204	4.90	8.44	8.3	40	86	C2-2 21.5	94	4.82
27	196	5.10	11.4	9.6	43	83	D10-10 23	94	4.29
28	99	10.1	16.0	5.2	34	84	D10-10 23	100	3.28
23	73.9	13.5	18.5	3.2	22	89	C2-2 21.5	102	2.34
21	57.8	17.3	18.1	3.4	12	98	C2-2 21.5	104	3.25

Note: data was primarily taken from IDO-17028 but was supplemented with extra thermocouple data (hot spot) for some of the checkout tests from IDO-16931

Note: all tests conducted from low power, ambient temperature, atmospheric pressure, under a 2 ft hydrostatic head, with only natural circulation flow

5/16/2004, 7:13 PM PhD_SE-Day_reactor-expt-data-LEU-rod.xls Spert I OC ramps

Table B-16: Spert I P-Core Fuel Loading Accident Summary Data

Test No.	Rho in ($)	Period (msec)	1/period (sec)	Pmax (MW)	Etot (MW-sec)
1	0.89	415	2.41	1.6	5.9
2	0.99	110	9.09	4.7	5.3
3	1.05	36	27.8	27	8.5
4	1.1	22	45.5	61	8.9
5	1.16	14	71.4	160	9.1
6	1.35	7	143	456	12

Note: data taken from IDO-16606, Table 1, p.3

2/20/04, 11:35 PM PhD_SE-Day_reactor-expt-data.xls Spert I P-18|19 FLA

B.7 Figures

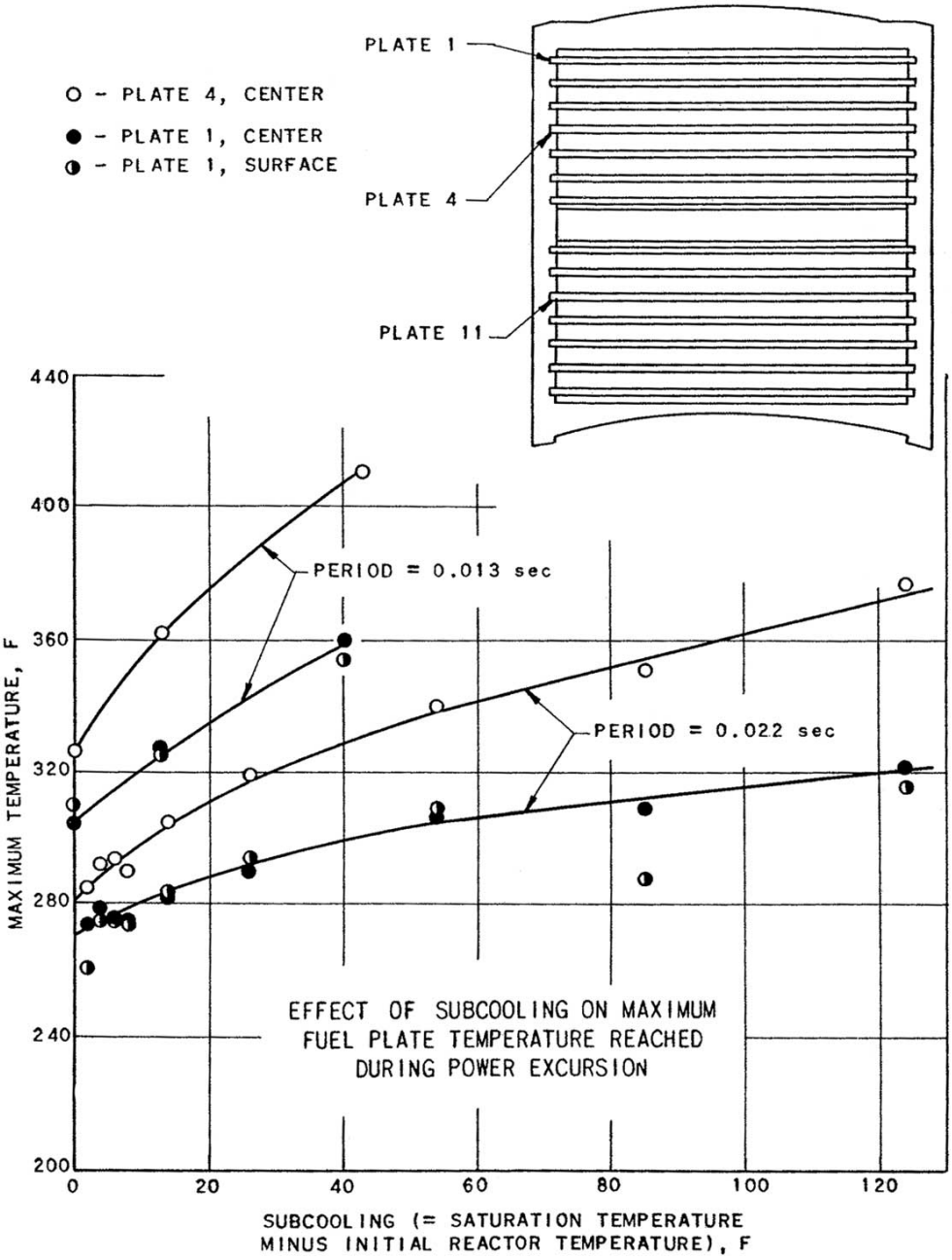

Figure B-1: Borax I Subcooling Temperature Data from 1953 Tests (reproduced from Ref. B-1)

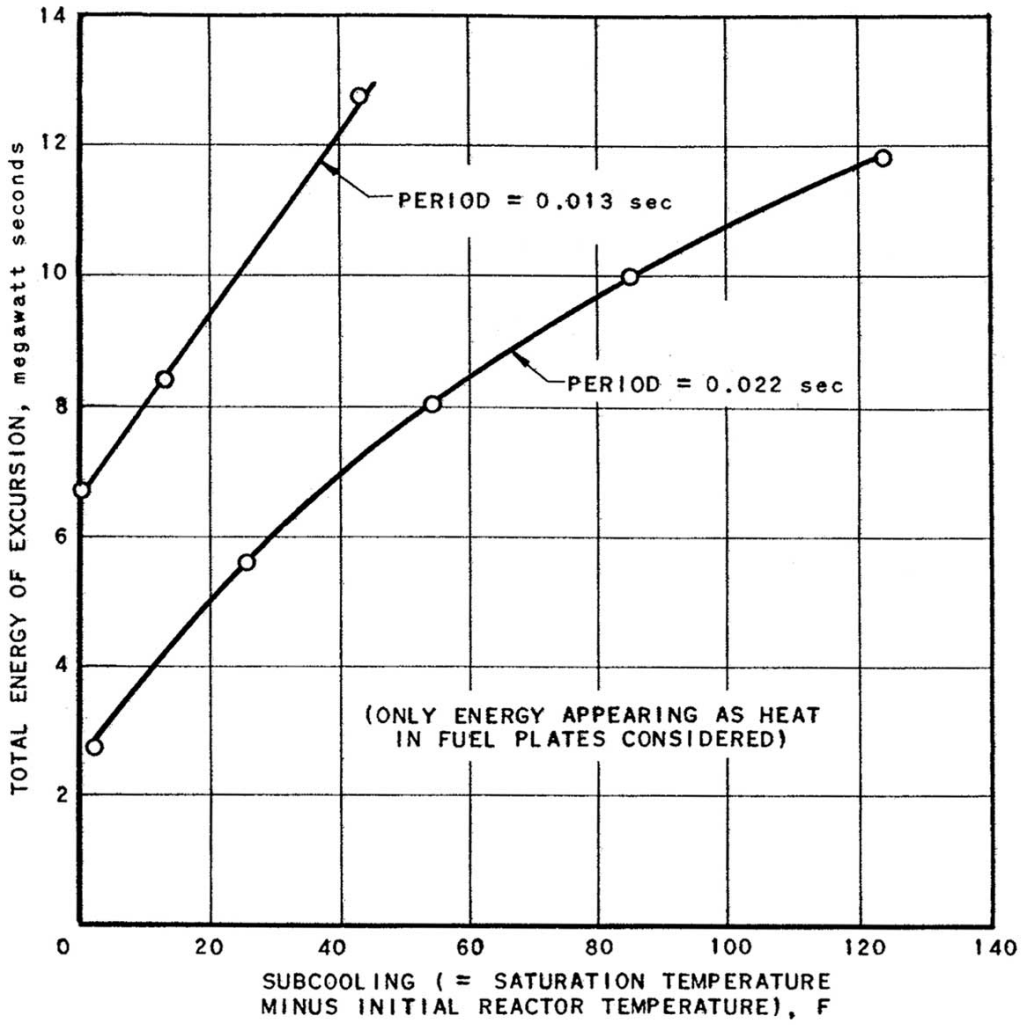

Figure B-2: Borax I Subcooling Energy Data from 1953 Tests
(reproduced from Ref. B-1)

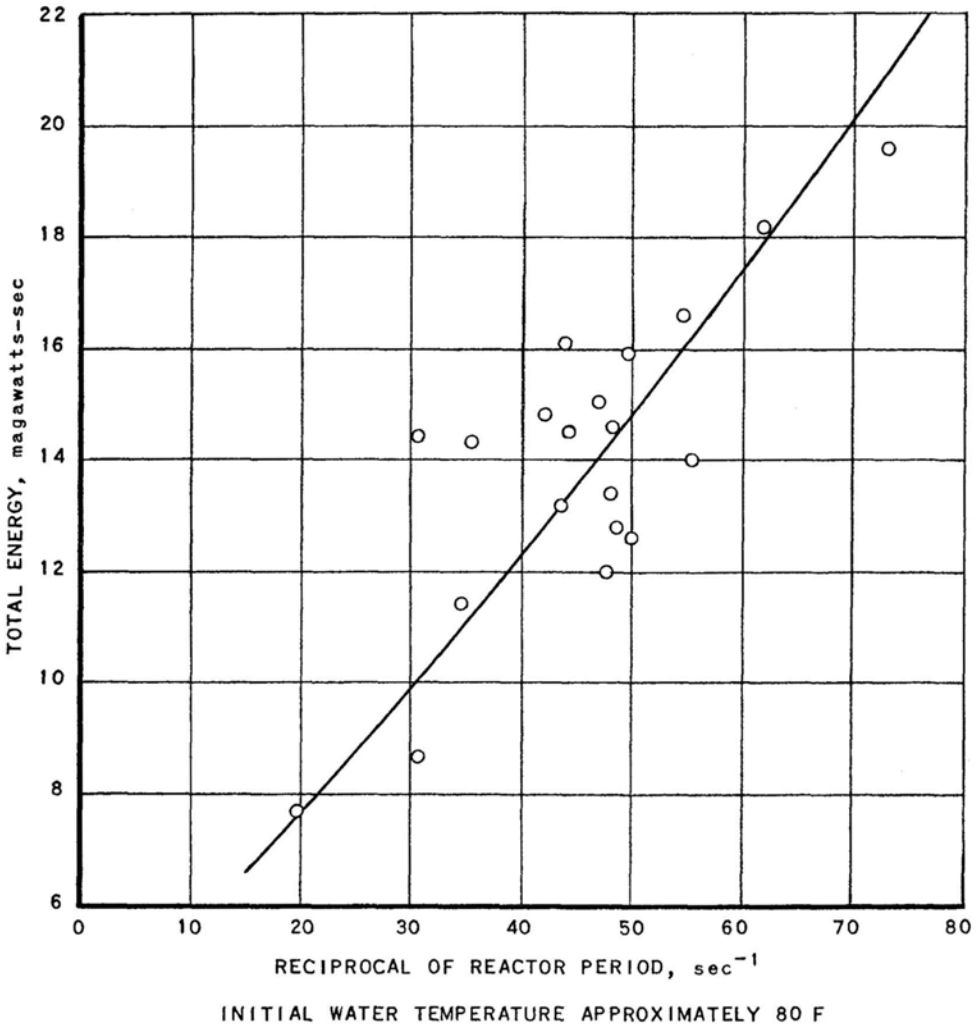

Figure B-3: Borax I Subcooling Energy Data from 1954 Tests
(reproduced from Ref. B-2)

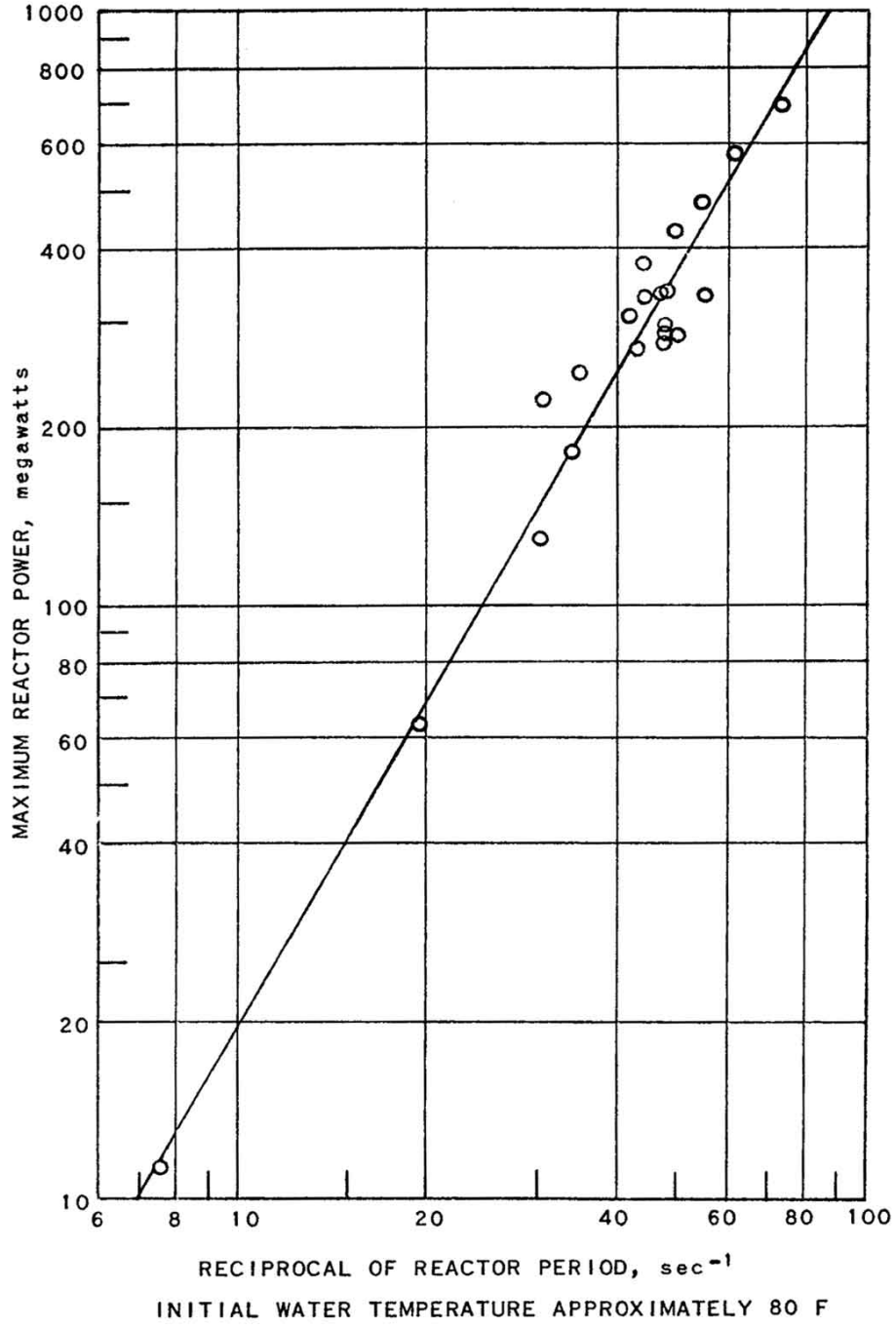

Figure B-4: Borax I Subcooling Power Data from 1954 Tests (reproduced from Ref. B-2)

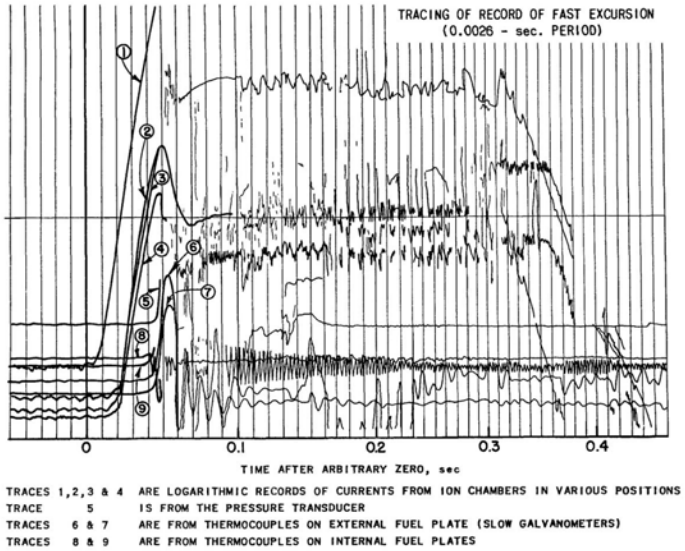

Figure B-5: Data Record from Borax I Destructive Test (reproduced from Ref. B-2)

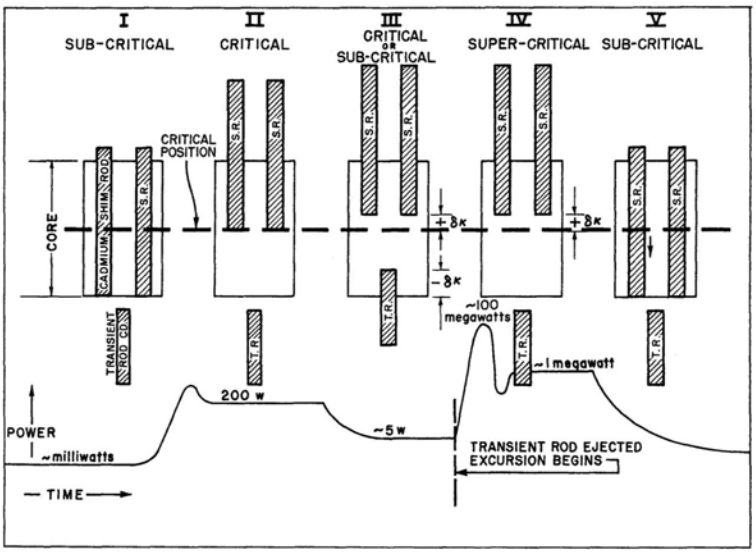

Figure B-6: Spert Step Insertion Test Sequence (reproduced from Ref. B-4)

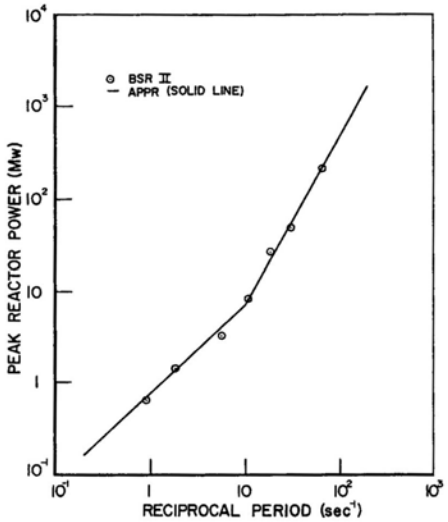

Figure B-7: Spert I BSR-II Step Insertion Test Maximum Power Data, including P-Core (APPR) Data (Ref. B-21)

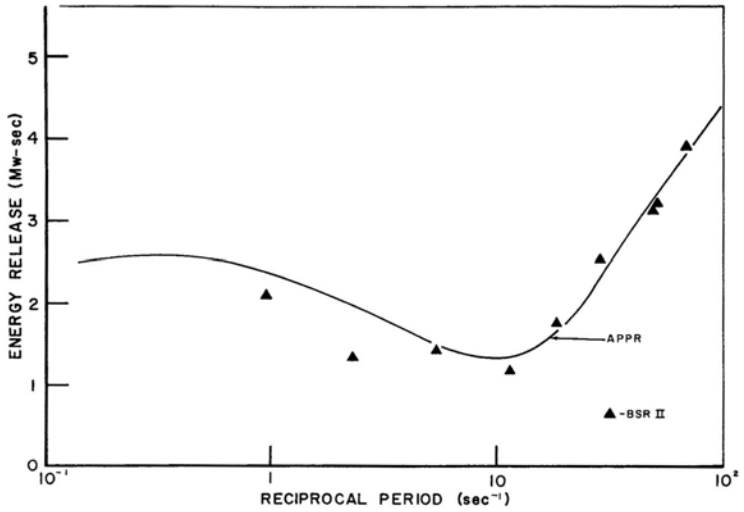

Figure B-8: Spert I BSR-II Step Insertion Test Maximum Energy Data, including P-Core (APPR) Data (Ref. B-21)

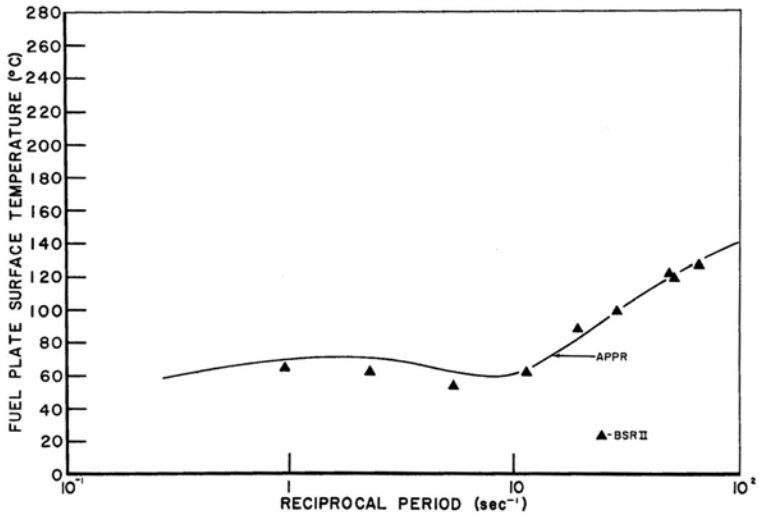

Figure B-9: Spert I BSR-II Step Insertion Test Maximum Temperature at the Time of Maximum Power Data, including P-Core (APPR) Data (Ref. B-21)

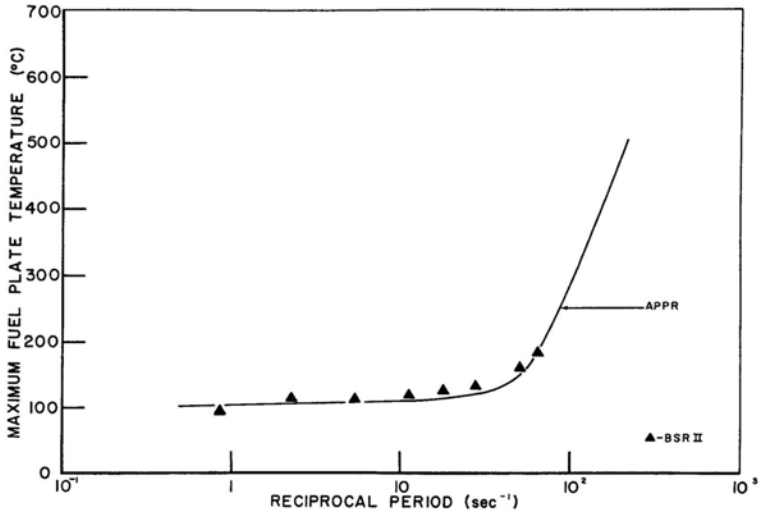

Figure B-10: Spert I BSR-II Step Insertion Test Maximum Temperature Data, including P-Core (APPR) Data (Ref. B-21)

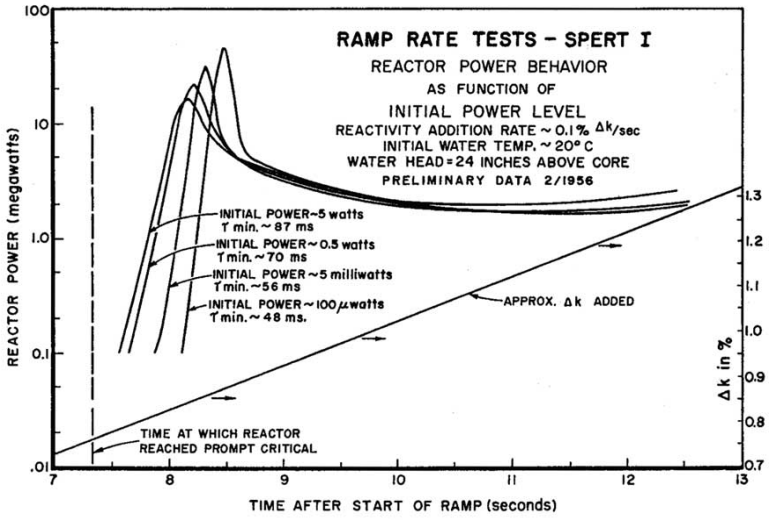

Figure B-11: Sperт I A Ramp Tests from Ambient Low Power Conditions (reproduced from Ref. B-4)

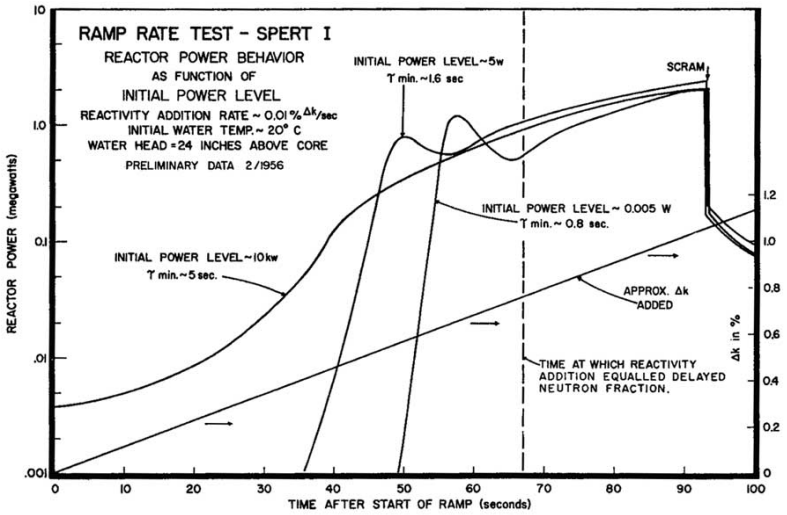

Figure B-12: Sperт I A Ramp Tests from Ambient Low Power Conditions (reproduced from Ref. B-4)

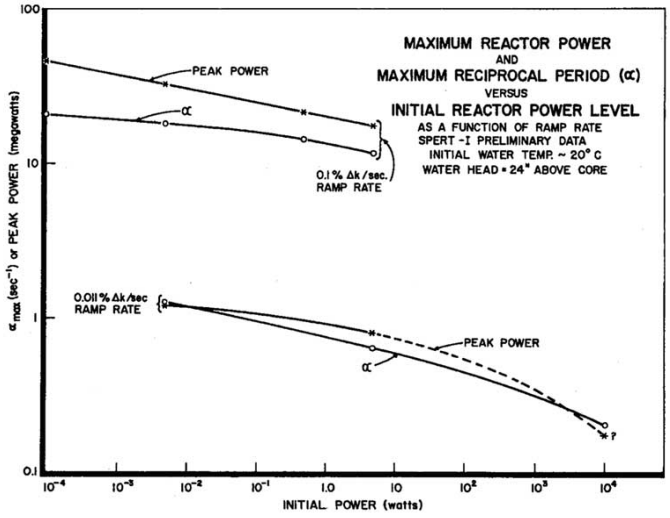

Figure B-13: Maximum Reciprocal Period and Maximum Power as Functions of Initial Power from Spert I A Ramp Tests from Ambient Low Power Conditions (reproduced from Ref. B-4)

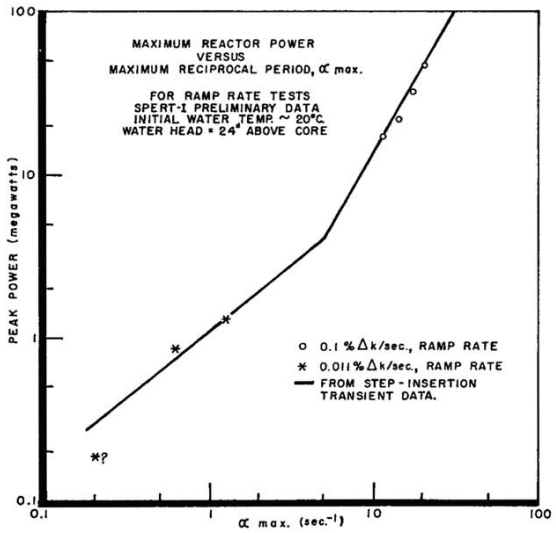

Figure B-14: Maximum Power as a Function of Reciprocal Period for Spert I A Ramp Tests from Ambient Low Power Conditions (reproduced from Ref. B-4)

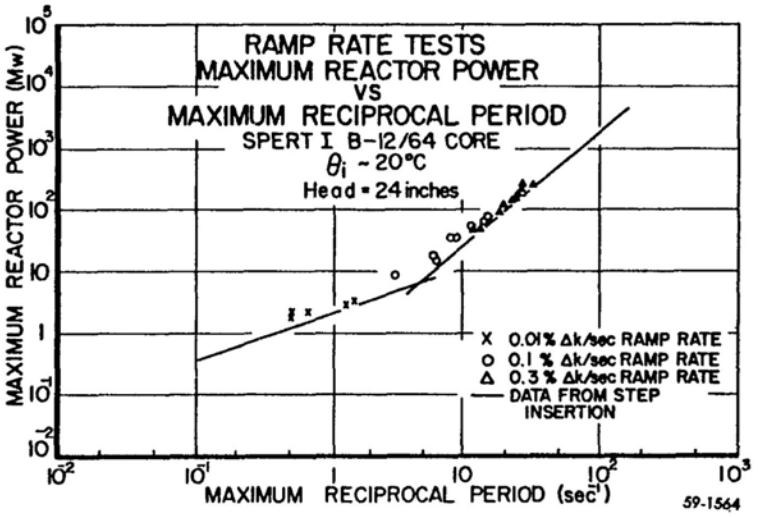

Figure B-15: Maximum Power as a Function of Reciprocal Period for Spert I B-12/64 Step and Ramp Tests from Ambient Low Power Conditions (reproduced from Ref. B-36)

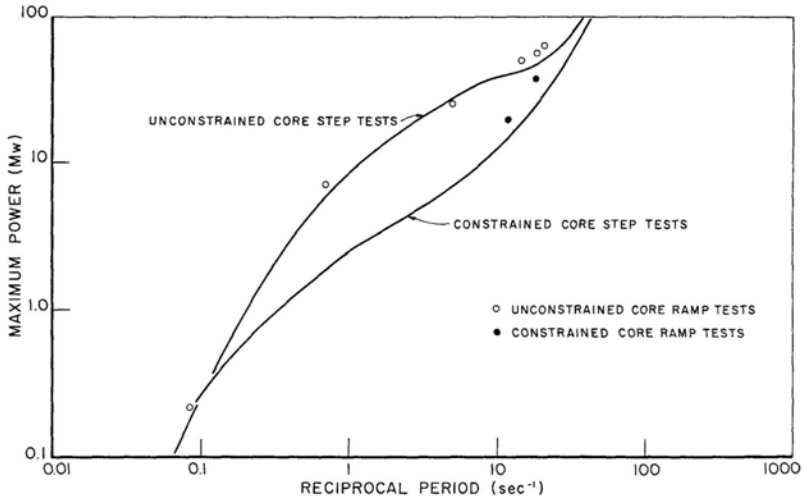

Figure B-16: A Comparison of Peak Power *vs.* Reciprocal Period for Spert I SA Step and Ramp Initiated Transients (reproduced from Ref. B-27)

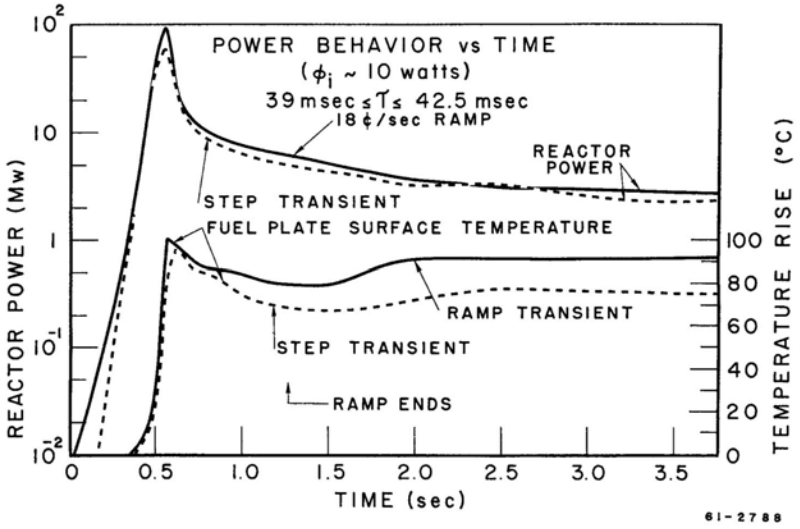

Figure B-17: Reactor Power and Fuel Plate Surface Temperature for 18c/sec Ramp Test and 40 msec-Period Step Test in Spert III C (reproduced from Ref. B-37)

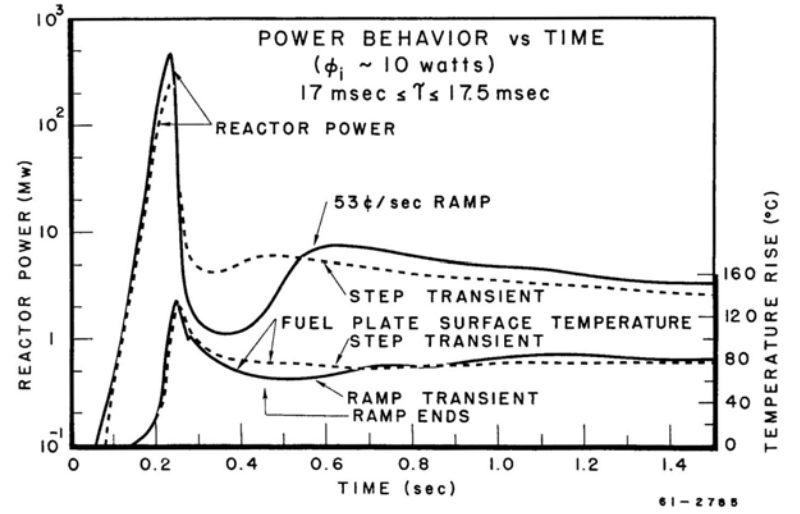

Figure B-18: Reactor Power and Fuel Plate Surface Temperature for 53c/sec Ramp Test and 17 msec-Period Step Test in Spert III C (reproduced from Ref. B-37)

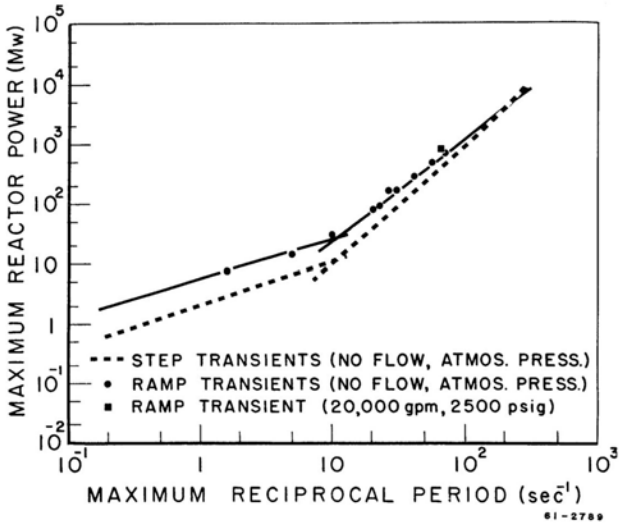

Figure B-19: A Comparison of Peak Power *vs.* Reciprocal Period for Spert III C-19/52 Step and Ramp Initiated Transients (reproduced from Ref. B-37)

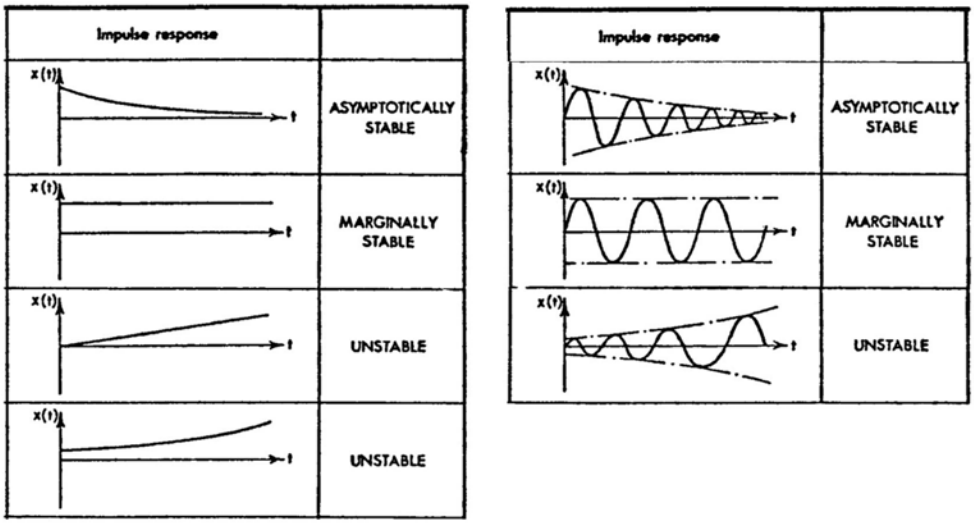

Figure B-20: Examples of Stable, Marginally Stable and Unstable Behaviour (modified from Ref. B-38)

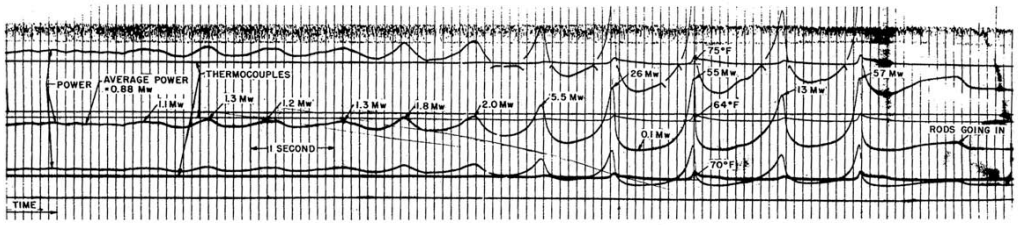

FAST GALVANOMETER RECORDS SHOWING TRANSITION FROM OSCILLATORY BOILING TO "CHUGGING" AT ATMOSPHERIC PRESSURE. 2.6% k_{eff} COMPENSATED BY STEAM (END OF RUN 2, 9/18/53)

THE THREE POWER RECORDS ARE FROM ION CHAMBERS OF DIFFERENT SENSITIVITIES, ON LOGARITHMIC SCALE. THE UPPERMOST TRACE IS UNRELIABLE BECAUSE OF A STICKING GALVANOMETER. THE TOP TEMPERATURE TRACE IS FROM THE CENTER OF FUEL PLATE 4. THE MIDDLE TRACE IS FROM THE CENTER OF PLATE 1, AND THE LOWEST TRACE FROM THE SURFACE OF PLATE 1.

Figure B-21: Chugging Power and Temperature Trace from the Borax I Tests (Ref. B-1)

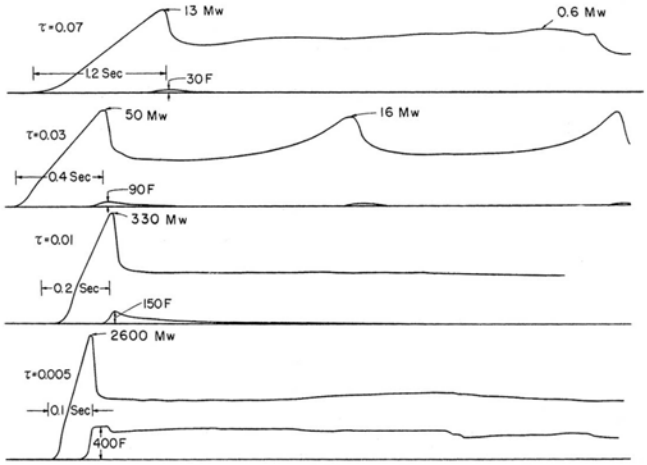

REPRESENTATIVE RECORDS OF EXCURSIONS AT SATURATION TEMPERATURE WITH VARIOUS EXCESS REACTIVITIES

THESE WERE TRACED DIRECTLY FROM THE GALVANOMETER RECORDS. NOTE THAT THE TIME SCALE CHANGES FROM RUN TO RUN.

THE PERIOD (τ) OF THE EXCURSION IS MARKED ON EACH RUN IN SECONDS. THE TEMPERATURE RECORD IS FROM THE CENTER OF FUEL PLATE 11

Figure B-22: Examples of Power and Temperature Response to Step Reactivity Insertions in Borax I, the Second Trace from the Top Shows Chugging Behaviour (Ref. B-1)

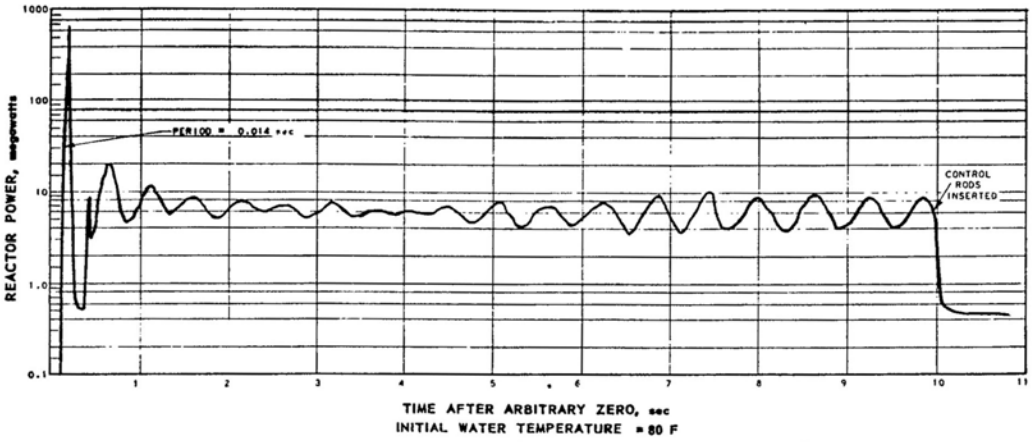

Reactor power variation during 10-second run following initial excursion of 14-millisecond period

Figure B-23: Power Oscillations during a Subcooled Step Reactivity Insertions in Borax I (Ref. B-39)

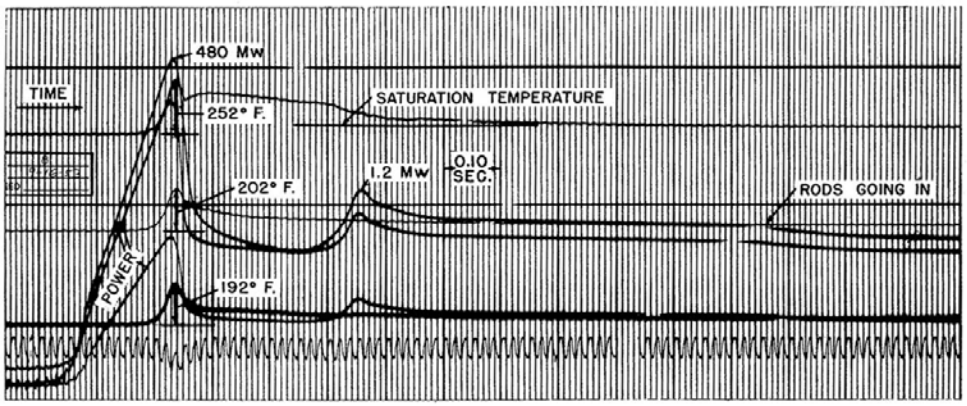

This record is from an excursion of 0.013 second period, with 43F subcooling. The top temperature trace is from the center of fuel Plate 4. The middle trace is from the center of Plate 1, and the bottom trace is from the surface of Plate 1. The three power traces on each record are from ion chambers of three different sensitivities, on logarithmic scales.

Figure B-24: Secondary Power Peak during a Subcooled Step Reactivity Insertions in Borax I (Ref. B-1)

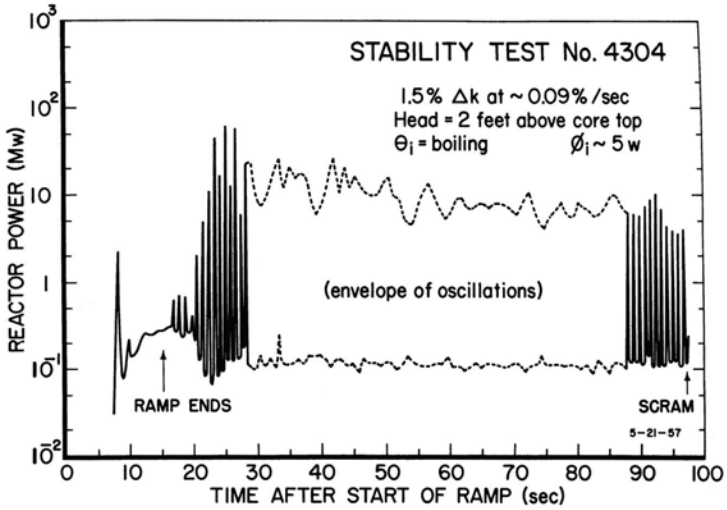

Figure B-25: Power Trace for Spert I A-17/28 Stability Test, 2-Foot Hydrostatic Head, Saturation Conditions (Ref. B-42)

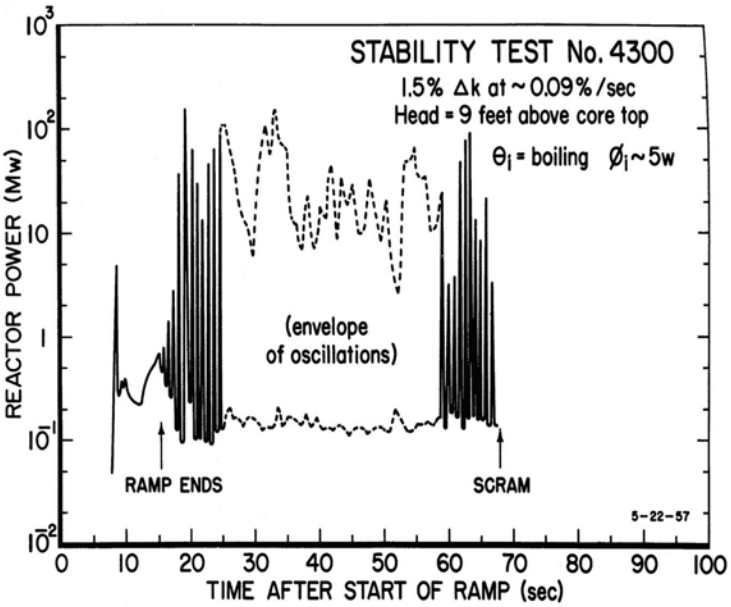

Figure B-26: Power Trace for Spert I A-17/28 Stability Test, 9-Foot Hydrostatic Head, Saturation Conditions (Ref. B-42)

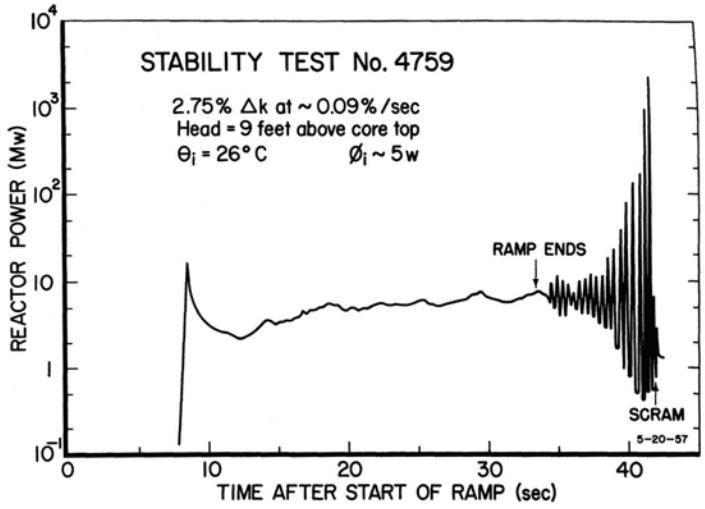

Figure B-27: Developing Chugging in Power Trace for Spert I A-17/28 Stability Test, 9-Foot Hydrostatic Head, Saturation Conditions (Ref. B-42)

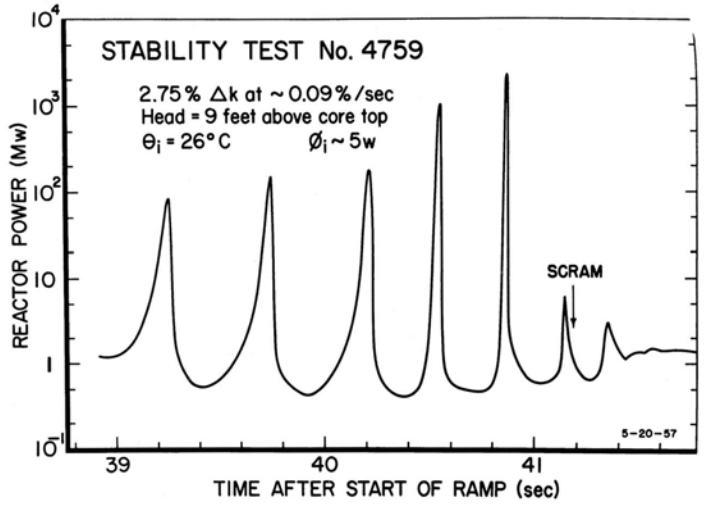

Figure B-28: Closeup of Developing Chugging in Power Trace for Spert I A-17/28 Stability Test, 9-Foot Hydrostatic Head, Saturation Conditions (Ref. B-42)

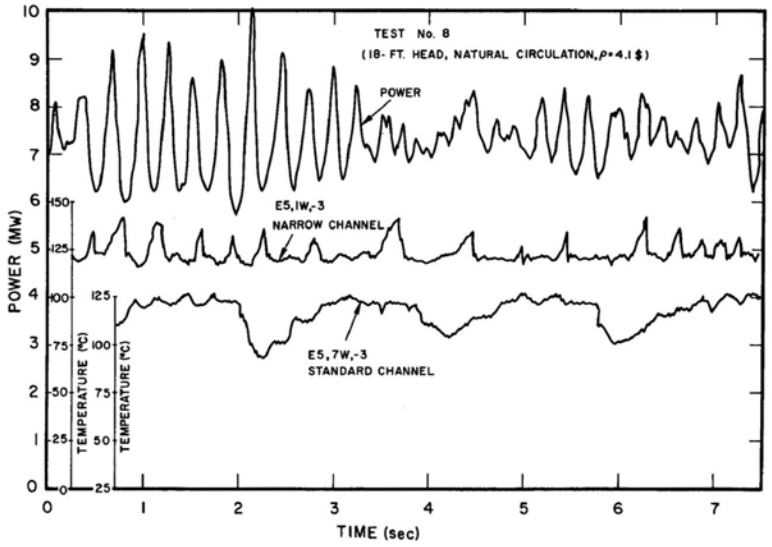

Figure B-29: Reactor Power and Cladding Surface Temperature Behaviour in a Narrow and a Standard Coolant Channel During an 18-Foot Head, Natural-Circulation Stability Test in Spert IV D-12/25 (Ref. B-45)

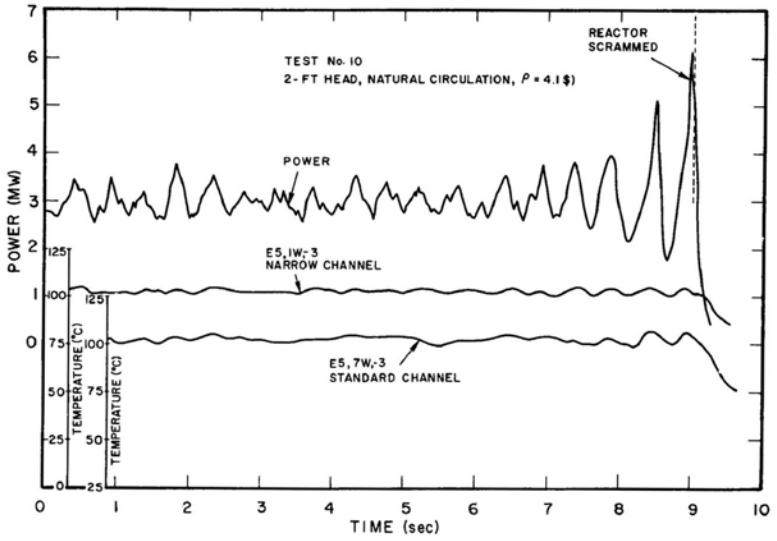

Figure B-30: Reactor Power and Cladding Surface Temperature Behaviour in a Narrow and a Standard Coolant Channel During an 2-Foot Head, Natural-Circulation Stability Test in Spert IV D-12/25 (Ref. B-45)

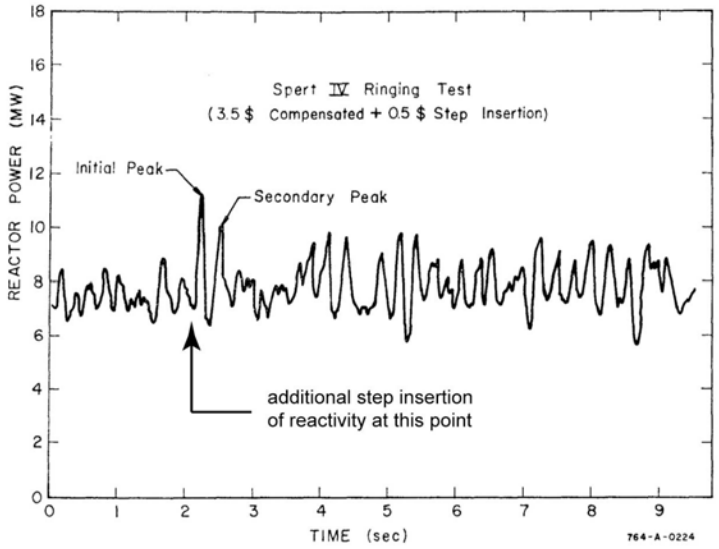

Figure B-31: Reactor Power Trace During a Ringing Test in Spert IV D-12/25 (Ref. B-31)

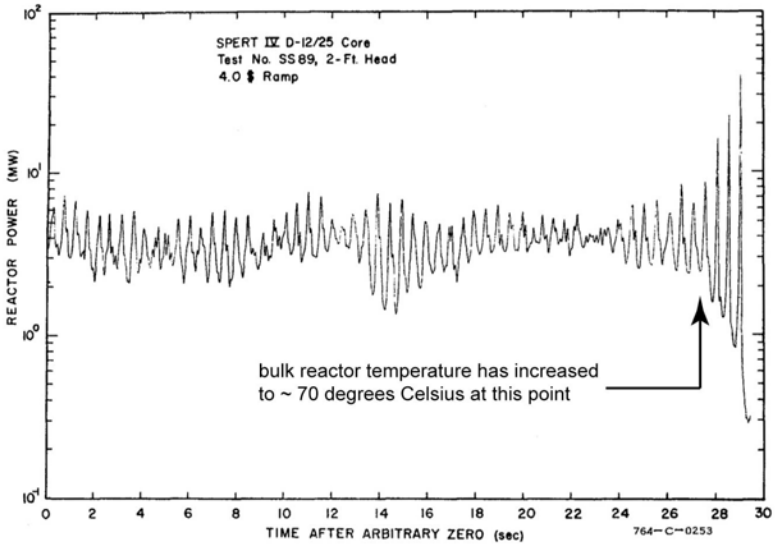

Figure B-32: Power Trace from Spert IV D-12/25 Chugging Test Showing the Onset of Chugging (Ref. B-25)

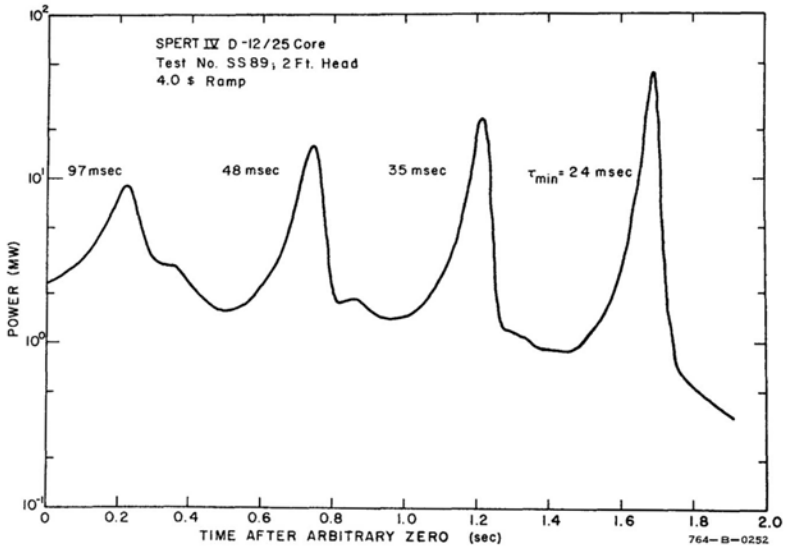

Figure B-33: Power Trace from Spert IV D-12/25 Chugging Test Showing the Last Four Power Oscillations (Ref. B-25)

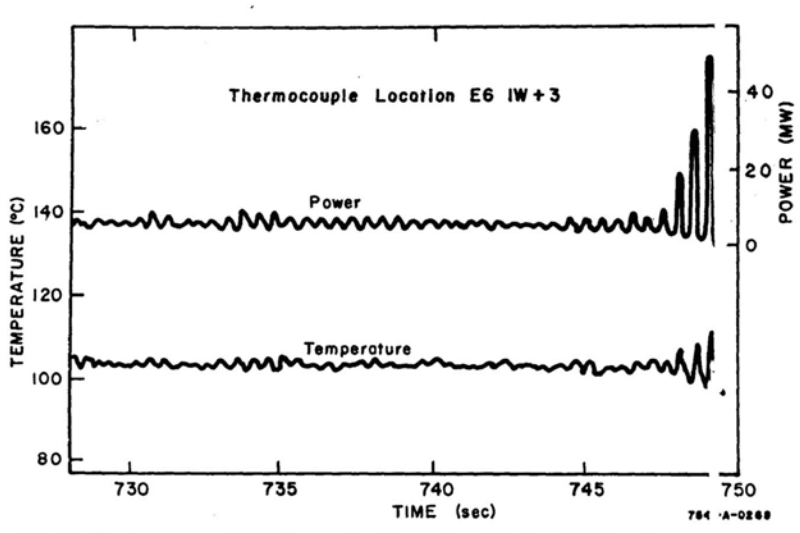

Fig. 30 Reactor power and cladding surface temperature behavior at the time the power became unstable during test No. SS 89.

Figure B-34: Reactor Power and Cladding Surface Temperature Behaviour at the Time of Onset of Chugging from Spert IV D-12/25 Chugging Test (Ref. B-17)

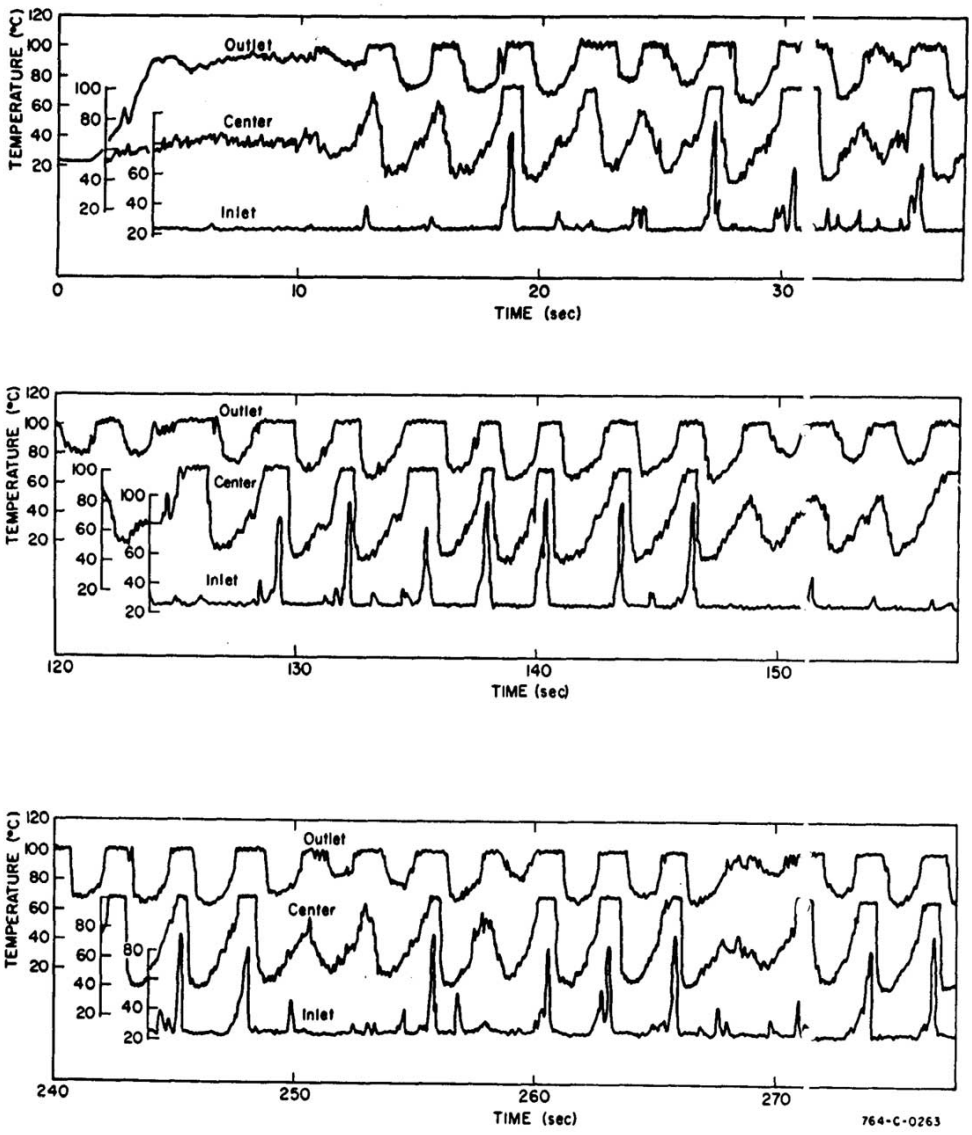

Fig. 31 Inlet, center, and outlet water channel temperature behavior for selected times during first half of test No. SS 89.

Figure B-35: Inlet, Centre, and Outlet Water Channel Temperature Behaviour for Selected Times During Spert IV D-12/25 Chugging Test (Ref. B-17)

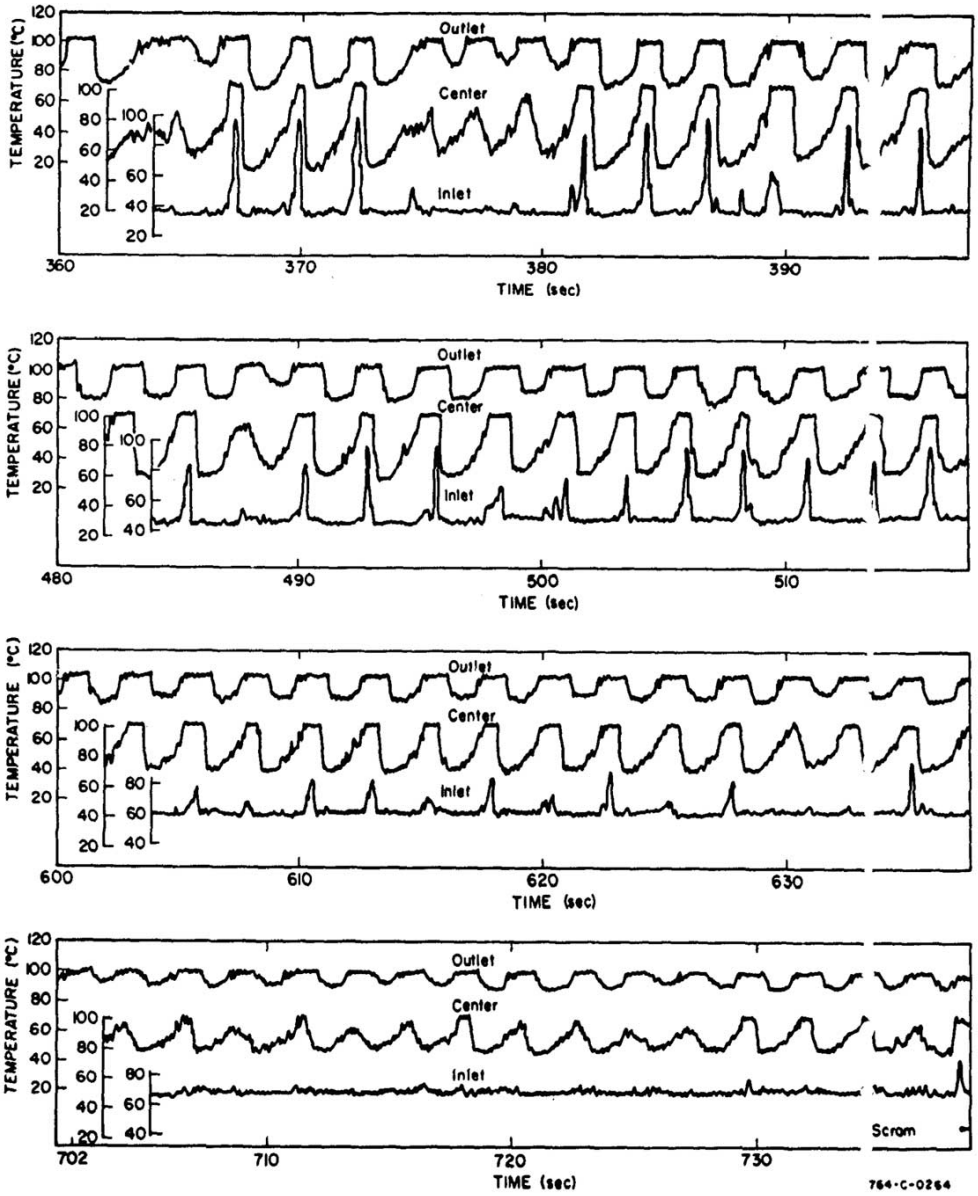

Fig. 32 Inlet, center, and outlet water channel temperature behavior for selected ti ss during last half of test No. SS 89.

Figure B-36: Inlet, Centre, and Outlet Water Channel Temperature Behaviour for Selected Times During Spert IV D-12/25 Chugging Test (Ref. B-17)

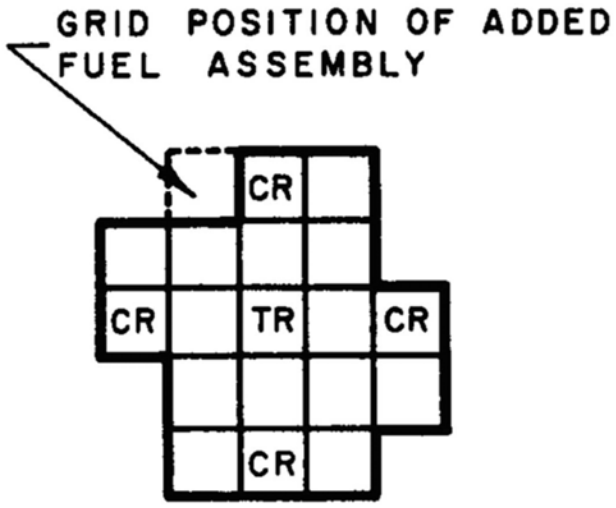

Figure B-37: Spert I P-18/18 Core with Indicated Position of Fuel Assembly in Fuel Drop Tests (reproduced from Ref. B-48)

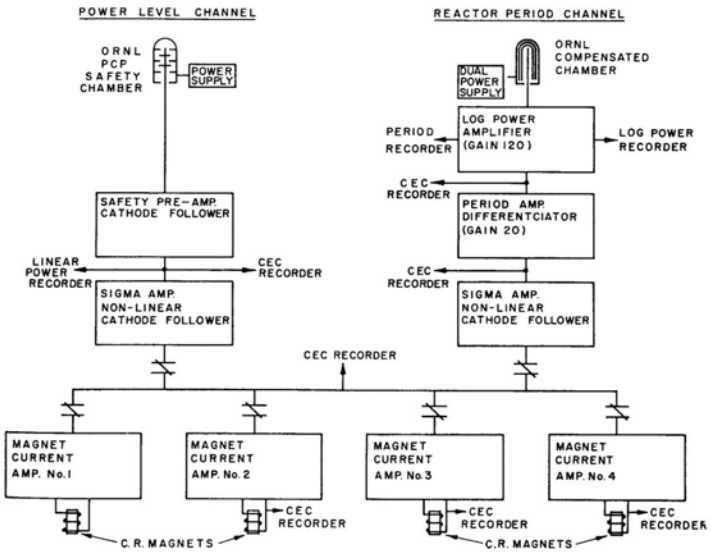

Figure B-38: BSR-II Safety System for the Spert I Installation (reproduced from Ref. B-49)

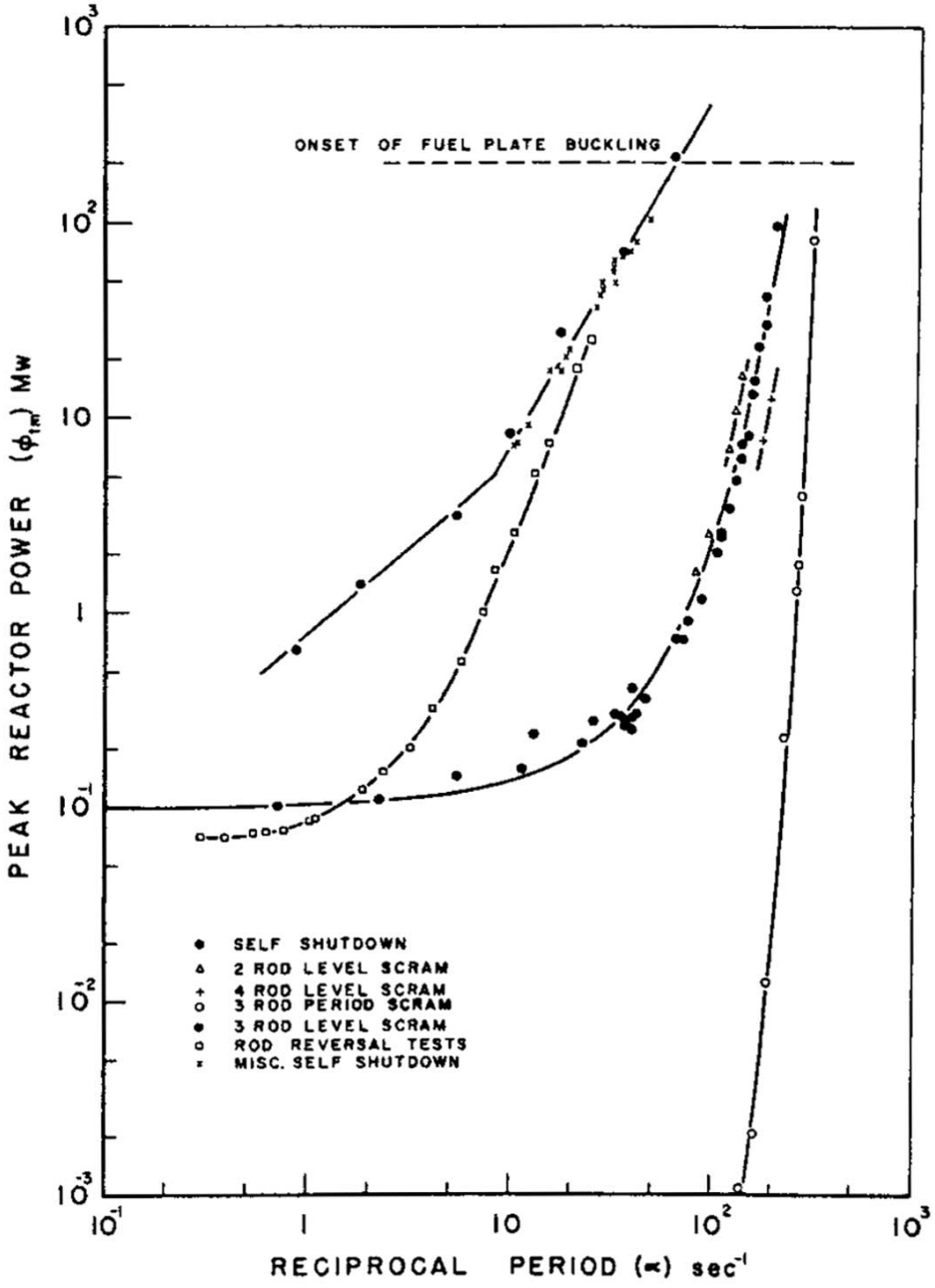

Figure B-39: Peak Power *vs.* Reciprocal Period for Various Modes of Shutdown for the Spert I BSR-II Core (reproduced from Ref. B-21)

APPENDIX C - STATISTICS, CURVE FITTING & HEU DATA REGRESSION ANALYSIS

TABLE OF CONTENTS

LIST OF TABLES

LIST OF FIGURES

(this page is intentionally left blank)

C STATISTICS, CURVE FITTING & HEU DATA REGRESSION ANALYSIS

C.1 Statistics & Curve Fitting

The Reactor Test Data, summarized in Chapter 3, exhibits notable trends in the primary quantities, *i.e.*, power, energy, and fuel plate surface temperature, with the reciprocal reactor period. In this appendix a formal curve fitting analysis is made of the transient summary data, *i.e.*, P_{max}, E_{tm}, and ΔT_{max}, with respect to the reciprocal reactor period.

C.1.1 Curve Fitting Methods

C.1.1.1 Linear Regression

Linear regression is used to fit functional relationships to the Reactor Test data. The behaviour of the transient summary data (P_{max}, E_{tm}, ΔT_{max}) as functions of the reciprocal period (α_o) suggest the following functions:

$$y = b\,x^m$$
$$y = b\,e^{mx}$$

The power relation of the first equation is applicable to the P_{max} and E_{tm} *vs.*α_o data whereas the exponential relation of the second equation is applicable to the ΔT_{max} *vs.* α_o data. This is discussed further in Section C.2.

These functions can be linearized by simply taking the logarithms of both sides of the equations, yielding:

$$\ln(y) = m\ln(x) + \ln(b)$$
$$\ln(y) = m\,x + \ln(b)$$

Standard linear regression analysis is then applied with the new variables being ln(y), ln(x), and x, to determine the slopes (m) and the intercepts (ln(b)) of the relations.

The idea of linear least squares regression is to minimize the sum of the squares of the vertical variances between the data points and the calculated regression line. This

is shown pictorially in Figure C-1.

Depending on the form of the uncertainties over the range of the independent variable either simplified or weighted linear regression is applicable. These are both standard approaches and are described in Reference C-1. In the case where the absolute uncertainty varies from one data pair to the next the contribution of each data pair to the regression analysis is weighted by the inverse square of the uncertainties. In the case of constant absolute uncertainties for each data pair the simplified least squares equations can be used.

C.1.1.2 Transformation of Uncertainties

The uncertainties on the test data must be transformed along with the linearization of the describing functions. This is straight-forward using standard error propagation:

$$v = \ln(y)$$

$$\sigma_v^{\,2} = \sigma_y^{\,2}\left(\frac{\partial v}{\partial y}\right)^2$$

$$= \sigma_y^{\,2}\left(\frac{1}{y}\right)^2$$

$$\sigma_v = \frac{\sigma_y}{y}$$

The result shows that the relative error on the measured quantity becomes an absolute error once the variable is transformed *via* the logarithm, *e.g.*,

$$\sigma_y = 5\%$$

$$\sigma_{\ln(y)} = \frac{\sigma_y}{y} = 0.05$$

The random uncertainties related to the test data are summarized Chapter 3. These take the form of percent errors in the measured values, which results in an increasing

absolute uncertainty as the reciprocal period is increases. As shown above, these uncertainties are then converted to constant factors upon linearization.

C.1.1.3 Indirect Uncertainty Contribution from Period Data

One of the assumptions behind linear least squares fitting is that all uncertainty in the data can be ascribed to the dependent variable. This is true when the precision of the measurement of the independent variable, x, is much better than that of the dependent variable, y, *i.e.*,

$$\sigma_x \frac{dy}{dx} \ll \sigma_y$$

In the case where the uncertainty in the independent variable is on the order of that associated with the dependent variable the fitting is still reasonably accurate if the uncertainty in the independent variable, x, is translated to additional uncertainty in the dependent variable, y, using the first order relation:

$$\sigma_{y,I} = \sigma_x \frac{dy}{dx}$$

This is referred to as the "indirect" contribution to the uncertainty in y from x, and is designated with the subscript I. The indirect contribution is then combined with the direct contribution to the uncertainty, $\sigma_{y,D}$, which is the measured uncertainty in y, as:

$$\sigma_y^{\,2} = \sigma_{y,D}^{\,2} + \sigma_{y,I}^{\,2}$$

This approach is outlined in Reference C-1 and is adopted in the case of the reactor test data since the random uncertainty on the reciprocal period is on the order of the random uncertainty in the other primary data.

C.1.2 Reference Data Set

Examination of the correlated data plots of the linearized test data, *i.e.*,

$$\ln\left(P_{max}\right) vs. \ln\left(\alpha_o\right)$$
$$\ln\left(E_{tm}\right) vs. \ln\left(\alpha_o\right)$$
$$\ln\left(\Delta T_{max}\right) vs. \ln\left(\alpha_o\right)$$

over the short period range, indicates common slopes for the data from each individual core (*i.e.*, each data set). That is, the slopes of curve fits through the data are common to the data from each test core, and the differences which do exist are in the vertical offset of the data, *i.e.*, the *y*-intercept values on the linearized plots.

Of interest in the data analysis are the differences in the vertical offsets of the different data sets. As a means to this end, a representative value for the slope through the data is chosen and applied to each data set. For the step insertion test data on the HEU Al-clad plate cores from ambient temperature, low-power, atmospheric pressure initial conditions the Spert I D-12/25 data are chosen as the reference data set from which the slope is determined.

The Spert I D-12/25 data set was chosen for multiple reasons:

- the data set contains the most data pairs,
- the variance of the data appears small relative to the data from other cores, especially for the temperature data, which is not unexpected given the refinement of equipment, procedures, and data analysis over the course of the Spert Project, and
- the data covers the entire range of periods up to the onset of fuel damage *via* melting.

The Spert I D-12/25 data set is used as the reference for all of the primary measured quantities, *i.e.*, for the power, energy, and temperature data. The applicability of using the slope from the Spert I D-12/25 regression fit on the other data sets is evaluated as part of the "goodness of fit" analysis.

For the remaining data sets (*i.e.*, data from the other test cores) the slope from the regression analysis on the linearized reference data set is used and the *y*-intercept value is calculated. This *y*-intercept value is calculated by simply taking the weighted average of the values calculated from each data point, *i.e.*,

$$y = m\,x + b$$
$$b_i = y_i - m\,x_i$$
$$\langle b \rangle = \frac{\sum(w_i b_i)}{\sum(w_i)}$$

where m is the slope value from the reference data set, x_i and y_i are the measured data pairs, and w_i is the weight of the data pair, *i.e.*,

$$w_i = \frac{1}{\sigma_{y_i}^{\,2}}$$

In the case of constant uncertainties for all data pairs the calculation simplifies to,

$$\langle b \rangle = \frac{\sum(b_i)}{N}$$

where N is the number of data pairs for the data set. The standard deviation on the $\langle b \rangle$ value is found from,

$$\sigma_{\langle b \rangle} = \sqrt{\frac{\sum\left(b_i - \langle b \rangle\right)^2}{N-1}}$$

C.1.3 Goodness of Fit Testing

The goodness of the curve fit is evaluated in a number of ways herein. These are described in the following sections.

C.1.3.1 Coefficient of Determination, R^2

The first method of evaluation is calculation of the coefficient of determination, R^2. This parameter indicates the degree to which the dependent variable can be predicted from the independent variable, or stated another way it shows how well the data are correlated in terms of the selected fitting function relative to a random scatter.

The R^2 parameter ranges in values between zero and one. A value of zero indicates no correlation between the variables, *i.e.*, that there is no linear relationship between the variables, *i.e.*, a horizontal straight line through the average of the *y*-values is the best fit straight line to the data. A value of unity indicates that all data points fall exactly on the regression line without scatter.

A convenient formula for calculating R^2 in unconstrained linear regression (*i.e.*, linear fitting which does not necessarily pass through the origin) is:

$$\begin{aligned} R^2 &= 1 - SS_{reg} / SS_{tot} \\ &= 1 - \frac{\sum \left(y_i - y_i^* \right)^2}{\sum \left(y_i - \langle y \rangle \right)^2} \end{aligned}$$

where SS_{reg} is the sum of the squares of the vertical variances of each data point relative to the regression line, and SS_{tot} is the sum of the squares of the vertical variances of each data point relative to a horizontal line through the average *y*-value.

The horizontal line through the average of the *y*-values is the null hypothesis, *i.e.*, no relation between variables. The theory behind the calculation is shown in Figure C-2 and is described in Reference C-2.

C.1.3.2 Confidence and Prediction Bands

The variance (or standard deviation) on the calculated regression fitting parameters, *i.e.*, slope and intercept, and on the data with respect to the fitting line can be calculated as part of the least squares analysis. These results can be used to construct both confidence and prediction bands on the plots of the data.

Confidence bands indicate the variation in the fitting line about the calculated line of best fit and are a function of the standard deviation about the calculated slope as well as the distance from the mean of the independent variable:

$$y_i^* \pm Ws \sqrt{\left(\frac{1}{N} + \frac{\left(x_i - \langle x \rangle \right)^2}{\sum \left(x_i - \langle x \rangle \right)^2} \right)}$$

where y_i* is the fitted value of y at point x_i, N is the number of data points, $\langle x \rangle$ is the mean value of x, s is the standard deviation of the data to the fitting line, and,

$$W = \sqrt{\left(2\,F(0.95, 2, N-2\right)}$$

where F represents the F-distribution for the upper 95 percentile (Ref. C-3). This is shown pictorially in Figure C-3 where the dashed lines are the confidence bands about the solid line of best fit.

The confidence bands provide confidence intervals simultaneously for all points about the fitted line, and represents a range within which the fitting line is 95% likely to exist. The variation of the fitting line within the confidence bands is shown in Figure C-4.

A related concept are prediction bands. These show the confidence region within which the data points are contained about the fitting line. Prediction bands are shown in Figure C-5. The curves defining the prediction intervals are further from the fitting curve than the confidence bands for the curve itself. A good approximation for calculating the prediction bands is made by simply adding one under the square root sign in the equation for the confidence bands (Ref. C-4), *i.e.*,

$$y_i^* \pm Ws\sqrt{\left(1 + \frac{1}{N} + \frac{\left(x_i - \langle x \rangle\right)^2}{\sum\left(x_i - \langle x \rangle\right)^2}\right)}$$

Given the approach adopted herein, the slope from the reference data set is used for fitting to the remaining data sets. As a result, the confidence bands are only relevant to the reference data set. Prediction bands are calculated as indicated above for the reference data set but are simply estimated as:

$$y_i^* \pm t^* s$$

for the remaining data sets given that the fitting curve slope is already fixed, where t* is the upper 95 percentile of the two-tailed Students t-distribution. For reasonably large values of N, (*i.e.*, large number of data points), *i.e.*, $N > 30$, t* is approximately equal to 2.0 and W is approximately 2.5.

As an indication of the goodness of fit the sizes of the confidence and prediction bands can be examined relative to the standard error on the measurement of the data. Prediction bands should certainly be of the same order of magnitude as the standard measurement error. Significantly larger prediction bands are an indication that either the model may need to be altered or more data are ideally needed to support the model.

C.1.3.3 Patterns in the Residuals

An additional check for the goodness of fit, or perhaps more along the lines of the applicability of the linear model in the first place, is to examine the residuals for patterns. The residuals of the data are simply the differences between the data points and the predicted values from the fitting function, *i.e.*,

$$r_i = \left(y_i - y_i^* \right)$$

where r_i is the residual for data point "i", and y_i* is the predicted value at x_i. Assuming the validity of the fitting function, the data should be scattered randomly about the fitting line. In other words, there should be as many positive as negative residuals and no patterns should be evident over the range of x values. Patterns indicate a bias in the model.

C.2 Regression Analysis for the Ambient-Temperature Test Data

The curve fitting methodology used in the regression analysis is described in the previous section.

The quantitative parameters determined by the regression analysis are suitable for use in parametric studies of the differences between the test data from the various test cores.

In the following sections the regression analysis results for the ambient temperature transient test data sets are summarized.

C.2.1 Power Data

C.2.1.1 Fitting Model

The power data are described in terms of the reciprocal period by:

$$P_{max} = b_1 \alpha_o^{\ m}$$

which when linearized is of the form:

$$\ln\left(P_{max}\right) = m \ln\left(\alpha_o\right) + \ln\left(b_1\right)$$

Examination of the direct random uncertainty on the P_{max} measurement and the indirect contribution from the random uncertainty on the measurement of the period (see Section C.1) results in a "total" random uncertainty of the form:

$$\begin{aligned}\sigma_{\ln(P_{max})} &= \sqrt{\sigma^2_{\ln(P_{max}),D} + \sigma^2_{\ln(P_{max}),I}} \\ &= \sqrt{\left(\frac{\sigma_{P_{max}}}{P_{max}}\right)^2 + \left(m\frac{\sigma_{\alpha_o}}{\alpha_o}\right)^2}\end{aligned}$$

which is constant over the range of alpha as the relative errors in P_{max} and α_o are constant over the range of α_o. Given this constant uncertainty on the $\ln(P_{max})$ variable, weighted least squares is equivalent to the simplified (non-weighted) least squares analysis.

In addition to the P_{max} data, it is useful to consider the related power density data. Both the maximum average and peak power densities are included and simply related to the P_{max} data *via* the fuel meat volume (V_f) and the power peaking factor (*PPF*). The working equations relevant to these results are:

$$\ln\left(\frac{P_{max}}{V_f}\right) = m \ln\left(\alpha_o\right) + \ln\left(b_2\right)$$

$$\ln\left(\frac{P_{max}}{V_f}\times PPF\right) = m\ln\left(\alpha_o\right) + \ln\left(b_3\right)$$

where,

$$\ln\left(b_2\right) = \ln\left(b_1\right) - \ln\left(V_f\right) + \ln\left(1000\right)$$

$$\ln\left(b_3\right) = \ln\left(b_1\right) - \ln\left(V_f\right) + \ln\left(PPF\right) + \ln\left(1000\right)$$

The ln(1000) term arises from a change in units from MW to kW. The total random uncertainty in the power density data is of the same form, *i.e.*, constant with respect to period, as for the P_{max} data. The magnitude of the uncertainty on the maximum peak power density includes an additional uncertainty related to the measured power peaking factor (*PPF*) (see Chapter 3).

C.2.1.2 Regression Analysis Results

C.2.1.2.1 Reference Data Set

Application of the least squares analysis to the Spert I D-12/25 reference data set results in a linear fit of:

$$\ln\left(P_{max}\right) = m\ln\left(\alpha_o\right) + \ln\left(b_1\right), \quad \alpha_o \geq 29\,\text{sec}^{-1}\ (\tau \leq 35\,\text{msec})$$

$$m = 1.597$$
$$\sigma_m = 0.0285$$
$$\ln\left(b_1\right) = -1.456$$
$$\sigma_{\ln(b_1)} = 0.1345$$

The standard deviation of the fitted data, and the coefficient of determination of the fit are:

$$s = 0.0492$$
$$R^2 = 0.9966$$

The reference data with the fitting function as well as confidence and prediction

bands are shown in Figure C-6.

C.2.1.2.2 Remaining Data Sets

The regression analysis results for all data sets are summarized in Table C-1. The associated *y*-intercept values for the maximum average power density (P_{max}/V_f) and the maximum peak power density (P_{max}/V_f x *PPF*) are also included in this table using the relations noted in Section C.2.1.1.

The results of the curve fitting are shown in Figures C-7, C-8, and C-9 for the P_{max}, P_{max}/V_f, and P_{max}/V_f x *PPF* data over the short period range.

C.2.1.3 Goodness of Fit

C.2.1.4 Reference Data Set

With respect to the curve fitting to the reference data set, the coefficient of determination is close to unity indicating a good choice of fitting function and a strong correlation between the independent and dependent variables.

The standard error on the slope value, σ_m, is small and the confidence bands on the fitting curve are narrow (see Fig. C-6), both indicating little statistical variance in the slope of the fitting curve. Additionally the residuals, *i.e.*, the deviations between the measured and curve fit predictions, show no discernable pattern over the range of the reciprocal period indicating that the model is not missing any component in the data trend (Fig. C-10).

The quality of the data is good. The standard deviation (standard error) in the fit to the Spert I D-12/25 data is small. This standard error translates to a relative standard deviation on the predicted P_{max} data (the reverse of the linearization process). As it is on the order of the relative error in the power data measurements which indicates that the quality of the fit is as good as the quality of the measured data. It follows that the prediction bands on the Spert I D-12/25 fit (Fig. C-6) are similarly consistent with the maximum estimated error (95% confidence) on the measured data.

The conclusion is that the regression analysis on the reference data set results in statistically well defined fitting parameters. The fitting model captures the behaviour of the data and the statistics of the fitting are consistent with the measurement uncertainty on the data.

C.2.1.5 Remaining Data Sets

The goodness of fit to each of the data sets follows in the same terms as for the Spert I D-12/25 regression results.

The applicability of using a common slope for all of the data sets can be evaluated by comparing the R^2 and standard errors for the fits using the Spert I D-12/25 derived slope to regression fits based entirely on the individual data sets, *i.e.*, where the slope is determined individually from each data set. A comparison of these parameters is shown in Table C-2.

The R^2 values for the fitting using the common slope were not significantly lower than those based on slope fitting for each individual data set. Similarly the standard error was not significantly increased by applying the common slope to each of the data sets. In fact, due to the small sample size in some cases the standard error was slightly reduced, based on the statistical calculation with one more degree of freedom (*i.e.*, when the data are not using a degree of freedom to calculate the slope).

Both of these comparisons support the idea of using a common slope to fit the data from different test cores.

With the exception of the Borax I case, the standard errors associated with each of the data sets are less than 0.10 (relative standard deviation in the P_{max} *vs.* α_o data is therefore less than 10%). For the Borax data set, the standard error is 0.175 (relative error in P_{max} *vs.* α_o of 17.5%). These standard errors are not greatly in excess of the total uncertainty in the power data, *i.e.*:

$$Borax\ measured\ data \quad \frac{\sigma_{P_{max}}}{P_{max}} = 11.4\%$$

$$Spert\ measured\ data \quad \frac{\sigma_{P_{max}}}{P_{max}} = 9.4\%$$

where the indirect uncertainty contribution from the period measurement has been taken into account. The fitting uncertainty in the Borax data set may be partially attributed to the small sample size, $N = 19$, but is likely more an indication that the measurement uncertainty may be underestimated.

The regression results have also been examined with respect to the distribution of

residuals as a function of the reciprocal period for each data set. As seen for the Reference Data Set a random distribution indicates comprehensive modelling. A possible positive slope in the distribution of the residuals is noted for some of the data sets, in particular the Spert I A-17/28 and Spert IV D-12/25 data. This trend may also be evident in the Spert I B-24/32 data. The Spert I A-17/28 residuals distribution is shown as an example in Figure C-11. The distribution indicates that a slightly greater slope may in fact be more applicable to the $\ln(P_{max})$ *vs.* $\ln(\alpha_o)$ test data. Development is left as future work.

The generally high R^2 values, and the comparable measurement and fitting standard error both indicate the appropriate choice of the fitting function and the quality of the measured data. The slight trends in some of the residual patterns suggests the possibility of a slight underestimation of the common slope in the $\ln(P_{max})$ *vs.* $\ln(\alpha_o)$ data but is not pursued further at this point. It should be noted that the size of the residuals are relatively small as can be seen by the magnitude of scatter of the data points with respect to their fitting lines (see for example, Fig. C-7) so any detectable patterns may not be of great concern with respect to the vertical offsets of the various data sets. Additionally, the noted patterns in some of the residuals should be considered with respect to the small sample sizes in all but the Reference data set and perhaps the Spert I A data set.

It should be noted that systematic errors on the measured data add a component of uncertainty to the vertical placement of the data on the correlated data plots. While not of concern for comparisons of data within a given set, *i.e.*, during the fitting process for a given data set, these uncertainties must be considered when comparing the vertical placement (*i.e.*, the *y*-intercept) values between different data sets.

C.2.2 Energy Data

C.2.2.1 Fitting Model

The energy to the time of peak power data are described in terms of the reciprocal period by the same functional form as the peak power data, *i.e.*:

$$E_{tm} = b_1 \, \alpha_o^{\,m}$$

which when linearized is of the form:

$$\ln\left(E_{tm}\right) = m\ln\left(\alpha_o\right) + \ln\left(b_1\right)$$

The fitting parameters m, and b_1 have different values for the energy data as compared to the power data.

The form of the total random uncertainty is also the same as that for the P_{max} data incorporating both the direct component from the energy measurement as well as the indirect component from the uncertainty in the period measurement. The total random uncertainty is given by:

$$\begin{aligned}\sigma_{\ln(E_{tm})} &= \sqrt{\sigma^2_{\ln(E_{tm}),D} + \sigma^2_{\ln(E_{tm}),I}} \\ &= \sqrt{\left(\frac{\sigma_{E_{tm}}}{E_{tm}}\right)^2 + \left(m\frac{\sigma_{\alpha_o}}{\alpha_o}\right)^2}\end{aligned}$$

which is constant over the range of alpha as the relative errors in E_{tm} and α_o are constant over the range of α_o. Given this constant uncertainty on the $\ln(E_{tm})$ variable, weighted least squares is equivalent to the simplified (non-weighted) least squares analysis.

As for the case of the power data, it is useful to consider the related energy density data. The maximum average and peak energy deposition densities to the time of peak power are found *via* normalisation to the fuel meat volume and scaling *via* the power peaking factor. The working equations relevant to these results are:

$$\ln\left(\frac{E_{tm}}{V_f}\right) = m\ln\left(\alpha_o\right) + \ln\left(b_2\right)$$

$$\ln\left(\frac{E_{tm}}{V_f}\times PPF\right) = m\ln\left(\alpha_o\right) + \ln\left(b_3\right)$$

where,

$$\ln\left(b_2\right) = \ln\left(b_1\right) - \ln\left(V_f\right) + \ln\left(1000\right)$$

$$\ln\left(b_3\right) = \ln\left(b_1\right) - \ln\left(V_f\right) + \ln\left(1000\right) + \ln\left(PPF\right)$$

The ln(1000) term arises from a change in units from MW to kW. The total random

uncertainty in the energy density data is of the same form, *i.e.*, constant with respect to period, as for the E_{tm} data. The magnitude of the uncertainty on the maximum peak energy deposition density includes an additional uncertainty related to the measured power peaking factor (*PPF*) (see Chapter 3).

C.2.2.2 Regression Analysis Results

C.2.2.2.1 Reference Data Set

Application of the least squares analysis to the Spert I D-12/25 reference data set results in a linear fit of:

$$\ln\left(E_{tm}\right) = m\ln\left(\alpha_o\right) + \ln\left(b_1\right), \quad \alpha_o \geq 29\,\text{sec}^{-1}\ (\tau \leq 35\,\text{msec})$$

$$m = 0.5737$$
$$\sigma_m = 0.0174$$
$$\ln\left(b_1\right) = -0.9978$$
$$\sigma_{\ln(b_1)} = 0.0823$$

The standard deviation of the fitted data, and the coefficient of determination of the fit are:

$$s = 0.0879$$
$$R^2 = 0.9226$$

The reference data with the fitting function as well as confidence and prediction bands are shown in Figure C-12.

C.2.2.2.2 Remaining Data Sets

The regression analysis results for all of the data sets are summarized in Table C-3. The associated *y*-intercept values for the maximum average energy deposition density (E_{tm}/V_f) and the maximum peak energy deposition density (E_{tm}/V_f x *PPF*) are also included in this table using the relations noted in Section C.2.2.1.

The results of the curve fitting are shown in Figures C-13, C-14, and C-15 for the E_{tm},

E_{tm}/V_f, and E_{tm}/V_f x *PPF* data over the short period range.

C.2.2.3 Goodness of Fit

The same approach is followed for the energy data as for the power data with respect to evaluating the goodness of the various fits.

C.2.2.3.1 Reference Data Set

Relative to the statistics on the power data curve fitting those for the energy data curve fitting are not as precise. However, in general the quality of the curve fitting to the energy data is still reasonable. With respect to the Spert I D-12/25 reference data set, the coefficient of determination is not as close to unity but is still reasonable.

In addition, the standard deviation is almost double that of the power data fit to the reference data set. This is reflected in noticeably wider confidence and prediction bands on the energy data (see Fig. C-12). These indicate a higher statistical variance on the slope of the reference fit as well as higher variance in the measured data with respect to the fit.

The standard deviation (standard error) in the fit to the Spert I D-12/25 data is comparable to the estimated total random error in the measured data:

$$curve\ fit \quad \frac{\sigma_{E_{tm}}}{E_{tm}} = 8\%$$

$$measured\ data \quad \frac{\sigma_{E_{tm}}}{E_{tm}} = 6\%$$

This indicates that the quality of the fit is as good as the quality of the measured data. As a result the 95% prediction bands on the Spert I D-12/25 fit (see Fig. C-12) are similarly consistent with the maximum estimated error (95% confidence) on the measured data.

The residuals show perhaps a slight curvature in their distribution with respect to the reciprocal period (Fig. C-16). Any curvature in the $\ln(E_{tm})$ *vs.* $\ln(\alpha_o)$ data is not addressed by the present model. This is not of great concern considering the other goodness of fit tests.

C.2.2.3.2 Remaining Data Sets

The applicability of using a common slope for all of the data sets is evaluated by comparing the R^2 and standard errors for the fits using the Spert I D-12/25 derived slope to regression fits based entirely on the individual data sets, *i.e.*, where the slope is determined individually from each data set. A comparison of these parameters is shown in Table C-4.

There is little difference in both the R^2 values and the standard errors for each data set from the curve fitting using the common slope and for full regression analysis on each individual data set. As a result, the applicability of the fitting function and the goodness of fit for each of the data sets is similar to that for the Spert I D-12/25 reference data set as described above.

All of the R^2 values and standard errors are in the same range for each of the data sets. This supports the approach of using a common slope to fit the data from different test cores. The relative standard deviations from the curve fitting and the measured energy data are:

$$curve\ fit \quad \frac{\sigma_{E_{tm}}}{E_{tm}} \leq 11\%$$

$$measured\ data \quad \frac{\sigma_{E_{tm}}}{E_{tm}} = 6\%$$

where the indirect uncertainty contribution from the period measurement is taken into account. This comparison suggests that either the curve fitting could be improved or the measured data random uncertainty is underestimated. Examination of the distribution of residuals suggests the former may be the case.

The current fitting model does not capture what looks like either some curvature in the $\ln(E_{tm})$ *vs.* $\ln(\alpha_o)$ data, or at least a bias towards positive residuals for larger reciprocal periods (shorter period tests). Examples of the residuals showing patterns are shown in Figures C-17 and C-18 for the Spert I A-core and Spert IV D-core data sets. These patterns are not clear in the residuals of all data sets but may be hidden due to sample size. Patterns in the residuals warrants further statistical examination given the small sample sizes of all but the Spert I D-12/25 and Spert I A-17/28 data sets.

As in the case of the power data, it should be noted that systematic errors on the measured energy data add a component of uncertainty to the vertical placement of the data on the correlated data plots. While not of concern for comparisons of data within a given set, *i.e.*, during the fitting process for a given data set, these uncertainties must be considered when comparing the vertical placement (*i.e.*, the *y*-intercept) values between different data sets.

C.2.3 Temperature Data

C.2.3.1 Available Test Data

The curve fitting to the maximum temperature rise data follows the methodology used for the power and energy data described above.

Of notable difference is the reduced sample size of the temperature data for the ambient initial temperature tests data set. Given the varying systematic errors associated with different thermocouples (see Chapter 3), only data from a single thermocouple is considered for each test core.

In addition, the three transient tests from the Spert I D-12/25 Destructive Test Series which resulted in fuel plate melting are not included for the Spert I D-12/25 regression fitting. The change in phase results in a different relationship between deposited energy and temperature rise as shown in the correlated ΔT_{max} *vs.* α_o data plot.

C.2.3.2 Fitting Model

The maximum temperature rise data can be described in terms of the reciprocal period by:

$$\Delta T_{max} = b_1 e^{m \alpha_o}$$

which when linearized is of the form:

$$\ln\left(\Delta T_{max}\right) = m\ \alpha_o + \ln\left(b_1\right)$$

This is a different functional form than used for fitting the P_{max} and E_{tm} data.

As a result of the different dependence on the reciprocal period, the form of the total random uncertainty is also different from that associated with the power and energy data. Incorporating the indirect contribution from the period uncertainty results in an absolute uncertainty which varies with reciprocal period (see Section C.1 above), *i.e.*:

$$\sigma_{\ln(\Delta T_{max})} = \sqrt{\sigma^2_{\ln(\Delta T_{max}),D} + \sigma^2_{\ln(\Delta T_{max}),I}}$$
$$= \sqrt{\left(\frac{\sigma_{\Delta T_{max}}}{\Delta T_{max}}\right)^2 + \left(m\,\sigma_{\alpha_o}\right)^2}$$

Given this varying uncertainty on the $\ln(\Delta T_{max})$ data, weighted least squares regression analysis is required.

Although perhaps not physically meaningful in terms of the self-limiting process the average temperature rise is also considered. This variable is related to the maximum temperature rise by the power peaking factor (*PPF*) in the same manner as the power and energy densities. The relevant working equation is:

$$\ln\left(\frac{\Delta T_{max}}{PPF}\right) = m\,\alpha_o + \ln\left(b_2\right)$$

where,

$$\ln\left(b_2\right) = \ln\left(b_1\right) - \ln\left(PPF\right)$$

The magnitude of the uncertainty on the average temperature rise includes an additional uncertainty related to the measured power peaking factor (*PPF*) (see Chapter 3).

C.2.3.3 Regression Analysis Results

C.2.3.3.1 Reference Data Set

Application of the least squares analysis to the Spert I D-12/25 reference data set results in a linear fit of:

$$\ln\left(\Delta T_{max}\right) = m\,\alpha_o + \ln\left(b_1\right), \quad \alpha_o \geq 29\ sec^{-1}\left(\tau \leq 35\ msec\right)$$

$$m = 0.01138$$
$$\sigma_m = 0.00036$$
$$\ln(b_1) = 4.261$$
$$\sigma_{\ln(b_1)} = 0.0362$$

The standard deviation of the fitted data, and the coefficient of determination of the fit are:

$$s = 0.1048$$
$$R^2 = 0.9629$$

The reference data with the fitting function as well as confidence and prediction bands is shown in Figure C-19.

C.2.3.3.2 Remaining Data Sets

The regression analysis results for all of the data sets are summarized in Table C-5. The associated *y*-intercept values for the average temperature rise ($\Delta T_{max}/PPF$) is also included in this table using the relation noted in Section C.2.3.2. Note that the quantity $\Delta T_{max}/PPF$ may not be physically meaningful given the relation of the average to peak temperature response being a function of local coolant conditions post peak power.

The results of the curve fitting are shown in Figure C-20 for the ΔT_{max} data over the short period range. The regression lines through the Borax I and Spert I B-24/32 data are difficult to distinguish as they lie almost on top of each other. The same applies to the regression lines for the Spert I A-17/28, Spert I D-12/25, and Spert IV D-12/25 data which are very close to lying on top of each other.

C.2.3.4 Goodness of Fit

C.2.3.4.1 Reference Data Set

The curve fitting to the Spert I D-12/25 maximum temperature rise data is comparable statistically to that for the associated energy data. The coefficient of determination is reasonable as is the standard deviation.

A plot of the reference data with the regression fitting line, 95% confidence bands, and 95% prediction bands is shown in Figure C-19. There is no clear pattern in the reference data set residuals (Fig. C-21).

The quality of the curve fit to the temperature data is still reasonable. The standard deviation (standard error) in the fit to the Spert I D-12/25 data, corresponding to a relative error in the ΔT_{max} data, is comparable to the estimated total random error in the measured data:

$$curve\ fit \quad \frac{\sigma_{\Delta T_{max}}}{\Delta T_{max}} = 10\%$$

$$measured\ data \quad \frac{\sigma_{\Delta T_{max}}}{\Delta T_{max}} = 5\% \rightarrow 11\%$$

The range of relative uncertainty in the measured data over the short period range, increases with increasing reciprocal period. This, indicates that the quality of the fit is good considering the quality of the measured data. As a result the 95% prediction bands on the Spert I D-12/25 fit (see Fig. C-19) are similarly consistent with the maximum estimated error (95% confidence) on the measured data.

Any curvature in the $\ln(\Delta T_{max})$ *vs.* $\ln(\alpha_o)$ data is not addressed by the present model. This is not of great concern considering the other goodness of fit tests.

C.2.3.4.2 Remaining Data Sets

The comparison of results from the fitting using the reference slope and individual regression for each data set is given in Table C-6. Compared to the fitting to the power and energy data the success of fitting the exponential function to the temperature data is not as good. This is reflected in the lower R^2 values and larger standard deviations for the fits to the individual core data sets. The lower R^2 values and larger standard errors can likely be attributed at least in part to the smaller sample size compared to the power and energy sample sizes.

The R^2 value for the Borax data set is negative but only indicates that there is considerable variance in the three data points for this set. More data are needed to generate more meaningful statistics with respect to the fitted line.

The standard errors are largest for the Spert I A-core and Spert IV D-core data,

approaching a relative error of 15% in the fitted data. Still this is not much higher than the maximum uncertainty in the measured data, *i.e.*, 11%. These differences are not great and may be due mainly to small sample sizes. The overall uncertainties do illustrate the effect of indirect uncertainties in the period measurement compared to the estimated 5% direct uncertainty in the temperature measurements.

Further indication that the room for improvement lies in the fitting model is indicated from the pattern in the residuals of the Spert I A-17/28 and Spert IV D-12/25 data relative to the fitting lines. A pattern in the residuals indicates that the modelling function is perhaps not picking up some aspect of the data behaviour. These residual plots are shown in Figures C-22 and C-23. No meaningful patterns were detectable in the residuals of the other data sets due to the small sample sizes. As noted above, there did not appear to be as noticeable a pattern in the reference data set (Spert I D-12/25) residuals.

Despite these indications the model is retained for the purposes of this analysis. Additional development, perhaps based on less empirical foundations, is left as future work. The rational for retaining the model is two-fold. Firstly, for most of the data sets, except the Spert I D-12/25 set, the sample size (*i.e.*, number of data pair measurements) is small. For example, the largest data set besides the reference set is for the Spert I A core where $N = 10$. For small sample sizes the statistics are not expected to be first rate. Further development of a fitting model may not be justified given the uncertainty due to lack of data.

Secondly, and perhaps most importantly, the objective of the analysis is to account for the variation between data sets for a given reciprocal period. Given the large systematic uncertainties in the data fine tuning the fitting model is unlikely to improve the final results. Any improvement in the fitting model, while theoretically pleasing, should be done in conjunction with a more precise and quantitative accounting of the systematic errors on each data set.

C.3 References

C-1. P. R. Bevington, D. K. Robinson, Data Reduction and Error Analysis for the Physical Sciences, Second Edition, McGraw-Hill Companies Inc., 1992, ISBN 0-07-911243-9.

C-2. H.J. Motulsky, A. Christopoulos, Fitting models to biological data using linear and nonlinear regression. A practical guide to curve fitting, 2003, Graphpad Software Inc., San Diego, CA, www.graphpad.com

C-3. Personal communication between S. E. Day and F. M. Hoppe, Department of Mathematics & Statistics, McMaster University, September 23, 2004.

C-4. Personal communication between S. E. Day and F. M. Hoppe, Department of Mathematics & Statistics, McMaster University, October, 2004.

C.4 Tables

Table C-1: Regression Results for Ambient Temperature Tests Power Data

ln(Pmax) vs. ln(α) Core	N	Reference Data Set m	Pmax (MW) ln(b1)	standard error s	R2	Pmax/Vf (kW/cc) ln(b2)	Pmax/Vf x PPF (kW/cc) ln(b3)
Borax I	19	1.597	-0.194	0.170	0.803	-2.589	-1.916
Spert I A-17/28	27	1.597	-0.806	0.097	0.986	-2.831	-2.137
Spert I B-24/32	6	1.597	-0.627	0.094	0.974	-3.344	-2.428
Spert I B-16/40	3	1.597	-0.384	0.041	0.995	-2.919	-2.177
Spert I B-12/64	9	1.597	0.110	0.082	0.977	-2.607	-1.818
Spert I D-12/25	41	1.597	-1.456	0.049	0.997	-3.105	-2.229
Spert IV D-12/25	9	1.597	-1.248	0.075	0.992	-2.897	-2.043

note: fitting uses reference slope from full linear regression on reference data set

Working Equations	1	Pmax = b1 α^m
	2	Pmax/Vf = b1/Vf α^m = b2 α^m
	3	Pmax/Vf x PPF = b1/Vf x PPF α^m = b3 α^m

Table C-2: Fitting Comparison for Ambient Temperature Tests Power Data

Core	N	Standard Deviation in Fitted Data		R2	
		Ref. Slope	Indiv. Fit	Ref. Slope	Indiv. Fit
Borax I	19	0.170	0.175	0.803	0.804
Spert I A-17/28	27	0.097	0.078	0.986	0.991
Spert I B-24/32	6	0.094	0.081	0.974	0.985
Spert I B-16/40	3	0.041	0.045	0.995	0.997
Spert I B-12/64	9	0.082	0.087	0.977	0.977
Spert I D-12/25	41	0.049	0.049	0.997	0.997
Spert IV D-12/25	9	0.075	0.021	0.992	0.999

note: the Spert I D-12/25 data set is considered as the reference data set

Table C-3: Regression Results for Ambient Temperature Tests Energy Data

ln(Etm) vs. ln(α) Core	N	Reference Data Set m	Etm (MW-sec) ln(b1)	standard error s	R2	Etm/Vf (kW-sec/cc) ln(b2)	Etm/Vf x PPF (kW-sec/cc) ln(b3)
Borax I	-	-	-	-	-	-	-
Spert I A-17/28	26	0.574	-0.321	0.091	0.916	-2.346	-1.652
Spert I B-24/32	6	0.574	0.008	0.057	0.883	-2.709	-1.792
Spert I B-16/40	3	0.574	0.015	0.020	0.992	-2.520	-1.778
Spert I B-12/64	9	0.574	0.629	0.070	0.915	-2.088	-1.299
Spert I D-12/25	41	0.574	-0.998	0.088	0.923	-2.647	-1.772
Spert IV D-12/25	9	0.574	-0.949	0.106	0.891	-2.598	-1.743

note: fitting uses reference slope from full linear regression on reference data set

Working Equations	1	Etm = b1 α^m
	2	Etm/Vf = b1/Vf α^m = b2 α^m
	3	Etm/Vf x PPF = b1/Vf x PPF α^m = b3 α^m

Table C-4: Fitting Comparison for Ambient Temperature Tests Energy Data

Core	N	Standard Deviation in Fitted Data		R2	
		Ref. Slope	Indiv. Fit	Ref. Slope	Indiv. Fit
Borax I	-	-	-	-	-
Spert I A-17/28	26	0.091	0.081	0.916	0.935
Spert I B-24/32	6	0.057	0.055	0.883	0.913
Spert I B-16/40	3	0.020	0.015	0.992	0.998
Spert I B-12/64	9	0.070	0.060	0.915	0.945
Spert I D-12/25	41	0.088	0.088	0.923	0.923
Spert IV D-12/25	9	0.106	0.106	0.891	0.904

note: the Spert I D-12/25 data set is considered as the reference data set

Table C-5: Regression Results for Ambient Temperature Tests Temperature Rise Data

ln(ΔTmax) vs. α Core	N	Reference Data Set m	ΔTmax (deg C) ln(b1)	standard error s	R2	ΔTmax/PPF (deg C) ln(b2)
Borax I	3	0.0114	4.376	0.080	-0.443	3.703
Spert I A-17/28	10	0.0114	4.247	0.149	0.803	3.553
Spert I B-24/32	6	0.0114	4.371	0.086	0.819	3.455
Spert I B-16/40	3	0.0114	4.591	0.033	0.986	3.849
Spert I B-12/64	4	0.0114	4.767	0.061	0.952	3.978
Spert I D-12/25	25	0.0114	4.261	0.105	0.963	3.385
Spert IV D-12/25	7	0.0114	4.255	0.149	0.868	3.400

note: fitting uses reference slope from linear regression on reference data set

Working Equations 1 $\Delta Tmax = b \exp(m*\alpha)$

2 $\Delta Tmax/PPF = b1/PPF*\exp(m*\alpha) = b2*\exp(m*\alpha)$

Table C-6: Comparison of Reference Fit and Individual Fits for Ambient Temperature Tests Temperature Rise Data

Core	N	Standard Deviation in Fitted Data		R2	
		Ref. Slope	Indiv. Fit	Ref. Slope	Indiv. Fit
Borax I	3	0.080	0.004	-0.443	0.997
Spert I A-17/28	10	0.149	0.061	0.803	0.967
Spert I B-24/32	6	0.086	0.041	0.819	0.959
Spert I B-16/40	3	0.033	0.016	0.986	0.997
Spert I B-12/64	4	0.061	0.053	0.952	0.963
Spert I D-12/25	25	0.105	0.105	0.963	0.963
Spert IV D-12/25	7	0.149	0.081	0.868	0.961

note: the Spert I D-12/25 data set is considered as the reference data set

C.5 Figures

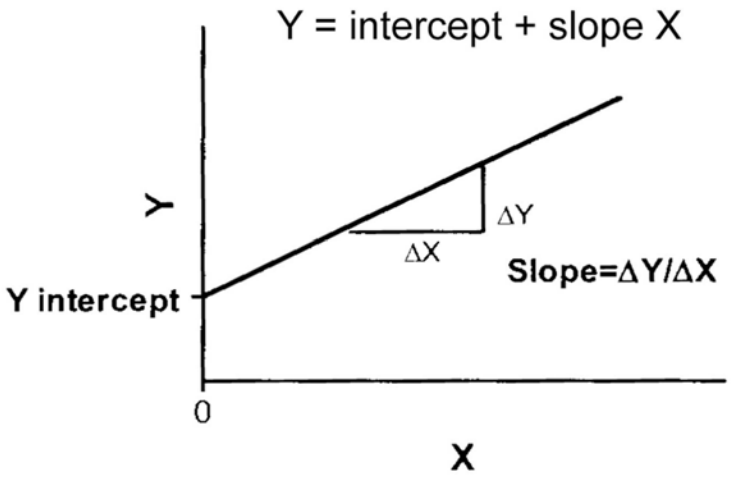

Figure C-1: Linear Regression (Ref. C-2)

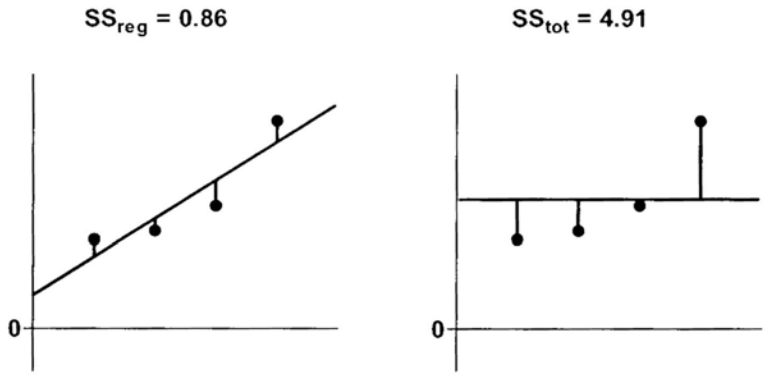

$$r^2 = 1 - \frac{SS_{reg}}{SS_{tot}} = 1 - \frac{0.86}{4.91} = 0.82$$

Figure C-2: Coefficient of Determination, R^2 (Ref. C-2)

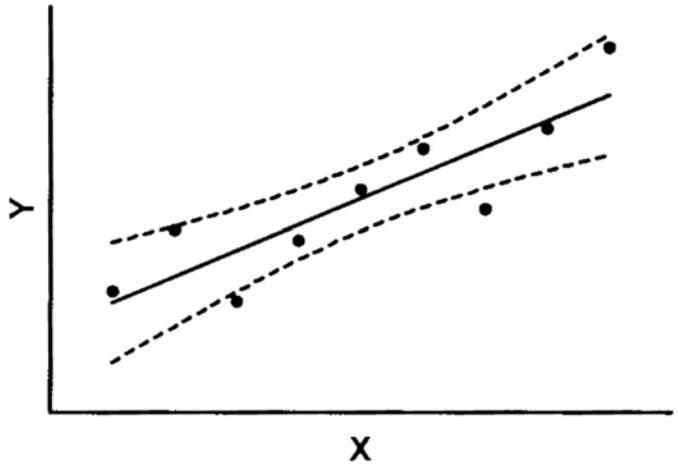

Figure C-3: Confidence Bands about a Regression Line (Ref. C-2)

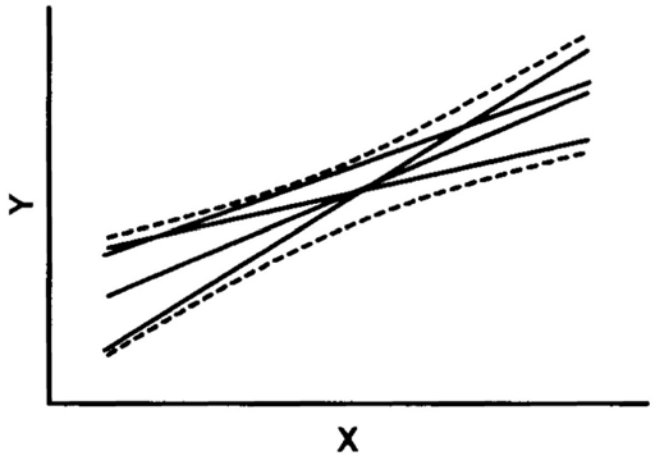

Figure C-4: Variation of a Regression Line within Confidence Bands (Ref. C-2)

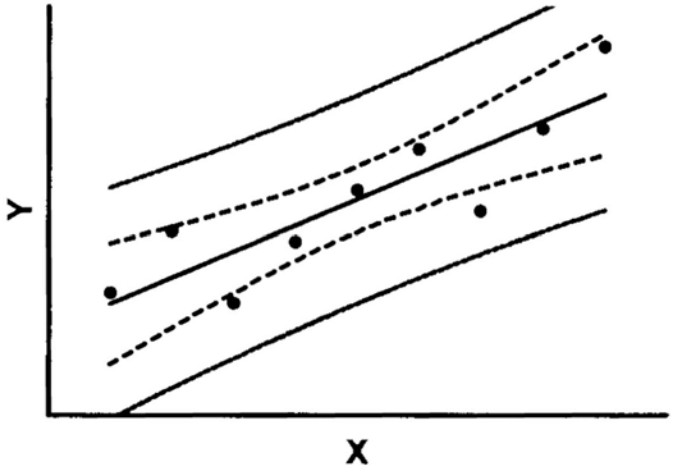

Figure C-5: Prediction and Confidence Bands about a Regression Line (Ref. C-2)

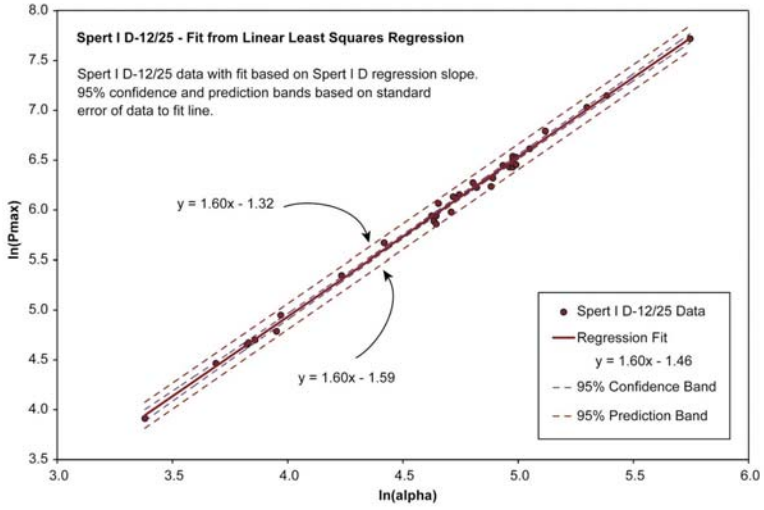

Figure C-6: Reference Data Set Regression Fit for Ambient Conditions Power Data

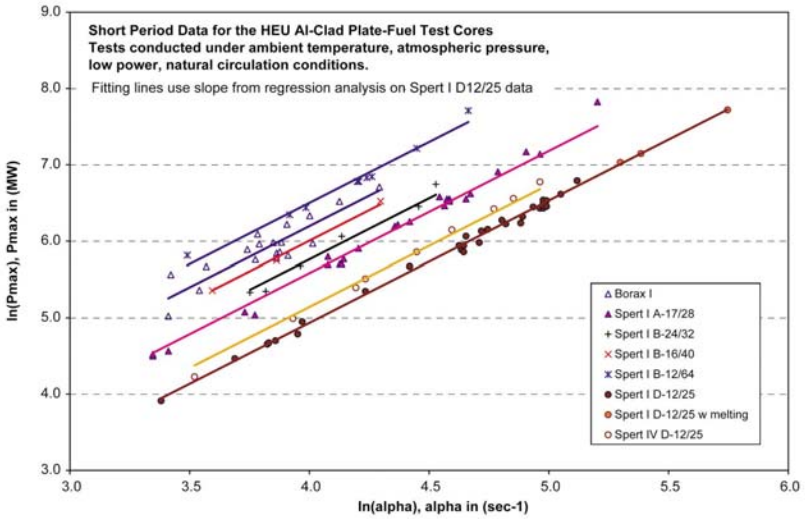

Figure C-7: Regression Fits for Ambient P_{max} Data

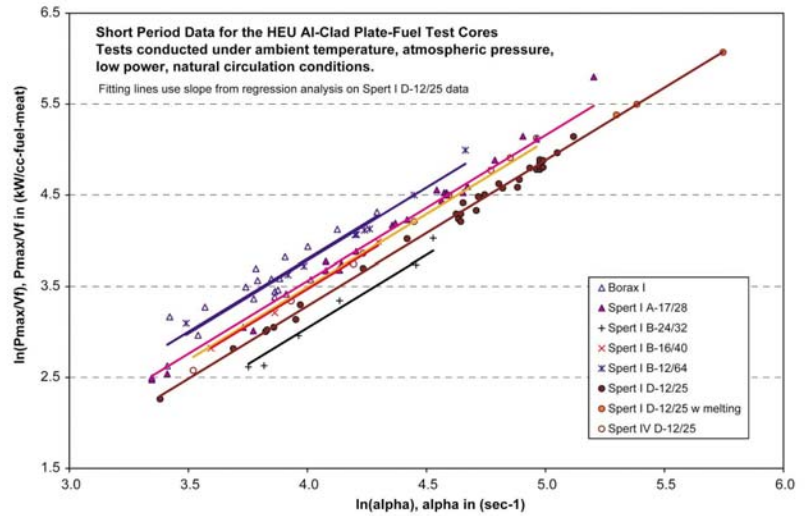

Figure C-8: Regression Fits for Ambient P_{max}/V_f Data

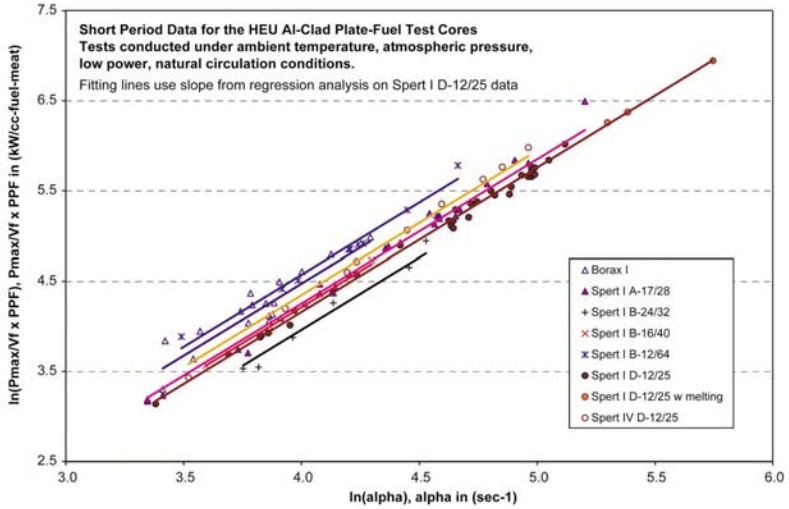

Figure C-9: Regression Fits for Ambient P_{max}/V_f x *PPF* Data

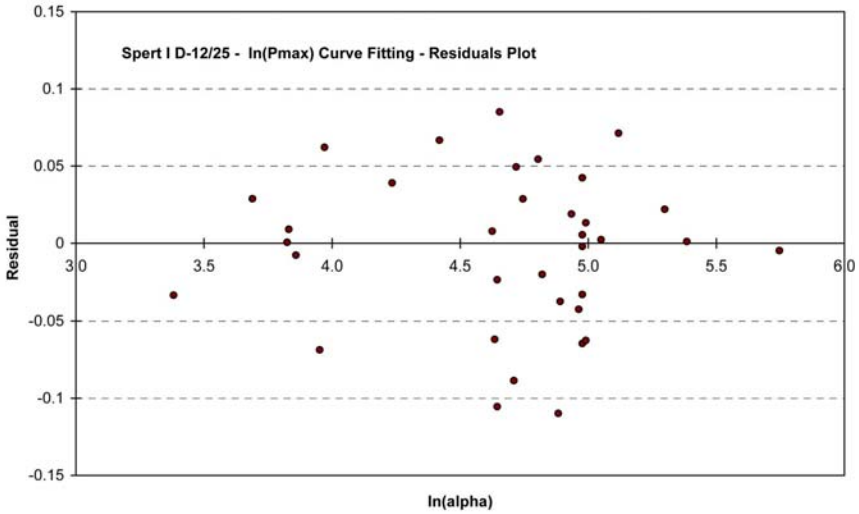

Figure C-10: Residual Distribution for Fit to Ambient Conditions P_{max} Reference Data Set

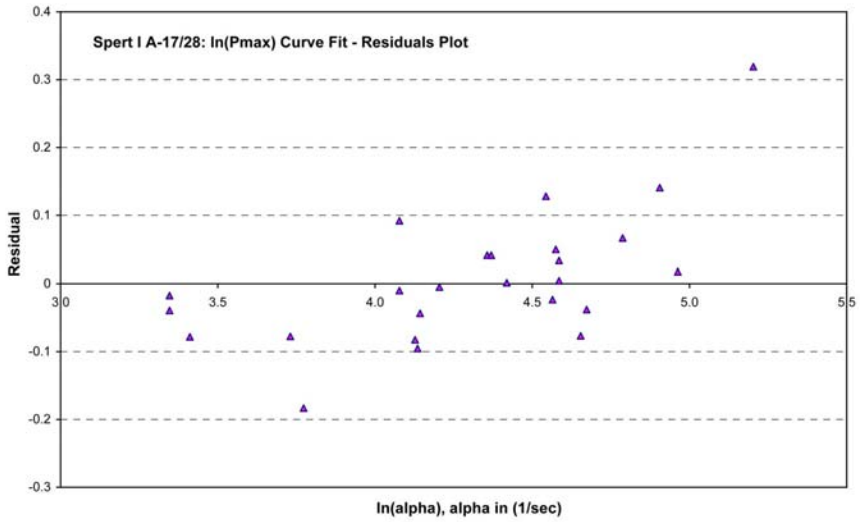

Figure C-11: Residual Distribution for Fit to Spert I A-17/28 Ambient Conditions P_{max} Data Set

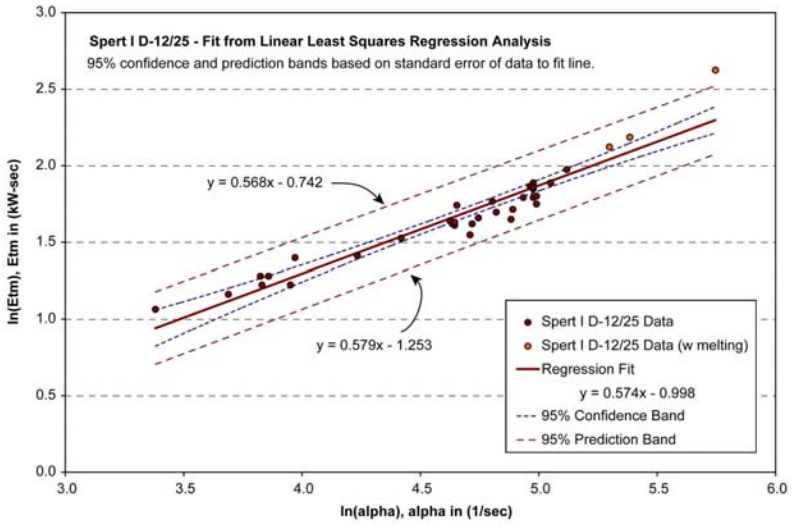

Figure C-12: Reference Data Set Regression Fit for Ambient Conditions Energy Data

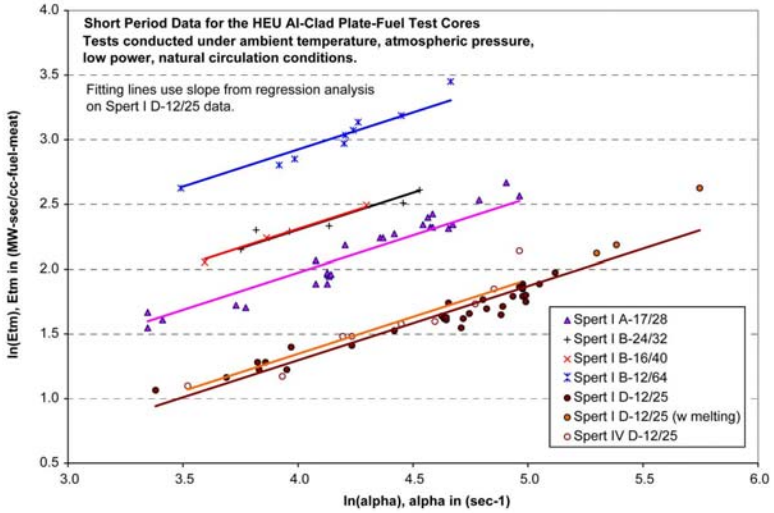

Figure C-13: Regression Fits for Ambient E_{tm} Data

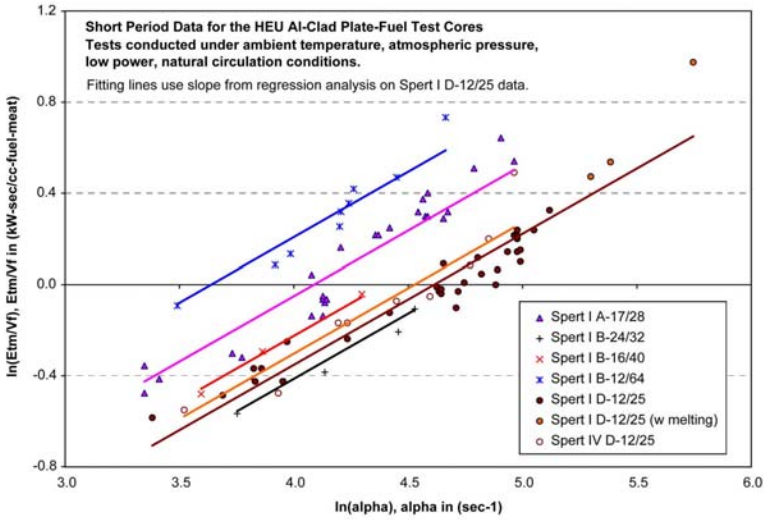

Figure C-14: Regression Fits for Ambient E_{tm}/V_f Data

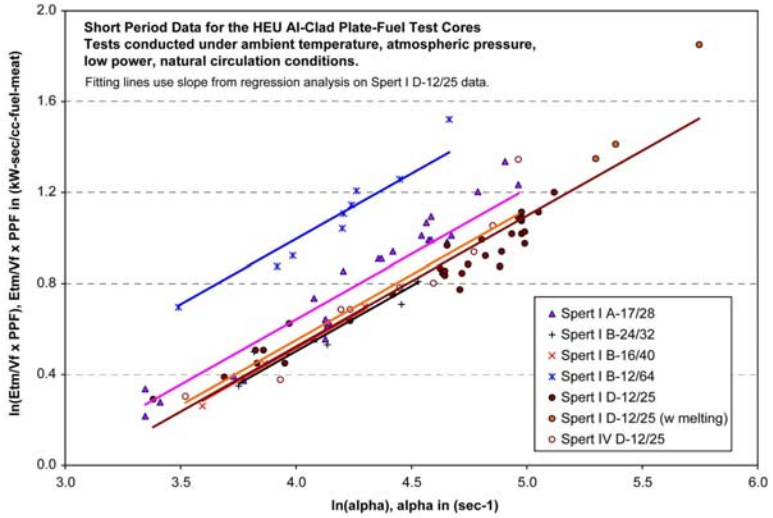

Figure C-15: Regression Fits for Ambient E_{tm}/V_f x *PPF* Data

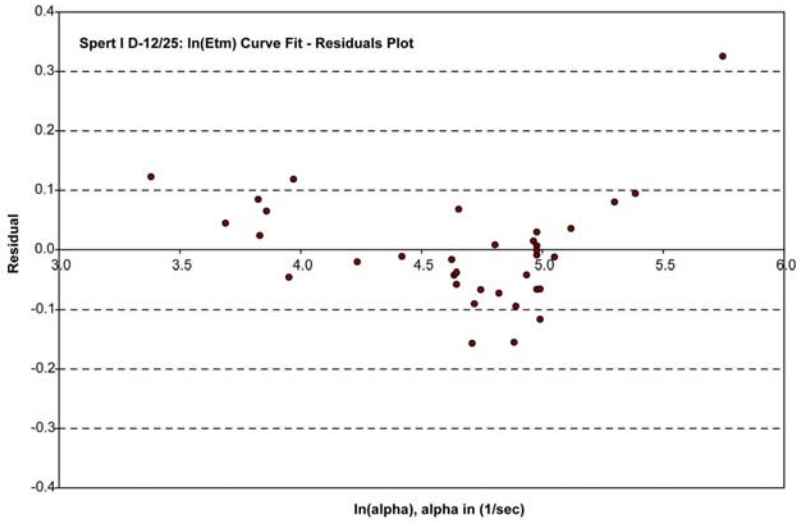

Figure C-16: Residual Distribution for Fit to Ambient Conditions E_{tm} Reference Data Set

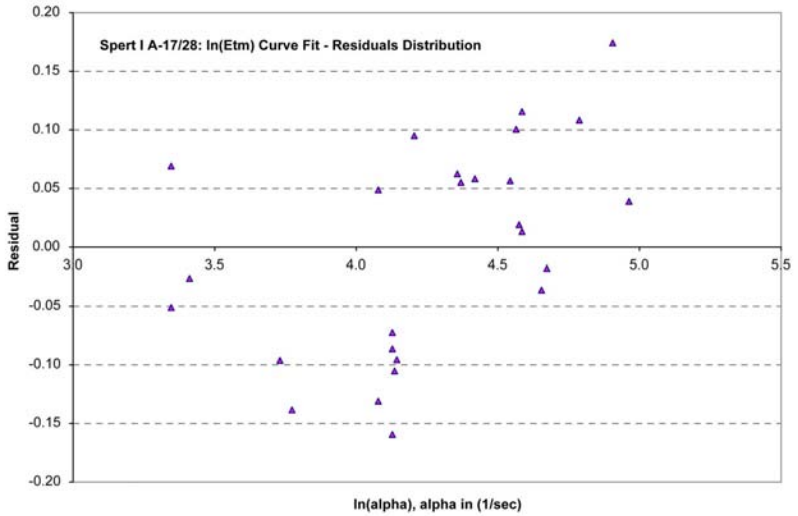

Figure C-17: Residual Distribution for Fit to Spert I A-17/28 Ambient Conditions E_{tm} Data Set

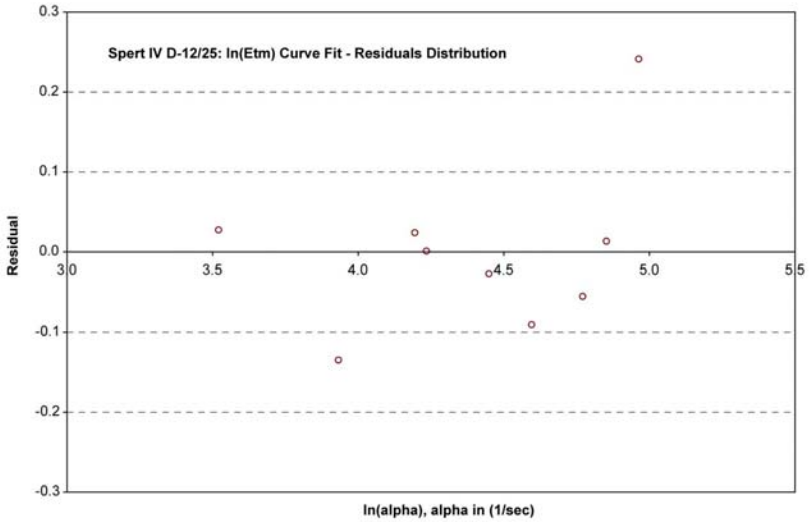

Figure C-18: Residual Distribution for Fit to Spert IV D-12/25 Ambient Conditions E_{tm} Data Set

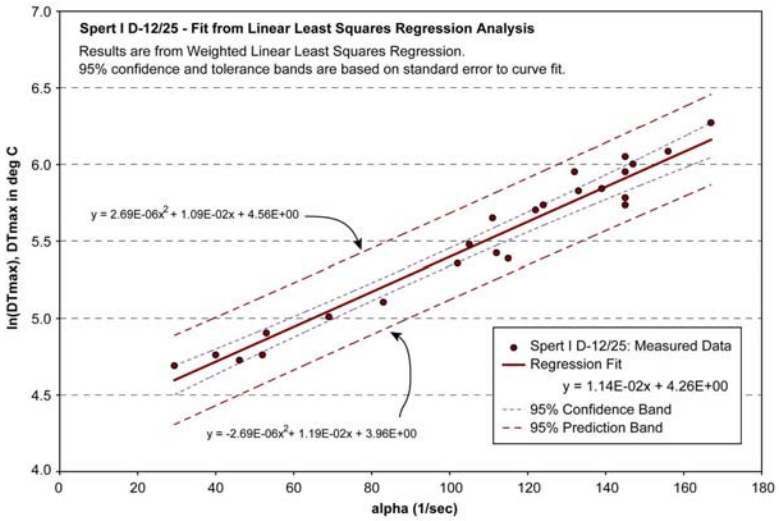

Figure C-19: Reference Data Set Regression Fit for Ambient Conditions Temperature Rise Data

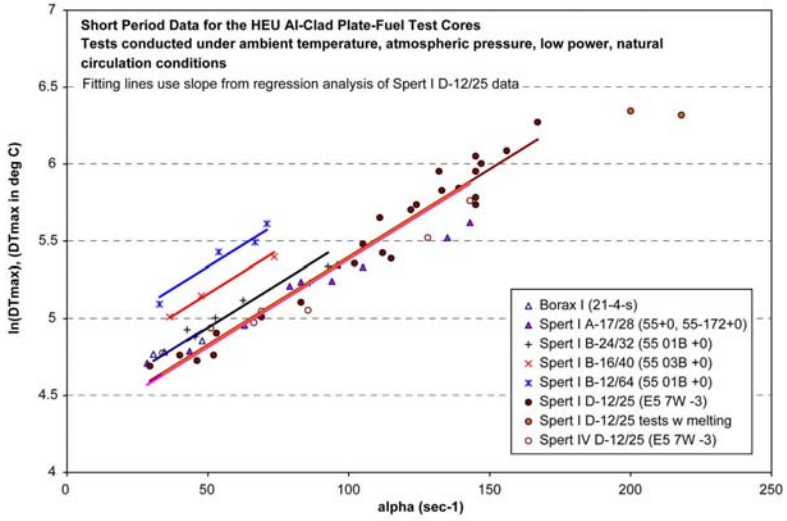

Figure C-20: Regression Fits for Ambient ΔT_{max} Data

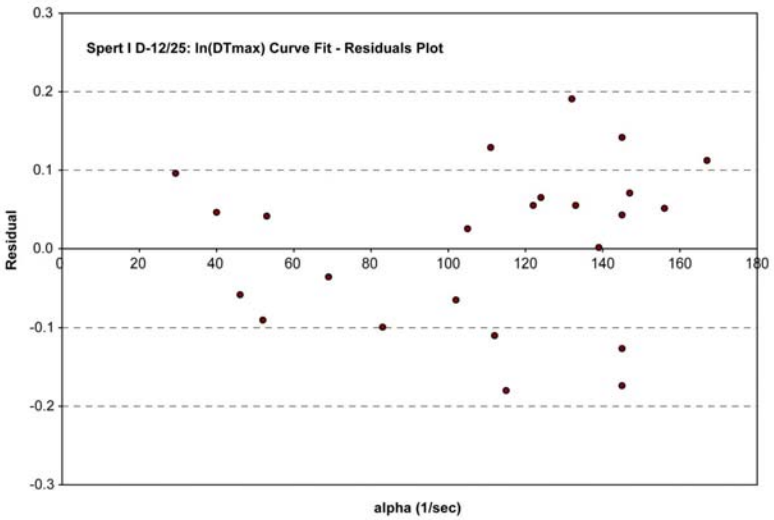

Figure C-21: Residual Distribution for Fit to Ambient Conditions ΔT_{max} Reference Data Set

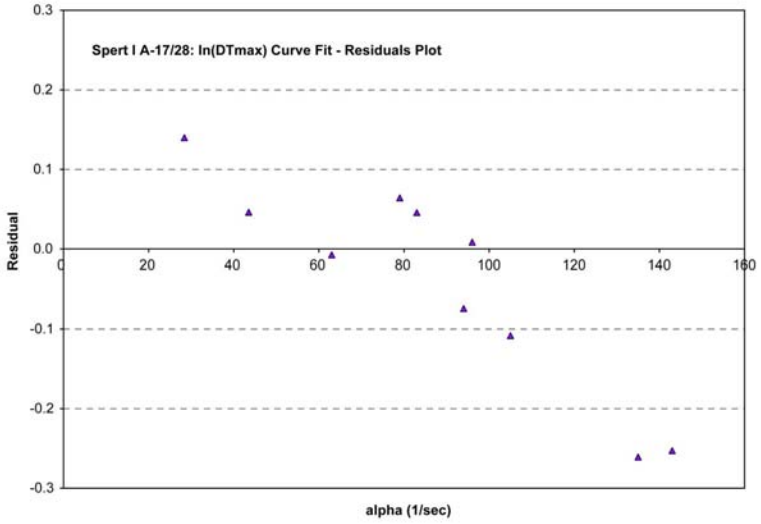

Figure C-22: Residual Distribution for Fit to Spert I A-17/28 Ambient Conditions ΔT_{max} Data Set

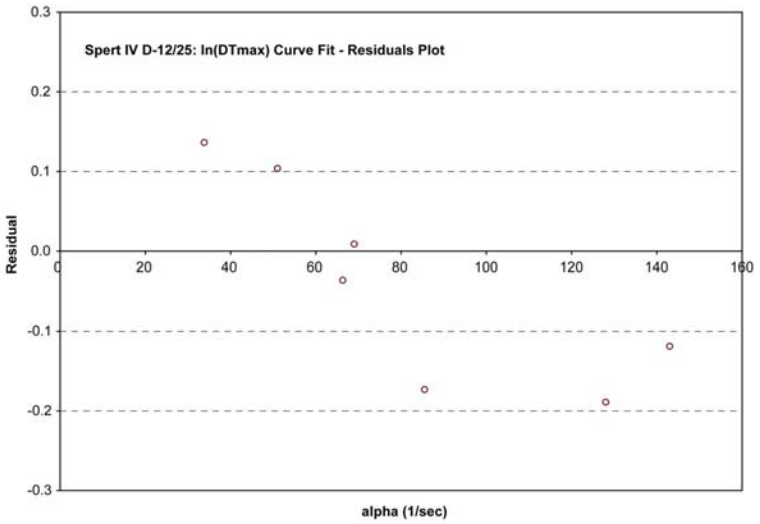

Figure C-23: Residual Distribution for Fit to Spert IV D-12/25 Ambient Conditions ΔT_{max} Data Set

(this page is intentionally left blank)

APPENDIX D - VOID REACTIVITY EFFECT MEASUREMENTS IN MNR

TABLE OF CONTENTS

LIST OF TABLES

LIST OF FIGURES

(this page is intentionally left blank)

D VOID REACTIVITY EFFECT MEASUREMENTS IN MNR

D.1 Introduction

This Appendix contains a report on void reactivity measurements conducted in the McMaster Nuclear Reactor (MNR) core in January 1999, January 2003, and January 2005. This report is also published as MNR-TN-2005-03, R0 (authored by S. E. Day, and M. P. Butler).

The results are part of ongoing nuclear characterization of MNR and are relevant to operations, general research, and safety analysis.

Trends in the experimental results with location of the void within an assembly and in the core as well as with assembly burnup are examined. Representative values for simulation and general safety analysis considerations are identified.

The results herein represent the best current estimates of the coolant void reactivity effect in the MNR core.

D.2 Description of Experiments

The open pool design of an MTR-type reactor such as MNR allows for ready access to the core for experimental purposes. Between January 1999 and January 2005 three void substitution experiments were conducted in MNR. These involved placing aluminum sheets (void plates) in the coolant channels of standard 18-plate LEU fuel assemblies. The cores for these experiments contained a mixture of both HEU and LEU assemblies.

Given the low neutron absorption and scattering of aluminum the plates simulate void in the coolant channels. By noting the position of the shim (shutdown) rods and the regulating (fine control) rod with and without the aluminum plates the reactivity worth of the void can be calculated.

D.2.1 Experimental Set Up

Two designs of plates were manufactured at the McMaster University machine shop. These plates were designed to fit in the coolant channels between fuel plates of a standard 18-plate fuel assembly.

The two plate models are similar in dimension. The "Jan99" plates measure 0.13 cm x 6.35 cm x 72.2 cm prior to rolling. A hole was drilled near the top of each plate to accommodate a hook. The size of the hole is 1 cm ID centered horizontally and offset 1 cm from the top of each plate.

The plates used in the 2003 and 2005 experiments (Fig. D-1), measure 0.13 cm x 6.35 cm x 72.7 cm prior to rolling. In the Jan03/Jan05 plates a cutaway section of 3.81 cm x 7.62 cm (3" x 1.5") was made at the top end of each plate to leave room for the fuel handling tool. A 0.3175 cm (1/8") diameter hole was drilled through each tab centered 1.27 cm from the top of the plate.

All were rolled to match the curvature (13.97 cm = 5" radius) of the fuel plates.

In the assembly, the plates sit on the top of the bottom end fitting and extend past the top of the fuel plates, thereby extending through the entire vertical active fuel region. The placement of the plates is shown in Figure D-2.

D.2.2 Core Maps and Supplemental Assemblies

The experiments were conducted on cores 49A (Jan/99), 51A (Jan/03), and 52E (Jan/05). The corresponding core maps are shown in Figures D-3, D-4, and D-5. The locations of the experiments in the core are shown in Figure D-6.

For the January 1999 experiment, fuel assembly MNR-304 (including voids) was used to substitute MNR-303. Both are "standard", *i.e.*, 18-plate 225 g U-235, LEU assemblies with no previous irradiation at the time of the experiment, *i.e.*, zero burnup.

For the January 2003 experiment, Core 51A contained assembly MNR-304 in position 3D. This was substituted with a spent end-of-life assembly, MNR-301, and a slightly irradiated assembly, MNR-321. The former is an earlier generation LEU type with a higher initial U-235 loading (284g U-235/assembly compared to 225g U-235/assembly) while the latter is a standard LEU assembly.

For the January 2005 experiment, only fuel assembly MNR-324 was used in the experiment. This slightly irradiated (5% burnup) assembly is part of the Core 52A configuration, located in position 4C.

D.2.3 Experimental Procedure

Each of the experiments was conducted in early January following the annual maintenance shutdown. This minimized radiation fields during the experiments and provided a xenon-free and thermally cold core. Critical rod positions were measured at low power (*i.e.*, 100 W) and given no at-power operation before or during the experiments, avoided any secondary reactivity effects (*i.e.*, those due to temperature or changes in fission product concentration).

The experimental procedure involved the following steps:

1. With the core shutdown and the rods at the safety bank position the assembly of interest was moved to a transfer station suspended from the apron at the side of the pool above the east shelf (Fig. D-7).
2. With the assembly positioned in the holder, aluminum void plates were added or removed using a hook tool (Fig. D-8). The void plates were handled using long tongs and kept on a designated work space to avoid contamination from the pool water and exposure to radiation fields. Given the significant fields from the assemblies resting in the transfer station and from the irradiated void plates, manipulation time was kept to a minimum.
3. The assembly was then transferred to the core. The top view of the core with an assembly containing void plates positioned in site 4C is shown in Figure D-9.
4. The reactor was brought to critical at low power (100 W) and the rod positions were noted.

Void plate positions in the assemblies could be noted with the naked eye but were checked using binoculars. During the entire experiment the primary flow was kept off.

D.3 Calculations

D.3.1 Calculation of Reactivity Change

To determine the reactivity effect of void in the fuel assembly coolant channels the shim and regulating rod critical positions were noted for both the cooled and voided

core configurations. The rod positions were then translated to reactivity worth values using the calibrated rod worth tables. These reactivity values were then used to determine the change in reactivity due to the presence of the void plates, *i.e.*:

$$\Delta\rho_{void} = \left(\rho_{shims}^{voided} + \rho_{reg}^{voided}\right) - \left(\rho_{shims}^{cooled} + \rho_{reg}^{cooled}\right)$$

where "voided" refers to the core configuration including the aluminum void plates, and "cooled" refers to the core configuration without the void plates. The corresponding void reactivity coefficient, α, is simply the change in reactivity due to the void over the amount of void causing the reactivity change, *i.e.*,

$$\alpha \equiv \frac{\Delta\rho_{void}}{void\ volume}$$

Typically the volume of void is expressed in either cubic centimetres (cc) or percent volume of coolant displaced (%). The volume considered for the %-void is the total coolant volume within the 17 coolant channels surrounding the 16 fuel plates and within the active height of the core. The coolant channel dimensions are:

- thickness (average) = 0.300 cm
- width = 6.632 cm
- height = 60.0 cm
- number = 17

D.3.2 Correction for Aluminum Absorption

Similar experiments using aluminum void plates/strips were conducted as part of the nuclear characterization of the Spert test cores. An estimate of the effect of using aluminum rather than a true void is thus available based on the comparison of corrected and not-corrected values reported in the literature (Ref. D-1). As a result, the MNR measured reactivity changes are scaled by:

$$\Delta\rho_{corrected} = c_{ac}\ \Delta\rho_{measured}$$

where c_{ac} is the absorption correction factor. The Spert measurements indicate that the absorption in the aluminum accounts for approximately 20% of the negative reactivity effect. Therefore a value of 0.8 is used for the correction factor in the

above formula.

D.4 Experimental Results

D.4.1 Results

The parameters and results of the void experiments are summarized in Tables D-1 and D-2, respectively. All results in the table have been corrected for aluminum absorption. The January 1999 results have been reported previously (Ref. D-2) but are not adjusted for aluminum absorption in this reference.

D.4.2 Uncertainties in the Measurements

Various sources of uncertainties exist with respect to the individual void reactivity results. These sources of error are:

- uncertainty in shim and reg rod positions
- uncertainty in calibrated differential rod worths
- uncertainty in the aluminum correction

This uncertainty in the rod position is considered **random** in nature, while the uncertainties due to the calibration of the rod worth and the aluminum correction are common to all measurements and as a result are considered **systematic** in nature.

With respect to the sources of random error, the uncertainty in the shim and regulating rod positions are estimated as 0.2 and 0.3 percentage points on the percent-withdrawal scale. This is an over-estimation of the noise on the digital display for the rod positions and is meant to incorporate any additional uncertainties in the rod position from the indicator potentiometer and motors.

These uncertainties on the rod location lead to varying absolute uncertainties on the associated rod worth due to the shape of the worth curve with position. The result is an uncertainty of up to 2% on the individual rod worth measurements due to uncertainty in rod position.

The method of calculating the change in reactivity worth of a given experiment is explained previously in Section D.3. This calculation involves the reactivity associated with the positions of both the shim and regulating rods with and without

the void plates being present in the core. The associated uncertainty is a combination of the uncertainties on the individual reactivity values. Using the linear propagation of errors approach (Ref. D-3), and assuming that each component is independent, the uncertainty for the change in reactivity values is found from:

$$y = f\left(x,u,v,...\right)$$

$$\sigma_y^2 = \sigma_x^2\left(\frac{\partial y}{\partial x}\right)^2 + \sigma_u^2\left(\frac{\partial y}{\partial u}\right)^2 + \sigma_v^2\left(\frac{\partial y}{\partial v}\right)^2 + ...$$

Considering the calculation for the reactivity change, the relative uncertainty in the calculated values is found from:

$$\frac{\sigma_{\Delta\rho_{void}}}{\Delta\rho_{void}} = \sqrt{\left(\frac{\sigma_{\Delta\rho_{shims}^{voided}}}{\Delta\rho_{shims}^{voided}}\right)^2 + \left(\frac{\sigma_{\Delta\rho_{reg}^{voided}}}{\Delta\rho_{reg}^{voided}}\right)^2 + \left(\frac{\sigma_{\Delta\rho_{shims}^{cooled}}}{\Delta\rho_{shims}^{cooled}}\right)^2 + \left(\frac{\sigma_{\Delta\rho_{reg}^{cooled}}}{\Delta\rho_{reg}^{cooled}}\right)^2}$$

Where each term under the square root represents the relative error in one of the rod reactivities. For example, the first term is the relative uncertainty in the reactivity worth for the shim rods in the voided core. A maximum relative uncertainty of 2% for each component leads to an overall random uncertainty of no more than 4% in the final void reactivity change results, *i.e.*:

$$\frac{\sigma_{\Delta\rho_{void}}}{\Delta\rho_{void}} = \sqrt{\left(0.02\right)^2 + \left(0.02\right)^2 + \left(0.02\right)^2 + \left(0.02\right)^2}$$

$$= 0.04$$

$$= 4\%$$

For the "Jan03" experiments it is assumed that the rod worth calibrations on Core 51A do not change significantly with substitution of the assembly in position 3D (*i.e.*, the rod calibrations were performed with assembly MNR-304 in position 3D while the experiment considered three assemblies of varying burnup in this position).

When comparing results from the different experiments, differences in the cores for the three experiments should also be considered. Although similar, the three core configurations differ in burnup and assembly distribution. As a result the void

reactivity effect distribution may vary between the three cores. To account for this an additional component of 5% is considered as contributing to the random error on the measurements. This estimate is an engineering judgement based on the variation of radial power density peaking factors with fuel environment (Ref. D-4). This is then combined with the random error estimate from the rod positions to give an overall random uncertainty of:

$$\frac{\sigma_{\Delta\rho_{void}}}{\Delta\rho_{void}} = \sqrt{(0.04)^2 + (0.05)^2}$$
$$= 0.064$$
$$= 6.4\%$$

which is applicable to comparisons of results from the different experiments.

With respect to the sources of systematic error, the uncertainties arising from the rod worth calibration and the correction due to aluminum absorption are estimated at no more than 5% each. Combining these two independent sources of error in a similar manner to that used for the random errors leads to an overall systematic error estimate of no more than 7% of the reactivity worth measurements.

The measurements were all made on the cold clean core, under low power conditions, following the annual maintenance shutdown and prior to any extended operation at power. As a result, independent reactivity effects due to changes in pool temperature and xenon concentration are negligible.

In summary,

$\sigma_{\Delta\rho_{void}}\big|_{random} \leq 4\%$ ← *when considering a given core configuration*

$\sigma_{\Delta\rho_{void}}\big|_{random} \leq 6.4\%$ ← *when comparing between different cores*

$\sigma_{\Delta\rho_{void}}\big|_{systematic} \leq 7\%$ ← *applicable to all experimental results*

The random errors are relevant to curve fitting to the experimental data whereas a total error,

$$\sigma^2_{total} = \sigma^2_{random} + \sigma^2_{systematic}$$

where the σ values are relative errors, can be applied to any final result or individual reactivity value. Total uncertainty values pertaining to the void reactivity effect results are:

$$\sigma_{\Delta\rho_{void}}\Big|_{total} \leq 8.1\% \quad \leftarrow \textit{when considering data from a single core}$$
$$\sigma_{\Delta\rho_{void}}\Big|_{total} \leq 9.5\% \quad \leftarrow \textit{when considering data from different cores}$$

where the former is a combination of the 4% and 7% error components and the latter is a combination of the 6.4% and 7% error components.

D.5 Analysis of the Experimental Results

D.5.1 Effect of Assembly Burnup

The 2003 results (Fig. D-10) illustrate the void effect as a function of assembly burnup (*i.e.*, depletion). The curve fit is from a non-weighted linear least squares regression. The void effect is larger in a fresh assembly relative to a depleted assembly, and decreases by approximately 35% from beginning-of-life (fresh) to end-of-life (50% depletion). The effect is approximately linear with burnup.

D.5.2 Effect of Non-Uniform Voiding

The 2005 experiment was designed to investigate the effect of non-uniform voiding in an assembly located in the hot-core location (4C) adjacent to the central flux trap (5C). The large moderator volume in the flux trap was of interest to examine the void effect within and at different locations within the adjacent assembly. The results are summarized in Table D-2 and are shown in Figure D-11 in terms of volume of void.

The roughly uniform loading of the six fuel plates indicates a void reactivity of:

$$-7.05\times10^{-3}\ \frac{mk}{cc} \quad = \quad -0.143\ \frac{mk}{\%\ void}$$

The effect of location of the void is illustrated by the results for the three void-plates

in the south and north halves of the assembly. The south half of the assembly is closest to the flux trap. The effect is noticeable, reduced relative to the average by 23% in the half of the assembly close to the flux trap. Conversely the effect is 27% larger (relative to the average) in the half of the assembly furthest away from the flux trap. The average of the two 3-plate results differs from the linear fit through the 6-plate data by 2%. This is within the random uncertainty estimate for the average value indicating a linear relationship between the location of the void and position in the assembly relative to the flux trap is reasonable.

D.5.3 Effect of Radial Location in the Core

Comparison of the results from the three experiments at different locations in the core (Tab. D-3) gives an indication of the radial distribution of the void effect. These results are compared based on void reactivity per void volume and are shown in Figure D-12. The three measurements are from beginning-of-life assemblies of approximately the same burnup (*i.e.*, 0%, 2%, and 5% U-235 depletion). Differences in the burnup and the core configurations on which these measurements were made are accounted for in the associated uncertainties.

In all cases the voiding produces negative reactivity. On the periphery of the core (7E) the effect is only 20% of that in the central position (4C). The void effect in site 3D is two thirds of that in the central site 4C. The relationship of void reactivity worth against position can be approximated by a quadratic relation, *i.e.*:

$$\alpha(x) = -\left(4.60\times10^{-6}\right)x^2 + \left(3.28\times10^{-4}\right)x - \left(7.05\times10^{-3}\right), \quad for\ \alpha\ in\ (mk/cc)$$

$$\alpha(x) = -\left(9.17\times10^{-5}\right)x^2 + \left(6.61\times10^{-3}\right)x - \left(1.43\times10^{-1}\right), \quad for\ \alpha\ in\ (mk/\%)$$

where $\alpha(x)$ is the void reactivity worth as a function of radial position in the core, and x is the distance in cm from site 4C.

D.5.4 Safety Analysis Reference Values

All of the measured void reactivity results are relevant to analysis of the MNR core. As well as providing benchmarking data for simulation models the experimental results can be used to estimate useful input data for kinetics simulation and general safety analysis considerations.

Two parameters of interest are the central and uniform void coefficients of reactivity. These parameters were measured for the Borax and Spert test cores and therefore provide a basis for comparison with the MNR core. The central void coefficient is a representative quantity describing voiding in the central (*i.e.*, hottest) region of the core while the average or uniform void coefficient describes a voiding of a uniform nature across the entire core (*e.g.*, 5% voiding in all assemblies simultaneously). As such, both parameters may be useful kinetics input data depending on the specific scenario under consideration.

The 2005 measurements provide a central void reactivity estimate of:

$$\begin{aligned}\alpha_{central} &= -7.05\times10^{-3} \pm 0.51\times10^{-3}\,(mk/cc) \\ &= -0.143 \pm 0.010\,(mk/\%)\end{aligned}$$

This central void coefficient is for fresh fuel in the limiting (*i.e.*, highest) power density core site, and thus an upper limit on the magnitude of the MNR coolant void reactivity.

The uniform void coefficient was not measured directly but must be between the peripheral and central measured values (see Section D.5.3). An estimate of the uniform void coefficient is found by taking the average of the fitting equation over the three radially distributed points of Figure D-12, *i.e.*:

$$\langle \alpha \rangle = \frac{\int_0^X \alpha(x)\, x\, dx}{\int_0^X x\, dx}$$

An outer limit of $X = 24$ cm was used for this calculation, corresponding to a radial cylindrical representation of a 36 assembly core. This value corresponds to a beginning-of-life burnup. A further adjustment using the dependence on burnup scales this estimate to a mid-life core, as in the case of the MNR Reference Core. The adjustment for burnup uses half the total change (35.5% change in void worth) over the depletion range of MNR fuel:

$$\langle \alpha \rangle_{mid-life} = \langle \alpha \rangle_{BOL} \left(1 - \frac{0.355}{2} \right)$$

These calculations result in an estimate of the uniform void coefficient of:

$$\begin{aligned} \langle \alpha \rangle_{mid-life} &= -3.3 \times 10^{-3} \pm 0.8 \times 10^{-3} \left(mk / cc \right) \\ &= -0.067 \pm 0.022 \left(mk / \% \right) \end{aligned}$$

The value has been corrected for aluminum absorption. The uncertainty associated with the experimental data is likely not an adequate estimate for the uniform void coefficient estimate considering the assumptions in the calculation. A more conservative uncertainty of ± 25% is recommended. This is a best estimate based on engineering judgement only.

Both the central and uniform void coefficient estimates are reasonable approximations for the MNR Reference Core in the absence of further experiments and simulation.

Similar experiments conducted as part of the Spert Project on a variety of MTR-type cores indicate that the void effect is linear with void volume at least up to about 35% void volume centrally and 10% uniformly over the core.

D.6 Closing Remarks

The coolant void reactivity effect has been successfully measured in standard 18-plate MNR fuel in a variety of core locations and for varying assembly burnup.

The measurements show that voiding in the coolant channels in MNR produces a negative reactivity change, even in the most highly moderated regions of the core (*i.e.*, next to the graphite reflector and the central flux trap).

Measurements at three core positions show the variation of the void effect with radial location in the core. The void effect at the core periphery is only 20% of that in the central hot assembly.

A clear trend is evident between the void reactivity effect and the assembly burnup.

The void effect is reduced by approximately 35% over the lifetime of an assembly (i.e., fresh to 50% U-235 depletion) in a given core location.

Estimates of central and uniform coolant void coefficients for MNR are:

$$\alpha_{central} = -7.05\times10^{-3} \pm 0.51\times10^{-3}\ \left(mk/cc\right)$$
$$\alpha_{uniform} = -3.3\times10^{-3} \pm 0.8\times10^{-3}\ \left(mk/cc\right)$$

where the void volume is considered to extend the active height of the fuel. The central coefficient was measured directly in the experiments and represents a maximum for the core (fresh assembly in the limiting core position). The uniform coefficient is a first approximation to a working value based on a typical core size and average depletion. These values represent the current best estimates for MNR safety analysis work and can be used for comparison with the Borax and Spert test core values.

D.7 References

D-1. G. O. Bright, editor, “Quarterly Progress Report - July, August, September, 1957 - Reactor Projects Branch”, US AEC Technical Report IDO-16416, Phillips Petroleum Co., October 1, 1957.

D-2. M. P. Butler, "Re: Void Effect Measurement", McMaster Nuclear Reactor internal memo to ROCC, McMaster University, February 5, 1999.

D-3. P. R. Bevington, D. K. Robinson, Data Reduction and Error Analysis for the Physical Sciences, 2nd Edition, McGraw-Hill, 1992.

D-4. S. E. Day, “Power Peaking Factors in MNR”, McMaster Nuclear Reactor Technical Note MNR-TN-010705, McMaster University, July 5, 2001.

D.8 Tables

Table D-1: Void Effect Experiment Parameters

Number	Date	Core Loading	Core Site	Assembly Number	Assembly Burnup (% U235)	Number of Plates	Volume of Void (cc)	Volume of Void (%)
1	1999	49A	7E	MNR-304	0%	4	198	9.8
2	2003	51A	3D	MNR-301	48%	8	397	19.5
3	2003	51A	3D	MNR-304	20%	8	397	19.5
4	2003	51A	3D	MNR-321	2%	8	397	19.5
5	2005	52E	4C	MNR-324	5%	6	298	14.7
6	2005	52E	4C	MNR-324	5%	3 (north)	149	7.3
7	2005	52E	4C	MNR-324	5%	3 (south)	149	7.3

All assemblies are LEU standard U3Si2-Al 225 g U-235/assembly, excpet MNR-301 which is 284 g U-235/plate
Volume in % refers to the coolant volume witin the 17 coolant channels and the active height of the fuel

Table D-2: Void Effect Experiment Results

Number	Change in Reactivity (mk)	Change in Reactivity (mk/cc)	Change in Reactivity (mk/%)	Relative Uncertainty Random	Relative Uncertainty Systematic	Relative Uncertainty Total
1	-0.28	-1.41E-03	-0.029	4.0%	7.0%	8.1%
2	-2.91	-7.32E-03	-0.149	2.0%	7.0%	7.3%
3	-2.49	-6.27E-03	-0.128	2.3%	7.0%	7.4%
4	-1.88	-4.72E-03	-0.096	2.6%	7.0%	7.5%
5	-2.10	-7.05E-03	-0.143	1.6%	7.0%	7.2%
6	-0.81	-5.45E-03	-0.088	1.7%	7.0%	7.2%
7	-1.33	-8.95E-03	-0.145	1.6%	7.0%	7.2%

Results are corrected for Al absorption in accordance with similar measurements in the Spert Project (IDO-16416)

Table D-3: Void Effect Results for Varying Core Location

Number	Core Site	Distance from 4C (cm)	Void Effect (mk/cc)	Void Effect (mk/%)	% Change from 4C
5	4C	0.0	-7.05E-03	-1.43E-01	0%
4	3D	8.0	-4.72E-03	-9.60E-02	-33%
1	7E	28.8	-1.41E-03	-2.86E-02	-80%

Assemblies of similar burnup are compared
Results are corrected for Al absorption in accordance with similar measurements in the Spert Project (IDO-16416)

D.9 Figures

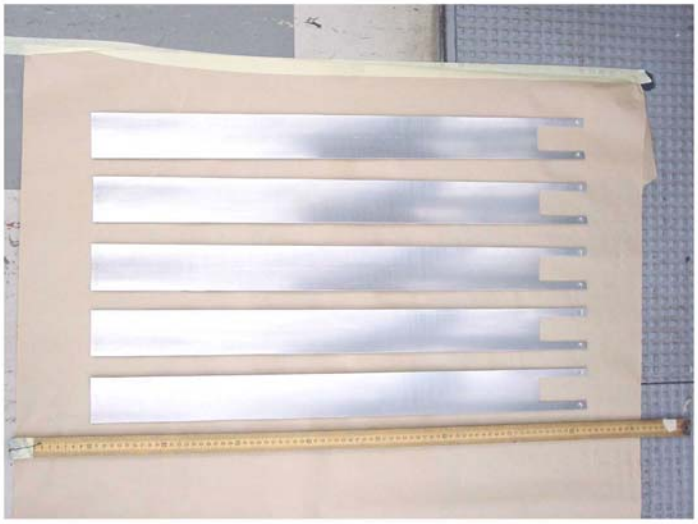

Figure D-1: Aluminum Void Plates

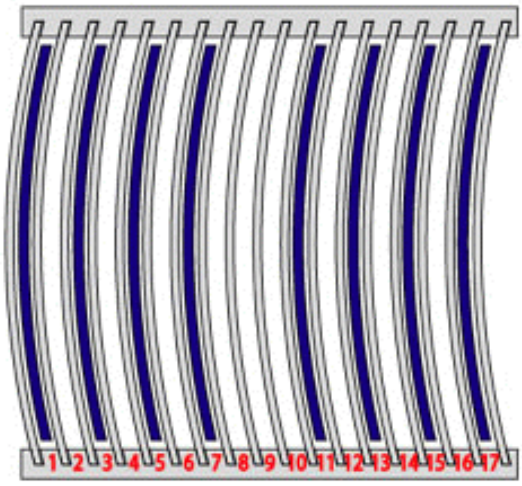

Figure D-2: MNR 18-Plate Assembly Housing Void Plates

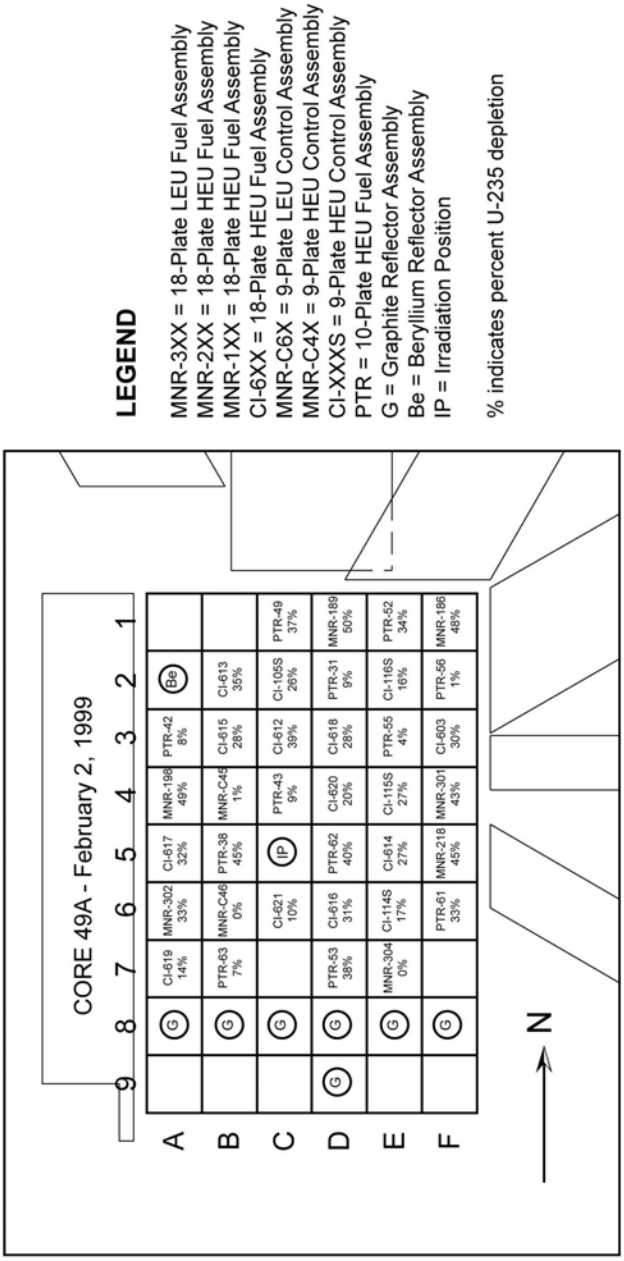

Figure D-3: MNR Core 49A

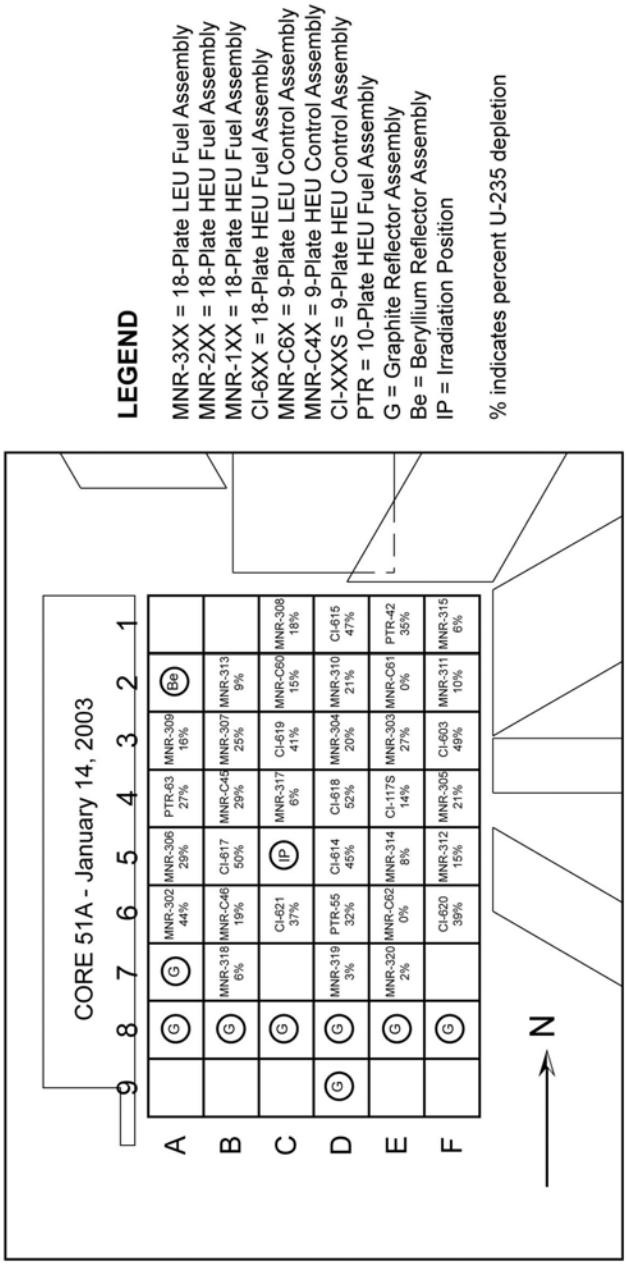

Figure D-4: MNR Core 51A

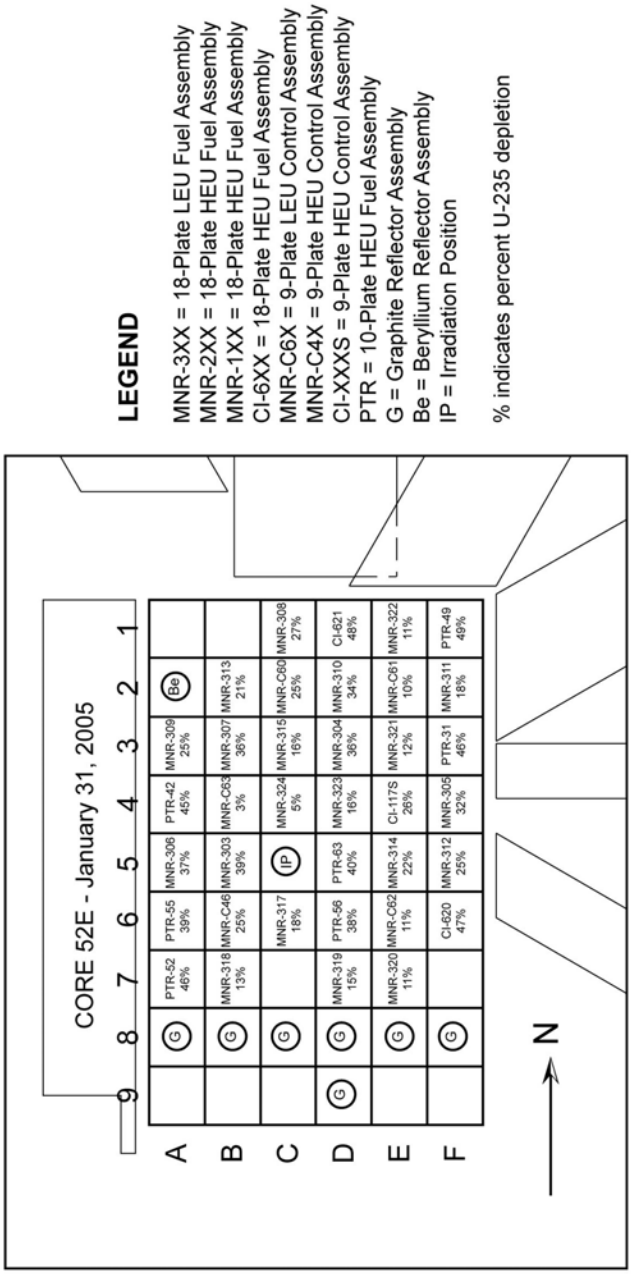

Figure D-5: MNR Core 52E

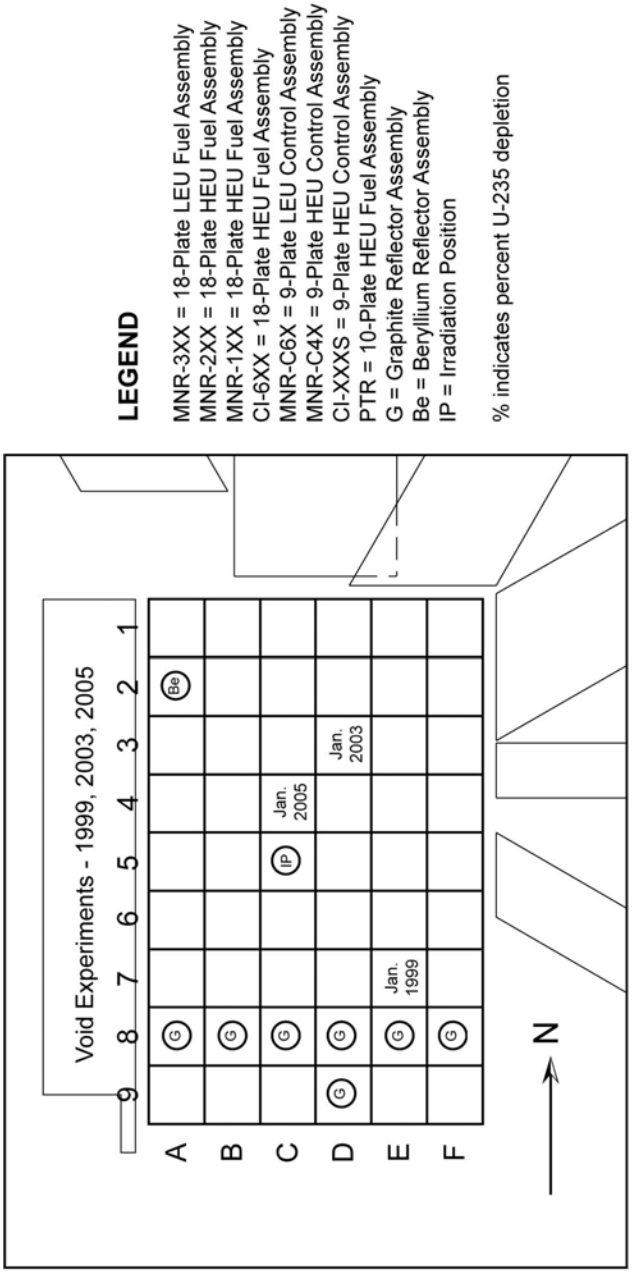

Figure D-6: Location of Void Effect Experiments

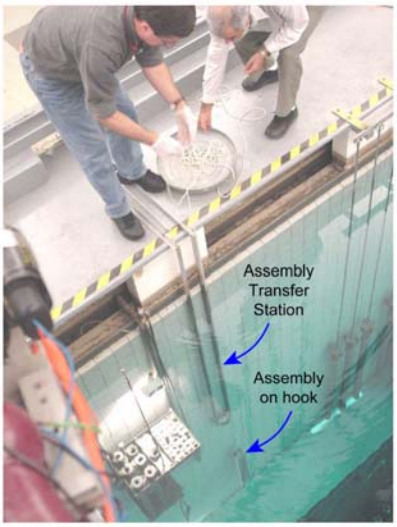

Figure D-7: Moving a Fuel Assembly to the Transfer Station

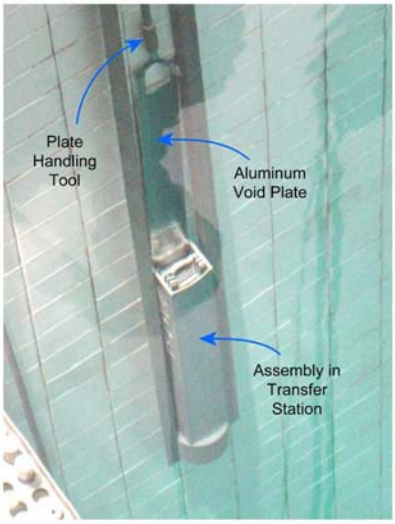

Figure D-8: Inserting a Void Plate into a Fuel Assembly

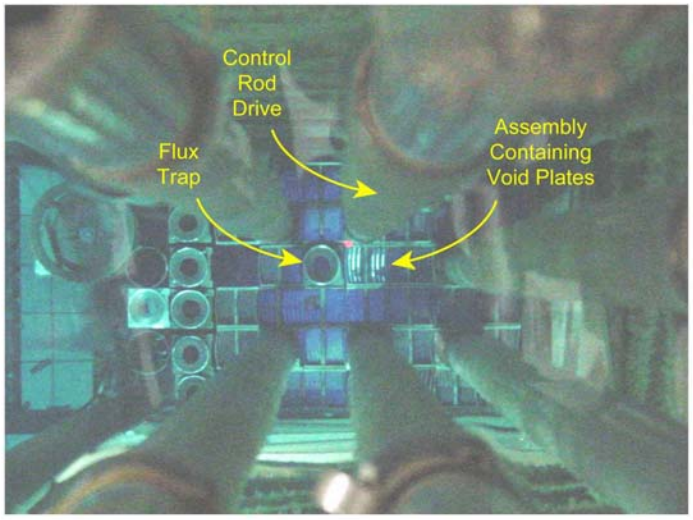

Figure D-9: Assembly Containing Void Plates in Core

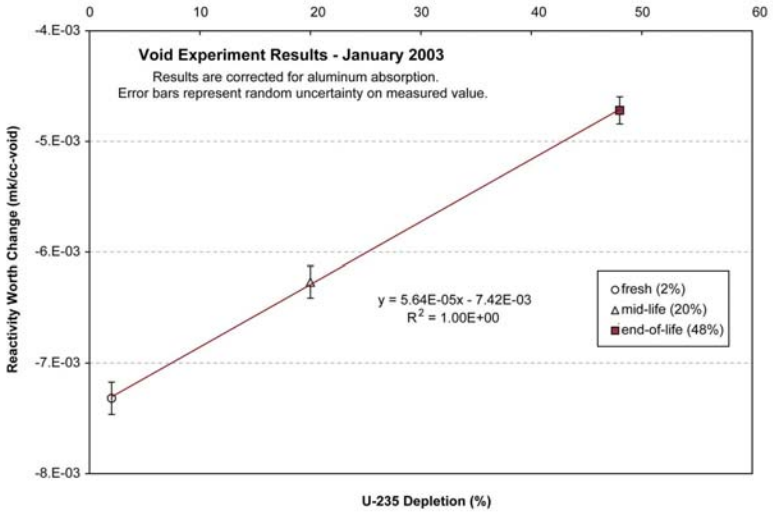

Figure D-10: Void Effect (in mk/cc) as a Function of Burnup

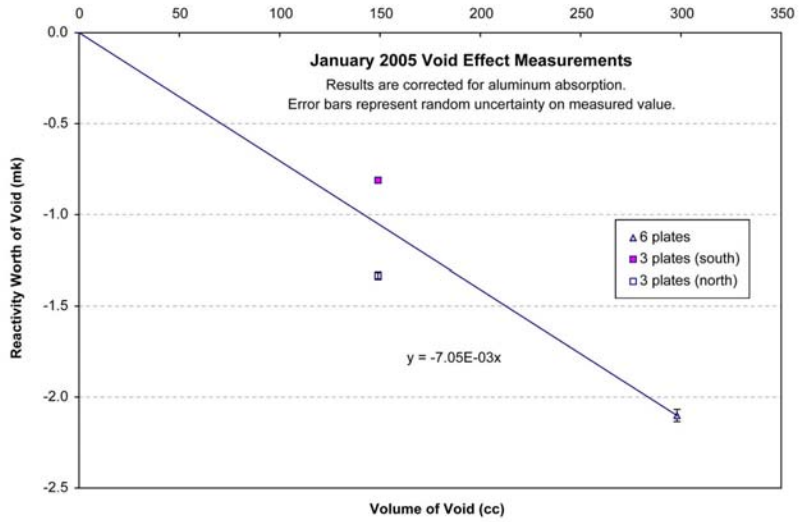

Figure D-11: Void Effect as a Function of Void Volume (cc)

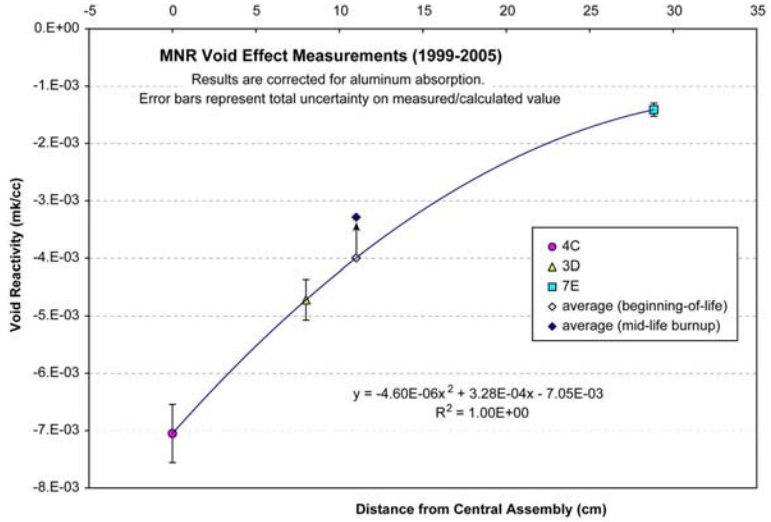

Figure D-12: Void Effect (mk/cc) in a BOL Assembly as a Function of Radial Position in the Core

APPENDIX E - PARAMETRIC ANALYSIS OF THE FUEL TEMPERATURE COEFFICIENT IN LEU MTR FUEL

TABLE OF CONTENTS

LIST OF TABLES

LIST OF FIGURES

(this page is intentionally left blank)

E PARAMETRIC ANALYSIS OF THE FUEL TEMPERATURE COEFFICIENT IN LEU MTR FUEL

E.1 Objective

The objective of this study is to determine order of magnitude sensitivity of the fuel temperature coefficient of reactivity for LEU MTR fuel with various system parameter variations.

E.2 Background

Research analysis at the McMaster Nuclear Reactor (MNR) has addressed self-limiting reactivity limits for MTR fuel. This work has been based largely on the existing experimental data of the Borax and Spert projects conducted in the 1950s and 1960s in the United States at the National Reactor Testing Station (NRTS). These experiments were performed mostly on Highly Enriched Uranium (HEU) MTR fuel.

Low Enrichment Uranium (LEU) MTR fuel is the current industry standard. The main difference in response of LEU fuel compared to HEU fuel is due to the increased fuel temperature feedback in the former - thus improving the self-limiting capability of the fuel. Simulation work performed at Argonne National Laboratory (ANL) as part of the Reduced Enrichment for Research and Test Reactors (RERTR) Program used the PARET code (Ref. E-1) to determine reactivity limits precluding clad melting for both HEU and LEU MTR fuel (Refs. E-2, E-3). The HEU PARET models were benchmarked against Spert transient data (Refs. E-2, E-4, E-5) while the PARET code had previously been shown to be accurate for LEU fuel modelling (Ref. E-6). The ANL work includes sensitivity analysis on the prompt neutron generation time and the fuel meat thermal conductivity.

This study is performed to identify further sensitivities of the fuel temperature coefficient of reactivity to other system parameters which may exist in LEU MTR fuel.

E.3 Theory

The fuel temperature reactivity is a function of two factors which change with changing fuel temperature: (i) neutron spectrum changes, and (ii) cross section resonance broadening.

Neutron spectrum changes occurs in the thermal energy range due to changes in scattering from the fuel material nuclides. Note that for a fast power excursion significant increases in fuel temperature will occur before a noticeable amount of heat has been transferred to the coolant. The spectrum effect results in an important positive reactivity effect in natural uranium and Slightly Enriched Uranium (SEU), *i.e.*, 1-2%, oxide fuel such as seen for CANDU systems. The contributing factors are the scatter from light nuclides in the fuel itself, *e.g.*, oxygen in the oxide fuel, and results in an increased fission rate from the low-lying Pu-239 resonance at 0.3 eV upon the spectrum hardening. This spectrum effect becomes significant as the natural uranium or SEU fuel is irradiated and the inventory of Pu-239 builds up while the U-235 inventory is depleted. The fission and capture cross sections of U-235 and the capture cross section of U-238 behave approximately as 1/v (where v is the neutron speed) in the thermal region and therefore thermal neutron spectrum hardening has little to no effect on the overall reaction rates of these nuclides (Ref. E-7).

In terms of LEU MTR fuel this spectrum effect is expected to be of less significance as most associated fuel materials are based on the heavier aluminum and silicon or molybdenum elements as opposed to oxygen and also as the fraction of Pu-239 fissions is much smaller compared to those from the much more concentrated U-235 inventory.

The second factor, a negative contribution to reactivity, known commonly as the Doppler effect, arises from increased capture due mainly to cross section resonance broadening of U-238 capture resonances. The net negative reactivity contribution of the Doppler effect occurs because U-238 has a significant capture cross section comprised of resonances in the epithermal energy range whereas the U-238 fission cross section is negligible in the resonance energy range becoming significant only at higher energies as it is a threshold reaction. Contributions from the other main isotopes U-235 and Pu-239 are small as the capture and fission cross sections have similar structures with the resonances coinciding in energy. As a result the capture to fission ratios of these isotopes are expected to vary only slightly with changing fuel temperature.

The Doppler effect is expected to be the significant contributing factor to the fuel temperature reactivity coefficient in LEU MTR fuel.

Factors of interest in studying the characteristics of resonance-related reaction rates are those which may impact the importance of the resonance energy range, *i.e.*, those which effect the thermalization of the neutron spectrum, and those effecting the reaction rates in the resonance energy range.

The neutron energy spectrum determines the relative importance of energy dependent reactions in a nuclear reactor core. For example, a highly thermalized system is expected to be less effected by changes in epithermal resonance-related reactions than a second system for which the neutron energy spectrum is larger in the epithermal range. Similarly, the leakage characteristics of a reactor core may be important to changes in resonance-related reactions since leakage is preferentially from higher neutron energies.

Where the neutron population is thermalized, with respect to resonance absorbers, may also be important and depends upon the reflector characteristics of the core as well as the presence of in-core flux traps. A system in which a significant amount of the thermalization occurs in the reflector or in in-core traps, *i.e.*, away from the resonance absorbers in the fuel, is expected to have a smaller Doppler coefficient of reactivity.

Finally, lumping of the fuel effects both the thermalization and self-shielding effects of the system while the composition of the core changes with exposure of the fuel and determines the overall balance of reactions in the core. With these various factors in mind, parameters which may have a potential effect on the fuel temperature feedback coefficient include:

- fuel loading (self-shielding)
- fuel assembly metal-to-water ratio (spectrum weighting)
- fuel depletion (fuel composition)
- in-core flux traps (moderation)
- core size (leakage)
- core reflection (leakage and moderation)

This study considers various changes to system parameters for an MTR LEU system and investigates the effect on the fuel temperature coefficient of reactivity as a result of these parametric variations.

E.4 Analysis Approach

As a first approximation core effects (in-core flux traps, core size, core reflection, and changes in leakage) are ignored as calculations are performed at a cell geometry level using the lattice code WIMS-ANL. The cell multiplication factor is used to determine the change in reactivity with respect to changes in fuel temperature while the reaction rates of the various fuel isotopes are examined to determine significant contributing factors to these changes in reactivity.

Fixed parameters in this study are:

- enrichment = 20%
- fuel meat thickness = 0.051 cm
- clad thickness = 0.038 cm
- fuel meat material = U_3Si_2-Al

Cell models used in this study encompass the following variations:

(i) fuel depletion
- 0% U-235 depletion (fresh fuel)
- 25% U-235 depletion (MNR mid-life burnup)
- 50% U-235 depletion (MNR exit-burnup)
- 70% U-235 depletion (end-of-life fuel)

(ii) fuel meat loading
- light loading (2.0 g-U/cc)
- medium loading (3.7 g-U/cc) (MNR standard LEU loading)
- heavy loading (8.0 g-U/cc)

(iii) coolant water channel thickness
- thin channels (0.200 cm)
- medium channels (0.300 cm) (MNR standard LEU geometry)
- wide channels (0.700 cm)

The fuel depletion encompasses the exposure range applicable to MNR (EOL = 50% U-235 depletion). The U-235 loading range envelopes the MNR LEU fuel loading of about 3.7 g/cc and projected high density fuels as currently being explored by the RERTR program. The lower limit of the U-235 loading (light loading) is based on a projection of the lightly loaded Borax and Spert HEU fuel to LEU values. The

water channel thickness variation bounds that found between 24-plate (thin channels) to 9-plate (wide channels) per assembly fuel based on the fixed fuel meat and cladding thicknesses. The specifications for the five different cases considered in this study are summarized in Table E-1.

A simple three-region half-plate 1-D slab cell model was used for this analysis. Leakage was not modelled in the calculations.

The version of WIMS-ANL and the associated microscopic cross section library used in this study were:

```
WIMS-ANL version 4.0 (December 2000)
ENDF/B-6 69-group libraries (10/05/00)
```

Additional runs for comparison using more recent versions of WIMS-ANL (5.00 and 5.01) and more recent versions of the libraries (ENDF/B-6 69-group 20020416, and 172-group 20020703) were examined and no significant differences were found.

The 69-group ENDF/B-VI library supplied with the WIMS-ANL code contains actinide cross sections at the following temperatures in the range of interest: 300K, 560K, 1000K and 1600K. WIMS-ANL cases were run over this temperature range for the four different U-235 depletions (0%, 25%, 50% and 70%).

The U-235, U-238 and Pu-239 absorption, fission, and capture (n,γ) reaction rates were determined for a three-group energy structure, shown in Table E-2. These reaction rates as well as the associated atom densities and the cell infinite multiplication factor, k_{inf}, were extracted from the standard WIMS-ANL output file.

E.5 Results & Discussion

The raw data results are summarized in Tables E-3 to E-7. From the multiplication factor results the reactivity change associated with the fuel temperature increases were calculated. Reactivity is defined as:

$$\rho \equiv \frac{k-1}{k}$$

Correspondingly, the fuel temperature reactivity change, in units of milli-k is defined

as:

$$\rho_{FT} = \left(\left(\frac{k_{T_i} - 1}{k_{T_i}} \right) - \rho_o \right) * 1000$$

where k_{Ti} is the multiplication factor of the cell at average fuel temperature T_i and ρ_o is the reactivity at a reference average fuel temperature, in this case 300K, *i.e.*,

$$\rho_{300K} = \frac{k_{300K} - 1}{k_{300K}}$$

The reactivity change due to fuel temperature increase for the MNR standard LEU fuel (base) case is shown in Figure E-1. The fuel temperature reactivity feedback was found to have a quadratic dependency on the fuel temperature. This figure shows the temperature dependence of the feedback for the various U-235 depletions.

The fuel temperature of reactivity for MTR LEU plate fuel is found to increase in magnitude with increasing U-235 depletion. This is due to the relative change in the U-235 content compared to the practically constant U-238 content as the fuel depletes. The result is that a higher percentage of the absorptions in the fuel is in U-238, which is the main contributor to the temperature dependence, for higher depletion situations. The dependence of the fuel temperature reactivity effect on depletion was found to be similar for all of the cases examined as illustrated by the consistent shape of the curves in Figure E-2.

The fuel temperature reactivity effect for MTR LEU plate fuel is found to increase in magnitude with increasing metal-to-water ratio (decreasing coolant channel thickness with a fixed fuel plate volume) of the assembly, *i.e.*, with less water in the fuel lattice (Figure E-3). This is consistent with the idea that a harder (due to under-moderation) neutron spectrum results in a higher importance on the resonance energy range and in general a lower resonance escape probability. The dependence of the reactivity effect is approximately linear with metal-to-water ratio over the range examined and is found to be independent of U-235 depletion. Variation in the magnitude of the fuel temperature effect relative to the thin coolant channel case is found to be on the order of 50% (Figure E- 4) over the range of metal-to-water ratios examined.

The fuel temperature reactivity effect for MTR LEU plate fuel is found to increase with higher uranium densities in the fuel meat (see Figure E-5). This is expected since the U-238 isotope is a higher percentage of the fuel than the U-235 or Pu-239 isotopes. Therefore, increasing the loading translates preferentially to more U-238 resonance absorption. The dependence of the reactivity effect is approximately linear over the range of uranium densities examined. The slight non-linearity is consistent with increased self-shielding with higher uranium densities. Variation in the magnitude of the fuel temperature effect relative to the light uranium density case is found to be on the order of up to 70% (Figure E-6) over the range of uranium densities examined.

The trends shown in Figures E-3, E-4, E-5 and E-6 are relatively insensitive to depletion so only the fresh fuel cases are shown. The parameter value of the IAEA 10MW Benchmark LEU fuel (Ref. E-8) is indicated on the figures.

Reaction rate results are not included in this report as an error was discovered in the WIMS-ANL reaction rate edit which resulted in erroneous results (Ref. E-9). This error did not seem to affect the multiplication factor results upon which the reactivity calculations are based.

E.6 Conclusions

Variation of the fuel temperature effect on reactivity was studied for typical LEU MTR fuel with special attention to the dependence on U-235 depletion, metal-to-water ratio of the fuel, and total uranium density in the fuel meat. Core effects such as leakage and reflection were not incorporated into the analysis.

The fuel temperature reactivity effect is observed to increase with increasing metal-to-water ratio, uranium density, and fuel depletion, over the range of parameter variation studied.

For conservative ranges of variation of the metal-to-water ratio and the uranium density in LEU MTR fuel the fuel temperature effect on reactivity may be expected to vary on the order of 50% and 70% respectively. Assuming that these two sensitivities are linearly independent a total variation of up to 120%, or a factor of up to 2.2, may be expected for the combined effect of variation of these two parameters.

In addition, the fuel temperature reactivity effect is observed to increase with increasing burnup of the fuel, akin to the uranium density effect. Thus the reactivity effect can be expected to be larger for operating cores compared to fresh cores. The increase in magnitude of the reactivity effect will depend on the average burnup of the core. A conservative estimate of a 20% increase for an average burnup of 25% is not unreasonable based on the results herein.

Assuming the primary factor contributing to the fuel temperature reactivity effect is U-238 resonance absorption (as indicated by preliminary examination of the cell-averaged microscopic cross sections in this study as well as stated in Reference E-5), the variation with depletion and loading also indicates the order of magnitude variation which could be expected in a partially converted MTR core, *i.e.*, that containing some HEU assemblies and some LEU assemblies. For example, as a first estimate on a 50% HEU / 50% LEU core the fuel temperature reactivity coefficient may be expected to be about half that of the average LEU burnup value determined from the cell calculations. The more HEU assemblies the smaller the fuel temperature reactivity coefficient. Of course, this is just a very rough estimate, and the assembly locations, and core burnup, power density, and temperature distributions must be considered in the case of a specific core configuration and core models should be constructed to extend the results herein.

E.7 References

E-1. C. F. Obenchain, "PARET - A Program for the Analysis of Reactor Transients", US AEC Technical Report IDO-17282, Phillips Petroleum Co., January 1969.

E-2. W. L. Woodruff, "The PARET Code and the Analysis of the SPERT I Transients", Argonne National Laboratory Technical Report ANL/RERTR/TM-4, pp. 560-579, from the Proceedings of the International Meeting on Research and Test Reactor Core Conversion from HEU to LEU Fuels, 1982.

E-3. J. E. Matos, K. E. Freese, "Safety Analyses for HEU and LEU Equilibrium Cores and HEU-LEU Transition Core for the IAEA Generic 10 MW Reactor", ANL, IAEA-TECDOC-643, v.2, Appendix A-2, 1992.

E-4. W. L. Woodruff, "A Kinetics and Thermal-Hydraulics Capability for the Analysis of Research Reactors", Nuclear Technology, v. 64, pp. 196-206, February 1984.

E-5. J. E. Matos, E. M. Pennington, K. E. Freese, W. L. Woodruff, "Safety-Related Benchmark Calculations for MTR-Type Reactors with HEU, MEU and LEU Fuels", ANL, IAEA-TECDOC-643, v.3, Appendix G-1, 1992.

E-6. T.G. Taxelius, editor, "Quarterly Technical Report - Spert Project - July, August, September, 1967", US AEC Technical Report IDO-17271, Phillips Petroleum Co., July 1968.

E-7. J.J. Duderstadt, L.J. Hamilton, Nuclear Reactor Analysis, John Wiley & Sons, Inc., 1976, Chapter 2, p.46.

E-8. "Research Reactor Core Conversion from the use of Highly Enriched Uranium to the use of Low Enriched Uranium Fuels Guidebook", International Atomic Energy Agency technical report IAEA-TECDOC-233, Appendix F, 1980.

E-9. Personal communication with J. Deen, Argonne National Laboratory, April 2004.

E.8 Tables

Table E-1: Case Specifications

Case Name	Coolant Channel Thickness	Fuel Meat Uranium Density
Base (MNR Std LEU)	0.300 cm	3.7 g/cc
Thin	0.200 cm	3.7 g/cc
Wide	0.700 cm	3.7 g/cc
Light	0.300 cm	2.0 g/cc
Heavy	0.300 cm	8.0 g/cc

Table E-2: Reaction Rate Group Structure Based on WIMS-ANL 69-Group ENDF/B-VI Library

Group	Upper Energy, eV	Library Groups
Fast (1)	10000000	1 - 14
Resonance (2)	9188	15 - 27
Thermal (3)	4	28 - 69
Lower Bound	0.00001	

Table E-3: K-inf Results for the Base Case (l225) Model

	Burnup (% U-235 Depletion)			
T_f (K)	0	25	50	70
300	1.648327	1.530425	1.378561	1.177635
560	1.637843	1.520693	1.369585	1.169739
1000	1.625259	1.509019	1.358866	1.160358
1600	1.612994	1.497645	1.348470	1.151309

Table E-4: K-inf Results for the Thin Coolant Channel Model

	Burnup (% U-235 Depletion)			
T_f (K)	**0**	**25**	**50**	**70**
300	1.661243	1.541796	1.392372	1.213307
430	1.654134	1.535176	1.38617	1.207697
560	1.648066	1.529517	1.380855	1.202881
1000	1.631852	1.514435	1.366793	1.190213

Table E-5: K-inf Results for the Wide Coolant Channel Model

	Burnup (% U-235 Depletion)			
T_f (K)	**0**	**25**	**50**	**70**
300	1.505917	1.375390	1.195041	0.977997
430	1.502933	1.372653	1.192622	0.975981
560	1.500375	1.370306	1.190544	0.974247
1000	1.493933	1.364389	1.185319	0.969903

Table E-6: K-inf Results for the Light Uranium Loading Model

	Burnup (% U-235 Depletion)			
T_f (K)	**0**	**25**	**50**	**70**
300	1.535048	1.407514	1.232832	1.013403
430	1.531024	1.403808	1.229530	1.010635
560	1.527578	1.400632	1.226696	1.008260
1000	1.518992	1.392716	1.219654	1.002376

Table E-7: K-inf Results for the Heavy Uranium Loading Model

	Burnup (% U-235 Depletion)			
T_f (K)	**0**	**25**	**50**	**70**
300	1.683747	1.557578	1.413860	1.25242
430	1.676139	1.550477	1.407019	1.246028
560	1.669648	1.544411	1.401152	1.240536
1000	1.65183	1.527794	1.385219	1.22569

E.9 Figures

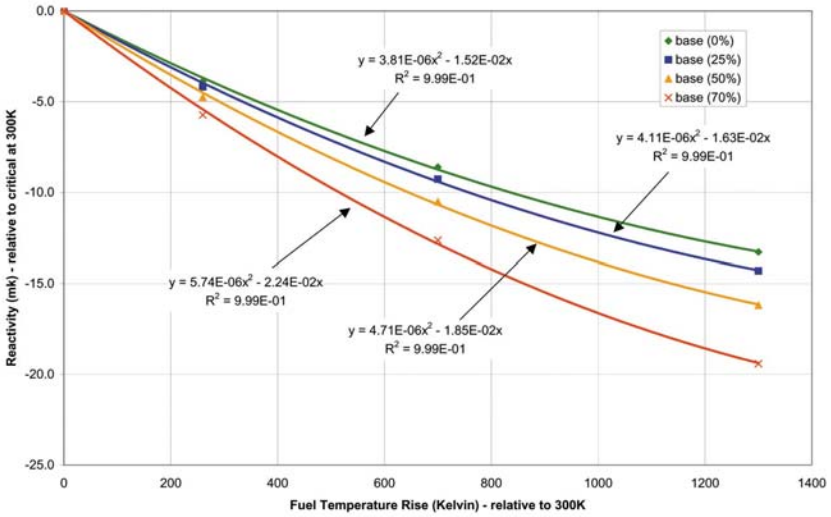

Figure E-1: Reactivity Change as a Function of Fuel Temperature for the Base Case at Various Fuel Depletions.

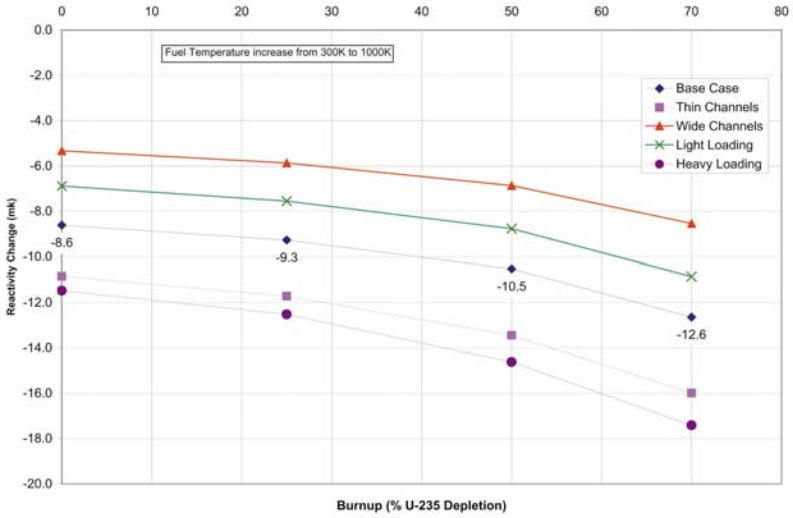

Figure E-2: Magnitude of the Fuel Temperature Reactivity Effect with Varying Burnup for All Cases.

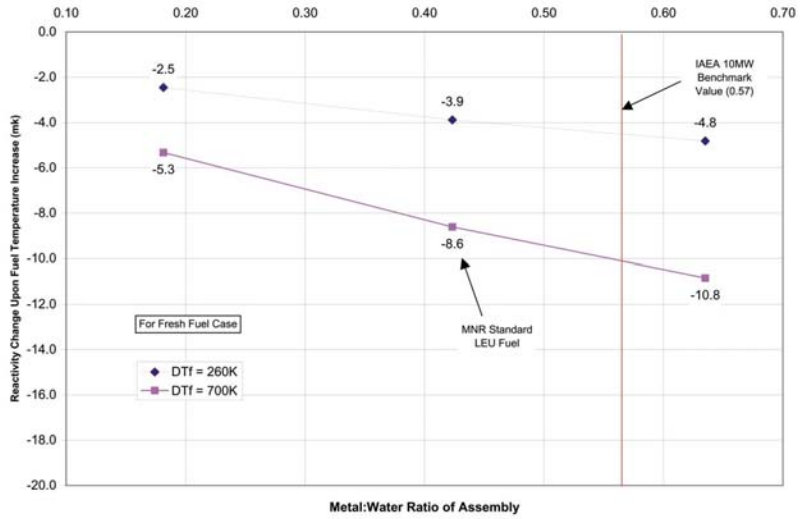

Figure E-3: Fuel Temperature Reactivity Change for Varying Metal:Water

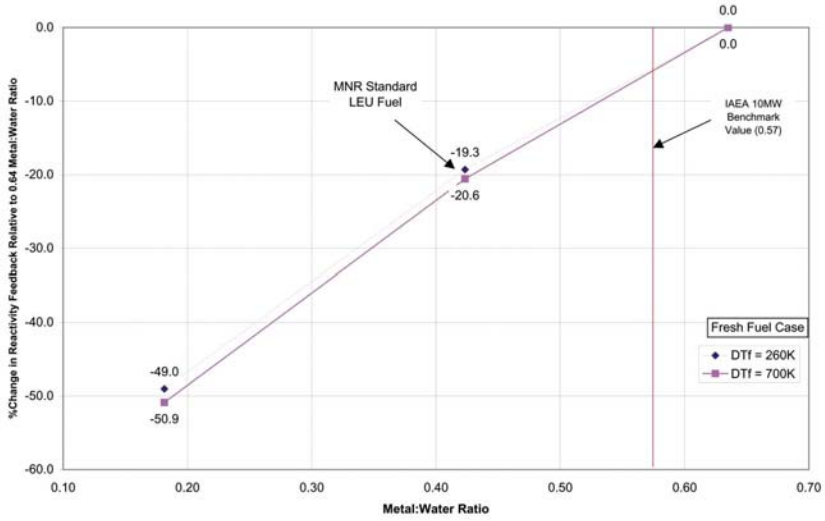

Figure E-4: Relative Change in Fuel Temperature Reactivity for Varying Metal:Water

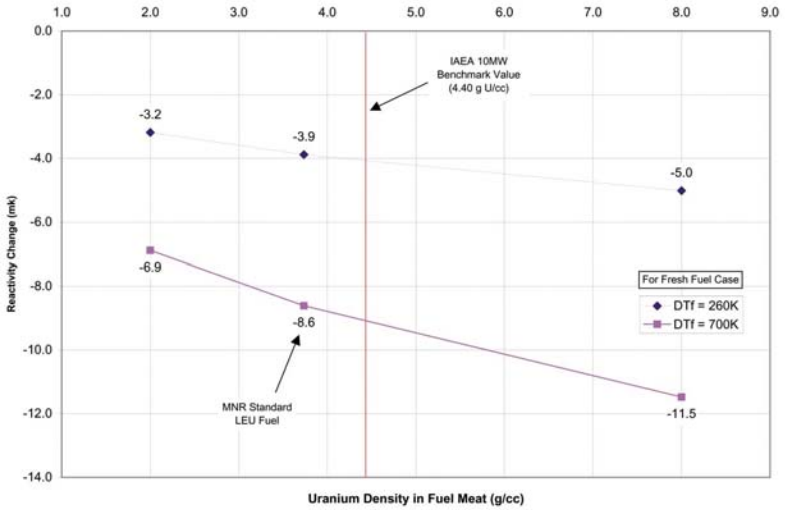

Figure E-5: Fuel Temperature Reactivity Effect for Varying Total Uranium Density

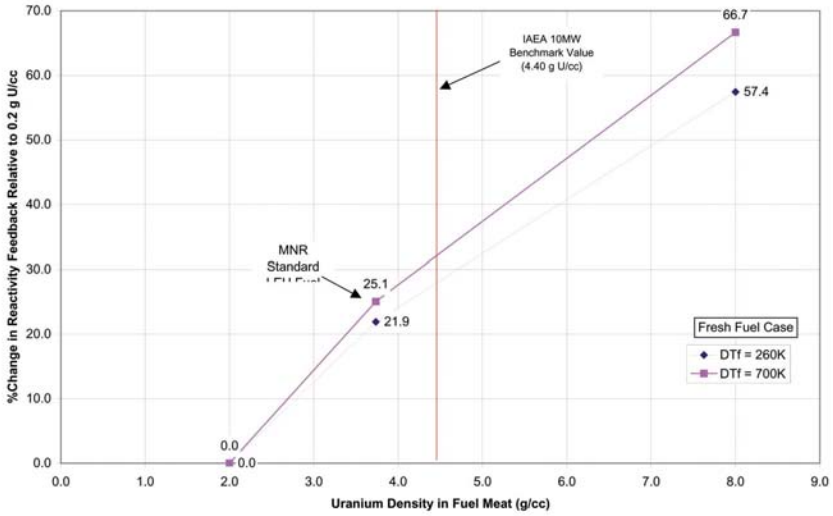

Figure E-6: Relative Change in Fuel Temperature Reactivity Effect for Varying Total Uranium Density

APPENDIX F - PARET INPUT FILES AND INFORMATION

TABLE OF CONTENTS

(this page is intentionally left blank)

F PARET INPUT FILES AND INFORMATION

This appendix contains the PARET input files for the Spert I D-12/25, IAEA HEU, and IAEA LEU cores. Modifications made to the files as supplied by ANL are indicated as are notes on the execution of these files. In addition general notes on the PARET modelling of Spert and the IAEA 10 MW benchmark reactor are included.

F.1 Input Files

F.1.1 Spert I D-12/25($1.50/0.07s ramp)

F.1.1.1 Notes

The following are notes on the spert150.inp PARET input file as supplied by W.Woodruff/N.Hanan, ANL (Dec.2003). The model is for a $1.50 step reactivity insertion in the Spert I D-12/25 core from low power, ambient conditions with natural circulation flow only and no SCRAM shutdown.

GENERAL INFORMATION (1000 series cards)
entry
1 -2 = two channels, -ve is SI units
2 21 = axial nodes
3 7 = radial nodes
4 0 = slab geometry
5 1 = reactivity specified
6 1 = vapour fraction & quality calc in (1) both subcooled & saturation ranges
7 0 = inlet pressure specified
8 0 = reduce & expand kinetics timestep
9 6 = number of delayed neutron groups
10 -1 = printout option
11 0 = no average temperature printout in addition to detailed printout
12 10 = max heat transfer iterations

13 5E-6 = initial power (MW)
14 5.20321E-3 = total vol of fuel in core (m3)
15 101360. = operation pressure (Pa)
16 -20.0 = moderator inlet (-ve) temperature (C)
17 7.62000E-4 = plate half thickness incl. clad (m)

18 2.54000E-4 = fuel half thickness (m)
19 2.54000E-4 = distance to inner surf of clad (=18) (m)
20 0.068680 = plate width (m)
21 0.062231 = fuel width (m)
22 0.6096 = active fuel height (m)
23 0.0 = inlet non-fueled section length (m)

24 0.0 = outlet non-fueled section length (m)
25 7.00000E-3 = Beff
26 6.00000E-5 = prompt neutron generation time (sec)
27 9.80664 = g (m/s2)
28 0.004556 = heat source descrip for moderator (unitless)

29 0.40 = transient time (sec)
30 0.80 = const. in void generation equation (unitless)
31 1.0 = exponent in void generation equation (unitless)
32 997.79 = moderator reference density (kg/m3) - may be over-ridden
33 0.0 = const. coeff. in fuel temp feedback equ'n

34 0.0 = lin. coeff. in fuel temp feedback equ'n
35 0.0 = quad. coeff. in fuel temp feedback equ'n
36 0.0 = cub. coeff. in fuel temp feedback equ'n
36 0.0 = temp. offset coeff. in fuel temp feedback equ'n
38 1.0 = exponent in fuel temp feedback equ'n
39 0.001 = upper limit on kinetics timestep test (rec. 0.001)

40 0.0 = steady-state DNB heat fluxes calc'ed in code are used
41 0.0005 = nucleate boiling collapse time (sec)
42 0.001 = transition boiling bubble collapse time (sec)
43 0.03 = frac. of clad surf. heat flux in sub-cool nucleate boiling
44 0.05 = frac. of clad surf. heat flux in sub-cool transition boiling
45 0.05 = frac. of clad surf. heat flux in sub-cool film boiling

46 0.13 = nat. convection heat transfer constant no.1
47 0.33333 = nat. convection heat transfer constant no.2

ADDITIONAL GENERAL INFORMATION (1111 series cards)

1111

1a 0.0842957 = total xsec flow area of all flow channels in core (m3)
2a 1.000 = flux weighting factor for channel 1 (rec. unity by ANL)
1.000 = flux weighting factor for channel 2 (rec. unity by ANL)
1112
1b 1 = Seider-Tate single phase correlation
2b 1 = McAdams two phase correlation
3b 1 = transition model two phase transient scheme
4b 0 = original DNB correlation
5b 2 = revised, with entrance effects for h, single phase heat trans. subroutine

6b 4.03500E+5 = ave core heat flux (W/m2) (only used with 4b = 3 & 4)
7b not incl. = bubble detachment parameter (only used with 4b = 3)
8b not incl. = Cp (J/kg-K) (used with 4b = 3 & 4)

1113
1c 1.2 = rate of ctrl rod movement (w scram or withdrawal) (m/sec)
2c 0.025 = delay time on rod move after trip (sec)
3c 1.20000E+5 = overpower trip point (MW)
4c default = low flow trip point (%), default 0.0%

1114
1d 0.0 = ht. above reactor for nat. circ. effects (m)
2d 0.0 = ht. below reactor for nat. circ. effects (m)

THERMAL PROPERTIES OF FUEL ELEMENT MATERIALS (2000 series cards)
fuel
2001a10.0 = th. cond. equ'n quad. coeff.
2001a20.0 = th. cond. equ'n lin. coeff.
2001a3151.53 = th. cond. equ'n const. term (w/m-K)
2001a40.0 = th. cond. equ'n 1/over coeff.
2001a50.0 = th. cond. equ'n temp. offset coeff.

2002b1 0.0 = vol. heat cap. equ'n quad. coeff.
2002b2 1014.0 = vol. heat cap. equ'n lin. coeff. (J/m3-K2)
2002b3 2.01140E+6 = vol. heat cap. equ'n const. term (J/m3-K)
2002b4 0.0 = vol. heat cap. equ'n 1/over coeff.
2002b5 0.0 = vol. heat cap. equ'n temp. offset coeff.

clad

2003a10.0 = th. cond. equ'n quad. coeff.
2003a20.0 = th. cond. equ'n lin. coeff.
2003a3183.11 = th. cond. equ'n const. term (w/m-K)
2003a40.0 = th. cond. equ'n 1/over coeff.
2003a5 0.0 = th. cond. equ'n temp. offset coeff.

2004b1 0.0 = vol. heat cap. equ'n quad. coeff.
2004b2 1243.4 = vol. heat cap. equ'n lin. coeff. (J/m3-K2)
2004b3 2.07090E+6 = vol. heat cap. equ'n const. term (J/m3-K)
2004b4 0.0 = vol. heat cap. equ'n 1/over coeff.
2004b5 0.0 = vol. heat cap. equ'n temp. offset coeff.

RADIAL OR HALF-PLATE DESCRIPTION (3000 series cards)

3001
1 6.35000E-5 = radial increment length (m)
2 5 = radial node out to which increment applies
3 1 = composition code (1=fuel)
4 0.955 = radial source descrip. (frac. of heat generated in composition)

3002
1 2.54000E-4 = radial increment length (m)
2 7 = radial node out to which increment applies
3 2 = composition code (1=clad)
4 0.0 = radial source descrip. (frac. of heat generated in composition)

AXIAL DESCRIPTION (4000 series cards)

4001
1 2.90285E-2 = axial region length (m)
2 21 = node number up to which increment applies

INDIVIDUAL CHANNEL INFORMATION (5000 series cards)
channel 1 (51XX series)
2a 1 = flow-forced channel (see Table 10)
3a 0 = pressure drop (Pa) (zero for 2a = 1)
4a 0.0030353 = radial distance from center of slab to center of channel (m)
5a 0.00370 = reactivity feedback wt. factor for channel (rec. vol. frac. of core)
6a 0.55 = loss coeff. for inlet of channel

7a 0.65 = loss coeff. for outlet of channel
8a 0.10 = inlet area ratio
9a 0.55 = outlet area ratio
10a 0.4214 = overall density/void coeff. ($/%-of-core-voided)
11a 0.028008 = overall coolant temperature coeff. ($/C)

1b 0.0 = length of inlet plenum (m)
2b 0.6096 = length of outlet plenum (m)
3b 0.8635 = inlet plenum equiv. diameter (m)
4b 0.36576 = outlet plenum equiv. diameter (m)

2c 2.4 (peak) = axial flux peaking factors (one for each axial node)
3c 1.0 (all) = moderator density feedback wt. factors (one for each axial node)
4c 1.0 (all) = fuel temperature feedback wt. factors (one for each axial node)
5c 1.0 (all) = coolant temperature feedback wt. factors (one for each axial node)

channel 2 (52XX series)
same as for channel 1 except
5a 0.99630 = reactivity feedback wt. factor for channel (rec. vol. frac. of core)
2c 1.311 (peak) = axial flux peaking factors (one for each axial node)

DELAYED NEUTRON INFORMATION (6000 series cards)

6-groups (agrees with entry #9 on 1000 series cards)

group	del. neut. fraction	decay const. (sec-1)
1	0.03443	0.01240
2	0.21797	0.03050
3	0.19904	0.11100
4	0.38861	0.30100
5	0.11701	1.14000
6	0.04294	3.01000

POWER OR REACTIVITY VS. TIME (9000 series cards)

1a 3 = number of pairs of entries in table

extern. inserted react. ($)	time (sec)
0.0	0.0

1.50	0.070
1.50	100.0

MODERATOR INLET MASS VELOCITY VS. TIME (10000 series cards)

1a 2 = number of pairs of entries in table

inlet mass vel. ((kg/s/m2)	time (sec)
2.99727	0.0
2.99727	100.0

PERCENT LINEAR THERMAL EXPANSION OF THE CLAD VS. TEMPERATURE (11000 series cards)

1a 16 = number of pairs of entries in table

% linear therm. exp.	temperature (K)
0.0	0.0
0.0	293.15
0.07668	323.15
0.1406	348.15
0.2045	393.15
0.3323	423.15
0.4601	473.15
0.5879	523.15
0.7157	573.15
0.8435	623.15
0.9713	673.15
1.0991	723.15
1.2269	793.15
1.3291	823.15
1.4825	873.15
1.7381	973.15

TOTAL PRESSURE DROP VS. TIME (12000 series cards)

1a 2 = number of pairs of entries in table

tot. pr. drop across chan. (N/m2 = Pa)	time (sec)
0.00	0.0
0.00	0.0

TABLE OF TIME INCREMENT VS. TIME (14000 series cards)

1a 5 = number of pairs of entries in table

time incr. (sec)	as of time (sec)
0.005	0.0
0.001	0.10
0.0005	0.28
0.0001	0.30
0.00005	0.32

TABLE OF PRINT FREQUENCY VS. TIME (16000 series cards)

1a 6 = number of pairs of entries in table

print time incr. for major output (sec)	freq. of int. output (every X steps)	as of time (sec)
0.100	5	0.0
0.005	2	0.100
0.001	1	0.33
0.005	2	0.335
0.005	5	0.355
0.010	10	0.370

TABLE OF PUMP MASS VELOCITY FRACTION VS. TIME (17000 series cards)

1a 2 = number of pairs of entries in table

cool. mass vel. frac. in chan. rel. to initial	time (sec)
1.0	0.0
1.0	500.0

TABLE OF ROD WORTH VS. ROD LOCATION OR LAPSED TIME (18000 series cards)

1a 2 = number of pairs of entries in table
Note: rod rate specified in card 1113 so table is in distance not time

reactivity of rod bank ($)	rod position (m)
0.0	0.0
-10.0	0.600

F.1.1.2 Modifications

(a) The total transient time and the time step increments have been lengthened to be similar to those used in the IAEA HEU 10MW Reactor case (bnch150h.inp) as supplied by ANL (Dec/04).

Originally:
total transient time = 0.40 sec (1000 series cards, entry 29)
(Table 14 from input)
14000, 5
14001, 0.005 0.0 0.001 0.10 0.0005 0.28
14002, 0.0001 0.30 0.00005 0.32
(Table 16 from input)
16000, 6
16001, 0.100 5 0.0 0.005 2 0.100
16002, 0.001 1 0.33 0.005 2 0.335
16003, 0.005 5 0.355 0.010 10 0.370
Modified:
total transient time (1000 series cards) = 0.80 sec
(Table 14 from input)
14000, 3
14001, 0.005 0.0 0.001 0.20 0.005 0.50
(Table 16 from input)
16000, 4
16001, 0.100 5 0.0 0.005 2 0.200
16002, 0.005 1 0.3 0.100 5 0.500

(b) Includes (a). Single phase heat transfer subroutine selection altered from revised with entrance effects (option 2), to the original (option 0).

1112 card, entry 5.

(c) timesteps reduced in size.

Originally:

```
14000,    3
14001, 0.005     0.0      0.001     0.20      0.005     0.50
16000,    4
16001,  0.100      5      0.0       0.005      2       0.200
16002,  0.005      1      0.3       0.100      5       0.500
```

Modified:

```
14000,    3
14001,  0.005    0.0      0.0001    0.20      0.001     0.38
16000,    4
16001,  0.10       5      0.0       0.02       2       0.20
16002,  0.02       1      0.30      0.05       5       0.38
```

(a) The case still does not finish gracefully. Stopped immediately after peak clad temperature is reached due to negative coolant enthalpy values. The change in time step increment size to a coarser mesh noticeably changes the Etm, Tclad and BSP results.

For comparison:

	as supplied	coarse dt
rho_in ($)	1.50	1.50
period (msec)	16.9	16.8
Pmax (MW)	221	220
Etm (MW-sec)	4.82	4.67
Ttm (clad, C)	212	219
Tmax (clad, C)	> 320	> 350
tm (sec)	0.334	0.333
t_Tmax (sec)	-	-
BSP	1.35	1.26

(b) no change was observed in the result upon altering the HTRAN option. The case still terminated prematurely on negative coolant enthalpies.

	rev HTRAN	orig HTRAN
rho_in ($)	1.50	1.50
period (msec)	16.8	16.8
Pmax (MW)	220	220
Etm (MW-sec)	4.67	4.67
Ttm (clad, C)	219	219
Tmax (clad, C)	> 350	> 350
tm (sec)	0.333	0.333
t_Tmax (sec)	-	-

BSP	1.26	1.26

(c) changing the time step increments avoided the negative enthalpy problem as the case executed to the end of the specified transient time. Also there was a significant impact on the Etm and Tclad results. For comparison:

	coarse dt	fine dt
rho_in ($)	1.50	1.50
period (msec)	16.8	16.8
Pmax (MW)	220	220
Etm (MW-sec)	4.67	4.82
Ttm (clad, C)	219	216
Tmax (clad, C)	> 350	328
tm (sec)	0.333	0.334
t_Tmax (sec)	-	0.353
BSP	1.26	1.31

F.1.1.3 Input

The following input incorporates modifications (b) and (c) noted above.

```
     0   200
*  SPERT I D12/25 TEST  $1.50 RAMP FROM 5W - Original Model Input - HTRAN0 -
fine dt
1001,     -2          21     7     0     1     1
1002,             0     0     6    -1     0    10
1003,    5.00000-6   5.20321-3     101360.       -20.0   7.62000-4
1004,    2.54000-4   2.54000-4    0.068680    0.062231     0.6096      0.0
1005,          0.0   7.00000-3   6.00000-5     9.80664    0.004556
1006,         0.80        0.80         1.0      997.79         0.0
1007,          0.0         0.0         0.0         0.0         1.0    0.001
1008,          0.0      0.0005       0.001        0.03        0.05     0.05
1009,         0.13     0.33333
1111,    0.0842957       1.000       1.000
1112,       1     1     1     0           0   4.03500+5
1113,         1.20       0.025   1.20000+5
1114,    0.0         0.0
2001,          0.0         0.0      151.53         0.0         0.0
2002,          0.0      1014.0   2.01140+6         0.0         0.0
2003,          0.0         0.0      183.11         0.0         0.0
2004,          0.0      1243.4   2.07090+6         0.0         0.0
3001,  6.3500000-5     5     1       0.955
3002,    2.54000-4     7     2         0.0
4001,    2.90285-2    21
5100,       1     0   0.0030353     0.00370        0.55       0.65     0.10
5100,         0.55      0.4214    0.028008
5101,    0.0         0.6096       0.8635     0.36576
5102,   0.7793        1.0          1.0        1.0
5103,   1.1671        1.0          1.0        1.0
5104,   1.4062        1.0          1.0        1.0
5105,   1.6255        1.0          1.0        1.0
5106,   1.8223        1.0          1.0        1.0
5107,   1.9936        1.0          1.0        1.0
```

```
5108,   2.1371       1.0         1.0         1.0
5109,   2.2510       1.0         1.0         1.0
5110,   2.3334       1.0         1.0         1.0
5111,   2.3833       1.0         1.0         1.0
5112,   2.4000       1.0         1.0         1.0
5113,   2.3833       1.0         1.0         1.0
5114,   2.3334       1.0         1.0         1.0
5115,   2.2510       1.0         1.0         1.0
5116,   2.1371       1.0         1.0         1.0
5117,   1.9936       1.0         1.0         1.0
5118,   1.8223       1.0         1.0         1.0
5119,   1.6255       1.0         1.0         1.0
5120,   1.4062       1.0         1.0         1.0
5121,   1.1671       1.0         1.0         1.0
5122,   0.7793       1.0         1.0         1.0
5200,      1     0   0.0030353     0.99630        0.55       0.65     0.10
5200,          0.55       0.4214    0.028008
5201,    0.0         0.6096       0.8635     0.36576
5202,   0.4257       1.0         1.0         1.0
5203,   0.6376       1.0         1.0         1.0
5204,   0.7682       1.0         1.0         1.0
5205,   0.8880       1.0         1.0         1.0
5206,   0.9955       1.0         1.0         1.0
5207,   1.0891       1.0         1.0         1.0
5208,   1.1675       1.0         1.0         1.0
5209,   1.2297       1.0         1.0         1.0
5210,   1.2747       1.0         1.0         1.0
5211,   1.3020       1.0         1.0         1.0
5212,   1.3111       1.0         1.0         1.0
5213,   1.3020       1.0         1.0         1.0
5214,   1.2747       1.0         1.0         1.0
5215,   1.2297       1.0         1.0         1.0
5216,   1.1675       1.0         1.0         1.0
5217,   1.0891       1.0         1.0         1.0
5218,   0.9955       1.0         1.0         1.0
5219,   0.8880       1.0         1.0         1.0
5220,   0.7682       1.0         1.0         1.0
5221,   0.6376       1.0         1.0         1.0
5222,   0.4257       1.0         1.0         1.0
6001,  0.03443      0.01240     0.21797    0.03050      0.19904    0.11100
6002,  0.38861      0.30100     0.11701    1.14000      0.04294    3.01000
9000,      3
9001,      0.0          0.0        1.50      0.070         1.50      100.0
10000,     2
10001,  2.99727     0.0         2.99727     100.0
11000,    16
11001,  0.0          0.0        0.0         293.15      0.07668   323.15
11002,  0.1406     348.15       0.2045      393.15      0.3323    423.15
11003,  0.4601     473.15       0.5879      523.15      0.7157    573.15
11004,  0.8435     623.15       0.9713      673.15      1.0991    723.15
11005,  1.2269     793.15       1.3291      823.15      1.4825    873.15
11006,  1.7381     973.15
12000,     2
12001,  0.00        0.0         0.00         0.0
14000,     3
14001,   0.005      0.0         0.0001      0.20        0.001        0.38
16000,     4
16001,   0.10          5        0.0         0.02           2         0.20
16002,   0.02          1        0.30        0.05           5         0.38
17000,     2
17001,   1.0        0.0         1.0         500.0
18000,     2
```

```
18001,   0.0        0.0         -10.0       0.600
```

F.1.2 IAEA 10 MW HEU Benchmark Reactor ($1.50 step)

F.1.2.1 Notes

This file contains notes on the bnch150h.inp PARET input file as supplied by N.Hanan, ANL (Dec.2003). The model is for a $1.50 step reactivity insertion in the IAEA 10MW benchmark HEU core from low power, ambient conditions with natural circulation flow only and no SCRAM shutdown.

** indicates different values than used in the Spert I D-12/25 model

GENERAL INFORMATION (1000 series cards)
entry
1 -2 = two channels, -ve is SI units
2 21 = axial nodes
3 7 = radial nodes
4 0 = slab geometry
5 1 = reactivity specified
6 1 = vapour fraction & quality calc in (1) both subcooled & saturation ranges
7 0 = inlet pressure specified
8 0 = reduce & expand kinetics timestep
9 6 = number of delayed neutron groups
10 -1 = printout option
11 0 = no average temperature printout in addition to detailed printout
12 10 = max heat transfer iterations

(1-12 are the same as used for the spert150.inp model)

13 ** 1E-6 = initial power (MW)
14 ** .010622139 = total vol of fuel in core (m3)
15 ** 1.70000E+5 = operation pressure (Pa)
16 ** 1.58650E+5 = moderator inlet (+ve) enthalpy (compare to 20C used for spert150.inp)
17 ** 6.35000E-4 = plate half thickness incl. clad (m)

18 ** 2.55000E-4 = fuel half thickness (m)
19 ** 2.55000E-4 = distance to inner surf of clad (=18) (m)

```
20 **  6.65000E-2 = plate width (m)
21 **  6.30000E-2 = fuel width (m)
22 **  0.6000     = active fuel height (m)
23     0.0        = inlet non-fueled section length (m)

24     0.0        = outlet non-fueled section length (m)
25 **  7.60710E-3 = Beff
26 **  55.9600E-6 = prompt neutron generation time (sec)
27     9.80664    = g (m/s2)
28 **  0.00975    = heat source descrip for moderator (unitless)

29 **  0.80       = transient time (sec)
30     0.8000     = const. in void generation equation (unitless)
31     1.0        = exponent in void generation equation (unitless)
32 **  993.20     = moderator reference density (kg/m3) - may be over-ridden
33     0.0        = const. coeff. in fuel temp feedback equ'n

34 **  3.60000E-5 = lin. coeff. in fuel temp feedback equ'n
35     0.0        = quad. coeff. in fuel temp feedback equ'n
36     0.0        = cub. coeff. in fuel temp feedback equ'n
36     0.0        = temp. offset coeff. in fuel temp feedback equ'n
38     1.0        = exponent in fuel temp feedback equ'n
39     0.001      = upper limit on kinetics timestep test (rec. 0.001)

40     0.0        = steady-state DNB heat fluxes calc'ed in code are used
41     0.0005     = nucleate boiling collapse time (sec)
42     0.001      = transition boiling bubble collapse time (sec)
43     0.03       = frac. of clad surf. heat flux in sub-cool nucleate boiling
44     0.05       = frac. of clad surf. heat flux in sub-cool transition boiling
45     0.05       = frac. of clad surf. heat flux in sub-cool film boiling

46 **  0.14       = nat. convection heat transfer constant no.1
47 **  0.33       = nat. convection heat transfer constant no.2

ADDITIONAL GENERAL INFORMATION (1111 series cards)

1111
1a **  .085792725 = total xsec flow area of all flow channels in core (m3)
2a     1.00       = flux weighting factor for channel 1 (rec. unity by ANL)
```

```
        1.00      = flux weighting factor for channel 2 (rec. unity by ANL)
1112
1b      1 = Seider-Tate single phase correlation
2b      1 = McAdams two phase correlation
3b      1 = transition model two phase transient scheme
4b      0 = original DNB correlation
5b **   0 = original single phase heat trans. subroutine (revised w entrance effects
used in spert150.inp)

6b      4.03500E+5 = ave core heat flux (W/m2) (only used with 4b = 3 & 4)
7b      not incl.  = bubble detachment parameter (only used with 4b = 3)
8b      not incl.  = Cp (J/kg-K) (used with 4b = 3 & 4)

1113
1c      1.2       = rate of ctrl rod movement (w scram or withdrawal) (m/sec)
2c      0.025     = delay time on rod move after trip (sec)
3c **   12.0      = overpower trip point (MW)
4c      0.0 (def)  = low flow trip point (%), default 0.0%

1114
1d      0.0       = ht. above reactor for nat. circ. effects (m)
2d      0.0       = ht. below reactor for nat. circ. effects (m)

THERMAL PROPERTIES OF FUEL ELEMENT MATERIALS (2000 series cards)
fuel
2001a10.0       = th. cond. equ'n quad. coeff.
2001a20.0       = th. cond. equ'n lin. coeff.
2001a3 ** 158.0    = th. cond. equ'n const. term (w/m-K)
2001a40.0       = th. cond. equ'n 1/over coeff.
2001a5  0.0       = th. cond. equ'n temp. offset coeff.

2002b1          0.0       = vol. heat cap. equ'n quad. coeff.
2002b2 ** 1067.00  = vol. heat cap. equ'n lin. coeff. (J/m3-K2)
2002b3 ** 2.07210E+6 = vol. heat cap. equ'n const. term (J/m3-K)
2002b4          0.0       = vol. heat cap. equ'n 1/over coeff.
2002b5          0.0       = vol. heat cap. equ'n temp. offset coeff.

clad
2003a10.0       = th. cond. equ'n quad. coeff.
```

2003a20.0 = th. cond. equ'n lin. coeff.
2003a3 ** 180.0 = th. cond. equ'n const. term (w/m-K)
2003a40.0 = th. cond. equ'n 1/over coeff.
2003a5 0.0 = th. cond. equ'n temp. offset coeff.

2004b1 0.0 = vol. heat cap. equ'n quad. coeff.
2004b2 ** 1242.00 = vol. heat cap. equ'n lin. coeff. (J/m3-K2)
2004b3 ** 2.06910E+6 = vol. heat cap. equ'n const. term (J/m3-K)
2004b4 0.0 = vol. heat cap. equ'n 1/over coeff.
2004b5 0.0 = vol. heat cap. equ'n temp. offset coeff.

RADIAL OR HALF-PLATE DESCRIPTION (3000 series cards)

3001
1 ** 6.37500E-5 = radial increment length (m)
2 5 = radial node out to which increment applies
3 1 = composition code (1=fuel)
4 0.955 = radial source descrip. (frac. of heat generated in composition)

3002
1 ** 1.90000E-4 = radial increment length (m)
2 7 = radial node out to which increment applies
3 2 = composition code (1=clad)
4 0.0 = radial source descrip. (frac. of heat generated in composition)

AXIAL DESCRIPTION (4000 series cards)

4001
1 ** 2.85714E-2 = axial region length (m)
2 21 = node number up to which increment applies

INDIVIDUAL CHANNEL INFORMATION (5000 series cards)
channel 1 (51XX series)
2a 1 = flow-forced channel (see Table 10)
3a 0 = pressure drop (Pa) (zero for 2a = 1)
4a ** 1.75000E-3 = radial distance from center of slab to center of channel (m)
5a ** 0.00181 = reactivity feedback wt. factor for channel (rec. vol. frac. of core)
6a 0.55 = loss coeff. for inlet of channel
7a 0.65 = loss coeff. for outlet of channel

8a ** 1.0 = inlet area ratio
9a ** 1.0 = outlet area ratio
10a ** 0.3257 = overall density/void coeff. ($/%-of-core-voided)
11a ** 0.015370 = overall coolant temperature coeff. ($/C)

1b 0.0 = length of inlet plenum (m)
2b ** 0.0 = length of outlet plenum (m)
3b ** 0.3048 = inlet plenum equiv. diameter (m)
4b ** 0.3048 = outlet plenum equiv. diameter (m)

2c 2.52(peak) = axial flux peaking factors (one for each axial node)
3c 1.0 (all) = moderator density feedback wt. factors (one for each axial node)
4c 1.0 (all) = fuel temperature feedback wt. factors (one for each axial node)
5c 1.0 (all) = coolant temperature feedback wt. factors (one for each axial node)

channel 2 (52XX series)
same as for channel 1 except
5a 0.99819 = reactivity feedback wt. factor for channel (rec. vol. frac. of core)
2c 1.50(peak) = axial flux peaking factors (one for each axial node)

DELAYED NEUTRON INFORMATION (6000 series cards)

6-groups (agrees with entry #9 on 1000 series cards)

all**	group	del. neut. fraction	decay const. (sec-1)
	1	3.89740E-2	1.27200E-2
	2	2.07990E-1	3.17390E-2
	3	1.88670E-1	1.16020E-1
	4	4.09410E-1	3.11030E-1
	5	1.28790E-1	1.3999
	6	2.61780E-2	3.8689

POWER OR REACTIVITY VS. TIME (9000 series cards)

1a 3 = number of pairs of entries in table

extern. inserted react. ($)	time (sec)
0.0	0.0
1.50	0.50 **

1.50 100.0

MODERATOR INLET MASS VELOCITY VS. TIME (10000 series cards)

1a 2 = number of pairs of entries in table

inlet mass vel. ((kg/s/m2)	time (sec)
3.21580E+3 **	0.0
3.21580E+3 **	100.0

PERCENT LINEAR THERMAL EXPANSION OF THE CLAD VS. TEMPERATURE (11000 series cards)

1a ** 2 = number of pairs of entries in table

all**	% linear therm. exp.	temperature (K)
	0.0	98.0
	0.0	1000.0

TOTAL PRESSURE DROP VS. TIME (12000 series cards)

1a 2 = number of pairs of entries in table

tot. pr. drop across chan. (N/m2 = Pa)	time (sec)
0.00	0.0
0.00	0.0

TABLE OF TIME INCREMENT VS. TIME (14000 series cards)

1a ** 3 = number of pairs of entries in table

time incr. (sec)	as of time (sec)
0.005	0.0
0.001	0.55 **
0.005 **	0.75 **

TABLE OF PRINT FREQUENCY VS. TIME (16000 series cards)

1a ** 4 = number of pairs of entries in table

print time incr. for major output (sec)	freq. of int. output (every X steps)	as of time (sec)
0.100	5	0.0
0.005	2	0.50 **
0.005 **	1	0.60 **
0.100 **	5	0.70 **

TABLE OF PUMP MASS VELOCITY FRACTION VS. TIME (17000 series cards)

1a 2 = number of pairs of entries in table

cool. mass vel. frac. in chan. rel. to initial	time (sec)
1.0	0.0
1.0	20.0 **

TABLE OF ROD WORTH VS. ROD LOCATION OR LAPSED TIME (18000 series cards)

1a 2 = number of pairs of entries in table
Note: rod rate specified in card 1113 so table is in distance not time

reactivity of rod bank ($)	rod position (m)
0.0	0.0
-10.0	0.600

F.1.2.2 Modifications

The following are notes on the modifications made to the bnch150h.inp file supplied by N.Hanan, ANL (Dec. 2004).

The modifications made to the file are:
(a) over-power trip point increase from 12 MW to 1.2E+5 MW, which effectively means the scram will not be activated on over-power as the power is not expected to reach this level.
(b) changed the single phase heat transfer subroutine selection from the original (option 0) to the revised, with entrance effects (option 2). This entry is made on the

1112 card.
(c) timestep shortened during transient (14000 series cards)
originally:
14000, 3
14001, 0.005 0.0 0.001 0.55 0.005 0.75
shortened:
14000, 3
14001, 0.005 0.0 0.0001 0.55 0.005 0.75
(d) removing modification (b)
(e) Including (d). Initial temperature changed from ~42C (using enthalpy) to 38C as specified in IAEA-TECDOC-643, App.G-0. This is entry 16 on the 1000 series cards.

(a) taking out the over-power trip significantly increases the burst parameters. For comparison:

	SCRAM	SELF-LIMITED
rho_in ($)	1.50	1.50
period (msec)	14.5	14.5
Pmax (MW)	132	357
Etm (MW-sec)	3.26	6.98
Ttm (clad, C)	136	215
Tmax (clad, C)	158	333
tm (sec)	0.656	0.666
t_Tmax (sec)	0.671	0.697
BSP	1.69	1.34

Note: that near the end of the run, well past the power peak and temperature peaks the code bombs out with negative temperatures of the coolant being calculated. This same problem was found with the Spert I D-12/25 self-limited model (spert150.inp) but in that case the termination was prior to the useful part of the transient.

(b) Including (a). Altering the single phase heat transfer subroutine selection from option 0 (original), to option 2 (revised with entrance effects), on the 1112 card has no effect on the burst parameter results. For comparison:

	S-L (OLD HT)	S-L (REVISED HT)
rho_in ($)	1.50	1.50
period (msec)	14.5	14.5
Pmax (MW)	357	357
Etm (MW-sec)	6.98	6.98
Ttm (clad, C)	215	215

Tmax (clad, C)	333	333
tm (sec)	0.666	0.666
t_Tmax (sec)	0.697	0.697
BSP	1.34	1.34

(c) Including (a) & (b). Shortening the time steps around the initial power peak and afterwards during the clad temperature peak do not significantly affect the burst parameters but do noticeably change the maximum clad temperature and timing of this parameter. For comparison:

	S-L (orig dt)	S-L (fine dt)
rho_in ($)	1.50	1.50
period (msec)	14.5	14.5
Pmax (MW)	357	356
Etm (MW-sec)	6.98	7.00
Ttm (clad, C)	215	213
Tmax (clad, C)	333	306
tm (sec)	0.666	0.666
t_Tmax (sec)	0.697	0.681
BSP	1.34	1.35

(d) Only (a) & (c). No difference was found in the burst parameters or the maximum clad temperture and timing with the change in the single phase heat transfer routine selection. For comparison:

	S-L (a-c)	S-L (Old HTRAN0)
rho_in ($)	1.50	1.50
period (msec)	14.5	14.5
Pmax (MW)	356	356
Etm (MW-sec)	7.00	7.00
Ttm (clad, C)	213	213
Tmax (clad, C)	306	306
tm (sec)	0.666	0.666
t_Tmax (sec)	0.681	0.681
BSP	1.35	1.35

(e) Changing the initial temperature from ~42C to 38C makes a slight impact on the burst parameters and the peak clad temperature, most notably on Pmax and Etm. For comparison:

	Ti~42C	Ti=38C
rho_in ($)	1.50	1.50
period (msec)	14.5	14.5
Pmax (MW)	356	371
Etm (MW-sec)	7.00	7.21

Ttm (clad, C)	213	214
Tmax (clad, C)	306	315
tm (sec)	0.666	0.666
t_Tmax (sec)	0.681	0.685
BSP	1.35	1.34

F.1.2.3 Input

The following is input file with modifications (e) as noted above.

```
     0
*  PARET:  HEU BENCHMARK  2 CHAN  $1.50/0.5S RAMP    Old HTRAN0 Opt - Self
Lim - Fine dt, Ti=38C
1001,     -2          21     7     0     1     1
1002,            0     0     6    -1     0    10
1003,    1.00000-6  .010622139   1.70000+5   -38.0      6.35000-4
1004,    2.55000-4   2.55000-4   6.65000-2   6.30000-2  0.6000     0.0
1005,   0.0         0.0076071     55.960-6   9.80664   0.00975
1006,   0.80        0.8000       1.0        993.20       0.0
1007,    3.60000-5    0.0        0.0         0.0         1.0       0.001
1008,   0.0           0.0005     0.001       0.03        0.05      0.05
1009,   1.4           0.33
1111,   .085792725  1.00        1.00
1112,      1     1     1     0     0        4.035000+5
1113,     1.2       0.025       1.2E+5        0.0
1114,    0.0        0.0
2001,   0.0         0.0         158.0       0.0         0.0
2002,   0.0          1.06700+3   2.07210+6   0.0         0.0
2003,   0.0        0.0          180.0       0.0         0.0
2004,   0.0          1.24200+3   2.06910+6   0.0         0.0
3001,    6.37500-5     5     1   0.955
3002,    1.90000-4     7     2   0.0
4001,    2.85714-2    21
5100,      1     0   1.75000-3  0.00181      0.55       0.65       1.0
5100,  1.0         0.3257         1.5370-2
5101,   0.0         0.0         0.3048      0.3048
5102,   0.1885      1.0         1.0         1.0
5103,   0.7172      1.0         1.0         1.0
5104,   1.0530      1.0         1.0         1.0
5105,   1.3674      1.0         1.0         1.0
5106,   1.6541      1.0         1.0         1.0
5107,   1.9073      1.0         1.0         1.0
5108,   2.1218      1.0         1.0         1.0
5109,   2.2934      1.0         1.0         1.0
5110,   2.4184      1.0         1.0         1.0
5111,   2.4945      1.0         1.0         1.0
5112,   2.5200      1.0         1.0         1.0
5113,   2.4945      1.0         1.0         1.0
5114,   2.4184      1.0         1.0         1.0
5115,   2.2934      1.0         1.0         1.0
5116,   2.1218      1.0         1.0         1.0
5117,   1.9073      1.0         1.0         1.0
5118,   1.6541      1.0         1.0         1.0
5119,   1.3674      1.0         1.0         1.0
5120,   1.0530      1.0         1.0         1.0
5121,   0.7172      1.0         1.0         1.0
```

```
5122,   0.1885      1.0         1.0         1.0
5200,      1     0   1.75000-3  0.99819      0.55       0.65       1.0
5200,  1.0          0.3257         1.5370-2
5201,   0.0         0.0         0.3048      0.3048
5202,   0.1122      1.0         1.0        1.0
5203,   0.4269      1.0         1.0        1.0
5204,   0.6268      1.0         1.0        1.0
5205,   0.8139      1.0         1.0        1.0
5206,   0.9846      1.0         1.0        1.0
5207,   1.1353      1.0         1.0        1.0
5208,   1.2630      1.0         1.0        1.0
5209,   1.3651      1.0         1.0        1.0
5210,   1.4395      1.0         1.0        1.0
5211,   1.4848      1.0         1.0        1.0
5212,   1.5000      1.0         1.0        1.0
5213,   1.4848      1.0         1.0        1.0
5214,   1.4395      1.0         1.0        1.0
5215,   1.3651      1.0         1.0        1.0
5216,   1.2630      1.0         1.0        1.0
5217,   1.1353      1.0         1.0        1.0
5218,   0.9846      1.0         1.0        1.0
5219,   0.8139      1.0         1.0        1.0
5220,   0.6268      1.0         1.0        1.0
5221,   0.4269      1.0         1.0        1.0
5222,   0.1122      1.0         1.0        1.0
6001,     3.89740-2    1.27200-2    2.07990-1    3.17390-2    1.88670-1
1.16020-1
6002,    4.09410-1   3.11030-1   1.28790-1   1.3999      2.61780-2   3.8689
9000,      3
9001    0.00        0.0        1.50         0.50       1.50          100.0
10000,     2
10001,   3.21580+3   0.0         3.21580+3   100.0
11000,     2
11001,   0.0         98.0        0.0         1000.0
12000,     2
12001,   0.0         0.0         0.0         0.0
14000,     3
14001,   0.005       0.0         0.0001      0.55        0.005        0.75
16000,     4
16001,   0.10          5        0.0         0.005          2         0.50
16002,   0.005         1        0.60        0.010          2         0.70
17000,     2
17001,    1.0        0.0          1.0      20.
18000,     2
18001,    0.0        0.0         -10.      0.6
```

F.1.3 IAEA 10 MW LEU Benchmark Reactor ($1.50 step)

F.1.3.1 Notes

This file contains notes on the bnch150l.inp PARET input file as supplied by N.Hanan, ANL (Dec.2003). The model is for a $1.50 step reactivity insertion in the IAEA 10MW benchmark LEU core from low power, ambient conditions with natural circulation flow only and no SCRAM shutdown.

** indicates different values than used in the Spert I D-12/25 model (spert150.inp)
+ indicates different values than used in the HEU IAEA 10MW reactor model (bnch150h.inp)

GENERAL INFORMATION (1000 series cards)
entry
1 -2 = two channels, -ve is SI units
2 21 = axial nodes
3 7 = radial nodes
4 0 = slab geometry
5 1 = reactivity specified
6 1 = vapour fraction & quality calc in (1) both subcooled & saturation ranges
7 0 = inlet pressure specified
8 0 = reduce & expand kinetics timestep
9 6 = number of delayed neutron groups
10 -1 = printout option
11 0 = no average temperature printout in addition to detailed printout
12 10 = max heat transfer iterations

(1-12 are the same as used for the spert150.inp model)

13 ** 1E-6 = initial power (MW)
14 ** .010622139 = total vol of fuel in core (m3)
15 ** 1.70000E+5 = operation pressure (Pa)
16 ** 1.58650E+5 = moderator inlet (+ve) enthalpy (compare to 20C used for spert150.inp)
17 ** 6.35000E-4 = plate half thickness incl. clad (m)

18 ** 2.55000E-4 = fuel half thickness (m)
19 ** 2.55000E-4 = distance to inner surf of clad (=18) (m)
20 ** 6.65000E-2 = plate width (m)
21 ** 6.30000E-2 = fuel width (m)
22 ** 0.6000 = active fuel height (m)
23 0.0 = inlet non-fueled section length (m)

24 0.0 = outlet non-fueled section length (m)
25 **+ 7.2753E-3 = Beff
26 **+ 43.740E-6 = prompt neutron generation time (sec)
27 9.80664 = g (m/s2)

28 **+ 0.00000 = heat source descrip for moderator (unitless)

29 **+ 3.00 = transient time (sec)
30 0.8000 = const. in void generation equation (unitless)
31 1.0 = exponent in void generation equation (unitless)
32 ** 993.20 = moderator reference density (kg/m3) - may be over-ridden
33 0.0 = const. coeff. in fuel temp feedback equ'n

34 **+ 3.31000E-3 = lin. coeff. in fuel temp feedback equ'n
35 0.0 = quad. coeff. in fuel temp feedback equ'n
36 0.0 = cub. coeff. in fuel temp feedback equ'n
36 0.0 = temp. offset coeff. in fuel temp feedback equ'n
38 1.0 = exponent in fuel temp feedback equ'n
39 0.001 = upper limit on kinetics timestep test (rec. 0.001)

40 0.0 = steady-state DNB heat fluxes calc'ed in code are used
41 0.0005 = nucleate boiling collapse time (sec)
42 0.001 = transition boiling bubble collapse time (sec)
43 0.03 = frac. of clad surf. heat flux in sub-cool nucleate boiling
44 0.05 = frac. of clad surf. heat flux in sub-cool transition boiling
45 0.05 = frac. of clad surf. heat flux in sub-cool film boiling

46 ** 0.14 = nat. convection heat transfer constant no.1
47 ** 0.33 = nat. convection heat transfer constant no.2

ADDITIONAL GENERAL INFORMATION (1111 series cards)

1111
1a ** .085792725 = total xsec flow area of all flow channels in core (m3)
2a 1.00 = flux weighting factor for channel 1 (rec. unity by ANL)
1.00 = flux weighting factor for channel 2 (rec. unity by ANL)
1112
1b **+ 2 = Petrukov-Popov single phase correlation (requires 5b=0) (Seider-Tate used for spert150.inp and bnch150h.inp)
2b 1 = McAdams two phase correlation
3b 1 = transition model two phase transient scheme
4b 0 = original DNB correlation
5b + 2 = revised, with entrance effects for h, single phase heat trans. subroutine (original used for bnch150h.inp)

6b 4.03500E+5 = ave core heat flux (W/m2) (only used with 4b = 3 & 4)
7b not incl. = bubble detachment parameter (only used with 4b = 3)
8b not incl. = Cp (J/kg-K) (used with 4b = 3 & 4)

1113
1c 1.2 = rate of ctrl rod movement (w scram or withdrawal) (m/sec)
2c 0.025 = delay time on rod move after trip (sec)
3c ** 12.0 = overpower trip point (MW)
4c **+ 85.0 = low flow trip point (%), default 0.0% (default used in spert150.inp and bnch150h.inp)
5c **+ 365.0 = prev. operation time (days) for decay heat calcs (default 24.0 days)

1114
1d 0.0 = ht. above reactor for nat. circ. effects (m)
2d 0.0 = ht. below reactor for nat. circ. effects (m)

THERMAL PROPERTIES OF FUEL ELEMENT MATERIALS (2000 series cards)
fuel
2001a10.0 = th. cond. equ'n quad. coeff.
2001a20.0 = th. cond. equ'n lin. coeff.
2001a3 **+ 50.0 = th. cond. equ'n const. term (w/m-K)
2001a40.0 = th. cond. equ'n 1/over coeff.
2001a5 0.0 = th. cond. equ'n temp. offset coeff.

2002b1 0.0 = vol. heat cap. equ'n quad. coeff.
2002b2 **+ 61.0800 = vol. heat cap. equ'n lin. coeff. (J/m3-K2)
2002b3 **+ 2.06000E+6 = vol. heat cap. equ'n const. term (J/m3-K)
2002b4 0.0 = vol. heat cap. equ'n 1/over coeff.
2002b5 0.0 = vol. heat cap. equ'n temp. offset coeff.

clad
2003a10.0 = th. cond. equ'n quad. coeff.
2003a20.0 = th. cond. equ'n lin. coeff.
2003a3 ** 180.0 = th. cond. equ'n const. term (w/m-K)
2003a40.0 = th. cond. equ'n 1/over coeff.
2003a5 0.0 = th. cond. equ'n temp. offset coeff.

2004b1 0.0 = vol. heat cap. equ'n quad. coeff.

2004b2 ** 1242.00 = vol. heat cap. equ'n lin. coeff. (J/m3-K2)
2004b3 ** 2.06910E+6 = vol. heat cap. equ'n const. term (J/m3-K)
2004b4 0.0 = vol. heat cap. equ'n 1/over coeff.
2004b5 0.0 = vol. heat cap. equ'n temp. offset coeff.

RADIAL OR HALF-PLATE DESCRIPTION (3000 series cards)

3001
1 ** 6.37500E-5 = radial increment length (m)
2 5 = radial node out to which increment applies
3 1 = composition code (1=fuel)
4 **+ 1.000 = radial source descrip. (frac. of heat generated in composition)

3002
1 ** 1.90000E-4 = radial increment length (m)
2 7 = radial node out to which increment applies
3 2 = composition code (1=clad)
4 0.0 = radial source descrip. (frac. of heat generated in composition)

AXIAL DESCRIPTION (4000 series cards)

4001
1 ** 2.85714E-2 = axial region length (m)
2 21 = node number up to which increment applies

INDIVIDUAL CHANNEL INFORMATION (5000 series cards)
channel 1 (51XX series)
2a 1 = flow-forced channel (see Table 10)
3a 0 = pressure drop (Pa) (zero for 2a = 1)
4a ** 1.75000E-3 = radial distance from center of slab to center of channel (m)
5a ** 0.00181 = reactivity feedback wt. factor for channel (rec. vol. frac. of core)
6a 0.55 = loss coeff. for inlet of channel
7a 0.65 = loss coeff. for outlet of channel
8a ** 1.0 = inlet area ratio
9a ** 1.0 = outlet area ratio
10a **+ 0.4047 = overall density/void coeff. ($/%-of-core-voided)
11a **+ 0.010820 = overall coolant temperature coeff. ($/C)

1b 0.0 = length of inlet plenum (m)

2b ** 0.0 = length of outlet plenum (m)
3b ** 0.3048 = inlet plenum equiv. diameter (m)
4b ** 0.3048 = outlet plenum equiv. diameter (m)

2c ** 2.52(peak) = axial flux peaking factors (one for each axial node)
3c 1.0 (all) = moderator density feedback wt. factors (one for each axial node)
4c 1.0 (all) = fuel temperature feedback wt. factors (one for each axial node)
5c 1.0 (all) = coolant temperature feedback wt. factors (one for each axial node)

channel 2 (52XX series)
same as for channel 1 except
5a ** 0.99819 = reactivity feedback wt. factor for channel (rec. vol. frac. of core)
2c ** 1.50(peak) = axial flux peaking factors (one for each axial node)

DELAYED NEUTRON INFORMATION (6000 series cards)

6-groups (agrees with entry #9 on 1000 series cards)

all**+ group	del. neut. fraction	decay const. (sec-1)
1	3.83850E-2	1.27270E-2
2	2.08620E-1	3.17160E-2
3	1.88730E-1	1.16700E-1
4	4.07220E-1	3.12140E-1
5	1.29940E-1	1.3985
6	2.71000E-2	3.8521

POWER OR REACTIVITY VS. TIME (9000 series cards)

1a 3 = number of pairs of entries in table

extern. inserted react. ($)	time (sec)
0.00	0.0
1.50	0.50 **
1.50	100.0

MODERATOR INLET MASS VELOCITY VS. TIME (10000 series cards)

1a 2 = number of pairs of entries in table

inlet mass vel. ((kg/s/m2)	time (sec)
3.21580E+3 **	0.0
3.21580E+3 **	100.0

PERCENT LINEAR THERMAL EXPANSION OF THE CLAD VS. TEMPERATURE (11000 series cards)

1a ** 2 = number of pairs of entries in table

all**	% linear therm. exp.	temperature (K)
	0.0	98.0
	0.0	1000.0

TOTAL PRESSURE DROP VS. TIME (12000 series cards)

1a 2 = number of pairs of entries in table

tot. pr. drop across chan. (N/m2 = Pa)	time (sec)
0.00	0.0
0.00	0.0

TABLE OF TIME INCREMENT VS. TIME (14000 series cards)

1a ** 3 = number of pairs of entries in table

time incr. (sec)	as of time (sec)
0.005	0.0
0.001	0.55 **
0.001 **+	0.75 **

TABLE OF PRINT FREQUENCY VS. TIME (16000 series cards)

1a ** 4 = number of pairs of entries in table

print time incr. for major output (sec)	freq. of int. output (every X steps)	as of time (sec)
0.100	5	0.0
0.002 **+	2	0.50 **

0.002 **+	1	0.60 **
0.050 **+	5	0.70 **

TABLE OF PUMP MASS VELOCITY FRACTION VS. TIME (17000 series cards)

1a 2 = number of pairs of entries in table

cool. mass vel. frac. in chan. rel. to initial	time (sec)
1.0	0.0
1.0	20.0 **

TABLE OF ROD WORTH VS. ROD LOCATION OR LAPSED TIME (18000 series cards)

1a 2 = number of pairs of entries in table
Note: rod rate specified in card 1113 so table is in distance not time

reactivity of rod bank ($)	rod position (m)
0.0	0.0
-10.0	0.600

F.1.3.2 Modifications

The following are notes on the modifications made to the bnch150l.inp file supplied by N.Hanan, ANL (Dec. 2004).

The modifications made to the file are:
(a1) over-power trip point increase from 12 MW to 1.2E+5 MW, which effectively means the scram will not be activated on over-power the power is not expected to reach this level.
(a2) low-flow trip point reduced from 85% to 0.0% (default). It is not clear if this will have any effect during the flow reversals due to boiling. (Note: total transient time reduced from 3.00 sec to 1.20 sec)
(b) Includes (a). Single phase correlation selection changed from option 2 (Petrukov-Popov) to option 1 (Seider-Tate)
(c) Includes (a) & (b). Changed heat source description from "no heat source in the moderator" to those values used in the IAEA HEU model (cards1000 series, entry 28; card 3001, entry 4).

(d) Includes (a), (b), & (c). Time step increment reduced during initial power peak and clad temperature peak.

originally:

```
14000,    3
14001,  0.005    0.0      0.001     0.55      0.001     0.75
```

modified:

```
14000,    3
14001,  0.005    0.0      0.0001    0.55      0.005     0.75
```

(e) Includes (a) to (d). Changed the single phase heat transfer subroutine selection from the revised, with entrance effects (option 2), to the original (option 0). This entry is made on the 1112 card.

(f) Including (e). Initial temperature changed from ~42C (using enthalpy) to 38C as specified in IAEA-TECDOC-643, App.G-0. This is entry 16 on the 1000 series cards.

(a1) taking out the over-power trip significantly increases the burst parameters. For comparison:

IAEA LEU	SCRAM	SELF-LIMITED
rho_in ($)	1.50	1.50
period (msec)	11.9	11.9
Pmax (MW)	147	274
Etm (MW-sec)	2.94	4.91
Ttm (clad, C)	135	172
Tmax (clad, C)	158	254
tm (sec)	0.613	0.619
t_Tmax (sec)	0.626	0.638
BSP	1.67	1.51

Note: the negative temperature problem which causes early termination of the code (seen for the IAEA HEU and SPERT I D-12/25 self-limiting cases) was not experienced in this case.

(a2) no difference observed when low-flow trip point set back to default

(b) significant different on Etm and Ttm as well as BSP. For comparison:

IAEA LEU	P-P	S-T
rho_in ($)	1.50	1.50
period (msec)	11.9	11.9
Pmax (MW)	274	273
Etm (MW-sec)	4.91	5.24
Ttm (clad, C)	172	180
Tmax (clad, C)	254	255

tm (sec)	0.619	0.621
t_Tmax (sec)	0.638	0.639
BSP	1.51	1.61

(c) Pmax is not significantly changed but Etm is reduced and Ttm and Tmax are also reduced. BSP changes noticeably. For comparison:

IAEA LEU	no mod heat	mod heat
rho_in ($)	1.50	1.50
period (msec)	11.9	11.9
Pmax (MW)	273	274
Etm (MW-sec)	5.24	5.08
Ttm (clad, C)	180	171
Tmax (clad, C)	255	249
tm (sec)	0.621	0.621
t_Tmax (sec)	0.639	0.644
BSP	1.61	1.56

(d) The finer time step spacing makes notable differences on the energy generation and the maximum clad temperatures as well as the BSP.

For comparison:

IAEA LEU	orig dt	fine dt
rho_in ($)	1.50	1.50
period (msec)	11.9	11.9
Pmax (MW)	274	274
Etm (MW-sec)	5.08	5.29
Ttm (clad, C)	171	179
Tmax (clad, C)	249	252
tm (sec)	0.621	0.621
t_Tmax (sec)	0.644	0.640
BSP	1.56	1.63

(e) Changing the single phase heat transfer subroutine does not make any significant difference on the burst parameters or the maximum clad surface temperature or timing.

For comparison:

IAEA LEU	rev HTRAN	orig HTRAN
rho_in ($)	1.50	1.50
period (msec)	11.9	11.9
Pmax (MW)	274	274
Etm (MW-sec)	5.29	5.29
Ttm (clad, C)	179	179
Tmax (clad, C)	252	252

tm (sec)	0.621	0.621
t_Tmax (sec)	0.640	0.643
BSP	1.63	1.63

(f) Changing the initial temperature from ~42C to 38C makes a slight impact on the burst parameters and the peak clad temperature. For comparison:

	Ti~42C	Ti=38C
rho_in ($)	1.50	1.50
period (msec)	11.9	11.9
Pmax (MW)	274	279
Etm (MW-sec)	5.29	5.31
Ttm (clad, C)	179	177
Tmax (clad, C)	252	249
tm (sec)	0.621	0.621
t_Tmax (sec)	0.643	0.641
BSP	1.63	1.60

F.1.3.3 Input

The following is the input file for modification (f) noted above.

```
     0
*   PARET:  LEU BENCHMARK  2 CHAN  $1.50/0.5S RAMP   HTRAN0 Opt, HS-mod,
SELF-LIM, Fine dt, Ti=38C
1001,     -2          21     7     0     1     1
1002,            0     0     6    -1     0    10
1003,    1.00000-6  .010622139   1.70000+5   -38.0       6.35000-4
1004,    2.55000-4   2.55000-4   6.65000-2   6.30000-2  0.6000     0.0
1005,   0.0         0.0072753     43.740-6   9.80664   0.00975
1006,   1.20        0.8000        1.0        993.20       0.0
1007,    3.31000-3    0.0         0.0         0.0         1.0        0.001
1008,   0.0           0.0005      0.001       0.03        0.05       0.05
1009,   1.4           0.33
1111,   .085792725  1.00         1.00
1112,      1     1     1     0     0         4.035000+5
1113,     1.2       0.025       1.20000E+5      0.0         365.0
1114,    0.0        0.0
2001,   0.0         0.0          50.0       0.0         0.0
2002,   0.0          6.10800+1   2.06000+6   0.0         0.0
2003,   0.0        0.0          180.0       0.0         0.0
2004,   0.0          1.24200+3   2.06910+6   0.0         0.0
3001,    6.37500-5     5     1   0.955
3002,    1.90000-4     7     2   0.0
4001,    2.85714-2    21
5100,      1     0   1.75000-3  0.00181      0.55       0.65       1.0
5100,  1.0         0.4047         1.0820-2
5101,   0.0         0.0         0.3048      0.3048
5102,   0.1885      1.0         1.0         1.0
5103,   0.7172      1.0         1.0         1.0
5104,   1.0530      1.0         1.0         1.0
5105,   1.3674      1.0         1.0         1.0
```

```
5106,   1.6541      1.0         1.0         1.0
5107,   1.9073      1.0         1.0         1.0
5108,   2.1218      1.0         1.0         1.0
5109,   2.2934      1.0         1.0         1.0
5110,   2.4184      1.0         1.0         1.0
5111,   2.4945      1.0         1.0         1.0
5112,   2.5200      1.0         1.0         1.0
5113,   2.4945      1.0         1.0         1.0
5114,   2.4184      1.0         1.0         1.0
5115,   2.2934      1.0         1.0         1.0
5116,   2.1218      1.0         1.0         1.0
5117,   1.9073      1.0         1.0         1.0
5118,   1.6541      1.0         1.0         1.0
5119,   1.3674      1.0         1.0         1.0
5120,   1.0530      1.0         1.0         1.0
5121,   0.7172      1.0         1.0         1.0
5122,   0.1885      1.0         1.0         1.0
5200,      1     0   1.75000-3  0.99819      0.55       0.65       1.0
5200,  1.0         0.4047         1.0820-2
5201,   0.0         0.0         0.3048      0.3048
5202,   0.1122      1.0         1.0       1.0
5203,   0.4269      1.0         1.0       1.0
5204,   0.6268      1.0         1.0       1.0
5205,   0.8139      1.0         1.0       1.0
5206,   0.9846      1.0         1.0       1.0
5207,   1.1353      1.0         1.0       1.0
5208,   1.2630      1.0         1.0       1.0
5209,   1.3651      1.0         1.0       1.0
5210,   1.4395      1.0         1.0       1.0
5211,   1.4848      1.0         1.0       1.0
5212,   1.5000      1.0         1.0       1.0
5213,   1.4848      1.0         1.0       1.0
5214,   1.4395      1.0         1.0       1.0
5215,   1.3651      1.0         1.0       1.0
5216,   1.2630      1.0         1.0       1.0
5217,   1.1353      1.0         1.0       1.0
5218,   0.9846      1.0         1.0       1.0
5219,   0.8139      1.0         1.0       1.0
5220,   0.6268      1.0         1.0       1.0
5221,   0.4269      1.0         1.0       1.0
5222,   0.1122      1.0         1.0       1.0
6001,     3.83850-2    1.27270-2    2.08620-1    3.17160-2    1.88730-1
1.16700-1
6002,    4.07220-1   3.12140-1   1.29940-1   1.3985      2.71000-2   3.8521
9000,      3
9001    0.00        0.0        1.50         0.50       1.50          100.0
10000,     2
10001,   3.21580+3   0.0         3.21580+3   100.0
11000,     2
11001,   0.0         98.0        0.0         1000.0
12000,     2
12001,   0.0         0.0         0.0         0.0
14000,     3
14001,   0.005       0.0         0.0001      0.55        0.005        0.75
16000,     4
16001,   0.10          5        0.0         0.005          2         0.50
16002,   0.005         1        0.60        0.010          2         0.70
17000,     2
17001,    1.0        0.0          1.0      20.
18000,     2
18001,    0.0        0.0         -10.      0.6
```

F.2 PARET Benchmarked Options

The following is information on the input options used in the PARET benchmarking of the Spert I B-24/32, B-12/64, and D-12/25 transients.

Information taken from Woodruff, Nucl. Tech., v.64, Feb. 1984, p.196:

General information:
2 channels (hot, average; card 10XX, entry 1)
initial power = 5E-6 MW (card 10XX, entry 13)
moderator inlet temp. = 20C (card 10XX, entry 16)

const. in void generation eqn = 0.80 (card 10XX, entry 30)
exponent in void generation eqn = 1.0 (card 10XX, entry 31)

NB bubble lifetime = 0.0005 sec (card 10XX, entry 41)
TB bubble lifetime = 0.001 sec (card 10XX, entry 42)
NB frac. of surf. heat flux producing voids = 0.03 (card 10XX, entry 43)
TB frac. of surf. heat flux producing voids = 0.05 (card 10XX, entry 44)
FB frac. of surf. heat flux producing voids = 0.05 (card 10XX, entry 45)

single-phase heat trans. = Rosenthal & Miller (card 111X, entry 1b) ***
**** option not listed in Input Description and Seider-Tate in spert150.inp (see below)
two-phase heat trans. = McAdams (card 111X, entry 2b)
transient two-phase scheme = transition model (card 111X, entry 3b)
CHF estimates = original DNB correlation (card 111X, entry 4b)

channel information:
avg channel cosine peak of 1.311 from Buckling used in reactivity coefficient calculations.
hot channel cosine peak taken from overall peak/avg flux ratios reported from Spert flux wires
Used in: 5000 series cards
(note: inlet is bottom of the core for upward nat circ., outlet
plenum is taken as the height of hydrostatic head above the core)
inlet plenum height = 0 cm (card 51XX. entry 1b)
oulet plenum height = 61cm (card 51XX, entry 2b)
exit loss coefficient, inlet plenum = 0.55 (card 51XX, entry 6a)

exit loss coefficient, outlet plenum = 0.65 (card 51XX, entry 7a)

initial inlet flow = 0.003 m/sec (= 3 kg/sec/m2, for card series 10000)

	B-24/32	B-12/64	D-12/25
prompt neutron gen. time (msec)	50.0	77.0	60.0
Beff	0.007	0.007	0.007
cool. temp. coeff. ($/C)	-2.528E-2	-4.157E-2	-2.801E-2
void/density coeff. ($/%-void)	-0.3571	-0.150	-0.4214
Doppler coeff. ($/C)	--	--	--
Peak/Avg Power	2.5	2.2	2.4

rho insertion time = 0.070 sec (card series 9000)

RESULTS: using these options the clad temperature was overestimated - either by 7% or 22% depending on TB fraction of surface heat flux producing voids (parameter). The onset of film boiling does not necessarily result in "burnout" or CHF conditions (*i.e.*, clad melting). Agreement is best for short period ranges where the feedback is predominantly from coolant voiding.

IAEA 10MW BENCHMARK CORES:

Input Options:
The PARET options and parameters used are identical to those used for the Spert I models, with the following:
single-phase heat trans. = S-T (card 111X, entry 1b)

	HEU	LEU
prompt neutron gen. time (msec)	55.96	43.74
Beff	7.607E-3	7.275E-3
cool. temp. coeff. ($/C)	-1.537E-2	-1.082E-2
void/density coeff. ($/%-void)	-0.3257	-0.4047
Doppler coeff. ($/C)	-3.6E-5	-3.31E-3

RESULTS: Clad melting temperature taken as 582C for Al 6061.
$1.50/0.5sec unprotected

	HEU	LEU
Period (msec)	14.5	11.9
Pmax (MW)	371	283
Etm (MW-sec)	7.30	5.56
tm (sec)	0.667	0.622

Ttm (C)	220	181
Tmax (C)	308	263
tmax (sec)	0.685	0.642

Step Insertion:
Rho limit precluding clad surface melt (HEU) = $2.35
Rho limit precluding clad surface melt (LEU) = $2.80
0.5 sec Ramp Insertion:
Rho limit precluding clad surface melt (HEU) = $3.20
Rho limit precluding clad surface melt (LEU) = $7.40

Rho limit (for both HEU and LEU) and ratio of LEU/HEU increases significantly with increasing rho insertion time.